NUREG/CR–4550
SAND86–2084
Vol. 3, Rev. 1, Part 3

Analysis of Core Damage Frequency: Surry Power Station, Unit 1 External Events

Prepared by
M. P. Bohn, J. A. Lambright, S. L. Daniel, J. J. Johnson,
M. K. Ravindra, P. O. Hashimoto, M. J. Mraz, W. H. Tong

Sandia National Laboratories
Operated by
Sandia Corporation

Prepared for
U.S. Nuclear Regulatory Commission

NUREG/CR–4550
SAND86–2084
Vol. 3, Rev. 1, Part 3

NUREG/CR--4550-Vol.3-Rev.1-Pt.3

TI91 006719

Analysis of Core Damage Frequency: Surry Power Station, Unit 1 External Events

Manuscript Completed: November 1990
Date Published: December 1990

Prepared by
M. P. Bohn, J. A. Lambright, S. L. Daniel, J. J. Johnson*,
M. K. Ravindra*, P. O. Hashimoto*, M. J. Mraz*, W. H. Tong*

Sandia National Laboratories
Albuquerque, NM 87185

Prepared for
Division of Systems Research
Office of Nuclear Regulatory Research
U.S. Nuclear Regulatory Commission
Washington, DC 20555
NRC FIN A1228

*EQE, Inc.

ABSTRACT

The U.S. Nuclear Regulatory Commission has sponsored probabilistic risk assessments of five operating commercial nuclear power plants as part of a major update of the understanding of risk as provided by the original WASH-1400 risk assessments. In contrast to the WASH-1400 studies, the NUREG-1150 risk assessments include a detailed analysis (for two plants) of risks due to earthquakes, fires, floods, etc. (which are collectively known as "external events"). This report presents the external events probabilistic risk assessment for the Surry Power Station (Unit 1).

In keeping with the philosophy of the internal events analyses for NUREG-1150, which are intended to be "smart" PRAs making full use of all insights gained during the past ten years' developments in risk assessment methodologies, the corresponding external event analyses performed by newly-developed methods which are an improvement over past methodologies in terms of completeness and reproducibility and which, in many cases, provide significant simplifications in calculational effort. These methods have been development at Sandia National Laboratories (SNL) under the sponsorship of the NRC's Division of Systems Research as part of their Dependent Failure Methodology Development Program.

As a first step, an extensive screening analysis was performed which showed that all external events had a negligible contribution except fires and seismic events. Detailed analyses for fire and seismic events were then performed. The final analysis of internal fires resulted in a total (mean) core damage frequency of 1.13E-5 per year. The final analysis of the seismic risk resulted in a total (mean) core damage frequency of 1.16E-4 per year using hazard curves developed by Lawrence Livermore National Laboratory (LLNL). The mean seismic core damage frequency was also calculated using hazard curves developed by the Electric Power Research Institute (EPRI) and found to be 2.50E-5 per year. Uncertainty analyses were performed for both fire and seismic events, and dominant components and sources of uncertainty were identified.

TABLE OF CONTENTS

CONTENTS (Continued)

CONTENTS (Continued)

CONTENTS (Concluded)

FIGURES

FIGURES (continued)

TABLES

TABLES (continued)

FOREWORD

This is one of numerous documents that support the preparation of the NUREG-1150 document by the NRC Office of Nuclear Regulatory Research. Figure 1 illustrates the front-end documentation. There are three interfacing programs performing this work: the Accident Sequence Evaluation Program (ASEP), the Severe Accident Risk Reduction Program (SARRP), and the Phenomenology and Risk Uncertainty Evaluation Program (PRUEP). The Zion PRA was performed at the Idaho National Engineering Laboratory and at Brookhaven National Laboratory.

Table 1 is a list of the original primary documentation and the corresponding revised documentation. There are several items that should be noted. First, in the original NUREG/CR-4550 report, Volume 2 was to be a summary of the internal analyses. This report was deleted. In Revision 1, Volume 2 now is the expert judgment elicitation covering all plants. Volumes 3 and 4 include external events analyses for Surry and Peach Bottom, respectively.

The revised NUREG/CR-4551 covers the analysis included in the original NUREG/CR-4551 and NUREG/CR-4700. However, it is different from NUREG/CR-4550 in that the results from the expert judgment elicitation are given in four parts to Volume 2 with each part covering one category of issues. The accident progression event trees are given in the appendices for each of the plant analyses.

Originally, NUREG/CR-4550 was published without the designation "Draft for Comment." Thus, the final revision of NUREG/CR-4550 is designated Revision 1. The label Revision 1 is used consistently on all volumes except Volume 2, which was not part of the original documentation. NUREG/CR-4551 was originally published as a "Draft for Comment" so, in its final form, no Revision 1 designator is required to distinguish it from the previous documentatation.

There are several other reports published in association with NUREG-1150. These are:

NUREG/CR-5032, SAND87-2428, Modeling Time to Recovery and Initiating Event Frequency for Loss of Off-site Power Incidents at Nuclear Power Plants, R. L. Iman and S. C. Hora, Sandia National Laboratories, Albuquerque, NM, January 1988.

NUREG/CR-4840, SAND88-3102, Procedures for External Event Core Damage Frequency Analyses for NUREG-1150, M. P. Bohn and J. A. Lambright, Sandia National Laboratories, Albuquerque, NM, November 1990.

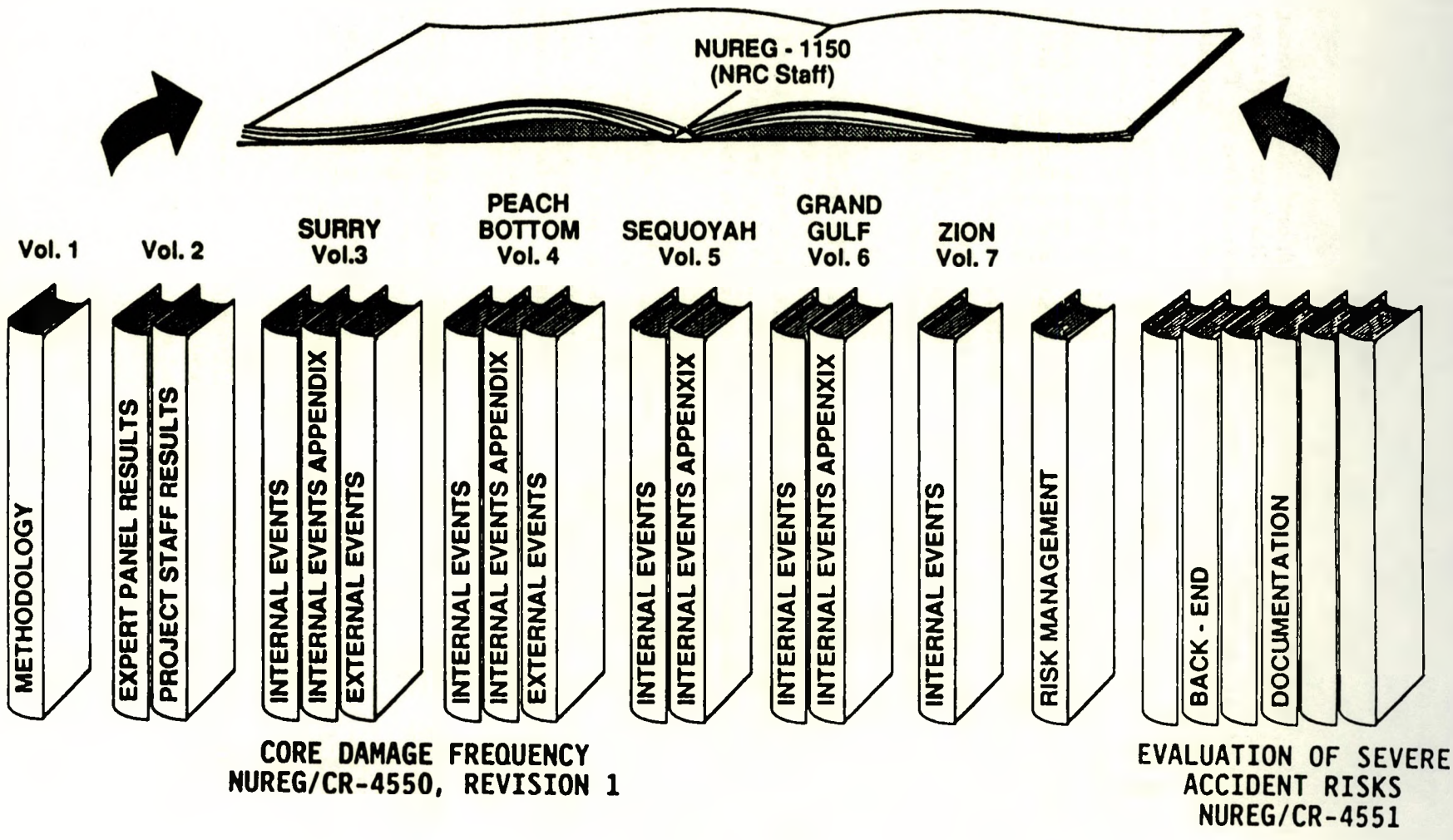

FIGURE 1. DOCUMENTATION FOR NUREG-1150.

Table 1.

NUREG-1150 Analysis Documentation

Original Documentation

NUREG/CR-4550
Analysis of Core Damage Frequency From Internal Events

Volume 1 Methodology
2 Summary (Not Published)
3 Surry Unit 1
4 Peach Bottom Unit 2
5 Sequoyah Unit 1
6 Grand Gulf Unit 1
7 Zion Unit 1

NUREG/CR-4551
Evaluation of Severe Accident Risks and the Potential for Risk Reduction

Volume 1 Surry Unit 1
2 Sequoyah Unit 1
3 Peach Bottom Unit 2
4 Grand Gulf Unit 1

NUREG/CR-4700
Containment Event Analysis for Potential Severe Accidents

Volume 1 Surry Unit 1
2 Sequoyah Unit 1
3 Peach Bottom Unit 2
4 Grand Gulf Unit 1

Revised Documentation

NUREG/CR-4550, Revision 1
Analysis of Core Damage Frequency

Volume 1 Methodology
2 Part 1 Expert Judgment Elicit.--Expert Panel
Part 2 Expert Judgment Elicit.--Project Staff
3 Part 1 Surry Unit 1 Internal Events
Part 2 Surry Unit 1 Internal Events App.
Part 3 Surry Unit 1 External Events
4 Part 1 Peach Bottom Unit 2 Internal Events
Part 2 Peach Bottom Unit 2 Internal Events App.
Part 3 Peach Bottom Unit 2 External Events
5 Part 1 Sequoyah Unit 1 Internal Events
Part 2 Sequoyah Unit 1 Internal Events App.
6 Part 1 Grand Gulf Unit 1 Internal Events
Part 2 Grand Gulf Unit 1 Internal Events App.
7 Zion Unit 1 Internal Events

NUREG/CR-4551, Evaluation of Severe Accident Risks

Volume 1 Methodology
2 Part 1 Expert Judgment Elicit.--In-vessel
Part 2 Expert Judgment Elicit.--Containment
Part 3 Expert Judgment Elicit.--Structural
Part 4 Expert Judgment Elicit.--Source-Term
Part 5 Expert Judgment Elicit.--Supp. Calc.
Part 6 Expert Judgment Elicit.--Proj. Staff
Part 7 Expert Judgment Elicit.--Supp. Calc.
Part 8 Expert Judgment Elicit.--MACCS Input
3 Part 1 Surry Unit 1 Anal. and Results
Part 2 Surry Unit 1 Appendices
4 Part 1 Peach Bottom Unit 2 Anal. and Results
Part 2 Peach Bottom Unit 2 Appendices
5 Part 1 Sequoyah Unit 2 Anal. and Results
Part 2 Sequoyah Unit 2 Appendices
6 Part 1 Grand Gulf Unit 1 Anal. and Results
Part 2 Grand Gulf Unit 1 Appendices
7 Part 1 Zion Unit 1 Anal. and Results
Part 2 Zion Unit 1 Appendices

NUREG/CR-4772, SAND86-1996, Accident Sequence Evaluation Program Human Reliability Analysis Procedure, A, D. Swain III, Sandia National Laboratories, Albuquerque, NM, February 1987.

NUREG/CR-5263, SAND88-3100, The Risk Management Implications of NUREG-1150 Methods and Results, A. C. Camp et al., Sandia National Laboratories, Albuquerque, NM, December 1988.

A Human Reliability Analysis for the ATWS Accident Sequence with MSIV Closure at the Peach Bottom Atomic Power Station, A-3272, W. J. Luckas, Jr. et al., Brookhaven National Laboratory, Upton, NY, 1986.

A brief flow chart for the documentation is given in Figure 2. Any related supporting documents to the back-end NUREG/CR-4551 analyses are delineated in NUREG/CR-4551. A complete list of the revised NUREG/CR-4550, volumes and parts is given below.

General

NUREG/CR-4550, Volume 1, Revision 1, SAND86-2084, Analysis of Core Damage Frequency: Methodology Guidelines for Internal Events.

NUREG/CR-4550, Volume 2, SAND86-2084, Analysis of Core Damage Frequency from Internal Events: Expert Judgment Elicitation on Internal Events Issues - Part 1: Expert Panel Results, Part 2: Project Staff Results.

Part 1 and 2 of Volume 2, NUREG/CR-4550 are bound together. This volume was not part of the original documentation and was first published in April 1989 and distributed in May 1989 with the title: Analysis of Core Damage Frequency from Internal Events: Expert Judgment Elicitation. In retrospect, a more descriptive title would be: Analysis of Core Damage Frequency: Expert Judgment Elicitation on Internal Events Issues.

SURRY

NUREG/CR-4550, Volume 3, Revision 1, Part 1, SAND86-2084, Analysis of Core Damage Frequency: Surry Unit 1 Internal Events.

NUREG/CR-4550, Volume 3, Revision 1, Part 2, SAND86-2084, Analysis of Core Damage Frequency: Surry Unit 1 Internal Events Appendices.

NUREG/CR-4550, Volume 3, Revision 1, Part 3, SAND86-2084, Analysis of Core Damage Frequency: Surry Unit 1 External Events.

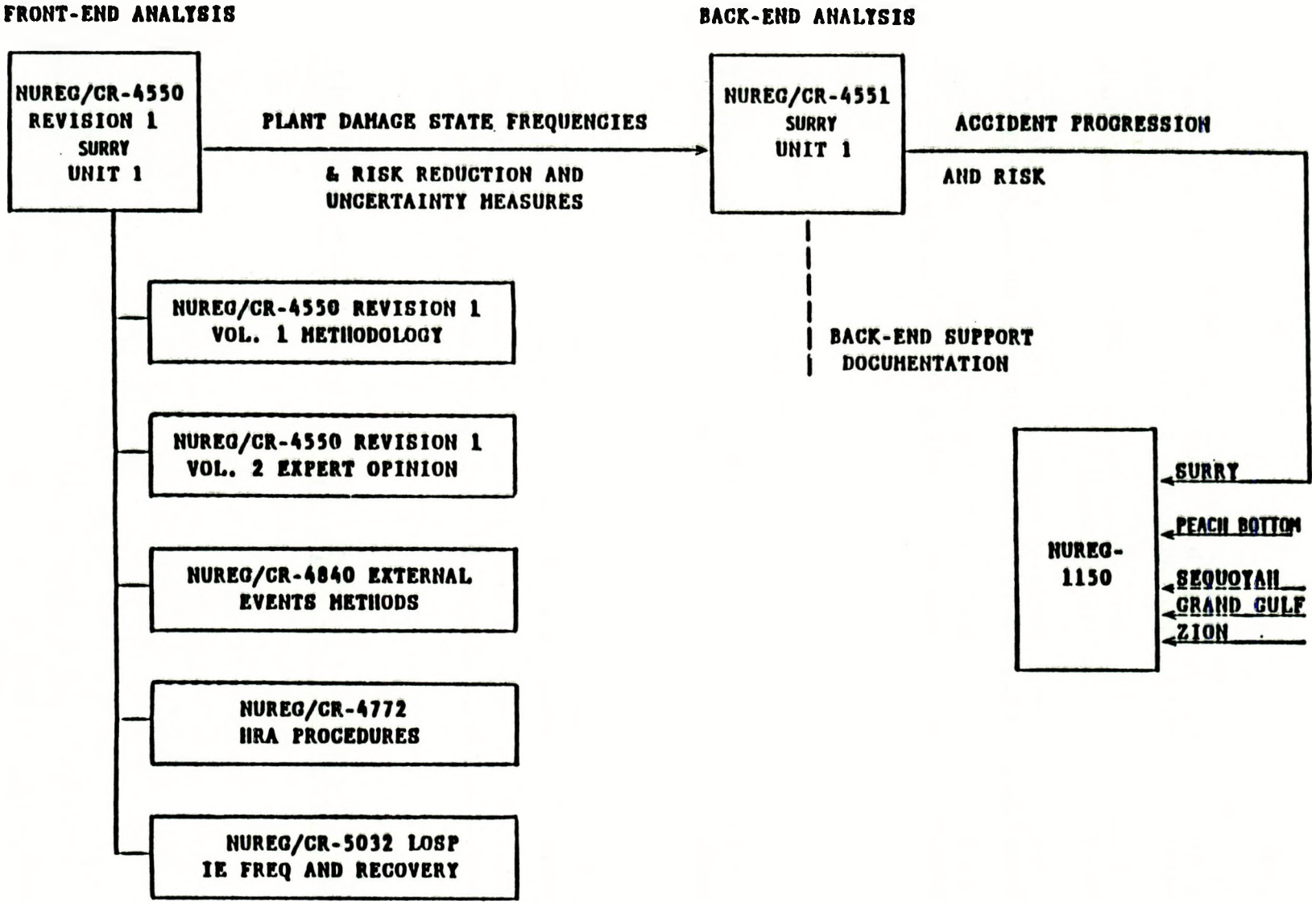

Figure 2. Surry Related Documentation.

Peach Bottom

NUREG/CR-4697, EGG-2464, Containment Venting Analysis for the Peach Bottom Atomic Power Station, D. J. Hansen et al., Idaho National Engineering Laboratory (EG&G Idaho, Inc.) February 1987.

NUREG/CR-4550, Volume 4, Revision 1, Part 1, SAND86-2084, Analysis of Core Damage Frequency: Peach Bottom Unit 2 Internal Events.

NUREG/CR-4550, Volume 4, Revision 1, Part 2, SAND86-2084, Analysis of Core Damage Frequency: Peach Bottom Unit 2 Internal Events Appendices.

NUREG/CR-4550, Volume 4, Revision 1, Part 3, SAND86-2084, Analysis of Core Damage Frequency: Peach Bottom Unit 2 External Events.

Sequoyah

NUREG/CR-4550, Volume 5, Revision 1, Part 1, SAND86-2084, Analysis of Core Damage Frequency: Sequoyah Unit 1 Internal Events.

NUREG/CR-4550, Volume 5, Revision 1, Part 2, SAND86-2084, Analysis of Core Damage Frequency: Sequoyah Unit 1 Internal Events Appendices.

Grand Gulf

NUREG/CR-4550, Volume 6, Revision 1, Part 1, SAND86-2084, Analysis of Core Damage Frequency: Grand Gulf Unit 1 Internal Events.

NUREG/CR-4550, Volume 6, Revision 1, Part 2, SAND86-2084, Analysis of Core Damage Frequency: Grand Gulf Unit 1 Internal Events Appendices.

Zion

NUREG/CR-4550, Volume 7, Revision 1, EGG-2554, Analysis of Core Damage Frequency: Zion Unit 1 Internal Events.

EXECUTIVE SUMMARY

The U.S. Nuclear Regulatory Commission (USNRC) is sponsoring probabilistic risk assessment of five operating commercial nuclear power plants as part of a major update of the understanding of risk as provided by the original WASH-1400 assessments. In contrast to the WASH-1400 studies, two of the NUREG-1150 risk assessments will include a detailed analysis of risks due to earthquakes, fires, floods, etc., which are collectively known as "external events." The two plants for which external events were analyzed are Surry and Peach Bottom, a PWR and a BWR, respectively. This report presents the results obtained for the Surry (Unit 1) external events core damage frequency assessment.

In keeping with the philosophy of the internal events analyses for NUREG-1150, which are intended to be "smart" PRAs making full use of all insights gained during the past ten years' developments in risk assessment methodologies, the corresponding external event analyses have been performed by newly-developed methods. The methods have been developed under NRC sponsorship and represent, in many cases, both advancements and simplifications over techniques that have been used in past years. They also include the most up-to-date data bases on equipment seismic fragilities, fire occurrence frequencies and fire damageability thresholds. These methods were developed at Sandia National Laboratories under the sponsorship of the USNRC's Division of Systems Research as part of their Dependent Failure Methodology Development Program. The first application of these new methods was to the seismic analysis of six power plants as part of the NRC program for the resolution of Unresolved Safety Issue USI A-45 - Adequacy of Decay Heat Removal Systems. Extension of these methods to fire, flood, etc., has been continuing during recent years.

In contrast to most past external event analyses, wherein rudimentary systems models were developed reflecting each external event under consideration, the NUREG-1150 external event analyses are based on the full internal event PRA systems models (event trees and fault trees) and make use of extensive computer-aided screening to reduce them to accident sequence cut sets important to each external event. This provides two major advantages in that both consistency and scrutability with respect to the internal event analysis is achieved, and the full gamut of random and test/maintenance unavailabilities are automatically included, while only those probabilistically important survive the screening process. Thus, full benefit of the internal event analysis is obtained by performing the internal and external event analyses sequentially.

The external event analysis began with a review of the FSAR, related design documents and the systems descriptions in the internal events PRA. Important components were located on general arrangement drawings. The utility fire study prepared to meet Appendix R of 10CFR50 requirements formed the basis for the initial identification of fire and flood area boundaries and barriers. Shortly thereafter, a plant visit of 3 days duration was made, involving an integrated team of specialists in the various external events. Based on the plant walkdown and the screening analysis described in Chapter 3, all external hazards were screened out based on probability considerations except for seismic and fire events.

The seismic risk assessment was the critical path item due to the time required to assemble the structural drawings and models. A best estimate structural dynamic response calculation for each building containing equipment important to safety was made using models used in the original design. The results were distributions for floor slab accelerations, and estimates of variability and correlations. Component fragilities were obtained either from a generic data base or derived on a plant-specific basis as needed. Dual probabilistic screening methods were used to determine important cutsets while allowing for explicit incorporation of correlation. The seismic hazard itself was obtained by extrapolation from the results of the NRC-sponsored Eastern Seismic Hazard Characterization Program performed at Lawrence Livermore National Laboratory (LLNL) and the industry-sponsored Electric Power Research Institute (EPRI) Seismic Hazard Methodology for the Central and Eastern United States Program.

The detailed fire analysis tasks were performed in parallel. Fire initiator frequencies were obtained from an updated historical data set developed at SNL. Partitioning of building fire frequencies (for which data are available) down to sub-area frequencies was based on cable loading, electrical cabinet locations and transient combustible estimates based on walkdown observations and a transient combustible data base developed at Sandia. Component damage temperatures (rather than auto-ignition temperatures) were based on SNL fire tests. The COMPBRN III code was used to predict component temperatures in fire areas where growth and separation are important considerations. Critical area analyses using the SETS code provided sequence cut sets for quantification, including barrier failure and random failures as appropriate. A fire detection/suppression histogram developed at SNL was used to incorporate firefighting timing into the analysis.

Similar approaches were used for internal and external floods, tornadoes, winds, etc. A major economy is achieved by analyzing fires and floods together, and seismic, wind and tornado events together, due to the commonality of the analysis processes. For example, it is a minor task to extend the seismic fragility derivations to be applicable to wind fragilities. Similar economies arise in the screening steps for fires and floods.

Detailed analysis of internal fires resulted in a total (mean) core damage frequency of 1.13E-5 per year. A detailed seismic analysis resulted in a total (mean) core damage frequency of 1.16E-4 per year using hazard curves developed by Lawrence Livermore National Laboratory. The mean seismic core damage frequency was also calculated using hazard curves developed by the Electric Power Research Institute and found to be 2.50E-5 per year. Uncertainty analyses were performed for both fire and seismic events, and dominant components and sources of uncertainty were identified.

In general, it was found that only a few accident sequences dominated the seismic and fire analysis results. For the seismic analysis, the most dominant sequence is a loss of offsite power (LOSP) transient sequence in which the auxiliary feedwater system fails (due to loss of a condensate storage tank) and the high pressure injection (HPI) system (and hence, the feed and bleed function) fails due to either failure of the refueling water storage tank or failures of the onsite AC power system. The second most significant seismic sequence is also a loss of offsite power transient sequence, except that this transient sequence leads to a seal LOCA. This is caused by failure of both the HPI system and the component cooling water (CCW) system which leads to the seal LOCA. The HPI system fails as described above while the CCW system fails due to loss of onsite AC power. Together, these two sequences constitute approximately 67% of the computed seismic core damage frequency.

The fire core damage frequency was found to be due to hypothesized fire events in four areas: (a) the emergency switchgear room, (b) the auxiliary building, (c) the control room, and (d) the cable vault/tunnel. In the case of the emergency switchgear room, cable vault/tunnel, and the auxiliary building, a reactor coolant pump seal LOCA leads to core damage. The fire itself fails cabling for both the HPI and CCW systems resulting in a seal LOCA. For the control room, a general transient with a subsequent stuck-open PORV leads to a small LOCA. Failure to control the plant from the auxiliary shutdown panel results in core damage. Together, these four areas gave rise to 99% of the fire risk.

1.0 INTRODUCTION

1.1 The NUREG-1150 Risk Analyses

This report describes the Level 1 external events probabilistic risk assessment (PRA) performed for the Surry commercial nuclear power plant as part of the NRC-sponsored Accident Sequence Evaluation Program (Ref. 1) power plant risk reevaluations, often referred to as the NUREG-1150 program (after the principal document summarizing the results of the program). In contrast to the original WASH-1400 risk assessments (Ref. 2), both internal and external events risk analyses are being performed in this program.

A Level 1 PRA consists of an analysis of plant design and operation focusing on accident sequences that could lead to core damage, their basic causes, and frequencies. Two kinds of accident initiators are considered for a Level 1 PRA, initiating events that occur within the power plant systems themselves and accident initiators caused by events external to the power plant systems. Examples of external initiators include earthquakes, floods and high winds. The results of both analyses provide assessments of plant safety, design and procedural adequacy, and insights into how the plant functions from the perspective of preventing core damage. This report documents work performed for the Level 1 external events PRA. It describes the methodology used, assumptions, data and models that provide the basis for the work, and the final results.

The methods utilized in the NUREG-1150 external events PRAs represent both advancements, and, in many cases, simplifications over techniques that have been used in past years. They include the most up-to-date data bases on equipment seismic fragilities, fire occurrence frequencies and fire damageability thresholds. In addition, they provide for minimization of execution time and cost reduction through the use of past PRA experience, generic data bases and defensible methodological simplification where possible. A full description of these procedures is given in Bohn and Lambright (Ref. 3). The methods were developed to meet the following objectives:

a. To be consistent with the internal event PRA analyses. The same event trees/fault trees and random, common mode failure and test and maintenance data are used.

b. To be transparent. A standard report format provides the data to enable the reader to reproduce the any of the point estimate results.

c. To be realistic. Best estimate data and models are used. All important plant-specific failure modes are analyzed.

d. To be consistent. The external event analyses are intended to be consistent with the internal event analyses due to common generic data, and methodology, and common level of detail.

1.2 The External Event Methodology

The simplified PRA procedures described in this section are based on the following general concepts:

a. The external event analyses are based on the internal event risk assessment plant system models and fault trees, and (other than preliminary data gathering) are not started until the internal events systems analysis (event trees and fault trees) has been finalized.

b. Vigorous and systematic screening of the full range of external events to which the plant could conceivably be exposed (e.g., aircraft crash, external flooding, tornado, extreme wind, etc.) is performed to eliminate early all unimportant contributing events.

c. Simultaneous and coordinated evaluation of all non-negligible external events is performed to minimize data gathering efforts and prevent duplication of effort. For example, building fragilities for extreme winds can be derived directly from seismic fragilities. Also, simultaneous evaluation produces insights into interactions (for example, seismic-fire interactions) not otherwise readily perceived.

d. In the analysis of each types of external event, computer-aided screening techniques and generic failure data are used prior to detailed component failure analysis calculations.

The general steps in the analysis of any external event risk analysis are shown below:

a. Determine the hazard.

b. Model plant and systems.

c. Solve fault trees with screening techniques to determine non-negligible cut sets.

d. Determine responses, fragilities, and correlation for basic events in non-negligible cut sets.

e. Evaluate point estimate sequence and core damage frequencies.

f. Perform uncertainty analysis and sensitivity studies.

These general steps apply to the full range of external events to which a power plant may be exposed. Table 1.1 presents a reasonably complete list of such events. Past PRA experience (Ref. 3) shows that only a very few of these are significant contributors to risk at any given site. In fact, the seismic and fire events are commonly the most important

contributors. In addition, external flooding, tornado or aircraft crashes are less frequent (and usually less significant) contributors.

Simplifications in Step (a), hazard determination, have been identified for both the seismic and fire analyses. Computer-aided screening techniques are used for Step (c) for fire, flood and seismic analyses to reduce the required number of plant-specific component failure calculations. For Step (d), response determination, seismic design fixed-base structural models are utilized in conjunction with an accurate and fully defensible soil-structure interaction model. While not a simplification, this process has been made very efficient by standardization, and use of variabilities and correlation factors derived from previous detailed seismic PRA work. Thus, in each step, defensible simplifications are identified which results, overall, in a cost-effective yet defensible analysis.

The procedures used here have been applied (in whole or in part) to six power plants as part of the U.S. NRC-sponsored Unresolved Safety Issue A-45 resolution program (Ref. 4), and have been applied at the N-Reactor (Ref. 5) and Savannah River (Ref. 6) Department of Energy reactor facilities.

Table 1.1

List of External Events

Major PRA Consideration	Minor PRA Consideration
Seismic	Lightning
Fire	Low Lake/River Level
Internal Flood	Ice Cover
	Avalanche
	Forest Fire
	Industrial Facility Accident
	Landslide
	Meteorite
	Volcanic Activity
	Hail

Occasional PRA Consideration
External flood
Transportation accidents
Pipe line accidents
Aircraft impact
Extreme winds
Tornado

1.3 Steps in the Analysis

1.3.1 Plant Walkdown and Data Gathering

The Surry external events analysis began with a plant visit in April 1987. The initial visit served as the basis for the initial plant information request submittal. Prior to the first plant visit, the external events team was briefed by the internal events systems analyst as to the general character of safety systems, support systems, system success criteria and critical interdependencies identified to date. In addition, applicable Final Safety Analysis Report (FSAR) sections were reviewed, and a basic set of plant general arrangement drawings were obtained for each team member.

The team consisted of the following personnel:

PRA Project Manager - M. P. Bohn
Team Leader - J. A. Lambright
Structural Fragility Analysts - J. J. Johnson, P. O. Hashimoto
Fire and Flood PRA Analyst - J. A. Lambright
External Event Screening Analyst - R. Ravindra

During the initial walkdown, team members visited all areas containing safety or support equipment except the containment. Two full days were adequate for this initial visit. At the completion of this initial visit, the following had been obtained.

a. A list of components suspected of being vulnerable to seismic damage and requiring site specific fragility analysis.

b. A list of potential secondary seismic structural failures (masonry walls, etc.) and components potentially damaged by these secondary failures.

c. A copy of the civil/structural drawing index for the plant from which needed drawings may be identified.

d. Sketches of typical anchorage details for important tanks, heat exchangers, electrical cabinets, etc.

e. A visual evaluation of structural connectivity of floor slabs, wall-to-ceiling connections, location of diaphragm cut-outs etc., which define load carrying paths. These were to be compared with structural drawings later.

f. For each room or compartment containing essential safety equipment, an identification of fire sources (power cables, pump motors, solvents, etc.), locations of fire barriers, fire/smoke detectors, separation of cable trains, etc., and a list of equipment in the room.

g. For each room or compartment, an identification of flooding sources (tanks, high or low pressure piping), floor drains, pumps, flood walls, flood detectors, etc.

h. A brief list of key plant personnel or utility engineering/licensing personnel to be contacted later if specific questions arose.

Following the initial plant visit, a list of needed drawings and documentation was prepared and sent to the designated plant contact. A second visit to the plant was made by the fire analysis personnel to allow for cable path tracing and verification. This was undertaken after the preliminary fire screening analysis had been performed based on a review of the plant Appendix R submittal. A final plant visit was made in September 1988. During this final visit initial conclusions as to plant vulnerabilities were reviewed with plant personnel, assumptions were verified, and final required data was obtained.

1.3.2 Screening of Other External Events

As mentioned in Section 1.1, the full range of possible external events was considered, but based on the FSAR and the initial plant visit, the vast majority of the external hazards was shown to have negligible impact. The set of general screening criteria which was used is given in the PRA Procedures Guide (Ref. 7) and is summarized as follows:

An external event can be excluded if:

a. The event is of equal or lesser damage potential than the events for which the plant has been designed. This requires an evaluation of plant design bases in order to estimate the resistance of plant structures and systems to a particular external event. For example, it is shown by Kennedy, Blejwas and Bennett (Ref. 8) that safety-related structures designed for earthquake and tornado loadings in Zone 1 can safely withstand a 3.0 psi static pressure from explosions. Hence, if the PRA analyst demonstrates that the overpressure resulting from explosions at a source (e.g., railroad, highway or industrial facility) cannot exceed 3 psi, these postulated explosions need not be considered.

b. The event has a significantly lower mean frequency of occurrence than other events with similar uncertainties and could not result in worse consequences than those events. For example, the PRA analyst may exclude an event whose mean frequency of occurrence is less than some small fraction of those for other events. In this case, the uncertainty in the frequency estimate for the excluded event is judged by the PRA analyst as not significantly influencing the total risk.

c. The event cannot occur close enough to the plant to affect it. This is also a function of the magnitude of the event. Examples of such events are landslides, volcanic eruptions and earthquake fault ruptures.

d. The event is included in the definition of another event. or example, storm surges and seiches are included in external flooding; the release of toxic gases from sources external to the plant is included in the effects of either pipeline accidents, industrial or military facility accidents, or transportation accidents.

These criteria are usually sufficient to exclude all but a few "other" external events. For those remaining, a simple bounding analysis (Ref. 9) will often provide sufficient justification for exclusion. The screening and bounding analyses for Peach Bottom are given in Chapter 3.

1.3.3 Seismic Risk Assessment Methodology

A nuclear power plant is designed to ensure the survival of all buildings and emergency safety systems in a worst-case ("safety shutdown") earthquake. The assumptions underlying this design process are deterministic and subject to considerable uncertainty. It is not possible, for example, to accurately predict the worst earthquake that will occur at a given site. Soil properties, mechanical properties of buildings, and damping in buildings and internal structures also vary significantly. To model and analyze the coupled phenomena that contribute to the total risk of radioactive release requires consideration of all significant sources of uncertainty as well as all significant interactions. Total risk is then obtained by considering the entire spectrum of possible earthquakes and integrating their calculated consequences. This point underscores an important requirement for a seismic PRA; the nuclear power plant must be examined in its entirety, as a system.

A second important aspect which must be addressed in a seismic PRA is that during an earthquake, all parts of the plant are excited simultaneously. Thus, during an earthquake, redundant safety system components experience highly correlated base motion, and there is a high likelihood that multiple redundant components would be damaged if one is. Hence, the planned-for redundancy would be comprised. This "common-cause" failure possibility represents a potentially significant risk to nuclear power plants during earthquakes.

The simplified seismic risk methodology reported here is based, in part, on the results of two earlier NRC-sponsored programs. The first was the Seismic Safety Margins Research Program. In the SSMRP, a detailed seismic risk assessment methodology was developed. This program culminated in a detailed evaluation of the seismic risk at the Zion nuclear power station, Bohn (Ref. 10). In this evaluation, an attempt

was made to accurately compute the responses of all walls and floor slabs in the Zion structures, moments in the all important piping systems, accelerations of all important valves, and the spectral acceleration at each safety system component (pump, electrical buss, motor control center, etc.). Correlation between the responses of all components was computed from the detailed dynamic response calculations. The important safety and auxiliary systems functions were analyzed, and fault trees were developed which traced failure down to the individual component level. Event trees related the system failures to accident sequences and radioactive release modes. Using these detailed models and calculations, it was possible to evaluate the seismic risk at Zion, and determine quantitatively the risk importance of the components, initiating events, and accident sequences.

The second is the NRC-sponsored Eastern Seismic Hazard Characterization program (Ref. 11) which performed a detailed earthquake hazard assessment of all sites east of the Rocky mountains. Results of these two programs formed the basis for a number of simplifications used in the seismic methodology reported here.

There are seven steps required for calculating the seismic risk at a nuclear power plant:

a. Determine the local earthquake hazard (hazard cure and site spectra).

b. Identify accident scenarios for the plant which lead to radioactive release (initiating events and event trees).

c. Determine failure modes for the plant safety and support systems (fault trees).

d. Determine the responses (accelerations or forces) of all structures and components (for each earthquake level).

e. Determine fragilities (probabilistic failure criteria) for the important structures and components.

f. Compute the probability of core damage using the information from Steps (a) through (e).

g. Estimate uncertainty in the core damage frequencies.

Only the level of detail differentiates a simplified seismic analysis from a detailed seismic PRA. The seven steps of the NUREG-1150 seismic risk analysis procedure are summarized below.

Step a - Seismic Hazard Characterization

The NUREG-1150 seismic analyses make use of hazard curves obtained from two recent programs aimed at developing sets of hazard curves based on

consistent data bases and assunptions. The first is the Eastern United States Seismic Hazard Characterization Program supported by the USNRC at Lawrence Livermore National Laboratory. The second is the industy-sponsored Seismic Hazard Methodology program performed by the Electric Power Research Institute. In both these programs, hazard curves were developed for all U.S. commercial nuclear power plant sites east of the Rocky Mountains.

Step b - Initiating Events and Event Trees

The scope of NUREG-1150 includes all potential initiating events, including loss of coolant accidents (vessel rupture, and large, medium, and small LOCAs) and transient events. Two types of transients are being considered: those in which the power conversion system (PCS) is initially available (denoted Type T3 transients) and those in which the PCS is failed as a direct consequence of the initiating event (denoted Type T1 transients). The event trees derived for the internal event analyses are utilized.

The reactor vessel rupture and large LOCA event frequencies were based on a Monte Carlo analysis of steam generators and reactor coolant pump support failures. The medium and small LOCA event frequencies are obtained from detailed piping failure calculations performed in the SSMRP.

The frequency of Type T1 transients is based on the probability of seismically-induced loss of offsite power (LOSP). This is the dominant type of transient (for the majority of plants for which LOSP causes loss of main feedwater). The frequency of the Type T3 initiating event is computed from the condition that the sum of the initiating event probabilities must be unity. The hypothesis is that, given an earthquake of reasonable size, at least one of the initiating events will occur.

Step c - Fault Trees

Fault trees for the safety systems at Surry have been developed in the internal events analysis for random failures only. These fault trees are used, with modification to include basic events for seismic failure modes. The trees are re-solved for pertinent seismic cut sets to be included in the probabilistic calculations. Probabilistic culling is used in re-solving these trees in such a way as to assure that important correlated seismic failure modes are not lost.

Step d - Component and Structure Failure Descriptions

Component seismic fragilities are obtained both from a generic fragility data base and from plant-specific fragilities developed for components identified during the plant walkdown.

The generic data base of fragility functions for seismically-induced failures was originally developed as part of the SSMRP (Ref. 10). Fragility functions for the generic categories were developed based on a combination of experimental data, design analysis reports, and an

extensive expert opinion survey. The experimental data utilized in developing fragility curves were obtained from the results of component manufacturer's qualification tests, independent testing lab failure data and data obtained from the U.S. Corps of Engineers extensive SAFEGUARD Subsystem Hardness Assurance Program (Ref. 12). These data were statistically combined with the expert opinion survey data to produce fragility curves for each of the generic component categories as reported in Reference 10. This generic data base was then updated by an evaluation of 19 site-specific seismic PRAs to yeild the final generic fragility data base used for the Surry and Peach Bottom NUREG-1150 PRAs.

Detailed structural fragility analyses were performed for all important safety related structures at the Surry plant. In addition, an analysis of liquefaction for the underlying soils was performed. These were included directly in the risk assessment.

Step e - Seismic Response of Structures and Components

Building and component seismic responses are estimated from peak ground accelerations at several probability intervals on the hazard curve. Three basic aspects of seismic response--best estimates, variability, and correlation--are generated. Zion analysis results from SSMRP and simplified methods studies form the basis for assigning scaling, variability and correlation of responses.

In each case, SHAKE code (Ref. 13) calculations are performed to assess the effect of the local soil column (if any) on the surface peak ground acceleration and soil structure interactions. This permits an evaluation of the effects of non-homogenous underlying soil conditions which can strongly affect the building responses.

Fixed base mass-spring (eigen-system) models are either obtained from the plants architect/engineer or are developed from the plant drawings as needed. Using these models one can compute the floor slab accelerations using the CLASSI code (Ref. 14). This code takes a fixed-base eigensystem model of the structure and input-specified frequency dependent soil impedances and computes the structural response (as well as variation in structural response if desired).

Variability in responses (floor and spectral accelerations) is assigned based on the SSMRP results. The recommended uncertainties (expressed as standard deviations of the logarithms of the responses) are shown below:

Quantity	Random
Peak Ground Acceleration	0.25
Floor Zero Period Acceleration	0.35
Floor Spectral Acceleration	0.45

Correlation between component failures is being included explicitly. In computing the correlation between component failures (in order to quantify the cut sets) it is necessary to consider correlations both in the responses and in the fragilities of each component. Inasmuch as

there are no data as yet on correlation between fragilities, the fragility correlations between like components are taken as zero, and the possible effect of such correlation can be quantified in a sensitivity study. The correlation between responses is assigned according to a set of rules that are explained in Chapter 4.0.

Step f - Probabilistic Failure and Core Damage Calculations

Given the input from the five steps above, the SETS (Ref. 15) code and mean basic event frequencies are used to calculate the required output (mean probabilities of failure, core damage, etc.).

Step g - Estimate Uncertainties

Complete uncertainty distributions were computed for all accident sequences and core damage frequencies using a Monte Carlo approach.

1.3.4 Internal Fire Assessment Methodology

Based on nuclear power plant operating experience over the last 20 years, it has been observed that typical nuclear power plants will have three to four significant fires over their operating lifetime. Previous probabilistic risk assessments (PRAs) have shown that fires are a significant contributor to the overall core damage frequency, contributing anywhere from 7 percent to 50 percent of the total (considering contributions from internal, seismic, flood, fire, and other events). Because of the relatively high core damage contribution, fires are always examined in detail. An overview of the simplified fire PRA methodology is as follows:

A. Initial Plant Visit

Based on the internal event and seismic analyses, the general location of cables and components of the systems of interest is known. The plant visit provides the analyst with a means of seeing the physical arrangements in each of these areas. The analyst will have a fire zone checklist which will aid the screening analysis and in the quantification step.

The second purpose of the initial plant visit is to confirm with plant personnel that the documentation being used is, in fact, the best available information and to get clarification about any questions that might have arisen in a review of the documentation. Also, a thorough review of firefighting procedures is conducted.

B. Screening

It is necessary to select important fire locations within the power plant under investigation having the greatest potential for producing risk-dominant accident sequences. The objectives of location selection are

somewhat competing and should be balanced in a meaningful risk assessment study. The first objective is to maximize the possibility that all important locations are analyzed, and this leads to the consideration of a potentially large number of candidate locations. The second objective is to minimize the effort spent in the quantification of event trees and fault trees for fire locations that turn out to be unimportant. A proper balance of these objectives is one that results in an ideal allocation of resources and efficiency of assessment.

The screening analysis is comprised of:

1. Identification of relevant fire zones.

2. Screening fire zones on probability of fire-induced initiating events.

3. Screening of fire zones on both order and frequency of cut sets.

4. Numerical evaluation and culling based on probability for each remaining fire zone.

C. Quantification

After the screening analysis has eliminated all but the probabilistically-significant fire zones, quantification of dominant cut sets is completed as follows:

1. Determine temperature response in each fire zone.

2. Compute component fire fragilities.

3. Assess the probability of barrier failure for all remaining combinations of fire zones.

4. Perform a recovery analysis.

Finally, an uncertainty analysis is performed to estimate error bounds on the computed fire-induced core damage frequencies. The Surry fire analysis is presented in Chapter 5.

1.4 References

1. U.S. Nuclear Regulatory Commission, Severe Accident Risks: An Assessment for Five U. S. Nuclear Power Plants, NUREG-1150, Second Draft for Peer Review, Vol. 1, June 1989.

2. U.S. Nuclear Regulatory Commission, Reactor Safety Study: An Assessment of Accident Risks in U.S. Nuclear Power Plants, WASH-1400, NUREG-75/014, 1975.

3. M. P. Bohn, and J. A. Lambright, Procedures for the External Event Core Damage Frequency Analyses for NUREG-1150, Sandia National Laboratories, Albuquerque, NM, NUREG/CR-4840, SAND88-3102, November 1990.

4. D. M. Ericson, Jr. et al, Shutdown Decay Heat Removal Analysis: Plant Case Studies and Special Issues, NUREG/CR-5230, SAND88-2375, April 1989.

5. J. A. Lambright and M. P. Bohn, Analysis of Core Damage Frequency Due to External Events at the DOE N-Reactor, Sandia National Laboratories, SAND89-1147, August 1990.

6. J. A. Lambright, Analysis of Core Damage Frequency Due to Fire at the Savannah River K-Reactor, Sandia National Laboratories, SAND89-1786, August 1990.

7. U.S. Nuclear Regulatory Commission, PRA Procedures Guide, NUREG/CR-2300, January 1983.

8. R. P. Kennedy, Blejwas, T. E., and D. E. Bennett, Capacity of Nuclear Power Plant Structures to Resist Blast Loadings, Sandia National Laboratories, NUREG/CR-2462, SAND83-1250, September 1983.

9. M. K. Ravindra and H. Banon, Methods for External Event Screening Quantification, Sandia National Laboratories, NUREG/CR-4839, SAND87-7156, August 1990.

10. M. P. Bohn, et al., Application of the SSMRP Methodology to the Seismic Risk at the Zion Nuclear Power Plant, Lawrence Livermore National Laboratory, Livermore, CA, NUREG/CR-3428, 1983.

11. D. L. Bernreuter, et al., Seismic Hazard Characterization of the Eastern United States: Methodology and Interim Results for Ten Sites, Lawrence Livermore National Laboratory, NUREG/CR-3756, April 1984.

12. U.S. Army Corps of Engineers, Subsystem Hardness Assurance Report, HNDDSP-72-156-ED.R, Vols I and II, 1975.

13. P. B. Schnabel, J. Lysmer, and H. B. Seed, SHAKE--A Computer Program for Earthquake Response Analysis of Horizontally Layered Sites, Earthquake Engineering Research Center, University of California, Berkeley, CA, EERC 72-12, 1972.

14. H. L. Wong and J. E. Luco, Soil-Structure Interaction: A Linear Continuum Mechanics Approach (CLASSI), Dept. of Civil Engineering, University of Southern California, Los Angeles, CA, CE79-03, 1980.

15. R. B. Worrell, SETS Reference Manual, Sandia National laboratories, Albuquerque, NM, SAND83-2675, NUREG/CR-4213, May 1985.

2.0 PLANT DESCRIPTION

2.1 Plant, Site and General Characteristics

The twin PWR units (Surry 1 and Surry 2) of Virginia Electric and Power Company are each rated at 781 MW. The reactor and generator for both the units were supplied by Westinghouse Electric Corporation. The plant began commercial operation in 1972-1973. Stone and Webster Engineering Corporation was the Architect/Engineer/Constructor for these plants. A type 3D containment design was used. Other Class I structures include the auxiliary building; control room area, including switchgear and relay rooms; fuel building; auxiliary generator cubicles; auxiliary containment buildings that contain main steam and feedwater isolation valves; recirculation spray and low-head safety injection pump cubicles; safeguards ventilation room and circulating water intake structures, including the high-level canal. All these structures have been designed to meet both earthquake and tornado criteria.

2.2 Description of Plant Systems

2.2.1 Introduction

This section discusses the system descriptions and system models of the major frontline and support systems identified as important to safety. In addition to the event trees discussed in Section 2.3, component fault trees also developed by the internal events analysts were utilized. Use of the same event trees, fault trees, and accident sequences developed during the internal events analysis ensured consistency between these major studies.

The discussion of the systems that follow includes:

a. A brief functional description of the system with reference to the one-line diagrams that were developed to indicate which components were included in the model;

b. Safety-related success criteria that were applied to the system;

c. Interfaces and safety actuation provisions between the frontline systems and the support systems.

2.2.2 Containment Spray System

The containment spray system (CSS) provides the initial containment pressure reduction following an accident by spraying cool water from the reactor water storage tank (RWST) to condense steam in the containment.

The Surry CSS is composed of two 100 percent capacity spray injection trains. The CSS has no recirculation or pump cooling capability. Each spray train draws water from the RWST through independent suction lines.

Each CSS pump takes suction through a normally open MOV and an in-line filter assembly. Each CSS pump discharges through a pair of normally closed MOVs arranged in parallel and through a check valve to its associated containment spray header. Both CSS pumps also feed a common third spray header (located on the outside of the crane wall) through separate check valves. A simplified schematic of the CSS is shown in Figure 2.1.

The CSS automatically starts on receipt of a Hi-Hi (25 psia) containment pressure signal from the consequence limiting control system (CLCS). The CLCS signals open the pump inlet and outlet valves and start the CSS pumps. An agastat timer in the pump start circuit delays pump start for 30 seconds after receipt of the signal. The success criterion for the CSS is one of the two CSS trains that provides flow to any one containment spray header.

2.2.3 High Pressure Injection/Recirculation System

The Surry charging system provides normal coolant makeup to the reactor coolant system (RCS) and cooling flow to the reactor coolant pump (RCP) seals under normal operating conditions. The high pressure injection/ recirculation (HPI/HPR) system uses the same charging pumps to provide primary coolant injection and recirculation following an accident, as well as maintaining flow to the RCP seals. The HPI system also functions to deliver boric acid to the RCS from the boric acid transfer system if emergency boration is required.

Under normal operating conditions, one of the three charging pumps provides normal RCS makeup and cooling to the RCP seals by taking suction from the volume control tank (VCT) through two motor-operated valves (MOVs) in series.

Upon indication of a loss of RCS coolant or steam line break (i.e., low pressurizer level, high containment pressure, high pressure differential between main steam header and any steam line, or high steam flow with low average temperature (T_{AVG}) or low steam line pressure), the safety injection actuation system (SIAS) initiates emergency coolant injection. The SIAS signals the normal charging line isolation valves to close, the standby charging pumps to start, the valves from the VCT to close, the normally open pump inlet and outlet MOVs to open, and a parallel set of normally closed MOVs to open to provide suction from the RWST. Also on receipt of an SIAS signal, a parallel set of normally closed MOVs open to provide flow from the pump discharge header to the three RCS cold legs. An additional path to the RCS cold legs through a manually operated normally closed MOV is also available. Flow through this line to the RCS is treated as a recovery action. The line to the RCP seals remains open throughout the event. The HPI system may also be used in the "feed and bleed" cooling mode. The only difference in this mode of operation from that discussed above is that a SIAS signal is not necessarily generated so the HPI system is manually placed in service.

In the recirculation mode of operation, the charging pumps draw suction from the discharge of the low pressure safety injection pumps in the low

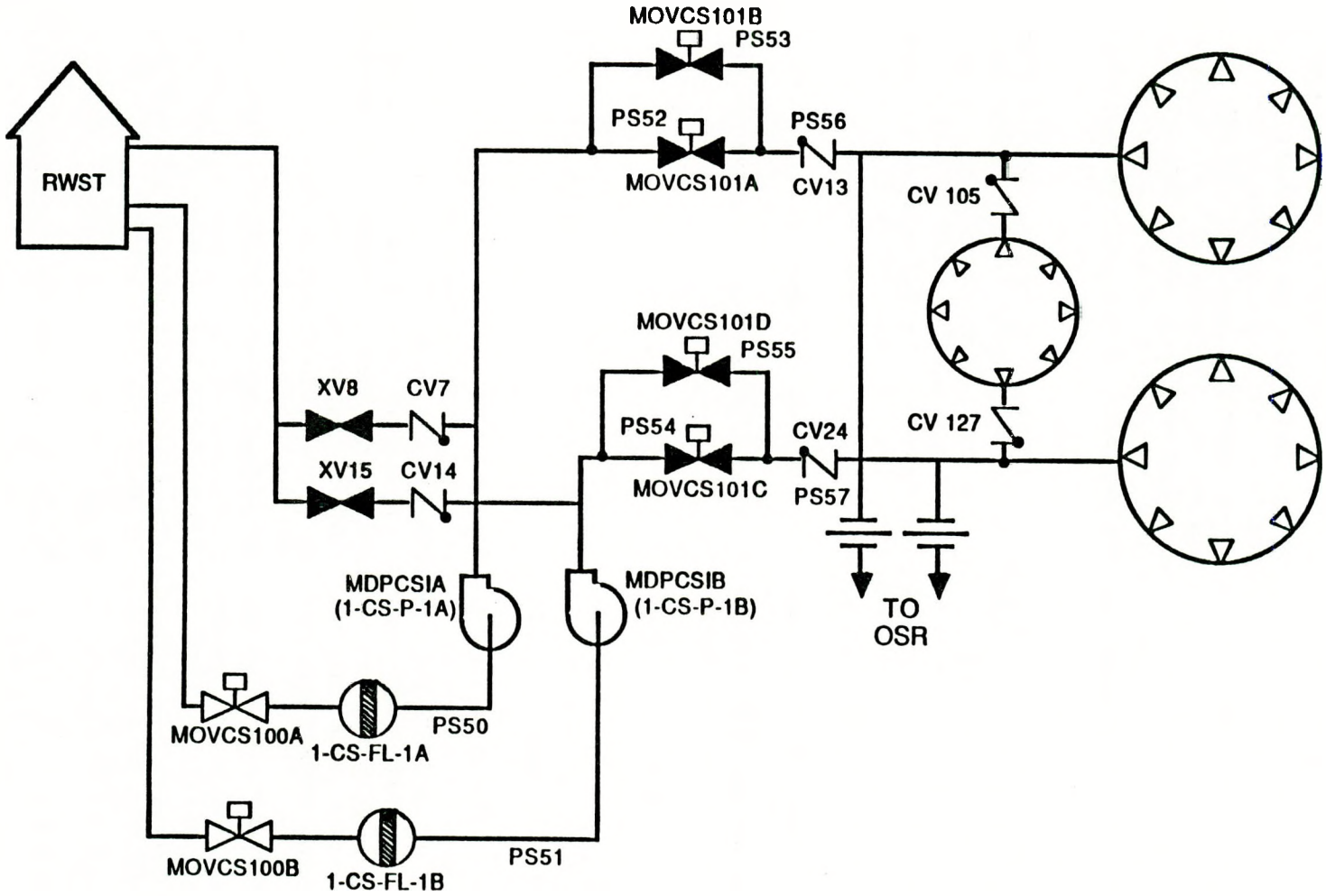

Figure 2.1. Containment Spray System Schematic

pressure recirculation (LPR) system. Upon receipt of a low RWST level signal, the recirculation mode transfer (RMT) system signals the charging pump suction valves from the RWST to close and the suction valves from the LPR pump discharges to open.

In the emergency boration mode, the HPI functions as described in the HPI description above with the exception that the boric acid transfer (BAT) pumps deliver boric acid from the BAT tanks to the charging pump suction header. To perform this operation, the operator must switch the normally operating BAT pump to fast speed operation and open the MOV allowing flow into the charging pump suction header. To enhance boric acid addition to the RCS, the emergency procedure calls for the PORVs be opened (to provide pressure reduction). A simplified schematic of the HPI/HPR system, including the relevant portions of the BAT system is presented in Figure 2.2.

The success criteria for the HPI modes of operation require flow from any one of three charging pumps to the RCS cold legs in response to a LOCA (automatic actuation), flow from any one of three charging pumps to the RCS cold legs in the "feed and bleed" mode (manual actuation), flow from any one of the three charging pumps to the RCP seals, or flow from any one of three charging pumps to the RCS with flow from one of two BAT pumps operating at fast speed (emergency boration mode).

The success criterion for the HPR mode of operation is continued flow from any one of the three charging pumps taking suction from the discharge of the low pressure recirculation system, given successful low pressure system operation.

2.2.4 Accumulator System

The accumulators provide an initial influx of borated water to reflood the reactor core following a large LOCA or a medium LOCA on the upper end of the LOCA size definition.

The accumulator system consists of three tanks filled with borated water and are pressurized with nitrogen. Each of the accumulators is connected to one of the RCS cold legs by a line containing a normally open MOV and two check valves in series. The check valves serve as isolation valves during normal reactor operation and open to empty the contents of the accumulator when the RCS pressure falls below 650 psig. A simplified schematic of the accumulators is shown in Figure 2.3.

The success criterion for the accumulators following a large LOCA, which assumed a cold leg break, is injection of the contents of the two accumulators associated with the intact cold legs into the RCS. The success criterion for the accumulators following a medium LOCA is injection of the contents of two or more accumulators into the RCS.

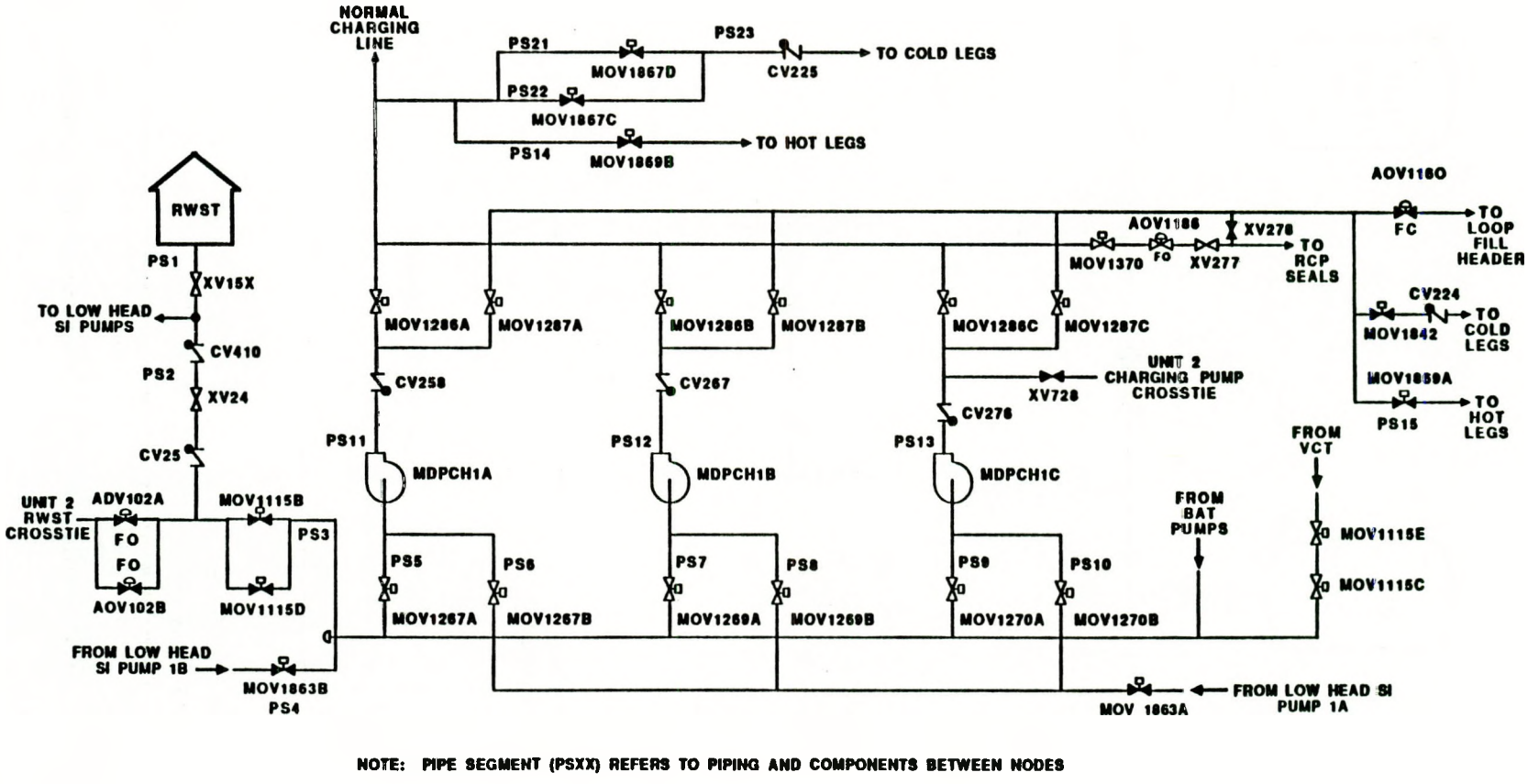

NOTE: PIPE SEGMENT (PSXX) REFERS TO PIPING AND COMPONENTS BETWEEN NODES

Figure 2.2. High Pressure Injection/Recirculation System Schematic (1 of 2)

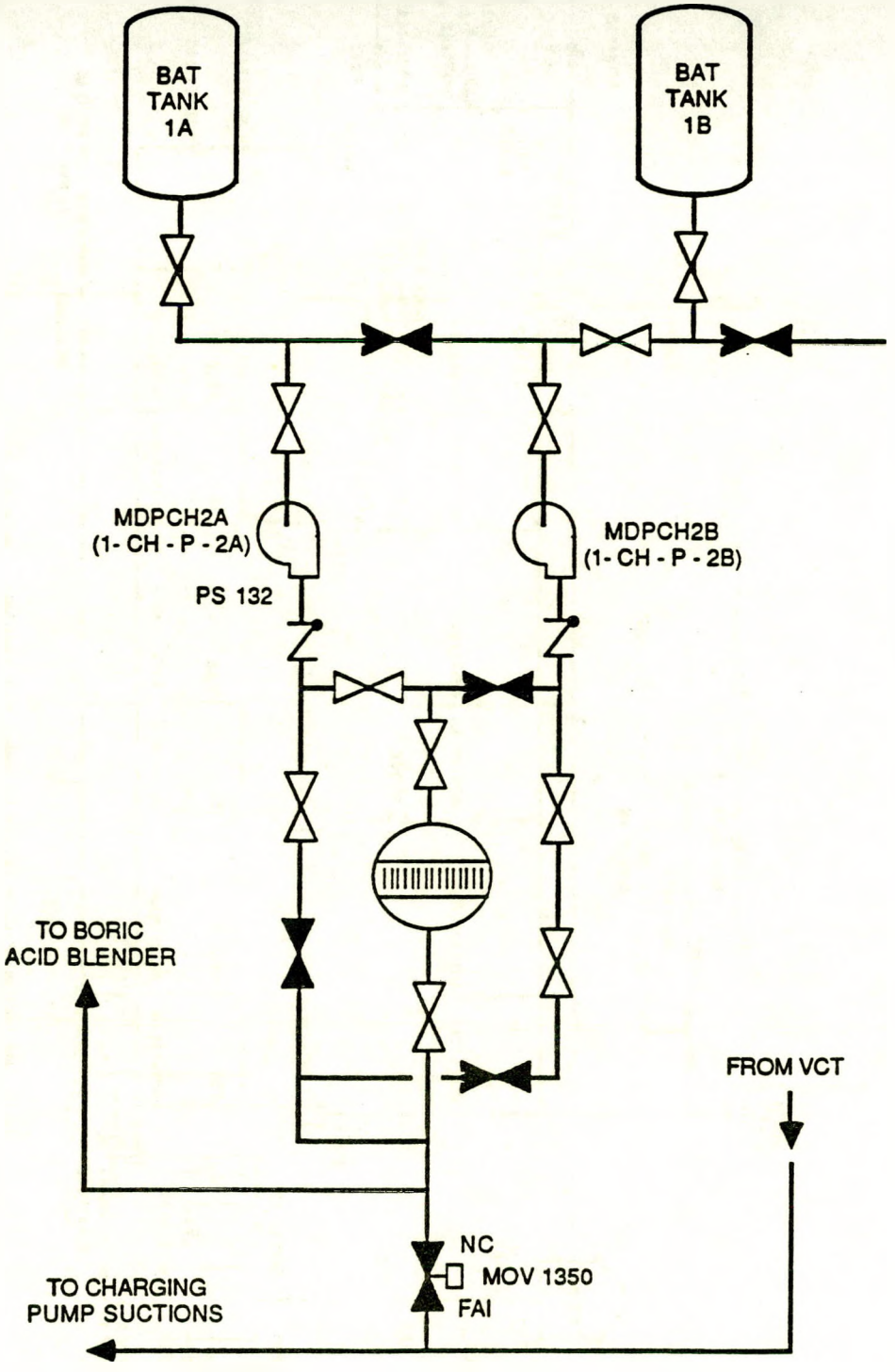

Figure 2.2. High Pressure Injection/Recirculation System Schematic (2 of 2)

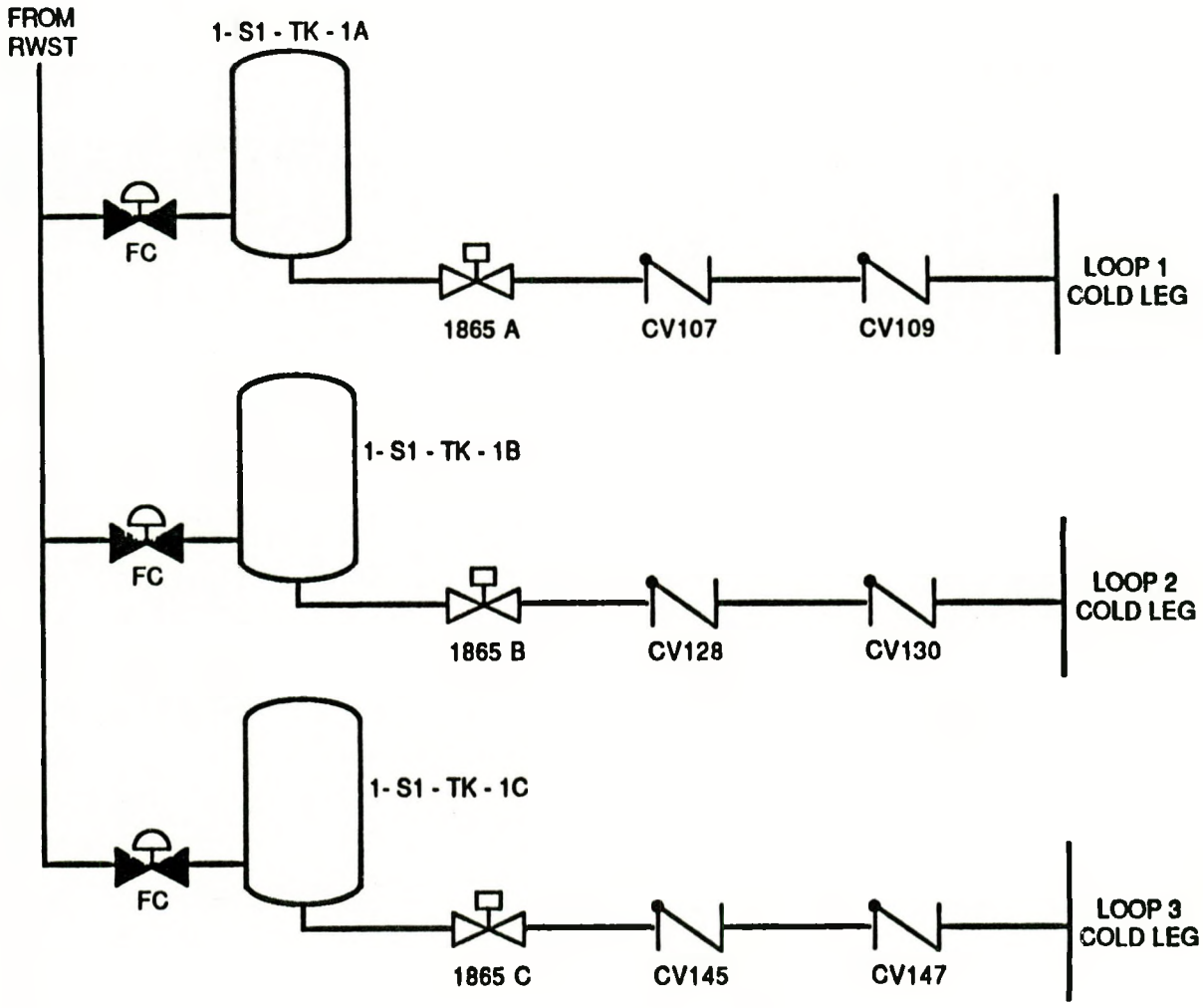

Figure 2.3. Accumulator System Schematic

2.2.5 Low Pressure Injection/Recirculation System

The Surry low pressure injection/recirculation (LPI/LPR) system provides emergency coolant injection and recirculation following a loss of coolant accident when the RCS depressurizes below 300 psig. In addition to the direct recirculation of coolant during the recirculation phase once the RCS is depressurized, the LPR discharge provides the suction source for the HPR system following drainage of the RWST.

The Surry LPI/LPR system is composed of two 100 percent capacity pump trains. The LPI/LPR has no heat removal capability. In the injection mode, the pump trains share a common suction header from the RWST. Each pump draws suction from the header through a normally open MOV, check valve, and locked open manual valve in series. Each pump discharges through a check valve and normally open MOV in series to a common injection header. The injection header contains a locked open MOV and branches to three separate lines, one to each cold leg. Each of the lines to the cold legs contain two check valves in series to provide isolation from the high pressure RCS.

In the recirculation mode, the pump trains draw suction from the containment sump through a parallel arrangement of suction lines to a common header. Flow from the suction header is drawn through a normally closed MOV and check valve in series. Discharge of the pumps is directed to either the cold legs through the same lines used for injection or to a parallel set of headers which feed the charging pumps, depending on the RCS pressure.

In the hot leg injection mode, system operation is identical to normal recirculation with the exception that the normally open cold leg injection valve must be manually closed from a remote location and one or more normally closed hot leg recirculation valves must also be manually opened from a remote location.

Upon indication of a loss of RCS coolant or a main steam line break (i.e., low pressurizer level, high containment pressure, high pressure differential between main steam header and any steam line or high steam flow with low T_{AVG} or low steam line pressure), the safety injection actuation system (SIAS) initiates LPI operation. The SIAS signals the low pressure pumps to start. All valves are normally aligned to their injection position. If primary system pressure remains above the LPI pump shutoff head, the pumps will discharge to the RWST through two normally open minimum flow recirculation lines until the RCS pressure is sufficiently reduced to allow inflow.

Upon receipt of a low RWST level signal, the recirculation mode transfer system (RMTS) signals the low pressure pump suction valves from the RWST and the valves in the minimum flow recirculation lines to the RWST to close and the suction valves from the containment sump to open. A simplified schematic of the LPI/LPR system is shown in Figure 2.4.

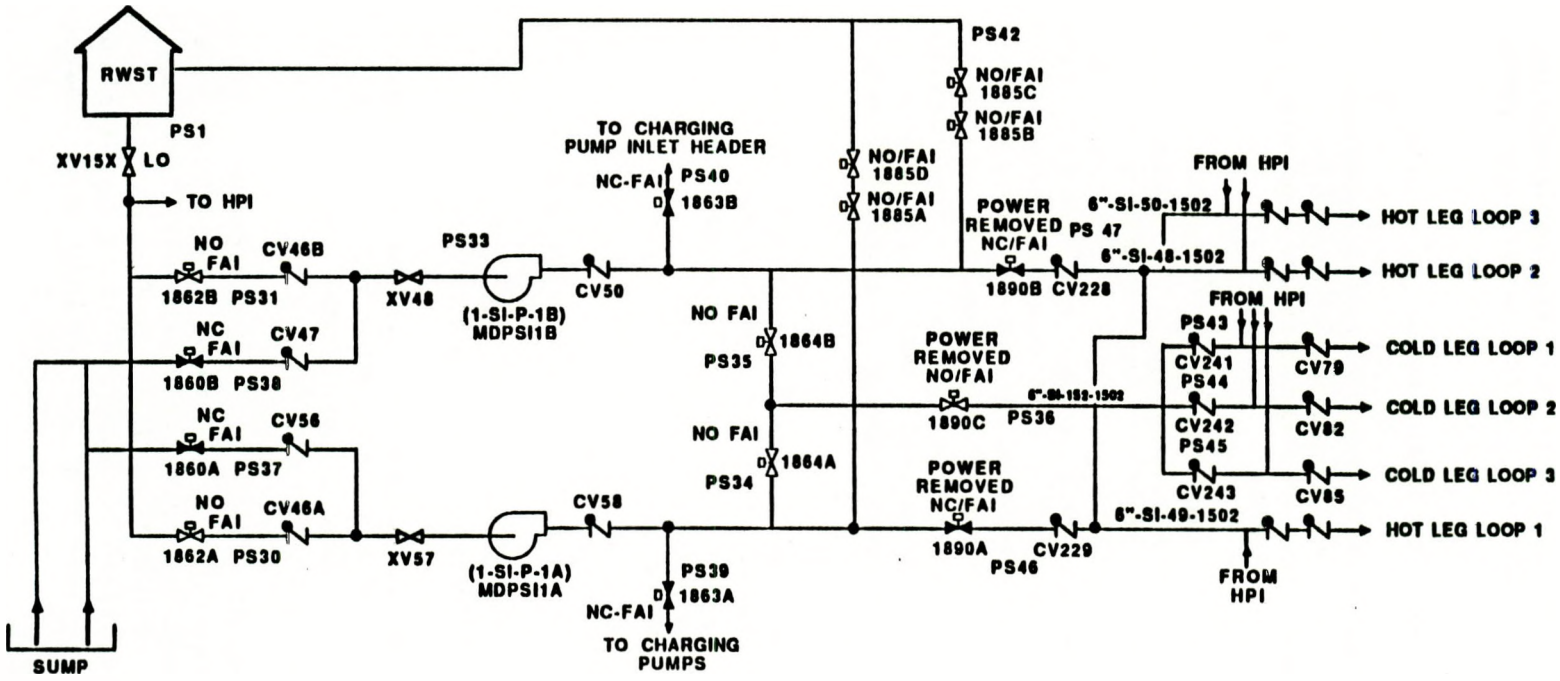

Figure 2.4. Low Pressure Injection/Recirculation System Schematic

The success criterion for the LPI mode of operation is flow from one or more low pressure pumps to the RCS cold legs in response to a loss of primary coolant inventory. The success criteria for the LPR modes of operation are continued flow from either of the two low pressure pumps to the cold legs and switchover to hot leg recirculation at 16 hours or sufficient flow from either of the two low pressure pumps to the charging pump suction header.

2.2.6 Inside Spray Recirculation System

The inside spray recirculation (ISR) system provides long term containment pressure reduction and containment heat removal following an accident by drawing water from the containment sump and spraying the water into the containment atmosphere.

The Surry ISR system is composed of two independent 100 percent capacity recirculation spray trains. Each spray train draws water from the containment sump through independent suction strainers and lines. The ISR and outside spray recirculation system (OSR) draw from the same sump, although the sump is compartmentalized and each ISR train has a separate sump compartment. Each ISR system pump discharges to a service water heat exchanger. The cooled water is then directed to an independent spray header. In order to ensure adequate net positive suction head (NPSH) for the ISR pumps during the initial phases of a LOCA, a recirculation line diverts a small amount of the cooled ISR flow back to the sump, close to the pump inlet. A simplified schematic of the ISR system is shown in Figure 2.5.

The ISR system automatically starts on receipt of a Hi-Hi (25 psia) containment pressure signal from the consequence limiting control system (CLCS). The CLCS signals start the ISR pumps. An agastat timer in the pump start circuit delays pump start for two minutes to ensure adequate sump inventory and the correct diesel generator loading sequence in the event of loss of offsite power. The success criterion for the Surry ISR system is that at least one of the two ISR trains provides flow to its containment spray header with service water being supplied to the heat exchanger.

2.2.7 Outside Spray Recirculation System

The outside spray recirculation (OSR) system provides long term containment pressure reduction and containment heat removal following an accident by drawing water from the containment sump and spraying the water into the containment atmosphere.

The Surry OSR system is composed of two independent, 100 percent capacity recirculation spray trains. The spray trains draw water from the containment sump through two parallel suction strainers and lines which are headered together. The OSR and ISR draw from the same sump, although the sump is compartmentalized. Each OSR train has its own separate compartment. Each OSR system pump has an individual suction line from the

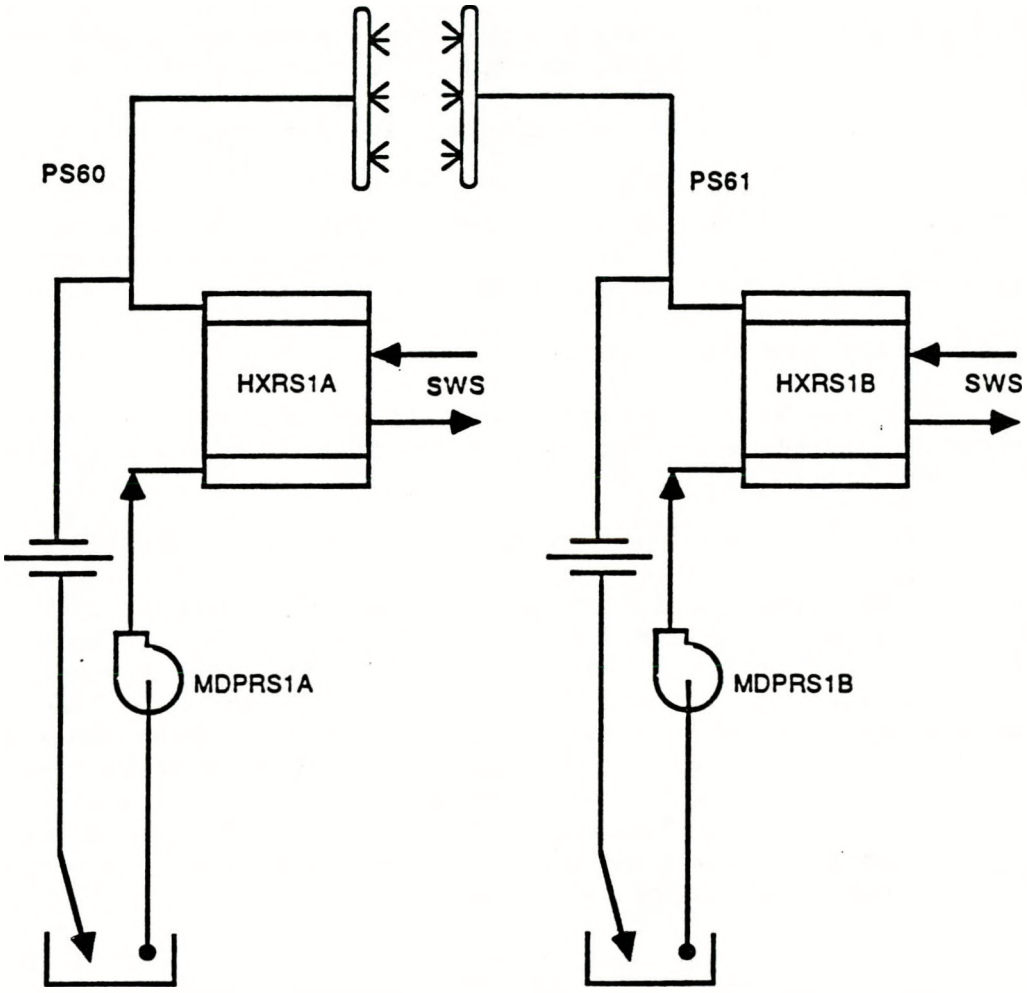

Figure 2.5. Inside Spray Recirculation System Schematic

header with a normally open MOV. Each pump discharges through a normally open MOV, check valve and a service water heat exchanger. The cooled water is then directed to an independent spray header. In order to ensure adequate NPSH for the OSR system pumps during the early phase of a LOCA, a line is provided which diverts a small amount of the cool CSS flow to the sump, close to the pump suction strainers. A simplified schematic of the OSR system is shown in Figure 2.6.

The OSR system automatically starts on receipt of a Hi-Hi (25 psia) containment pressure signal from the consequence limiting control system (CLCS). The CLCS signals start the OSR system pumps and ensure that the pump inlet and discharge valves are open. An agastat timer in the pump start circuit delays pump start for five minutes to ensure adequate sump inventory and the correct diesel generator loading sequence in the event of loss of offsite power.

The success criterion for the OSR system is that at least one of the two OSR system trains provides flow to its containment spray header, with service water provided to the heat exchanger.

2.2.8 Auxiliary Feedwater System

The auxiliary feedwater (AFW) system provides feedwater to the steam generators to provide heat removal from the primary system after reactor trip.

The Surry AFW is a three train system, two electric motor driven pumps and one steam turbine driven pump. Each pump draws suction through an independent line from the 110,000 gallon condensate storage tank (CST). In addition, a 300,000 gallon CST, a 100,000 gallon emergency makeup tank and the fire main can be used as water supplies for the AFW pumps. Each AFW pump discharges to two parallel headers. Each of these headers can provide auxiliary feedwater flow to any or all of the three steam generators (SGs). Flow from each header to any one SG is through a normally open MOV and a locked open valve in series, paralleled with a line from the other header. These lines feed one line containing a check valve which joins the main feedwater line to a steam generator. A simplified schematic of the AFW is shown in Figure 2.7.

The motor driven AFW pumps automatically start on receipt of an SIAS signal, loss of main feedwater, low steam generator level in any steam generator, or loss of offsite power. The turbine driven AFW pump automatically starts on receipt of indication of low steam generator level in two of the three steam generators or undervoltage of any of the three main RCS pumps. These signals also ensure that the system MOVs are in the correct position. The success criterion for the AFW following all events is flow from any one AFW pump to any of the three steam generators.

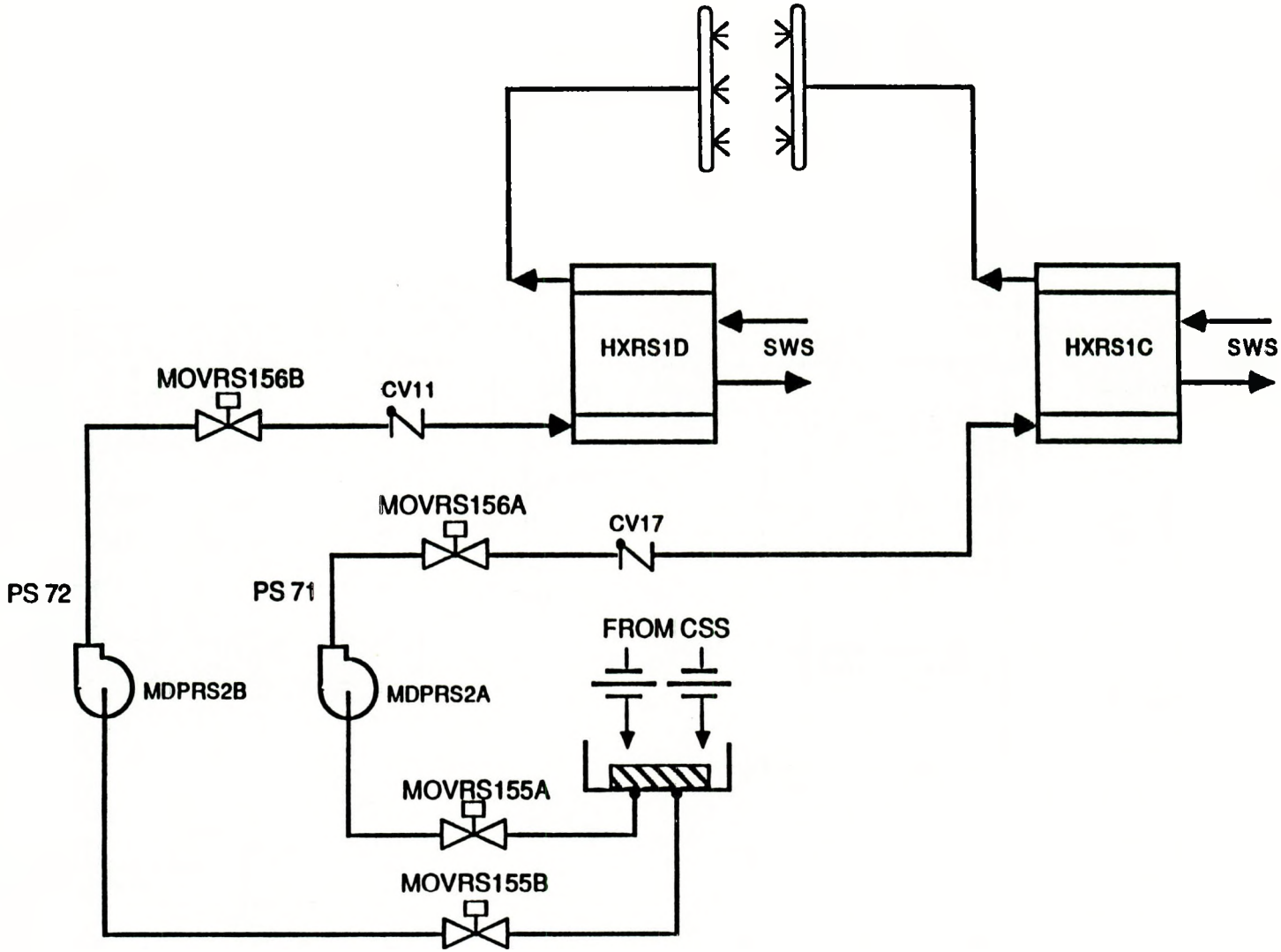

Figure 2.6. Outside Spray Recirculation System Schematic

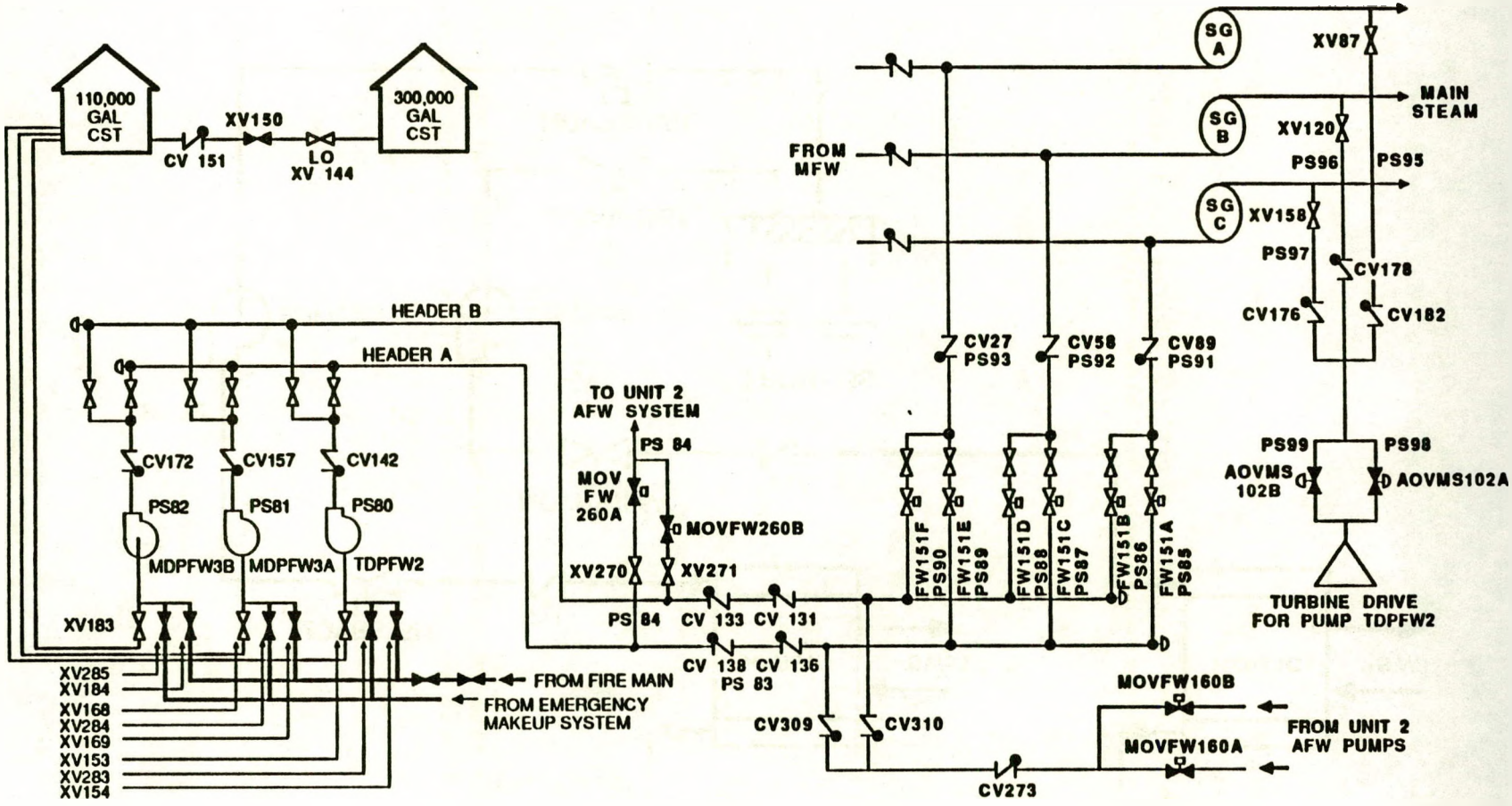

Figure 2.7. Auxiliary Feedwater System Schematic

2.2.9 Primary Pressure Relief System

The primary pressure relief system (PPRS) provides protection from over-pressurization of the primary system to ensure that primary integrity is maintained. The PPRS also provides the means to reduce the RCS pressure if necessary.

The Surry PPRS is composed of three code safety relief valves (SRV) and two power operated relief valves (PORVs). The code safety valves were important only for the ATWS analysis. The PORVs provide RCS pressure relief at a set point below the SRVs. The PORVs discharge to the pressurizer relief tank. Each PORV is provided with a motor operated block valve. A simplified schematic of the PPRS is shown in Figure 2.8.

The PORVs automatically open on high RCS pressure or are manually opened at the discretion of the operator. The block valves are normally open unless a PORV is leaking.

The success criterion for the PPRS following a transient event demanding PORV opening is that the PORVs successfully reclose. The success criterion for the PPRS following a transient and failure of the AFWS is that both PORVs successfully open on demand. The success criterion for the PPRS following a small LOCA with failure of the AFWS and for the support system function provided to HPI in the emergency boration mode is that one or more PORVs successfully open on demand.

2.2.10 Power Conversion System

The power conversion system (PCS) can be used to provide feedwater to the steam generators following a transient.

The PCS, as modeled in this study, consists of the main feedwater pumps, the condensate pumps, the condensate booster pumps, and the hotwell inventory. Because Surry has electrically driven MFW pumps, it is possible to supply feedwater using the MFW system, without having the turbine bypass and steam condensing systems available. The inventory of the hotwell (with the CST as a backup supply) was calculated to be sufficient for all mission times of interest. The feedwater regulating valves will close after a reactor scram, due to plant control logic. The feedwater pumps remain on, and the miniflow valves will open. Feedwater can then be provided to the SGs, through the feedwater regulating valve bypass valve. The success criterion for the PCS are restoration of flow from one or more main feedwater pumps to one or more steam generators.

2.2.11 Charging Pump Cooling System

The charging pump cooling (CPC) system is a support system which provides lube oil cooling and seal cooling to the three charging pumps in the HPI/HPR system.

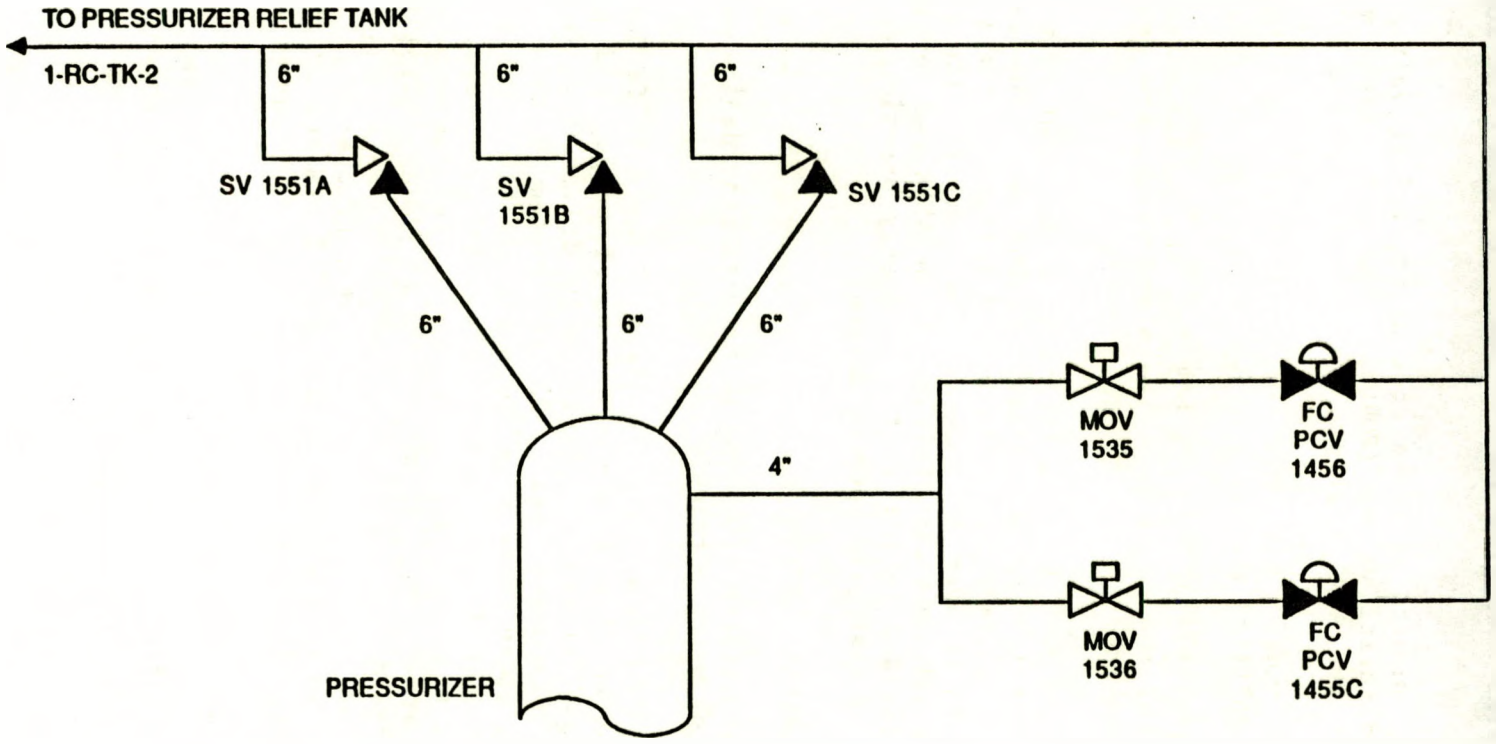

Figure 2.8. Primary Pressure Relief System Schematic

The Surry CPC system provides two specific cooling functions for the charging pumps, lube oil cooling and seal cooling. The CPC system is composed of two subsystems, the charging pump service water system and the charging pump cooling water system. The charging pump service water system is an open cooling system which provides cooling to the lube oil coolers and to the intermediate seal coolers in the charging pump cooling water system. The charging pump cooling water system is a closed cycle system which provides cooling to the charging pump seal coolers.

The charging pump service water system is composed of two 100 percent capacity pump trains, each providing flow to one intermediate seal cooler and all three charging pump lube oil coolers. Flow is drawn from the condenser inlet lines through independent lines by the charging pump service water pumps. Upstream of each pump are two separate, independent strainer assemblies. Each pump discharges through two check valves. Downstream of the check valves the flow is split with a portion of the flow directed to an intermediate seal cooler and the other portion directed to a common header feeding the lube oil coolers. From this header, flow is directed through the lube oil coolers for the operating charging pumps. Temperature control valves control the flow through the lube oil coolers to prevent overcooling of the lube oil. The service water flow is discharged to the discharge canal.

The charging pump cooling water system is a closed cycle system composed of two 100 percent capacity pump trains, each containing a charging pump cooling water pump and intermediate seal cooler which provide cooling water to the charging pump seal coolers. Each pump draws suction from the outlet of either of the two intermediate seal coolers and discharge to a common header. The common header provides flow to the seal coolers for each charging pump. Two seal coolers in parallel are provided for each charging pump. The discharge of the seal coolers is returned to the intermediate seal coolers where it is cooled by the charging pump service water system. Makeup to the charging pump cooling water system to account for seal leakage is provided by a surge tank which is supplied by the component cooling water system. A simplified schematic of the CPC system is shown in Figure 2.9.

One of the charging pump service water pumps and one of the charging pump cooling water pumps are normally in operation. Upon indication of low discharge pressure of one of the pumps, the parallel pump receives a signal to start. With the exception of the pumps and the lube oil cooler temperature control valves, all other components in the system are manually actuated.

2.2.12 Service Water System

The service water system (SWS), as defined for this analysis, is a support system which provides cooling to the heat exchangers in the ISR system and OSR system. The SWS provides heat removal from the containment following an accident.

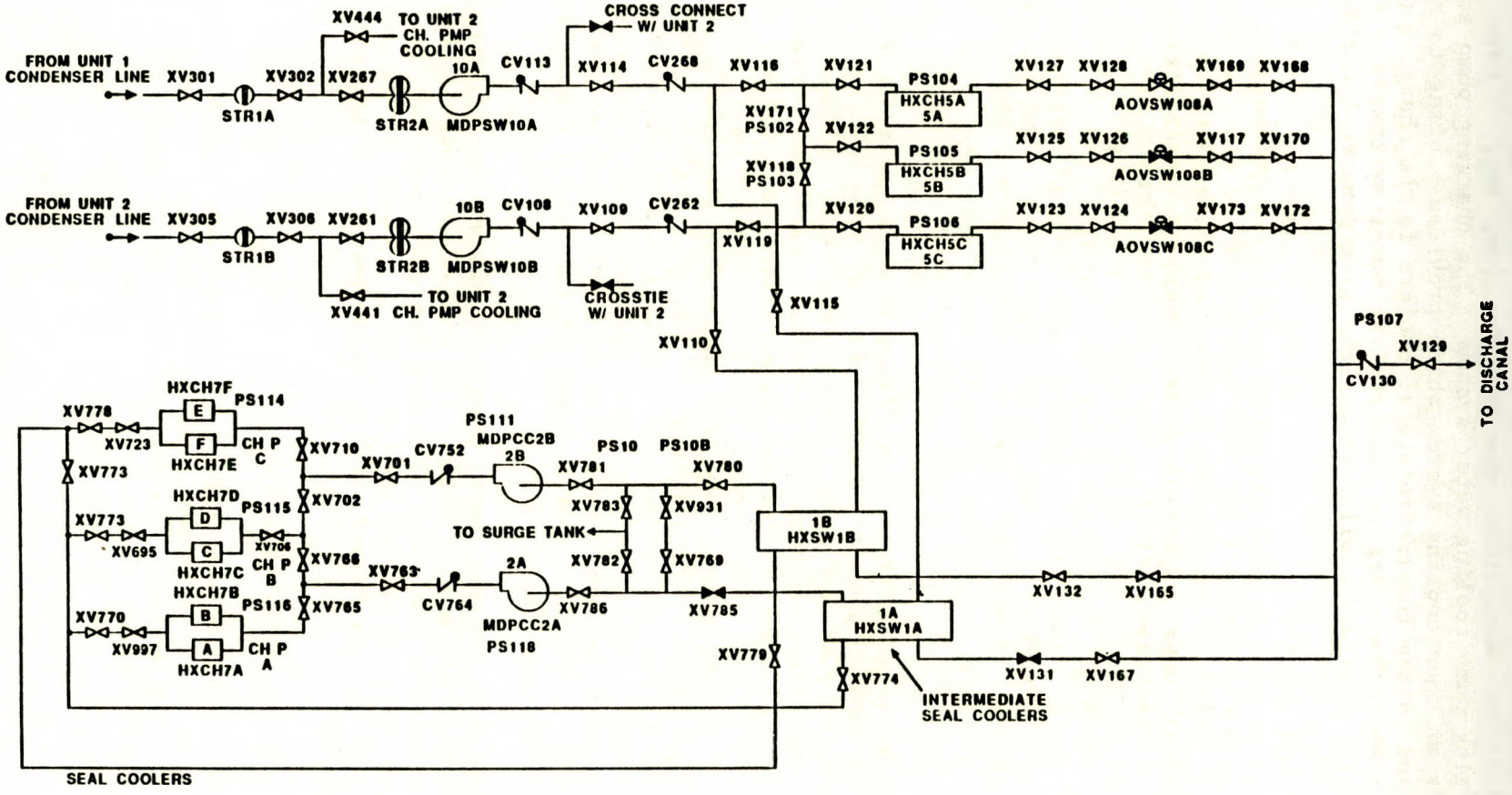

Figure 2.9. Charging Pump Cooling System Schematic

The Surry SWS is a gravity flow system. The service water supply to the containment spray heat exchangers consists of two parallel inlet lines which provide SW from the condenser cooling pipes each through two normally closed MOVs in parallel to individual headers. The headers each provide flow to one ISR and OSR heat exchanger. The two headers are cross connected by two normally open MOVs in series such that flow from either inlet line can be used to cool all four ISR and OSR heat exchangers. Service water flows through each heat exchanger and discharges through a normally open MOV to two headers which flow to the discharge tunnel. A simplified schematic of the SWS is shown in Figure 2.10.

The SWS automatically starts on receipt of a Hi-Hi (25 psia) containment pressure signal from the consequence limiting control system (CLCS). The CLCS signals open the header inlet valves. No other actions are required to place the SWS in service.

2.2.13 Component Cooling Water System

The component cooling water (CCW) system, as defined for this analysis, includes only that portion of the CCW system required to provide cooling water to the RCP thermal barriers.

The CCW system is composed of two CCW pumps in parallel and two CCW heat exchangers. The CCW system is a closed cycle system. The CCW pumps take suction from the return line from the RCS pump thermal barriers and are headered together at their discharges. The header feeds the two CCW heat exchangers arranged in parallel. The discharge of the heat exchangers is delivered to the thermal barriers. After cooling of the thermal barriers, the flow is returned to the CCW pump suction. Makeup to the CCW system is provided from a surge tank in the system. A simplified schematic of the portions of the CCW system required for thermal barrier cooling is shown in Figure 2.11.

One CCW pump and heat exchanger are normally in operation. In the event of failure of either component, the parallel component is manually placed in service. Following a loss of offsite power, the stub buses powering the CCW pumps are shed from the emergency buses and must be manually reconnected to restore power to the CCW pumps. The throttle valve on the thermal barrier cooling water outlet closes on loss of instrument air or receipt of a consequence limiting control system (CLCS) Hi-Hi signal, resulting in loss of flow to the thermal barriers. The success criterion for the Surry CCW system is that continued CCW flow is provided to the RCS pump thermal barriers following reactor shutdown.

2.2.14 Emergency Power System

The emergency power system (EPS) provides AC and DC power to safety-related components following reactor scram.

The EPS consists of two 4160 V AC buses, four 480 buses, four 120 V AC vital instrumentation buses, two 125 V DC buses, one dedicated and one

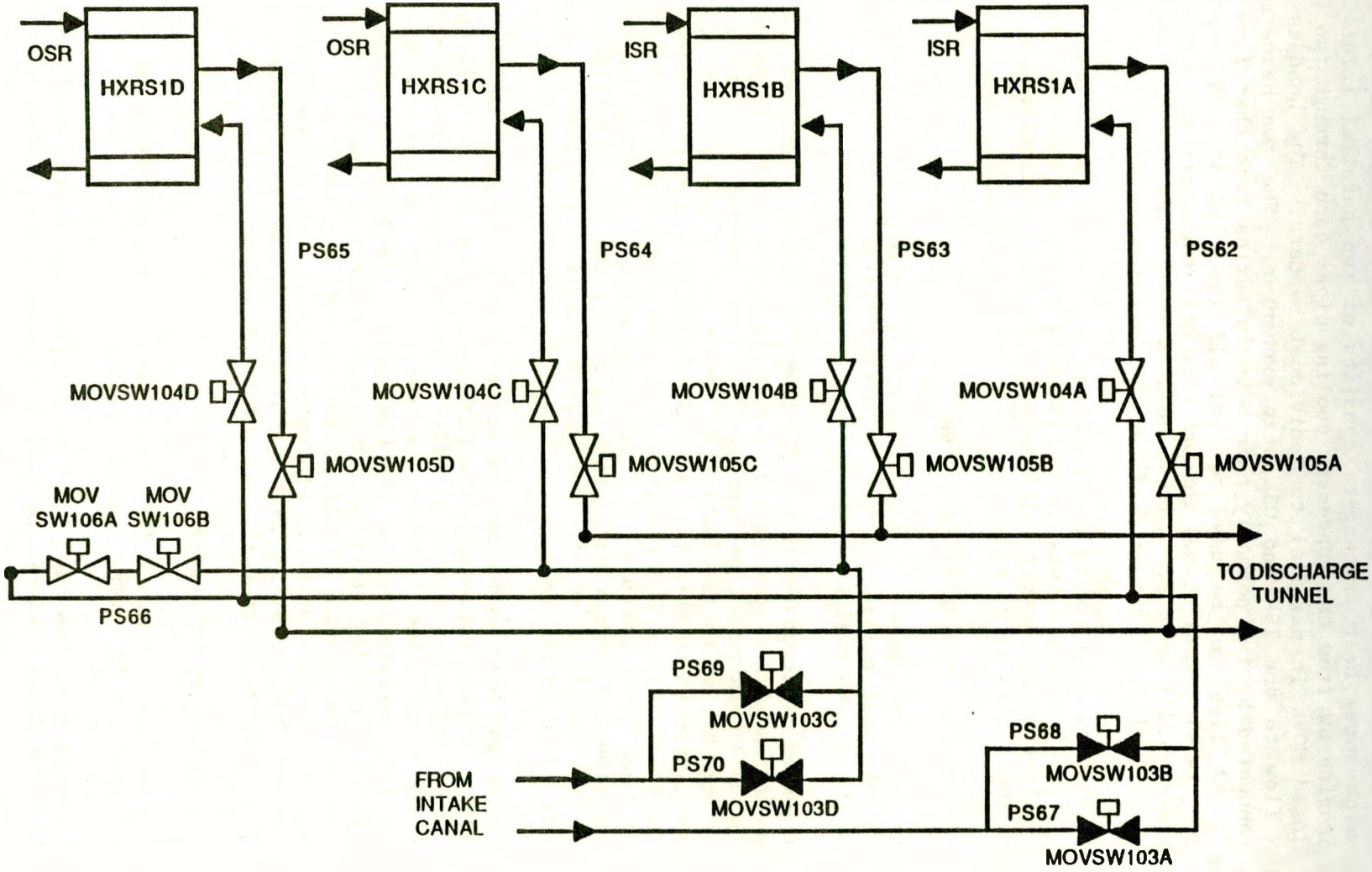

Figure 2.10. Service Water System Schematic

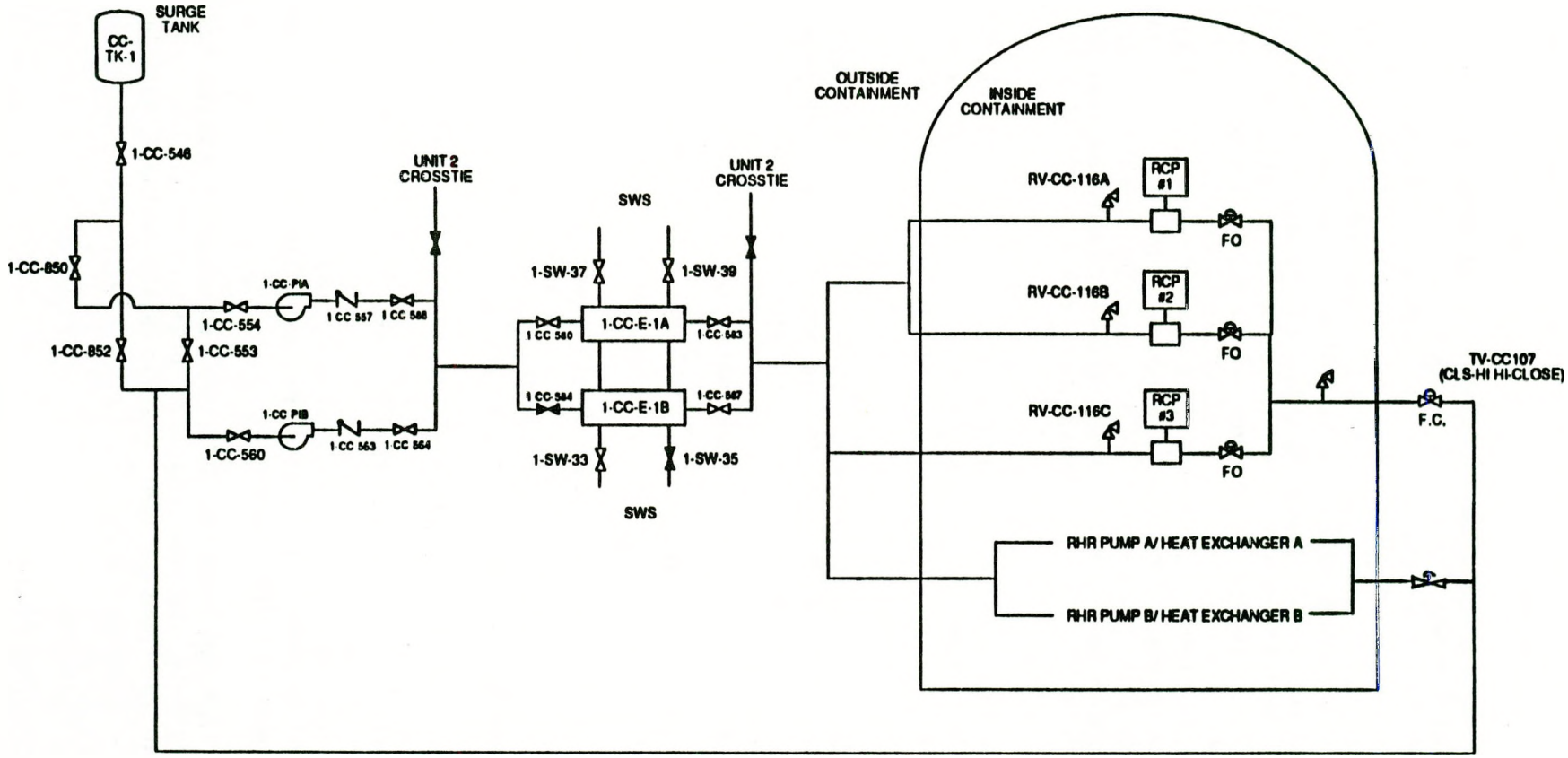

Figure 2.11. Component Cooling Water System Schematic

shared diesel generator, and their associated motor control centers, breakers, transformers, chargers, inverters, and batteries.

Each 4160 V AC bus is normally powered from offsite power sources. On loss of offsite power the breakers open, the diesel generators start and their associated breakers close to load the diesels on the emergency buses. Surry has three diesel generators, one dedicated to each unit and a third swing diesel generator shared by the units. The dedicated diesel at Unit 1 is attached to the 1H 4160 V AC bus while the swing diesel can be connected to the 1J 4160 V AC bus. In the event that the swing diesel is demanded by both units, the diesel will be aligned to the unit at which a safety-injection actuation system SIAS or CLCS Hi-Hi exists. If signals exist at both units, the diesel will be aligned to the unit whose breaker closes first. Each diesel is a self-contained, self-cooled unit with its own battery for starting power. The 4160 V AC buses provide power to the large pumps such as the high pressure injection pumps, the stub buses which each power one CCW and residual heat removal pump and is shed on undervoltage on the main bus, and the 480 V AC buses through transformers.

The following description applies to the 1H related buses. Since the 1H and 1J related buses are symmetrical, the description is equally applicable to the 1J related buses with the appropriate changes to the designators.

The 1H 4160 V AC bus feeds two 480 V AC buses (1H and 1H-1) through transformers. The 1H 480 V AC bus is primarily used to power pumps such as the A train low pressure injection pump. The 1H-1 480 V AC bus feeds two motor control centers (MCCs), MCC 1H1-1 and 1H1-2, which provide power to a multitude of MOVs and small pumps such as the charging pump cooling water pumps. MCC 1H1-1 also provides power to two battery chargers used to charge DC battery A, and to the 1-I 120 V AC vital instrumentation by DC bus 1A through an inverter.

The 1A 125 V DC bus provides control power to the switchgear for the pumps powered from the 1H buses. The 1A 125 V DC bus is powered from a 480 V AC bus, as noted above, and in the event of loss of the AC power source is powered from DC battery A.

A simplified electrical diagram of the EPS is included in Figure 2.12.

2.2.15 Safety Injection Actuation System

The safety injection actuation system (SIAS) automatically initiates the high and low pressure injection systems following an indication of the need for primary coolant makeup.

The Surry SIAS is composed of two independent trains used to automatically actuate the low and high pressure injection systems and the motor driven AFW pumps. The signals which actuate SIAS are shown in Figure 2.13.

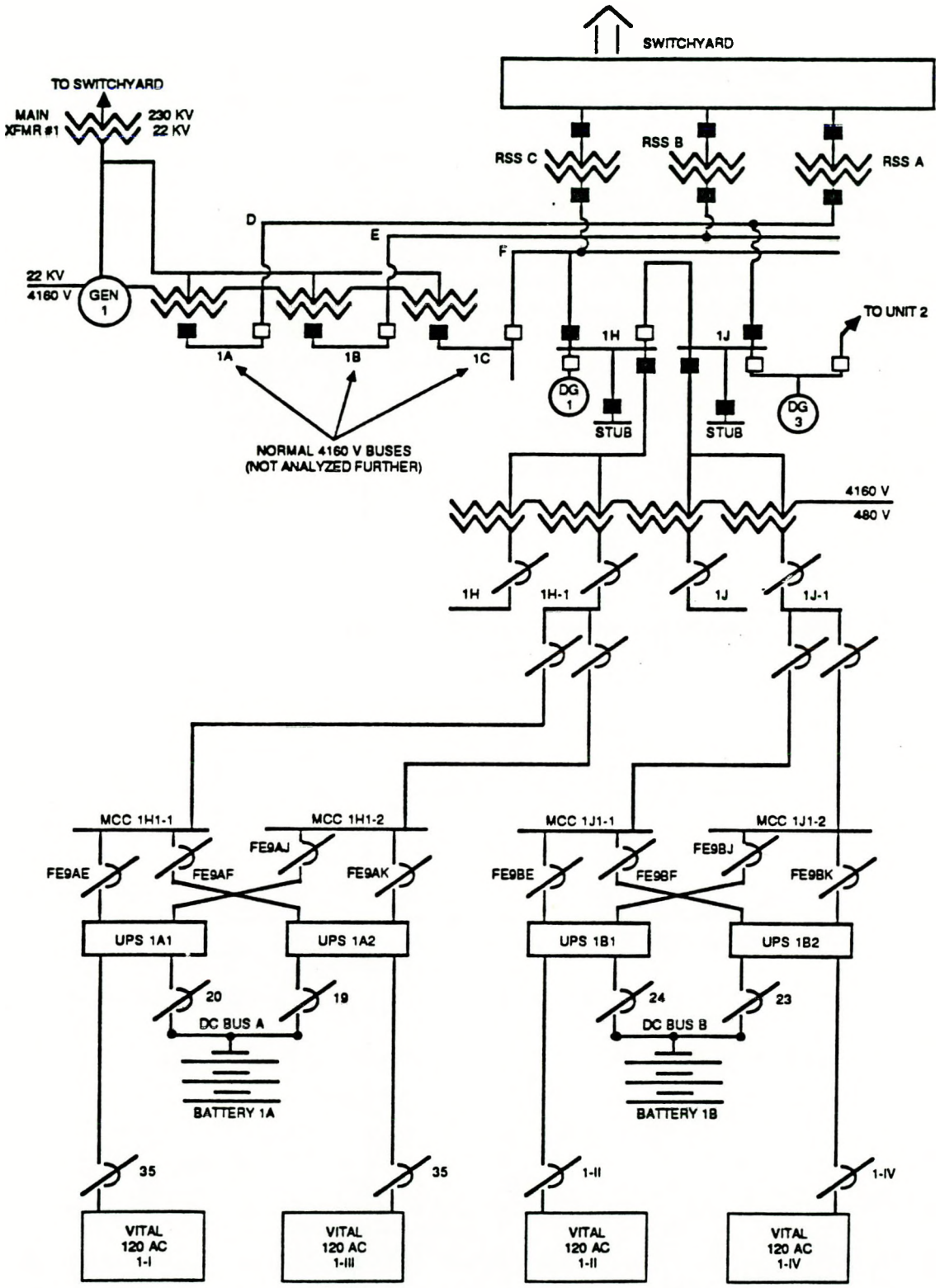

Figure 2.12. Emergency Power System Schematic (1 of 2)

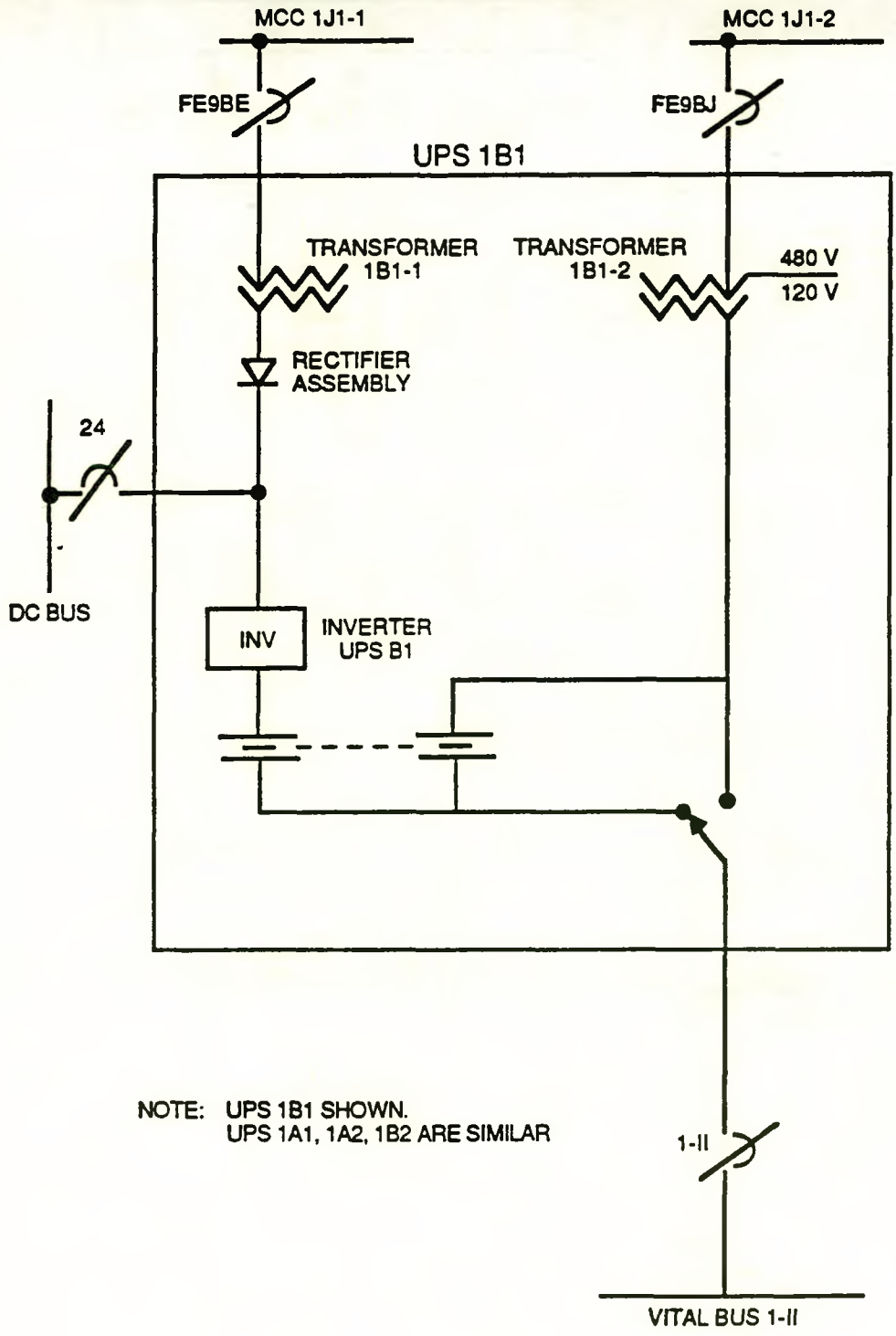

Figure 2.12. Emergency Power System Schematic (2 of 2)

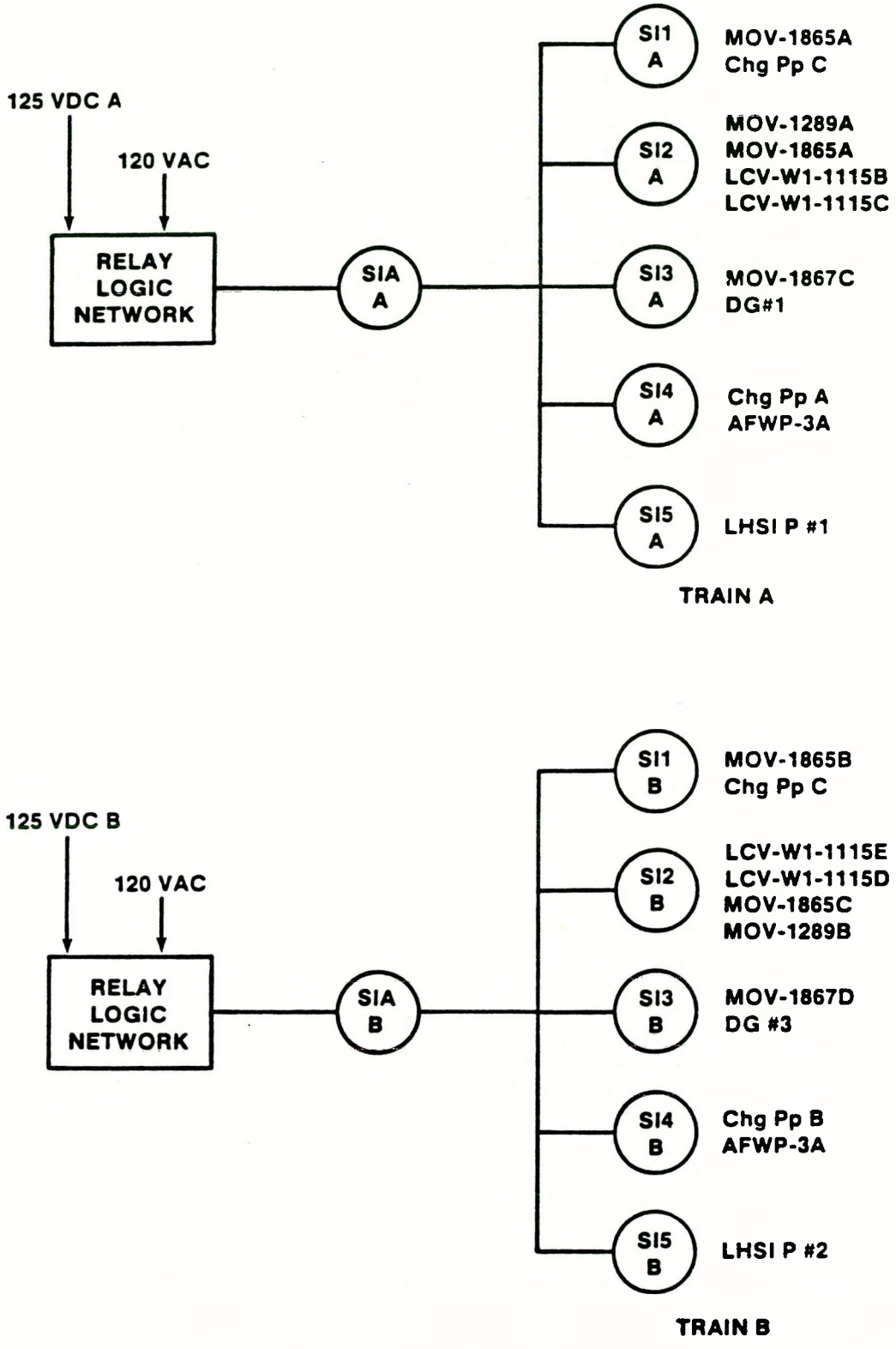

Figure 2.13. Safety Injection Actuation System Logic Diagram

2.2.16 Consequence Limiting Control System

The consequence limiting control system (CLCS) automatically actuates the containment safeguards systems following receipt of an indication of Hi-Hi (25 psia) containment pressure.

The Surry CLCS is composed of four containment pressure sensors, each feeding a signal comparator. The output of each signal comparator is input into two separate three out of four logic trains. These logic trains automatically actuate the containment safeguards system components. A simplified CLCS logic diagram is shown in Figure 2.14.

2.2.17 Recirculation Mode Transfer System

The recirculation mode transfer (RMT) system automatically initiates the switchover of the suction of the low pressure injection pumps from the RWST to the containment sump and the suction of the high pressure injection pumps from the RWST to the low pressure injection pump discharges on low RWST level.

The Surry RMT system is composed of four independent RWST level sensors, each feeding two separate two out of four relay matrices. These two relay matrices automatically actuate the components required to perform the switchover to the recirculation mode of the low and high pressure systems. A simplified RMT system logic diagram is shown in Figure 2.15.

2.2.18 Residual Heat Removal System

The residual heat removal (RHR) system provides shutdown cooling when the reactor coolant system (RCS) depressurizes below 450 psig and is less than 350°F. The RHR is a front line system (although nonsafety grade) designed to provide long-term decay heat removal. The following sections provide a physical description of the RHR system, and identify the interfaces and dependencies of the RHR system with other front line and support systems. A simplified RHR system schematic is shown in Figure 2.16.

The Surry RHR system is composed of two pumps and two RHR heat exchangers in parallel. The RHR pumps take suction from the RCS loop 1 hot leg through two normally shut motor-operated valves (MOVs) and a manual isolation valve. The discharge of the pumps is headered together and feeds two heat exchangers arranged in parallel. The RHR pumps and heat exchangers are cooled by component cooling water (CCW). An air operated valve (AOV) controls bypass flow around the heat exchangers, another controls flow through the heat exchangers. The two AOVs work together to control the cooldown rate of the RCS. The discharge of the flow control valves feeds into the SI/accumulator piping and is delivered to the RCS loop 2 and loop 3 cold legs. Each path has a normally shut MOV isolating the RHR from the high pressure RCS during normal plant operations. Make-up to the RHR system is provided by the RCS.

The RHR is manually initiated. An interlock prevents opening the RHR isolation MOVs until RCS pressure is below 450 psig. Following a loss

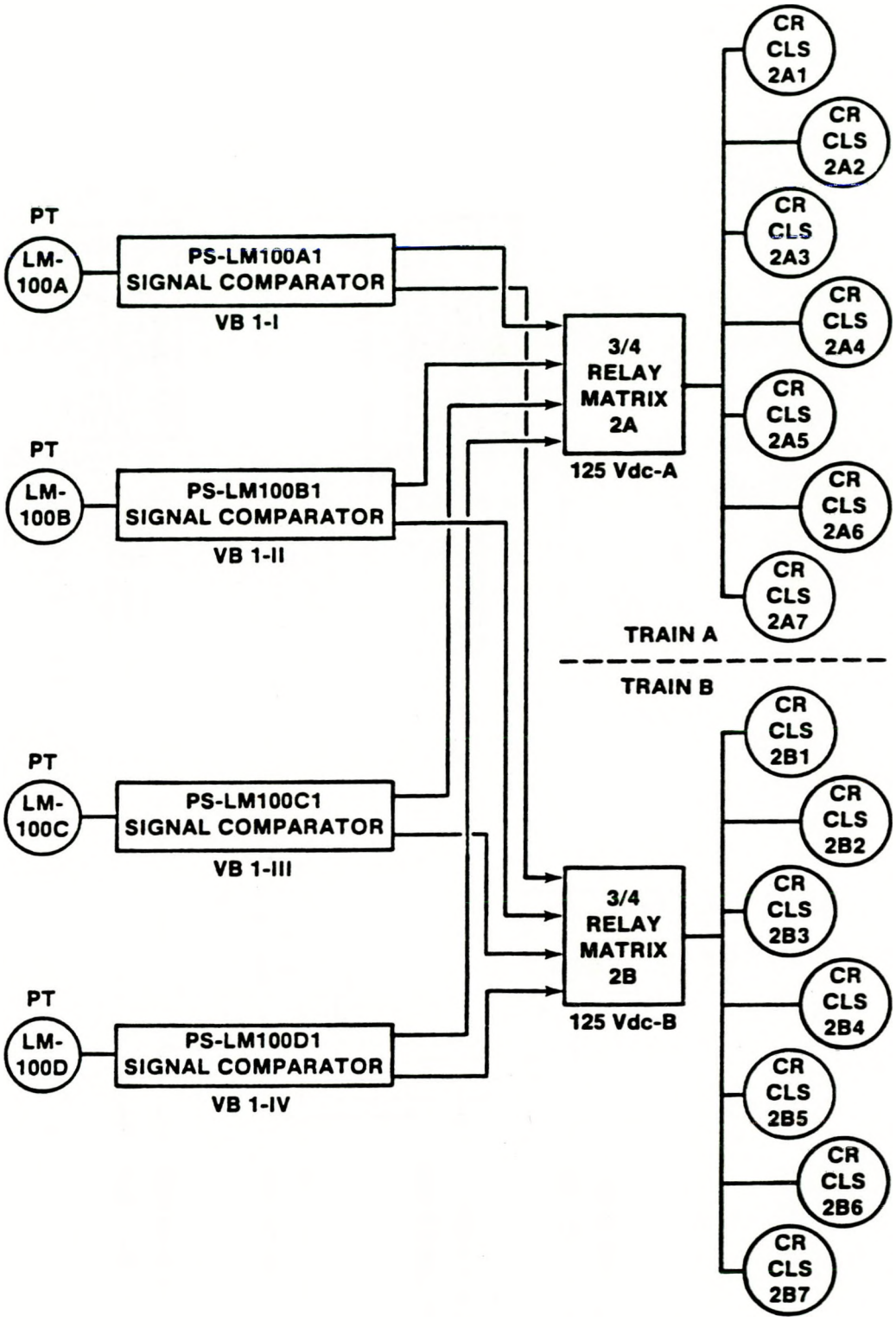

Figure 2.14. Consequence Limiting Control System Logic Diagram

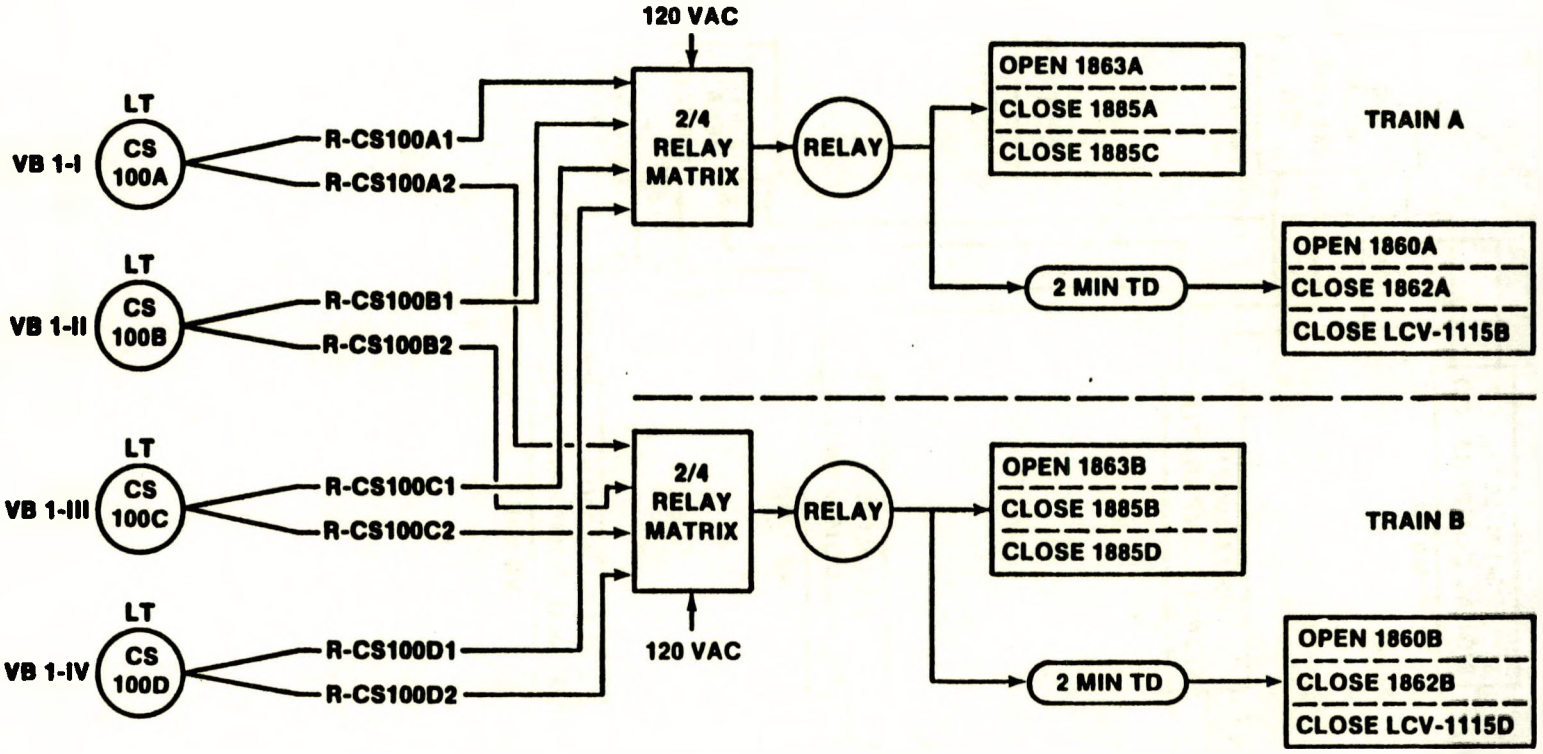

Figure 2.15. Recirculation Mode Transfer System Logic Diagram

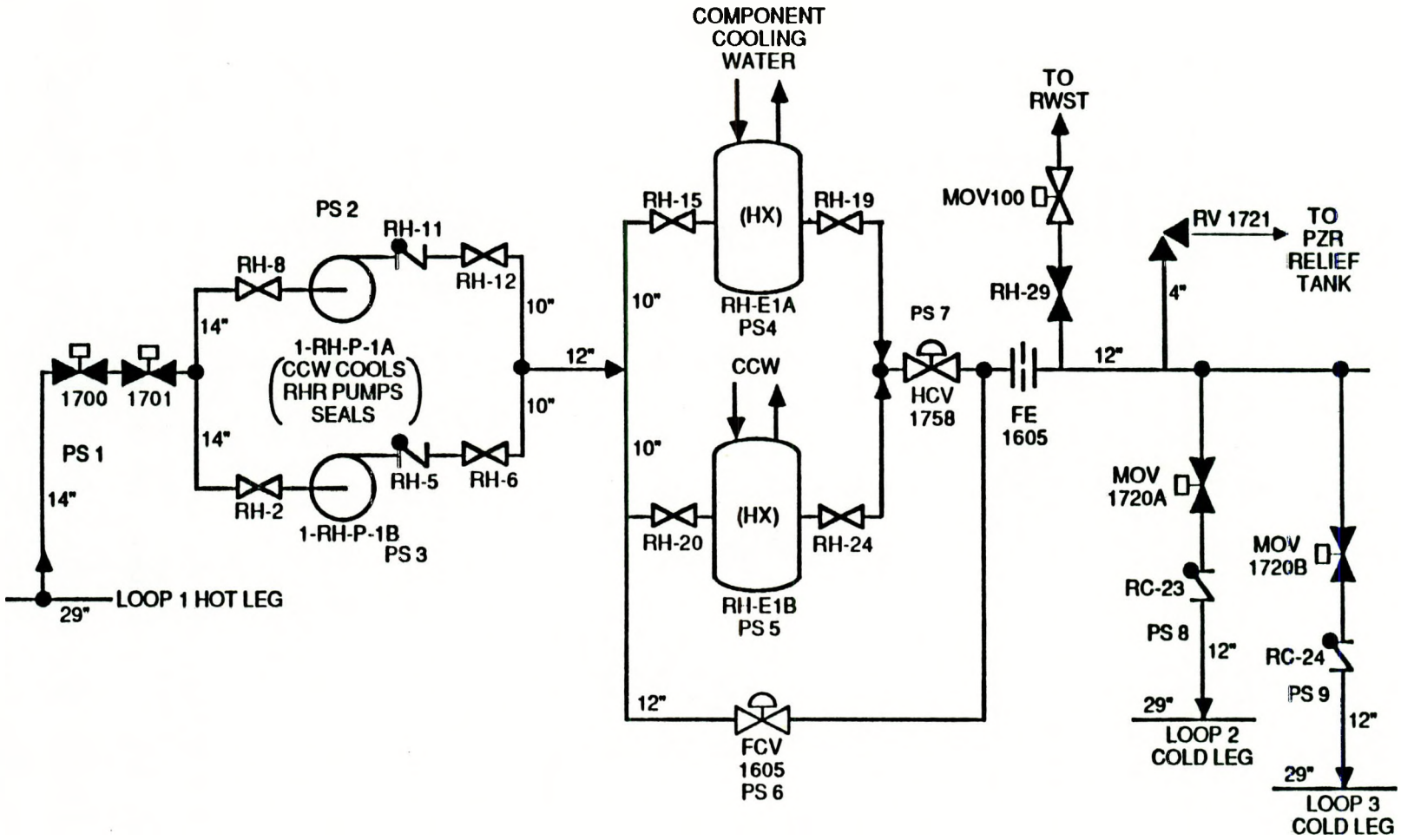

Figure 2.16. Residual Heat Removal System Schematic

of offsite power, the stub buses powering the RHR pumps are shed from the emergency buses and must be manually reconnected to restore power to the RHR pumps.

2.3 Initiating Events and Accident Sequences

2.3.1 Introduction

This task involved the identification of potentially significant external event induced initiators at nuclear plants, identifying the applicability of them to the Surry plant, and grouping the initiators into categories based on similar plant response and similar success criteria for successful initiator mitigation. It is not the intent of a focussed PRA to explicitly evaluate (i.e., perform event sequence quantification) every possible initiating event. The intent is rather to evaluate those initiators which have previously been shown to be important and to ensure that all other potential initiators can be adequately represented by those initiators chosen for explicit evaluation.

The final list of initiating events which formed the basis for accident sequence quantification are shown in Table 2.1. These either seismically or fire-induced event sequences are described in the following sections. Table 2.2 details a description of the event headings for the event trees.

From this list of potential initiating events the non-recoverable loss of a DC bus was eliminated because the frequency of fire-induced failures was an order of magnitude below that of the internal event frequency and it is judged to be highly unlikely that the postulated fire would spread beyond these buses and cause other damage. Also, interfacing LOCAs were screened because a valid fire-related mechanism that had not been addressed by the Appendix R submittal could not be identified. It should also be noted that small LOCA (S_2) fire and very small LOCA (S_3) fire and seismic sequences had to be transient-induced.

2.3.2 T_1 (Loss of Offsite Power) Event Tree

This section presents and discusses the event trees for the offsite power initiating event. This event is identified by the symbol T_1 in the event tree.

Loss of offsite power will deenergize the normal and emergency 4160V buses, which will de-energize all lower level buses. The DC buses and the vital buses would be available, unless random failures of these buses were postulated.

The reactor protection system will de-energize, thus signaling the control rods to insert. The main feedwater and condensate system will be unavailable for the duration of the event.

Table 2.1

Initiating Event Categories Used in the External Events Analysis

Abbreviation	Description	External Event Category
T_1	Loss of Offsite Power	Seismic/Fire
T_3	Transients with MFW Initially Available	Seismic/Fire
T_{5A}	Non-Recoverable Loss of DC Bus A	Fire
T_{5B}	Non-Recoverable Loss of DC Bus B	Fire
A	Large LOCA, 6 in. to 29 in.	Seismic
S_1	Medium LOCA, 2 in. to 6 in.	Seismic
S_2	Small LOCA, 1/2 in. to 2 in.	Seismic/Fire
S_3	Very Small LOCA, less than 1/2 in.	Seismic/Fire
V	Interfacing LOCA	Fire

The T_1 event will affect both Unit 1 and Unit 2. Should DG 2 (dedicated to Unit 2) fail to start or run, DG 3 would be aligned to Unit 2, thereby making it unavailable for Unit 1. In the event that both DG 1 and DG 2 fail to start, DG 3 was always assumed to align to Unit 2.

The four primary functions required in response to T_1 are reactor scram, primary system integrity, auxiliary feedwater, and RCP seal cooling. If all these functions are provided, the transient is mitigated at a very early stage. Failure to provide reactor scram transfers to the ATWS tree. Failure of PORVs to reclose transfers to the S_2 LOCA tree. Failure to provide RCP seal cooling results in a seal vulnerable condition which is evaluated separately.

Failure to provide AFW leads to a demand for "feed and bleed" cooling. For feed and bleed, failure to provide charging flow and open two PORVs leads to core damage. Successful feed and bleed cooling leads to a demand for the containment systems and coolant recirculation systems. These sequences are developed on the tree.

The event tree for T_1 is shown in Figure 2.17. One event tree was used to evaluate the loss of offsite power initiating event which assumes at least one diesel initially available at Unit 1.

Table 2.2

Event Tree Headings

Part 1: Description of Events

Abbr.	Heading	Description of Event
A	LARGE LOCA	IE - large LOCA (6 in. to 29 in.)
CS	CONT SYS	Top level event for containment heat removal. Includes CSS, ISR, and OSR system functions
CV	CORE VULNR TO CD	Probability of core damage for core vulnerable states (the core is being cooled but containment cooling has failed)
D1	HPI	Failure of charging pump system in high pressure injection mode
D2	HPI	Failure of charging pump system in feed and bleed mode
D3	SEAL COOL	Failure of charging pump system in seal injection flow mode
D5	ACC	Failure of accumulators in injection mode
D6	LPI	Failure of low head safety injection system in injection mode
H1	LPR	Failure of low head safety injection system in recirculation mode
H2	HPR	Failure of charging pump system in high pressure recirculation mode
K	RPS	Failure of reactor protection system
L	AFW	Failure of auxiliary feedwater system for transients with reactor trip
L3	AFW	Auxiliary feedwater: failure of 1/3 AFWPs to 1/2 SGs
M	MFW	Failure of main feedwater

Table 2.2 (Continued)

Event Tree Headings

Part 1: Description of Events

Abbr.	Heading	Description of Event
OD	OPER DEPRES	Operator fails to depressurize RCS during small break initiators
P	PRV	Failure of both PORVs to open for feed and bleed
P1	PORV	Failure of one PORV to open for S_2L sequences
PL	PWR LEVEL	Power level less than 25% of rated power
Q	RCI	Failure of pressurizer SRV/PORV to close after transient
QC	RCI	Failure of PORV to reclose after very small LOCA (SI causes relief valve to open)
R	MAN SCRAM	Failure to effect manual reactor trip
S1	MEDIUM LOCA	IE - medium LOCA (2 in. to 6 in.)
S2	SMALL LOCA	IE - small LOCA (1/2 in. to 2 in.)
S3	VERY SMALL LOCA	IE - very small LOCA (less than 1/2 in.)
SL	RCP SEAL LOCA	RCP seal leakage, limited to less than 2 lb/sec/pump
T1	LOSP	IE - loss of offsite power
T3	TURB TRIP W/MFW	IE - turbine trip with MFW available
W	CCW	Failure of component cooling water to thermal barriers of all reactor cooling system pumps
W3	RHR	Residual heat removal in shutdown cooling mode

Table 2.2 (Continued)

Event Tree Headings

Part 2: Definition of Events

C - Less than 1/2 CSS trains taking suction from RWST and injecting into associated containment spray sparger.

D_1 - Less than 1/3 high pressure injection pumps taking suction from RWST and injecting through MOV 1867 C/D into 1 of 3 RCS cold legs. Initiated by SI signal.

D_2 - Same as D_1, except must be initiated by operator.

D_3 - Less than 1/3 charging pumps injecting through MOV 1370.

D_4 - Less than 1/3 charging pumps injecting through the normal charging lines with the BAT pumps on fast speed, MOV 1350 open, and one PORV open within 10 min from initiator. SI alignment not required.

D_5 - For A, less than 2/2 accumulators injecting into their associated cold legs. For S_1, less than 2/3 accumulators injecting into their associated cold legs.

D_6 - Less than 1/2 LHSI trains taking suction from the RWST and injecting through MOV 1890C to 1/3 RCS cold legs.

F_1 - Less than 1/2 ISR trains taking suction from the sump and injecting through associated spray sparger, with service water being provided to the secondary side of the heat exchanger.

F_2 - Less than 1/2 OSR trains taking suction from the sump and injecting through associated spray sparger, with service water being provided to the secondary side of the heat exchanger.

H_1 - Less than 1/2 LHSI pumps taking suction from the sump and injecting to MOV 1890C, or injecting to the charging pump suction. Plus switch to hot leg recirculation at 16 hr for A and S_1 LOCAs.

H_2 - Less than 1/3 charging pumps taking suction from the LHSI discharge and injecting through MOV 1867 C/D.

K - Failure of automatic insertion of sufficient control rods to produce subcriticality at hot shutdown.

L - Less than 1/3 AFW pumps delivering water to 1/3 steam generators.

Table 2.2 (Concluded)

Event Tree Headings

Part 2: Definition of Events

L_2	-	Less than 2 motor-driven feed water pumps (MDFWP) or 1 turbine-driven auxiliary feed water pump (TDAFWP) delivering flow to 2 to 3 stream generators.
L_3	-	Less than 1/3 AFW pumps delivering water to 1/2 steam generators.
M	-	Failure of at least 1 main feedwater pump delivering flow to at least one steam generator, and a source of water from the hotwell or CST which is sufficient for 24 hr.
P	-	Failure of at least 2 PORVs and associated block valves to open. Initiated by manual action.
P_1	-	Less than 1/2 PORVs and associated block valves open. Initiated by operator.
Q	-	Failure of pressurizer PORVs to reclose or be manually isolated after a transient.
W	-	Failure of component cooling water supplied to the lower bearing heat exchanger of all reactor coolant pumps.

The T_1 event tree represents sequences where at least one diesel is available at Unit 1. Sequence 1 of the T_1 event tree represents successful mitigation of the initiator; diesel generators start, auxiliary feedwater is available, and the charging system provides seal injection flow to the RCP seals. The plant is in a stable condition and attention can be directed to restoration of the offsite power. Sequence 2 is similar to 1, except that seal injection flow from the charging system is unavailable. RCP seal cooling is provided by CCW to the thermal barrier heat exchangers. Sequence 3 represents a condition with no seal cooling available. Both CCW to the thermal barriers and seal injection flow have failed. Auxiliary feedwater is available, however, and all essential safety functions are being provided at the time seal cooling is lost. This represents a seal vulnerable condition and is handled with the seal LOCA model. Sequence 4 represents failure of all steam generator heat removal with successful core cooling via feed and bleed, using one charging pump and opening of both PORVs. ECCS recirculation from the sump and successful operation of the containment spray recirculation heat exchangers provide long term cooling. Sequences 5 and 6 lead to core damage through failure to provide long term feed and bleed cooling in the recirculation mode. Sequence 5 is due to failure of the high pressure recirculation system. Sequence 6 is due to failure of

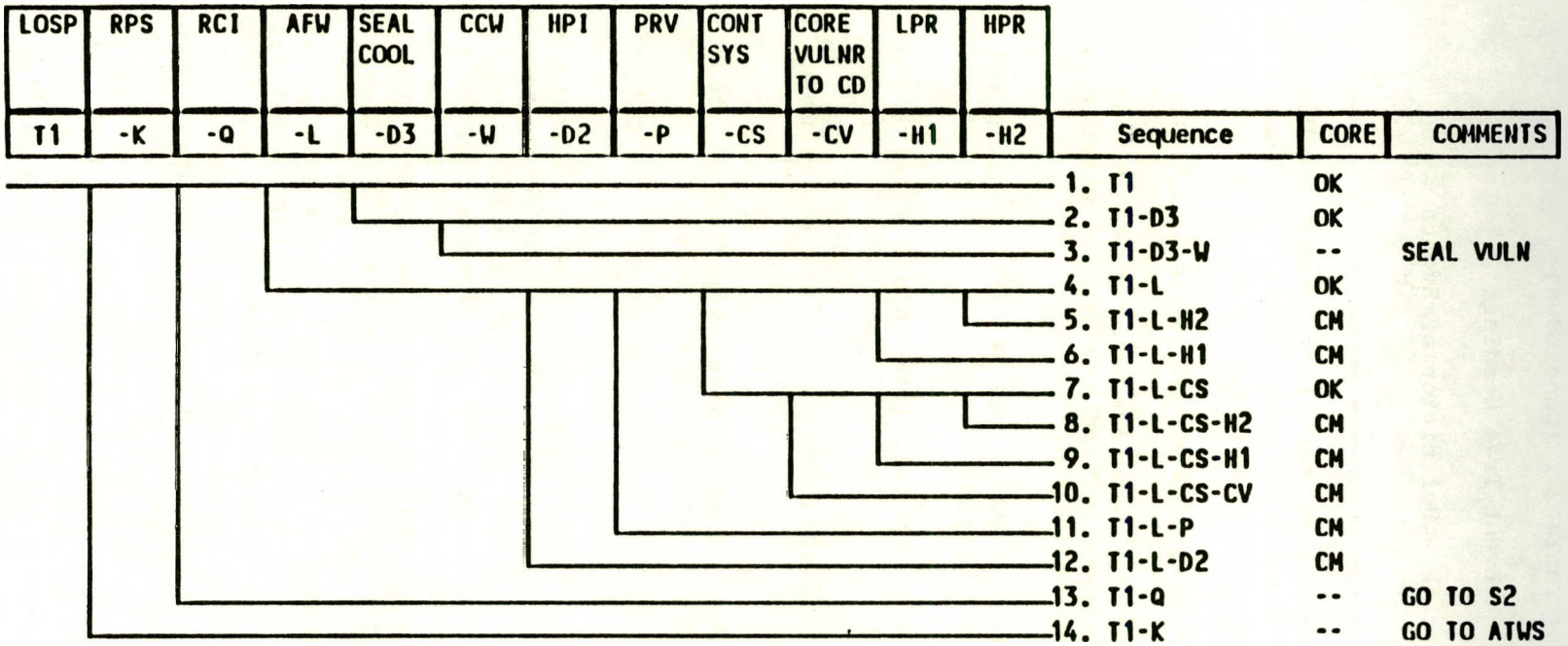

Figure 2.17. Event Tree for T_1--Loss of Offsite Power

the low pressure recirculation system. Sequences 7 through 10 represent the occurrence of a core vulnerable state and its possible outcomes. A core vulnerable state occurs when containment heat removal fails after feed and bleed is initiated. Coolant makeup to the core is being provided and heat is being removed from the RCS through the PORVs. However, containment heat removal (CHR) has failed, thereby leading to gradual containment pressure increase. Should the containment pressure increase continue, unmitigated by containment venting or restoration of CHR systems, containment overpressure failure will occur. Events occurring during containment failure could cause failure to ECCS systems, which in turn would lead to core damage. This is represented by Sequence 10. Sequence 7 represents containment failure, but survival of the ECCS and continued core cooling. Sequences 8 and 9 represent containment failure, followed by ECCS failure due to causes other than containment failure.

Sequence 11 represents failure of steam generator heat removal followed by failure to establish feed and bleed cooling, due to failure to open both PORVs. Sequence 12 is similar to 11, except feed and bleed core cooling fails due to failure to establish safety injection flow with the charging system. Sequence 13 represents transient induced LOCAs caused by a transient related PORV demand, followed by failure to reclose PORV. This condition transfers to the S_2 event tree for further evaluation. Sequence 14 is an ATWS condition.

2.3.3 T_3 (Turbine Trip with MFW Available) Event Tree

This section presents and discusses the event tree for the turbine trip initiating event group in which the main feedwater system remains available. Transients in which one or both MFW pumps remain available are considered. This event is identified by the symbol T_3 in the event tree.

This initiating event group represents a fire or seismic induced manual scram or turbine trip. PORV demand for this class of initiators is considered to be a random occurrence, due to degraded control system performance or degraded balance-of-plant (BOP) components performance. The probability of PORV demand was assigned a value of .014, for high power initiators only, based on historical Westinghouse experience. The MFW control system at Surry is such that if the reactor trip breakers are closed and T_{AVE} is less than 543°F, the main feedwater regulating valves will close, the miniflow lines will open, and the MFW pumps will stay on. This was assumed to be the course of all T_3 initiating events. Although the MFW pumps are isolated from the steam generators, they remain a viable source of SG inventory makeup, should AFW be unavailable. AFW is the preferred source of SG makeup, but MFW pumps can easily be used by opening the feedwater regulating valve bypass valve. Because AFW is the preferred source of SG makeup, it appears on the tree before main feedwater.

Four primary functions were required to successfully mitigate the T_3 events. These functions are reactor scram, RCS integrity, SG inventory makeup, and RCP seal cooling. If all these functions are provided, the transient will be mitigated at a very early stage. Failure to provide

reactor scram transfers to the ATWS tree. Failure of PORVs to reclose transfers to the S_2 LOCA tree. Failure to provide RCP seal cooling leads to a seal vulnerable condition.

Failure to provide feedwater leads to a demand for "feed and bleed" cooling. For feed and bleed, failure to provide charging flow and open two PORVs leads to core damage. Successful feed and bleed and cooling leads to a demand for containment systems and coolant recirculation systems.

The event tree for T_3 is shown in Figure 2.18. The first sequence represents successful stabilization of the reactor at hot shutdown. Reactor scram is successful. AFW starts and provides water to at least one of three steam generators. Heat removal is via the steam dumps to the condenser. Seal cooling is provided by seal injection flow. At this juncture in the tree, the reactor is stable in hot shutdown. This is considered successful termination and no further system availability questions are asked. Particularly, the availability of RHR which is necessary to reach cold shutdown is not asked. Sequence 2 is also a success state, with seal cooling being provided by CCW to the thermal barrier. Sequence 3 is a seal vulnerable condition. All critical safety functions are being provided, but RCP seal cooling is not available. The potential for this sequence to lead to core damage depends on the susceptibility of seals to failure after loss of all cooling and the potential recovery options to restore seal cooling prior to seal failure. The seal vulnerable evaluation will be cone on an individual sequence basis, should the quantification show this state to be important.

Sequence 4 represents stable hot shutdown with SG inventory being provided by main feedwater, after failure of auxiliary feedwater. This is a success state similar to Sequence 1, except of a much lower probability. Questions of seal cooling were not asked on this branch, because the additional sequences would be subsets of Sequences 2 and 3. Sequence 5 represents loss of auxiliary feedwater and all main feedwater, but successful feed and bleed cooling, using containment heat removal systems and reactor coolant recirculation systems. Long term feed and bleed cooling requires high pressure coolant recirculation. Sequence 6 represents core damage due to failure to provide high pressure recirculation for long term cooling. Sequence 7 is similar to 6, except that the low pressure recirculation systems are unavailable.

Sequences 8 through 11 represent successful feed and bleed cooling, but failure of containment heat removal. In Sequence 8, containment failure does not lead to structural or phenomenological failure of the ECCS, therefore, core cooling is successful. Sequences 9 and 10 represent ECCS survival of the containment failure, but failure due to random other causes. Sequence 11 represents ECCS failure due to containment failure. Thus, Sequence 11 represents containment failure prior to core damage.

Sequences 12 and 13 represent failure to initiate feed and bleed cooling after loss of auxiliary feedwater. In Sequence 12 feed and bleed fails due to failure of 2 of 2 PORVs to open, while in Sequence 13, feed and bleed fails due to failure to establish safety injection flow.

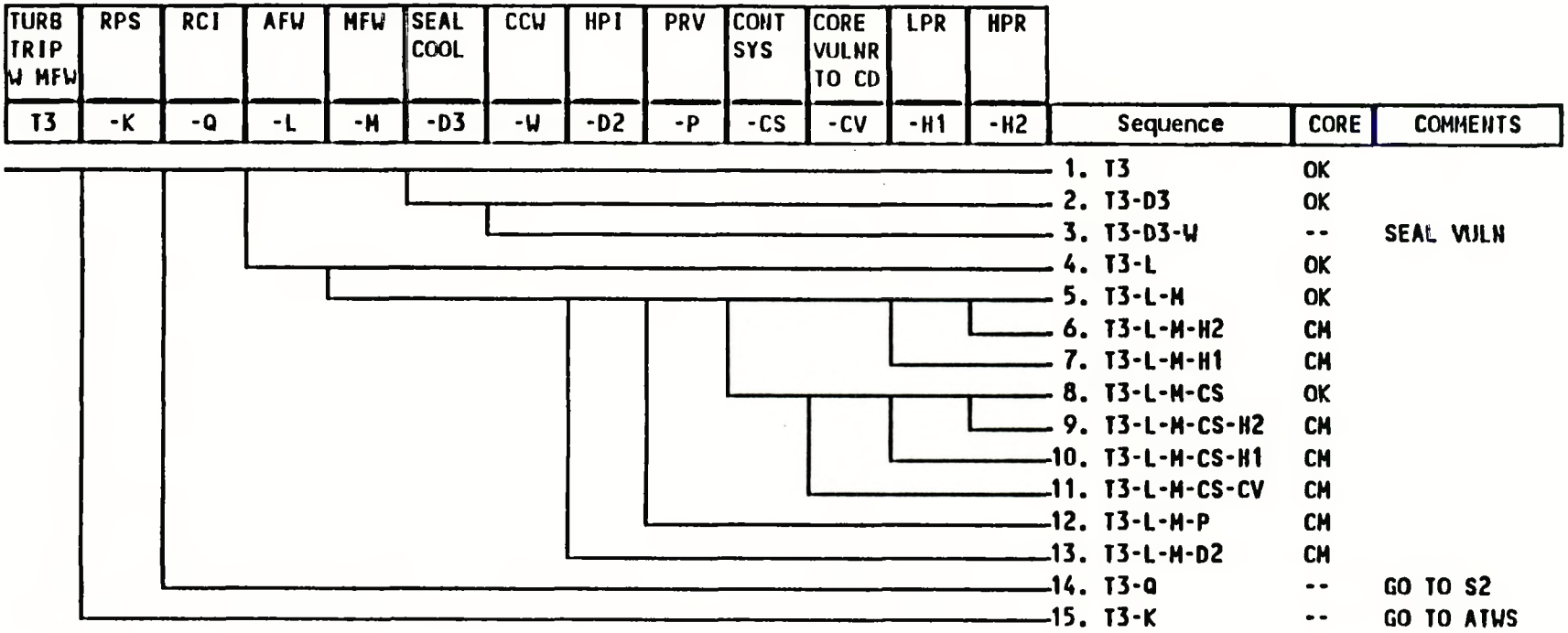

Figure 2.18. Event Tree for T_3 - Turbine Trip With MFW

Sequence 14 is a transient induced LOCA, which transfers to the S_2 tree for further evaluation. Sequence 15 is an ATWS sequence.

2.3.4 Large LOCA Event Tree

This section presents and discusses the event tree for the large LOCA initiating event. This event is identified by the symbol A in the event tree and covers break sizes ranging from 6 to 29 in. The event tree for large LOCAs is shown in Figure 2.19.

Sequence 1 represents a completely successful response to the initiator in which all systems function as intended. The accumulators inject water immediately to accommodate the initial high volume surge of water from the reactor cooling system. Low pressure injection subsequently provides the high volume, low pressure flow required for continued core cooling. The containment heat removal systems successfully maintain containment pressures and temperatures at acceptable levels, and recirculation cooling is established from the containment sump to provide long-term cooling.

Sequence 2 leads to core damage because of a failure to provide low pressure recirculation cooling. No other system can provide the volume of flow needed under large LOCA conditions. Sequences 3, 4, and 5 represent the occurrence of a core vulnerable state and its possible outcomes. A core vulnerable state occurs when containment heat removal fails after core cooling has been established by low pressure injection. Under such circumstances, heat is being transferred from the core to the containment via the water flowing through the opening in the RCS pressure boundary. As a result, the pressure and temperature in the containment rise due to the lost containment heat removal (CHR) capability. If the containment pressure continues to increase without being mitigated by containment venting or restoration of CHR systems, containment overpressure failure will occur. Events occurring during containment failure could cause ECCS systems to fail, which would lead to core damage. Such a scenario is represented by Sequence 5. Sequence 3 represents containment failure, but the ECCS survives and continues to cool the core. Sequence 4 represents containment failure together with independent failure of the ECCS (i.e., due to causes other than the containment failure).

Sequence 6 represents failure to the ECCS to respond early in the scenario to provide the high volume, low pressure injection flow needed to cool the core, thereby leading to core damage. In Sequence 7 the accumulators fail to inject water immediately as the pressure in the reactor coolant system drops suddenly as a result of the large break in the cooling system pressure boundary. This sudden loss of coolant inventory causes core damage.

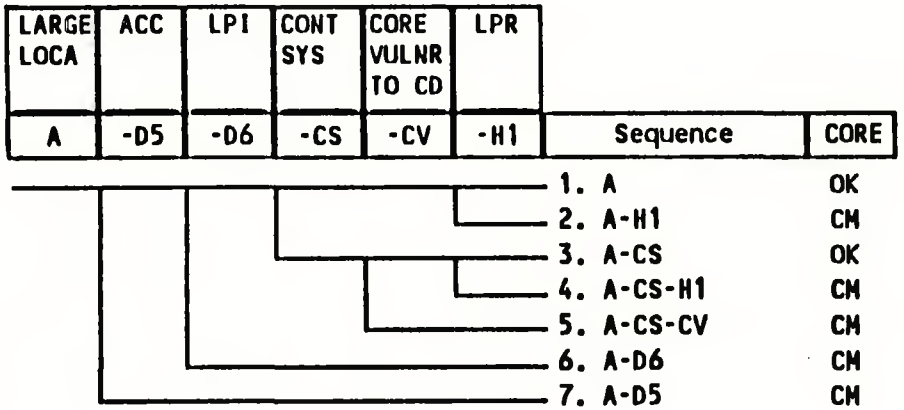

Figure 2.19. Event Tree for A - Large LOCA

2.3.5 Medium LOCA Event Tree

This section presents and discusses the event tree for the medium LOCA initiating event. This event is identified by the symbol S_1 in the event tree and covers leak sizes ranging from 2 to 6 in.

Success criteria for S_1 are distinctively different A and S_2. These differences were derived from requirements for AFW, accumulators, HPI/R and LPI/R.

The S_1 events will maintain the reactor moderately pressurized during the early time frame, thus requiring early inventory makeup from HPI. As the pressure declines the accumulators and LPI are required. A requirement for high pressure recirculation is not necessary, because pressure will be below shutoff head for low-head safety injection (LHSI) pumps at the time of recirculation. The event tree for medium LOCAs is shown in Figure 2.20.

Sequence 1 represents a completely successful response to the initiator in which all systems function as intended. High pressure injection immediately provides the high pressure initial flow required for core cooling. The accumulators inject water to accommodate the initial high-volume surge of water from the reactor cooling system. The containment heat removal systems successfully maintain containment pressures and temperatures at acceptable levels, and low pressure injection and recirculation cooling are established to provide long term cooling.

Sequence 2 leads to core damage because of the failure to provide low pressure recirculation cooling. No other system can provide the volume of flow needed under the low pressure conditions that follow a medium LOCA. Sequence 3 denotes failure to establish low pressure injection, which is required before enough water accumulates in the containment sump to allow recirculation cooling.

Sequences 4, 5, 6, and 7 represent the occurrence of a core vulnerable state and its possible outcomes. A core vulnerable state occurs when containment heat removal (CHR) fails after core cooling has been established by high pressure injection. Under such circumstances, heat is being transferred from the core to the containment via the water flowing through the opening in the RCS pressure boundary. As a result, the pressure and temperature in the containment rise due to the failed containment heat removal capability. If the containment pressure continues to increase without being mitigated by containment venting or restoration of CHR systems, containment overpressure failure will occur. Events occurring during containment failure could cause ECCS systems to fail, which would lead to core damage. Such a scenario is represented by Sequence 7. Sequence 4 represents containment failure, but the ECCS survives and continues to cool the core. Sequences 5 and 6 represent containment failure together with independent failure of the ECCS (i.e., due to causes other than the containment failure).

In Sequence 8 the accumulators fail to inject water immediately as the pressure in the reactor coolant system drops suddenly as a result of the

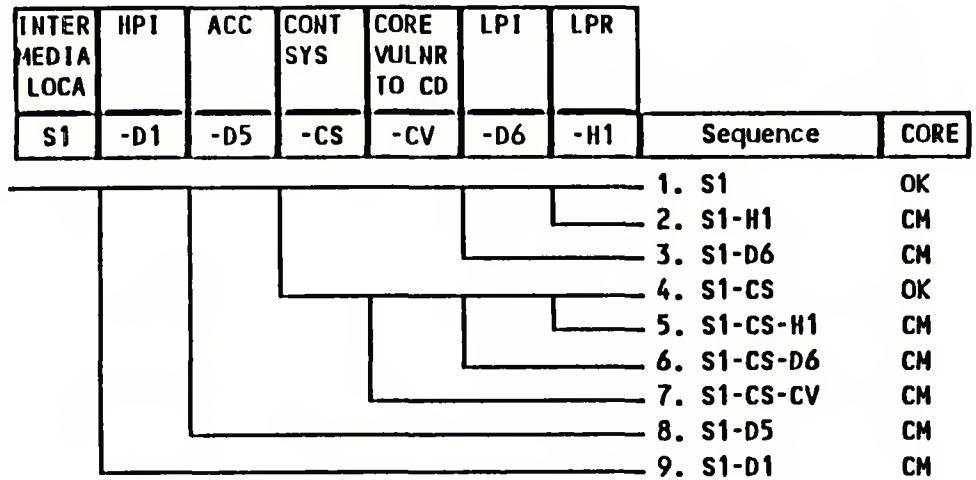

Figure 2.20. Event Tree for S_1 - Medium LOCA

medium break in the cooling system pressure boundary. This sudden loss of coolant inventory causes core damage. Sequence 9 represents failure of the ECCS to respond early in the scenario to provide the high pressure injection flow needed to cool the core, thereby leading to core damage.

2.3.6 Small LOCA Event Tree

This section presents and discusses the event tree for the small LOCA initiating event. This event is identified by the symbol S_2 in the event tree and covers leak sizes ranging from 1/2 to 2 in.

S_2 success criteria are a combination of transient and LOCA type criteria. The break is not sufficient to depressurize the reactor, so that large volume ECCS systems are not effective. Thus the need for control rod insertion, because the ECCS boration function will not be performed.

AFW is required for successful S_2 mitigation, because the break size itself is not sufficient to carry away decay heat and pump heat. If AFW is unavailable, "feed and bleed" cooling is viable if the operator opens one PORV. The event tree for S_2 is shown in Figure 2.21.

Sequence 1 represents a completely successful response to the initiator in which all systems function as intended. The reactor protection system successfully scrams the reactor. High pressure injection provides the initial high pressure flow required to replace the lost inventory. The auxiliary feedwater system provides core heat removal via the steam generators. The containment heat removal systems successfully maintain containment pressures and temperatures at acceptable levels. The operator successfully depressurizes the RCS, and recirculation cooling is established to provide long-term cooling, using the low pressure recirculation systems. Low pressure recirculation from the sump was required for successful mitigation, because shutdown cooling on RHR may not be possible due to break location.

Sequence 2 leads to core damage because of a failure to provide low pressure recirculation cooling. Sequence 3 represents successful mitigation after the failure of the operator to depressurize the RCS. Failure to depressurize the RCS leads to the requirement for high pressure recirculation. If either low or high pressure recirculation fails, core damage results as indicated by Sequences 4 and 5.

Sequences 6 through 11 cover the case in which the containment heat removal systems fail after core inventory is being maintained via high pressure injection and core cooling has been established by the AFW system. Whether or not this can lead to a core vulnerable state depends on whether or not the operator depressurized the RCS. If operator depressurization occurs, SG heat removal is not effective and a core vulnerable state can occur. Under such circumstances, heat is gradually being transferred from the core to the containment via the water flowing through the opening in the RCS pressure boundary. As a result, the pressure and temperature in the containment rise gradually due to the

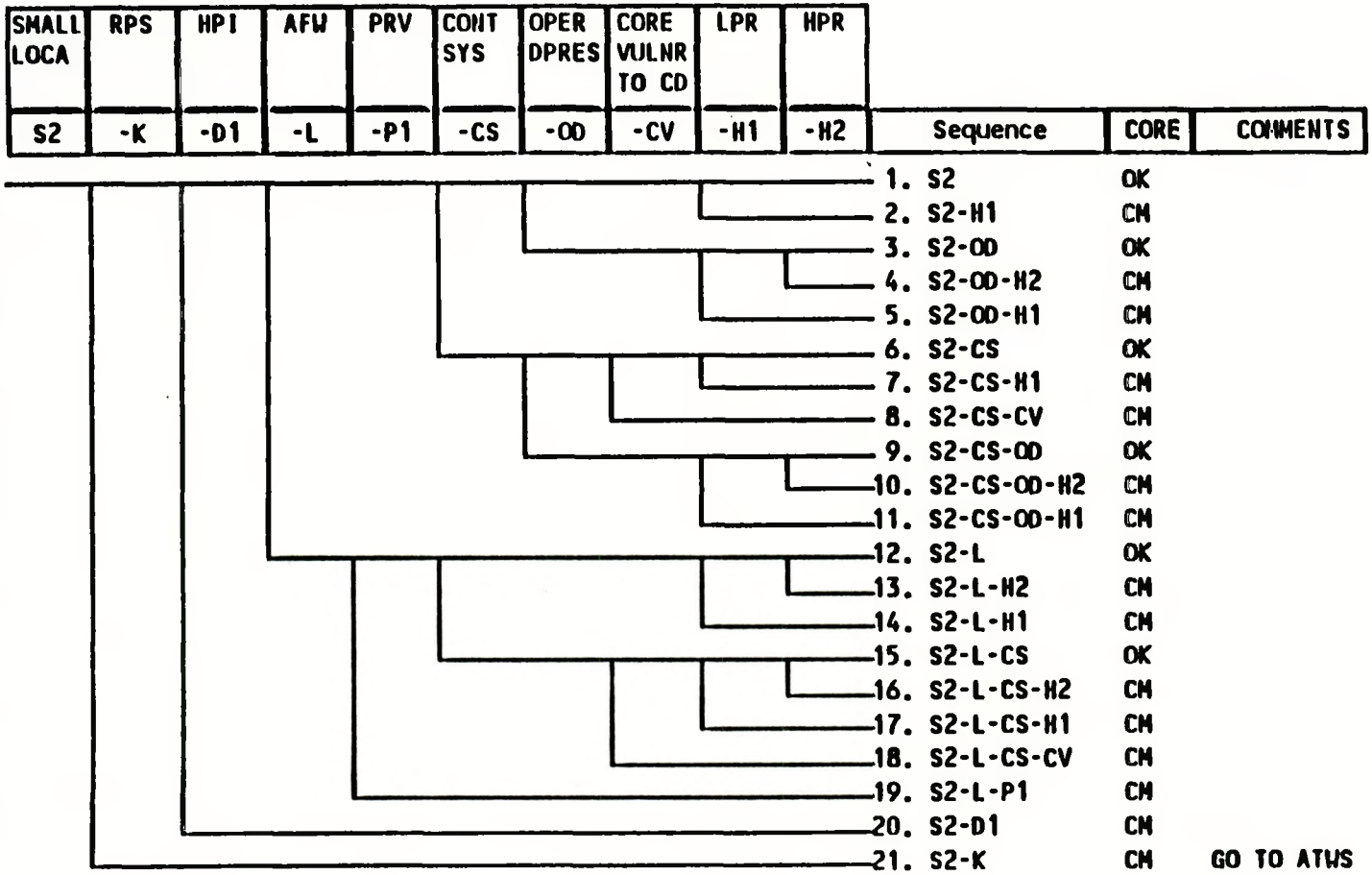

Figure 2.21. Event Tree for S_2--Small LOCA

lost containment heat removal (CHR) capability. If the containment pressure continues to increase without being mitigated by containment venting or restoration of CHR systems, containment overpressure failure will occur. Continued heat removal through the steam generators has been shown to be sufficient to prevent containment overpressure failure in these cases. Events occurring during containment failure could cause ECCS failure which would lead to core damage. Such a scenario is represented by Sequence 8. Sequence 6 represents containment failure, but the ECCS survives and continues to cool the core. Sequence 7 represents containment failure together with the independent failure of the ECCS (i.e., due to causes other than the containment failure). If the operator keeps the RCS pressurized and thus supports steam generator heat removal (as represented by Sequences 9, 10, and 11), then the containment overpressure failure is averted, even though containment heat removal systems have failed. Under such circumstances the containment is not expected to fail, and the "CV" question is not asked. Sequence 9 represents successful functioning of the ECCS in the recirculation mode. Sequences 10 and 11 represent ECCS failure, which results in core damage. Sequences 12 through 19 address the sequences with auxiliary feedwater failure. If AFW is lost, core cooling can be accomplished by opening a PORV to increase the breakflow. Now sufficient water is lost from the RCS to carry away all decay heat. The charging pump is known to be successful at this point in the event tree. Sequence 19 represents failure of either PORV to open.

Sequences 12 through 18 address the potential for a core vulnerable state due to failure of CHR. A core vulnerable state occurs when containment heat removal fails after feed and bleed core cooling has been established. Under such circumstances, heat is being transferred from the core to the containment. The pressure and temperature in the containment rise due to the lost containment heat removal capability. If the containment pressure continues to increase without being mitigated by containment venting or restoration of CHR systems, containment overpressure failure will occur. Events occurring during containment failure could cause ECCS systems to fail, which would lead to core damage. Such a scenario is represented by Sequence 18. Sequence 12 is AFW success and no core damage. Sequences 13 and 14 are AFW success but long-term recirculation failure leads to core damage. Sequence 15 represents containment failure, but the ECCS survives and continues to cool the core. Sequences 16 and 17 represent containment failure together with independent failure of the ECCS (i.e., due to causes other than the containment failure).

In Sequence 20 the ECCS fails to respond to the small LOCA initiator and to provide the initial high pressure injection flow needed to cool the core. In Sequence 21 the RPS fails to scram the reactor.

2.3.7 Very Small LOCA Event Tree

This section presents and discusses the event tree for the very small LOCA initiating event. This event is identified by the symbol S_3 in the event tree. This group of LOCAs includes spontaneous seal LOCAs and very small breaks, with leak sizes equivalent to less than approximately 1/2 in. break.

The system success criteria are very similar to the S_2 criteria. However, timing considerations due to the impact of the very small leak rate have a significant impact on the recirculation requirements.

Heat removal from the RCS by the AFW combined with the containment fan coolers ad natural cooling/condensation processes are expected to maintain containment pressure well below the spray actuation point. With only the HPI flow draining the RWST, S_3 breaks could remain in the injection phase for a long time.

If the operator takes action to depressurize the RCS, thus reducing the leak rate from the RCS, the reactor can be depressurized and in cold shutdown long before depletion of RWST inventory forces a switch to recirculation. The event tree for S_3 is shown in Figure 2.22.

Sequence 1 represents a completely successful response to the initiator in which all systems function as intended. The reactor protection system successfully scrams the reactor. High pressure injection provides the high pressure initial flow required for continued core cooling. The RCS relief valves reclose if opened, auxiliary feedwater cooling is initiated, the operator depressurizes the RCS, and the residual heat removal system is available to provide shutdown cooling.

Sequence 2 addresses the case where residual heat removal system is unavailable and low pressure recirculation cooling is required to provide long-term core cooling. If LPR fails (as in Sequence 3), then core damage will result.

Sequences 4, 5, and 6 address the cases where the operator does not depressurize the RCS. Continued blowdown leads to RWST depletion which forces recirculation. Sequence 4 represents successful switch to high pressure recirculation. Sequences 5 and 6 represent core damage due to failure of high and low pressure recirculation.

Sequences 7 through 21 represent all cases in which the primary mode of steam generator feedwater supply is lost. In Sequences 7 through 13, main feedwater supplies steam generator feed flow. These sequences have much the same characteristics as Sequences 1 through 6.

Sequences 14 through 21 address the case that both AFW and MFW have been lost. In this instance, it is necessary to establish feed and bleed cooling. Both PORVs must open to allow water to flow from the RCS, to remove decay heat. A single charging pump is required to supply makeup to replenish the PORV discharge. If feed and bleed cooling is lost (Sequence 21), then core damage results. Sequence 14 represents successful feed and bleed cooling followed by long term cooling in the recirculation mode. If either high pressure or low pressure recirculation cooling is lost (as in Sequences 15 and 16), then core damage results.

Sequences 17 through 20 represent the occurrence of a core vulnerable state during successful feed and bleed cooling. A core vulnerable state

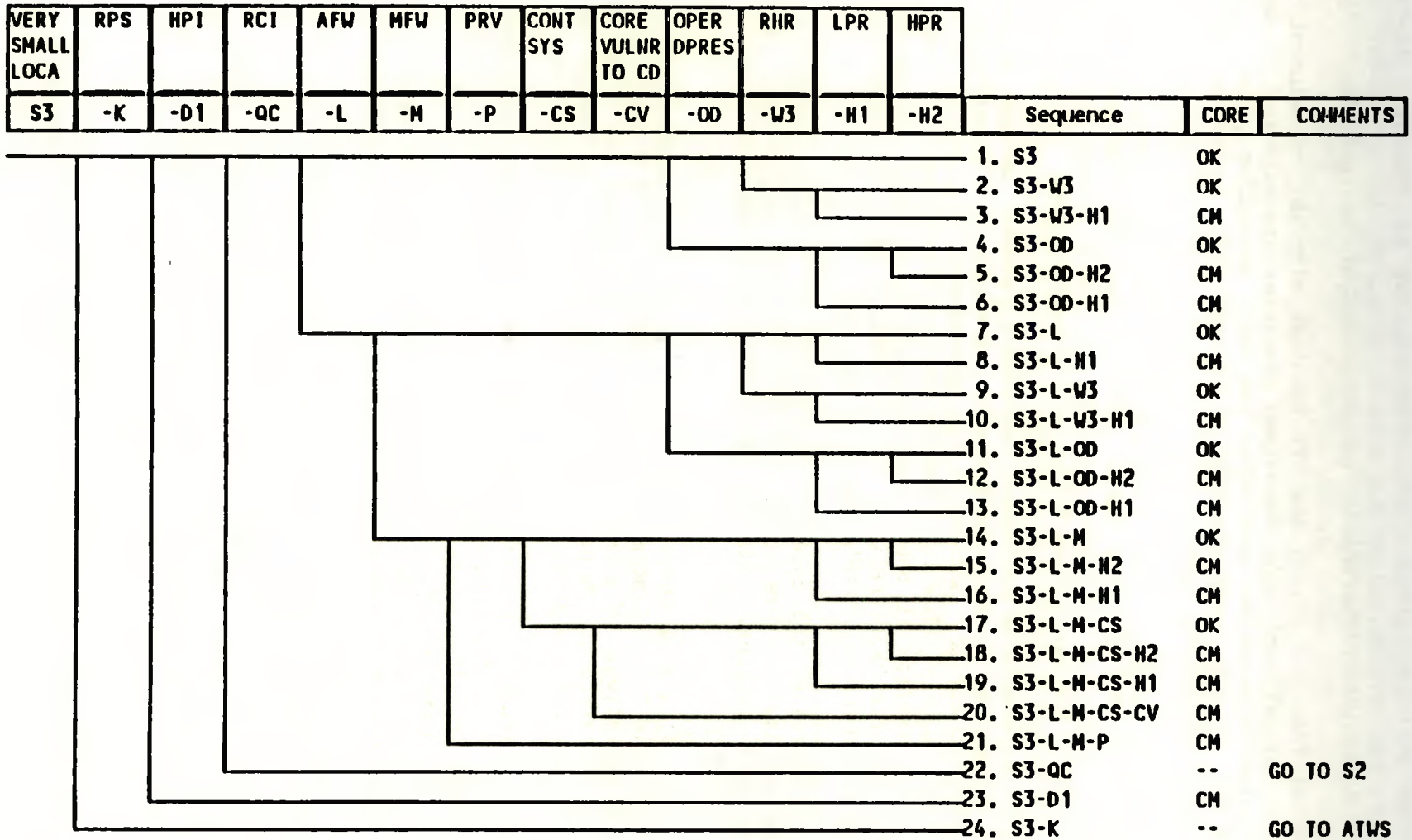

Figure 2.22. Event Tree for S_3--Very Small LOCA

occurs when containment heat removal fails after core cooling has been established in the feed and bleed mode. Under such circumstances, heat is being transferred from the core to the containment. (A core vulnerable state cannot occur in Sequences 2 through 13 in the event tree because an insufficient amount of hot water is transferred into the containment to cause overpressure.) As a result, the pressure and temperature in the containment rise due to the lost containment heat removal capability. If the containment pressure continues to increase without being mitigated by containment venting or restoration of CHR systems, containment overpressure failure will occur. Events occurring during containment failure could cause ECCS systems to fail, which would lead to core damage. Such a scenario is represented by Sequence 20. Sequence 17 represents containment failure, but the ECCS survives and continues to cool the core. Sequences 18 and 19 represent containment failure together with independent failure of the ECCS (i.e., due to causes other than the containment failure). Sequence 22 represents the case in which SI flow causes the RCS relief valves to open, and one of the valves fails to reseat. This leads to a larger LOCA size, which requires analysis via the small LOCA event tree. In Sequence 23 the ECCS fails to respond to the LOCA initiating event and to provide the initial high pressure injection flow needed to cool the core. In Sequence 24 the RPS fails to scram the reactor.

3.0 SCOPING QUANTIFICATION STUDY

A scoping quantification study was performed for Surry Power Station site to determine which external events should be included in the detailed PRA study. This scoping study considered all potential external hazards at the site except for seismic and fire events, since these two events were already scheduled for a detailed risk analysis. The PRA Procedures Guide (Ref. 1) was used as a guideline for systematic identification of the external events at the site. Next, an initial screening process was carried out to eliminate as many events as possible from the list. For this purpose, a set of screening criteria was developed and then each external event was examined for possible elimination based on these criteria. After the initial screening process was completed, it was found that the following events could not be screened out based on the general screening criteria:

a. Aircraft Impact
b. External Flooding
c. Extreme Winds and Tornados
d. Industrial or Military Facility Accidents
e. Pipeline Accidents
f. Release of Chemicals from On-Site Storage
g. Transportation Accidents
h. Turbine Generated Missiles
i. Internal Flooding

A bounding analysis was done for each of these events. The degree of sophistication in the bounding analysis for each event depended on whether the event could be eliminated based on only a hazard analysis or whether a complete analysis including hazard analysis, fragility evaluation and plant response analysis was required.

This chapter covers the screening and bounding analyses for the external events as part of the scoping quantification study of the Surry Power Station. Section 3.1 is a general description of the plant and its location. Section 3.2 deals with the identification and screening of external events for this site. A number of the events could be screened based on the Surry Updated Final Safety Analysis Report (FSAR) (Ref. 2) and its supporting documents as discussed in Section 3.3. Finally, the remaining external hazards were screened out using a bounding analysis as described in Section 3.4. Section 3.5 summarizes the results of the screening study.

3.1 General Description

3.1.1 Site

The Surry Power Station is located in Gravel Neck, Virginia at approximately 37° 10 ft N, 76° 42 ft W. The peninsular site is bordered by the James River and the Hog Island Waterfowl Refuge. This wildlife area is marshy and covered by many streams and creeks. The site is 8 miles from the town of Surry and is at the end of Route 650 (a state secondary route). This road provides the only land access to the area. Also, a

public access road to the waterfowl refuge runs through the power plant site. The topography in macro and micro scales is shown in Figures 3.1 through 3.3.

The site occupies 840 acres and the area within 10 miles of the site is predominantly rural, with a few small urbanized segments. The neighboring area is characterized by farmlands, marshy wetlands, swamps, and small streams. The water table is near the surface throughout the area and drainage is toward Hampton Roads, on the Atlantic Ocean and near the mouth of the Chesapeake Bay. The ground surface at the site is generally flat, with steep banks sloping towards the river and to the low-level waterfowl refuge. Pre-construction elevation within the site boundaries varied from river level to 39 ft, with a mean elevation of 34 ft. Station ground grade for the site was established at 26.5 ft above the mean sea level.

The resident population in 1980 was estimated to be 1,759 within 5 miles of the site and 61,711 within 10 miles. The nearest city is Newport News, with a population of 114,903 which is, however, only 4-1/2 miles across the James River. In addition, there is a transient population of 25,000 per year at the public recreational facilities (beaches, boat landings, fishing areas, etc.), 2.16 million at the Busch Gardens/ Anheuser-Busch brewery (6 miles north of the site), and 1.5 million to 2.5 million per year at the historical attractions in the Williamsburg-Jamestown area (4 to 7 miles north of the site). Further details regarding population projections are available in FSAR.

The roads, railways, and airports in the vicinity of the site are shown in Figures 3.2 and 3.4. The location of the natural gas pipelines is shown in Figures 3.3 and 3.5. As seen from these, two pipelines cross the southeast corner of the site. The closest industrial facilities to the site are a brewery plant (6 miles), a synthetic fibers factory (5 miles), and some food processing units. The U.S. Army Transportation Center at Fort Eustis is within 5 miles of the site. There are no known mines or stone quarries within 5 miles of the site.

The Surry site experiences a high variability in temperature extremes. For example, extreme temperatures recorded at nearby Richmond range from -12°F to 105°F. Temperature data from Norfolk indicates a range of 5°F to 104°F. The maximum recorded precipitation for a 24-hour period was 8.79 in. at Richmond and 11.4 in. at Norfolk. The maximum 24-hour snowfall observed at the two stations was 21.6 in. and 12.4 in., respectively. The local climatological data indicates an average of 29 days per year of heavy fog (i.e., visibility of 1/4 mile or less) for Richmond and 21 days for Norfolk. The site experiences a wide spectrum of extreme winds and tornadoes. The one hundred year wind speed is estimated to be 105 mph and using a gust factor of 1.3, the highest instantaneous gust expected is 137 mph. During the period 1951 through 1982, a total of 30 tornadoes were reported within 50 miles of the site. In addition, an average of two storms/hurricanes per year bring torrential rainfall to the tidewater areas, and high tides result in flood conditions for low-lying areas along the coast.

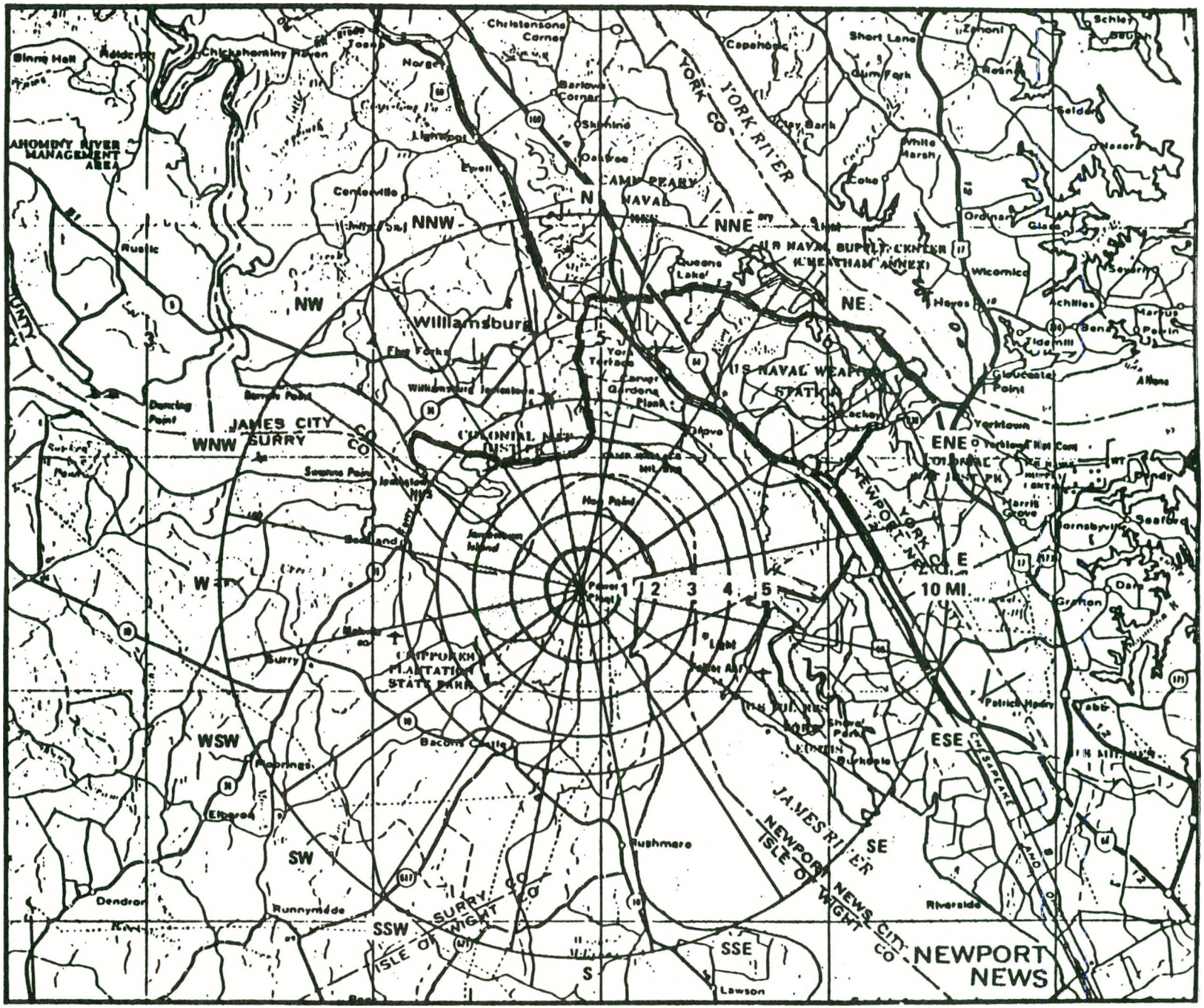

Figure 3.1 Immediate Environs of Plant Site: Surry Power Station

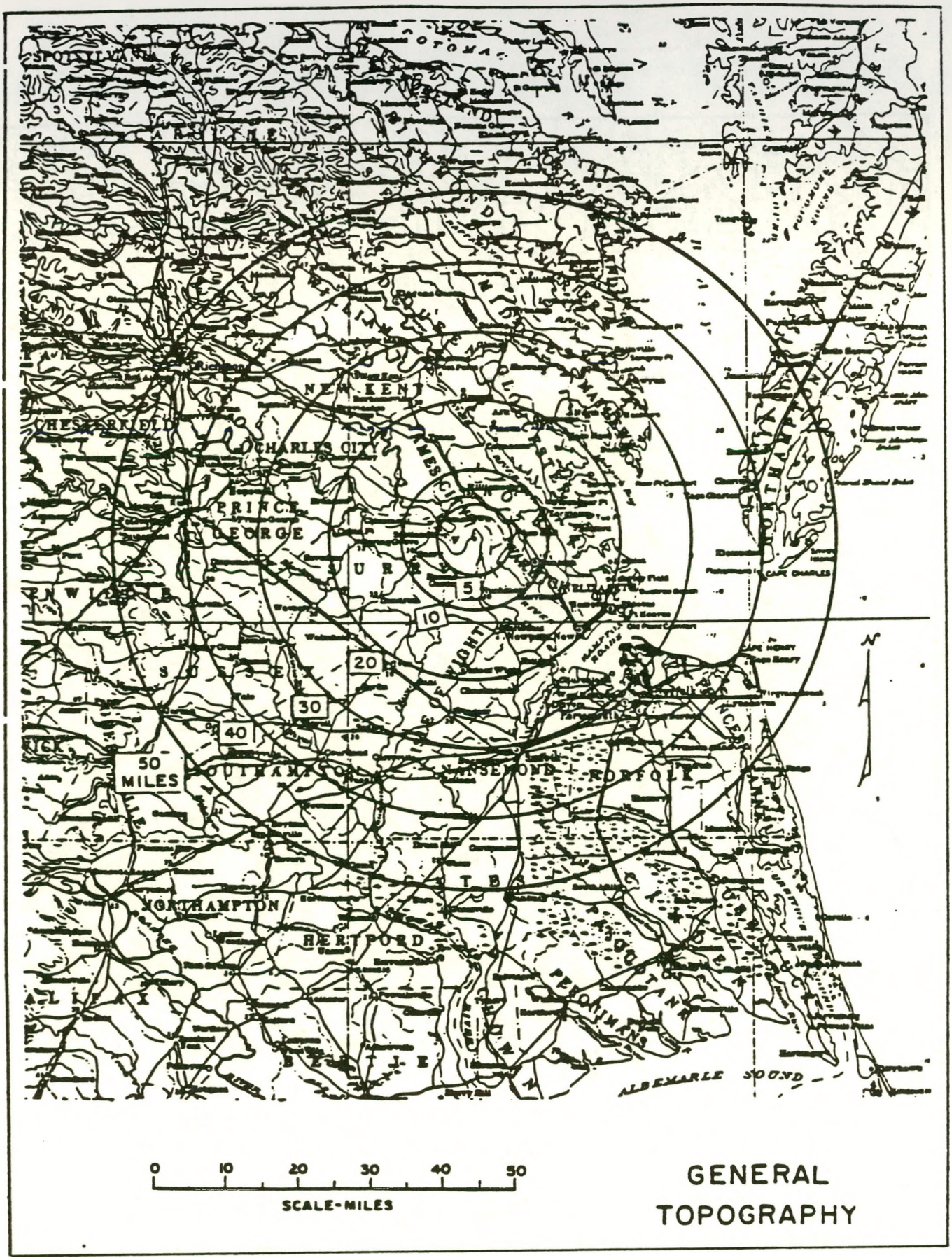

Figure 3.2. General Topography: Surry Power Station

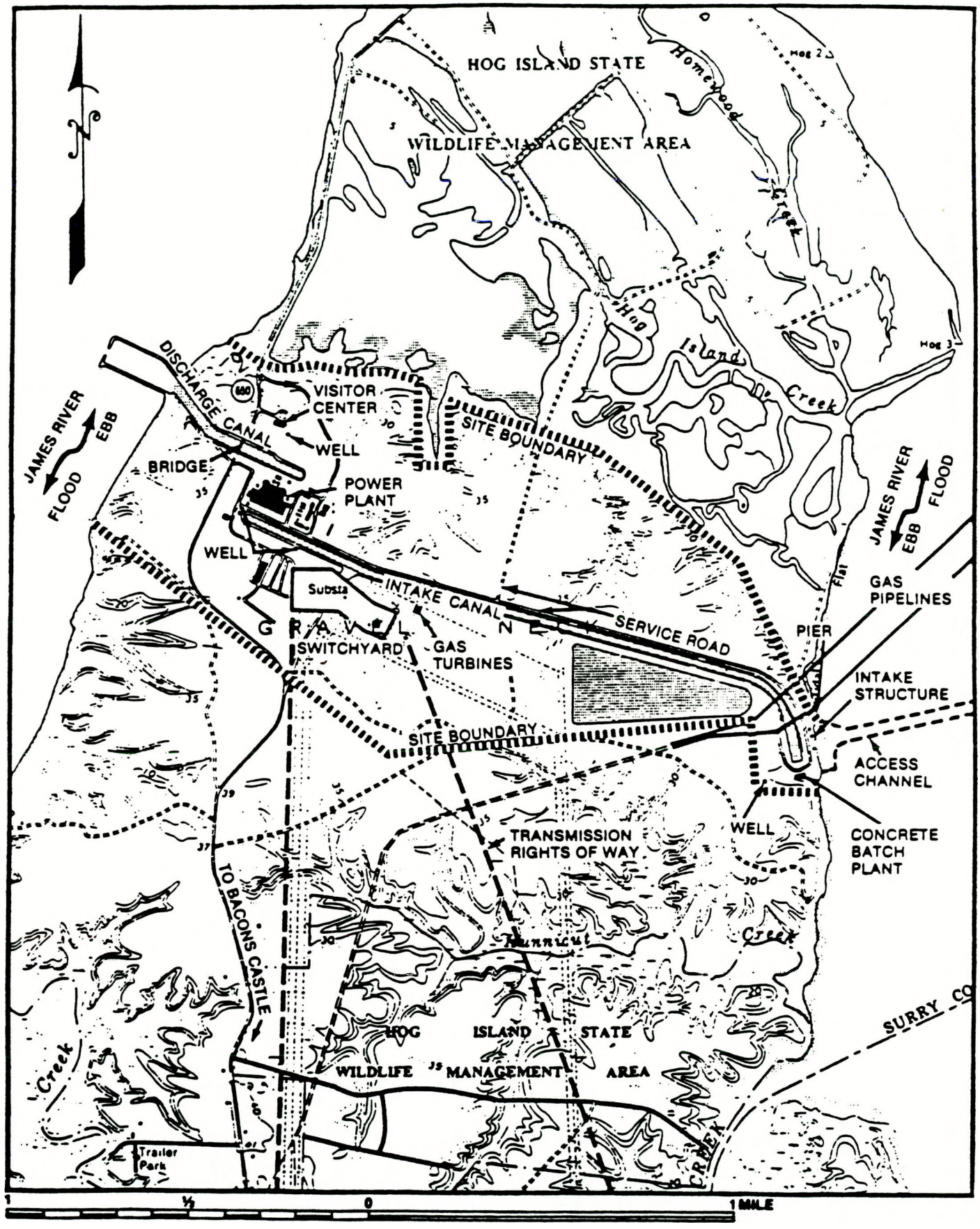

Figure 3.3. Local Topography: Surry Power Station

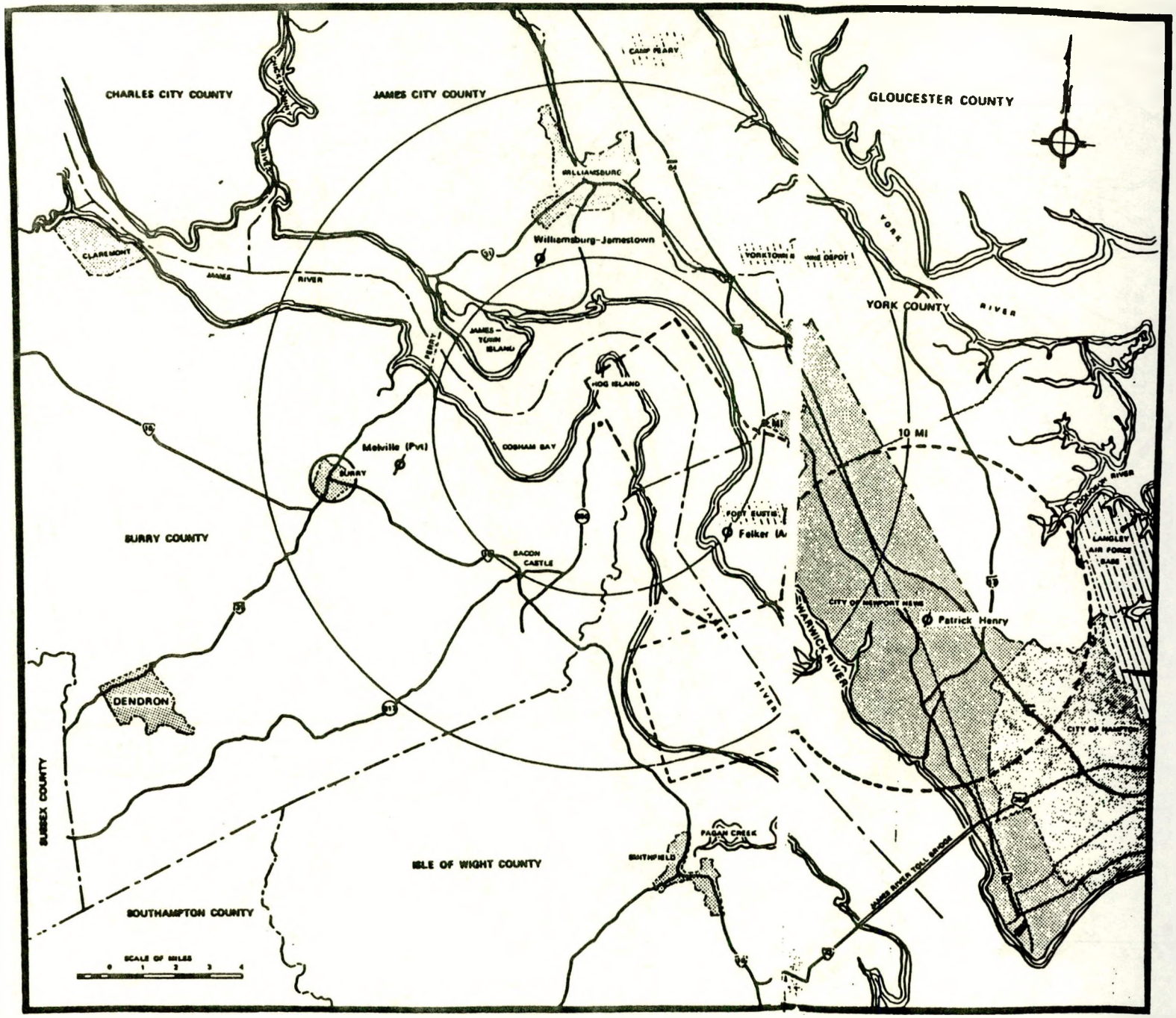

Figure 3.4. Airports Within 10 Miles of Plant Site

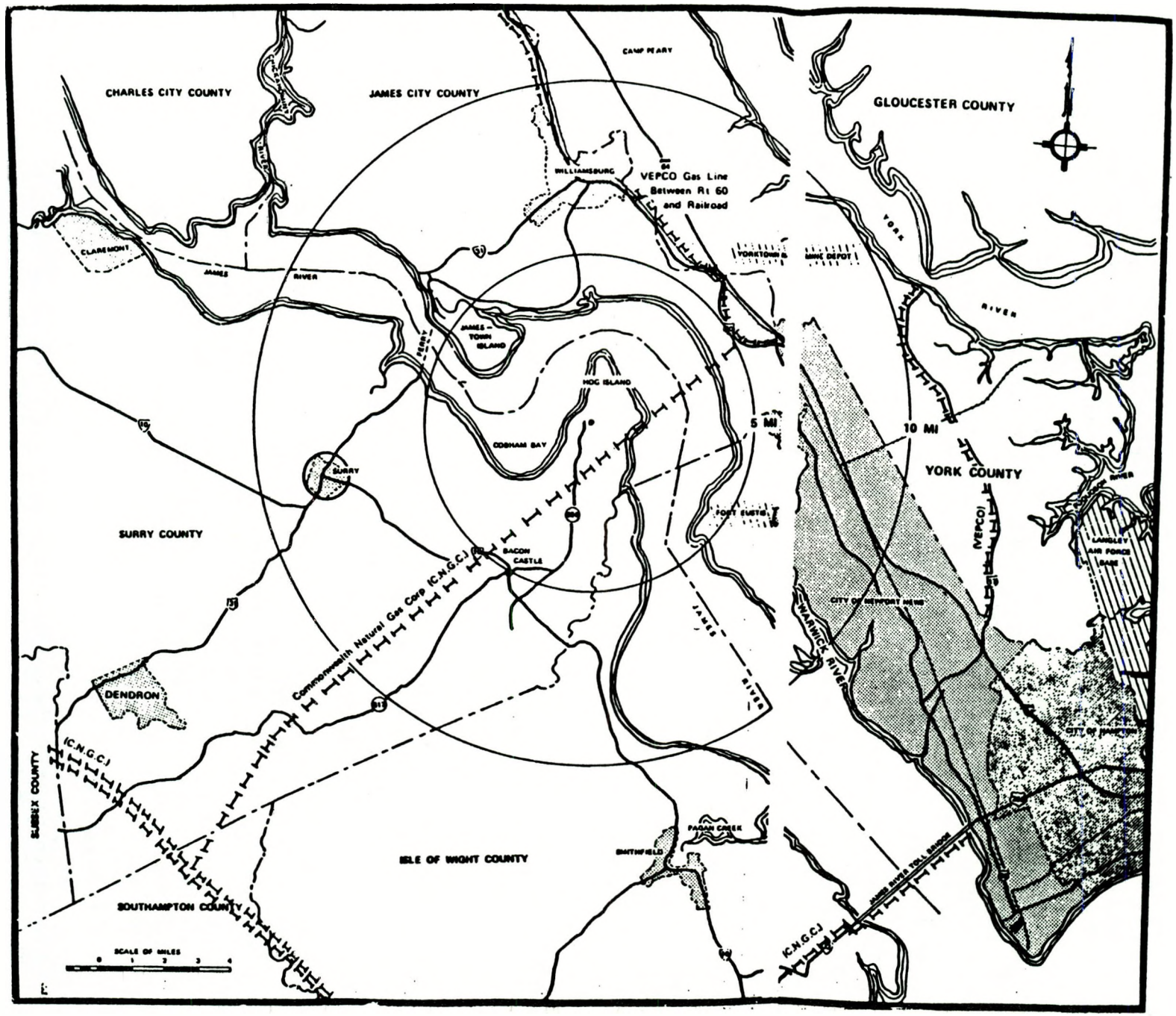

Figure 3.5. Natural Gas Pipelines Within 10 Miles of Plant Site

3.1.2 Plant

The twin PWR units (Surry 1 and Surry 2) belonging to the Virginia Power Company are each rated at 781 MW. The reactor and generator for both the units were supplied by Westinghouse Electric Corporation. The plant began commercial operation in 1972-73. Stone and Webster Engineering Corporation was the Architect/Engineer/Constructor for these plants.

The reactor containment structure is a steel-lined, reinforced concrete unit with vertical cylindrical walls and a hemispherical dome. The supporting flat base of the foundation mats is approximately 66 ft below finished ground grade. The containment structure below grade is constructed inside a cofferdam. Dimensions for each of these units are as follows:

a.	Inside diameter	126 ft-0 in.
b.	Springline of dome above the top of foundation mat	122 ft-1 in.
c.	Thickness of mat	10 ft-0 in.
d.	Thickness of dome	2 ft-6 in.
e.	Thickness of cylindrical walls	4 ft-6 in.
f.	Thickness of steel liner:	
	(i) base mat	0.25 in.-.75 in.
	(ii) hemisphere	0.5 in.
	(iii) cylindrical wall	0.375 in.

Access to the containment structure for personnel and equipment is provided by two hatch penetrations with internal diameters of 7 ft-0 in. and 14 ft-0 in. respectively. Besides these, there are several smaller penetrations for pipes and conduits.

Other Class I structures (i.e., except the reactor containment) are the auxiliary building; control room area, including switchgear and relay rooms; fuel building; auxiliary generator cubicles; auxiliary containment buildings that contain main steam and feedwater isolation valves; recirculation spray and low-head safety injection pump cubicles; safeguards ventilation room and circulating water intake structures, including the high-level canal. All these structures were designed to meet both earthquake and tornado design criteria.

3.1.3 Site Visit

The screening analysis began with a site visit conducted in April 1987. The purpose of the site visit was twofold: first, to confirm the information in the FSAR which was used in the Surry scoping quantification

study, and second to collect new information and look for possible changes in the plant and site conditions which could affect the risk from external hazards to the site. The site visit included a tour of the plant structures as well as a survey of the plant boundary and surrounding areas. Following is a highlight of the issues which were resolved by the site visit:

a. No major changes or deviations from the information in the Surry FASR (which could affect the external event screening) were observed in the plant or its surroundings.

b. A survey of the structures in Surry revealed that all the doors which open to the outside of the plant are above the plant grade which is considerably higher than the probable maximum hurricane-induced flood level. The circulating water intake structure and emergency service water pumphouse have doors and air intake louver openings at levels below the probable maximum surge level. However, the doors are leaktight and the air intake is not used in the event of a probable maximum surge.

c. During the site visit, a survey of the objects in the plant boundary which could potentially become tornado-generated missiles was carried out. The site visit confirmed that the potential number of missiles at the Surry site is less than the number used in the tornado missile simulation study (Ref. 3) utilized in the bounding analysis study discussed in Section 3.4.2.

d. The site visit confirmed that there are no new industries, major airports, pipelines, or major highways in the vicinity of the site that are not described in the Surry FSAR.

3.2 Initial Screening of External Events

An extensive review of information on the site region and plant design was made to identify all external events to be considered. The data in the Surry FSAR as well as other data obtained from the utility, and the information gathered in the site visit were reviewed for this purpose.

A set of screening criteria was utilized to identify those external hazards which could be screened from further consideration based on very general considerations, as described in Section 1.3.2. These criteria, based on those in the PRA Procedures Guide (Ref. 1), are listed again below:

An external event can be excluded from further consideration if:

Criterion 1 The event is of equal or lesser damage potential than the events for which the plant has been designed. This requires an evaluation of plant design bases in order to estimate the resistance of plant structures and systems to a particular external event.

Criterion 2 The event has a significantly lower mean frequency of occurrence than other events with similar uncertainties and could not result in worse consequences than those events.

Criterion 3 The event cannot occur close enough to the plant to affect it. This is also a function of the magnitude of the event.

Criterion 4 The event is included in the definition of another event.

Criterion 5 The event is slow in developing and there is sufficient time to eliminate the source of the treat or to provide an adequate response.

The use of these criteria minimizes the possibility of omitting any significant risk contributors while at the same time reducing the amount of detailed bounding analysis required.

Table 3.1 is a listing of external hazards for the Surry Station based on the augmentation of Table 10-1 of the PRA Procedures Guide (Ref. 1). For each external event, the applicable screening criteria and a brief description of the basis for the screening (if any) is included in the table.

In summary, the findings of the preliminary screening are that, aside from seismic and fire events which have already been included in the detailed external hazards analyses, the following events were identified as requiring further bounding study.

a. Aircraft Impact

b. External Flooding

c. Extreme Winds and Tornadoes

d. Military and Industrial Facilities Accidents

e. Pipeline Accidents

f. Release of Chemicals in On-site Storage

g. Transportation Accidents

h. Turbine Missiles

i. Internal Flooding

The bounding analyses performed for these events are discussed in Sections 3.3 and 3.4.

Table 3.1

Preliminary Screening of External Events for
Surry Nuclear Power Station

Events	Applicable Screening Criteria	Remarks
Aircraft Impact	--	A bounding analysis is performed for this event.
Avalanche	3	Topography is such that no avalanche is possible.
Biological Events	1	The only biological event which may affect the safety of the plant is fish in the river, i.e., fish may block flow of water in the intake structure. This event is not further considered because there would be adequate warning, and therefore, remedial action can be taken before supply of the intake canal is exhausted.
Coastal Erosion	3	The site is located on the banks of the James River on three sides. The area is covered by marshy wetlands and swamps. Therefore, erosion is not a significant possibility.
Drought	1	The stretch of the river between Richmond and the mouth of the river is essentially a tidal estuary. There are no known or planned river control structures and the possibility of water shortage is unlikely. However, under certain circumstances, winds from the northeast could cause abnormally low river levels at the site for up to 24 hours. However, the design of the plant can accommodate this event. The high-level intake canal contains a minimum of 45 million gallons of water for use in recirculation spray-heat exchangers during a LOCA incident in one unit combined with loss of power in both units. This storage volume can be used up to 100 hours to maintain the station in a safe shutdown condition.

Table 3.1 (Cont'd)

Preliminary Screening of External Events for
Surry Nuclear Power Station

Events	Applicable Screening Criteria	Remarks
External Flooding	--	A bounding analysis is performed for this event.
Extreme Winds and Tornadoes	--	A bounding analysis is performed for this event.
Fog	4	Fog can affect the frequency of occurrence of other hazards such as highway accidents or aircraft landing and take-off accidents. The effects of fog on highway, railway, or barge accidents are implicitly taken into account by assuming a worst possible transportation accident near the site. Transportation accidents are considered in detail for the present study.
Forest Fire	3	Site itself is cleared, while scrub pine exists beyond site boundary. Fires cannot directly affect the plant. Fire suppression systems at Surry not automatically activated, so no chance of incidental actuations.
Frost	1	Loads induced on structures due to frost are much lower than snow and ice loads, i.e., frost loads can be safely neglected in the plant hazard analysis.
Hail	1	Hail is less damaging than other missiles which are generated outside of the plant such as tornado missiles and turbine missiles. Therefore, hail is not considered further in the scoping study.
High Tide or High River Stage	4	Included under external flooding.

Table 3.1 (Cont'd)

Preliminary Screening of External Events for
Surry Nuclear Power Station

Events	Applicable Screening Criteria*	Remarks
High Summer Temperature	1	As mentioned under drought, it is possible to safely shut down the plant due to unavailability of water. Therefore, high temperatures on record were indirectly included under drought conditions.
Hurricane	1	The effects are included under flooding and tornado effects.
Ice Cover	1	Ice or snow loading is considered in the plant design. Ice blockage of the river is included in flood.
Industrial or Military Facility Accident	--	A bounding analysis is performed for this event.
Internal Flooding	--	A bounding analysis is performed for this event.
Landslide	3	The Surry plant is built on flat land where landslides are not possible.
Low Lake or River Water Level	4	This event is considered under drought.
Low Winter Temperature	1,4	Thermal stresses and embrittlements are insignificant and are covered by design codes and standards for plant design. Generally, there is adequate warning of icing on the ultimate heat sink (i.e., river) so that remedial action could be taken.

Table 3.1 (Cont'd)

Preliminary Screening of External Events for
Surry Nuclear Power Station

Events	Applicable Screening Criteria	Remarks
Meteorite	2	This event has a very low probability of occurrence. A study by Solomon et al. (Ref. 4) showed that the probability of a meteorite impacting any nuclear power plant in the U.S. is negligible, and therefore, meteorites need not be considered in this study.
Pipeline Accident	--	A bounding analysis is performed for this event.
Intense Precipitation	4	Included under internal and external flooding.
Release of Chemicals in On-site Storage	--	A bounding analysis is done for this event.
River Diversion	3	This event is not credible for the site under consideration.
Sandstorm	3	This is not relevant for this region.
Seiche	4	Included under external flooding.
Snow	1	Plant is designed for snow load, ponding effects, and combinations of snow with other loads.
Soil Shrink-Swell Consolidation	1	Plant structures are all designed for the effects of consolidation. Such effects occur over a long period and they do not pose a hazard during plant operation, i.e.e, the plant can be safely shut down if needed.
Storm Surge	4	Included under external flooding.
Transportation Accidents	--	A bounding analysis is done for this event.

Table 3.1 (Concluded)

Preliminary Screening of External Events for
Surry Nuclear Power Station

Events	Applicable Screening Criteria	Remarks
Tsunami	3	Tsunamis are rare on the East Coast. Plant location is inland from sea coast.
Toxic Gas	4	Included in transportation accident, on-site chemical release, and industry and military facilities accidents.
Turbine-Generated Missiles	--	A bounding analysis is performed for this event.
Volcanic Activity	3	The site is not close to any active volcanos.
Waves	4	This event included under external flooding.

3.3 Screening of External Events Based on FSAR and Site Hazard Studies

This section describes the external events which could be screened out based on the updated FSAR information supplemented with new data. Section 3.3.1 discusses the military and industrial facilities accidents, Section 3.3.2 deals with the transportation accidents and Section 3.3.3 covers on-site chemical release. It is concluded that these events can be screened out.

3.3.1 Accidents in Industrial and Military Facilities

According to the Surry FSAR, the areas to the north and south of the site, except for the Williamsburg area, are principally rural and agricultural. The nearest industrial facility is located 4-1/2 miles from the site, and this is the only industrial facility within a five mile radius. Table 3.2, which is duplicated from an NUS Corporation study on toxic chemicals at the Surry site (Ref. 5), lists all the chemical compounds used by, and/or stored, at this facility

There are three possible effects from an industrial accident near the site: (1) incident over-pressure on plant structures due to an explosion, (2) seepage of toxic chemicals into the control room, which could incapacitate the operators, and (3) flammable vapor clouds leading to a heat hazard at the site. Industrial accidents at distances farther than 5 miles to the site are not expected to cause significant over-pressure loads on the plant structures. For example, of all the chemicals stored at the industrial facility (Table 3.2), only acrylonitrile and methyl acrylate are explosive. Assuming an explosion of the entire quantity of these chemicals, the peak over-pressure experienced on wall panels at the site would be less than 1 psi. As the Surry plant Category 1 structures are designed for tornado wind loads, with a minimum capacity of 3 psi against blast loads, an over-pressure hazard due to industrial accidents can be screened out.

Release of toxic chemicals near nuclear power plants can potentially result in the control room being uninhabitable. This condition can happen if (1) large quantities of toxic chemicals are released, (2) there are favorable wind conditions and insufficient dilution of chemicals such that these chemicals reach the control room air intakes, and (3) there are no detection systems and air isolation systems in the control room. According to Regulatory Guide 1.78 (Ref. 6), chemicals stored or situated at distances greater that 5 miles need not be considered as an external hazard. This is due to the fact that if a release occurs at such a distance, atmospheric dispersion will dilute and disperse the incoming plume to such a degree that there should be sufficient time for the control room operators to take appropriate action. As the amount of stored chemicals is small and at a distance of nearly 5 miles from the site, the accidents in the only industrial facility near the plant do not pose an unacceptable risk. This same conclusion was reached in the NUS Corporation study (Ref. 5).

Table 3.2

Chemical Compounds Used and/or Stored Near Surry

Chemical	Container Size	Quantity per Unit	Type Container	Distance Miles	Berm
Acrylonitrile	50,000 gal (5,000 gal)	1 4 ea	Metal Tank	4.9	50'x30'x4.5' (30'x15'x4.5')
Methyl Acrylate	25,000 gal (5,000 gal)	1 1	Metal Tank	4.9	30'x20'x5.5' (30'x15'x4.5')
Sulfuric Acid	5,000 gal	3 ea	Metal Tank	4.9	40'x20'x2'
Hydrochloric Acid	5,000 gal	3 ea	Metal Tank	4.9	40'x20'x2'

3.3.2 Transportation Accidents

The plant is located on the banks of the James River, which is a navigable river used for transportation of bulk goods. The type of chemicals and their quantities are shown in Table 3.3. Virginia Highway 10 is the only major surface route near the plant besides the state secondary access Route 650 to the site. The access road ends at the Hog Island Waterfowl Refuge, north of the site. Small amounts of chemicals required in plant operations are transported along the access road and these hazards are considered under on-site chemicals in Section 3.3.3. The chemicals transported on Virginia 10 are given in Table 3.4 (from Reference 5). There is no rail traffic within a five mile radius of the station and the risk from the air transport mode is considered separately in Section 3.4.5.

A transport accident near the site can pose risk in one of the following ways: (1) a chemical explosion due to a transportation accident may cause damage to Category I structures and safety-related equipment, and (2) toxic chemicals which are spilled in a transportation accident may drift into the control room and cause incapacitation of the operators. A chemical explosion near the plant structures may cause over-pressure, dynamic pressures, blast-induced ground motion, or blast generated missiles. However, from previous research in this area, it has been determined that over-pressures would be the controlling consideration for explosions resulting from transportation accidents (Regulatory Guide 1.91, Ref. 7). An accident over-pressure at the site can also occur due to vapor cloud explosions drifting towards the structures. This type of explosion involves complex phenomena which depend on the material involved, combustion process, and topographical and meteorological conditions. According to a study by Eichler and Napadensky (Ref. 8), present theoretical and empirical knowledge is too limited to quantitatively evaluate realistic accidental vapor cloud explosion scenarios. However, vapor cloud explosions are implicitly included in the TNT equivalents which are used to represent transportation accidents. According to the Regulatory Guide 1.91 (Ref. 7), chemical explosions which would result in free-field over-pressures of less than 1 psi at the site do not need to be considered in the plant design. Based on experimental data on hemispherical charges of TNT, a 1 psi pressure would be translated into a safe distance R (ft) which is defined as:

$$R > kw^{1/3}$$

where $k = 45$ and w is an equivalent weight of TNT charge.

According to Table 3.4, the maximum possible explosive charge is due to 8,500 gallons of gasoline, which is an (approximate) equivalent of 50,000 lbs. of TNT charge. Using the relation given above, the distance for a pressure pulse less than 1 psi is calculated to be 1,658 ft. Based on this result, it is concluded that explosions on Virginia 10 highway will not pose an over-pressure hazard to the plant structures.

Table 3.3

Chemical Compounds Shipped on the James River

Chemical	Container Size	Quantity per Unit	Type Container	Distance Miles
Diaminocyclo Nexane Corrosive Liquid	55 gal/barrels 80 to 140	4,400 to 7,700 gal	Closed Van Ocean Vessel	1 1/2
Ethanol/Inflammable Liquid	55 gal/barrels 80 to 140	4,400 to 7,700 gal	Closed Van Ocean Vessel	1 1/2
Tiazinetrione Dry Oxidizer	50 lb bags Pelletized	40,000 to 60,000 lb	Closed Van Ocean Vessel	1 1/2
Napthyl Methyl Carbonate - Poison	50 lb bags Pelletized	40,000 to 60,000 lb	Closed Van Ocean Vessel	1 1/2
Ethyl Alcohol Flammable Liquid	55 gal/barrels 80 to 140	4,400 to 7,700 gal	Closed Van Ocean Vessel	1 1/2
Sodium Meta Periodate - Oxidizer	50 lb bags Pelletized	40,000 to 60,000 lb	Closed Van Ocean Vessel	1 1/2
Nitro Imidayol Poison - Solid	50 lb bags Pelletized	40,000 to 60,000 lb	Closed Van Ocean Vessel	1 1/2
Ethyacloxysilane Corrosive Liquid	55 gal/barrels 80 to 140	4,400 to 7,000 gal	Closed Van Ocean Vessel	1 1/2
Dinitrochloro Benzene - Poison	50 lb bags Pelletized	40,000 to 60,000 lb	Closed Van Ocean Vessel	1 1/2

Table 3.3

Chemical Compounds Shipped on the James River (Continued)

Chemical	Container Size	Quantity per Unit	Type Container	Distance Miles
Monochloracetic Acid Corrosive	50 lb bags Pelletized	40,000 to 60,000 lb	Closed Van Ocean Vessel	1 1/2
2-Methox 4-2-3 Dyhydro 4-H Inflammable Liquid	55 gal/barrels 80 to 140	4,400 to 7,700 gal	Closed Van Ocean Vessel	1 1/2
Ortho-Phenylenediamine Poison	50 lb bags Pelletized	40,000 to 60,000 lb	Closed Van Ocean Vessel	1 1/2
Chloro Benzo Tri Fluoride Inflammable Liquid	55 gal/barrels 80 to 140	4,400 to 7,700 gal	Closed Van Ocean Vessel	1 1/2
Caustic Alkali Liquid Corrosive	55 gal/barrels 80 to 140	4,400 to 7,700 gal	Closed Van Ocean Vessel	1 1/2
Thionyl Chloride Corrosive	55 gal/barrels 80 to 140	4,400 to 7,700 gal	Closed Van Ocean Vessel	1 1/2
Gasoline, #6 Oil, Diesel Oil, #2 Oil	Steel Tanks 8 Compartments	168,000 gal ea 1,300,000 total	Barge	1 1/2
Phenol	Steel Tanks 2 Compartments	1,325 tons ea 2,650 total	Barge	1 1/2
Oleum	Steel Tanks 2 Compartments	1,500 tons ea 3,000 total	Barge	1 1/2

Table 3.3

Chemical Compounds Shipped on the James River (Concluded)

Chemical	Container Size	Quantity per Unit	Type Container	Distance Miles
Sulfur (Liquid at 260°F to 275°F)	Steel Tanks 2 Compartments	10,000 tons ea 20,000 total	Barge	1 1/2
Liquid Fertilizer (Uran)	Steel Tanks 2 Compartments	5,000 tons ea 10,000 total	Barge	1 1/2
Ammonium Sulfate	50 lb bags Pelletized	1,500 to 12,000 tons	Barge	1 1/2
Ammonium Sulfate	50 lb bags Pelletized	8,000 to 25,000 tons	Closed Van Ocean Vessel	1 1/2

Table 3.4

Chemical Compounds Transported by Truck on Virginia Highway 10

Chemical	Container Size	Quantity per Unit	Type Container	Distance Miles
Sulfuric Acid	25 ton truck tank	3,300 gal	Metal Tank	4 1/2
Nitric Acid	25 ton truck tank	4,000 gal	Metal Tank	4 1/2
Muratic Acid	25 ton truck tank	5,000 gal	Metal Tank	4 1/2
Petroleum Gasoline, Oil	25 ton truck tank	8,500 gal	Metal Tank	4 1/2

Assuming a typical maximum probable equivalent TNT charge of 1 x 10^7 lbs. for any of the chemicals transported on a river barge and the distance of the barge from the nearest plant structure to be 1.5 miles, an over-pressure of around 1 psi will be experienced. This is well within the design limit of 3 psi, postulated for tornado-designed structures.

Flammable vapor clouds also do not present any explosive hazard. According to a study by Eichler, Napadensky and Mavec (Ref. 9), the accidents in an empty barge due to vaporization of liquid left in the tank would lead to a maximum TNT equivalent explosive load of 1000 lbs. Since this type of accident does not produce a more severe condition, it is not considered further.

A toxic chemical spill near the site would pose a danger to the plant if toxic chemicals penetrate into the control room through air intakes. This can happen if (1) large quantities of toxic chemicals are released, (2) there are favorable wind conditions which would cause a drift of chemicals towards the control room air intakes at excessive concentrations, and (3) there are no detection systems and air isolation systems in the control room.

Among the various transportation modes near the site, a barge accident in the James River would result in the largest amount of chemical spill. The NUS Corporation study (Ref. 5) also estimated the danger from toxic chemicals spilled in an off-site transportation accident. According to this report, from the quantities, distances and properties of the chemicals, the toxicity limit and the estimated cloud center concentration at the control room air intake of most chemicals were not cause for concern. Only concentrations of gasoline exceeded the toxicity limit. It was estimated that the control room personnel would have 2,390 seconds (40 min.) of warning if notified immediately of the accident. This time includes the time required for the vapor cloud to drift to the air intake and then to build up to the toxicity limit in the control room. The amount of warning time available without knowledge of the accident is 192 seconds, if detectors are placed at the air intake.

In response to NRC review of this study, VEPCO agreed to modifications to assure control room habitability. With these modifications, the risk to control room personnel due to a transportation accident will be negligible.

3.3.3 Release of On-site Chemicals

The chemicals stored on-site at the Surry plant are listed in Table 3.5 and their storage locations are shown in Table 3.6. The NUS Corporation study (Ref. 5) analyzed the consequence of release of a single container of these chemicals, its dispersion and subsequent build-up in the control room air. The amounts of each chemical analyzed for spill and their toxicity limits are listed in Table 3.5. The results in terms of peak concentration of chemicals in the control room are given in Table 3.7. This table shows that most of these chemicals (morpholine, acetone,

Table 3.5

Surry On-Site Chemical Spill Analysis

Chemical	Quantity Assumed Spilled	Toxicity Limit (mg/m^3)
Morpholine	55 gal	105
Acetone	55 gal	4,800
Cyclohexylamine	55 gal	40
Sulfuric Acid	8,000 gal	2
Ammonium Hydroxide	3,000 gal	70
Carbon Dioxide	17 tons	18,000
Diesel Fuel	210,000 gal	1,355
Chlorine	64 lb	45
Hydrazine	55 gal	0.3
Dimethylamine	135 lb	28

cyclohexylamine, sulfuric acid, ammonium hydroxide, and diesel fuel) present no hazard to control room personnel. The peak concentration in the control room exceeds the toxicity limits due to release of dimethylamine, carbon dioxide, chlorine and hydrazine. The time required to reach the limits are also indicated. Time t_1 gives the warning time if detectors are present at the chemical storage location whereas t_2 represents the warning time available for detectors at the air intake.

Pacific Northwest Laboratories reviewed the NUS Corporation report on control room habitability (Ref. 10) for the NRC. VEPCO agreed to certain modifications listed in USNRC letter of June 28, 1982 (Ref. 11). These modifications will provide safe, habitable conditions within control room under both normal and accidental toxic gas conditions and the risk from these hazards can be expected to be negligible.

3.4 Bounding Analyses

The bounding analyses for the external events which could not be screened out by the general criteria as described above are given in this section.

Table 3.6

Surry 1 and 2 Toxic Chemical Source Locations

Chemical	Distance From Air Intake (ft)	Location
Dimethylamine, Argon, Helium Hydrogen, Nitrogen, Oxygen, Carbon Dioxide, Acetylene, Breathing Air, Specialty Gas Mixes	125	Outside NNW of Intake East of Security Building
Morpholine, Anhydrous Hydrazine Acetone, Sodium Hypochloride, Cyclohexylamine	190	Outside NNW of Intake East of Security Building
Hydrogen Bank	276	Outside W of Intake, SW of Condensate Storage Tanks
Sulfuric Acid	410	Room Within Condensate Polishing Building, Berm Within Room, 2 (Self-Closing) Doors Between Emergency Intake. 567 ft. From Condensate Polishing Building HVAC Exhaust Stack to Normal Intake
Ammonium Hydroxide	426	Room Within Condensate Polishing Building, 2 (Self-Closing) Doors Between Emergency Intake. 620 ft. From Ammonium Room Exhaust Stack to Normal Intake
Hydrazine	374	Condensate Polishing Building. 1 (Self-Closing) Door Between Emergency Intake
Carbon Dioxide	157	Outside Adjacent to Double Doors South Side of Turbine Building
Sulfuric Acid	131	Inside Turbine Building Across From Emergency Intake

Table 3.6

Surry 1 and 2 Toxic Chemical Source Locations (Concluded)

Chemical	Distance From Air Intake (ft)	Location
Diesel Fuel	400	Outside Separate Tank 60'x 60'x 9' Dike
Chlorine	472	Inside Sewerage Treatment Building - Off Plot
Hydrazine Ammonium Hydroxide	1,476	Inside Warehouse Building - Off Plot

The probabilistic models used in these bounding analyses integrate the randomness and uncertainty associated with loads, response analysis, and capacities to predict the annual frequency of the plant damage from conservative models. If the mean frequency computed with a conservative model is predicted to be sufficiently low (e.g., less than 10^{-6}/year), the external event may be eliminated from further consideration. The bounding analyses thus provides a second screening of the external hazards, allowing additional hazards to be deleted from further consideration, and identifying those remaining external events which need to be analyzed in detail as part of the PRA.

In addition to calculating and screening on a best estimate frequency of core damage, the uncertainties in hazard and component fragilities may be used to find the high confidence (95 percent) bounds on the frequency of core damage. However, such an uncertainty analysis is required only if the best estimate of the core damage frequency of the external event leads to a value which is close to the (usual) mean rejection frequency of 10^{-6}/year.

Often, simplifications in the above analyses are introduced. As an example, in case of aircraft impact, back-face (inside) scabbing of the exterior barrier walls of safety-related structures can be assumed to result in core damage even though, actually, a suitable combination of component failures is necessary to lead to this damage state. However, if the resulting frequency of core damage computed with the conservative model is sufficiently small, no further consideration is required.

In addition, for some external events, it is possible to perform a bounding analysis without performing a structural response analysis. In effect, one shows that the frequency of exceeding the design loads is very small, and thus, infers that the hazard can be neglected due to the conservatism in

Table 3.7

Peak Concentration of Chemicals in Control Room

Chemical	TL	C_R	t_1	t_2
Morpholine	105	$9.2x10^{-1}$	*	*
Acetone	4,800	$2.7x10^{1}$	*	*
Cyclohexylamine	40	1.1	*	*
Sulfuric Acid	2	$4.3x10^{-3}$	*	*
Hydrazine	0.3	$2.1x10^{1}$	946	36
Diesel Fuel	1,355	$5.2x10^{1}$	*	*
Ammonium Hydroxide	70	3.8	*	*
Carbon Dioxide	$1.8x10^{4}$	$3.9x10^{4}$	159	61
Carbon Dioxide	$1.8x10^{4}$	$2.2x10^{4}$(E)	180(E)	82(E)
Chlorine	45	$8.9x10^{2}$	280	17
Dimethylamine	28	$6.5x10^{3}$	68	7

TL = Toxicity Limit (mg/m^3).

C_R = Peak concentration in control room (mg/m^3).

t_1 = Time from spill until TL is reached in control room air (seconds), * indicates TL not reached.

t_2 = Time from reaching TL at intake to reaching TL in control room.

E = Emergency air intake.

the design process. These, and other simplifications are utilized as appropriate in the following bounding analyses.

3.4.1 Extreme Winds and Tornadoes

Extreme winds from tornadoes, hurricanes or wind storms present a likely threat to the nuclear power plants due to (a) direct damages from the dynamic wind loadings, (b) missiles generated and, (c) pressure differentials. The winds associated with hurricanes and storms are usually less intense and lower in magnitude than those associated with tornadoes. Hence, it is sufficient to to consider risk to the structures due to tornadoes. This section describes the analysis of Surry structures for the effects of tornadoes.

Regulatory Guide 1.117 (Ref. 14) specifies the plant systems, structures, components, areas, etc., to be protected against tornadoes. Both seismic category I structures and non-category I structures were considered for this task. Seismic category I structures have been designed for extreme winds, seismic, and tornado loadings. Non-category I structures were generally designed against wind loads.

3.4.1.1 Plant Design Criteria for Category I Structures

The category I structures of Surry were designed to withstand a Design Basis Tornado (DBT) which is defined as follows:

Rotational velocity	300 mph
Translation velocity	60 mph
Pressure drop	3 psi in 3 sec
Overall diameter	1200 ft
Radius of maximum winds	200 ft

As per the FSAR, the structures can resist a maximum wind velocity associated with a tornado of 360 mph; and were also checked for tornado pressure loading, pressure drop and combinations of the two. For the purpose of structural analysis, dynamic wind pressures on the structures were converted into equivalent static forces which vary along the height of each structure. Since the natural periods of buildings at Surry are short compared with the rise in time of applied design pressures, the above assumption is well justified.

The safety related structures were also designed for the effects of postulated tornado missiles. The postulated tornado missiles used in the design of category I structures were as follows:

a. Wooden pole 40 ft long, 12 in. diameter, weighing 50 lbs/ft^3 and traveling in a vertical or horizontal direction at 150 mph.

b. 1-ton automobile traveling at 150 mph.

The FSAR gives details regarding different structures and systems designed for tornado loadings. (Table 3.8)

Table 3.8

Structures and Components Designed for Seismic and Tornado Criteria

Item	Earthquake Criterion	Tornado Criterion	Note	Typical Thickness of Concrete
Structures				
Reactor Containment				NA
Reinforced-concrete substructure	I	P		54" (Cylinder Walls)
Reinforced-concrete superstructure	I	T		30"
Reinforced-concrete interior shields and walls	I	NA		NA
Steel plate liner	I	P	P for containment integrity,	NA
Piping, duct, and electrical penetrations and shield wall	I	T	T for shield wall and critical system penetrations only	14"
Personnel access hatch	I	P		NA
Equipment access hatch	I	P		NA
Cable Vault and Cable Tunnel	I	T		24"
Pipe Tunnel to Containment from Auxiliary Building	I	T		24"
Auxiliary Steam-Generator Feed Pump Cubicle	I	T		36"

Table 3.8

Structures and Components Designed for Seismic and Tornado Criteria (Continued)

Item	Earthquake Criterion	Tornado Criterion	Note	Typical Thickness of Concrete
Structures				
Cubicle for Main Steam and Feedwater Isolation Valves	I	T		36"
Recirculation Spray and Low-Head Safety Injection Pump Cubicle and Pipe Tunnel				
Safeguards Ventilation Room	I	NA		NA
Auxiliary Building				
Reinforced-concrete Structure	I	T		18" to 24"
Steel superstructure	I	NA		NA
Vacuum equipment area	I	NA		NA
Fuel Building				
Reinforced-concrete structure	I	T	T for horizontal missile only, T for tornado P for horizontal missile only	Drawings Not Available
Steel superstructure	I	T		
Spent-fuel storage rack	I	P		

Table 3.8

Structures and Components Designed for Seismic and Tornado Criteria (Continued)

Item	Earthquake Criterion	Tornado Criterion	Note	Typical Thickness of Concrete
Structures				
Fuel Building (continued)				
Fuel-handling trolley support structure	I	P	T for tornado winds only	NA
Control Room	I	T		18"
Emergency Switchgear and Relay Room	I	T		18" to 24"
Battery Rooms	I	T		12"
Air-Conditioning Equipment Rooms	I	T	For control room and relay room only	18" to 24"
Reactor Trip Breaker Cubicle	I	T		
Auxiliary Diesel-Generator Cubicles				
Reinforced-concrete floor	I	T		24"
Walls, excluding louvers	I	T		24"
Structural steel-supported roof and roof slab	I	T	Protected by missile rack	

Table 3.8

Structures and Components Designed for Seismic and Tornado Criteria (Continued)

Item	Earthquake Criterion	Tornado Criterion	Note	Typical Thickness of Concrete
Structures				
Turbine Building	NA	NA	By design, building collapse will not damage any Class I structures and components during earthquake, or tornado-resistant structures and components during tornado.	NA
Circulating Water Pump Intake Structure	I	T	T for emergency service water pump cubicle only	12" to 36"
High-Level Intake Structures	I	T	T, no missile protection required	30" to 36"
Seal Pits	I	T	T, no missile protection required	18"
High-Level Intake Canal	I	NA		NA

Table 3.8

Structures and Components Designed for Seismic and Tornado Criteria (Concluded)

Item	Earthquake Criterion	Tornado Criterion	Note	Typical Thickness of Concrete
Structures				
Fire-Pump House	I	T	Engine-driven pump only	24"
Fuel-Oil Transfer Pump Vault	I	T		24"
Boron Recovery Tank Dikes	I	T		24"

I - Refers to Seismic Class I criteria. All Class I components and structures are designed to resist the operating-basis earthquake within allowable working stresses. A check has been made to determine that failure to function will not occur with a design-basis earthquake.

T - Refers to structures, systems, and components that will not fail during the design tornado.

P - Refers to systems and components that will not fail during the design tornado since they are designed to be protected by tornado resistance structures.

NA - Not applicable.

According to Ravindra and Banon (Ref. 15), if the plant has been designed against tornado effects, there are no-metal-sided walls or roofs in seismic category I buildings, if the reinforced concrete walls of seismic category I buildings are at least 18 in. thick, and if there are no non-redundant outdoor unprotected safety-related equipment, the contribution of tornado and extreme wind-induced accidents to the plant risk is judged to be very low. A review of the engineering drawings revealed that there are no metal sided walls or roofs in Seismic Category I buildings and the walls of these buildings are either 18 in. or more in thickness. It was also confirmed that the outdoor equipment such as the condensate storage tank and refueling water storage tank are either protected against tornado missiles or have redundant items that are protected from tornado effects. It is therefore concluded that the risk of damage from tornado and tornado missile impacts is negligibly small.

3.4.2 Pipeline Accidents

There are two natural gas pipelines passing through the southeast end of the site. These pipelines are operated by Commonwealth Natural Gas Corporation and Colonial Pipeline Company and come from across the James River and join another pipeline with a northwest-southeast orientation (Figure 3.5). The pipelines cross the canal near the intake structure (Figure 3.4) and one branch of the pipeline supplies natural gas to the combustion turbine building located south of the cooling canal. There are no automatic check valves in the vicinity of the power plant. The Surry FSAR shows that the probability of damage to plant structures due to a pipeline accident is negligibly small. However, according to Ravindra and Banon (Ref. 15), if there are pipelines transporting natural gas, propane and other flammable explosive or toxic gases near the nuclear power plant, a scoping analysis of the hazard posed by the pipelines should be performed. The safety hazards posed by pipelines include thermal radiation, blast overpressure, missile generation, and plant contamination by gas at an unacceptable concentration. Among these, hazards due to thermal radiation, missile generation and plant contamination by gas at an unacceptable concentration are negligible.

The annual frequency of failure of a large pipeline near the plant, P, is calculated as:

$$P = N\ D\ fs\ fw\ ft\ fd/L$$

where

N = number of gas transmission line failures per year in the United States

L = miles of transmission pipeline in the United States

D = length of pipe near site (miles)

fs = fraction of failures that are large

fw = fraction of time wind will blow toward the plant from pipeline

ft = fraction of failures due to construction-related failures and corrosion

fd = fraction of leaks going undetected

The distance from the gas pipeline at the closest approach to the nearest plant structures is approximately 0.82 miles. The length D of pipe considered is based on the quantity of natural gas that would produce an explosive force equivalent to 25,000 pounds of TNT, and as per FSAR, it is 2.6 miles. Other values for use in equation are estimated to be

ft = 0.25 N/L = # of pipeline ruptures/year/mile = 1.2×10^{-4}

L = 200,000 miles

fs = 0.329

fd = 0.10

fw = 0.5 (estimated from wind direction roses for the site.)

Hence, it is found that

$P = 1.2 \times 10^{-4} \times 2.6 \times 0.329 \times 0.5 \times 0.25 \times 0.1$

$= 1.2 \times 10^{-6}$

The annual frequency of failure of the pipeline near the plant is, therefore, 1.2×10^{-6}. It is judged that the probability of this event leading to core damage is extremely small.

3.4.3 Turbine Missiles

Failures of large steam turbines in both nuclear and fossil-fueled powerplants, although rare, have occurred occasionally in the past. These failures have occurred because of one or more of the following broad classes of reasons: (1) metallurgical and/or design inadequacies, (2) environmental effects, (3) out-of-phase or generator field failures and (4) failures of overspeed protection systems. The failures have resulted in loss of blades, disk cracking, rotor and disk rupture and even missiles. Interior missiles are highly energetic and have the potential to damage safety-related structures housing critical components.

In a total of 2,500 years of interior operation in nuclear power plants in the free world, only four failures have occurred: Calder Hall (1958), Hinkley Point (1969), Shippingport (1974), and Yankee Rowe (1980). Missiles were produced in the Hinkley Point and Calder Hall failures. Although the causative mechanisms of these failures have been identified and are generally corrected in the modern plants, there is no assurance

that turbine failures will not occur in the future. Recent discovery of widespread stress corrosion cracking in the disks and rotors of operating nuclear turbines has revived the industry's interest in the issue of such failures.

Turbines rotate at 1800 rpm with the low-pressure (LP) and high-pressure (HP) sections on a contiguous shaft. The LP sections have blade hubs (called "wheels" or "disks") shrunk onto the rotor. Depending on the manufacturer and rated capacity of the turbine, there could be 10 to 16 disks on each LP section. The disks are massive components each weighing between 4 and 8 tons. These disks, because of their relatively large radius, are the most highly stressed spinning components in the interior. With the interior unit running at less than 120 percent of the rated speed, the disks are stressed well below the yield strength of material so that failures can be caused only by undetected material flaws that may be aggravated by stress corrosion and fatigue. At 180 percent of the rated speed, the disks are stressed at or above their ultimate strength so that they burst into fragments. At intermediate speeds (i.e., 120 to 180 percent), rupture of disks may be caused by a combination of flaws and weaker material in the disks.

Turbine missiles are spinning, irregular fragments with weights in the range of 100 to 8,000 pounds, and velocities in the range of 30 ft/sec to 800 ft/sec. It is conventional to discuss two types of turbine missile trajectories: low trajectory missiles (LTM) and high trajectory missiles (HTM). The low trajectory missiles are those which are ejected from the turbine casing at a low angle toward a barrier protecting an essential system. High trajectory missiles are ejected vertically (almost) upward through the interior casing and may strike critical targets by falling on them. The customary ballistic distinction between LTM and HTM is the initial elevation angle (ϕ) of the missile (LTM is for $\phi < 45°$ and HTM is for $\phi > 45°$). Turbine manufacturers have specified that the maximum deflection angle for the missiles produced in the burst of the last disk on the rotor is 25°. Based on this, the NRC has defined a low trajectory missile strike zone in the Regulatory Guide 1.115 (Ref. 16) and recommended that the essential systems be located outside this LTM strike zone. If a turbine missile impacts a barrier enclosing a safety-related component, interest lies in knowing if the missile perforates or scabs the barrier to cause sufficient damage to the component. Using empirical formulas for scabbing derived on the basis of full-scale and model tests, it is estimated that concrete barriers should be at least 4 ft thick to prevent scabbing. The need for providing such barriers depends on the probability of turbine failure and the arrangement of safety-related components with respect to interior missile trajectories. In the design of a nuclear power plant, the designers have many alternative approaches for treating the potential effects of turbine failures (Sliter, Chu and Ravindra, Ref. 17). These approaches can be grouped as: (1) prevention of turbine failure, (2) prevention of missiles, (3) prevention of strike on critical components, and (4) performance of probabilistic analysis to demonstrate that the probability of turbine missile damage is acceptably low.

3.4.3.1 Probabilistic Methodology

The probability of serious damage from turbine missiles to a specific system in the plant is calculated as (Bush, Ref. 18):

$$P_4 = P_1 P_2 P_3$$

where

P_1 = probability of turbine failure leading to missile generation

P_2 = probability of missiles striking a barrier which encloses the safety system given that the missile(s) have been generated

P_3 = probability of unacceptable damage to the system given that one or more missiles strike the barrier

In practice, the evaluation of P_4 should include consideration of different speed conditions, distribution of missiles and all the safety-related components and systems in the plant.

Turbine missile damage in the older plants was usually considered on the basis of a deterministic safety review according to RG 1.115 and SRP2.2.3 (NUREG-0800, Ref. 19), i.e., the probability of unacceptable damage from turbine missiles (P_4) was implicitly shown to be less than 10^{-7} per year. The new guidelines concerning safety of nuclear power plants against turbine missile strikes are best summarized in NUREG-1068 which is a review of the Limerick PRA (Ref. 20). The following paragraphs have been reproduced from NUREG-1068 describing the NRC position on calculating the probability of turbine missile damage:

> In the past, analyses for construction permit and operating license review assumed the frequency of missile generation (P_1) to be approximately 10^{-4} per turbine year, based on the historical failure rate. The strike probability (P_2) was estimated (SRP 3.5.1.3) based on postulated missile sizes, shapes, and energies, and on available plant specific information such as turbine placement and orientation, number and type of intervening barriers, target geometry, and potential missile trajectories. The damage probability (P_3) was generally assumed to be 1.0. The overall frequency of unacceptable damage to safety-related systems (P_4), which is the sum over all targets of the product of these frequencies, was then evaluated for compliance with the NRC safety objective. This logic places the regulatory emphasis on the strike probability. That is, having established an individual plant safety objective of about 10^{-7} per year, or less, for the probability of unacceptable damage to safety-related systems as a result of turbine missiles, this procedure requires that $P_2 P_3$ be less than or equal to 10^{-3}.
>
> Although the calculation of strike probability (P_2) is not difficult in principle, for the most part reducing it to a straightforward ballistics analysis presents a problem in

practice. The problem stems from the fact that numerous modeling approximations and simplifying assumptions are required to make tractable the incorporation into acceptable models of available data on the (1) properties of missiles, (2) interactions of missiles with barriers and obstacles, (3) trajectories of missiles as they interact with or perforate (or are deflected by) barriers, and (4) identification and location of safety-related targets. The particular approximations and assumptions made tend to have a large effect on the resulting value of P_2. Similarly, a reasonably accurate specification of the damage probability (P_3) is no simple matter because of difficulty of defining the missile impact energy required to make given safety-related systems unavailable to perform their safety function, and the difficulty of postulating sequences of events that would follow a missile-producing turbine failure.

Because of the uncertainties involved in calculating P_2, the NRC staff concludes that P_2 analyses are "ball park" or "order of magnitude" type calculations only. Based on simple estimates for a variety of plant layouts, the NRC staff further concludes that the strike and damage probability product can be reasonably taken to fall in a characteristic narrow range that is dependent on the gross features of turbine-generator orientation because (1) for favorably oriented turbine generators, P_2 P_3 tend to lie on the range 10^{-4} to 10^{-3}, and (2) for unfavorably oriented turbine generators, P_2 P_3 tend to lie in the range 10^{-3} to 10^{-2}. For these reasons (and because of weak data, controversial assumptions, and modeling difficulties), in the evaluation of P_4, the NRC staff gives credit for the product of the strike and damage probabilities of 10^{-3} for an unfavorably oriented turbine, and does not encourage calculations of them. In the opinion of the NRC staff, these values represent where P_2 P_3 lie, based on calculations done by the NRC staff and others.

It is the view of the NRC staff that the NRC safety objective with regard to turbine missiles is best expressed in terms of criterion applied to the missile generation frequency which requires the demonstrated value of turbine missile generation frequency (P_1) be less than 10^{-5} for initial startup and that corrective action be taken to return P_1 to this value if it should become greater than 10^{-5} during operation.

It is the staff's view that the frequency of unacceptable damage to safety-related structures, systems and components as a result of turbine missiles is acceptably low (i.e., less than 10^{-7} per year) provided that the above criterion on turbine missile generation is met. This criterion is to be met by the maintenance of an appropriate in service inspection and testing program on the turbine throughout the plant's life as discussed in detail in the Limerick PRA.

From the preceding paragraphs, it is seen that the emphasis is on turbine maintenance and in service inspection to assure a value of the frequency of turbine missile generation (P_1) less than 10^{-5} per year.

Also, if a plant has an in service inspection program which assures missile generation frequency of less than 10^{-5} per year, then based on a minimum P_2 P_3 value of 10^{-2} per year, turbine missiles can be excluded from external events analysis. For plants which do not have an inspection program, but have a favorable turbine orientation, the argument for excluding turbine missiles from further consideration is as follows. Based on historical failure data (Ref. 18), the probability of turbine missile generation has been calculated to be approximately 10^{-4} per year. Also, Patton, et al (Ref. 21) conducted a comprehensive study which estimated the probabilities of turbine missile generation at operating speed and overspeed as 1.2×10^{-4} per year and 0.44×10^{-4} per year, respectively. Since damage due to turbine missiles in a favorably oriented turbine is almost entirely due to the high trajectory missiles, the P_2 P_3 probability estimate of 10^{-3} per year which was accepted by the NRC staff is judged to be conservative. Therefore, the frequency of turbine missile damage in plants which have favorably oriented turbines is conservatively estimated to be on the order of 10^{-7} per year.

3.4.3.2 FSAR Analysis

Westinghouse turbine generators which have never experienced any disk failure have been used at the Surry plant. It has been estimated that for failure at the normal rated speed or at 120 percent of rated speed, only 2 shrunk - on disks out of 16, in the low-pressure turbine could generate external missiles. All other fragments would be incapable of penetrating the turbine casing and would remain within the stationary turbine parts. It was judged that the external missiles produced by the two disks will range from 3,711 lb at 287 fps to 2,865 lb at 416 fps at 120 percent of rated speed. As all class I structures are designed for tornado, the penetration of these structural barriers by missiles is not expected. In addition, most important areas of the containment and other structures are also shielded by moisture separators/reheaters or other parts of the turbine building structure. The probability of turbine missiles entering the spent fuel-pool is estimated as approximately 10^{-5}.

According to NRC, if turbines are maintained and in service inspection is carried out periodically, the frequency of turbine missile generation less than 10^{-5} per year can be assured and the frequency of turbine missile damage can be expected to be less than 10^{-7} per year and a bounding analysis is not required. Site data on the frequency of inspection at Surry was not known. However, as per Surry FSAR, in addition to design provisions associated with turbine control and protection system, valves are exercised on a regular basis during unit operation to minimize the possibility of valve stem sticking. Analyses of oil samples are performed regularly. The turbine is periodically oversped to check the tripping speed. The remaining tripping devices are regularly checked. In addition, design, manufacturing and inspection

technique for turbine rotors and disk forgings make the possibility of an undetected flaw very remote. Thus, likelihood of a turbine risk hazard is considered negligible.

3.4.4 External Flooding

The Surry Nuclear Power Station is located on the banks of the James River on a peninsular site. The ground surface at the site is flat with a station grade of 26.5 ft above the mean sea level and steep banks sloping towards the river and to the low-level waterfowl refuge. Much of the region is characterized by marshes, swamps and streams. The water table is approximately at an elevation of 4 ft and drainage is towards Hampton Roads, on the Atlantic Ocean and near the mouth of the Chesapeake Bay. The effects of flooding on the plant components may include (1) inundation, (2) hydrostatic or dynamic forces, (3) Erosion, (4) sedimentation, and (5) corrosion. All these consequences, except inundation, are insignificant.

The water level in the James River at any time is determined by three components: (1) freshwater discharge from the James River watershed, (2) flow due to the oscillatory ebb and flood of the tide, and (3) flow due to circulation patterns caused by intrusion of saline water within the estuary. Therefore, the water level rise due to river discharge, high tide, hurricane, intense local precipitation, storm surge, ice blockage and the effects of waves is to be considered for the Surry site.

The drainage area of the river above the station site is 9517 square miles. The river between Richmond and the mouth of the river is a tidal estuary and is subjected to tidal motion. The semidiurnal tide has two high waters and two low waters in each lunar day. The oscillatory tides constitute the dominant motion near the site, much larger than downstream flow required to discharge the freshwater to sea. In addition, there is a net nontidal circulation due to movement of less saline water towards the sea and deeper saline layers up the estuary. The volume rate of this flow is smaller than the oscillatory tidal flow, but it is several times larger than the river discharge.

Due to the wide flood plain at the site, even severe meteorological events produce only a small rise in water level. For example, it is estimated in FSAR that for a 50 year river flood, the level at the site will not rise more than 1 ft. Even during Hurricane Agnes in 1972, peak flood discharge due to excessive rainfall led to flood levels of 4 ft to 5 ft in Richmond, but negligible levels at the site. Based on 11 years of observations at the site, there has been no significant high water level due to storm surge during the hurricanes. The highest water level ever reached at Norfolk in 100 years of records is 8.6 ft. A study of meteorological means and extremes in the Surry site region leads one to conclude that ice formation on the river is unlikely to obstruct the flow and cause flooding due to salinity of river below the site.

The analysis in FSAR identifies the flooding resulting due to storm surge from the probable maximum hurricane given below to be the most severe source of flooding at the site.

Central Pressure Index	26.97 in. of mercury
Radius of Maximum Winds	35 nautical miles
Forward Speed of Translation	22 knots
Maximum Wind Speed	135.4 mph

Based on theoretical models, the surge at the power station was computed and is shown in Figure 3.6. This includes the contribution of the highest astronomical tide, an initial rise to account for short period anomalies, and the rise due to atmospheric pressure reduction. For this hurricane, the size, period and length of the waves impinging on the east and west ends of the site, and the resulting run up on the slopes, was found to be small.

Calculations indicate that the probable maximum hurricane would not produce a high enough level of water at the site to be considered as a source of risk. For example, the maximum water elevation at the site was calculated to be approximately 22 ft, which is considerably less than the plant grade elevation of 26.5 ft. As only eight hurricanes have passed within a 100 mile radius of the site in the last 100 years, the likelihood of water level reaching the peak for the probable maximum hurricane is considered to be negligibly small. In any case, further protection is offered by engineered structures such as berms, seawalls, levees, etc. Moreover, for a flood to pose any danger to the plant, the water level has to reach the openings of safety related structures, most of which are either at or above the station ground grade (Table 3.9). Only the circulating water intake structure and emergency service water pumphouse located above it, are the exception. As the sill of the pump room door entrance and air intake louver openings are at 21 ft 2 in., assuming the maximum probable hurricane plus maximum wave run up on the east side, inundation of emergency service water pump diesels is possible, but leak tight construction for doors will prevent this. Moreover, external flooding events likely to damage the plant generally take time to develop. It can be safely assumed that ample warning time is available for emergency procedures. As per FSAR, air intake louvers can be sealed with warning of a design basis flood and air for the operation of diesel-driven emergency service water pumps can be provided by the motor-operated dampers located in the top of the pump house structure with a roof elevation of 33 ft 6 in., and beyond the reach of waves. Hence, the risk of external flooding is considered negligible.

3.4.5 Aircraft Impact

An assessment of the risk from aircraft crashes into the Surry structures is presented in this section. For this purpose, information in the FSAR was used. Section 3.4.5.1 describes the information in FSAR, and Section 3.4.5.2 describes the bounding analysis.

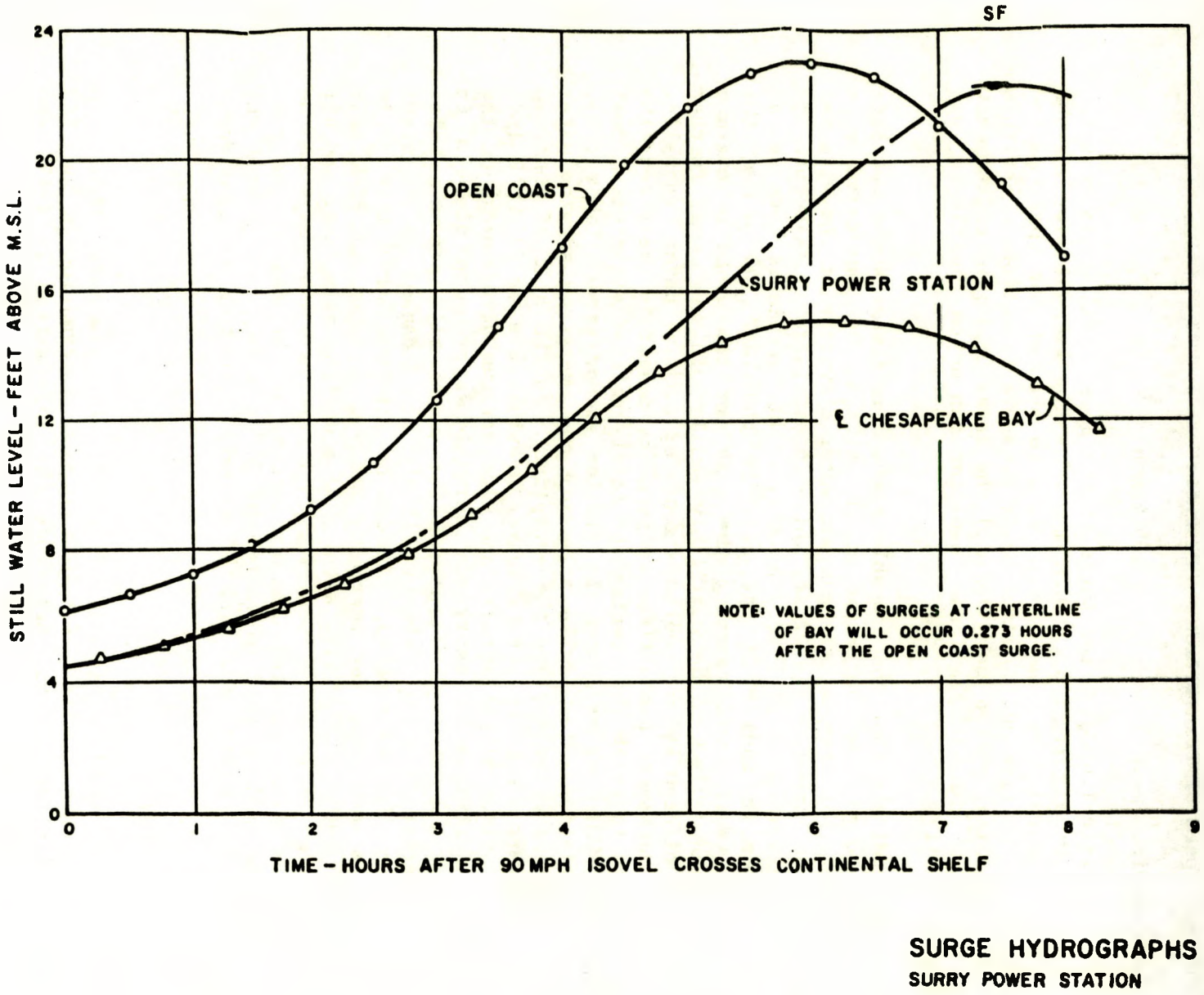

Figure 3.6. Computed Surge Levels at the Surry Power Station

Table 3.9

Maximum-Probable-Flood Protection
Levels for Class I Structures

Class I Structure	Flood Protection Level, Ft - MSL
Containment Structure	26.5
Cable Vault and Cable Tunnel	26.5
Pipe Tunnel Between Containment and Auxiliary Building	26.5
Main Steam and Feedwater Isolation Valve Cubicle	27.5
Recirculation Spray and Low-Head Safety Injection Pump Cubicle	26.5
Safeguards Ventilation Room	26.5
Auxiliary Building	26.5
Fuel Building	26.5
Control Room	27.0
Emergency Switchgear and Relay Room	26.5
Relay Room	26.5
Battery Room	26.5
Air-Conditioning Equipment Room	26.5
Reactor Trip Breaker Cubicle	45.25
Auxiliary Diesel-Generator Cubicle	26.5
Circulating Water Intake Structure (Emergency Service Water Pump House)	24.0
High-Level Intake Structure	36.0
Seal Pit	Not Applicable

3.4.5.1 FSAR Information

The Surry FSAR includes a description of airports and aircraft activity near the site. There are two main airports near the site. Williamsburg-Jamestown Airport, 5 miles north-northwest of the site, has a 3,200-ft long paved runway. Melville, 6 miles west-southwest of the site, is a private field with a 2,900-ft long unpaved runway. This airfield is used by a few small aircraft. These and other airports within 25 miles of the site are given in Table 3.10.

There are no federal airways within 5 miles of the plant. FSAR estimated the probability of an aircraft accident due to flights from the two airports within 5 miles of the site to be 7×10^{-7} per year and from Patrick Henry Airport to be 2.7×10^{-8} per year.

According to the Standard Review Plan, the possibility of aircraft accidents resulting in unacceptable radiological consequences is less than about 10^{-7} per year if the following requirements are met:

a. The plant-to-airport distance D is between 5 and 10 miles statute miles, and the projected annual numbers of operations is less than 500 D2, or the plant-to-airport distance D is greater than 10 statute miles, and the projected number of operations is less than 1,000 D2.

b. The plant is at least 5 statute miles from the edge of military training routes, including low-level training routes, except for those associated with a usage greater than 1,000 flights per year, or where activities (such as practice bombing) may create an unusual stress situation.

c. The plant is at least 2 statute miles beyond the nearest edge of a federal airway, holding pattern, or approach pattern.

The Standard Review Plan requires that a detailed review of aircraft impact risk be performed if the above requirements are not met or if sufficiently hazardous military activities are identified.

In the present case, there are two airports at 5 miles from the plant. The project annual number of operations at these airports is greater than 500(5)2(=12,500) operations. Therefore, a bounding analysis is required.

3.4.5.2 Aircraft Impact Bounding Analysis

The evaluation of probability of an aircraft crash at Surry Power Station is considered from Felker AAF (5 miles SE, 81,500 movements) and Williamsburg-Jamestown (5 miles NNW, 45,000 movements). Only accidents within a few miles of the airports are relevant here since there is no air corridor passing directly above the Surry station.

Table 3.10

Airports Within 25 Miles of the Site

Airport	Distance (mi)	Sector	Number of Movements/yr	Type of Airport
Felker AAF	5	SE	81,500	F, M (30)
Melville	6	SW	--	E, R (29)
Williamsburg-Jamestown	5	NNW	45,000	E, P (32)
Patrick Henry	11	ESE	172,000	F, C (80)
Langley AFB (100)	19	ESE	--	F, M
NAS Norfolk	24	SE	--	F, M (37)

F - Aerodromes with facilities (land)

E - Aerodromes with emergency or no facilities (land)

P - Public use

C - Civil

M - Military

R - Restricted

()- Length of longest runway in hundreds of ft

There is no exact way to model a problem of this type and some of the factors cannot be easily quantified. However, an approximate value of the strike probability/year can be estimated from

$$P = p\ f\ A$$

where

P = Probability of aircraft strike/year
p = Aircraft strike probability per square mile/flight of an aircraft along a given flight pattern
f = Number of movements or flights per year of aircraft along a given flight pattern
A = Effective target area of critical portions of the plant

The effective target area A includes the base area of the structure plus additional areas accounting for the possibility of skidding of an aircraft after hitting the ground as well as consideration of shadow areas of structures. The numerical values assumed here allow for aircraft hitting up to 100 ft short of a structure and sliding into it.

The structures considered as targets include containment building, auxiliary building, control building, fuel storage building, service water pumphouse and tank farm. The exposed area for these is calculated by assuming a 30° slope for the approaching aircraft. This 30° above horizontal shadow of the height of the structures is considered to be an average trajectory of a ground aviation aircraft in a landing or takeoff ground collision.

A review of the site plan shows that the containment building is the dominant one and shields a large number of adjacent buildings. The shielded structures are thus covered under any aircraft hitting the reactor dome. The area is calculated for four different directions of aircraft travel and the maximum value is chosen. Due to the complexity of the site plan, such area computations necessarily involve some approximations. Based on these computations and approximations, the target area is estimated to be less than 3×10^{-3} square miles, leading to a strike probability of 6.6×10^{-7}/year from the Felker AAF and 3.6×10^{-7}/year from the Williamsburg-Jamestown airport, i.e., a total probability of 1×10^{-6}/year. (This is different from the FSAR due to conservative bias in area computation.) Hence, the risk of aircraft crash and resulting plant damage is considered negligible.

3.4.6 Internal Flooding

3.4.6.1 Introduction

A nuclear power plant contains many potential sources of flooding and flood locations. In order to make the analysis of these floods tractable, a process was defined to identify candidate sources and critical flooding areas and to estimate their contribution to core damage frequency if required. The process consisted of the following steps:

a. Identification of important flood sources and critical flooding areas during the initial plant walkdown. Critical areas can be thought of as those plant areas where flooding could not only result in a plant trip but also damage safety related equipment needed to mitigate the effects on any potentially induced plant transient.

b. Definition of all initiating events which have the potential to be flood-induced for each flood source in each critical area. This step of the analysis results in the spectrum of potential flood rates but is also used in quantification of initiating event frequencies.

c. Perform a screening analysis. The screening analysis is comprised of the following steps:

    1. Eliminate all plant areas not identified either by the initial plant walkdown or by computer mapping of critical equipment.

    2. Perform a computer-aided critical area analysis which allows for the incorporation of random failures (i.e., failures not related to the flood itself) as well as all flood related damage. This is a similar process to what occurs in the fire analysis so refer to Chapter 5 for more details on this procedure. This step resulted in flood zone singles, singles with randoms, and double combinations that are listed in Table 3.11.

    3. Screen on frequency for each remaining flood scenario. For Surry this step resulted in elimination of all remaining flood areas and scenarios under consideration. Details of why each of the Table 3.11 areas were screened from further consideration are given in Section 3.4.6.2.

d. Quantify core damage sequences for each remaining flood scenario.

e. Perform an uncertainty analysis utilizing the TEMAC computer code for all remaining scenarios.

3.4.6.2 Screening based on critical area analysis.

As described above, a complete critical area analysis was performed for all the areas within the plant and for all the potential flood-induced accident sequences identified as part of a review of all internal events accident initiators. This analysis identified those singles, singles in conjunction with random failures, or multiple areas (with or without random failures) which, if all equipment in the zone is assumed to be failed by the flood, results in the occurrence of an accident scenario. The results are shown in Table 3.11. The zones themselves are defined in Table 5.3 of Chapter 5. The fire zones of that Table 5.3 correspond directly with the flood zones of Table 3.11. In addition, the equipment located in each fire zone is described in Appendix D. Table 3.11

Table 3.11

Surry Flooding Critical Area Analysis Summary

Single Zone	Single Zone Plus Randoms	Double Zones
Zone 1	Zone 15	None
Zone 3	Zone 19	
Zone 5	Zone 31	
Zone 17	Zone 45	
Zone 54	Zone 54	

Note: Zones are identical to the fire zones defined in Sect. 5.2

presents all the zones that survived the screening analysis and these are the zones which were analyzed for the possible occurrence of floods in this section. Note that the same zone (for example, Zone 2) can occur either as a single or as a single plus random in different accident sequences. (Of course, the same zone cannot occur as a single and as a single plus random in the same accident sequence or it would be non-minimal). As can be seen, a total of only ten zones survived the screening process. Four zones were identified as singles, while eleven zones in conjunction with random failures were identified. Note that each of these zones in general was associated with a number of different random failures, so each zone itself could actually occur in a number of different single plus random cut sets. Finally, eight combinations of two zones (again, some in combination with random failures) were identified. In the following, each one of these zones or zone plus random failure combinations are analyzed to determine any potential non-negligible flooding scenarios.

Cable Vault/Tunnel (Zone 1)

This area adjacent to the emergency switchgear room on 9'6" elevation. Most of the safety cabling for Unit 1 passes through the cable vault and tunnel. The only water source within this zone is a deluge fire suppression system. Two doors enter this area; one from the emergency switchgear room and the second via a spiral staircase leaves the area at a higher elevation going to the outside. The only water source in adjacent rooms is a 3 inch pipe running through the emergency switchgear room in a channel in the floor. Any break from this 3 inch line would be detected by one or more of the three existing flood alarms. The critical equipment in this area are power and control cables for the HPI and CCW systems. The lowest point that this cabling is relative to the floor is approximately three feet above floor level. As a consequence, water level in the tunnel would have to be approximately three feet high before postulated damage could occur. Given that the only adjacent water source is in the emergency room this scenario can be bounded and neglected in comparison to flooding within the emergency switchgear room itself which contains both safety trains of the emergency 4KV switchgear. Since the switchgear are lower relative to the floor than the cabling in the cable vault/tunnel it is clear that flooding in the emergency switchgear room would effect the 4KV switchgear which would result in station blackout) long before any failures of the HPI and CCW system occurred in the cable vault/tunnel area. Hence, this scenario may be screened out.

Emergency Switchgear Room (Zone 3)

This room is at elevation 9'6". As mentioned above, the only water source in this room is a three inch pipe laid in the channel in the floor and protected by three flood alarms. There are two doors into this area for Unit 1. It is connected to the Turbine Building (through the Unit 2 emergency switchgear room) through a fire door and a 2 foot flood barrier. This door leads out to the bottom floor of the Turbine Building also at elevation 9'6". Secondly, there is the door into the cable

vault/tunnel described above. This zone is a single inasmuch as failure of both 4KV switchgear due to flooding would result in station blackout and also a seal LOCA. It is estimated that flooding at least one foot high in the entire area would be required to fail the 4KV switchgear.

Two scenarios need be considered for the emergency switchgear room. The first is the case of the break of the 3 inch pipe within the room. In this case, for a problem to occur it would be necessary for all three flood alarms to simultaneously fail and for the sump pumps also to fail. Given the small volume of water available through the 3 inch pipe, and the low probability that all three flood alarms would fail this scenario can be screened from further consideration.

The second scenario would involve an unisolatable flood in the adjacent Turbine Building, raising the water level of the Turbine Building above the two foot flood barrier allowing water to flood the entire emergency switchgear room (of both Units 1 and Units 2).

An unisolatable flood is possible because intake canal level is (normally) approximately 8 feet above Turbine Building basement level. If the inlet piping failed (low pressure lines) two random value failures would also have to occur to make this scenario valid. Therefore, failure of the inlet piping can be eliminated from further consideration. Sump pump capacity is such that failure of the shell side of the condenser would not provide a sufficient water source to exceed the 2 foot barrier at the entrance to the emergency switchgear room. Therefore, any postulated mechanism for an unisolatable flood can be screened.

Mechanical Equipment Room (Zone 45)

This room contains a service water system which provides cooling to the lube oil supply for the HPI system. If this equipment were to fail, it would fail the HPI system. There is only one door into this room (from the emergency switchgear room) and the only water sources in the room are from the small pony pumps themselves and the three inch supply line in a channel in the floor. This zone is in a cut set in conjunction with two random failures. The two possible scenarios are flood induced failure of the HPI in conjunction with the stuck open relief valve (random) and random failure of the remaining service water pump located in a different flood zone. The second scenario would involve flood induced failure of the HPI system in conjunction with random failures of the CCW system and again, random failure of the other service water pump. These two scenarios can be eliminated based on the random failure probabilities and a conservative pipe break frequency estimate of 1E-3/yr.

Charging Pump Service Water Pump Room (Zone 54)

This zone is a single room on the wall of the Turbine Building (on the opposite side of the wall from the mechanical equipment room #3) and has a single door connecting this area into the Turbine Bay at elevation 9'6". This area contains one of the two charging pump service water system pumps and in addition, contains a cable for the other charging

pump service water system pump. The flood scenarios in this room could damage both trains of the charging pump service water system and hence, fail the HPI. Again, two scenarios can occur which are a small LOCA involving flood induced failure of the HPI in conjunction with a stuck open safety relief valve or a seal LOCA due to flood induced failures of the HPI in conjunction with random failure of the component cooling water system. The only water sources in the room are two small capacity pony pumps. However, floods in the Turbine Building could enter this area under the door. These two scenarios can be subsumed with the flooding scenarios associated with the emergency switchgear room inasmuch as both these scenarios require additional random failures whereas scenarios associated with the emergency switchgear room lead directly to a station blackout scenario. The cable associated with the charging pump service water system pump in the adjacent mechanical equipment room enters through the common Turbine Building wall at an elevation of approximately 4 foot above the floor level and then exits through the ceiling. Hence, a flood in this room would have to flood the entire area over 4 feet in order to fail both of the service water pumps. With a 1E-3/yr pipe break frequency, which is clearly conservative, and the stuck open relief valve probability of approximately 1E-4/demand this scenario can be screened out. Similarly, random failure of the component cooling water system is associated with a failure probability of approximately 1E-3/demand and thus, would also screen out in conjunction with failures of the pony motors or pipes within the room alone. Also, for the seal LOCA case, a readily available recovery action is to cross connect to the unit #2 component cooling water system.

Turbine Building (Zone 31)

The Turbine Building elevation 9'6" was found to be a single zone in conjunction with random failures in the vital area analysis. This arose due to the fact that cables from both charging pump service water system pumps enter the wall of the Turbine Building at approximately 7 foot elevation above the floor and hence, any flood which shorted those cables out would fail the HPI system in exactly the same scenarios as discussed for zones 45 and 54. However, a flood in the Turbine Building up to elevation 7 foot above the floor level would by then have exceeded the barrier into the emergency switchgear room and hence, gave rise to the scenarios associated with that zone which are more severe (station blackout) than the scenarios which would result in this case. In addition, these scenarios for the Turbine Building require random failures of the component cooling water system or stuck open relief valve as discussed for zone 45. Hence, this flood zone can be screened since it is subsumed by the scenarios associated with the emergency switchgear room.

Control Room (Zone 5)

This is at elevation 27 foot adjacent to the Turbine Building. The control room itself has no water sources other than those associated with air conditioning and normal domestic water supply. Rooms surrounding the

control room consists of lunch room and office space. Again, these adjacent areas have no significant sources of water. Above the control room is the normal (non-emergency) cable spreading room which has no water sources. Hence, the only flooding that could occur in this room would be due to flooding in the Turbine Building. This would require flooding the Turbine Building to elevation 27 feet which, as discussed above, would have already resulted in flooding of the emergency switchgear room with its associated station blackout scenarios. Hence, floods in the control room (which is a single vital area analysis) are subsumed by floods in the emergency switchgear room.

Auxiliary Building (Zone 17)

The Auxiliary Building is a single vital area analysis zone because it contains both the component cooling water pumps and the high pressure injection pumps and failure of those systems together leads to a seal LOCA. All these pumps are located at the bottom (two foot elevation) level. The cubicles for the high pressure injection pumps flood are isolated at the 2 foot floor elevation from the main floor area which contains the CCW pumps. These walls extend to the 13' elevation. Since there are no significant water sources either above or adjacent to this area and flooding would have to reach the 13' elevation, this zone was eliminated from further consideration.

Safeguards Area (Zone 19)

This area is comprised of the rooms surrounding the containment and contains the auxiliary feedwater system pumps and the low pressure injection pumps. There are several elevations in the safeguards area. The auxiliary feedwater and LPI pumps are on the ground floor elevation level. This zone occurs in cut sets associated with additional random failures and two types of scenarios are possible. The first is associated with a random failure of the feed and bleed function in conjunction with flood induced failure of the auxiliary feedwater system. Random failures of feed and bleed are due, for example, to random failures of the PORV or random failures of the HPI system. The second type of scenario is associated with a stuck open safety relief valve and involves flood induced failure of both the auxiliary feedwater system and the LPI system which thus results in failure of the long term recirculation function. Since the random failure probabilities for the PORVs, safety relief valves, and the HPI system are approximately 1E-4/demand and random pipe break frequency which might lead to a flood is smaller than 1E-3 per year it can be seem that these sequences (conservatively) are less than 1E-6/yr and hence, can be screened out from further consideration.

Containment (Zone 15)

The containment occurs as a single zone in conjunction with random failure of the auxiliary feedwater system. The containment flood must fail a PORV. The PORVs are located on the top of the pressurizers.

Cabling for the PORVs runs down the pressurizer, then is routed along the containment wall out through the upper elevations of the safeguards area and then directly into the cable vault/tunnel. This would require flooding of the containment structure to approximately the 18 foot elevation. This scenario can be screened by virtue of a frequency of pipe break being bounded by 1E-3 per year, the probability of a spurious actuation induced by the flood in the PORV (approximately 1E-1 per demand) and the random failure probability of the auxiliary feedwater system which is approximately 1E-3/demand. Taken together these factors demonstrate that the scenario can be screened from further consideration.

3.5 Summary

The scoping quantification study considered all possible external events at the site except for seismic and fire events, since these two events were included in a detailed external events analysis. The PRA Procedures Guide (Ref. 1), suitably augmented with other available information, was used as a guidelines for identification of all possible external events at the Surry site. Next, an initial screening process was carried out to eliminate events not applicable to Surry from the list. For this purpose, a set of screening criteria was developed and then each external event was examined for possible elimination based on these criteria. After the initial screening process was completed, the following events were found to be potential contributors to the plant risk.

a. Aircraft Impact
b. External Flooding
c. Extreme Winds and Tornadoes
d. Industrial or Military Facility Accident
e. Pipeline Accidents
f. Release of Chemicals from On-Site Storage
g. Transportation Accidents
h. Turbine Generated Missiles
i. Internal Flooding

The degree of sophistication in the bounding analysis for each event depended on whether the event could be eliminated based on only a hazard analysis or a complete analysis including hazard analysis, fragility evaluation and plant response analysis. The detailed plant response analysis was conservatively neglected in evaluating the impact of these external events.

The risk due to an aircraft striking the plant structures and causing unacceptable radiological consequences was screened out on the basis of the probability of strike and the design of different structures.

Evaluation of the potential for flooding as a result of the most conservative combination of Probable Maximum Flood (computed from conservative estimates of probable maximum precipitation) and wind-generated waves showed that the essential structures in the plant are located above the probable maximum surge level and the risk of flooding is negligibly small.

Tornadoes and tornado missile impacts were eliminated on the basis of a detailed computation of tornado strike probability and other features of plant structures and components designed to withstand the effects of a Design Basis Tornado.

The information available from the Virginia Power Company was used as the basis to assumed the safety of essential plant structures from damage due to turbine missiles.

Finally, explosions due to pipeline accidents, transportation accidents and both on-site and off-site chemical release were determined have a low probability of affecting the site.

Thus, all external hazards except fire and seismic events were found to be negligible contributors to the risk of core damage at the Surry plant. Detailed evaluations of fire and seismic events are contained in the remainder of this report.

3.6 References

1. USNRC, PRA Procedures Guide, NUREG/CR-2300, January 1983.

2. Virginia Electric & Power Company, Updated Final Safety Analysis Report, Surry Nuclear Power Station, Richmond, Virginia, 1983.

3. L. A. Twisdale and W. L. Dunn, Tornado Missile Simulation and Design Methodology, Vol. 1, Research Triangle Institute, NP-2005, August 1981.

4. K. A. Soloman et al., Estimate of the Hazards to a Nuclear Reactor From the Random Impact of Meteorites, UCLA - ENG - 7426, March 1974.

5. NUS Corporation, Surry Onsite Toxic Chemical Release Analysis (Vol. E) and Surry Offsite Toxic Chemical Release Analysis (Vol. II), #NUS-3735, 1981.

6. USNRC, "Assumptions for Evaluating Habitability of nuclear power Plant Control Room During a Postulated Hazardous Chemical Release," Regulatory Guide 1.78, U.S. AEC Directorate of Regulatory Standards, June 1974.

7. USNRC, "Evaluation of Explosions Postulated to Occur on Transportation Routes Near Nuclear Power Plants," USNRC Office of Standards Development, Revision 1, Regulatory Guide 1.91, February 1978.

8. T. V. Eichler and H. S. Napadensky, Accidental Vapor Phase Explosions on Transportation Routes near Nuclear Power Plants, USNRC, NUREG/CR-0075, May 1978.

9. T. V. Eichler et al, Evaluation of Risks to the Marble Hill Nuclear Generating Station from Traffic on the Ohio River, Engineering Division, IIT Research Institute, Chicago, Illinois, October 1978.

10. D. W. Murphy, Battelle Pacific Northwest Laboratories Letter to L. A. Hulman, USNRC, March 23, 1982, regarding Control Room Habitability Evaluation.

11. S. A. Varga, USNRC letter to R. H. Leasburg, VEPCO, June 28, 1982, Docket No. 50-280 and 50-281.

12. NUS Corporation, Severe Accident Risk Assessment, Limerick Generating Station, Philadelphia, Pennsylvania, prepared for NUS Corporation, Philadelphia Electric Company, 1983.

13. A. D. Swain and H. E. Guttman, Handbook of Human Reliability Analysis, NUREG/CR-1278, SAND80-0200, Sandia National Laboratories, Albuquerque, NM, August 1983.

14. USNRC - "Protection of Nuclear Power Plants Against Extreme Winds and Tornadoes," Regulatory Guide 1.117, 1977.

15. M. K. Ravindra and H. Banon, Methods for External Event Screening Quantification, NUREG/CR-4839, to be published.

16. USNRC - "Protection Against Low Trajectory Turbine Missiles," Rev. 1, Regulatory Guide 1.115, July 1977.

17. G. E. Sliter et al, "EPRI Research on Turbine Missile Effects in Nuclear Power Plants," Transactions of 7th International Conference on Structural Mechanics in Reactor Technology, Paper J815, Chicago, Illinois, 1983, pp. 403-409.

18. S. H. Bush, "Probability of Damage to Nuclear Components due to Turbine Failure, in Nuclear Safety, Vol. 14, No. 3, May - June 1973.

19. USNRC, Standard Review Plan for the Review of Safety Analysis Reports for Nuclear Power Plants, USNRC, Office of Nuclear Reactor Regulations, Washington, D. C., NUREG-0800 LWR Edition, July 1981.

20. M. A. Azarm et al., A Review of the Limerick Generating Station Severe Accident Assessment, NUREG/CR-3493, July 1984.

21. E. M. Patton et al, Probabilistic Analysis of Low-Pressure Steam Turbine Missile Generation Events, Battelle Pacific Northwest Laboratories, EPRI NP-2749, August 1973.

4.0 SEISMIC PRA

A detailed seismic risk assessment was performed for the Surry Plant. This analysis utilized dynamic response calculations for all important structures, a generic seismic fragility data base for components, and detailed component fragility derivations for a number of components identified during the plant visit as falling outside the generic data base. Hazard curves developed by the USNRC sponsored Seismic Hazard Characterization Program at Lawrence Livermore National Laboratory for the USNRC and by the Electric Power Research Institute were used. Mean values of accident sequence and core damage frequencies were obtained using a Monte Carlo approach. Each of these aspects of seismic risk are described in the following subsections.

4.1 Seismicity and Hazard Curves

The earthquake hazard at a given power plant site is characterized by a hazard curve and a site ground motion spectra. The hazard curve is a frequency plot which gives the probability of exceedance (per year) of different peak ground accelerations. The site response spectra describes the relative frequency content of the earthquakes expected at the site, and also the influence of the local soil column and layering in modifying the earthquake frequencies transmitted to the site.

4.1.1 General Considerations

For a given site, the hazard curve is derived from a combination of recorded earthquake data, estimated earthquake magnitudes of known events for which no data are available, review of local geological investigations, and use of expert judgment from seismologists and geologists familiar with the region in question. The region around the site (say within 100 km) is divided into zones, each zone having an (assumed) uniform mean rate of earthquake occurrence. This mean occurrence rate is determined from the historical record, as is the distribution of earthquake magnitudes. Then, for the region under consideration, an attenuation law is determined which relates the ground acceleration at the site to the ground acceleration at the earthquake source, as a function of the earthquake magnitude. The uncertainty in the attenuation law is specified by the standard deviation of the data (from which the law was derived) about the mean attenuation curve. These four pieces of information (zonation, mean occurrence rate and magnitude distribution for each zone, and attenuation law) are then combined statistically to compute the hazard curve.

The low level of seismic activity and the lack of instrumental records make it difficult to carry out seismic hazard analyses for the central and eastern United States using historic data alone. To augment the data base, current methodologies make use of the judgment of experts familiar with the area under consideration.

Approaches used to generate the subjective input, to assure reliability by feedback loops and cross-checking, and to account for biases and modes of judgment are described in detail in Bernreuter (Ref. 1).

4.1.2 Hazard Curves Used For Surry

The hazard curves used in the NUREG 1150 PRAs were taken from two sources. The first set of curves was obtained from the USNRC-sponsored Eastern US Seismic Hazard Characterization Program (Ref. 1) being performed by Lawrence Livermore Laboratories (LLNL). From this program one can obtain a median hazard curve and an estimate of the distribution about the median curve. This is shown in Figure 4.1 where the mean, median, the 15th percentile and 85th percentiles are shown. According to the principal investigator of this program, the distribution about the median is nearly log normal so for use in the NUREG 1150 analyses a log normal distribution was fit using the median and mean curves. From this fit any particular percentile curve of the hazard curve family can be computed. Table 4.1 lists the numerical values used in fitting the LLNL hazard curves.

A second set of hazard curves was obtained from the industry-sponsored Electric Power Research Institute's Seismic Hazard Methodology Development program (Ref. 2). The corresponding curves are shown in Figure 4.2. These were also fit with a log normal model. The numerical values used in fitting the EPRI curves are listed in Table 4.2.

Note that the mean hazard curves of Figure 4.1 and 4.2 are near or above the 85th percentile hazard curve shown. This mean hazard curve will be found to drive the calculation of mean core damage frequency estimates as explained in Section 4.4.

The two sets of hazard curves shown in Figures 4.1 and 4.2 are significantly different, both in regard to location of the mean hazard curve as well as to the range of uncertainty about the median curve. This is not too surprising inasmuch as the emphasis of the two programs was somewhat different. The EPRI Program focused on very detailed geological studies of the sites in question, and resulted in a somewhat finer zonation of each site. However, only three attenuation (ground motion) models were used. Further, while a number of teams of seismological and geological experts were assembled, each team was proscribed to reach a consensus on the final hazard curve families developed by that team.

By contrast, in the LLNL program, considerable emphasis was placed on the full range of attenuation models, and rather than a number of teams, a total of 11 seismicity experts and five ground motion experts were individually polled, and a full set of 2750 hazard curves were developed for each site by considering each expert's input equally likely. The curves developed in this process encompass somewhat more uncertainty than those produced by the EPRI process, and the increased uncertainty leads to higher probabilities of nonexceedance for the LLNL mean curve peak ground acceleration values than are obtained from the EPRI distributions.

At this time, both sets of hazard curves are viewed by the US NRC staff as being equally credible. As such, calculations of the seismic core damage and plant damage state frequencies at Surry are presented for both sets of hazard curves in this report.

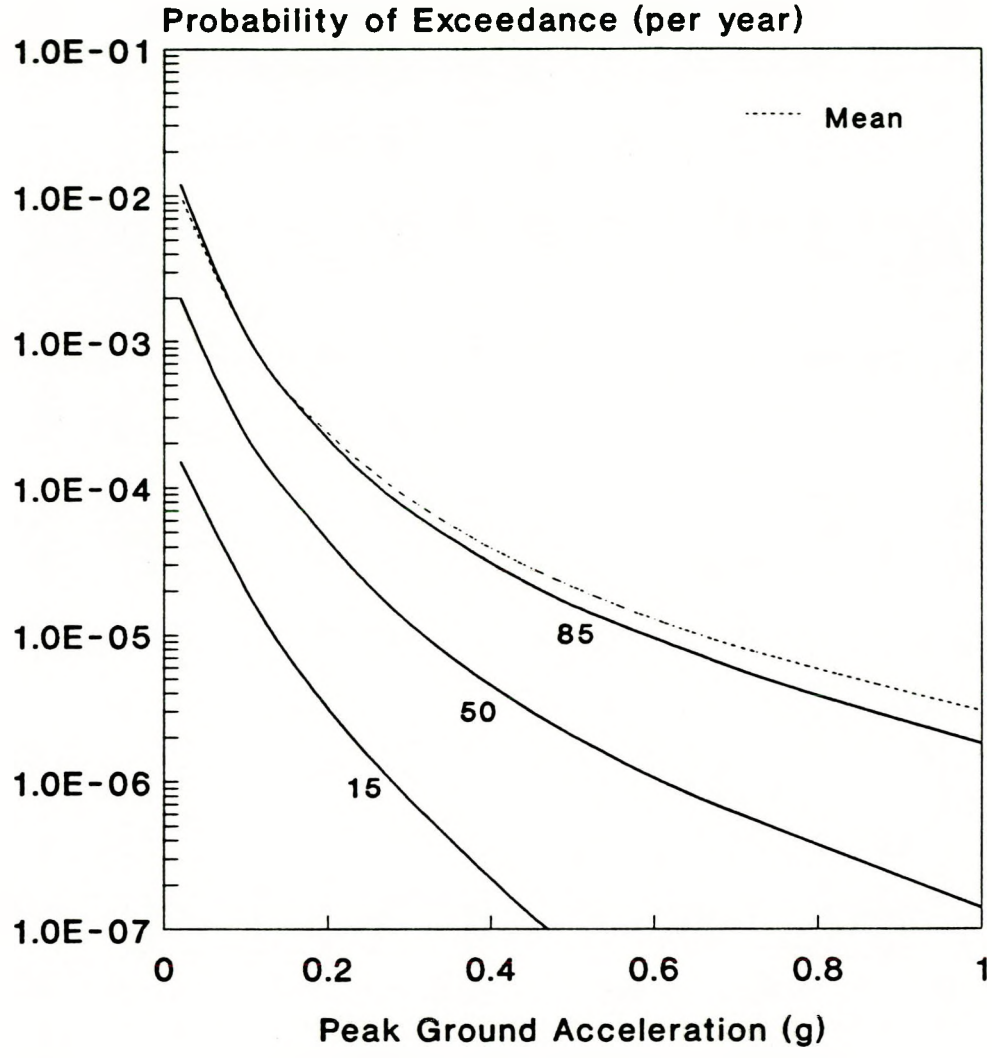

Figure 4.1. LLNL Surry Hazard Curve: Mean, Median, 15th and 85th Percentile Curves

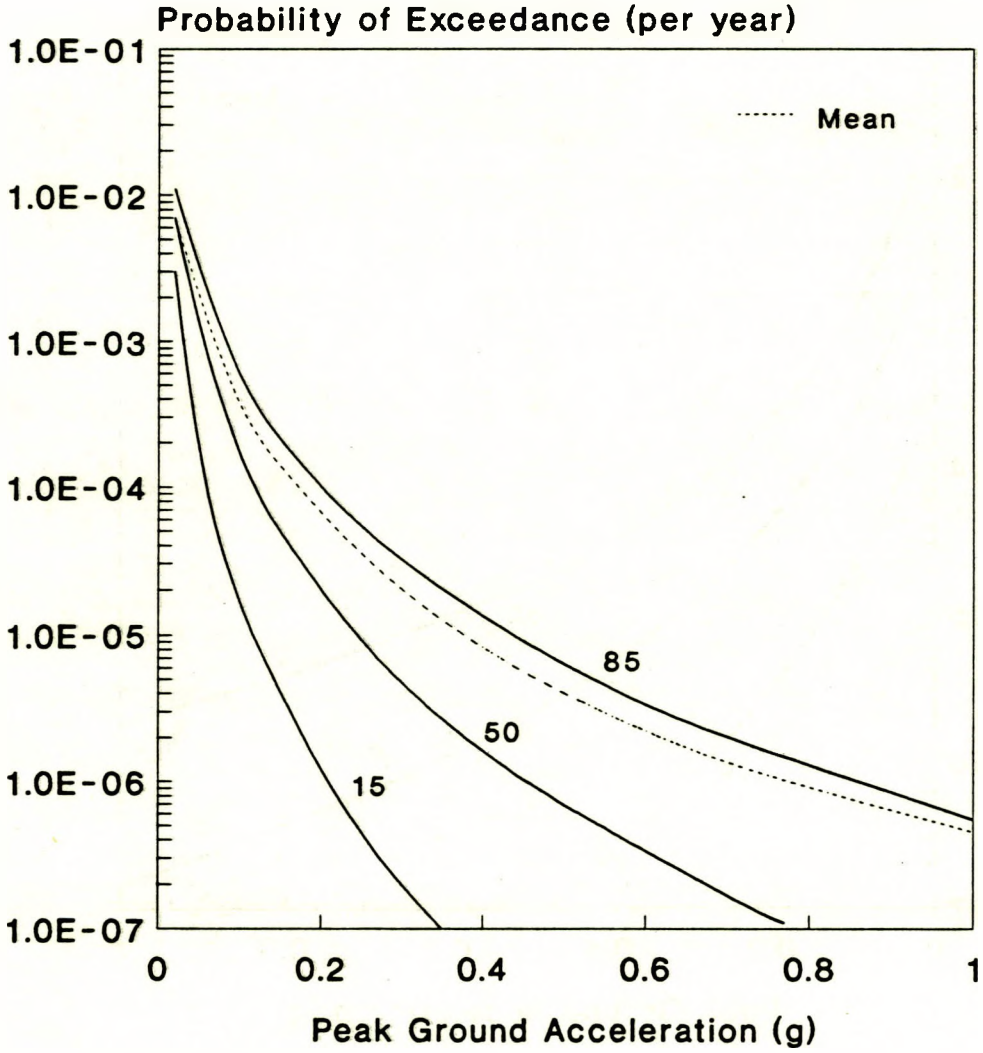

Figure 4.2. EPRI Surry Hazard Curve: Mean, Median, 15th and 85th Percentile Curves

Table 4.1

LLNL Mean and Median Hazard Curve Values

PGA(g)	Mean Hazard $P_{exceedance}$ per year	Median Hazard $P_{exceedance}$ per year
0.05	4.10E-3	1.67E-3
0.15	4.24E-4	9.45E-5
0.25	1.26E-4	2.03E-5
0.35	5.40E-5	6.85E-6
0.45	2.78E-5	2.92E-6
0.55	1.61E-5	1.43E-6
0.65	1.01E-5	7.75E-7
0.75	6.74E-6	4.77E-7

Table 4.2

EPRI Mean and Median Hazard Curve Values*

PGA(g)	Mean Hazard $P_{exceedance}$ per year	Median Hazard $P_{exceedance}$ per year
0.05	1.92E-3	1.11E-3
0.15	1.35E-4	4.68E-5
0.25	3.28E-5	8.52E-6
0.35	1.21E-5	2.56E-6
0.45	5.54E-6	1.01E-6
0.55	2.92E-6	4.77E-7
0.65	1.67E-6	2.38E-7
0.75	1.07E-6	1.19E-7

*Note that numerical values for the EPRI curve shown here differ slightly from those published in the final version of Reference 2. The final core damage frequency results reported here would be decreased by 12% using the latest EPRI hazard curves, with the relative importance of components and sequences being unchanged.

4.2 Response Calculations

4.2.1 Introduction

As previously described, seismic probabilistic risk assessments (PRAs) can be considered in a series of steps: seismic hazard characterization, seismic response of structures and components, structure and component failure descriptions, plant logic models, and probabilistic failure calculations. Section 4.2 deals with the frequency characteristics of the free field ground motion (an element of the seismic hazard characterization) and the seismic response of structures and components.

In a seismic PRA of a nuclear power generating plant's safety systems, only the components affecting the operation of the systems and those structures housing or supporting these components need to be analyzed. Plant logic models identify the components. Plant general arrangement and mechanical drawings are then used to locate the components and identify the relevant supporting structures. For the Surry Power Station the specific safety-related components are housed in the Reactor Building, Auxiliary Building, Safeguards Area, Emergency Generator Enclosure, Containment Spray Pump Enclosure, Control Room, and Intake Structure. Figure 4.3 illustrates the general plant layout showing relative location of these structures.

Seismic PRAs require as input best-estimate structural response, variations of response and correlation of response. A seismic PRA considers earthquakes over the entire range of the seismic hazard curve; hence, seismic responses must be determined over this range. Often, seismic response determined as part of the plant design process is available. However, this data reflects the conservatism associated with the seismic design analysis methodology and considers only low seismic excitation levels.

To determine structural response at the higher excitation levels required by a seismic PRA, either the design analyses must be extrapolated or reanalyses of the structures must be made. For this study, analytical models of each structure identified above as housing safety-related components were developed and used in a probabilistic response analysis to determine the best-estimate seismic response of these structures.

The balance of this section will describe and summarize:

a. site and seismic characteristics

b. probabilistic response analysis of each structure

c. in-structure responses which define the response of safety-related components

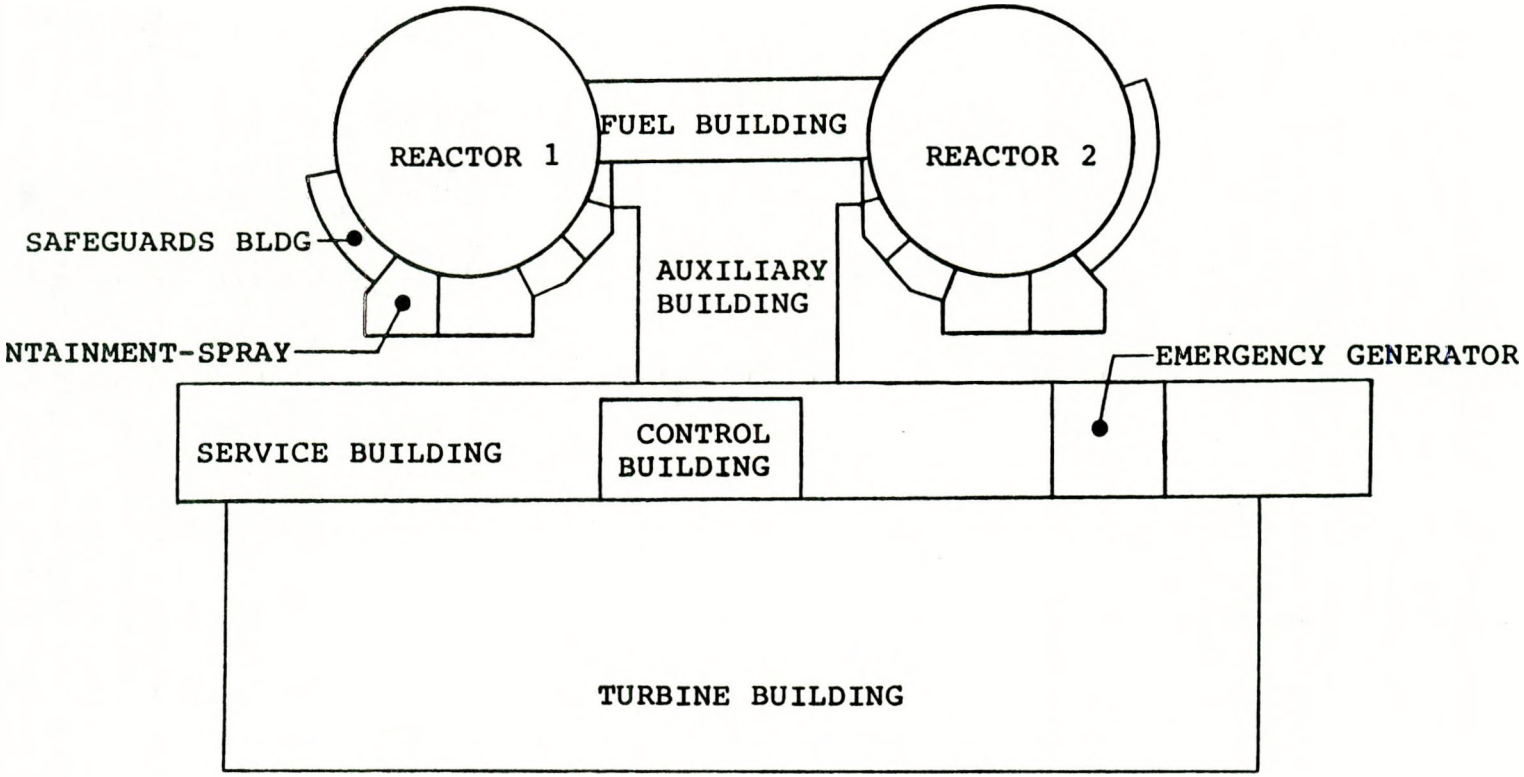

Figure 4.3 Surry Power Station General Arrangement

4.2.2 Site and Seismic Characteristics

4.2.2.1 Site Description.

The Surry Power Station site is characterized as a deep soil site of alternating strata of clay and sands of the Pleistocene age. The Pleistocene age strata lie unconformably on Miocene clays beginning at elevation -38. Original ground elevation through the area of the site was +34 ft. Finished grade exists at an elevation of +26.5 ft. The Miocene clay is heavily over-consolidated extending to -280 ft in elevation. Formations of the Eocene, Paleocene, Cretaceous and Crystalline age exists beyond the Miocene clay strata. Figures 4.4a and 4.4b show the Pleistocene and Miocene age strata and foundation elevations for the Surry Power Station structures.

4.2.2.2 Soil Properties and Earthquake Definition.

Two interrelated objectives for the initial portion of this investigation were to:

a. define strain compatible soil properties over the range of seismic excitation levels defined by the seismic hazard curves.

b. define the input motion for the probabilistic response analyses of the structures

The safe shutdown earthquake (SSE) for the Surry site is defined to have a peak horizontal ground acceleration of 0.15g. Three seismic excitation levels were considered and defined by their peak ground acceleration in the horizontal direction -- 0.15g (1 SSE), 0.30g (2 SSE), 0.45g (3 SSE). They are denoted acceleration ranges 1, 2, and 3 in subsequent discussions. These excitation levels were treated explicitly -- input motions and probabilistic response for other levels defined by the hazard curve can then be interpolated from the results.

In general, soil properties such as shear modulus and damping are a function of soil strain and consequently a function of excitation level, i.e., acceleration ranges 1, 2, and 3 defined above. With higher excitation levels, soil shear modulus tends to decrease while soil damping tends to increase. Equivalent linear visco-elastic soil properties as a function of excitation level were developed using the program SHAKE (Ref. 3). The soil deposit is idealized as a series of horizontal layers. Low strain soil properties were derived by relationships between blow counts and shear wave velocity for the sand strata (Ref. 4). The blow counts for the sand layers are given in Reference 5. Shear modulus for the clay strata, both Pleistocene and Miocene deposits, are reported in Reference 5 as derived from quick shear test results on undisturbed samples. There are three principle layers of strata with varying low strain soil properties as given in Table 4.3. Estimation of equivalent linear strain compatible properties is preceded by defining the relationship between soil shear modulus and strain (shear modulus degradation curve), and soil material damping and strain. No

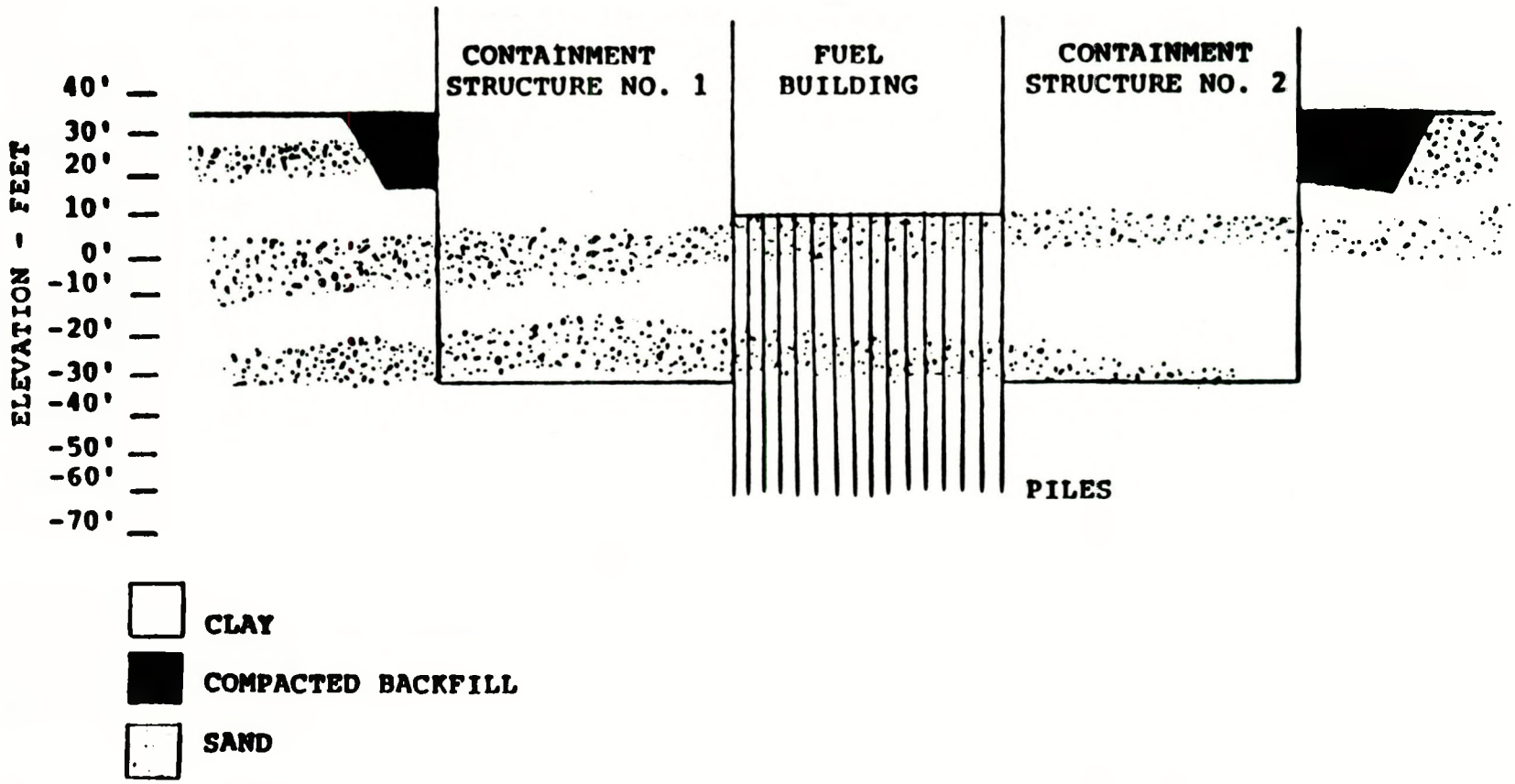

Figure 4.4a. Surry Power Station Subsurface Profile E-W Section

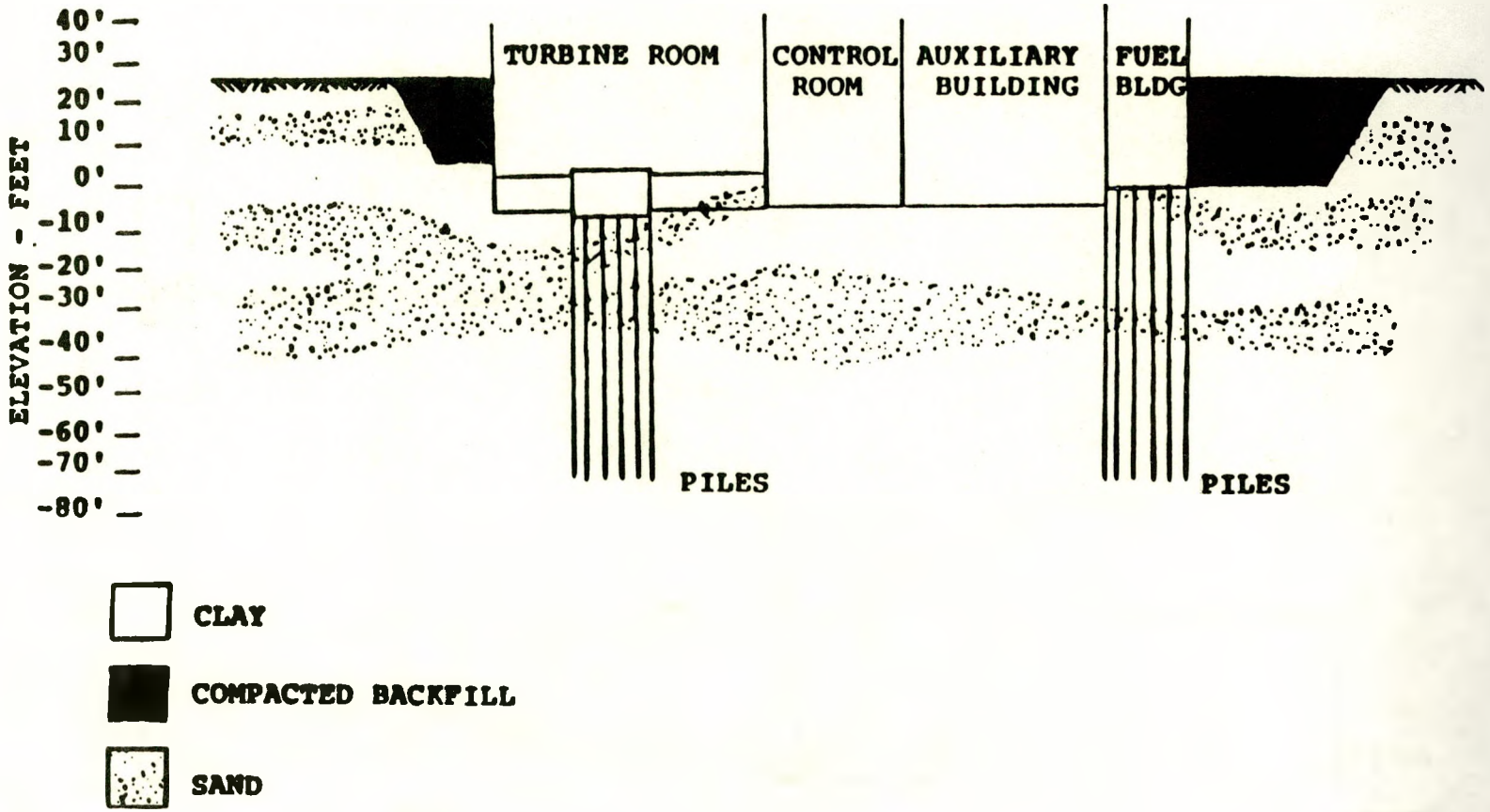

Figure 4.4b. Surry Power Station Subsurface Profile N-S Section

Surry Power Station specific data were available, thus curves developed by Seed and Idriss (Ref. 6) were used in the present investigation. Vertically propagating shear waves are assumed to be the wave progation mechanism by which horizontal motion propagates to the soil free surface. Nominal strain compatible soil properties for the three acceleration ranges computed using the SHAKE code are shown in Table 4.4 and Figure 4.5.

Table 4.3

Surry Power Station Low Strain Soil Properties

Layer No.	Thickness (ft)	Shear Wave Velocity (ft/s)	Unit Weight (pcf)
1	20	740	110
2	40	810	110
3	280	820	110

The input motion used to develop these values and also to perform the probabilistic analysis was developed from recorded earthquakes at soil sites. A suite of ten earthquake acceleration time histories was defined and scaled to each of the three excitation levels. Each of the acceleration time histories consists of recorded motions of actual earthquakes from similar soil sites. A total of five recorded earthquake acceleration time histories were selected and listed in Table 4.5. For the purpose of the analyses a total of ten input acceleration time histories in each orthogonal horizontal direction was created by rotation of the two horizontal components. The median acceleration response spectrum of the ten horizontal components is shown in Figure 4.6, along with median response spectra for two types of similar soil sites: soft to medium clay and deep cohesionless soil as reported in Reference 7. The comparison shows that frequency content and amplification for the median response of the ten horizontal components adequately the represent the expected motion at the Surry Power Station.

4.2.3 Probabilistic Response Analysis

In recognition of the importance of the effects of embedment and soil structure interaction (SSI), probabilistic soil-structure interaction building response analyses were used to generate median responses for the Surry Power Station structures housing safety-related components. The methodology used is that of SMACS (Ref. 8) as implemented in the computer program CLASSI (Ref. 9) utilizing the substructure approach. The substructure approach to SSI is composed of the following elements: specification of the free-field ground motion; determination of the

Table 4.4a

Surry Power Station Strain Compatible Soil Properties -- Acceleration Range 1

Elevation (ft)	Shear Modulus (KSF)	Shear Wave Velocity (fps)	Damping
27.5	1805.	727.	.016
21.5	1172.	586.	.026
16.5	883.	508.	.033
11.5	699.	452.	.038
6.5	825.	491.	.039
1.5	755.	470.	.041
-3.5	684.	447.	.044
-13.5	620.	426.	.047
-23.5	580.	412.	.049
-33.5	588.	415.	.049
-43.5	585.	414.	.049
-53.5	596.	418.	.049
-63.5	612.	423.	.047
-73.5	624.	427.	.047
-83.5	652.	437.	.046
-93.5	628.	429.	.047

Table 4.4b

Surry Power Station Strain Compatible Soil Properties -- Acceleration Range 2

Elevation (ft)	Shear Modulus (KSF)	Shear Wave Velocity (fps)	Damping
27.5	1388.	637.	.022
21.5	722.	460.	.037
16.5	534.	395.	.046
11.5	410.	346.	.055
6.5	490.	379.	.055
1.5	435.	357.	.061
-3.5	374.	331.	.068
-13.5	325.	308.	.074
-23.5	319.	306.	.074
-33.5	372.	330.	.069
-43.5	388.	337.	.068
-53.5	398.	341.	.066
-63.5	344.	317.	.072
-73.5	291.	292.	.078
-83.5	278.	285.	.080
-93.5	241.	266.	.088

Table 4.4c

Surry Power Station Strain Compatible Soil Properties -- Acceleration Range 3

Elevation (ft)	Shear Modulus (KSF)	Shear Wave Velocity (fps)	Damping
27.5	1190.	590.	.026
21.5	623.	427.	.041
16.5	444.	361.	.050
11.5	346.	318.	.063
6.5	409.	346.	.064
1.5	358.	324.	.070
-3.5	302.	298.	.076
-13.5	266.	279.	.082
-23.5	252.	272.	.084
-33.5	264.	278.	.083
-43.5	266.	279.	.083
-53.5	273.	283.	.082
-63.5	260.	276.	.084
-73.5	251.	271.	.086
-83.5	247.	269.	.087
-93.5	221.	255.	.092

Table 4.5

Free-Field Acceleration Time Histories for Probabilistic Response Analysis

Site	Date
El Centro	May 18, 1940
Hollywood Storage	July 21, 1952
Ferndale City Hall	December 21, 1954
Hollister	April 8, 1961
8244 Orion Los Angeles	February 9, 1971

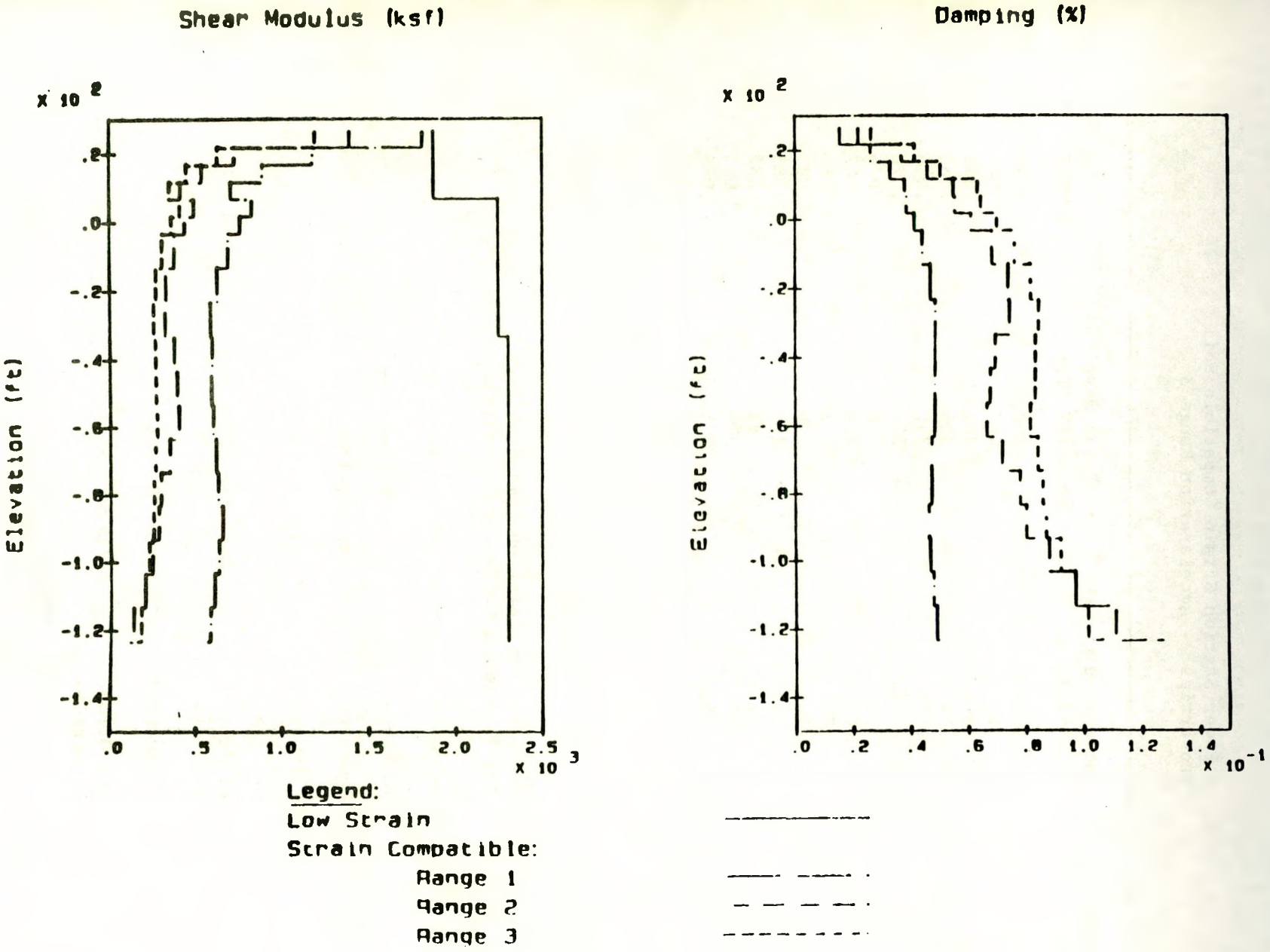

Figure 4.5. Variation of Soil Shear Modulus and Damping Ratio with Depth

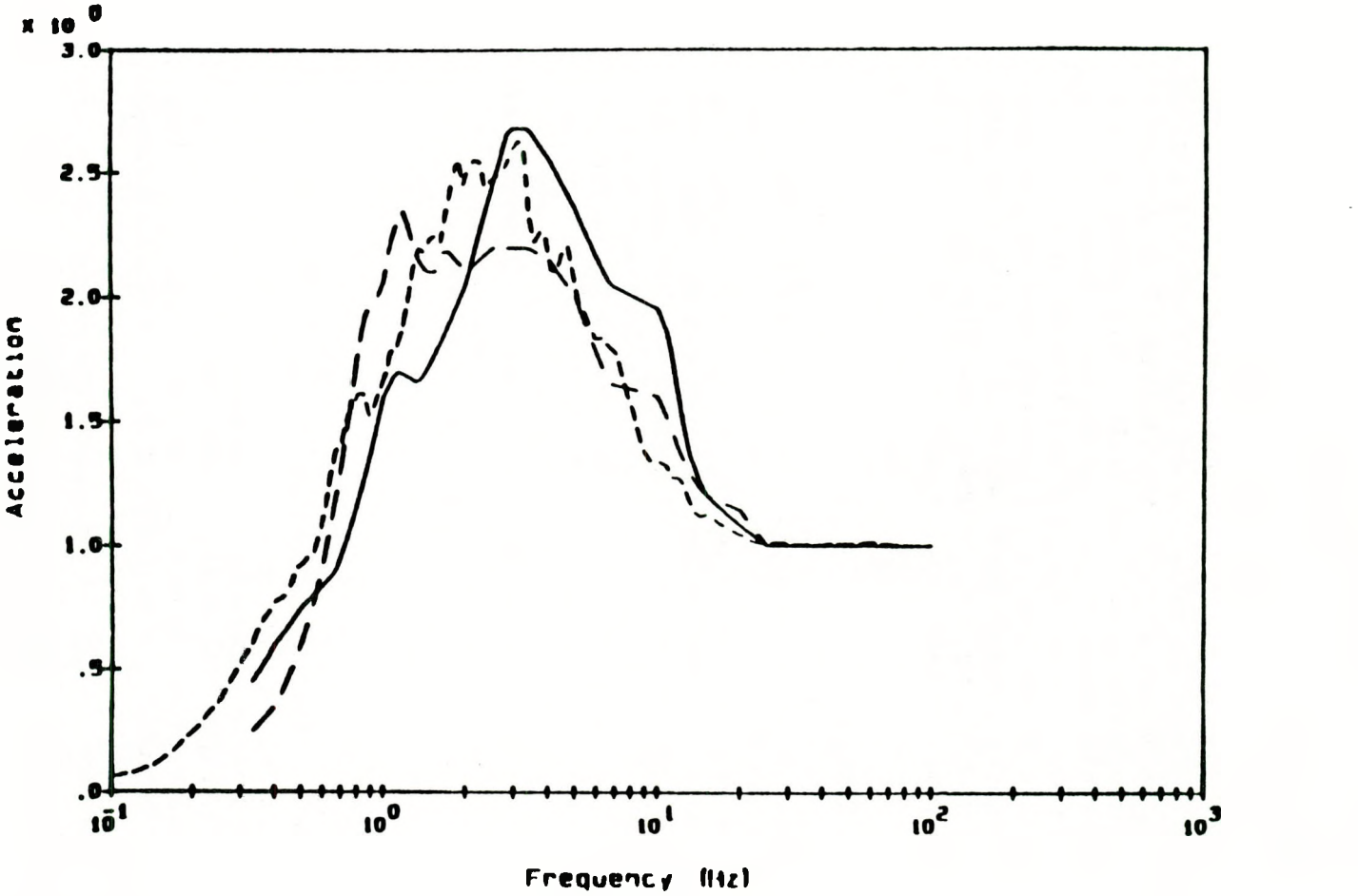

Figure 4.6. Surry Power Station Median Free-Field Input Motion Compared to Soft Cohesionless Soils and Clay Spectra (Ref. 7)

foundation input motion and impedances; calculation of the dynamic characteristics of the structure; and analysis of the coupled soilstructure system. Each element as pertaining to the Surry Power Station structural analyses is discussed below.

4.2.3.1 Free-Field Ground Motion

Specification of the free-field ground motion includes specifying its frequency characteristics, spatial variation, and control point. The frequency characteristics and spatial variation of the free-field motion were discussed above. The elevation at which the free-field is specified for each structure is the control point. Generally, this would be the existing free surface at elevation 27.5 ft for the Surry Power Station Site. However, some of the structures analyzed and founded at elevation -2 ft are surrounded by other structures on all sides founded at the same or deeper elevation. Thus the control point was conservatively defined as -2 ft for the Auxiliary Building, and Control Room Structure, while for other structures the control point was specified at elevation 27.5 ft.

4.2.3.2 Foundation Input Motion

The foundation input motion varies from the free-field motion for all cases except surface founded foundations, i.e., control point and foundation at the same elevation, subjected to vertically propagating shear and dilatational waves. A scattering function relates the three translational free-field components to the six degrees of freedom on the foundation. The scattering function is frequency dependent and complex valued. For this investigation all waves are assumed to be vertically propagating. The variation between free-field motion and foundation motion is due to the variation of free-field motion with depth and wave scattering at the soil foundation interface for embedded foundations. This follows since the foundation is modeled as rigid and massless, and points on the foundation are constrained to move according to its geometry in plan and depth of embedment.

4.2.3.3 Foundation Impedances.

Foundation impedances are the force-displacement characteristics of the soil. Foundation impedances depend on the soil layering and soil material behavior, frequency of excitation, and geometry and embedment of the foundation. For a rigid foundation, the force displacement characteristics are uniquely defined by a 6 x 6 matrix, complexed valued and frequency dependent, relating a resultant set of forces and moments to the six rigid-body degrees of freedom of the foundation. The foundations of all structures analyzed here are approximated as an equivalent surface-founded or embedded cylinder. The soil column is idealized as a half-space with properties taken at an elevation of half the characteristic length below its foundation. Depth of embedment for each structure's foundation model is given in Table 4.6 below.

Table 4.6

Surry Power Station Foundation Models
Depth of Embedment

	Embedment (ft)
Reactor Building	67
Auxiliary Building	0
Control Room Structure	0
Safeguards Area	19
Containment Spray Pump Enclosure	19.5
Emergency Generator Enclosure	13
Intake Structure	36.75

4.2.3.4 Structural Dynamic Characteristics.

Structural dynamic characteristics are described by their fixed-base eigensystem and modal damping factors. Eigensystems, fundamental modes of vibration and eigenvectors are determined from fixed-base lumped mass beam element models. The beam elements represent stiffness between floor levels located at the shear centroid of the reinforced concrete walls or diagonal steel bracing, including shear deformation. The contribution to lumped mass at each floor level is from the half height of the wall above and below, floor slab, and equipment at that floor. Nominal values of structure damping were taken to be 0.07, 0.085, and 0.10 (fractions of critical damping) for the three seismic acceleration ranges considered here. These were based on published damping values and assumed stress levels achieved.

4.2.3.5 Soil Structure Interaction Analysis.

The probabilistic SSI analysis procedure is to perform a series of deterministic analyses, each simulating an earthquake occurrence, including variability in seismic input, soil-structure interaction, and structure representation. The seismic input variability is normally introduced by considering an ensemble of earthquake motions. For this study, the five earthquake motions described earlier were used. A series of ten earthquake simulations for each acceleration range were performed each using the identical free-field input motion as a starting point. Soil structure interaction and structure response variability are introduced through a limited number of parameters -- soil shear modulus,

soil damping, structure frequency and structural modal damping. Variability in SSI was incorporated through modelling soil shear modulus and soil material damping as random variables with lognormal distributions with medians corresponding to the nominal values of Table 4.4 and coefficients of variation of 0.4 and 0.5, respectively. Variability in structure dynamic behavior was also modelled by treating structure frequency and modal damping as random variables. Parameter variations in each step of the response analysis were selected to represent random variability, and not to include modelling uncertainty. The assumed parameter variability corresponds to that developed in the SSMRP (Ref. 10). The parameter values for each of the ten simulations were selected from the probability distributions by dividing the distributions into equally probable segments, sampling from each segment and combining the samples using a Latin hypercube experimental design. The responses calculated from the simulations are combined to estimate median responses conditional on the occurrence of an earthquake described by a particular hazard curve parameter, e.g., peak ground acceleration.

Instructure spectra were calculated at 5 percent damping at the mass centroid of each floor elevation translational component for the ten input motions. The ten spectra were then combined to form median centered spectra assuming a lognormal distribution.

The structures for which best-estimate dynamic responses were computed based on the 10 selected time histories were shown in Table 4.6. Each structure considered is described below.

Reactor Building Internal Structure. The reactor building is a reinforced concrete structure, circular in plan (68 ft radius) supported on a 10-ft-thick reinforced concrete mat at elevation -39.5 ft and which extends in height to elevation 95 ft. The foundation supports two independent structures, the containment shell and the internal structure, coupled only at the base.

Figure 4.7 shows the 3-D fixed base model used to calculate the nominal eigenvalues and eigenvectors of the reactor building. Both the containment shell and internal structure are represented in the model. The internal structure's fundamental mode of vibration has a frequency of 6.48 Hz in the E-W direction and 6.89 Hz in the N-S direction accounting for 86 percent and 89 percent, respectively, of the mass participating in the horizontal directions.

Auxiliary Building. The auxiliary building is a reinforced concrete structure up to elevation 27.5 ft and steel frame to elevation 66 ft. It is rectangular in plan (150 ft x 111 ft) supported on a 4-ft-thick reinforced concrete mat at elevation -2 ft. The auxiliary building is surrounded on all sides by other structures founded at the same elevation or deeper.

Figure 4.8 shows the 3-D fixed base model used to calculate the nominal eigen values and vectors of the auxiliary building. The auxiliary building fundamental mode of vibration has a frequency of 20.8 Hz in the

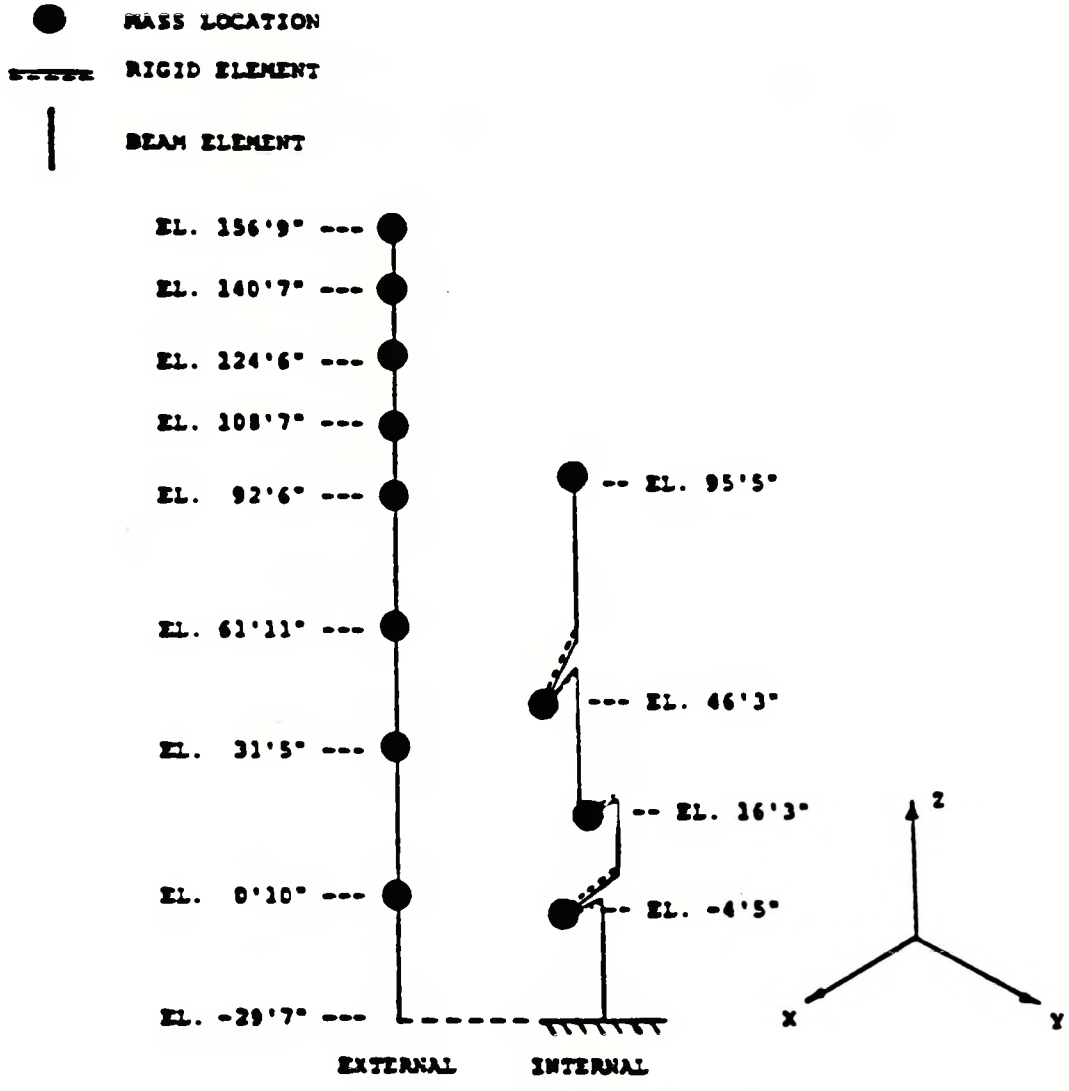

Figure 4.7. Surry Power Station Reactor Building Structural Model

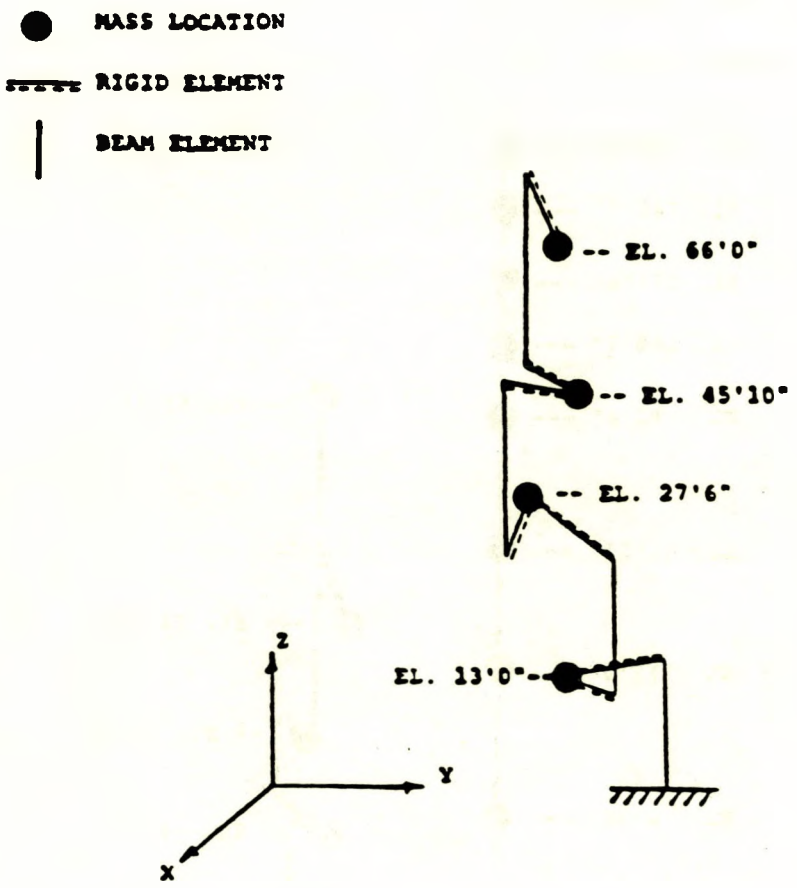

Figure 4.8. Surry Power Station Auxiliary Building Structural Model

E-W direction and 22.1 Hz in the N-S direction accounting for 80 percent and 65 percent, respectively, of the mass participating in the horizontal directions. The structural steel frame on the upper elevations has fundamental modes at approximately 6 Hz in both directions.

Control Room Structure. The control room resides inside the service building as a separate structure isolated by expansion joints resting on an independent foundation mat. It is constructed of reinforced concrete to elevation 45 ft and structural steel frame to 77 ft. The service building foundation in the control room area is tied into the adjacent turbine building strip footing running in the E-W direction. In addition the service and turbine building share the lateral force resisting system of a structural steel frame above elevation 45 ft. Stiffness and mass contributions from the turbine building are incorporated in the structural model to the extent structural details and load paths dictate. The control room area is rectangular in plan (185 ft x 75.5 ft) founded on a 4-ft-thick reinforced concrete mat at elevation -2 ft, surrounded on all sides by other structures founded at the same elevation.

Figure 4.9 shows the 3-D fixed base model used to calculate the nominal eigenvalues and eigenvectors of the control room structure. Contributions to the stiffness between floor levels and mass from the turbine building were incorporated in the model to the extent necessary as dictated by lateral force resisting systems and load paths by the single bent shown in Figure 4.9. The control room structure fundamental mode of vibration has a frequency of 17.0 Hz in the E-W direction and 22.6 Hz in the N-S direction accounting for 53 percent and 47 percent, respectively, of the mass participating in the horizontal directions. The structural steel frames of the upper elevations have fundamental modes between 1.8 and 6 Hz.

Safeguard Area. The safeguards area is of irregular shape, a segment of a circular arc conforming to the circular plan of the reactor building containment shell. It was idealized as a rectangular structure. The safeguard building is 68 ft x 14 ft, founded on a 2.5-ft-thick reinforced concrete mat at elevation 10.0 ft extending in height to elevation 42.5 ft. Reinforced concrete shear walls and diaphragms transmit lateral loads to its base. The roof is a steel frame metal deck and concrete slab.

Figure 4.10 shows the 3-D fixed base model used to calculate the nominal eigenvalues and eigenvectors of the safeguards area. The safeguards building significant modes of vibration are 34 Hz accounting for 56 percent of the mass in a direction tangential to the containment shell. In the orthogonal direction (towards the center of the reactor building) the first significant mode of vibration is 21.5 Hz with 57 percent of the mass participating.

Containment Spray Pump Enclosure. The containment spray pump enclosure is of irregular shape. It was idealized as a rectangular structure. The containment spray pump enclosure is 38 ft x 30 ft founded on a 2.5-ft-thick reinforced concrete mat at elevation 9.0 ft, extending in

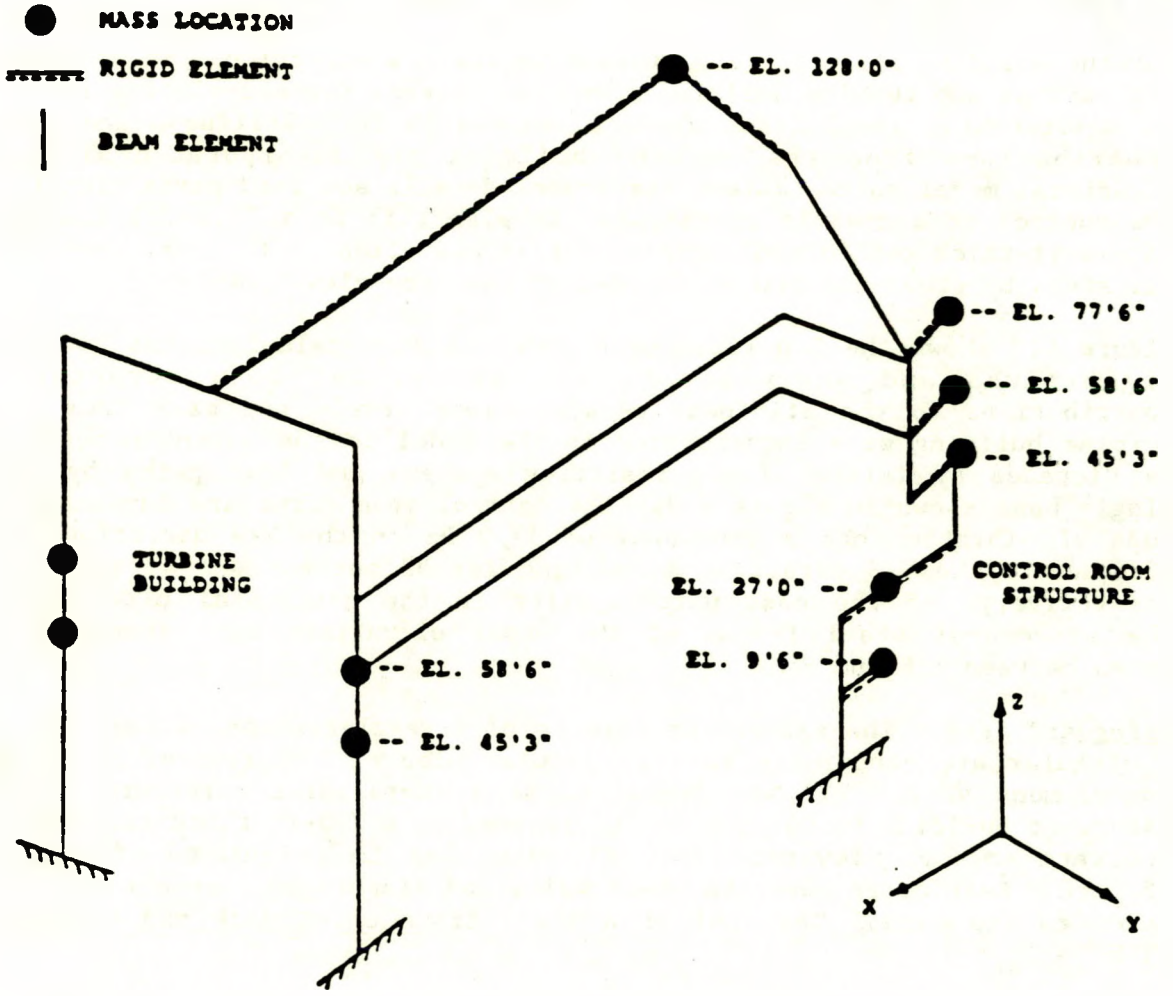

Figure 4.9. Surry Power Station Control Room Structure Structural Model

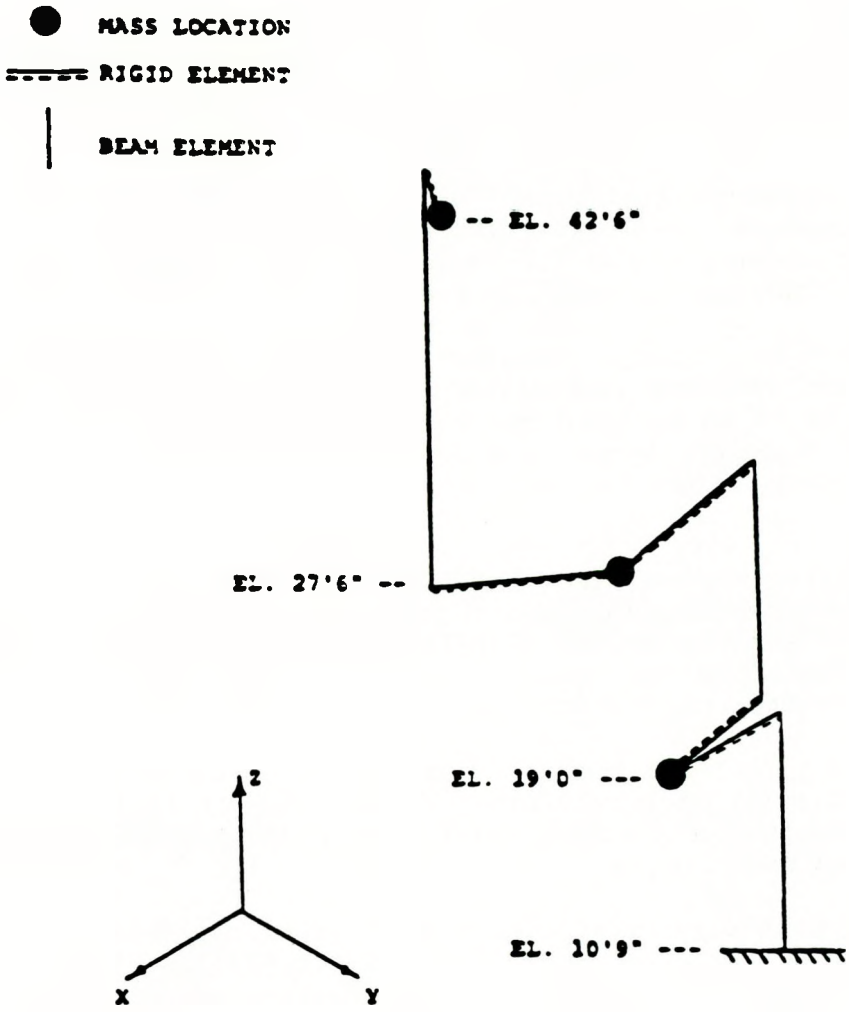

Figure 4.10. Surry Power Station Safeguards Area Structural Model

height to elevation 42.5 ft. Reinforced concrete shear walls and diaphragms transmit lateral loads to its base. The roof is a steel frame metal deck and concrete slab.

Figure 4.11 shows the 3-D fixed base model used to calculate the nominal eigen values and vectors. The containment spray pumps enclosure significant modes of vibration are at 10.82 and 21.0 Hz accounting for 20 and 52 percent of the mass in a N-S direction In the orthogonal direction, E-W the first significant mode of vibration is 21.6 Hz with 43 percent of the mass participating.

Emergency Generator Enclosure. The emergency generator enclosure is a rectangular structure 64 ft x 110 ft founded on a perimeter strip footing ranging in elevation from 3.5 ft to 20.5 ft. Reinforced concrete shear walls and diaphragms transmit lateral loads to its base.

The emergency generator enclosure foundation was modeled as a rigid, massless and embedded equivalent circular plate at an average footing elevation 13 ft in an idealized half-space. The soil strain compatible properties represent those at a depth of half the characteristic length (cl = 47.ft) below the foundation elevation.

Recognized as a very stiff structure relative to the soil and since the only required response is at the free-field elevation (27.5 ft), the entire mass properties of the structure (all six degrees of freedom) were calculated about the foundation reference point. A single rigid massless element translates the response to the desired elevation of 27.5 ft. Figure 4.12 shows the 3-D SSI model of the emergency generator enclosure.

Intake Structure. The intake structure is a rectangular structure 74 ft x 180 ft founded on a reinforced concrete mat 3 ft thick at elevation -9.25 ft. Reinforced concrete shear walls and diaphragms transmit lateral loads to its base.

Recognized as a very stiff structure relative to the soil and since the only required response is at the free-field elevation (27.5 ft) the structural model is simplified. The entire mass properties of the structure, all six degrees of freedom, were calculated about the foundation reference point. A single rigid, massless element translates the response to the desired elevation of 27.5 ft. Figure 4.13 shows the 3-D SSI model of the intake structure.

Response Results. For each of these structures, the dynamic structural response for each of the ten suites of time histories was computed at each of the three earthquake excitation levels. From the computed time history responses at the different floor levels, response spectra were generated. As examples of the output, the computed response spectra for the 2 SSE acceleration range for each structure are shown in Figures 4.14 through 4.20. In each figure, spectra in the E-W, N-S and Vert directions are shown. Each spectra plot has several building elevations

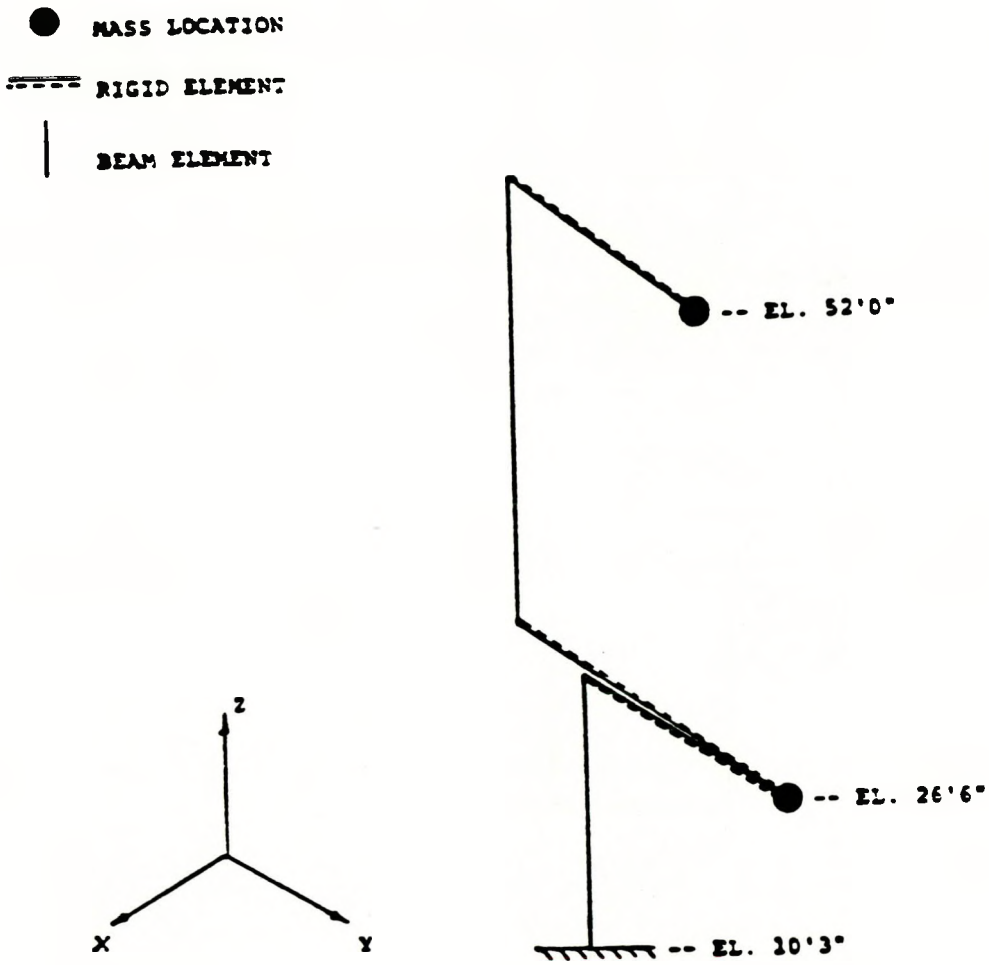

Figure 4.11. Surry Power Station Containment Spray Pump Enclosure Stuctural Model

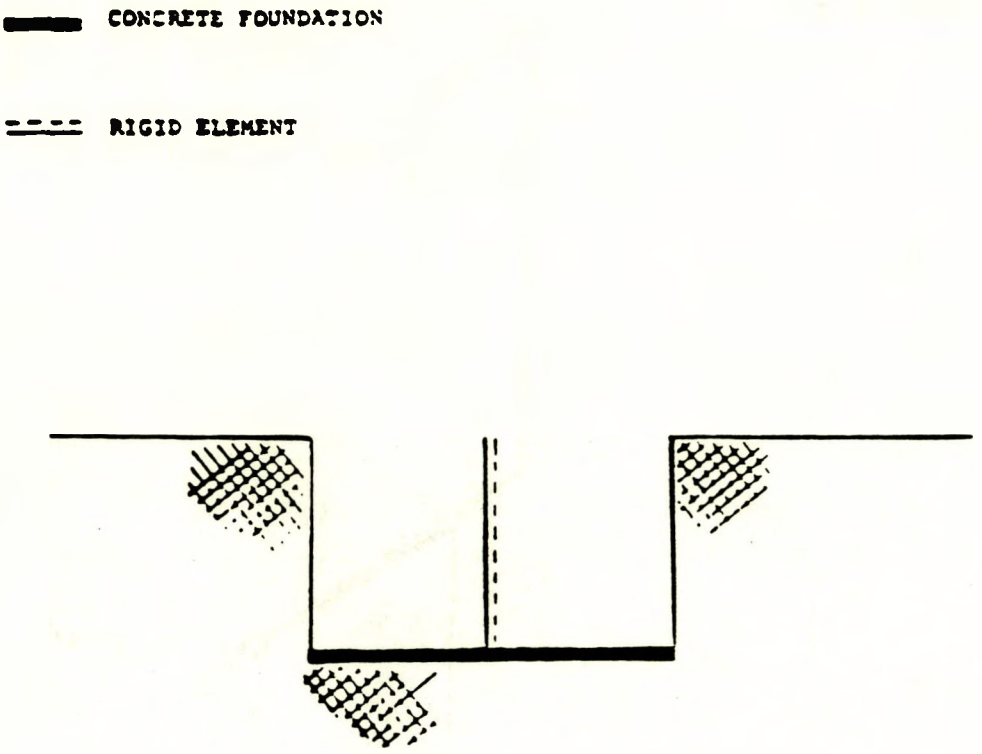

Figure 4.12. Surry Power Station Emergency Generator Enclosure SSI Model

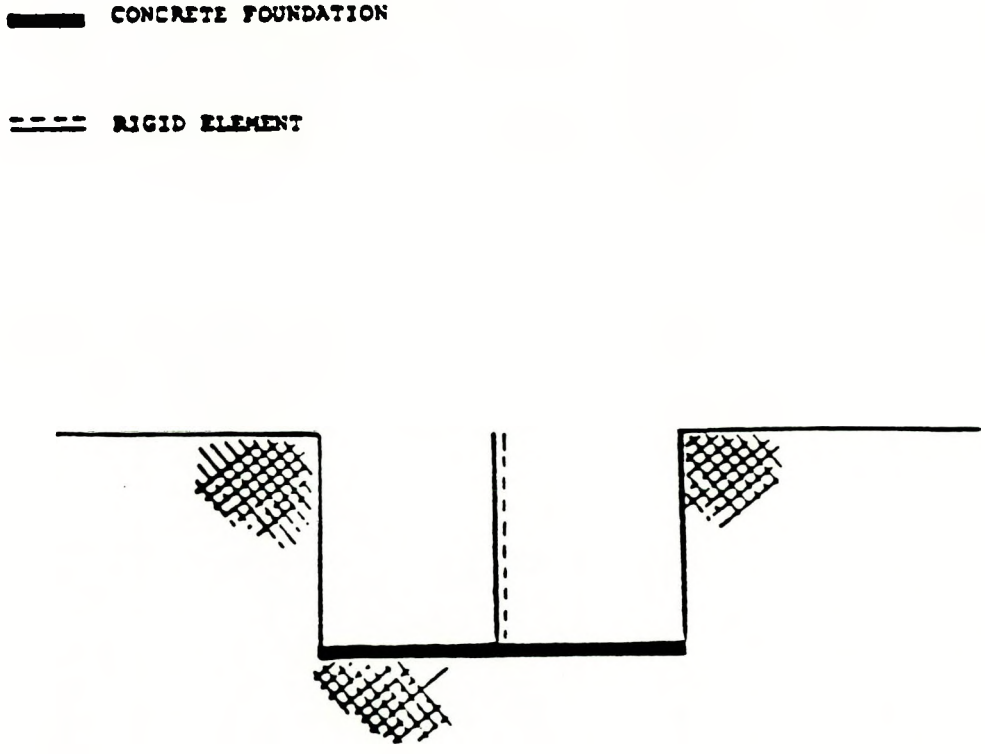

Figure 4.13. Surry Power Station Intake Structure SSI Model

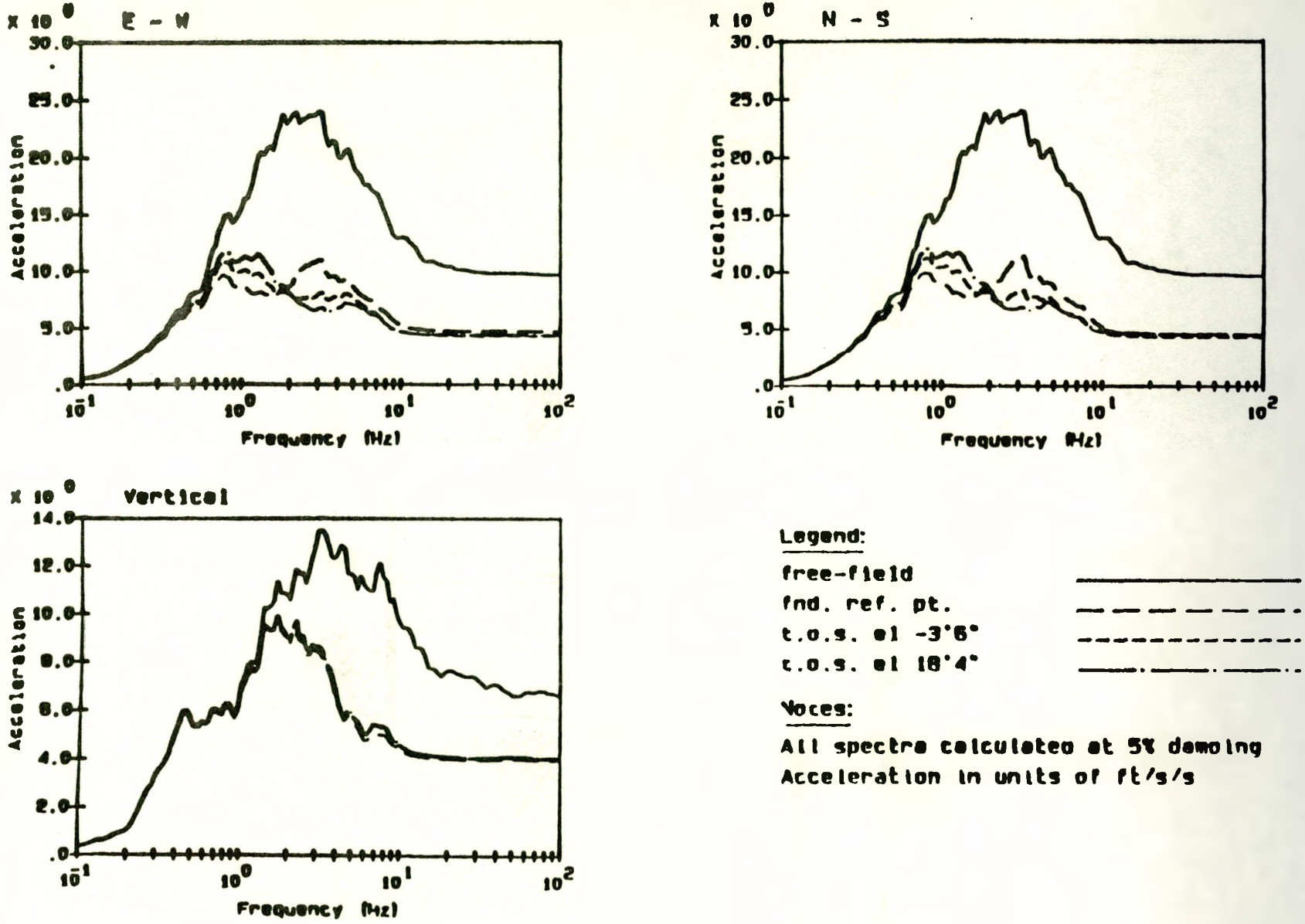

Figure 4.14a. Surry Nuclear Power Plant Reactor Containment Internal Building Instructure Response Acceleration Range 2

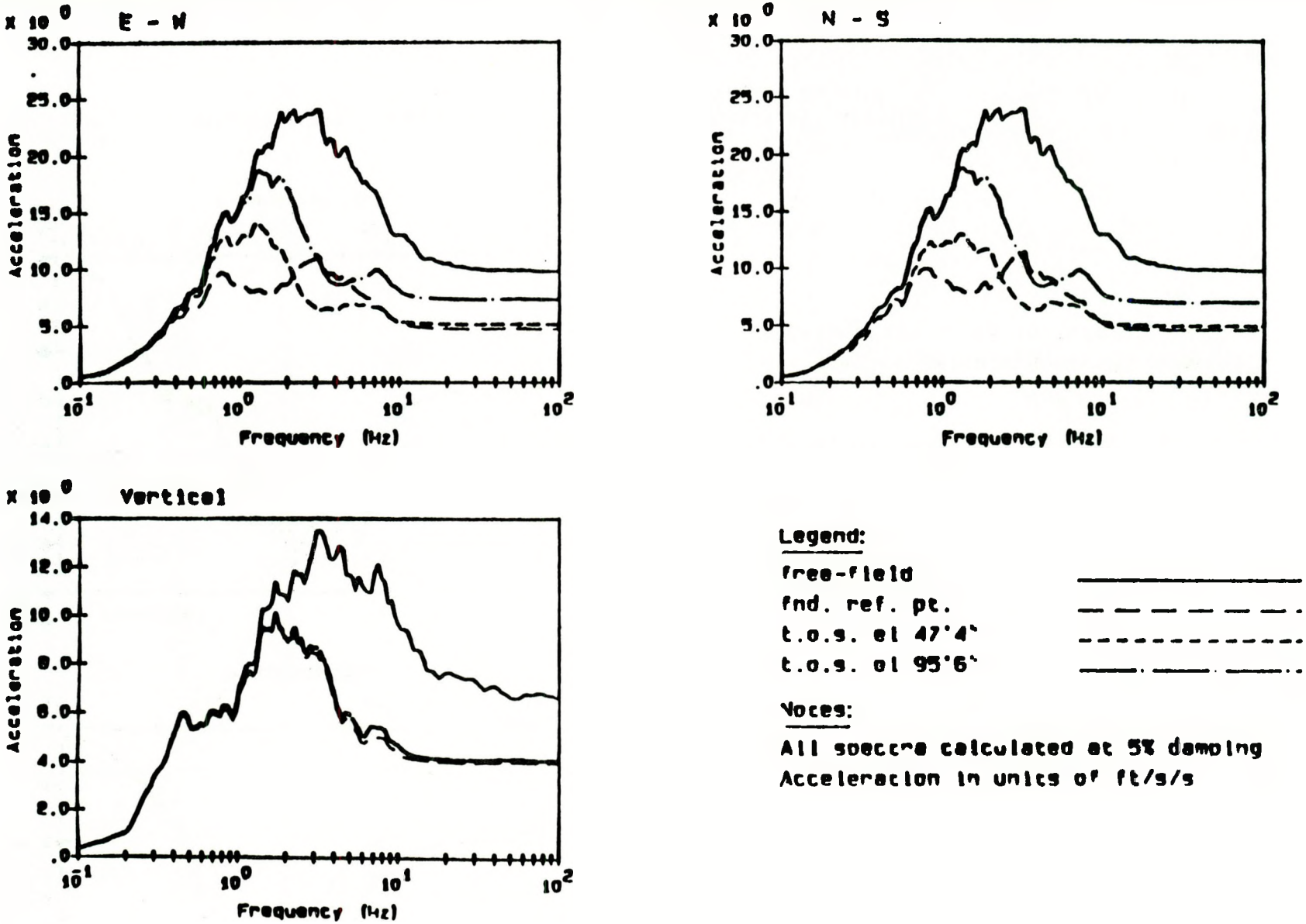

Figure 4.14b. Surry Nuclear Power Plant Reactor Containment Internal Building Instructure Response Acceleration Range 2

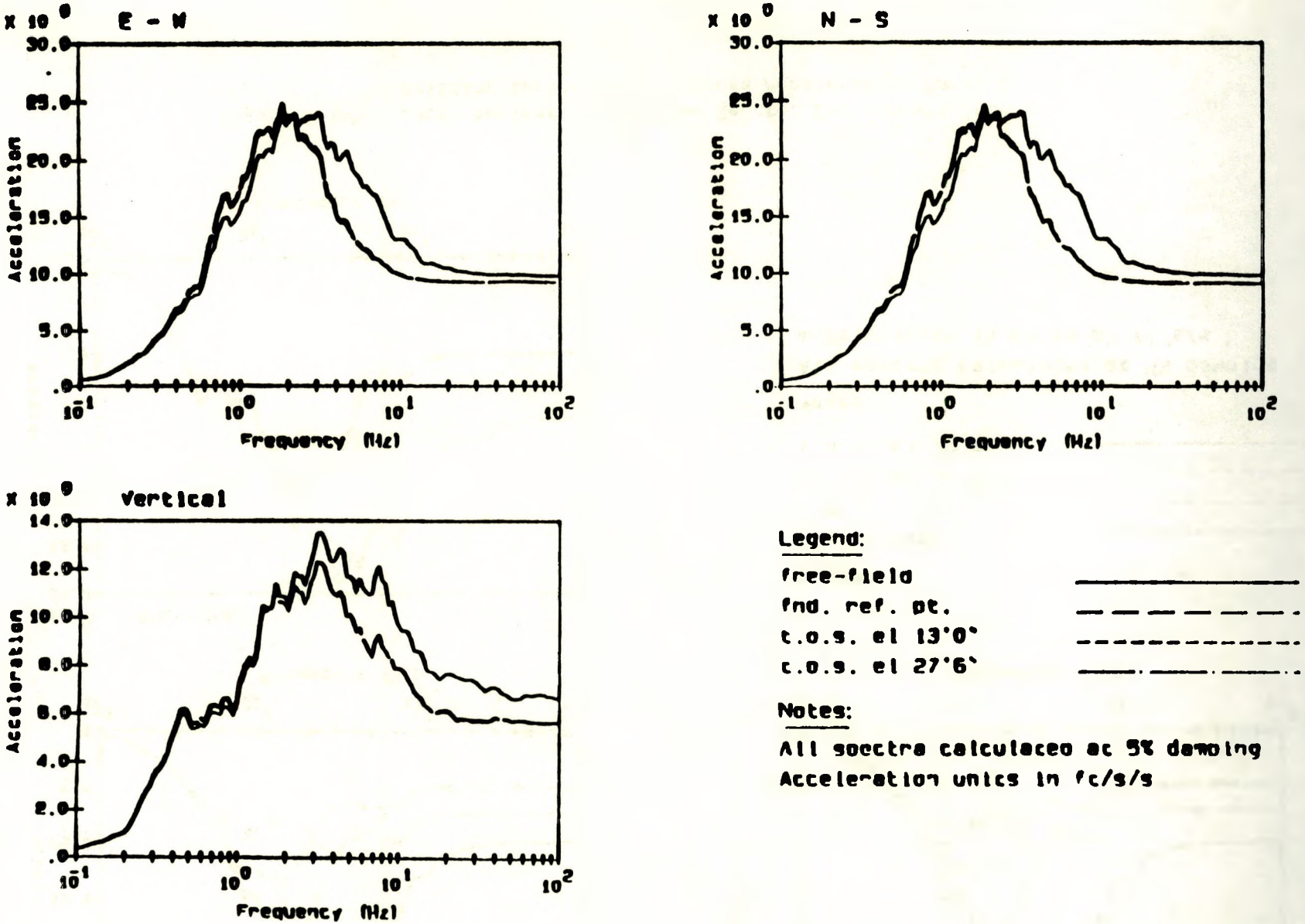

Figure 4.15a. Surry Nuclear Power Plant Auxiliary Building
Instructure Response Acceleration Range 2

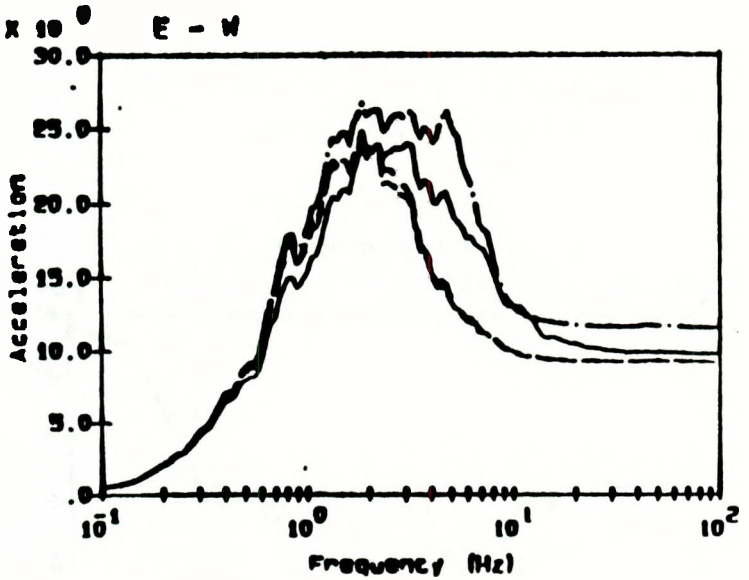

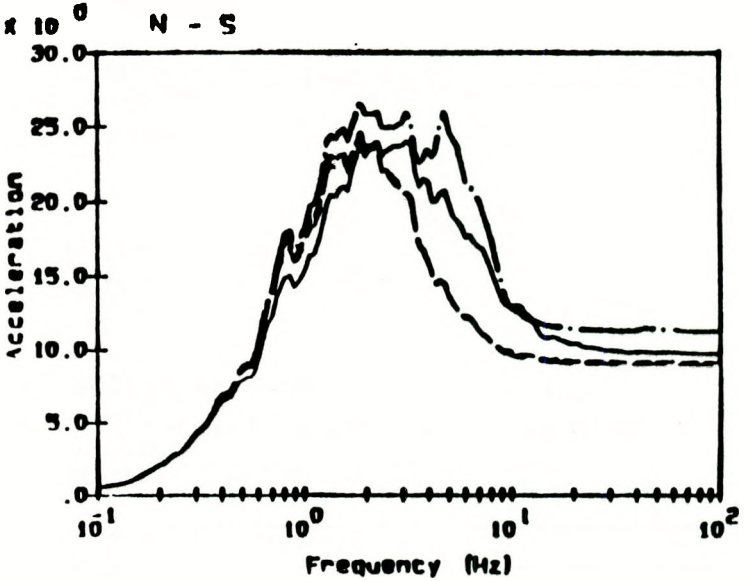

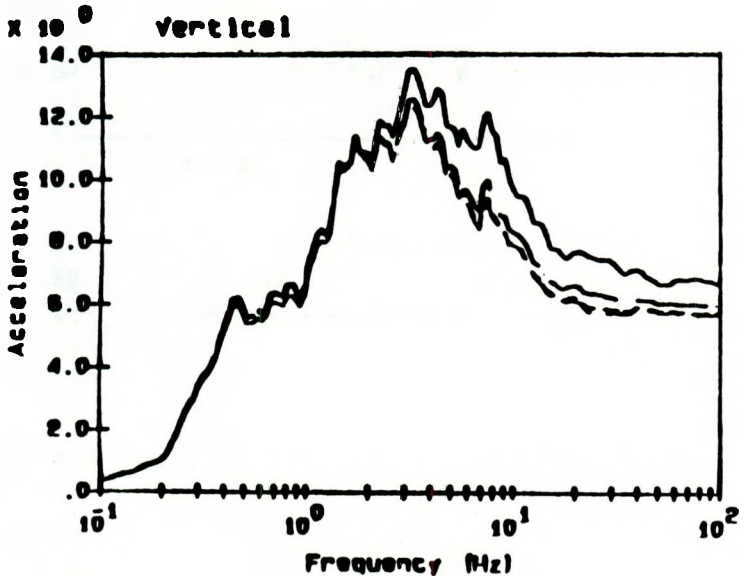

Legend:

free-field

fnd. ref. pt.

t.o.s. el 45'10"

t.o.s. el 66'0"

Notes:

All spectra calculated at 5% damping

Acceleration units in ft/s/s

Figure 4.15b. Surry Nuclear Power Plant Auxiliary Building Instructure Response Acceleration Range 2

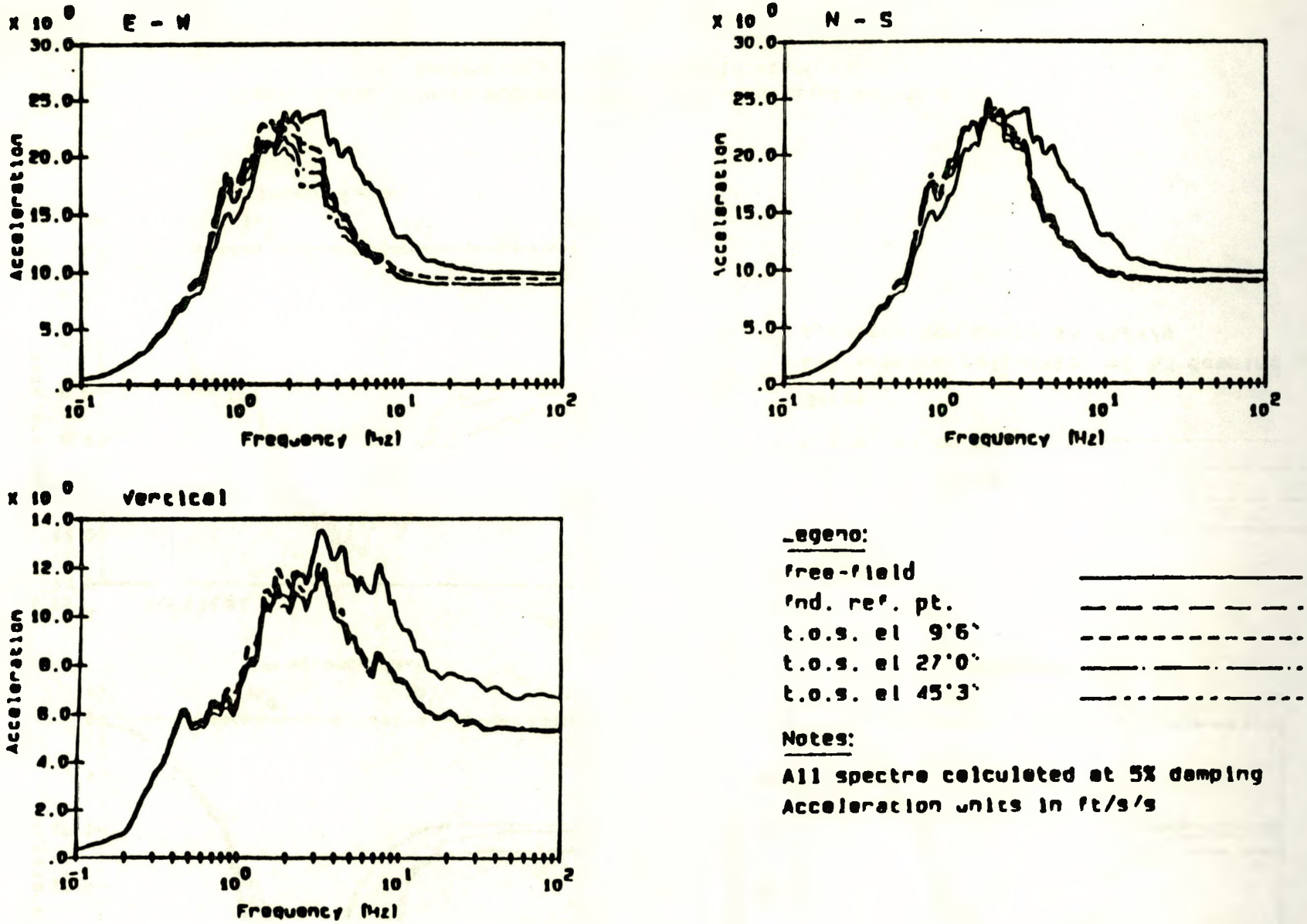

Figure 4.16a. Surry Nuclear Power Plant Control Room Structure Instructure Responses Acceleration Range 2

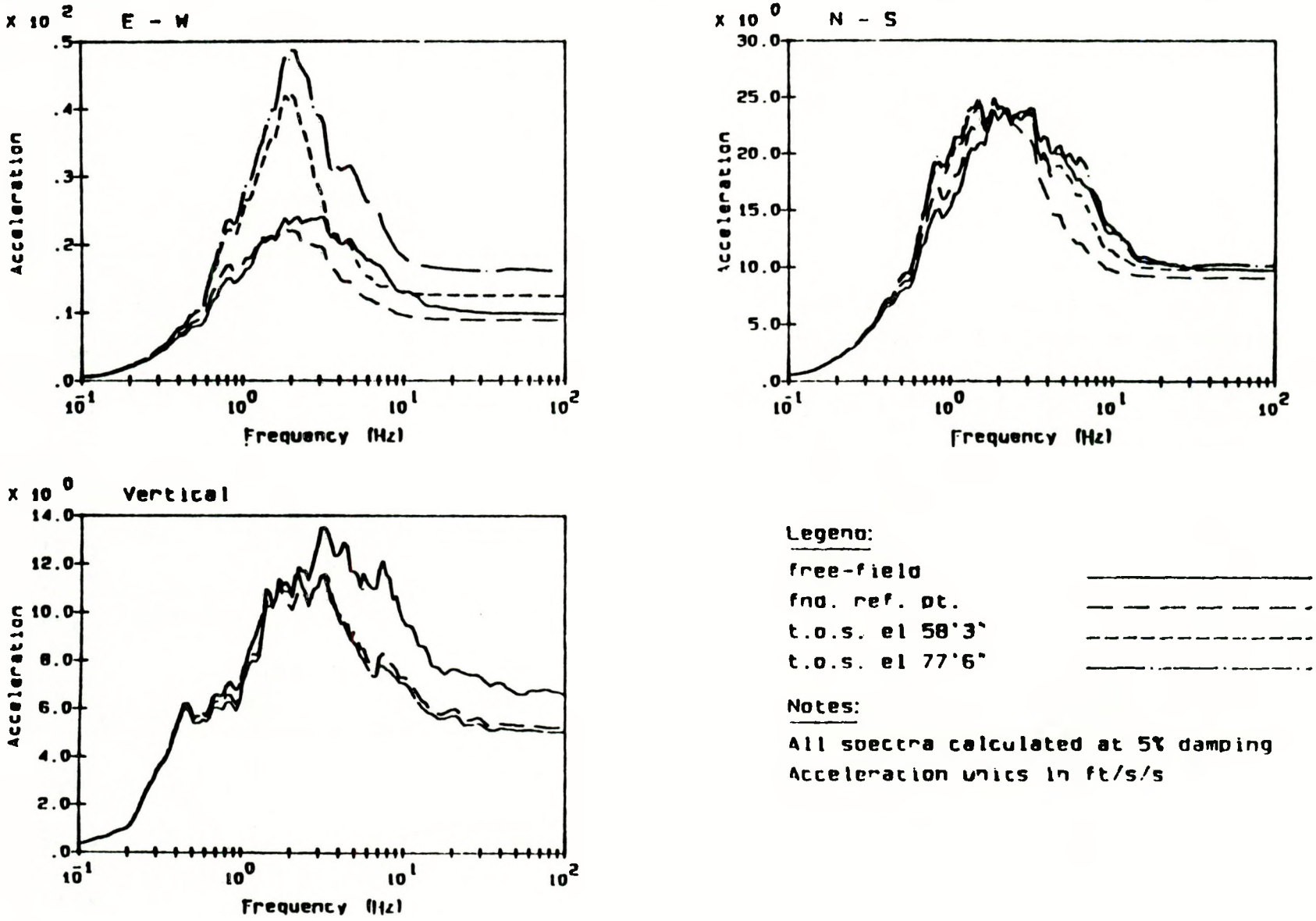

Figure 4.16b. Surry Nuclear Power Plant Control Room Structure Instructure Responses Acceleration Range 2

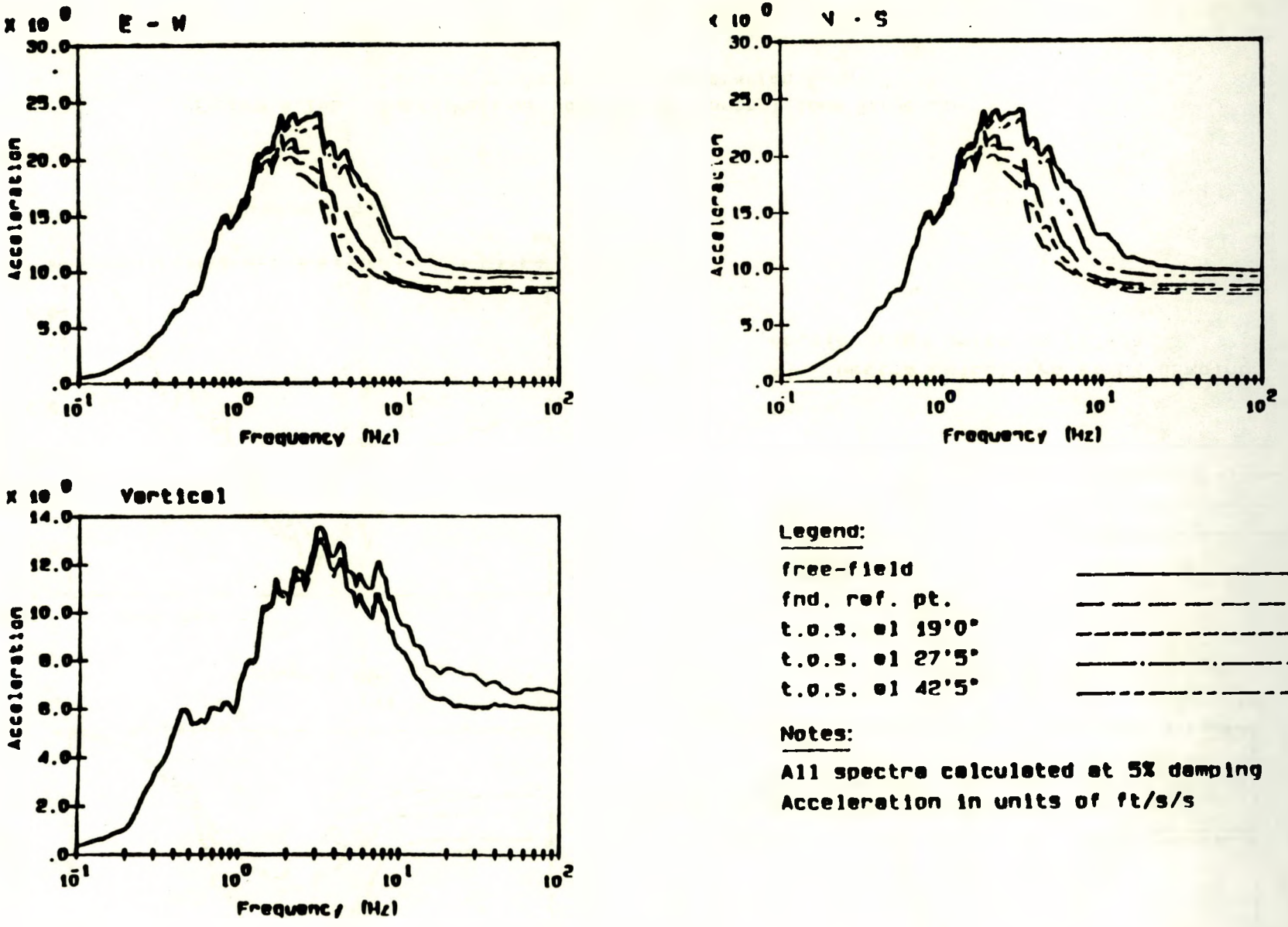

Figure 4.17. Surry Nuclear Power Plant Safeguards Building Instructure Responses Acceleration Range 2

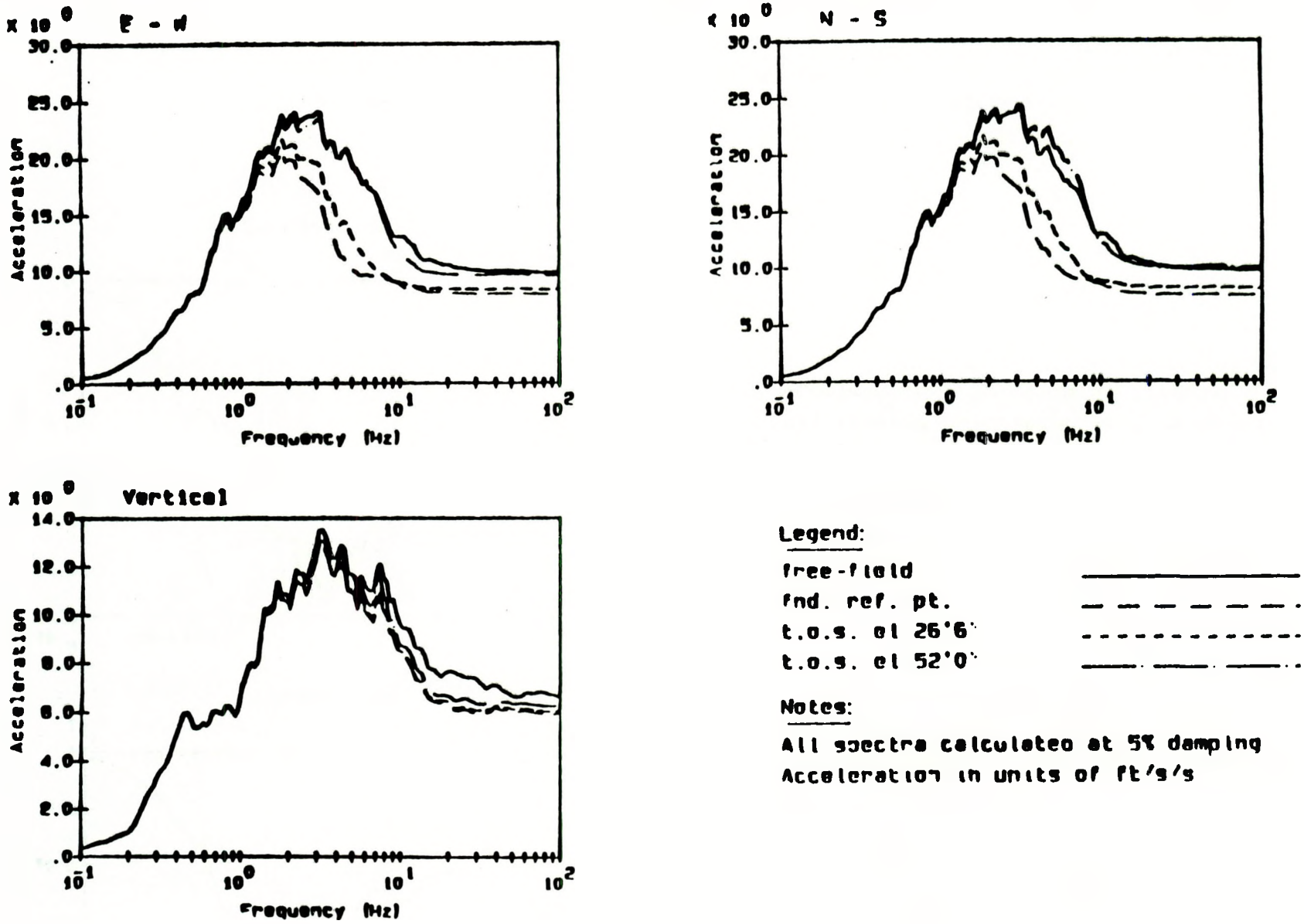

Figure 4.18. Surry Nuclear Power Plant Containment Spray Building Instructure Responses Acceleration Range 2

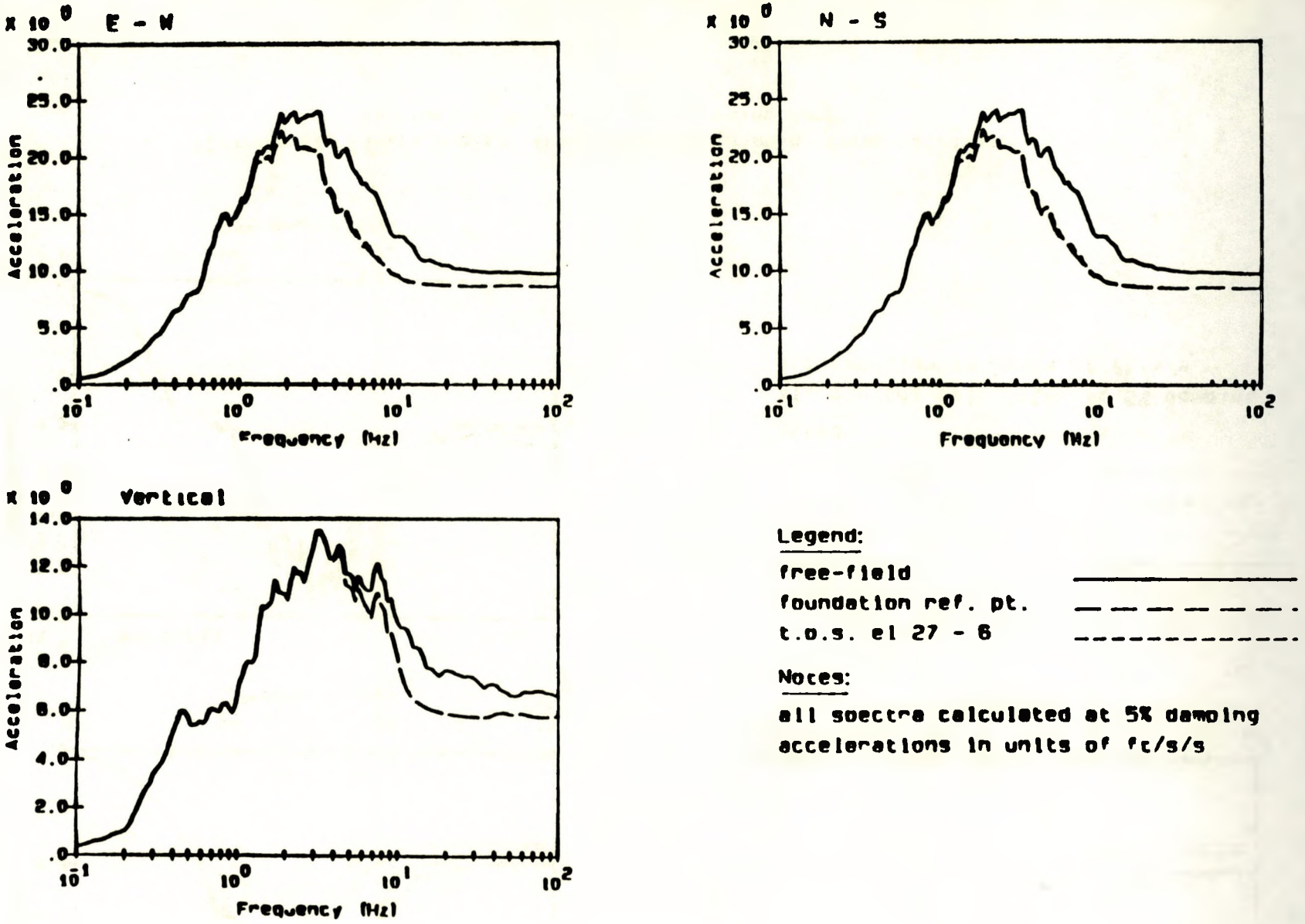

Figure 4.19. Surry Nuclear Power Plant Emergency Generator Enclosure Instructure Responses Acceleration Range 2

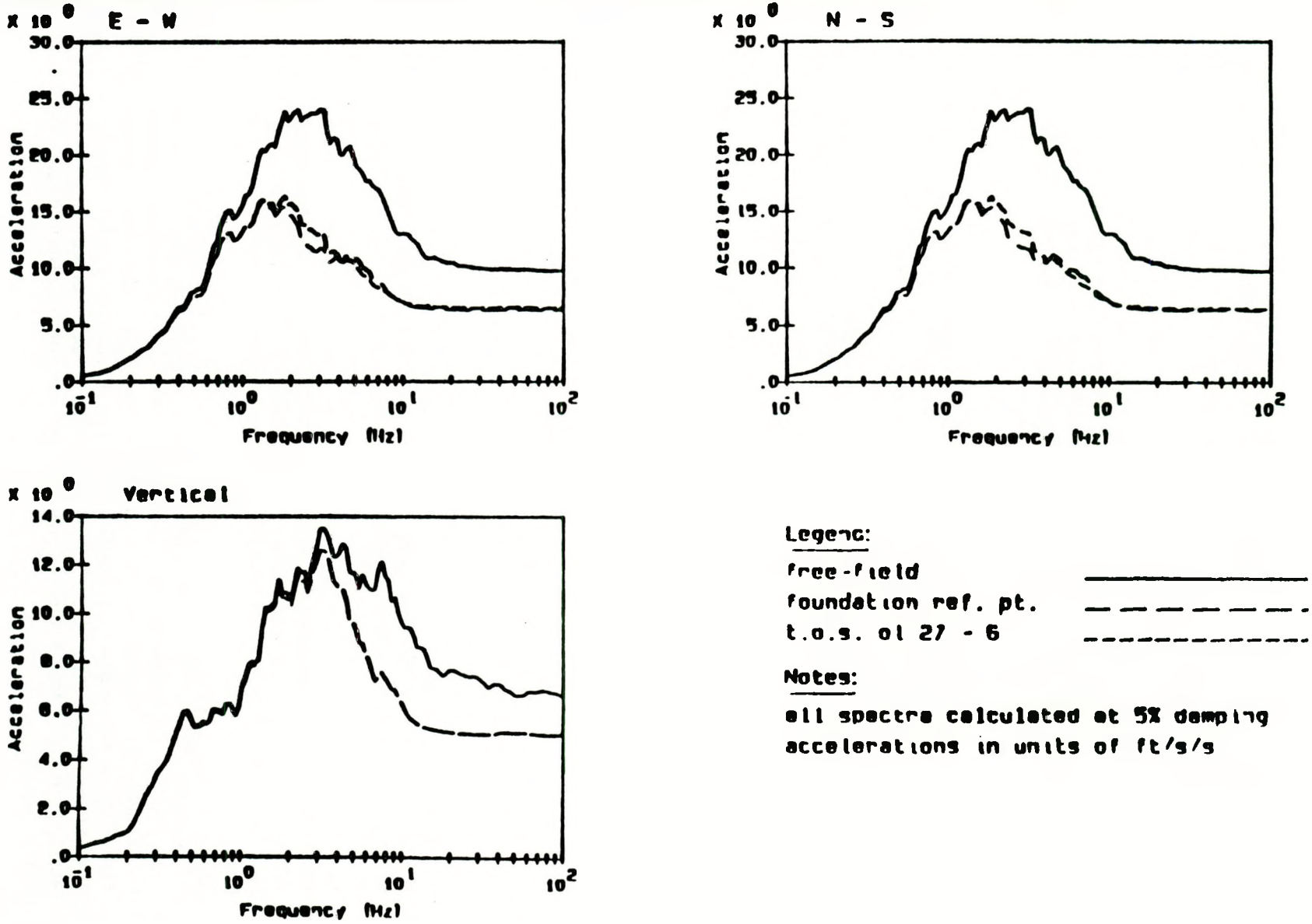

Figure 4.20. Surry Nuclear Power Plant Intake Structure Instructure Responses Acceleration Range 2

corresponding to major floor slabs). Similar spectra are given in Appendix A for the other acceleration ranges. Taken together, the spectra at the three different acceleration ranges provide all the response input needed.

4.2.4 Safety-Related Component Responses

The in-structure spectra presented and discussed in the previous section are used to determine safety-related component response. Assuming that the dynamic characteristics of a given component can be represented by a single dominant mode of vibration, the component response can be approximated by the spectral acceleration of the appropriate in-structure spectra at the frequency of the dominant mode.

Thus, at each structural location, numerical response values at different frequencies or frequency ranges are computed directly from these spectra. These ranges span the probable natural frequencies of the components housed at that location. The median zero period acceleration response is calculated from the ten values given by the probabilistic response analysis assuming a lognormal distribution. The median response over a frequency range is over the range from the median spectra given by the ten earthquake simulations. Given the natural frequency of the component of interest, the appropriate frequency interval and component response is then defined. Numerical values of the median component responses for the three levels of ground motion (1 SSE, 2 SSE, and 3 SSE) taken from these spectra are presented in Appendix B.

4.2.4.1. Responses in Terms of Peak Ground Acceleration

The responses in Appendix B are given at three peak ground acceleration values (0.15g, 0.30g, and 0.45g). One could directly interpolate between these three values to obtain any specified response at any arbitrary value of peak ground acceleration.

However, a more direct approach which greatly simplifies computation of the component failure probabilities is to compute the average ratio between the median PGA and the median response spectral acceleration at each specified component location. Figures 4.21 through 4.25 are plots of the response location accelerations in each building (at various building elevations) versus PGA. It can be seen that a linear relation exists up to free field accelerations of 0.4g or greater. Furthermore, for those curves which show significant non-linearity at higher acceleration levels, the linear relation provides a conservative estimate of the local response.

From these figures, ratios between the various responses and PGA were determined, as listed in Table 4.7. (Note that not all responses listed in Appendix B are included on this table, as not all floor slabs supported critical components identified on the seismic fault trees.) Using these response amplification ratios, the local spectral acceleration response at any floor level of any of the buildings can be computed at any pga level.

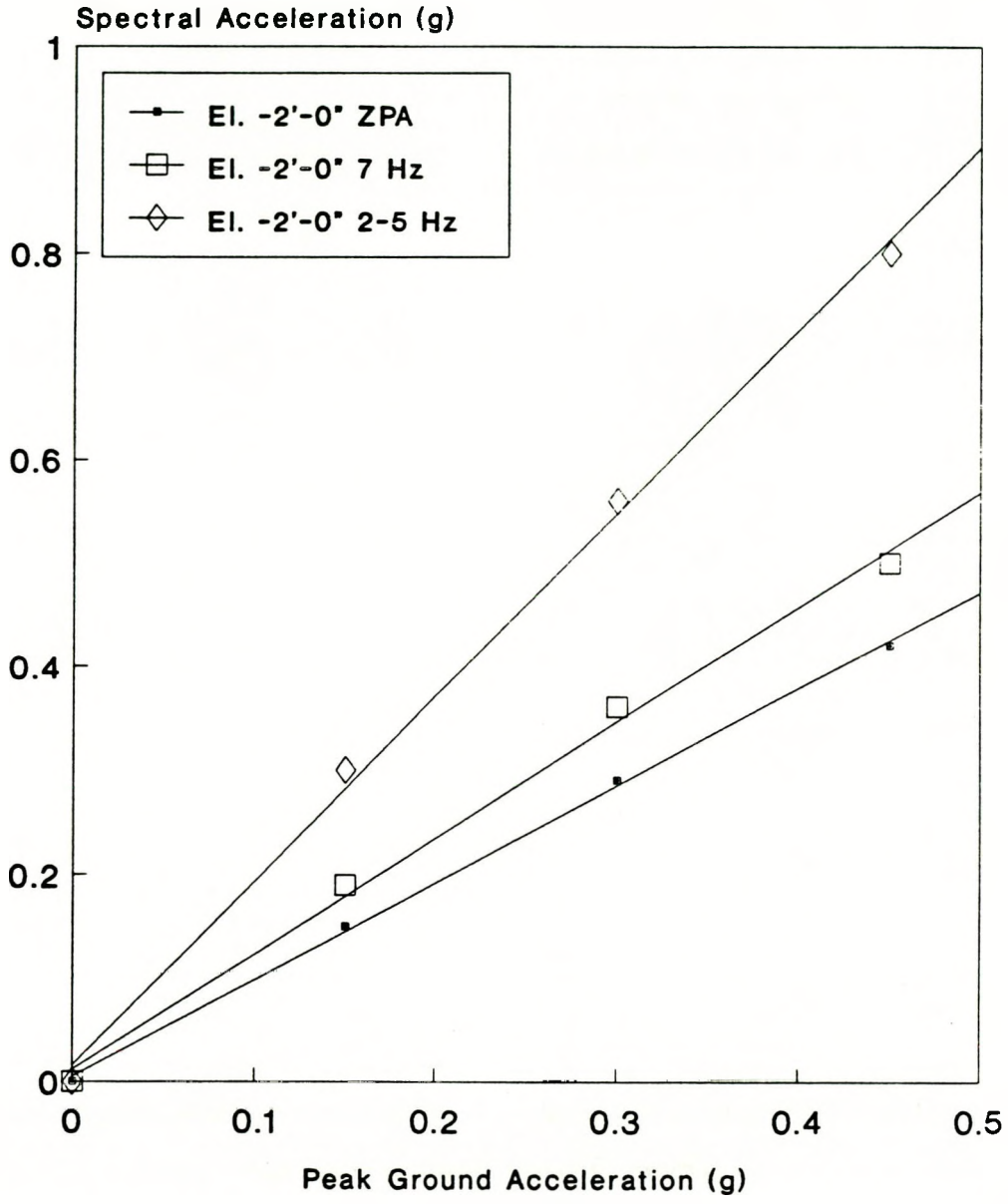

Figure 4.21a. Auxiliary Building Median Responses

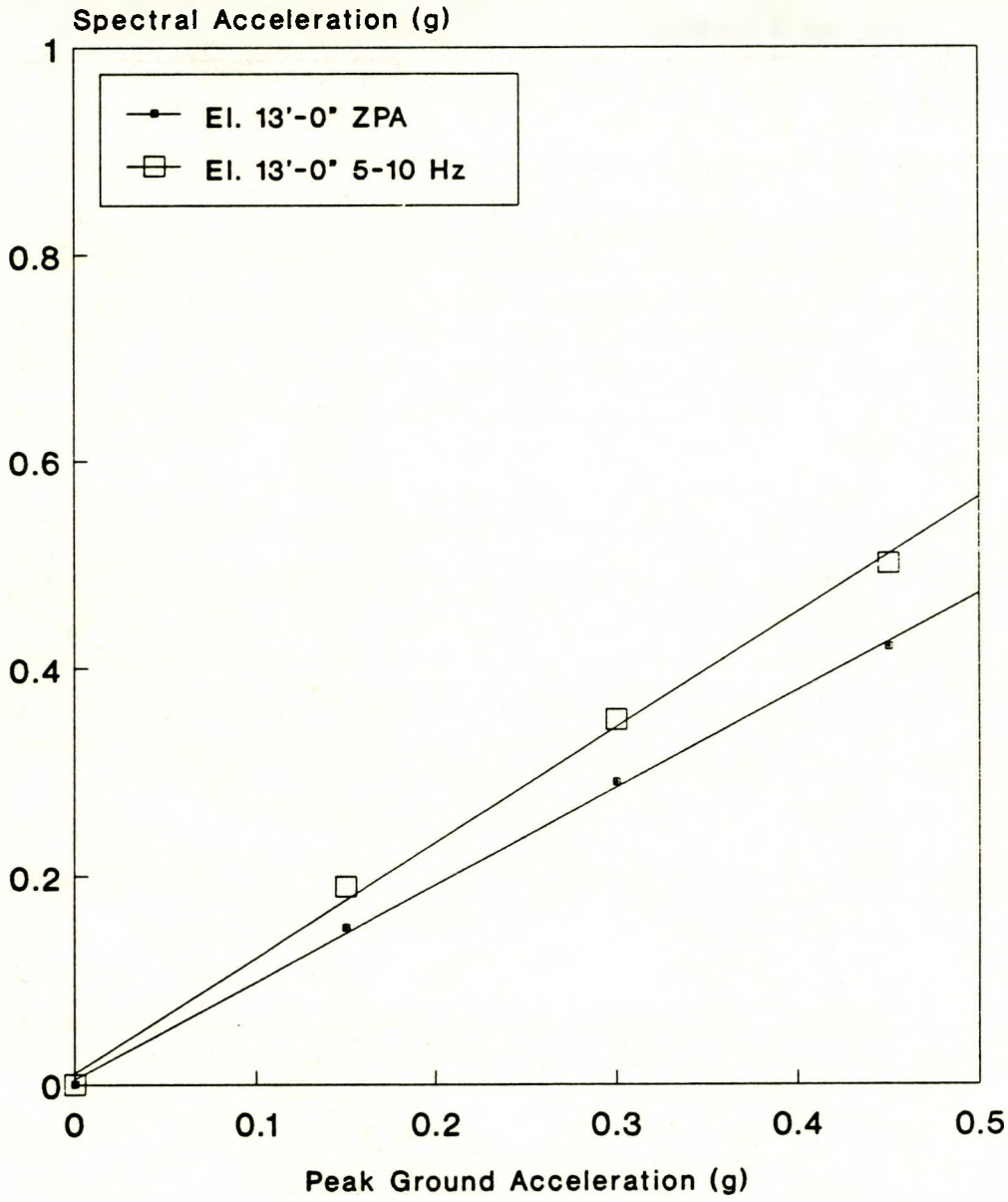

Figure 4.21b. Auxiliary Building Median Responses

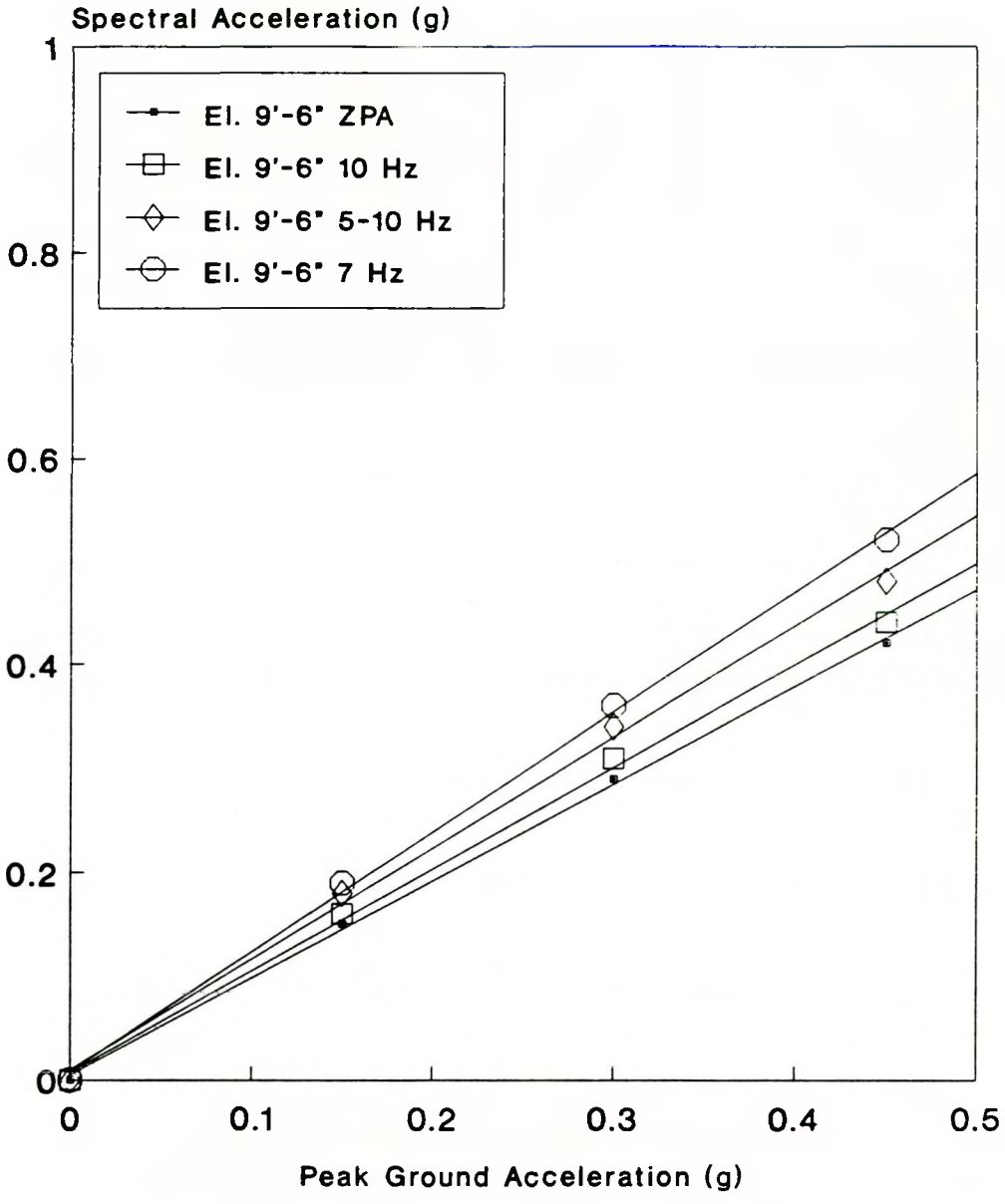

Figure 4.22 Control Room Structure Median Responses

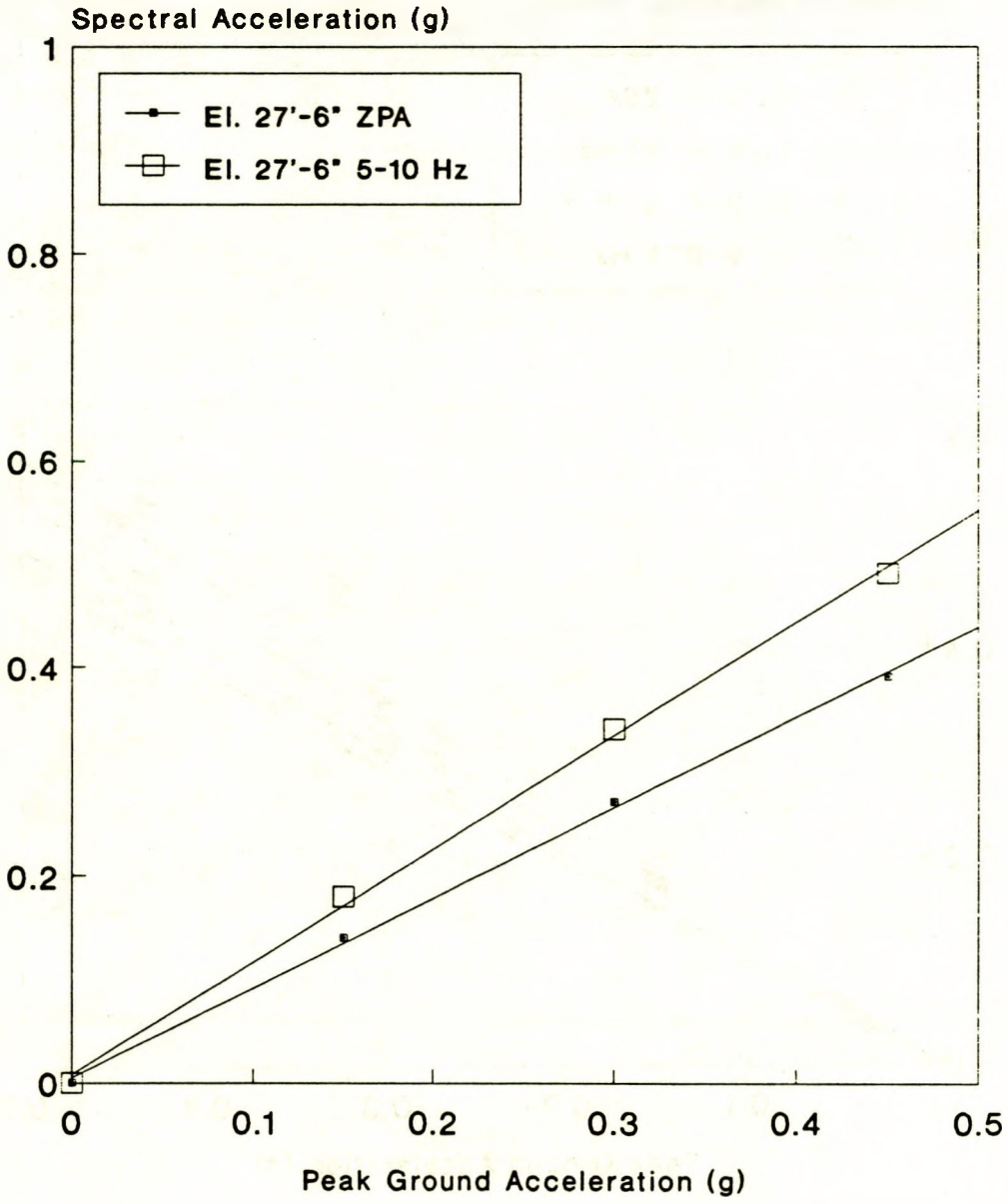

Figure 4.23. Emergency Generator Enclosure Median Responses

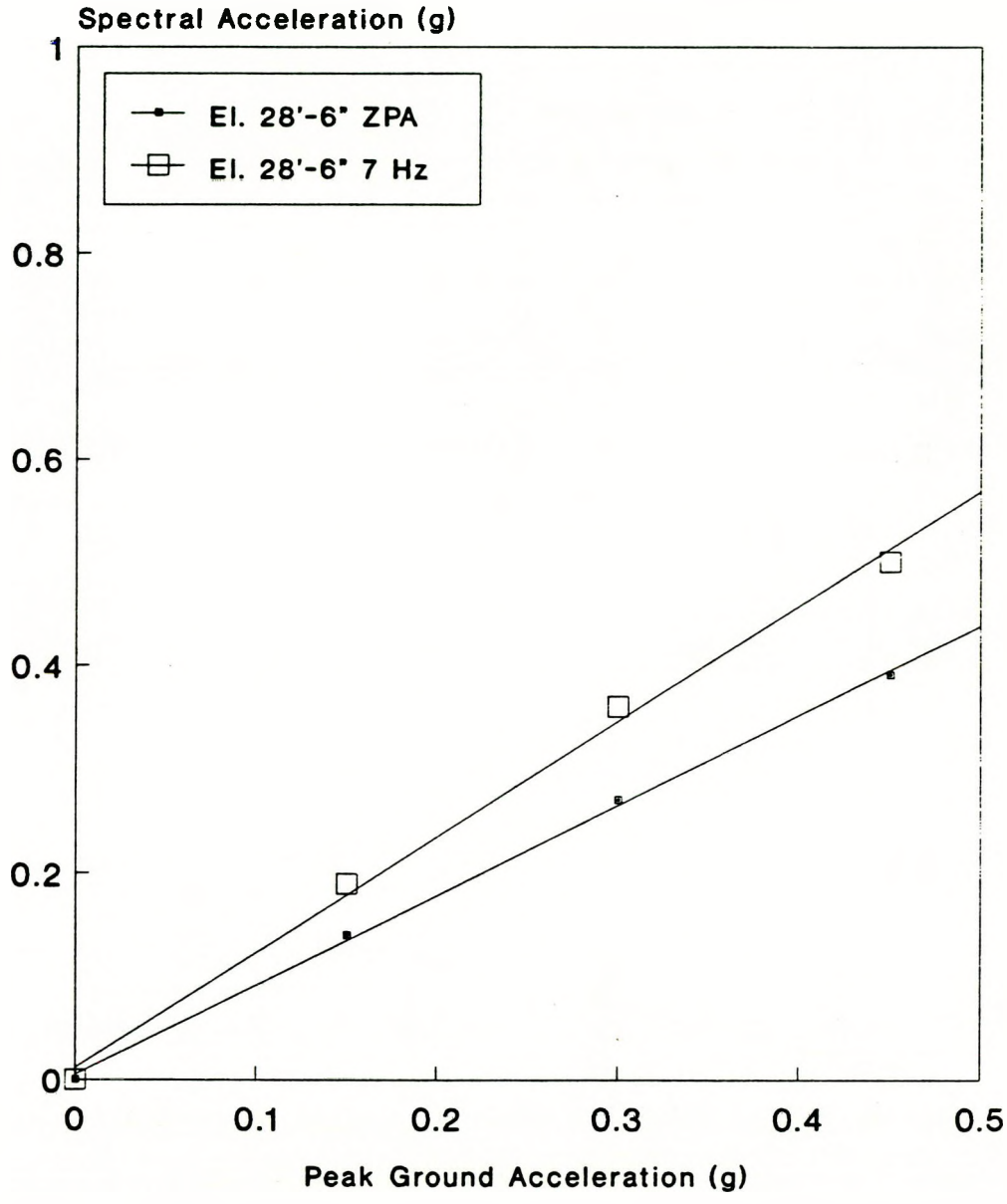

Figure 4.24. Safeguards Area Median Responses

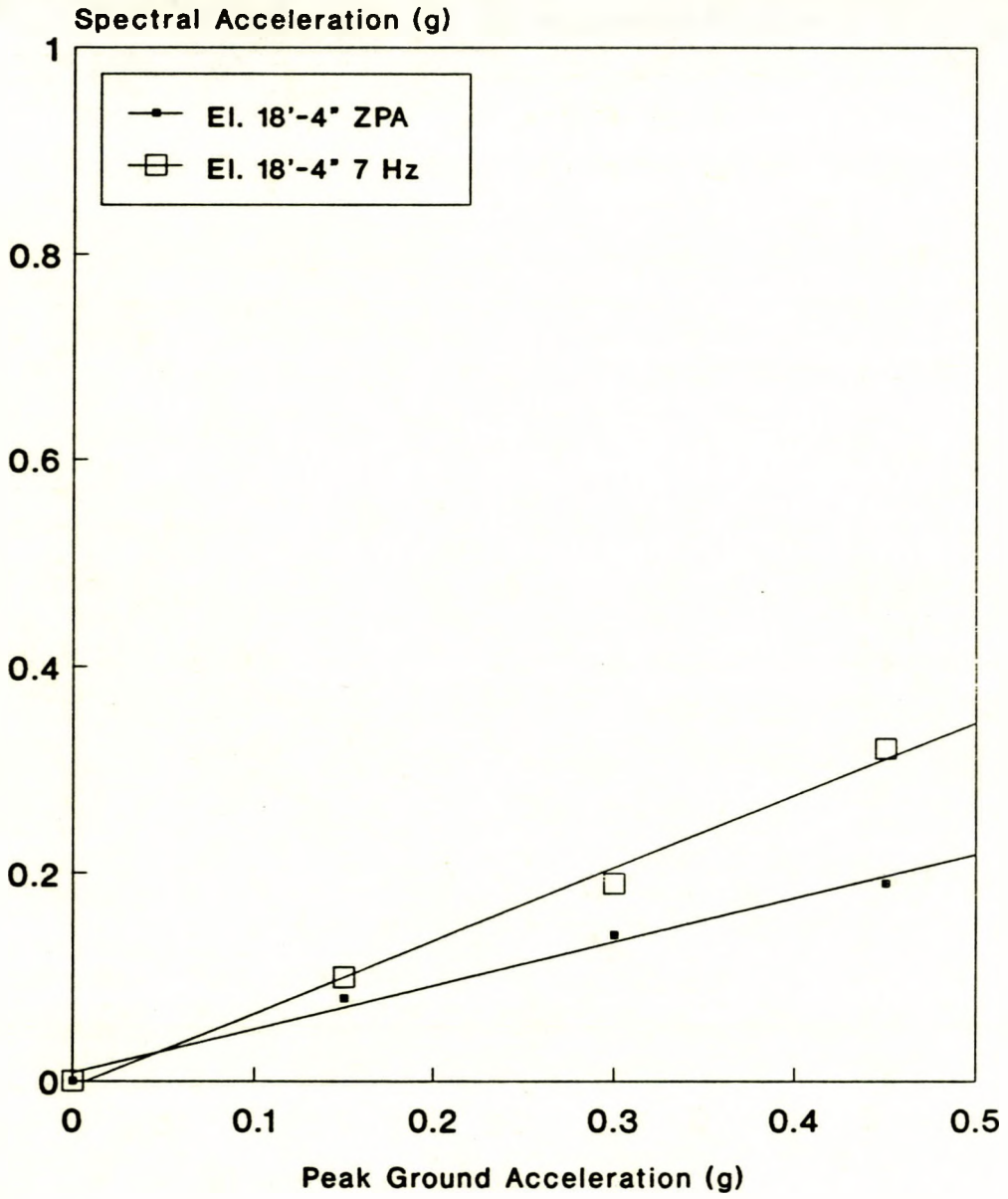

Figure 4.25. Reactor Building Median Responses

Table 4.7

Surry Seismic Response Locations

Response Number	Location	Elevation	Frequency	Multiple of PGA
1	Yard (PGA)		ZPA	1.0
2	Service Building (SB)	9'6"	ZPA	1.0
3	" "	"	5-10	1.2
4	" "	"	7	1.3
5	" "	"	10	1.1
6	" "	27'-0"	ZPA	0.9
7	" "	"	5-10	1.2
8	Aux. Building (AB)	-2'-0"	ZPA	1.0
9	" "	"	5	1.5*
10	" "	"	7	1.3
11	Safeguards Area (SG)	27'-6"	ZPA	0.9
12	" "	"	7	1.2
13	Turbine Building (TB)	15'-0"	ZPA	1.0+
14	Cable Vault/Tunnel (CVT)	15'-0"	5-10	1.2+
15	Reactor Building (RB)	18'-4"	ZPA	0.5
16	" "	"	7	0.6
17	" "	27'-7"++	7	0.8

*Estimated from 2-5 and 7 H values. Not used.
+Used Auxiliary Building at elevation 13'-0".
++Used RB 47'-4".

4.2.4.2 Variability in Response

Variability in responses (floor and spectral accelerations) was assigned based on SSMRP results (Ref. 10). Confidence bounds were computed for the final core damage probabilities using both random (irreducible) and systematic (modeling) uncertainties. The uncertainties (expressed as standard deviations of the logarithms of the responses) are shown below:

Quantity	Random	Systematic
Peak Ground Acceleration	0.25	See cross-
Floor Zero Period Acceleration	0.35	reference
Floor Spectral Acceleration	0.45	table in Appendix C

4.2.4.3 Correlation

In computing the probability of cut sets involving correlated component failures, it is necessary to consider correlations both in the responses and in the fragilities of each pair of components in the cut set. Once this is done, the correlation coefficient between any two component failures is computed from the expression

$$\rho = \frac{\beta_{R1}\beta_{R2}}{\sqrt{\beta_{R1}^2 + \beta_{F1}^2}\ \sqrt{\beta_{R2}^2 + \beta_{F2}^2}}\ \rho_{R1R2} + \frac{\beta_{F1}\beta_{F2}}{\sqrt{\beta_{R1}^2 + \beta_{F1}^2}\ \sqrt{\beta_{R2}^2 + \beta_{F2}^2}}\ \rho_{F1F2}$$

in which

ρ = correlation coefficient between the failure of components 1 and 2

β_{R1}, β_{R2} = standard deviation of the logarithms of the responses of components 1 and 2

β_{F1}, β_{F2} = standard deviations of the logarithms of the fragilities of components 1 and 2

ρ_{R1R2} = correlation coefficient between responses of components 1 and 2

ρ_{F1F2} = correlation coefficient between the fragilities of components 1 and 2

This relation shows that the correlation between the failure of any two components depends not only on the correlations between the respective responses and the respective fragilities, but also on the variances in the responses and fragilities.

With the correlation between the failure events in the cut set known, the evaluation of the cut set probability is performed by evaluating the multivariate probability distribution for the cut set. Methods for evaluating such correlated cut sets are described in Reference 3 of Chapter 1 of this report.

The pairwise correlations between the responses are assigned according to the rules on Table 4.8. Using the rules given and the definitions of the responses given on Table 4.7, the response correlation matrix shown in Table 4.9 results.

Inasmuch as there are no data as yet which prove or disprove correlation between fragilities, the fragility correlations between both like and unlike components were taken as zero.

In general, there exists some degree of correlation between any two components excited by the same earthquake by virtue of the common ground motion. However, it is not necessary to compute correlated failure probabilities when the degree of correlation between the failure events is small (e.g., less than 0.25) as the result will be very close to the uncorrelated value. By examining the response and (in general) the fragility correlations, it is possible to identify those pairs of components for which correlation effects may be neglected, and those for which correlation must be considered. In general, it is found that correlation between like components (identical components which are sensitive to the same spectral acceleration) in the same location should always considered as they are usually the most significant. However, while correlations between two unlike components can (in principle) exist, these are usually of lesser significance, and can usually be neglected, especially when dealing with components located on different floors of a building or in seperate buildings.

For Surry, a review of the response correlation table in conjunction with the fact that fragility correlations are taken as zero allowed screening of the components for those differing components which might be assigned correlation. For unlike components, it was found that only correlation between the RWST and the CST had any potential significance. By contrast, a number of identical components in the same location were found to be significantly correlated. These components are listed below:

a. 4 kV busses
b. 125 volt busses
c. diesel generators
d. PCS motor driven pumps
e. Pilot-operated relief valves

For these components, the correlation coefficient was computed and a proper evaluation of the correlated pairs of failures occurring in the various cut sets was made during quantification of the accident sequences.

Table 4.8

Rules for Assigning Response Correlation ρ_{R1R2}

1. Components on the same floor slab, and sensitive to the same spectral frequency range (i.e., ZPA, 5 to 10 Hz, or 10 to 15 Hz) will be assigned response correlation = 1.0.

2. Components on the same floor slab, sensitive to different ranges of spectral acceleration will be assigned response correlation = 0.5.

3. Components on different floor slabs (but in the same building) and sensitive to the same spectral frequency range (ZPA, 5 to 10 Hz or 10 to 15 Hz) will be assigned response correlation = 0.75.

4. Components on the ground surface (outside tanks, etc.) shall be treated as if they were on the grade floor of an adjacent building.

5. "Ganged" valve configurations (either parallel or series) will have response correlation = 1.0.

6. All other configurations will have response correlation equal to zero.

Table 4.9

Correlation Coefficients Between Responses - Surry

	1	2	3	4	5	6	7	8	9	10	11	12	13	14	15	16	17
1	1																
2		1	.5	.5	.5	.75											
3			1	.5	.5		.75										
4				1	.5												
5					1												
6						1	.5										
7							1										
8								1	.5								
9									1	.5							
10										1							
11											1	.5					
12												1					
13	Table is Symmetric												1				
14														1			
15	All correlations zero														1	.5	
16	except those shown.															1	.75
17																	1

4.3 Seismic Fragilities

Component failure is taken as either loss of pressure boundary integrity or loss of operability. Failure (fragility) is characterized by a cumulative distribution function which describes the probability that failure has occurred given a value of loading. Loading may be described by local spectral acceleration or moment, depending on the component and failure mode. The fragilities are related to the appropriate local response to permit an accurate assessment of the effects of common-cause seismic failures in the evaluation of the accident sequences.

4.3.1 Generic Fragilities

A generic data base of fragility functions for seismically-induced failures was developed in the SSMRP (Ref. 10). As a first step, all components were grouped into generic categories. For example, all motor operated valves located on piping with diameters between 2-1/2 and 8 inches were placed into a single generic category, and similarly, all motor control centers were placed into another generic category.

Fragility functions for the generic categories were developed based on a combination of experimental data, design analysis reports, and an extensive expert opinion survey. The experimental data utilized in developing fragility curves were obtained from the results of component manufacturer's qualification tests, independent testing lab failure data and data obtained from the extensive U.S. Corps of Engineers SAFEGUARD Subsystem Hardness Assurance Program. These data were critically examined for applicability and then statistically combined with the expert opinion survey data to produce the fragility curves for the SSMRP generic component categories reported in Reference 10.

Finally, a review of more recent site-specific component fragilities contained in the Lawrence Livermore data base (Ref. 11) was made. Based on these reviews, several of the SSMRP generic fragilities in Reference 10 were updated.

The final generic categories and the corresponding fragility medians and uncertainties are shown in Tables 4.10 and 4.11. These fragilities are used as the starting point in the simplified seismic PRA. As in the use of any generic data base, one must be cognizant of the source of the data and the equipment to which it applies. An important aspect of using this data is to examine the equipment in the plant being analyzed and compare it with the data base for which the generic fragilities were developed. Any deviation is noted and examined carefully, and new site-specific fragilities developed as necessary.

Fragilities for electrical components represent a special problem in that there is a wide variety of electrical gear found within a plant. Typically, all this gear is enclosed in switchgear cabinets or motor control centers. The two lowest failure modes that were identified in the SSMRP fragility data base were relay chatter and inadvertent trip of circuit

Table 4.10

Generic Component Categories

Fragility Category	Component Class	Typical Components	Frequency (Hz)
1	LOSP	Ceramic Insulators	ZPA
2	Relays		5-10
3	Circuit Breakers		5-10
4	Batteries		ZPA
5	Battery Racks		ZPA
6	Inverters		5-10
7	Transformers	4KV to 480V and 480 to 120V	10
8	Motor Control Centers	Control for ESF Pumps and Valves	5-10
9	Aux. Relay Cabinets		5-10
10	Switchgear (Inc. Transformers, Buses and Breakers)	416V and 480V	5-10
11	Cable Trays		ZPA
12	Control Panels and Racks	RPS Process Control	5-10
13	Local Instruments	Misc. Pressure and Temperature Sensors	5-35
14	Diesel Generators	4160 AC Emergency Power Units	22
15	Horizontal Motors	Motor-Generator Sets	ZPA
16	Motor-Driven Pumps and Compressors	AFWS, RHR, SIS, Charging Pumps, Lube Oil Pumps, Diesel Starting Compressors	7
17	Large Vertical, Centrifugal Pumps (Motor-Drive)	Service Water Pumps	5
18	Large Motor-Operated Valves (>10")		ZPA
19	Small Motor-Operated Valves (<10")		ZPA
20	Large Pneumatic/Hydraulic Valves	Includes MSIV, ADP, and PORV	ZPA
21	Large Check and Relief Valves		ZPA
22	Miscellaneous Small Valves (<8")		ZPA

Table 4.10

Generic Component Categories (Concluded)

Fragility Category	Component Class	Typical Components	Frequency (Hz)
23	Large Horizontal Vessels and Heat Exchangers	Pressurizer Relief Tank, CCW Heat Exchangers	ZPA
24	Small to Medium Heat Exchangers and Vessels	Boron Injection Tank	20
25	Large Vertical Storage Vessels with Formed Heads	RHR Heat Exchanger, Accumulator Tank	ZPA
26	Large Vertical Flat-Bottomed Storage Tanks	CST, RWST	
27	Air Handling Units	Containment Fan Coolers	5

Table 4.11

Generic Component Fragilities, in units of gravity (g)

Category	Generic Component	Median*	β_R	β_U
1	Ceramic Insulators	0.25	0.25	0.25
2	Relays	4.00	0.48	0.75
3	Circuit Breakers	7.63	0.48	0.74
4	Batteries	0.80	0.40	0.39
5	Battery Racks	2.29	0.31	0.39
6	Inverters	2.00	0.26	0.35
7	Dry Transformers	8.80	0.28	0.30
8	Motor Control Centers	7.63	0.48	0.74
9	Auxiliary Relay Cabinets	7.63	0.48	0.74
10	Switchgear	6.43	0.29	0.66
11	Cable Trays	2.23	0.34	0.19
12	Control Panels and Racks	11.50	0.48	0.74
13	Local Instruments	7.68	0.20	0.35
14	Diesel Generators	1.00	0.25	0.31
15	Horizontal Motors	12.10	0.27	0.31
16	Motor-driven Pumps and Compressors	2.80	0.25	0.27
17	Large Vertical Centrifugal Pumps	2.21	0.22	0.32
18	Large Motor-Operated Valves (>10 in.)	6.50	0.26	0.60
19	Small Motor-Operated Valves (<10 in.)	4.83	0.26	0.35
20	Large Pneumatic/Hydraulic Valves	6.50	0.26	0.35
21	Large Relief, Manual, and Check Valves	8.90	0.20	0.35
22	Miscellaneous Small Valves	12.50	0.33	0.43
23	Large Horizontal Vessels and Heat Exchangers	3.0	0.30	0.53
24	Small to Medium Vessels and Heat Exchangers	1.84	0.25	0.45
25	Large Vertical Vessels with Formed Heads	1.46	0.20	0.35
26	Large Vertical Tanks with Flat Bottoms	0.45	0.25	0.29
27	Air Handling Units	6.90	0.27	0.61

*All medians in terms of spectral acceleration at 5% damping and for frequency (or frequency range) shown on Table 4.10.

β_R = random uncertainty

β_U = systematic uncertainty

breakers. Virtually all the electrical switchgear and motor control centers in a nuclear power plant include these two types of components, so these two fragilities were used as the generic failure modes for electrical gear in the SSMRP analysis. Relay chatter is the lowest failure mode and, if included blindly in a risk analysis, would be the dominant failure. Because, in many cases, circuits are protected by time delay circuits and because, in most cases, chatter of relays would not cause a change in the state of a system being controlled, the NUREG 1150 analyses chose not to include relay chatter as a failure mode for electrical gear but rather to include circuit breaker trip as the lowest functional failure mode.

4.3.2 Surry Site Specific Component Fragilities

During the initial plant visit, the following components were identified as requiring plant-specific fragility derivations:

1. RWST and CST Tanks
2. CCW Heat Exchangers
3. 4Kv Busses
4. Diesel Generator Load Distribution Cabinets
5. 480 MCC Cabinets in Cable Vault Tunnel

The RWST and CST tanks were identified both because of their height-to-diameter ratios as well as due to the time period during which they were designed and installed. The CCW heat exchangers were mounted on concrete pedestals with relatively few anchor bolts. The 4kV busses and the diesel generator cabinet were anchored with relatively small welds. The 480 MCC cabinets in the cable vault/tunnel area were evidently bolted to a concrete mounting pad, however, due to the very high aspect ratio, it was suspected that the bolting might be marginal.

Based on these observations, site-specific fragilities were developed for the above-mentioned items. The resulting component site-specific fragilities are summarized on Table 4.12.

It should be pointed out that all the components above were found to have median failure acceleration levels well above the SSE. However, they did have less margin of safety above the SSE than the other components examined during the plant visit, and, hence, were anticipated to be significant contributors to the accident sequence probabilities.

4.3.3 Site Specific Building Fragilities

4.3.3.1 Method of Fragility Evaluation

The fragilities of Surry Unit 1 structures were generated using the basic methodology described in Reference 12, with certain modifications. The fragility of a structure can be expressed in terms of its peak ground acceleration capacity, A_m, as follows:

Table 4.12

Summary of Surry Site-Specific
Fragility Functions

Component	Failure Mode	Median Base Acceleration at Failure	β_R
RWST	Buckling with Anchor Bolt Yielding	0.46g	0.34
CST	Buckling with Anchor Bolt Yielding	0.45g*	0.35*
CCW HTX	Support Failure	0.29g	0.30
Diesel Generators	Load Center Weld Anchorage Failure	0.76g	0.25
480 MCCs (BAC-1H1-2, BAC-1J1-2)	Anchorage Failure	0.70g	0.25

* No CST drawings were located. Used value from generic data base, which was consistent with that computed for the RWST.

$$A = A_m e_R e_U$$

In this formulation, A_m is the median peak ground acceleration (PGA) capacity, and e_R and e_U are random variables with unit median, representing the inherent randomness about the median and the uncertainty in the median value. The variables e_R and e_U are assumed to be lognormally distributed with logarithmic standard deviations β_R and β_U, respectively. The properties of the lognormal distribution are presented in Reference 10.

For convenience, the median peak ground acceleration capacity, A_m, was formulated as the product of the SSE peak ground acceleration, A_{SSE} = 0.15g for Surry site, and a median factor of safety against this ground motion level, F_m. Thus, the median peak ground acceleration capacity can be expressed as:

$$A_m = F_m A_{SSE}$$

The median factor of safety, F_m, was in turn expressed as the product of the following two median factors of safety:

a. The median strength factor, F_s, which is defined as the ratio of the median structure strength to the median structure loads for the SSE ground motion input.

b. The median inelastic energy absorption factor, F_u, which accounts for the ability of the structure to withstand seismic loads in excess of those corresponding to yield through ductile, nonlinear response.

The strength and inelastic energy absorption factors have associated logarithmic standard deviations, β_s and β_u. From the properties of the lognormal distribution, the logarithmic standard deviation associated with the total factor of safety is calculated as follows:

$$\beta^2 = \left[\beta_s^2 + \beta_u^2\right]^{1/2}$$

These variabilities are composed of randomness and uncertainty, which are defined as follows:

a. Randomness consists of variabilities that cannot be reduced by more detailed evaluation or data collection.

b. Uncertainty consists of variabilities resulting from lack of knowledge.

The only source of random variability reported in this section results from the effect of certain earthquake characteristics on the structure

inelastic energy absorption capability. Uncertainties result from variables such as material strength, member capacity, member ductility, etc.

Structure seismic response contributes additional variability to the structural fragilities. Logarithmic standard deviations for seismic response variability are not included in the values reported in this section as they are included in the responses directly.

4.3.3.2 Development of Structural Capacities

The Surry structural fragilities were expressed in terms of factors which account for structure ultimate strength and inelastic energy absorption capability. The basic techniques used to determine the median values and associated variabilities of the terms were essentially those described in Reference 11, with certain modifications.

Structure Element Ultimate Strengths

Two major considerations are involved in the determination of the ultimate strengths of individual structural elements. One is the definition of the strengths of the materials composing the members. The other is the determination of the ultimate strength capacities of the structural members given the type of loading, material strength, member configuration, etc.

The Surry plant specific material strength data were not available. The following values, which were used in the fragility evaluation, were estimated based upon data from other nuclear power plants (Ref. 12):

Concrete Compressive Strength

Minimum Specified (psi)	Median (psi)	β
3000	4900	0.17
4000	6000	0.15

Steel Reinforcement Yield Strength

Grade	Median (ksi)	β
40	48	0.10
50	55	0.10
60	69	0.07

The Grade 50 steel was used for #14S and #18S reinforcement in the Surry fragility analyses.

The median ultimate strength capacities of the structural elements were found using the median material strengths and member configurations (i.e., geometry, reinforcement, etc.) in conjunction with available predictive formulation or approaches. The approaches and formulations used were those appropriate for the type of element (i.e., shear wall, reinforced concrete cylinder, etc.) and loading (i.e., shear, flexure, etc.). They were typically found to provide essentially median-centered capacities when compared to the results of available experimental testing. For example, the predictive equations used to determine the median ultimate strengths of the Surry shear walls subjected to in-plane shear and flexure are presented in Reference 13.

Median strength factors, F_{sm}, were calculated for individual structural elements as follows:

$$F_{sm} = \frac{V_{um,i}}{V_{SSE,i}}$$

$V_{um,i}$ = Median ultimate strength for element i

$V_{SSE,i}$ = Median load due to SSE ground motion input for element i

The median strength factor for a structure was generally taken to be the lowest value of the individual elements composing its primary seismic load-resisting system. This is slightly conservative if the structural elements are ductile and redundant. In certain cases, load redistribution among such structural elements was considered when determining the structure strength factor.

Variability of the structural element ultimate strengths was considered to be composed of uncertainty since it is associated with a lack of knowledge. Uncertainty attributed to material strength was based upon the estimated variabilities listed above. Comparisons of the predicted strength capacities to the available test results provided estimates of the uncertainty in the predictive strength formulations. Additional uncertainty attributable to variabilities associated with other sources, such as member geometry, reinforcement spacing, openings, workmanship, differences between field and laboratory conditions, accuracy of the predicted load distributions, etc., were also included.

Structure Inelastic Energy Absorption

The ability of a structure to withstand seismic levels in excess of those corresponding to yield through ductile, nonlinear response was accounted for by the inelastic energy absorption factor, F_u. This factor was based upon the Riddell-Newmark response deamplification factor, ϕ_u (Ref. 14).

The median inelastic energy absorption factor, F_{um}, corresponding to some ductility ratio, μ, is given by the following equation:

$$F_{um} = \frac{S_{ae}}{S_{au}}$$

S_{ae} = Median elastic spectral acceleration for median structure damping at the dominant structure frequency

S_{au} = Deamplified spectral acceleration at the dominant structure frequency

For frequencies in the amplified acceleration range (between about 1.8 Hz and 3 Hz) of the Surry median ground response spectrum:

$$S_{au} = \phi_u S_{ae} > S_{ahf}$$

$$\phi_u = (p\mu - q)^{-r}$$

$$p = q + 1$$

$$q = 3.0\ \beta^{-0.30}$$

$$r = 0.48\ \beta^{-0.08}$$

β = System damping

For frequencies in the amplified velocity region (less than 1.8 Hz), the q and r terms in the above equations are defined as:

$$q = 2.7\ \beta^{-0.40}$$

$$r = 0.66\ \beta^{-0.04}$$

For frequencies greater than the frequency at which the median spectral acceleration returns to the peak ground acceleration (about 15 Hz):

$$S_{au} = S_{ahf} = \mu^{-0.13}\ PGA$$

PGA = Peak ground acceleration

The Riddell-Newmark response deamplification factor was based upon a series of nonlinear analyses utilizing single-degree-of-freedom (SDOF) fixed base models subject to time histories of large magnitude, long duration earthquakes. Nonlinear response of the Surry structures would be expected to differ from the response calculated using these deamplification factors for the following reasons:

a. The Surry structures are founded on relatively soft soil. As a result, significant soil-structure interaction (SSI) is expected.

b. The Surry structures are typically multi-degree-of-freedom (MDOF) systems.

c. Small magnitude earthquakes are expected for the Surry site.

To account for these differences, an effective ductility, μ_e, was used in the equations above.

The system ductility, μ_{sys}, for use with the Riddell-Newmark deamplification factor is a measure of the nonlinearity throughout the structure. For fixed-base SDOF structures, the system ductility is equal to the story drift ductility, μ_{st}. However, for MDOF structures, the system ductility may be less than the story ductility if the ratio of the story demand to story capacity is not uniform through the structure. Also, nonlinear behavior has less effect on structures with significant SSI effects as compared to fixed base structures for the following reasons:

a. Structure nonlinearity causes only slight frequency shift in system modes dominated by soil flexibility.

b. Increased damping due to hysteretic behavior is small compared to soil radiation damping.

In the fragility evaluation, the system ductility, μ_{sys}, was reduced from the story ductility. From the study of Reference 15, the system ductility, μ_{sys} can be related to the story ductility by a factor M.

$$\mu_{sys} = \left[\frac{\mu_{st} - 1}{M}\right] + 1$$

The median story ductility for typical nuclear plant shear walls is estimated to be about five. Values for the factor M were estimated on a case by case basis depending on the extent of the soil-structure interaction effects and the distribution of structure nonlinearities. For the containment spray pump enclosure and the safeguards area, an M value of 4.5 was estimated. For the containment and the concrete internal structures where soil-structure interaction is more significant and localized nonlinearity is expected, M values of 6 and 7 were estimated, respectively. The service building, auxiliary building, emergency generator enclosure, and intake structure all essentially behave as rigid structures on flexible soil. This conclusion is based on the observation that there is little or no amplification of the foundation level input motion throughout the height of these structures. For these buildings, S_{au} was calculated using the equation for the rigid frequency range (>15 Hz) along with the median story ductility.

The Riddell-Newmark response deamplification factors were based only on large magnitude earthquakes. It is well known that lower magnitude earthquakes are not as damaging to structures and equipment as higher magnitude earthquakes with the same peak ground acceleration (Ref. 15). The lower magnitude earthquakes have lower energy content and shorter durations which develop fewer strong response cycles. Structures are able to withstand larger deformations (i.e., higher ductility) for a few cycles compared to the larger number of cycles resulting from longer duration events.

Earthquake magnitude effects were accounted for by using an effective ductility, μ_e, in the Riddell-Newmark response deamplification factor approach. The effective ductility was calculated as follows:

$$\mu_e = 1.0 + C_D \ (\mu_{sys} - 1.0)$$

where the duration coefficient, C_D, is a function of the earthquake magnitude and μ_{sys} is the previously defined system ductility.

The results of the analyses performed in Reference 15 were used to provide estimates of the duration coefficient, C_D, as a function of earthquake magnitude. For earthquakes having magnitudes ranging from 4.5 to 6.0, a duration coefficient of 1.4 was determined to be appropriate by correlating the inelastic energy absorption factor from the Riddell-Newmark formulation to the results of Reference 15. Similarly, a duration coefficient of 0.7 was estimated for earthquake magnitudes in the 6.5 to 7.5 range. A duration coefficient of 1.3 was estimated for the Surry structures. This is a representative value for eastern United States nuclear plants.

It should be noted that, for purposes of this study, structures are considered to fail functionally when inelastic deformations of the structure under seismic load are estimated to be sufficient to potentially interfere with the operability of safety-related equipment attached to the structure. The element and system ductility limits chosen for structures are estimated to correspond to the onset of significant structural damage. For many potential modes of failure, this is believed to represent a conservative bound on the level of inelastic structural deformation which might interfere with the operability of components housed within the structure. It is important to note that considerably greater margins of safety against structural collapse are believed to exist for these structures than many cases reported within this study. Thus, the structural element capacities reported herein should not be inferred as corresponding to structure collapse.

4.3.4 Structure Fragilities Derived for Surry

Fragilities for the Surry structures are listed in Table 4.13. In general, several potential failure modes were investigated for each structure. Fragilities for the governing failure modes are reported. These failure modes are typically associated with structural failure which would result in damage to the safety-related equipment located in the building.

Table 4.13

Surry Structural Fragilities Summary

Structure	Critical Failure Mode	A_m	β_R	β_U	Consequence of Failure	Incorporation in PRA
Containment Building	Shear failure near the base	7.7g	.09	.24	Loss of liner integrity and loss of reactor coolant pressure boundary	Not included since negligible
Concrete internal	Shear failure at the base	1.8g	.14	.27	Loss of lateral support of steam generators and coolant pumps and loss of primary coolant pressure boundary	Results in RVR initiating event
Safeguards Building	Shear wall failure	1.5g	.06	.23	Damage to equipment throughout the structure	No initiator results. LPI, HPR, LPR
	Impact damage to slab due to sliding	1.6g	.26	.31	Loss of anchorage of low head safety injection pumps mounted on the slab	Fails LPI, HPR
Spray Pump Enclosure	Shear wall failure	2.1g	.06	.23	Damage to equipment throughout the structure	No initiator. Fails CSS and OSR.
	Sliding Induced damage to the slab	1.8g	.26	.30	Potential damage to components housed in the enclosure	

Table 4.13

Surry Structural Fragilities Summary (Concluded)

Structure	Critical Failure Mode	A_m	β_R	β_U	Consequence of Failure	Incorporation in PRA
Service Building	Shear wall failure	1.7g	.05	.24	Damage to equipment throughout the structure	Causes T_1 (LOSP) initiator and fails all electrical (AC & DC) systems. Results in sequence T_1RQLD_2.
EGE	Shear wall failure	4.2g	.05	.21	Damage to equipment mounted on the wall or roof. Probably no damage to the diesel generators	Negligible, so not included.
Intake Structure	Failure of guide wall	2.0g	.05	.24	Damage to equipment throughout the structure.	No initiator results. Fails pumps which fill canal. Does not fail canal. Would affect only after 12 hrs.
	Sliding	1.7g	.33	.35	Damage to the service water pipes and other lifelines penetrating outer walls.	
Auxiliary Building	Shear wall failure	1.8g	.05	.23	Damage to equipment throughout the structure.	Results in seal LOCA. Does not cause LOSP. Fails HPI, CCW (D1, D2, D3, W) systems.

Notes:
1. Median capacities are calculated by multiplying the factor of safety A_m of the critical failure mode by 0.15g free field peak ground acceleration.
2. β_R and β_U reported are variabilities associated with capacity only except those reported for sliding which include variabilities of both capacity and response.

In developing the capacity factors, structural wall and beam resultant forces were determined from the dynamic response models. The building's structural dynamic characteristics are described by their fixed-base eigensystem and modal damping factors. Eigensystems, fundamental modes of vibration and eigenvectors, are determined from fixed base lumped mass beam element models. Beam elements represent stiffness between floor levels located at the shear centroid of the reinforced concrete walls or diagonal steel bracing, including shear deformation. The contribution to lumped mass at each floor level is from the half height of the wall above and below, floor slab, and equipment at the floor. National values of structure damping were taken to be 0.07, 0.085, and 0.10 (fractions of critical damping) for the three seismic acceleration ranges considered here. These were based on published damping values and assumed stress levels achieved. Failure modes for each structure are described below.

Containment and Internal Structures

The containment structure is a reinforced concrete structure consisting of a circular cylindrical wall capped by a hemispherical dome. The containment wall is supported by a basemat founded on soil. The bottom of the basemat is at elevation (-)39 ft-7 in. A continuously operating drainage system is provided to keep the groundwater below the top of the basemat such that the hydrostatic pressure is not significant. Principal dimensions of the containment structure are:

Mat	Radius	71 ft-4 5/8 in.
	Thickness	10 ft-0 in.
	Liner plate thickness	3/8 in.
Cylinder	Inside radius	63 ft-0 in.
	Wall thickness	4 ft-6 in.
	Liner plate thickness	3/8 in.
	Height to springline	122 ft-1 in.
Dome	Inside radius	63 ft-0 in.
	Wall thickness	2 ft-6 in.
	Liner plate thickness	3/8in.

Concrete with a design compressive strength of 3000 psi at 28 days was used to construct the wall. Grade 50 #18S reinforcing bars with a minimum specified yield strength of 50 ksi were provided in the meridional and hoop directions. Additional two layers of #18S diagonal reinforcement were provided in the cylindrical wall to resist horizontal seismic shear force.

Both the flexural and shear strengths were evaluated for the containment structure. The controlling failure mode was found to be shear failure of the cylindrical wall near the base. Horizontal shear forces due to seismic response of the containment structure introduce tangential shear stress in the wall. The median shear strength was determined using an

empirical equation derived from testing of scale model prestressed and reinforced concrete containment structures. Resistance to horizontal seismic shear force is provided by the concrete, meridional and hoop reinforcement and diagonal reinforcement. This mode of failure was found to have a median PGA capacity of 7.7g. Loss of liner integrity and loss of reactor coolant pressure boundary will result.

The concrete internal structure of the Surry containment structure consists of the primary shield wall, cylindrical crane wall, concrete floor slabs and refueling pool. The internal structure provides biological shielding and missile protection and also supports major components such as RPV, coolant pumps, etc. The main lateral load carrying elements of the internal structure are the crane wall and the primary shield wall. These structures are founded on the basemat common with the containment structure. Cadwelds were used to provide continuity of vertical wall reinforcing steel of these structures across the basemat liner plate. Dimensions of the crane wall and the primary shield wall are:

Crane wall	Outer radius	53 ft-0 in.
	Thickness	2 ft-9 in.
	Height	124 ft-5 in.
Primary shield wall	Inner radius	11 ft-0 in.
	Thickness	4 ft-6 in.
	Height	47 ft-11 in.

A review of the internal structure indicates that failure due to seismic response will probably occur toward the base of the structure. Near the base, the crane wall is perforated by several large openings that result in a series of wall segments, typically 2 ft-0 in. thick by 8 ft-0 in. wide spanning from the top of the basement at elevation (-)29 ft-7 in. to the slab at elevation (-)3 ft-9 in.

Failure of the concrete internal structure was found to be governed by shear at the base. Shear yielding is expected to occur first at those wall segments near the base of the crane wall. The primary shield wall was found to have higher capacity than the crane wall. Since the primary shield wall and the crane wall are structurally tied together by the floor slabs at elevation (-)3 ft-6 in., elevation 18 ft-4 in. and elevation 47 ft-4 in. and by radial walls, some load redistribution is expected to occur after ductile yielding of the crane wall. Additional load can be resisted by the primary shield wall. The median PGA capacity of the concrete internal structure accounting for this load redistribution was found to be 1.8g. Failure of the concrete internal structure will result in loss of lateral support for the steam generators, coolant pumps and RPV, and loss of primary coolant pressure boundary.

Safeguards Area

The safeguards area is a reinforced concrete enclosure located outside of the containment structure with planar dimensions of about 17 ft in the

radial direction of the containment structure by about 70 ft long in the circumferential direction. The structure is founded on a 2-ft-6-in.-thick basemat at elevation 12 ft-0 in. with a total height of about 30 ft. This area is enclosed on three sides by reinforced concrete walls and by the containment structure shell on the fourth side. The safeguards area is separated from the containment structure with a 3-in. gap throughout its height. Safety-related equipment in this enclosure include the containment recirculation spray pumps and low head safety injection pumps.

The controlling failure modes of the safeguards area were found to be concrete shear wall failure and structure sliding-induced failure. Both failure modes would occur in the short direction of this enclosure, i.e., radial direction of the containment structure. There are fewer concrete shear walls in this direction to resist the lateral force. Also, due to the backfill outside of the long wall, both static and dynamic lateral earth pressures are present in this direction. The governing shear wall was found to be the 1-ft wall between the safeguards area and the spray pump enclosure. The failure mode of this wall is governed by flexure. The median PGA capacity of this mode of failure was determined to be 1.5g. The potential consequence of this failure mode is damage to equipment throughout the safeguards area.

The second controlling failure mode was found to be sliding towards the containment structure. Resistance to sliding is primarily provided by friction at the base of the safeguards structure. No buoyancy force was considered as the ground water table is about 10 ft below the basemat. The median capacity for sliding was based on Newmark's approach (Ref. 16). Because structural backfill is present only at one side of the safeguards area, and causes relatively significant earth pressure, Newmark's sliding equation for the unsymmetric resistance case was used as shown below:

$$u_m = \left(\frac{1}{2.5} \right) \left[\frac{V^2}{2gN} \left(\frac{A}{N} - 1 \right) \right]$$

N = Coefficient of friction

A = Peak ground acceleration

V = Peak ground velocity

u_m = Structure displacement

The 2.5 median factor of safety associated with this equation was determined based on the data given in Reference 16. Should the structure slide 3 in. and impact the containment structure, there is a possibility of concrete spalling with subsequent damage to anchorage of the low head safety injection pumps anchored close to the edge of the slab. The sliding failure mode was found to have a median PGA capacity of about 1.6g.

Containment Spray Pump Enclosure

The containment spray pump enclosure is located outside of the containment structure and houses safety-related equipment such as the containment spray pumps and emergency auxiliary feedwater pumps. The building is enclosed by an "L" shaped reinforced concrete wall on two sides, by the containment structure shell on the third side and the main steam valve enclosure wall on the fourth side. The spray pump enclosure is founded on a 2-ft-6-in. concrete basemat at elevation 11 ft-6 in. Similar to the safeguards area, this enclosure is separated from all adjacent structures by a 3-in. gap throughout its height.

Two controlling failure modes were identified for the spray pump enclosure: Concrete shear wall flexural failure and structure sliding induced failure. The median PGA capacity of shear wall failure was found to be 2.1g. Torsional response of this enclosure was found to be significant due to the unsymmetric "L" shaped layout of the major shear walls and was considered in the evaluation. Similar to the safeguards area, the unsymmetric sliding equation was used to evaluate the median sliding capacity. Upon closing of the 3-in. gap after initiation of sliding, impact between the pump enclosure and the containment structure would occur with subsequent potential damage to the containment spray pumps and the auxiliary feedwater pumps. The median PGA capacity of the sliding failure mode was determined to be 1.8g.

Service Building

The service building consists of a reinforced concrete substructure from 2 ft-0 in. up to elevation 45 ft-3 in. and a structural steel superstructure above elevation 45 ft-3 in. The areas in the service building which house safety-related systems or equipment are the control room at elevation 27 ft-0 in. and the switchgear and battery rooms at elevation 9 ft-6 in. All safety-related equipment are enclosed in the reinforced concrete substructure. It is judged that the failure of the steel superstructure will not damage the safety-related equipment. Thus, the fragility evaluation of the service building is focused on the reinforced concrete substructure.

The seismic induced lateral forces are resisted by the typical 2-ft-thick reinforced concrete shear walls and concrete floor diaphragms. The governing failure mode was found to be the shear wall failure in flexure in the transverse (N-S) direction. The median PGA capacity was determined to be 1.7g. Damage to the safety-related equipment throughout the service building is expected as a result of this failure mode. In the longitudinal direction (E-W), the service building was found to have much more higher capacity.

Emergency Generator Enclosure

The emergency generator enclosure (EGE) is a single story reinforced concrete structure and houses the four emergency diesel generators and related equipment. The EGE structure consists of concrete roof slab and

load bearing concrete shear walls. The exterior walls are founded on strip footings at different elevations. The interior partitioning walls are founded on strip footings near grade. Each diesel generator is supported on its own mat near grade which is separated from the EGE structure.

The controlling shear wall failure in the transverse (N-S) direction of the EGE was found to have a median PGA capacity of 4g. Damage to equipment mounted on the walls is expected as a result of this failure mode. For exterior walls where significant backfill are present, the effect of both lateral earth pressure and hydrostatic pressure were considered in the wall capacity evaluation. The exterior walls were found to have higher PGA capacities. The roof diaphragm of the EGE was evaluated and was found to have higher capacity than the controlling shear wall.

Auxiliary Building

The auxiliary building is composed of a reinforced concrete substructure below elevation 27 ft-0 in. and a structural steel superstructure above elevation 27 ft-0 in. The top of the reinforced concrete foundation basemat is at elevation 2 ft. Numerous concrete walls and columns are present throughout the substructure of the auxiliary building. Most of the safety-related equipment are located in the concrete substructure. The superstructure consists of a metal roof deck at elevation 66 ft, an 8-in. concrete slab on metal deck at elevation 45 ft-10 in. and vertical braced frames. The seismic capacity of the steel superstructure was not evaluated. All safety-related equipment located above elevation 27 ft are enclosed by three separate reinforced concrete enclosures and should not be damaged by failure of the superstructure.

A number of shear walls and diaphragms were evaluated. The controlling failure mode was found to be failure of the east-west oriented reinforced concrete shear walls at the center core of the auxiliary building bounded by Column Lines H, K, 8, and 10. The median PGA acceleration capacity of this failure mode was found to be 1.8g with inelastic load redistribution among these center core walls considered. Failure of these walls is expected to lead to equipment damage throughout the auxiliary building. The floor diaphragms were found to have higher capacities.

Intake Structure

The intake structure is a reinforced concrete structure founded on a basemat bearing on the soil at approximately elevation (-)26 ft. Plan dimensions of the structure are approximately 177 ft in the north-south by 64 ft in the east-west. The reinforced concrete oil and pump storage room, which houses the safety-related service water pumps, is supported on the operating floor of the intake structure at elevation 12 ft-0 in. The major lateral force resisting system consists of concrete shear walls and slabs.

Both structural failure mode and sliding-induced failure mode were evaluated. Sliding was considered as a potential failure mode due to

lack of keyways at the basemat and foundation soil interface. The intake structure is backfilled on the north, south and west sides with the east side open to the water. Thus, sliding in the eastward direction was evaluated. Resistance to sliding is provided by the static friction between the basemat and the foundation soil. The normal water level was assumed at elevation 0 in. Reduction of the static friction resistance due to buoyancy force at the bottom face of the basemat was considered.

The median capacity for sliding was determined using Newmark's equation for symmetric resistance (Ref. 16) as given below:

$$u_m = \left[\frac{1}{2} \right] \left[\frac{V^2}{2gN} \left[1 - \frac{N}{A} \right] \right]$$

The median factor of safety associated with this equation was estimated to be 2.0. The equation for symmetric resistance was used in consideration of the massiveness of the intake structure. The sliding displacement at which damage to the service water lines is expected was estimated at three in. This criteria is based on the line configuration, the backfill depth above the lines outside of the intake structure and the line anchorage at the intake structure outer wall. The median PGA capacity for sliding-induced failure was found to be 1.7g.

A number of the shear walls and the diaphragms of the intake structure were evaluated. In addition to the seismic inertial loads, forces due to both static and dynamic effects of the backfill and the water inside and outside of the structure were considered. The controlling structure failure mode of the intake structure was found to be the flexural failure of interior guide walls with a medial PGA capacity of 2.0g. Failure of these walls is expected to lead to damage of service water pumps.

Masonry Block Walls

The reevaluation effort on I&E Bulletin No. 80-11 activities at Surry Power Station (Ref. 17) identified all safety-related (Class I and II) masonry block walls in the Category I structures of the Surry Power Station. Class I masonry walls are defined as those walls located in areas with high probability of impacting a significant amount of safety-related equipment if wall failure resulted. Class II masonry walls are those with limited safety-related equipment in its proximity. Some of these walls such as the ones in the pump and oil storage room of the intake structure were modified as a result of the reevaluation effort (Ref. 17). These modified walls were judged to have high capacities. Other walls were found acceptable without any modification necessary. The fragility evaluation os Surry masonry block wall is limited to these unmodified walls.

The 8-in. block wall in the control room of the service building was judged to have the lowest seismic capacity. This wall separates the control room and the computer room at elevation 27 ft-0 in. The wall was constructed with the lightweight C90 masonry units using Type N mortar. The wall spans vertically with a span of about 16 ft high between the

floors at elevation 27 ft and elevation 45 ft-3 in. It was assumed that the top joint of the wall is mortared into the overhead slab based on review of the available drawings of similar walls in the plant. The seismic capacity of the wall was determined assuming the wall can develop arching action. The median capacity of this wall governed by the compressive stress of the masonary unit was found to be about 3.5g. Failure of this wall is expected to damage equipment in the control and computer rooms.

4.3.5 Liquefaction

An analysis for the potential of soils liquefaction at the Surry site was made by GeoMatrix, Inc. as contained in Appendix D. Their analysis showed that some liquefaction would be expected at peak ground acceleration values of 0.3g to 0.4g. The effect of this liquefaction would be relative displacements between the containment and other important safety buildings (Auxiliary Building, Safeguards Area, Service Building and Turbine Building) of approximately 2 to 4 inches. However, this displacement is limited by the depth of the liquifying layers. A site examination of the piping systems and cable penetrations going from these buildings into the containment indicated that such displacements were not likely to cause failure. Hence, liquefaction, while it is to be expected at earthquake levels above the SSE, is not expected to affect the plant. Thus, liquefaction was not included explicitly in the Surry base case seismic PRA results.

4.4 Core Damage and Risk Computations

In the event of an earthquake or any other abnormal condition in a nuclear power plant, the plant safety systems act to bring the plant to a safe shutdown condition. In this step of the risk analysis process, we identify the possible paths that a nuclear plant would follow, given that an earthquake-related event has occurred which causes shutdown. These paths involve an initiating event and a success or failure designation for systems affecting the course of events, and are referred to as accident sequences.

4.4.1 Initiating Events

The seismic analysis performed for Surry is based on the same set of event trees developed for the internal event analyses of the plant. The initiating events considered are:

a. Reactor Vessel Rupture (ECCS ineffective)

b. Large LOCA

c. Medium LOCA

d. Small LOCA

e. Transient Type 1 (PCS failed by initiator)

f. Transient Type 3 (PCS initially available)

The reactor vessel rupture RVR and large LOCA (ALOCA) were computed based on the failure of the supports of the steam generators and reactor coolant pumps. Specific values for support fragility were taken from the SSMRP analysis of the Zion plant, however, a review of fragilities of other plants as contained in Reference 11 showed that the values used were typical. Surry is a 3-loop plant, and hence, the definition of the RVR event is the simultaneous failure of at least one steam generator or reactor coolant pump in at least two of the loops. Similarly the definition of the large LOCA is a failure of at least one steam generator or one reactor coolant pump in any one of the three loops. Since these failures are due to the same floor response and their fragilities are expected to be highly correlated, it was necessary to do an exact evaluation of these failure events explicitly including all correlation. In particular, it was necessary to include correlation between cut sets (combinations of component failures) as well as correlation between the failure events in each cut set. This was accomplished by performing a Monte Carlo evaluation of the Boolean equations describing the RVR and ALOCA events. This resulted in the failure probability distributions shown in Figure 4.26. The independent variable in these figures is the concrete internals response at 7 Hertz computed for Surry. This failure distribution was satisfactorily fit in log normal form and input as a component for the analysis.

The small and medium LOCA initiating events were computed based on the failure of appropriately sized piping in the reactor coolant loop. These distributions were generated from the calculations of piping failures for all the pipes considered in the SSMRP Zion analysis. These distributions are shown in Figure 4.27. The independent variable for this figure is peak ground acceleration, with a random variability of 0.25g. These distributions were also input in log normal component form for the analysis.

The Type 1 transient initiating event was based on the probability of loss of offsite power (LOSP). This has been found to be the dominant source of such transients in all seismic PRA's to date (wherein LOSP results in loss of the main feedwater system).

In computing the frequency of the initiating events, a hierarchy between them must be established. The order of this hierarchy is such that, if one initiating event occurs, the occurrence of other initiating events further down the hierarchy are of no consequence. Thus, for example, if a large LOCA occurs, we are not concerned if a small LOCA or transient occurs. Thus, the most serious initiating event is assumed to be the RVR event. The probability of the large LOCA event is then computed as the probability of the anchorage failures causing the large LOCA initiating event times the complement of the RVR event, and similarly, for the MLOCA, SLOCA and T_1 events. Figure 4.28 illustrates the hierarchy in an event tree format, and shows the expressions used to calculate the initiating event frequencies. Implicit in the hierarchy definition is the requirement that events in the hierarchy above a given initiating event cannot occur in the accident sequence for that event. For example, LOSP can occur as a basic event in any of the LOCA sequences, but cannot occur as a basic event in the T_3 accident sequence.

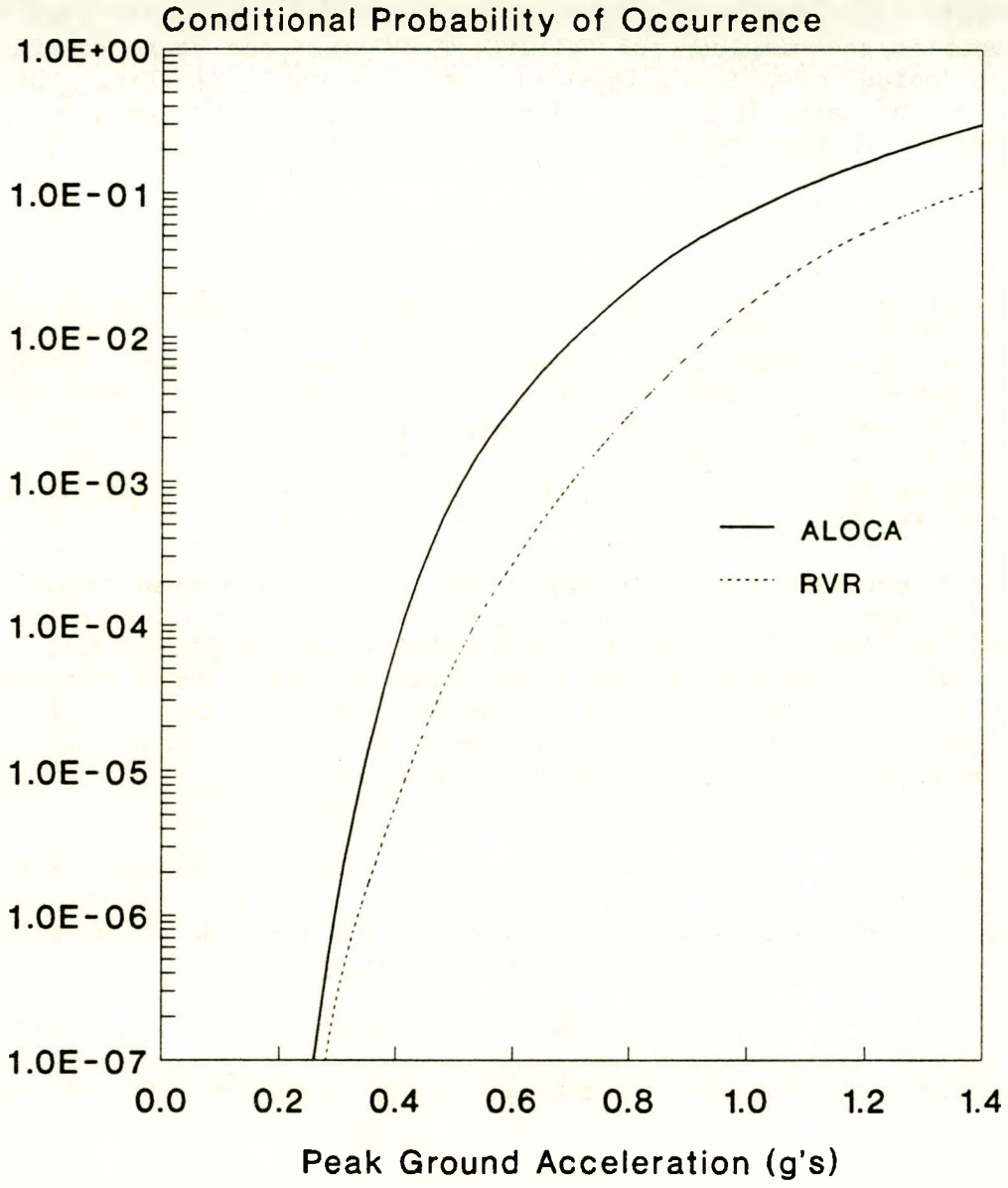

Figure 4.26 RVR Initiating Event Frequencies Due to Steam Generators & Reactor Coolout Pump Support Failures at Surry

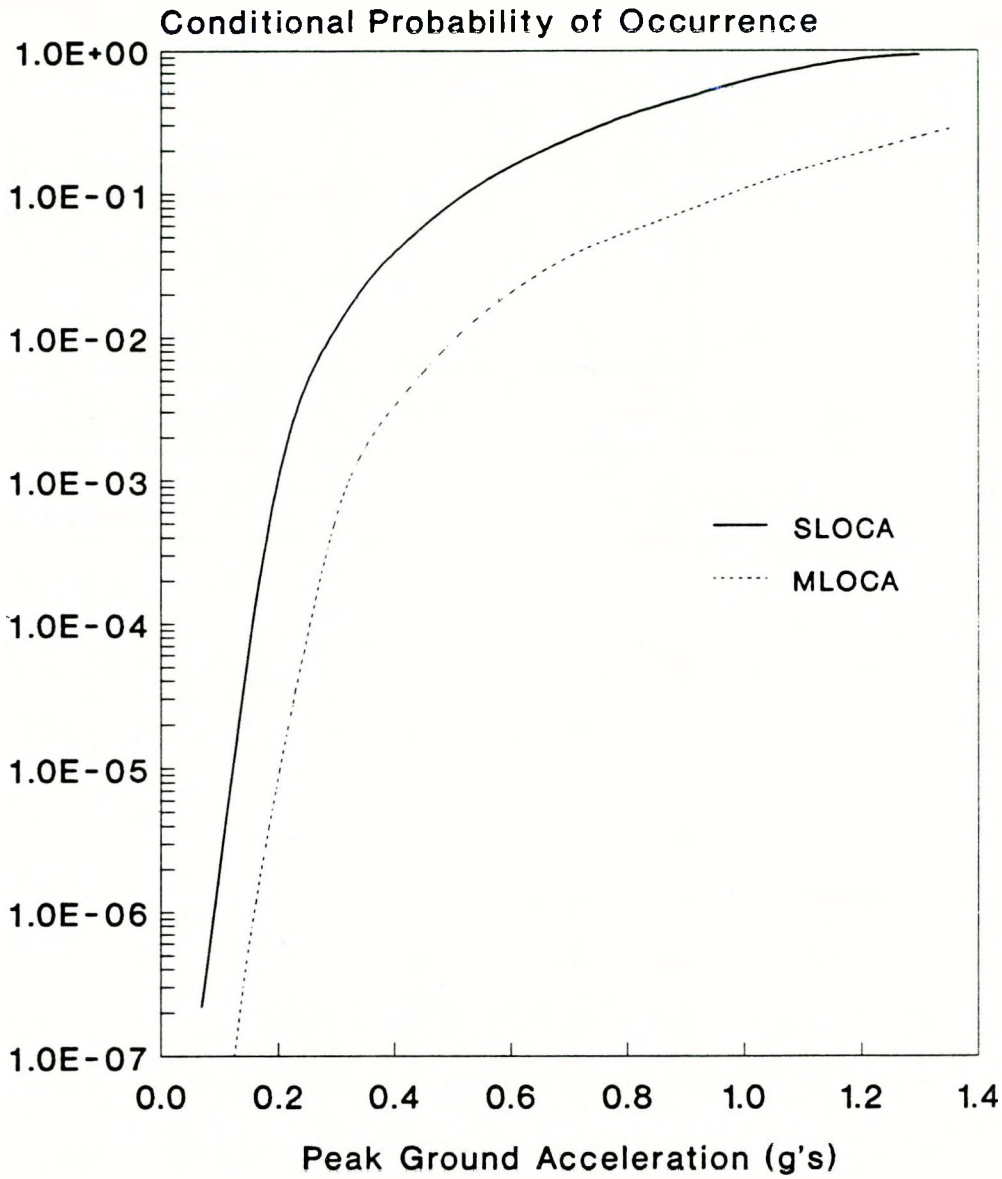

Figure 4.27 Frequencies of Pipe Breaks Causing LOCAS Derived from SSMRP Piping Calculations

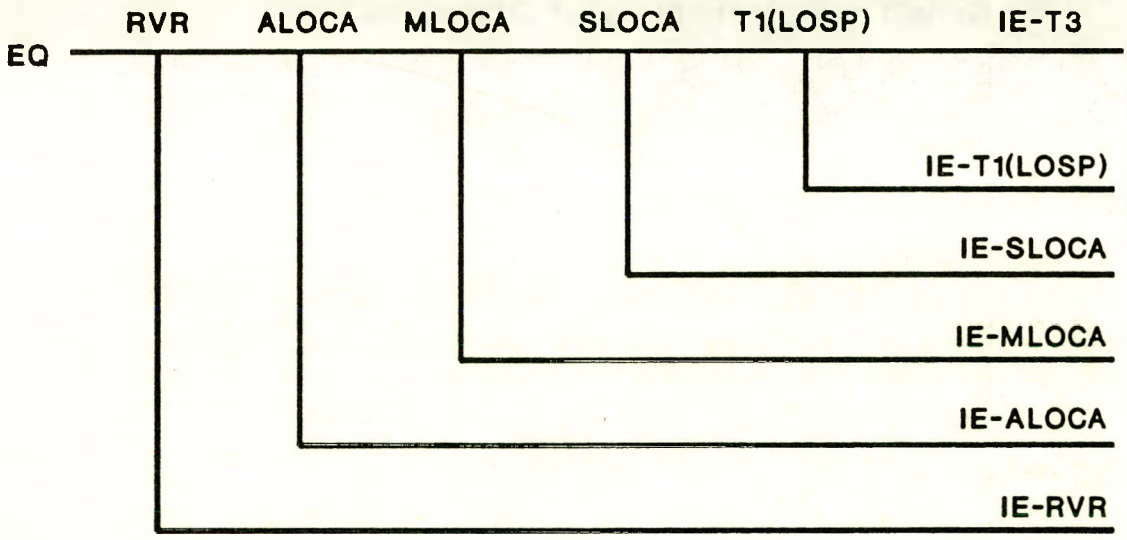

$$P[IE(RVR)] = RVR$$

$$P[IE(ALOCA)] = \overline{RVR} * ALOCA$$

$$P[IE(MLOCA)] = \overline{RVR} * \overline{ALOCA} * MLOCA$$

$$P[IE(SLOCA)] = \overline{RVR} * \overline{ALOCA} * \overline{MLOCA} * SLOCA$$

$$P[IE(T_1)] = \overline{RVR} * \overline{ALOCA} * \overline{MLOCA} * \overline{SLOCA} * LOSP$$

$$P[IE(T_3)] = 1 - P[IE(RVR)] - P[IE(ALOCA)] - P[IE(MLOCA)] - P[IE(SLOCA)] - P[IE(T_1)]$$

Figure 4.28 Initiating Event Hierarchy Event Tree

With the hierarchy established, the Type 3 initiating event probability is computed from the condition that the sum of the initiating event probabilities considered must be unity. The hypothesis is that, given an earthquake of reasonable size, at least one the initiating events will occur. At the least, we expect the operator to manually SCRAM the plant given an earthquake above the OBE level.

Numerical values for the initiating events at various earthquake levels are given in Section 4.4.5. Numerical values for the parameters of the fitted distributions are listed in Appendix C.

4.4.2 Event Trees

The event trees developed for the internal event analyses were used, so as to be able to compare the final core damage frequencies due to seismic and internal events on a common basis. The complete internal event trees were shown in Section 2.3. For the seismic computation of core damage frequency, wherein failure of the containment safety systems does not play a role, the internal event trees were simplified by deleting the containment systems. These trees, used for the seismic calculations, are shown in Figures 4.29 through 4.33. Note that no event that is shown for the RVR initiating event as the initiator itself leads directly to core damage since the ECCS mitigating systems are assumed ineffective. Assignment of the accident sequences and their cut sets to the different damage states was performed by examination of the cut sets in both the accident sequences and the containment system sequences.

4.4.3 Failure Modes of Safety Systems

To determine failure modes for the plant safety systems, fault tree methodology is used. This methodology systematically identifies all groups of components in a system which, if they failed simultaneously, would result in failure of that system.

Construction of a fault tree begins by identifying the immediate causes of system failure. Each of these causes is then examined for more fundamental causes, until one has constructed a downward branching tree, at the bottom of which are failures not further reducible, i.e., failures of mechanical or electrical components due to all causes such as structural failure, human error, maintenance outage, etc. These lowest order failures on the fault tree are called <u>basic events</u>. Failures of basic events due to seismic ground motions, random failures, human error, and test and maintenance outages are included in the seismic analyses.

The main difference between an internal event fault tree for a safety system and an external event fault tree is that consideration must be given to the physical location of the components, because the physical location determines to what extent secondary failures become important. Examples of this would be secondary failures due to local masonry wall collapse or due to a high temperature/steam environment from a broken steam line. Hence, in performing the seismic analyses, the locations of all important pieces of equipment must be determined from the general

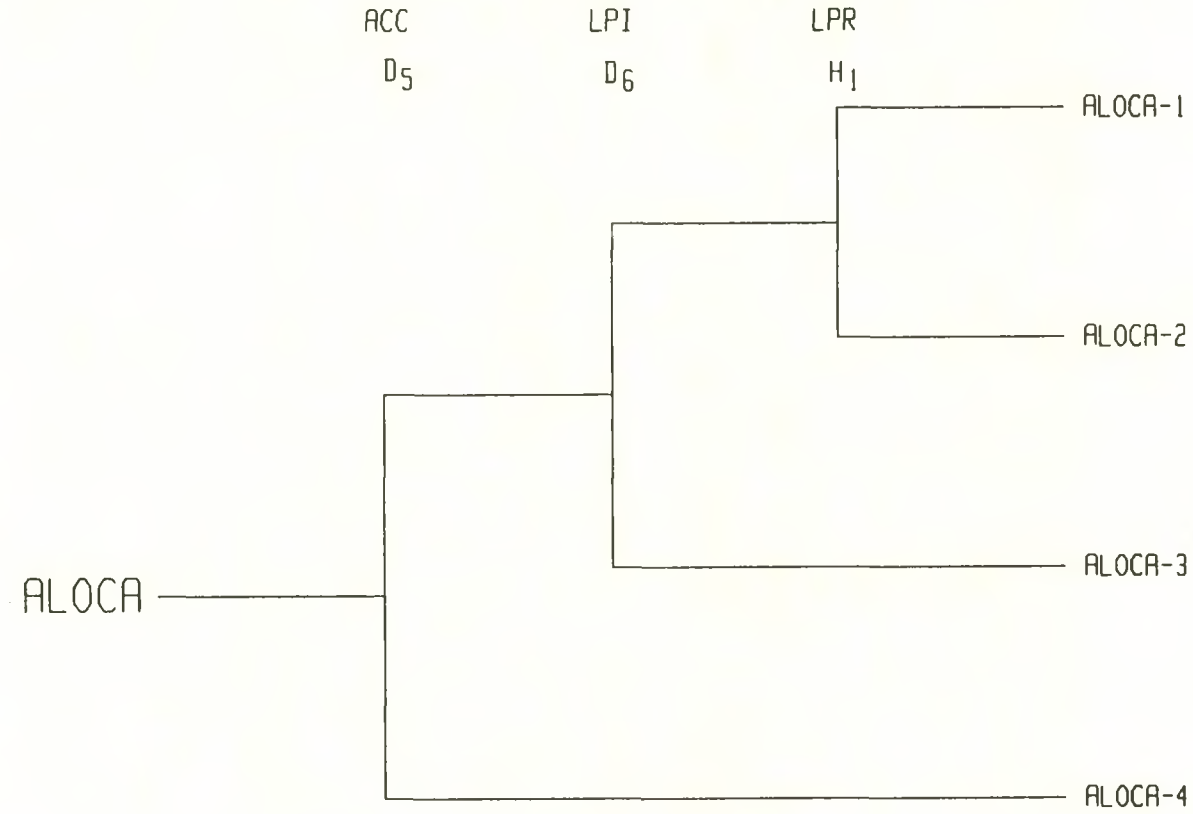

Figure 4.29 Large LOCA Seismic Event Tree

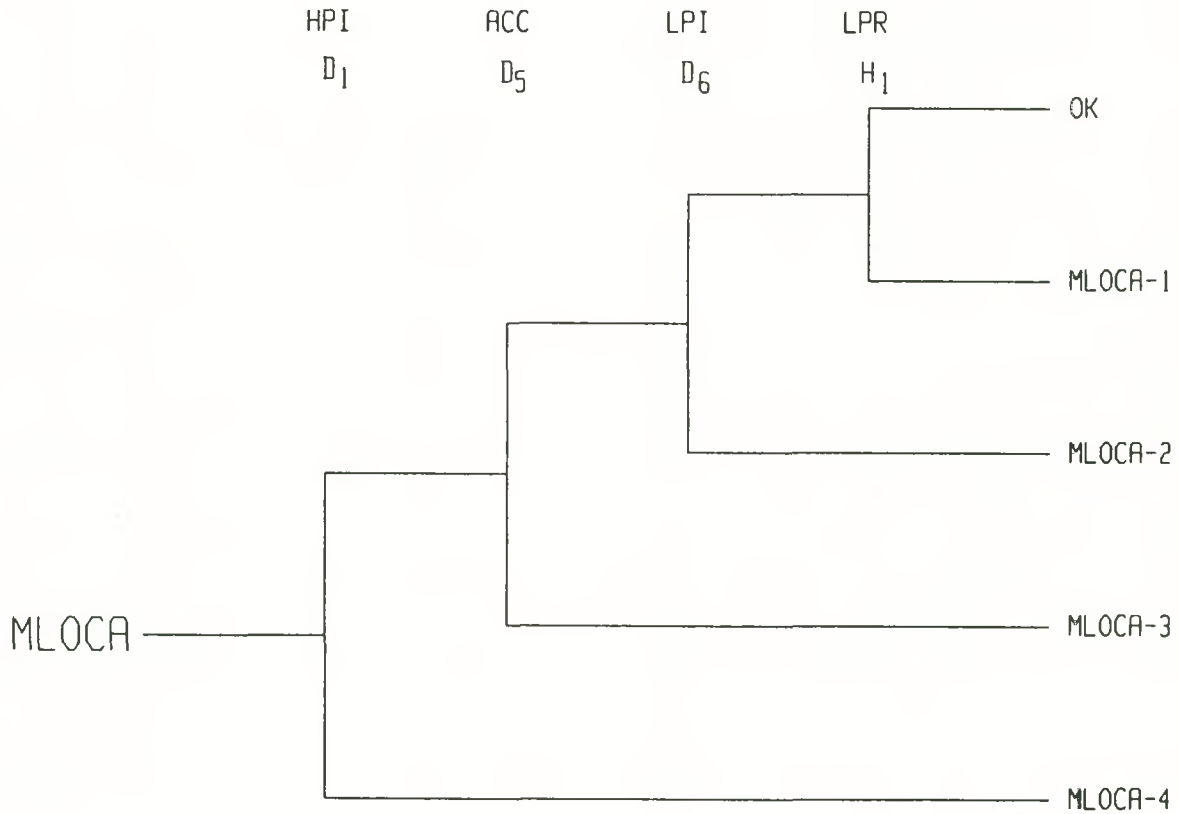

Figure 4.30 Medium LOCA Seismic Event Tree

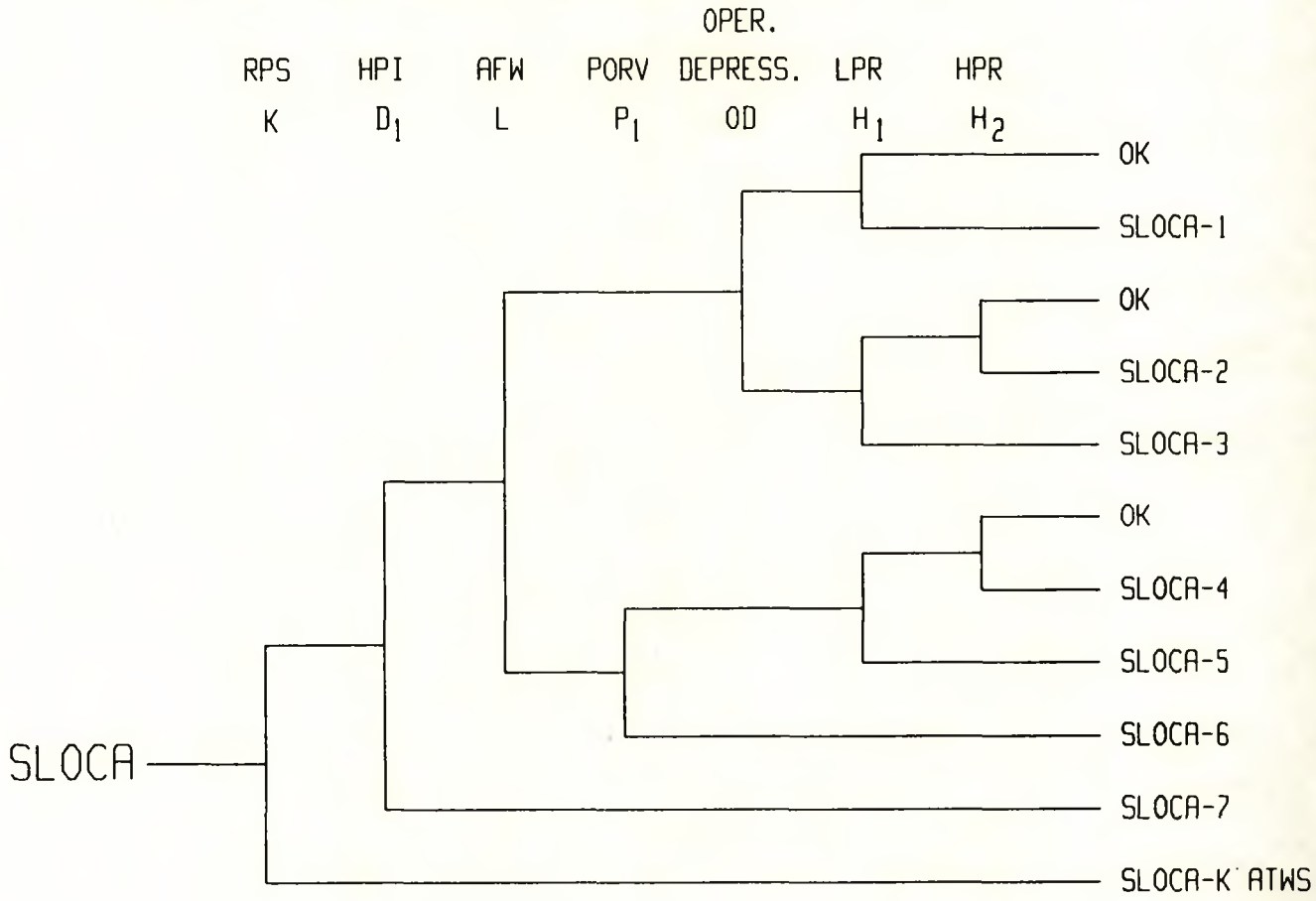

Figure 4.31 Small LOCA Seismic Event Tree

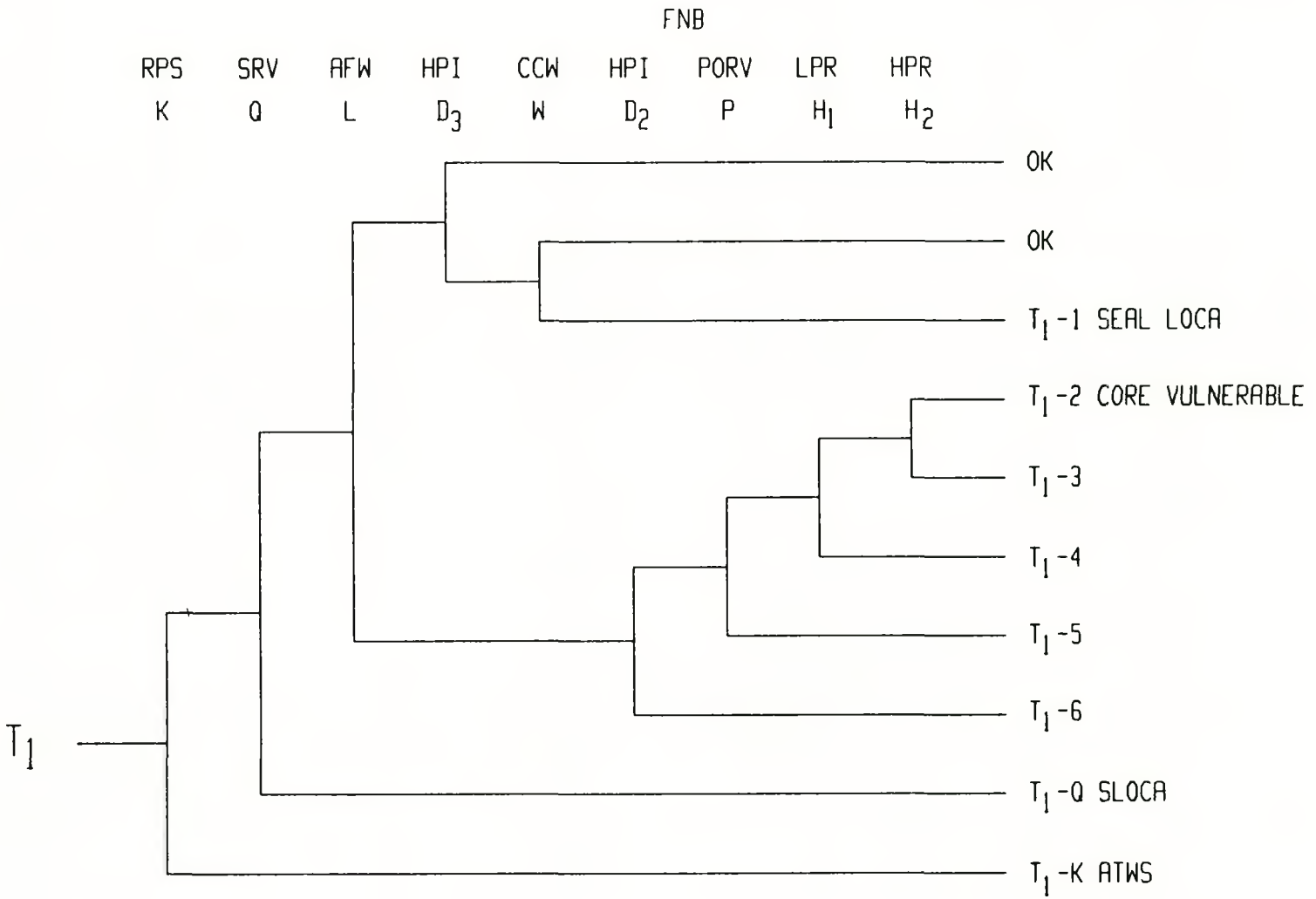

Figure 4.32 T_1 (Loss of Offsite Power) Seismic Event Tree

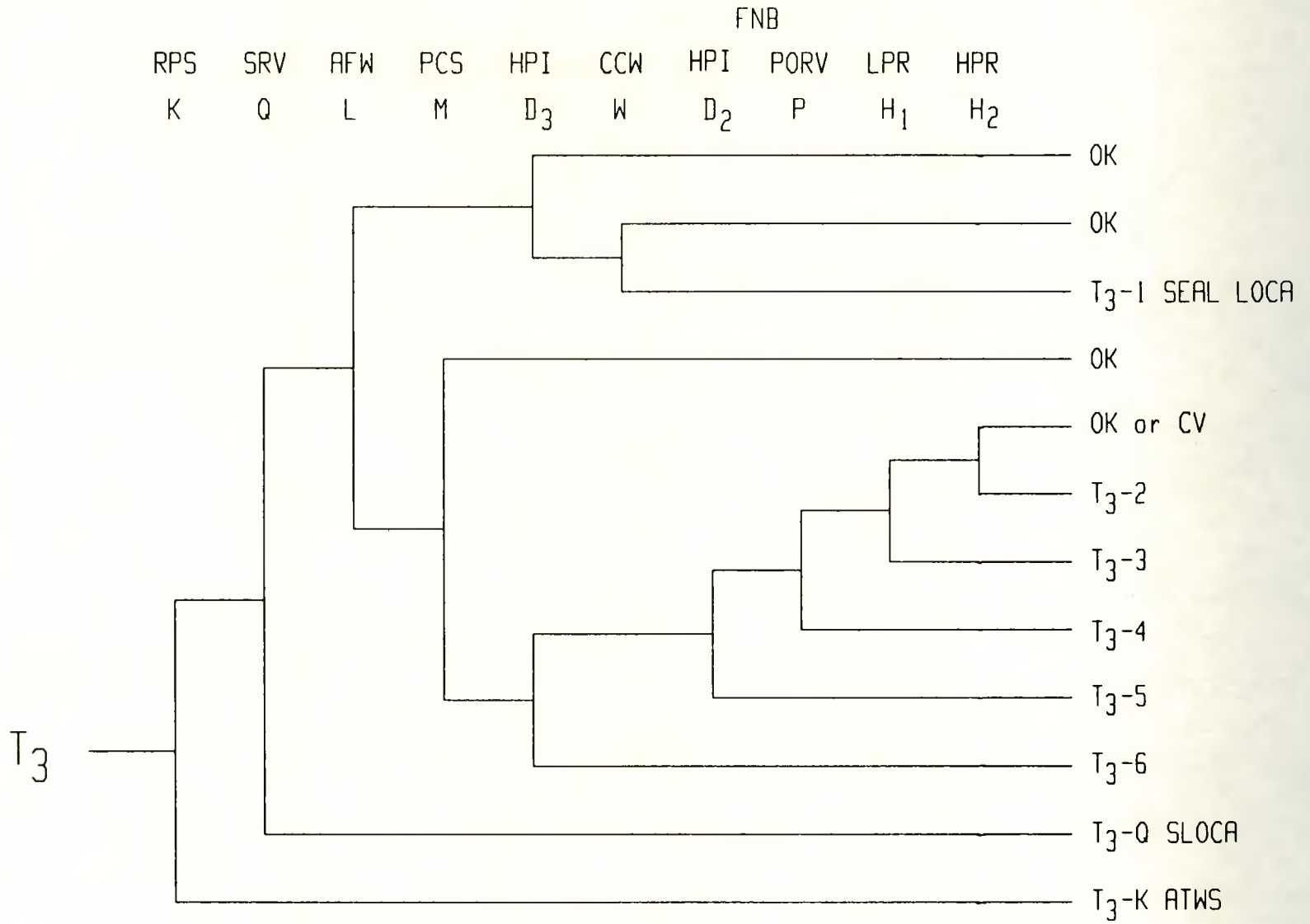

Figure 4.33 T_3 (Turbine Trip) Seismic Event Tree

arrangement drawings for the plant, and then a systematic examination for secondary failure possibilities is made during the plant walkdown.

As stated earlier, the internal event PRA fault trees form the basis for the fault trees used in the seismic analysis. This allows for a consistent level of detail between internal and external event analyses, and assures the consistent inclusion of random and test/maintenance outage unavailabilities in the seismic analysis.

Since the internal event fault trees are assumed to exist and seismic failure modes are to be added, one must modify the internal event fault trees to include:

a. Local structural failures (block walls, cranes, etc.)

b. Failure of critical passive components (tanks, cable tray failures, and pipes.) often missing in internal events analysis.

This is accomplished in several ways. First, the secondary or passive failure event can be added directly to the fault tree structure and the "gate" definition data file modified. Alternatively, the fragility definition of a relatively strong component on the tree may be redefined in terms of the (relatively weaker) associated secondary failure. Finally, events globally affecting a safety system or an accident sequence (such as building failure or liquefaction) can be added directly to the Boolean expression for the system failure or accident sequence.

4.4.4 Accident Sequence Evaluation

Accident sequence probabilities are used in determining the frequencies of core damage and of radioactive release for a given release category. Core damage frequency is defined as the sum of the frequencies of all accident sequences leading to core damage.

A. General Considerations

Each accident sequence consists of groups of events (successes or failures of safety systems) which must occur together. The failure of each safety system can be represented in terms of minimal cut sets, which are groups of component failure which will cause the safety system to fail. These cut sets and the accident sequences are combined together so that every accident sequence can be expressed in a Boolean expression of the form

$$ACC_j = IE_j \; [C_1C_2C_3 \text{ or } C_4C_5 \text{ or } \ldots \text{ or } C_iC_jC_k]$$

in which IE_j is the initiating event and the C_i are basic events (i.e., failure of individual components) identified on the system fault trees. If at least one of the component failure groups $C_iC_jC_k$ occurs, then the

accident sequence occurs. Computation of each accident sequence probability consists of determining the probability of each cut set, and then combining them to get the accident sequence probability.

Each basic event seismic failure probability is computed assuming that the response and fragility distributions are in log normal form. Calculations in the SSMRP showed that responses were reasonably fit by log normal distributions. The limited data on fragilities can be fit with log normal distributions as well as any other type. Hence, for convenience the log normal distribution is used for both. The equation used to calculate seismic failure frequencies is given as

$$P_f = \Phi \left[\frac{\ln \left(m_R / m_F \right)}{\sqrt{\beta^2_{FR} + \beta^2_{RR}}} \right]$$

where

Φ is the standard normal cumulative distribution function.

m_R, m_F are the medians of the response and fragility,

β_{FR}, β_{RR} are the corresponding random variabilities

Note that the use of log normal distributions is not essential to the calculation of process used in these calculations, and, in fact, any arbitrary pair of distributions could be used for the responses and fragilities provided they are physically meaningful.

When the individual basic failure events in a cut set $C_i C_j C_k$ are not independent, correlation between the basic events must be explicitly included. When only two of the basic events are correlated the joint probabilities may be computed directly by the use of tables. When more than two basic events in a cut set are correlated, numerical multiple integration may be used (such as contained in the SEISIM code developed in the SSMRP).

Finally, the accident sequences defined above are a function of peak ground acceleration, and as such, are conditional on the hazard curve. They are subsequently un-conditioned by integrating these sequences over the hazard curve as described subsequently.

B. Accident Sequence Quantification

Quantification of the accident sequences is a multi-step procedure involving several levels of screening. In the first step, the SETS code is used to evaluate all potential accident sequences using point estimate input screening values for all the seismic failure events (and using the internal events point estimate failure values for all random events). The same fault trees used by the internal events analysis are solved with

additions as noted in Section 4.4.3. The seismic screening values are taken as some conservative estimate, usually the component failure probabilities evaluated at three times the SSE. A dual probabilistic culling criterion is used in this culling process. This dual criterion is used in recognition of the fact that potentially large correlations can exist between basic events in the same cut set due to the pervasive nature of the seismic input motion. The result of this screening step is a reduced set of Boolean equations describing each of the safety and support systems.

In the second step, again utilizing the SETS code, these Boolean equations are merged together to form the accident sequences, again as defined for the internal events analysis. At this stage, truncation is performed based both on the order of the cut sets as well as the probability of the cut sets. The result of this step is Boolean equations describing each accident sequence and containing all the important seismic and random failure events.

The final step involves the actual quantification of the accident sequences. These accident sequence expressions are utilized both to compute point estimates of the accident sequence frequencies and to perform the uncertainty analysis calculations. A cross reference table is set up which relates each component to a component ID number, its random point estimate and error factor value, and to its associated seismic fragility category and seismic response category. This cross reference table thus provides all the information required to compute the probability of failure of any basic event (random or seismic or combined) at any peak ground acceleration level. The cross reference table for Surry is presented in Appendix C.

Finally, a complete uncertainty analysis is performed on the dominant accident sequences (and on the dominant cut sets in each accident sequence) as determined in the point estimate evaluations. A true Monte Carlo analysis was used for the NUREG 1150 studies. Thus, the expression for the unconditional accident sequence frequencies (and for core damage frequency), shown as below:

$$ACC_j = \int P(ACC_j, PGA) f_{eq}(PGA) d(PGA)$$

where

$P(ACC_j, PGA)$ is the conditional accident sequence frequency as a function of PGA, and
$f_{eq}(PGA)$ is the probability distribution function for the hazard curve,

is randomly sampled varying the hazard curve parameters, the random failure frequencies, and the seismic response and fragility parameters. From the accumulated values of accident sequence frequency and core damage frequency, exact statistics on their distributions are directly obtainable.

Note that in performing the uncertainty analyses, full correlation between random samples taken from each response category and from each fragility category was enforced. This is correct, and consistent with the philosophy utilized in the internal event NUREG 1150 uncertainty calculations.

In addition to the full uncertainty analysis (which produces exact mean values and exact percentiles of the distributions of the accident sequences and total core damage frequency) a "mean point estimate" is computed. The mean point estimate is useful for illustrating various intermediate results (conditional accident sequences frequencies, initiating event frequencies, etc.) which explain the flow of the calculations, for demonstrating convergence of the numerical integration, and for performing sensitivity studies in a cost effective manner. Specifically, the mean point estimate is used to understand the contributions of the various basic events to the total frequencies and to understand the contributions to the total uncertainty bands.

The mean point estimate is computed by using the mean random failure frequencies, the mean seismic hazard curve, and the mean values for the seismic failure event frequencies in evaluating the accident sequences. Only one reevaluation of the accident sequences is required. This mean point estimate will be seen to be nearly equal to the exact mean values of the accident sequence and core damage frequencies as obtained from the uncertainty analysis. This is to be expected because mean values probabilistically add to yield the mean value of each accident sequence (conditional on the hazard), and the only difference between the true mean and the mean point estimate has to do with integration of the conditional accident frequencies over the hazard curve. Experience has shown, however, that the difference between these is very small.

4.4.5 Base Case Surry Results

This section presents the results of the base case seismic risk analysis for the Surry Nuclear Power Plant. The base case is our best estimate of the current configuration of the plant and its emergency procedures. In particular, the seismic component failure probabilities were taken from the generic fragility data base (Table 4.11) with the exception of the site specific component and building fragilities given in Tables 4.12 and 4.13. As described in Section 4.4.2, a total of six initiating events are included for the seismic analysis.

A total of 28 accident sequences are identified on these trees which were solved for the Surry seismic analysis. These 28 sequences are presented in Table 4.14 along with identification of the Boolean sequences that were solved for each accident sequence. (The number of Booleans solved using the SETS code is less than the number of accident sequences because several accident sequences may utilize the same Boolean expression even though the initiating event may be different.) Also identified on this table are the complement expressions which must be included in the numerical sequence quantification at high PGA levels at which success proba-

Table 4.14

Seismic Accident Sequences

	Accident Sequence	Multiplier Expression	Boolean Expression	SETS ID No.	Complement Factor	Notes
	Vessel Rupture					
RVR-1	RVR	1	1		1	
	Large LOCA					
ALOCA-1	$A\overline{D_5D_6}$	1	1		$\overline{D_5D_6}$	Core Vulnerable
-2	$A\overline{D_5D_6}H_1$	1	$\overline{D_5D_6}H_1$	(1)	$\overline{D_5D_6}$	
-3	$A\bar{D}_5D_6$	1	$\bar{D}_5D_6$	(2)	$\bar{D}_5$	
-4	AD_5	1	D_5	(3)	1	
	Medium LOCA					
MLOCA-1	$S_1\overline{D_1D_5D_6}H_1$	1	$\overline{D_1D_5D_6}H_1$	(8)	$\overline{D_1D_5D_6}$	
-2	$S_1\overline{D_1D_5}D_6$	1	$\overline{D_1D_5}D_6$	(9)	$\overline{D_1D_5}$	
-3	$S_1\bar{D}_1D_5$	1	$\bar{D}_1D_5$	(10)	$\bar{D}_1$	
-4	S_1D_1	1	D_1	(11)	1	
	Small LOCA					
SLOCA-1	$S_2\overline{KD_1LOD}H_1$	$\bar{K}$	$\overline{D_1LOD}H_1$	(32)	$\overline{D_1LOD}$	
-2	$S_2\overline{KD_1LOD}\bar{H}_1H_2$	$\bar{K}$	$\overline{D_1LOD}\bar{H}_1H_2$	(29)	$\overline{D_1LH_1}$	
-3	$S_2\overline{KD_1LOD}H_1$	$\bar{K}$	$\overline{D_1LOD}H_1$	(28)	$\overline{D_1L}$	
-4	$S_2\bar{K}\bar{D}_1L\overline{P_1H_1}H_2$	$\bar{K}$	$\bar{D}_1L\overline{P_1H_1}H_2$	(23)	$\overline{D_1P_1H_1}$	
-5	$S_2\bar{K}\bar{D}_1L\bar{P}_1H_1$	$\bar{K}$	$\bar{D}_1L\bar{P}_1H_1$	(22)	$\overline{D_1P_1}$	
-6	$S_2\bar{K}\bar{D}_1LP_1$	$\bar{K}$	$\bar{D}_1LP_1$	(21)	$\bar{D}_1$	
-7	$S_2\bar{K}D_1$	$\bar{K}$	D_1	(11)	1	

Table 4.14

Seismic Accident Sequences (Continued)

	Accident Sequence	Multiplier Expression	Boolean Expression	SETS ID No.	Complement Factor	Notes
	T1(LOSP)					
T1-1	$T_1\overline{KQ}LD_1D_3W$	$\overline{KQ}$	$\bar{L}D_1D_3W$*	(33)	$\bar{L}$	Seal LOCA
-2	$T_1\overline{KQ}L\overline{D_2PH_1H_2}$	$\overline{KQ}$	$L\overline{D_2P}$	(34)	$\overline{D_2PH_1H_2}$	Core vulnerable
-3	$T_1\overline{KQ}L\overline{D_2PH_1}H_2$	$\overline{KQ}$	$L\overline{D_2PH_1}H_2$	(13)	$\overline{PD_2H_1}$	
-4	$T_1\overline{KQ}L\overline{D_2P}H_1$	$\overline{KQ}$	$L\overline{D_2P}H_1$	(12)	$\overline{PD_2}$	
-5	$T_1\overline{KQ}L\bar{D}_2P$	$\overline{KQ}$	$L\bar{D}_2P$	(14)	$\bar{D}_2$	
-6	$T_1\overline{KQ}LD_2$	$\overline{KQ}$	LD_2	(15)	1	
	T3 Transient					
T3-1	$T_3\overline{KQ}LD_1D_3W$	$\overline{KQ}$	D_1D_3W*	(26)	$\bar{L}$	Seal LOCA
-2	$T_3\overline{KQ}ML\overline{D_3D_2PH_1H_2}$	$\overline{MKQ}$	$L\overline{D_3D_2PH_1H_2}$	(20)	$\overline{D_3D_2PH_1}$	
-3	$T_3\overline{KQ}ML\overline{D_3D_2P}H_1$	$\overline{MKQ}$	$L\overline{D_3D_2P}H_1$	(19)	$\overline{D_3D_2P}$	
-4	$T_3\overline{KQ}ML\overline{D_3D_2}P$	$M\overline{KQ}$	$L\overline{D_3D_2}P$	(18)	$\overline{D_3D_2}$	
-5	$T_3\overline{KQ}ML\bar{D}_3D_2$	$M\overline{KQ}$	$L\bar{D}_3D_2$	(17)	$\bar{D}_3$	
-6	$T_3\overline{KQ}MLD_3$	$M\overline{KQ}$	LD_3	(16)	1	

*This sequence transfers to the SSLOCA tree, where it only needs D_1 to fail in order to cause a seal LOCA leading to core damage.

Table 4.15

Safety Systems Nomenclature

C	Containment spray system (CSS)
D_1	High pressure injection (HPI)
D_2	Same as HPI
D_3	High pressure injection for seal cooling
D_5	Accumulators (ACC)
D_6	Low pressure injection (LPI)
F_1	Inside spray recirculation (ISR)
F_2	Outside spray recirculation (OSR)
H_1	Low pressure recirculation (LPR-LH)
H_2	Low pressure recirculation (LPR-HH)
L	Auxiliary feedwater system (AFWS)
M	Main feedwater (PCS)
OD	Operator depressurization (OD)
P_1	Block valves and PORV system (one valve required) (PPS2)
P	Block valves and PORV system (both valves required) (PPS1)
W	Component cooling water system (CCW)

bilities may be significantly less than unity. The multiplier expression column lists those events specified by algebraic equations rather than by Boolean logical expressions. The analytical equations used for calculating the multipliers, the Boolean sequences, and the complement factors are presented in Appendix C. Table 4.15 describes the abbreviations used for the accident sequences in Table 4.14.

A total of 10 accident sequences survived the seismic screening process. These 10 non-negligible accident sequences were fully requantified using best estimate random failure frequencies and best estimate seismic fragilities and responses plus associated variabilities. The total mean core damage frequency for the Surry base case was computed to be 1.16E-4 per year using the LLNL hazard curves and 2.50E-5 per year using the EPRI hazard curves. The mean contributions of the accident sequences are shown on Table 4.16 for both hazard curves. Percentiles of the frequency distributions from the Monte Carlo analyses are shown on Tables 4.17 and 4.18. (Relative importance of the basic events to these results is given in the point estimate results presented later.)

Based on this final quantification, seven dominant sequences were identified. These dominant sequences are (in order of importance):

	LLNL Hazard	EPRI Hazard
T1-6	44%	40%
T1-1	23%	27%
T3-1	6%	8%
SLOCA-7	6%	5%
T1-5	6%	5%
T3-6	4%	3%
ALOCA-3	4%	3%

The percentage contributions were taken from the Monte Carlo uncertainty results on Table 4.16. Note that the same dominant accident sequences were obtained from the two different hazard curves, and it will be seen later that the order of importance of the major contributors is the same. A description of the dominant accident sequences follows.

Description of Accident Sequences

The dominant sequences computed for the Surry seismic risk are related to loss of AC power and failures of the auxiliary feedwater system and the high pressure injection systems. Given an event which does not cause a LOCA, there are two ways to remove heat. First, there is the auxiliary feedwater system and, second, there is the feed and bleed operation. This latter operation requires both high pressure injection and the pilot operated relief valves (PORVs). In addition, two seal LOCA sequences were identified. At Surry, there are two sources of cooling water for the reactor coolant pump seals, namely, the high pressure injection (HPI)

Table 4.16

Accident Sequence and Total Core Damage Mean Frequencies(1/yr)

Acc Seq	LLNL Hazard	EPRI Hazard
T1-6	5.1 e-5	1.0 e-5
T1-1	2.7 e-5	6.8 e-6
T3-1	7.2 e-6	2.1 e-6
SLOCA-7	6.8 e-6	1.3 e-6
T1-5	6.4 e-6	1.3 e-6
T3-6	4.9 e-6	8.7 e-7
ALOCA-3	4.3 e-6	7.4 e-7
ALOCA-2	3.4 e-6	5.9 e-7
RVR	3.3 e-6	5.5 e-7
MLOCA-4	1.5 e-6	1.7 e-7
Total	1.16 e-4	2.50 e-5

Table 4.17

Base Case Accident Sequence Frequency Distribution Percentiles (LLNL Hazard)

No.	Sequence	Mean	Var	5%	50%	95%
1	T1-6	5.1E-5	2.21E-08	1.29E-07	5.54E-06	1.80E-04
2	T1-1	2.7E-5	5.05E-10	6.91E-09	4.51E-07	1.69E-05
3	T3-1	7.2E-6	3.21E-08	2.53E-08	2.22E-06	9.22E-05
4	SLOCA-7	6.8E-6	2.84E-09	2.87E-10	9.85E-08	1.47E-05
5	T1-5	6.4E-6	1.87E-09	5.10E-09	3.79E-07	2.09E-05
6	T3-6	4.9E-6	3.42E-10	6.72E-10	1.43E-07	1.39E-05
7	ALOCA-3	4.3E-6	8.52E-10	1.72E-10	5.53E-08	7.40E-06
8	ALOCA-2	3.4E-6	1.05E-11	1.02E-10	3.50E-08	3.37E-06
9	RVR	3.3E-6	2.10E-10	5.31E-10	1.20E-07	1.43E-05
10	MLOCA-4	1.5E-6	2.40E-09	0.00E-01	4.34E-13	5.02E-06
	TOTAL	1.16-04	1.40E-07	3.92E-07	1.48E-05	4.38E-04

Table 4.18

Base Case Accident Sequence Frequency Distribution Percentiles (EPRI Hazard)

No.	Sequence	Mean	Var	5%	50%	95%
1	T1-6	1.0E-05	7.94E-10	9.50E-08	2.21E-06	4.51E-05
2	T1-1	6.8E-06	2.38E-11	4.43E-09	2.00E-07	4.70E-06
3	T3-1	2.1E-06	1.07E-09	1.65E-08	9.53E-07	2.41E-05
4	SLOCA-7	1.3E-06	2.71E-10	1.86E-10	5.55E-08	5.30E-06
5	T1-5	1.3E-06	3.60E-11	2.90E-09	1.43E-07	4.96E-06
6	T3-6	8.7E-07	9.34E-12	2.89E-10	5.03E-08	2.82E-06
7	ALOCA-3	7.4E-07	1.79E-11	6.48E-11	1.86E-08	1.93E-06
8	ALOCA-2	5.9E-07	3.85E-13	5.39E-11	1.28E-08	8.15E-07
9	RVR	5.5E-07	5.53E-12	2.44E-10	3.96E-08	2.67E-06
10	MLOCA-4	1.7E-07	1.37E-10	0.00E-01	1.27E-13	2.02E-06
	TOTAL	2.50E-05	5.04E-09	3.00E-07	6.12E-06	1.03E-04

system and secondly, the component cooling water (CCW) system. Both these systems must fail in order to fail cooling to the reactor coolant pumps.

The most important sequence is sequence T1-6. This is a loss of offsite power (LOSP) sequence in which both the auxiliary feedwater system and high pressure injection fail. The auxiliary feedwater system fails primarily due to failure of the condensate storage tank while the high pressure injection system fails either due to failure of the refueling water storage tank (RWST) or loss of onsite AC power. The loss of onsight AC power is due primarily to failure of the 4KV emergency switchgear anchorages, and secondarily to failure of the diesel generators to start given the seismic event.

The second most dominant sequence is T1-1. This is a loss of offsite power sequence leading to a seal LOCA. Note that this is a loss of offsite power sequence, however, the auxiliary feedwater system does succeed. However, failures of high pressure injection and component cooling water lead to a seal LOCA. Failures of these two systems are due either to the RWST or are onsite power related. There is a small contribution from the RHR heat exchanger support failures to the failure of the component cooling water system. The third most dominant sequence T3-1 is identical to sequence T1-1 except that now the transient is caused by some other failure (or manual scram) leading to shutdown, and offsite power is available. The predominant contribution to this sequence is due to failures of the 4KV emergency switchgear which effectively cause loss of all emergency AC power.

The fourth most important sequence is SLOCA-7 which is a small LOCA and which involves failure of the high pressure injection system. Again, the high pressure injection system fails either due to the RWST or onsite AC power failures as in the sequences already discussed.

The fifth most important sequence, T1-5, is also a loss of offsite power sequence in which both the AFWS and the feed and bleed function have failed. In this case, feed and bleed fails due to failure of the PORVs and their associated block valves. This is caused by failure of one train of AC power in conjunction with one set of block valves being closed. (At Surry, both sets of block valves and PORVs must be available for feed and bleed.)

Sequence T3-6 is the same as T1-6 except that offsite power is initially available. In this case, failures of the AFWS and the HPI systems are caused by failures of the water sources (the CST and the RWST, respectively).

The two sequences ALOCA-3 and ALOCA-2 are next in importance. In the former, the accumulators function properly but the low pressure injection system fails due to electric power failures. In the latter, both the accumulators and LPI succeed, but long term low pressure injection fails.

The RVR sequence is next in importance. It's occurrence is totally due to failure of the reactor coolant pump and steam generator supports.

Lastly, the medium LOCA sequence MLOCA-4 occurs due to failure of the HPI system. This occurs primarily because loss of power and also due to loss of the RWST.

Mean Point Estimate Using the LLNL Hazard Curves

As described earlier, this point estimate is based on using the mean values for all variables. The mean initiating event frequencies at different PGA values are given in Table 4.19 As can be seen, at the lower earthquake levels the transient sequence initiating events dominate, and as the earthquake acceleration level increases, the LOCA initiators increase until, finally, at the highest earthquake levels, there is a contribution from the reactor vessel rupture (RVR) event. Also note that, at each earthquake level, the initiating events sum to 1.0. Values of the dominant accident sequence conditional frequencies at various earthquake levels are presented in Table 4.20 These are the values that are integrated over the hazard curve to obtain the unconditional accident sequence frequencies.

Table 4.21 presents the mean core damage contributions at seven intervals over the hazard curve for each accident sequence. (Integration over the hazard curve was performed from 0.05g to 0.75g and in the uncertainty analysis computations, integration increments of 0.025g were utilized. However, for explanatory purposes the results presented here are based on an integration increment of 0.1g.) The right hand column presents the total contribution of each accident sequence to the total core damage frequency of 1.12e-4. As can be seen, the incremental contributions from the LOCA events do not become significant until the higher acceleration levels. The reactor vessel rupture sequence does not make a significant contribution until the highest PGA increment.

An important thing to note from Table 4.21 is the sum of the accident sequence contributions at each earthquake level, as shown at the bottom of each column on the table. The contributions are seen to be small at the first increment, increasing to a maximum at the fourth earthquake increment, and then decreasing at higher earthquake levels. This indicates that the bulk of the risk is occurring in the range of 0.25g to 0.65g which roughly corresponds to the range of 2-4 SSE. Further, this shows that the bulk of the risk has been captured by integrating over the range 0.05g to 0.75g.

Mean Point Estimate Using the EPRI Hazard Curve

Tables 4.22 through 4.24 presents similar results for the mean point estimate using the EPRI hazard curves. In this case, a total core damage frequency of 2.21E-5 was computed. This was very close to the Monte Carlo estimate of mean core damage frequency of 2.50E-5 computed using the same equations in the uncertainty analysis. Similar comments with

Table 4.19

Mean Initiating Event Frequencies - LLNL Hazard

	0.1g	0.2g	0.3g	0.4g	0.5g	0.6g	0.7g
RVR	1.79E-06	3.59E-04	4.03E-03	1.66E-02	4.22E-02	7.80E-02	1.19E-01
ALOCA	1.63E-05	1.71E-03	1.35E-02	4.37E-02	9.18E-02	1.43E-01	1.87E-01
MLOCA	4.59E-06	4.82E-04	4.12E-03	1.43E-02	3.14E-02	5.01E-02	6.57E-02
SLOCA	1.84E-04	6.73E-03	3.28E-02	7.79E-02	1.28E-01	1.63E-01	1.78E-01
T1(LOSP)	3.36E-02	3.25E-01	6.08E-01	7.06E-01	6.74E-01	5.65E-01	4.51E-01
T3	9.66E-01	6.66E-01	3.38E-01	1.41E-01	3.27E-02	0.00E-01	0.00E-01

Table 4.20

Mean Dominant Accident Sequence Frequencies - LLNL Hazard
(Conditional on hazard)

	0.1g	0.2g	0.3g	0.4g	0.5g	0.6g	0.7g
T1-2	7.56E-07	2.90E-03	8.18E-02	3.62E-01	5.83E-01	5.56E-01	4.51E-01
T1-3	4.01E-06	2.65E-03	2.83E-02	3.93E-02	1.51E-02	2.40E-03	2.15E-04
T1-1	6.70E-05	4.20E-03	3.76E-02	9.07E-02	1.07E-01	8.18E-02	4.96E-02
T3-1	3.18E-04	1.25E-02	4.43E-02	5.26E-02	2.08E-02	0.00E-01	0.00E-01
SLOCA-7	8.72E-07	7.46E-04	1.42E-02	6.11E-02	1.22E-01	1.62E-01	1.78E-01
ALOCA-3	6.98E-08	1.51E-04	4.13E-03	2.49E-02	7.13E-02	1.29E-01	1.79E-01
RVR	1.79E-06	3.59E-04	4.03E-03	1.66E-02	4.22E-02	7.80E-02	1.19E-01
MLOCA-4	2.17E-08	5.34E-05	1.78E-03	1.12E-02	2.99E-02	4.97E-02	6.57E-02
ALOCA-2	1.63E-05	1.71E-03	1.35E-02	4.37E-02	9.18E-02	1.43E-01	1.87E-01

Table 4.21

Mean Core Damage Contributions (Median) at Intervals of PGA - LLNL Hazard

	0.05-0.15g	0.15-0.25g	0.25-0.35g	0.35-0.45g	0.45-0.55g	0.55-0.65g	0.65-0.75g	Total
T1-6	1.87E-07	4.63E-06	1.47E-05	1.61E-05	9.46E-06	4.28E-06	1.81E-06	5.12E-05
T1-5	5.38E-08	1.78E-06	3.63E-06	1.50E-06	2.10E-07	1.40E-08	5.61E-10	7.19E-06
T1-1	4.01E-07	4.94E-06	9.61E-06	6.38E-06	2.62E-06	8.55E-07	2.48E-07	2.50E-05
T3-1	8.28E-07	2.19E-06	1.14E-06	3.15E-07	6.56E-08	1.18E-08	1.96E-09	4.55E-06
SLOCA-7	4.79E-09	3.07E-07	1.44E-06	2.22E-06	1.94E-06	1.34E-06	8.31E-07	8.08E-06
ALOCA-3	3.35E-10	6.16E-08	4.30E-07	9.45E-07	1.19E-06	1.13E-06	9.18E-07	4.67E-06
RVR	8.52E-09	1.42E-07	3.93E-07	5.94E-07	6.87E-07	6.95E-07	6.46E-07	3.17E-06
MLOCA-4	1.19E-10	2.20E-08	1.82E-07	4.08E-07	4.76E-07	4.16E-07	3.19E-07	1.82E-06
ALOCA-2	1.19E-10	1.93E-08	2.58E-07	8.08E-07	1.18E-06	1.15E-06	9.32E-07	4.35E-06
T3-6	2.73E-07	8.78E-07	5.81E-07	2.25E-07	6.99E-08	1.97E-08	5.27E-09	2.05E-06
Total	1.74E-6	1.49E-5	3.24E-5	2.95E-5	1.79E-5	9.91E-6	5.7E-6	1.12E-04

Table 4.22

Mean Initiating Event Frequencies - EPRI Hazard

	0.1g	0.2g	0.3g	0.4g	0.5g	0.6g	0.7g
RVR	1.79E-06	3.59E-04	4.03E-03	1.66E-02	4.22E-02	7.80E-02	1.19E-01
ALOCA	1.63E-05	1.71E-03	1.35E-02	4.37E-02	9.18E-02	1.43E-01	1.87E-01
MLOCA	4.59E-06	4.82E-04	4.12E-03	1.43E-02	3.14E-02	5.01E-02	6.57E-02
SLOCA	1.84E-04	6.73E-03	3.28E-02	7.79E-02	1.28E-01	1.63E-01	1.78E-01
T1(LOSP)	3.36E-02	3.25E-01	6.08E-01	7.06E-01	6.74E-01	5.65E-01	4.51E-01
T3	9.66E-01	6.66E-01	3.38E-01	1.41E-01	3.27E-02	0.00E-01	0.00E-01

Table 4.23

Mean Accident Sequence Frequencies (per year) Conditional on Hazard - EPRI Hazard

	0.1g	0.2g	0.3g	0.4g	0.5g	0.6g	0.7g
T1-2	7.56E-07	2.90E-03	8.18E-02	3.62E-01	5.83E-01	5.56E-01	4.51E-01
T1-3	4.01E-06	2.65E-03	2.83E-02	3.93E-02	1.51E-02	2.40E-03	2.15E-04
T1-1	6.70E-05	4.20E-03	3.76E-02	9.07E-02	1.07E-01	8.18E-02	4.96E-02
T3-1	3.18E-04	1.25E-02	4.43E-02	5.26E-02	2.08E-02	0.00E-01	0.00E-01
SLOCA-7	8.72E-07	7.46E-04	1.42E-02	6.11E-02	1.22E-01	1.62E-01	1.78E-01
ALOCA-3	6.98E-08	1.51E-04	4.13E-03	2.49E-02	7.13E-02	1.29E-01	1.79E-01
RVR	1.79E-06	3.59E-04	4.03E-03	1.66E-02	4.22E-02	7.90E-02	1.19E-01
MLOCA-4	2.17E-08	5.34E-05	1.78E-03	1.12E-02	2.99E-02	4.97E-02	6.57E-02
ALOCA-2	1.63E-05	1.71E-03	1.35E-02	4.37E-02	9.18E-02	1.43E-01	1.87E-01

Table 4.24

Mean Core Damage Contributions From Dominant Accident Sequences - EPRI Hazard

	0.05-0.15g	0.15-0.25g	0.25-0.35g	0.35-0.45g	0.45-0.55g	0.55-0.65g	0.65-0.75g	Total
T1-6	7.03E-08	1.20E-06	3.14E-06	2.98E-06	1.57E-06	6.56E-07	2.36E-07	9.85E-06
T1-5	2.02E-08	4.60E-07	7.74E-07	2.79E-07	3.48E-08	2.14E-09	7.28E-11	1.57E-06
T1-1	1.51E-07	1.28E-06	2.05E-06	1.19E-06	4.33E-07	1.31E-07	3.22E-08	5.26E-06
T3-1	3.11E-07	5.69E-07	2.42E-07	5.85E-08	1.08E-08	1.82E-09	2.55E-10	1.19E-06
SLOCA-7	1.80E-09	7.95E-08	3.08E-07	4.12E-07	3.21E-07	2.05E-07	1.08E-07	1.43E-06
ALOCA-3	1.26E-10	1.60E-08	9.16E-08	1.76E-07	1.97E-07	1.73E-07	1.19E-07	7.73E-07
RVR	3.20E-09	3.68E-08	8.38E-08	1.10E-07	1.14E-07	1.06E-07	8.39E-08	5.38E-07
MLOCA-4	4.48E-11	5.69E-09	3.87E-08	7.58E-08	7.87E-08	6.38E-08	4.14E-08	3.04E-07
ALOCA-2	4.48E-11	5.01E-09	5.50E-08	1.50E-07	1.95E-07	1.77E-07	1.21E-07	7.02E-07
T3-6	1.02E-07	2.28E-07	1.24E-07	4.19E-08	1.16E-08	3.01E-09	6.84E-10	5.11E-07
Total	6.55E-7	3.88E-6	6.90E-6	5.47E-6	2.96E-6	1.52E-6	7.42E-7	2.21E-5

to the variation of initiating event frequencies and accident sequence frequencies with earthquake level as described for the LLNL mean point estimate case apply.

4.4.6 Base Case Importance Studies

A. Basic Event Importance to Mean Values

The importance of the basic seismic failure events was evaluated by setting the seismic failure probability to zero, which gives a measure of the net reduction in risk that would occur if that component could never fail due to seismic shaking. The results of these calculations for both sets of hazard curves are shown in Table 4.25 and the results are both qualitatively and quantitatively similar. (Note that the sum of the risk reduction percentages do not and should not equal unity, since many of the important components occur together in the same cut sets, and hence, a zero failure probability of one component causes the entire cut set to vanish.)

It can be seen that the largest risk reduction occurs for ceramic insulators. This occurs, of course, because the ceramic insulators are the basis for the T_1 transient sequences. The two vertical water storage tanks (CST and RWST) have risk reductions of 26 percent and 10 percent respectively. The 4Kv busses together represent a risk reduction of 36 percent, which is due to the fact that all 4Kv power, including emergency power from the diesel generators, go through these busses. The two diesel generators represent a risk reduction of 22 percent when taken together. The remainder of the components have significantly less risk reduction potential.

B. Basic Event Importance to Overall Uncertainty

The relative contribution of the hazard curve, the seismic response and the seismic fragility uncertainties (β_u's) to the overall core damage frequency was ascertained. The results of these comparisons (for both sets of hazard curves) are shown on Tables 4.26 and 4.27 The base case mean, 95 percent and 50 percent core damage frequencies are shown in the first column. The second column shows the corresponding values with the hazard curve fixed at its median value (i.e., with no modeling uncertainty). For the LLNL hazard curve case, it can be seen that the error factor (EF) associated with these results is 3.6, whereas the corresponding error factor for the base case was 29.6. Similarly, for the EPRI hazard curve case, the base case error factor was 16.8 while with no uncertainty in the hazard curve, the error factor is reduced to 4.2. Clearly, the hazard curve is contributing the vast majority of the uncertainty in the base case results.

The third column shows the calculation wherein all the fragility and response modeling uncertainties are simultaneously set to zero. For the LLNL hazard curves, the error factor is 23.6. For the EPRI hazard curves, the corresponding error factor is 12.6. These results show that the reduction in the response or fragility uncertainties has only a

Table 4.25

Dominant Component Contributors to P(cm)
Ranked By Risk Reduction Potential

Component	LLNL Hazard	EPRI Hazard
Ceramic Insulators	50%	68%
4KV1H	36%	27%
4KV1J		
CST	26%	21%
DG1-FS	22%	13%
DG3-FS		
RWST	21%	22%
BAC-1H1-2	9%	8%
BAC-1J1-2		
AFW-XCONN	3%	2%
OEP-DG-3U2	3%	2%
CRB-FT-15H3	<1%	<1%
CRB-FT-15J3	<1%	<1%
DG1-MA	<1%	<1%
DG3-MA	<1%	<1%
OEP-DG-CCF-13	<1%	<1%
BATT1A	<1%	<1%
BATT1B	<1%	<1%

Table 4.26

Comparison of Contributions of Modeling Uncertainty in Response, Fragility and Hazard Curves to Core Damage Frequency
LLNL Hazard

	Base Case	Hazard $\beta_U=0$	$\beta_{FU}=0$ $\beta_{RU}=0$
Mean	1.16E-4	1.76E-5	6.31E-5
95%	4.38E-4	4.66E-5	2.30E-4
50%	1.48E-5	1.28E-5	9.73E-6
$\frac{P_{cm}(95\%)}{P_{cm}(50\%)}$	29.6	3.6	23.6

Table 4.27

Comparison of Contributions of Modeling Uncertainty in Response, Fragility and Hazard Curves to Core Damage Frequency
EPRI Hazard

	Base Case	Hazard $\beta_U=0$	$\beta_{FU}=0$ $\beta_{RU}=0$
Mean	2.50E-5	8.09E-6	1.29E-5
95%	1.03E-4	2.29E-5	4.86E-5
50%	6.12E-6	5.47E-6	3.86E-6
$\frac{P_{cm}(95\%)}{P_{cm}(50\%)}$	16.8	4.2	12.6

secondary effect on the overall core damage uncertainty (no matter which set of hazard curves is used).

These results show quite clearly that the uncertainty in the hazard curve is the dominant factor in both the mean value of core damage frequency and in the uncertainty of the core damage frequency. Further, as was seen in the discussion of the mean point estimate case, it is the mean hazard curve which drives the mean estimate of core damage frequency. Again, this shows the dominant influence of the hazard curve uncertainty (which determines the mean hazard curve) in determining the mean core damage frequency.

C. Effect of Hazard Curve Discretization

All the results discussed so far have been based on a model of the hazard curve uncertainty in which the variation is assumed to be log normal (at each value of PGA). The principal investigator of the Eastern US Seismic Hazard Characterization Program has indicated that this uncertainty distribution is approximately log normal, and this was substantiated by the calculated mean hazard curve shown earlier. However, the log normal distribution does have an extended tail. To assess the potential effect of contributions from the tail of the assumed distribution an alternate approach was taken.

In this sensitivity study, a family of ten hazard curves was generated from the assumed log normal distribution corresponding to confidence levels of 5 percent, 15 percent, . . . 95 percent. Each of these curves is assumed to be equally weighted.

Table 4.28 compares the LLNL mean hazard curve ordinates derived from the family of discrete hazard curves used above with the mean hazard curve obtained from the full log normal distribution model. As can be seen from this table, the mean hazard curve is significantly less for the discrete family. A point estimate calculation was made using the mean hazard curve for the family and mean seismic accident sequence frequencies which resulted in a mean point estimate value of core damage frequency given by 6.40E-5. This compares to the base case mean value of 1.12E-4. This reduction in core damage frequency from the base case is due to both eliminating the tails of the distribution and due to a shift in the mean hazard curve.

Table 4.29 compares the EPRI mean hazard curve ordinants derived from the family of discrete hazard curves with a full log normal distribution model. Again, repeating the analysis resulted in a mean core damage frequency of 1.67E-5 as contrasted to the base case result of 2.21E-5 per year.

From these results, one would infer that the use of a limited number of discrete hazard curves results in a reduction in computed core damage frequencies from 24 percent to 43 percent, and that the reduction is due to the reduction in the mean hazard curve which results from cutting off the tails of the full hazard curve distribution. From a PRA perspective,

Table 4.28

Comparison of Mean Hazard
Curve Probabilities From Ten
Discrete Hazard Curves and From
Hazard Curve with Assumed Log Normal Distribution
LLNL Hazard

PGA	10 Discrete Curves Mean Hazard Probability	Full Distribution Mean Hazard Probability
0.15g	3.63E-4	5.65E-4
0.25g	9.58E-5	1.70E-4
0.35g	3.74E-5	7.30E-5
0.45g	1.79E-5	3.77E-5
0.55g	9.78E-6	2.19E-5
0.65g	5.78E-6	1.37E-5
0.75g	3.70E-6	9.12E-6

Table 4.29

Comparison of Mean Hazard
Curve Probabilities From Ten
Discrete Hazard Curves and From
Hazard Curve with Assumed Log Normal Distribution
EPRI Hazard

PGA	10 Discrete Curves Mean Hazard Probability	Full Distribution Mean Hazard Probability
0.15g	1.10E-4	1.35E-4
0.25g	2.42E-5	3.28E-5
0.35g	8.34E-6	1.21E-5
0.45g	3.64E-6	5.54E-6
0.55g	1.85E-6	2.92E-6
0.65g	1.01E-6	1.67E-6
0.75g	5.96E-7	1.07E-6

reductions, while not insignificant, would not affect the conclusions resulting from a seismic PRA. Thus, one would conclude that knowledge of the exact form of the tails of the hazard curve distribution (as determined by the LLNL hazard curve development process) is not essential to a robust understanding of the plant's seismic risk and vulnerabilities.

4.4.7 Summary and Plant Specific Insights

This chapter has presented the seismic risk results for the Surry Plant using both industry-sponsored (EPRI) and NRC-sponsored (LLNL) hazard curve estimates. The differences between these sets of hazard curves resulted in a significant difference in computed total core damage frequency (1.16E-4 per year for the LLNL hazard curves and 2.50E-5 per year for the EPRI hazard curves). This rather significant difference is expected to bound the seismic risk at Surry.

However, the seismic risk was found to be dominated by relatively few accident sequences and the same dominant accident sequences were found using both sets of hazard curves. Furthermore, it was found that the relative contribution of individual component failures was the same (both qualitatively and quantitatively) for both sets of hazard curves. Thus, insights as to important contributors to risk at Surry and to the identification of important accident scenarios are relatively robust and did not depend on the particular hazard curves chosen.

In general, it was found that only a few accident sequences dominated the results. The most dominant sequence was a loss of offsite power (LOSP) transient sequence in which the auxiliary feedwater system fails (due to loss of the condensate storage tank) and the high pressure injection (HPI) system (and hence, the feed and bleed operation) fails due to either failure of the refueling water storage tank or failures of the onsite AC power system. The second most significant sequence is also a loss of offsite power transient sequence, except that this transient sequence leads to a seal LOCA. This is caused by failure of both the HPI system and the component cooling water (CCW) system which leads to the seal LOCA. The HPI system fails as described above while the CCW system fails due to loss of onsite AC power. Together, these two sequences constitute approximately 67% of the computed core damage frequency.

Finally, a sensitivity study in which the continuous lognormal uncertainty model for the hazard curves was replaced by a discrete family of hazard curves (and, hence, the extreme tails of the lognormal distribution were truncated) was made. This study showed that the tails of the hazard curve distribution did not dominate the core damage frequency results obtained.

4.5 References

1. D. L. Bernreuter et al., Seismic Hazard Characterization of 69 Nuclear Plant Sites East of the Rocky Mountains, Lawrence Livermore National Laboratory, NUREG/CR-5250, October 1988.

2. Electric Power Research Institute, Seismic Hazard Methodology for the Central and Eastern United States, EPRI NP-4726, Vol. 1-10, July 1986.

3. P. B. Schnabel, J. Lysmer, and H. B. Seed, SHAKE -- A Computer Program for Earthquake Response Analysis of Horizontally Layered Sites, Earthquake Engineering Research Center, University of California, Berkeley, CA, EERC 72-12, 1972.

4. Ohta and Goto, "Empirical Shear Wave Velocity Equations In Terms of Characteristic Soil Indexes," Earthquake Engineering & Structural Dynamics, Vol. 6, pp 169-187, 1978.

5. Surry Power Station Updated Final Safety Analysis Report, Section 2.0, June 1983.

6. H. B. Seed and I. M. Idriss, Soil Moduli and Damping Factors for Dynamic Response Analyses, Earthquake Engineering Research Center, University of California, Berkeley, CA, EERC 70-10, 1970.

7. H. B. Seed, C. Ugas, and J. Lysmer, Site Dependent Spectra for Earthquake Resistant Design, Earthquake Engineering Research Center, University of California, Berkeley, CA, EERC 74-12m, 1974.

8. J. J. Johnson, G. L. Goudreau, S. W. Bumpus, and O. R. Maslenikov, Seismic Safety Margins Research Program Phase I Final Report -- SMACS - Seismic Methodology Analysis Chain with Statistics (Project VIII), Lawrence Livermore National Laboratory, Livermore, CA, UCRL-53021, Vol. 9, NUREG/CR-2015, Vol. 9, 1981.

9. H. L. Wong and J. E. Luco, Soil-Structure Interaction: A Linear Continuum Mechanics Approach (CLASSI), Dept. of Civil Engineering, University of Southern California, Los Angeles, CA, CE79-03, 1980.

10. M. P. Bohn et al., Application of the SSMRP Methodology to the Seismic Risk at the Zion Nuclear Power Plant, UCRL-53483, NUREG/CR-3428, Lawrence Livermore National Laboratory, Livermore, CA, 1983.

11. L. E. Cover, et al., Handbook of Nuclear Power Plant Seismic Fragilities, NUREG/CR-3558, December 1983.

12. R. D. Campbell, et al., Compilation of Fragility Information From Available Probabilistic Risk Assessments, Lawrence Livermore National Laboratory Report UCID-20571 Rev. 1, September 1988.

13. D. A. Wesley and P. S. Hashimoto, Seismic Structural Fragility Investigation for the Zion Nuclear Power Plant, Lawrence Livermore National Laboratory, NUREG/CR-2320, October 1981.

14. R. Riddell and N. M. Newmark, Statistical Analysis of the Response of Nonlinear Systems Subjected to Earthquakes, UILU-ENG 79-2016, University of Illinois, August 1979.

15. R. P. Kennedy, et al, Engineering Characteristics of Ground Motion - Task I: Effects of Characteristics of Free-Field Motion on Structural Response, Lawrence Livermore National Laboratory, NUREG/CR-3805, May 1984.

16. N. M. Newmark, "Effects of Earthquakes on Dams and Embankments," Geotechnique, Volume XV, No. 2, 1965.

17. Letter from Virginia Electric and Power Company to NRC, Subject: IE Bulletin 80-11, Masonry Wall Design Final Report, Surry Power Station Units 1 and 2, dated October 29, 1981 (Serial No. 604).

5.0 SURRY FIRE ANALYSIS

5.1 Introduction

The objective of the analysis reported here was to estimate the contribution of fire-induced core damage and plant damage state frequencies. The overall fire-induced core damage frequency for Surry Unit 1 was found to be 1.13E-5 per year. The various fire area contributions are given in Table 5.1. The accident sequences these scenarios mapped into are listed in Table 5.2.

Table 5.1

Surry Fire Area Core Damage Frequency

	Core Damage Frequency (/yr)			
Fire Area	Mean	5th Percentile	Median	95th Percentile
Emergency Switchgear Room	6.09E-6	3.93E-9	3.15E-6	1.98E-5
Control Room	1.58E-6	1.20E-10	4.68E-7	6.95E-6
Cable Vault/Tunnel	1.49E-6	6.51E-10	6.99E-7	5.79E-6
Auxiliary Building	2.18E-6	5.32E-7	1.59E-6	5.64E-6
Charging Pump Service Water Pump Room	3.92E-8	1.43E-10	5.66E-9	1.58E-7
Total	1.13E-5	5.37E-7	8.32E-6	3.83E-5

Based on plant operating experience over the last 20 years, it has been observed that typical nuclear power plants will have three to four significant fires over their operating lifetime. Previous probabilistic risk assessments (PRAs) have shown that fires are a significant contributor to the overall core damage frequency, contributing anywhere from 7 percent to 50 percent of the total (considering contributions from internal, seismic, flood, fire, and other events). Because of the relatively high core damage contribution, fires need to be examined in more detail.

An overview of the simplified fire PRA methodology is as follows:

Table 5.2

Dominant Accident Sequence Core Damage Frequency Contributors

Sequence	Fire Area	Mean Core Damage Frequency (/yr)
$T_3D_3WD_1$	Emergency Switchgear Room	6.09E-6
	Auxiliary Building	2.18E-6
	Cable Vault/Tunnel	1.49E-6
T_3QD_1	Control Room	1.58E-6
	Charging Pump Service Water Pump Room	3.92E-8

A. Initial Plant Visit

Based on the internal event and seismic analyses, the general location of cables and components of the systems of interest is known. The plant visit provides the analyst with a means of seeing the physical arrangements in each of these areas. The analyst will have a fire zone checklist which will aid the screening analysis and in the quantification step. The second purpose of the initial plant visit is to confirm with plant personnel that the documentation being used is, in fact, the best available information and to get clarification about any questions that might have arisen in a review of the documentation. Also, a thorough review of firefighting procedures is conducted.

B. Screening

It is necessary to specify the important fire locations within the power plant under investigation that have the greatest potential for producing risk-dominant accident sequences. The objectives of this location selection are somewhat competing and should be balanced in a meaningful risk assessment study. The first objective is to maximize the possibility that all important locations are analyzed, this leads to the consideration of a potentially large number of candidate locations. The second objective is to minimize the effort spent in the quantification of event trees and fault trees for fire locations that turn out to be unimportant. A proper balance of these objectives is one that results in an ideal allocation of resources and efficiency of assessment.

The screening analysis is comprised of:

1. Identification of relevant fire zones. Those Appendix R identified fire zones which had either safety related equipment or power and control cables for that equipment were identified as requiring further analysis. This group of fire zones (areas) is briefly described in Section 5.2. All critical safety components within these fire areas are given in Appendix D.

2. Screen fire zones on probable fire-induced initiating events. Determination of the fire frequency for all plant locations and determination of the resulting fire-induced initiating events and "off-normal" plant states is delineated in Sections 5.3 and 5.4 respectively.

3. Screen fire zones on both order and frequency of cut sets.

4. Each fire zone remaining is numerically evaluated and culled on frequency.

The screening methodology (Section 5.5) describes how reduction of the initial group of locations from Section 5.2 to the five remaining with contributions to core damage frequency of greater than 10^{-8} per year was accomplished.

C. Quantification

After the screening analysis has eliminated all but the probabilistically-significant fire zones, quantification of dominant cut sets is completed as follows:

1. Determine temperature response in each fire zone.

2. Compute component fire fragilities. The latest version of the fire growth code COMPBRN with some modifications was used to calculate fire propagation and equipment damage. A description of these results for steps 1 and 2 is given in Section 5.6. These fire calculations were only performed for the fire areas that survived the screening analysis.

3. Assess the probability of barrier failure for all remaining combinations of fire zones. A barrier failure analysis was conducted for those combinations of two adjacent fire zones which, with or without additional random failures, remained after the screening analysis. The methodology to assign barrier failure probability to the fire zone combinations is described in Section 5.7.

4. Perform a recovery analysis. In similar manner to that used for the internal event analysis recovery of non-fire related random failures was addressed. Appropriate modifications to recovery probabilities were made as described in Section 5.8.

5. An uncertainty analysis is performed to estimate error bounds on the computed fire-induced core damage frequencies. As in the internal events analysis, the TEMAC code was utilized in the uncertainty analysis as described in Section 5.9.

In Section 5.10 a detailed description of all fire scenarios with contributions to core damage frequency of greater than 10^{-8} per year and their associated fire areas is given. Distributions and a description of all factors used in the final quantification of all fire areas are delineated.

5.2 Fire Locations Analyzed

In this section, the plant areas (fire zones) analyzed are listed in Table 5.3. A list of components contained in each of these fire zones is given in Appendix D. Table 5.3 also provides a brief physical description of each fire zone. This study was conducted with cable routing information on a limited set of components considered to be those most vital to mitigating the effects of any potential fire-induced "off-normal" plant state. Some of this cable routing information was obtained from the Appendix R submittal while other routings were obtained from utility routing information and confirmed during a plant walkdown.

These lists of components as well as cable traced vital components formed the basis of the computer aided screening analysis. All other fire areas not contained in Table 5.3 were screened, as they did not contain either vital equipment or cabling for that equipment.

The following subsections provide a discussion of the fire detection and manual or automatic fire extinguishment capabilities that presently exist in each fire zone.

5.2.1 Cable Vault/Tunnel (Fire Area 1)

Ionization smoke detectors are provided in Fire Area 1. These detectors alarm in the control room. In addition, heat detectors which actuate an automatic CO_2 system are located in the CV/T.

A manually activated deluge system, located at the top of the high ceiling vault, and a manually activated closed-head sprinkler system, located within the tunnel, covers Fire Area 1. Portable extinguishers and hose stations are available in each area for firefighting purposes.

5.2.2 Emergency Switchgear Room (Fire Area 3)

Fire detection consists of ionization detectors in conjunction with a manually actuated total flooding Halon system. There are also portable extinguishers located within the area and a hose station located in the turbine building at the door to the emergency switchgear room.

5.2.3 Control Room (Fire Area 5)

The control room has ionization smoke detectors mounted at the ceiling. There is no automatic suppression system.

Table 5.3

Surry Fire Areas Containing Safety Related Components

Fire Area	Physical Description
1	Outside containment penetration vault; Cable tunnel; Service building cable vault.
3	Emergency switchgear room (Elev. 9 ft 6 in. - Service Building) contains switchgear area, 2 battery rooms, and a relay room, as well as the auxiliary shutdown panel.
5	Main control room (Elev. 27 ft) in the Service Building for operation of primary and secondary systems of each unit.
6	Emergency Diesel Generator Room #1 for Unit 1 (Elev. 27 ft) in the Service Building.
7	Emergency Diesel Generator Room #2 for Unit 2 (Elev. 27 ft) in the Service Building.
8	Emergency Diesel Generator Room #3 as backup for Unit 1 or 2 (Elev. 27 ft) in the Service Building.
15	Primary Containment for Unit 1, multilevel structure with floor elevations of 46 ft 4 in., 27 ft 7 in., 18 ft 4 in., 13 ft (partial elevation only), and 3 ft 6 in., with personnel airlock access hatch at the 45 ft 10 in. elevation of the auxiliary building.

Table 5.3

Surry Fire Areas Containing Safety Related Components (Concluded)

Fire Area	Physical Description
17	Auxiliary Building, Fuel Building, and Decontamination Building. The buildings are located side by side in a north-south orientation, with the auxiliary building to the south, the decontamination building to the north, and the fuel building in the center. The auxiliary building is a four-story structure consisting of the 2 ft, 13 ft, 27 ft 6 in., and 45 ft 10 in. elevations.
19	This fire area, collectively referred to as the safeguards area, consists of the main steam valve house, containment spray pump house, and the safeguards area.
31	The Turbine Building consists of three primary elevations: the 9 ft 6 in. basement, the 35 ft mezzanine, and the 58 ft 6 in. turbine deck.
45	Mechanical Equipment Room #3 is located in the service building basement at elevation 9 ft 6 in.
54	The Charging Pump Service Water Pump Room is on the 9 ft 6 in. level adjacent to the main turbine building and mechanical equipment room #3.

Manual fire suppression is provided for by fire extinguishers interior to the control room and a hose station located in the turbine building.

5.2.4 Emergency Diesel Generator Rooms (Fire Areas 6, 7, and 8)

Each emergency diesel generator room is equipped with a total flooding low pressure carbon dioxide (CO_2) fire suppression system. The system can be manually actuated either locally at the CO_2 control panel directly outside the door or remotely in the control room. Doors and dampers are equipped with blow-off caps to close upon CO_2 initiation. Rate compensated heat detectors (190°F) are located in each room and provide remote annunciation to the control room.

All the EDG rooms have at least two fire extinguishers. Hose stations and a portable firefighting foam cart are located nearby in the turbine building corridor.

5.2.5 Primary Containment (Fire Area 15)

The boundary fire barrier for Fire Area 15 is of a heavy reinforced concrete construction with an inherent fire rating in excess of three hours. Fire detection consists of heat, smoke, and duct detectors, which are alarmed in the control room.

There are portable fire extinguishers located just outside the containment at the personnel hatch. Dry hose standpipes are available inside containment. Adequate hose lengths to reach all portions of the containment can be brought in during emergencies.

5.2.6 Auxiliary Building (Fire Area 17)

An automatic detection system that alarms in the control room is provided in the auxiliary building portion of Fire Area 17. Smoke detectors are located on each elevation of the auxiliary building, consisting of both ceiling-mounted smoke detectors and duct detectors. One ceiling-mounted detector and one duct detector is provided in each charging pump cubicle. Two ceiling-mounted detectors are installed above each unit's charging pump-component cooling water pumps. Portable extinguishers and manual hose stations are provided on all levels of the auxiliary building for fire fighting purposes.

5.2.7 Safeguards Area (Fire Area 19)

The safeguards area is equipped with ionization smoke detectors. All of the smoke detectors alarm in the control room. In addition, each area contains portable extinguishers. An exterior hose station, located in the yard, is available for manual firefighting purposes.

5.2.8 Turbine Building (Fire Area 31)

A full area automatic sprinkler system is installed on the 35 ft and the 9 ft 6 in. elevations. Upon sprinkler system water flow, an alarm is transmitted to the control room.

The major lube oil components have individual deluge systems actuated by heat detectors. These also provide annunciation to the control room upon system actuation.

There are a number of portable fire extinguishers and hose stations located in the turbine building as well as a portable firefighting foam cart.

5.2.9 Mechanical Equipment Room #3 (Fire Area 45)

Smoke detectors are provided in Fire Area 45. These detectors alarm in the control room. Some of these smoke detectors are designed to operate MOVs in the event of a fire to allow the redundant charging pump service water pumps to operate.

There are fire extinguishers in the area and hose stations are located in the turbine building at the door to the emergency switchgear room.

5.2.10 Charging Pump Service Water Pump Room (Fire Area 54)

Fire detection consists of two ionization detectors which alarm in the control room. This area could be entered from the turbine building for firefighting purposes.

5.3 Initiating Event Frequencies

Data on fires in Light Water Reactors have been analyzed in several studies (Refs. 1,2,3). Although they have been done independently, they have some common aspects. For example, almost all studies have used License Event Report (LER) data from the Nuclear Regulatory Commission (NRC). All have reported the overall frequency of fires of approximately 0.16 per reactor year on a plant wide basis.

To determine fire initiating event frequencies, there are two kinds of information needed: (1) the number of fire incidents that have occurred in specific compartments during commercial operation, and (2) the number of compartment years that the nuclear industry has accumulated. Most of the data for the first part comes from reports of insurance inspectors to American Nuclear Insurers (ANI), although other sources are also used, e.g., the U.S. Nuclear Regulatory Commission. While the NRC requires the reporting of fires that, in some way, affect the safety of the plant, the ANI has more stringent requirements in the sense that all fire events must be reported. Compartment years are computed by adding the age of all compartments (within a certain category of compartments) of units that were in commercial operation by the end of June 1985. The age is defined as the time between first commercial operation and the end of June 1985 (or date of decommissioning). The combination of specific fire locations and compartment age is given in Table 5.4. Even though fire events that occurred when the plant was shutdown were used, an event was only included if it could be postulated that it could also occur when the plant was at power. Eight areas are typically found in nuclear power plants. These are (1) the control room, (2) cable spreading room,

(3) diesel generator room, (4) reactor building, (5) turbine building, (6) auxiliary building, (7) electrical switchgear room, and (8) battery room. In most plants, the first three areas and the electrical switchgear room and battery room are single compartments while the other three are typically large buildings. A listing of all generic data used for each of the four types of fire areas that survived screening is given in Appendix E.

Table 5.4

Statistical Evidence of Fires in LWRs
(As of June 1985)

Area	Number of Fires r	Number of Compartment Years T
Control Room	3	681.0
Cable Spreading Room	2	747.3
Diesel Generator Room	37	1600.0
Reactor Building	15	847.5
Turbine Building	21	654.2
Auxiliary Building	43	673.2
Electrical Switchgear Room	4	1346.4
Battery Room	4	1346.4

To obtain fire zone specific initiating frequencies, a partitioning method is required. Partitioning allows the analyst to subdivide the frequency of fire occurrence from a large building (e.g., auxiliary building) to a specific room or area within that building. Also, further partitioning can occur within a specific room or area. One method of partitioning is comprised of ratioing the areas of fire zones within a building (e.g., auxiliary building). The assumption here is that the probability of fire occurrence is dependent only upon the amount of area a fire zone contains. Another method of partitioning would look at each fire zone and analyze factors important to probability of fire initiation. These factors are the amount of electrical components and cabling, the fire loading, whether the fire zone is controlled, and how often the fire zone is occupied.

The fire events and operating years for the eight plant areas were obtained using the fire data base developed by Wheelis (Ref. 4). To determine operating years for electrical switchgear rooms and battery rooms, auxiliary building operating years were doubled. A survey of all U.S. light water reactors indicated that there is an average of 2.25 trains of emergency switchgear and their associated batteries per plant. However, it is known that some plants such as Surry locate both trains of their emergency switchgear in one fire zone. So it was assumed that an average number would be close to two per plant.

To aid partitioning within a large building or within a specific fire zone in that building a checklist was used on the initial plant visit to determine the most probable fire initiating sources. Also, data on past fire occurrences was thoroughly reviewed. For instance, control room data indicate that fires have only occurred in electrical cabinets. Therefore, area ratios were developed based on cabinet area within this respective area. Since transient combustible initiated fires have never occurred, they were eliminated from further consideration.

The generic fire occurrence data was updated using a method developed by Iman (Ref. 5) to determine plant specific fire occurrence frequencies.

This Bayesian approach models the incidence rate for each plant relative to the incidence rates of all other plants, and the posterior distribution is found for the incidence rate for each plant.

For this analysis the gamma distribution is used as a model, although many other distributions could be used.

In this way plant specific fire initiating event frequencies and distributions were developed. Table 5.5 lists the Surry Unit #1 specific fire initiating event frequencies for the five types of fire areas with contributions to core damage frequency of greater than 10^{-8} per year. It should be noted that fire frequency for the CPSWPR was based strictly on generic data. There was no ready means of determining how many pump rooms there are on average per plant. Therefore, two were assumed and auxiliary building operating years were doubled. Since a breakdown of the number of pump rooms per plant could not be obtained, the distribution for the CPSWPR was assumed to be lognormal with an error factor of three.

Surry Unit #1 had no recorded fire occurrences in any of the five areas (cable spreading room, control room, electrical switchgear room, auxiliary building, pump room) that survived the screening process. Surry, however, did have four fire occurrences between 1972 and 1980 that occurred in other plant areas. These fires were located in the safeguards area, transformer yard, diesel generator room, and in a local control tunnel for a control room chiller. Since none of these areas survived the screening analysis described in Section 5.5 no attempt was made to update their fire initiating event frequency.

5.4 Determination of Fire-Induced "Off-Normal" Plant States

One of the most critical steps in a fire analysis is to determine on a plant specific basis which events in a wide range of possible initiating events have the potential to be induced due to a fire occurrence.

As in the NUREG-1150 internal events analysis, a comprehensive list of initiators was identified for further study. It is known from a review of previous fire PRAs that only a limited set of initiating events have the potential to be significant contributors to fire-induced core damage frequency. Typically, initiating events such as large or medium LOCAs caused directly by the fire have not been analyzed because the vulnerabilities of a piping system or tanks to fire events are considered to be insignificant.

Table 5.6 lists the initiating events that were analyzed during the screening process and provides a brief explanation as to why a particular initiating event was included or excluded from further study.

The same fault trees and event trees which were used in the internal events analysis were utilized in the fire analysis. Thus, the level of analytical detail was consistent with the level in the internal event analysis.

5.5 Detailed Description of the Screening Analysis

A comprehensive screening analysis is required to reduce the number of potential fire-induced scenarios to only those which have the potential to be probabilistically significant to core damage frequency.

The screening analysis is composed of the following four steps:

Step 1. Identification of Relevant Fire Zones

Fire zones containing equipment or cables associated with safety-related systems which mitigate the effects of the unscreened fire-induced "off-normal" plant states were identified. All other fire zones were then eliminated from further analysis. This resulted in the fire zones which are described in Section 5.2.

Step 2. Screen Fire Zones Based on Fire Area Analysis

The remaining fire zones underwent a fire area analysis (location mapping) of components as well as control and power cables for a limited set of "vital" components that were located within these areas. This information resulted in a transformation block used in conjunction with the SETS computer code (Refs. 6, 7) to solve all front line systems and then solve all of the identified sequences (Table 5.6) of Section 5.4.

Table 5.5

Surry Fire Initiating Event Frequencies (/yr)

Fire Area	Mean	5th Percentile	50th Percentile	95th Percentile
Control Room	1.8E-3	1.2E-6	9.6E-4	7.4E-3
Cable Vault/Tunnel	7.5E-3	3.0E-6	1.8E-3	1.6E-2
Electrical Switchgear Room	8.0E-3	2.0E-5	2.4E-3	1.7E-2
Auxiliary Building	6.6E-2	2.7E-2	5.9E-2	1.6E-1
Pump Room	3.7E-3		(Lognormal EF = 3)	

Table 5.6

Surry Fire-Induced Initiating Events Analyzed

Initiating Event	Comments
Loss of Offsite Power	Offsite power was excluded because redundant trains were found to be widely separated when routed through common areas which were of sufficient size to preclude buildup of a hot gas layer.
Transient with PCS initially available	Similar to the seismic methodology if no other initiator could occur it was assumed that the operator would either manually scram the plant or an automatic trip would occur due to the fire.
Transient-induced seal or stuck-open PORV LOCA	The probability of one unisolatable stuck-open relief valve was sufficiently high ($>10^{-5}$ demand) to require further analysis.
V-Sequence LOCA	Screened from further analysis because no probabilistically significant mechanism could be identified which had not been addressed by the Appendix R submittal.

The fire occurrence frequency for each zone was set to 1.0 and, given a fire, all components within that zone were assumed to fail. The output of this process was accident cut sets which has fire zone combinations as well as random failures (i.e., not fire-related) included.

Truncation of cut sets at a random failure probability of 10^{-5} was accomplished. This is equivalent to truncation of internal event cut sets at approximately 10^{-9} since the fire frequency is arbitrarily set for screening purposes to 1.0.

Cut sets which required three or more fire zones were eliminated. This was deemed appropriate since these cut sets imply the failure of two or more three-hour rated fire barriers. Cut sets which contained two fire zones were screened on the following three criteria: (1) no adjacency between zones, (2) no penetrations in the adjacency between zones, and (3) if there were penetrations by numerical culling with barrier penetration failure set to a screening value of 0.1. It is known from the analysis of many fire barriers that typical failure rates are on the order of 10^{-2} to 10^{-3}. Therefore, this screening value has been set high enough to insure potentially important fire zone combinations are not truncated in this screening step.

One additional important piece of information gained from these cut sets was identification of the remaining plant locations where zone to zone barriers needed to be analyzed. Dominant cut sets which contained adjacent fire zones were analyzed for barrier failure in the quantification process.

Step 3. Cull Fire Zones on Frequency

Cut sets not eliminated in the first two screening steps were resolved with fire zone specific initiating event frequencies that were calculated as described in Section 5.3.

Also, operator recovery of non-fire related random failures was included. For screening purposes only all short term (less than 24 hours) recovery actions (of non-fire failures) were increased from their respective internal events probabilities by a factor of five to allow for the additional confusion of the fire situation occurring in conjunction with other random failures. If recovery actions were long term (greater than 24 hours) no modification to internal event probabilities were deemed appropriate. It is felt that by this time the fire will be extinguished and any spurious signals will have terminated in open circuits.

It must be noted that Steps 2 and 3 of the screening process reduced the number of cut sets under consideration by at least two orders of magnitude. Also, there were only a few remaining sequences which had not been screened.

Step 4. Confirmatory Plant Visit

For those remaining fire zones all fire-related failure scenarios were identified. A scenario can be thought of as a combination of one or more fire related equipment failures within a fire zone with or without additional non-fire related (random) failures outside of the fire area. These failure combinations must minimally lead to core damage. Each fire zone can have one or more scenarios depending on the equipment combinations which must fail due to the fire in that particular area. A second plant visit was then conducted to determine which of these scenarios were valid based upon cable or equipment locations within a particular fire zone. For instance, if a given scenario required the fire-related failure of cabling for components A and B and it could be shown that these cables were always separated by greater than 40 ft within a room of sufficient size to preclude buildup of a hot gas layer, or one of the component's cabling was in a 3-hr rated fire wrap, then these types of scenarios were eliminated from further consideration. Past experience with fire code calculations, which is discussed in the following section, and fire testing, provided much of the basis for assessing the validity of the scenarios. About one-quarter of the remaining cut sets (scenarios) were eliminated as a result of this confirmatory plant visit.

Those scenarios remaining after screening on physical location of components or their associated cabling within a fire zone was determined had fire propagation calculations run to determine equipment damage. It must be noted for some fire areas that the exact location of a particular components cabling could not be determined. In such cases a best estimate of cable routing was used.

5.6 Fire Propagation Modeling

The COMPBRN fire growth code (Ref. 8) was used to calculate fire propagation and equipment damage. COMPBRN was developed specifically for use in nuclear power plant fire PRAs. The code calculates the time to damage critical equipment given that a fire has started. This failure time is then used in conjunction with experiential information on fire suppression in nuclear power plants to obtain the probability or frequency that a given fire will cause damage which leads to core damage before the fire can be suppressed. The latest version of the code, COMPBRN III (Ref. 9), with some additional modifications was used for the calculations.

COMPBRN follows a quasi-static approach to simulate the process of fire during the pre-flashover period in an enclosure. COMPBRN uses a zone model, breaking the fire environment into three zones: flame/plume, hot gas layer, and ambient (see Figure 5.1). Simple fire and heat transfer models and correlations are employed to predict the thermal environment as a function of time. The thermal response of various targets in the fire scenario is modeled to predict the amount of time for a fire to damage or ignite critical equipment. The critical equipment is generally taken to be a cable tray carrying cables necessary for safe shutdown of the plant, although other critical components such as pump motors may be modeled.

The original version of COMPBRN, now referred to as COMPBRN I, has been used to calculate damage times in the majority of fire PRAs to date. However, the code calculations are thought to be highly conservative due to the neglect of heat losses from the targets. A critical assessment of the code detailing this and other problems has been performed (Ref. 10). In response to these problems with COMPBRN I, two later versions of the code were developed: COMPBRN II and COMPBRN III (Ref. 9). Neither of the later versions of the code has been extensively validated or compared to data, but presumably represent various degrees of improvement.

As a part of a recent study (Ref. 3) on nuclear power plant fire risk assessment, the latest version of the code (COMPBRN III) was selected to requantify fire damage times from several fire PRAs. Initial attempts to use COMPBRN III in the requantification resulted in the observation of problems with and nonphysical behavior of the code. Many of the code calculations could not be explained on a physical basis. As a result of the observed nonphysical behavior of the code, an effort was undertaken to identify problem areas and to suggest and implement modifications to the code which would make the code predictions more reasonable on a physical basis. It was this modified version of the COMPBRN code which

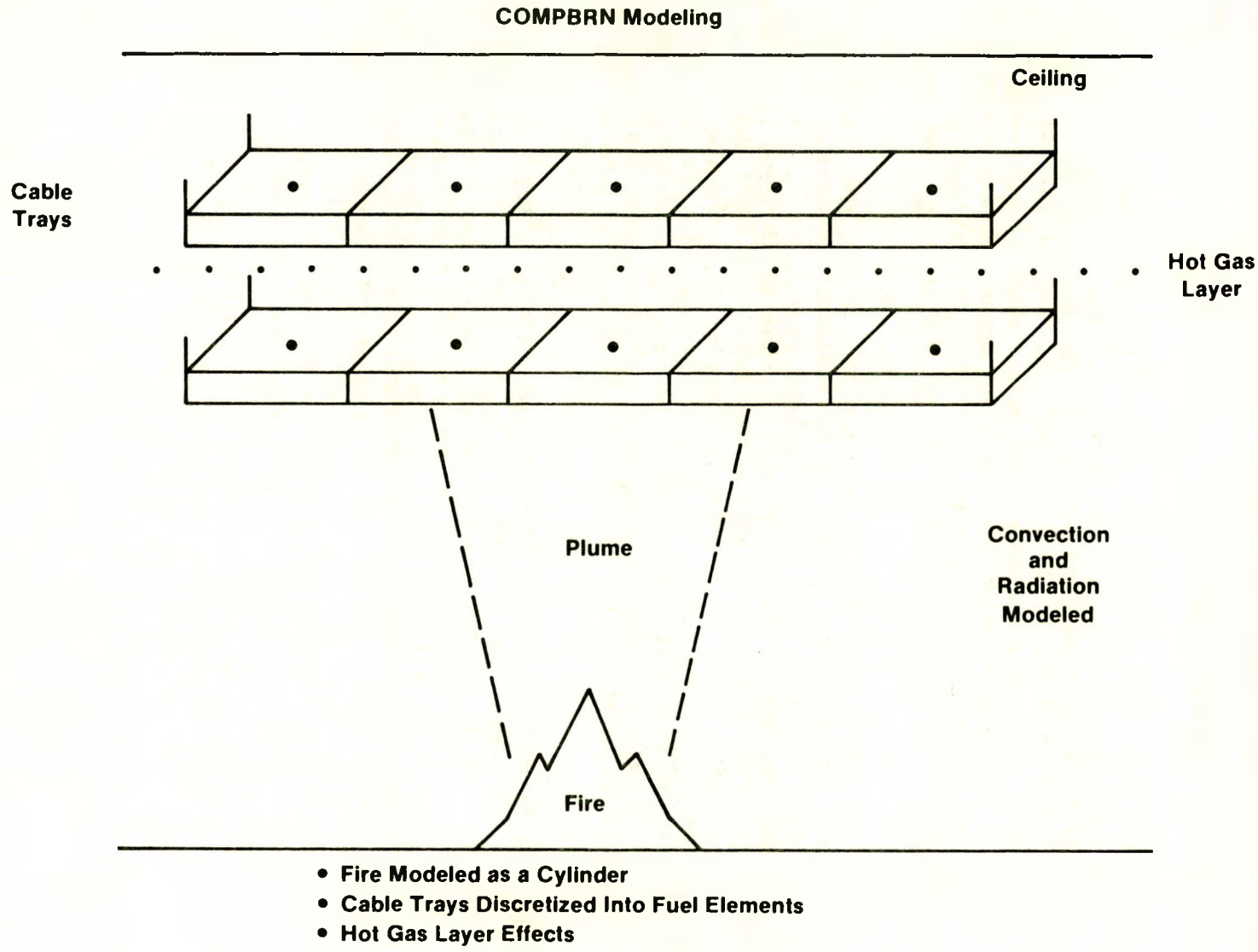

Figure 5.1. COMPBRN Zone Model

was used to provide the fire propagation analysis for this report. References 3 and 11 provide detailed discussions of the problems noted and recommended modifications for the COMPBRN III code. The following is a brief listing of the major problems which were identified and addressed in the modified version of the code:

a. An error, and nonconservative assumption, exists in the forced ventilation hot gas layer model, predicting low hot gas layer temperatures.

b. Radiative heat transfer directly above the flame is not modeled, yielding cooler temperatures directly above the flame than off to the side of the flame.

c. Two errors in the calculation of view factors overpredict the heat radiated to targets to the side as compared to objects directly above the flame.

d. Only convective heat transfer, not the dominant radiative heat transfer for objects directly engulfed in the flame, is modeled. Time to ignition is highly nonphysical.

e. The conduction algorithm is unstable, often resulting in premature termination of the code, especially for cases involving objects in the flame or thermal response of barriers.

f. The mass burning rate of burning objects is underpredicted due to lack of thermal feedback modeling.

g. Cable insulation ignition and damage failure threshold criteria are not currently well understood and the results are quite sensitive to the input parameters chosen.

Both small and large fires were postulated in the calculations. A small fire was assumed to be 2 ft. (.61 m) in diameter and consist of 1 gallon (3.8 l) of oil. A large fire was assumed to be 3 ft (.91 m) in diameter and consist of 10 gallons (38 l) of oil. Analysis of a data base on transient combustible fuel sources found at nuclear power plants* indicates that oil sources less than or equal to 1 gallon (3.8 l) were found approximately 70 percent of the time. Oil sources larger than this were found roughly 30 percent of the time. A similar partitioning between small and large quantities in terms of heat content (BTU or KJ) can be made for other credible transient combustible sources such as solvents or trash paper. Again, analysis indicates that a 70/30 partitioning between small and large fuel sources is appropriate (within ± 10 percent). It can also be shown that 10 gallons (38 l) of oil bounds any large solvent or trash paper combustible source in terms of heat content and is, therefore, an appropriate upper bound on transient combustible fuel source size.

A walkdown of the Surry Power Plant was performed to obtain vital information for the COMPBRN calculations. This information included the

*Transient Combustible Fuel Sources Found at Nuclear Power Plants (Data), Letter Report by W. Wheelis, Sandia National Labs, July 1984

location of critical equipment and cable trays, separation between redundant trains, types of cable present, and any shielding or fire barriers which may be present. Several "pinch points" were identified where critical cables from redundant trains passed from one room to another. Thin sheets of corrugated aluminum were observed on top of many cable trays. However, because of its low melting point this aluminum was neglected in the COMPBRN calculations to be conservative. Similarly, in several cases the power cables to critical pumps were routed in metal sleeves. In the COMPBRN calculations, these cables were assumed to be incapable of igniting. However, damage was assumed to occur when the surface temperature reached the temperature corresponding to cable failure.

Cable insulation ignition and damage thresholds are currently not well known (Ref. 12). For this study, a cable insulation ignition temperature of 773°K (932°F) was assumed along with a damage temperature of 623°K (662°F). For the large fire simulations these thresholds are not as critical to the fire damage time calculations because of the intensity of the flames.

A list of input parameters for the COMPBRN calculations is shown in Table 5.7. These parameters were selected to represent typical qualified cable insulation. It was assumed that the cabling in the areas of interest included typical brands of nuclear qualified cable insulation materials, such as Rockbestos Firewall III, Brand Rex, or Okonite. Because of the good flame resistance properties of these cables, no self-ignited (electrically initiated) cable tray fires were postulated.

The COMPBRN results are shown in Table 5.8 for the critical areas noted in Section 5.2. One general comment is in order: The modified version of COMPBRN III used in these calculations predicts that it is very difficult to ignite qualified cable insulation unless the cables are actually in the flames. For cases where the cables are not within the flames (or very close to them), the modified version of COMPBRN III predicts that they will not be damaged (infinite damage time). One exception to this is the charging pump service water pump room which is so small that the hot gas layer from a fire anywhere in the room would quickly damage critical cables. For cases where the cables are immersed in the flames from a transient combustible source, the modified version of COMPBRN III predicts that these cables ignite very quickly (1 to 4 min).

The modified version of COMPBRN III also calculated that a small fire would have to occur within 2 ft (.61 m) of a cable tray (horizontal distance) to damage it. Large fires were capable of damaging cable trays if they were located within 3 ft (.91 m) horizontally of the cable tray. Using these results the area in which a fire would have to occur to damage critical cables can be estimated. An area ratio can then be calculated by dividing this area by the total floor area of the room. This reduction factor can then be multiplied by the initiating frequency to estimate the frequency of fires which occur in a critical portion of a given room.

Table 5.7

Modified COMPBRN III Input Parameters

Cable Insulation Parameters	
Density	1715 kg/m^3
Specific Heat	1045 J/kg-K
Thermal Conductivity	0.092 W/m-K
Heat of Combustion	1.85-2.31E7 J/kg
Combustion Efficiency	0.6-0.8
Critical Temperature	
Piloted Ignition	773°K
Spontaneous Ignition	773°K
Damage	623°K
Surface Controlled Burning Rate	0.0001-0.0075 kg/m^2-S
Burning Rate Radiation Augmentation	1.86E-7 kg/J-m^2
Radiative Fraction	0.3-0.5
Smoke Attenuation Factor	1.4
Reflectivity	0.1-0.3
Oil Parameters	
Density	900 kg/m^3
Specific Heat	2100 J/kg-K
Heat of Combustion	4.67E7 J/kg
Combustion Efficiency	0.9
Surface Controlled Burning Rate	0.06
Radiative Fraction	0.3-0.5
Mass of Oil	3.4-34.0 kg

The area ratios for the rooms of interest are presented in Table 5.9. Note that for the charging pump service water pump room, an area ratio of 1.0 was assumed because the small size of the room enables the hot gas layer from a fire anywhere within the room to damage critical cables.

5.7 Barrier Failure Analysis

In the unscreened cut sets where a potential for barrier failure had been identified, barrier failure probability was estimated using barrier failure rates developed as described below.

Barriers were grouped into three types: (1) fire doors, security doors, water-tight doors, and fire curtains; (2) fire dampers and ventilation dampers; and (3) penetration seals and fire walls. The data base contains 628 records from when construction began on any given plant to the end of June 1985. The number of barriers of each type at a plant is required to estimate the rate at which a specific component fails. The number is not known precisely for each plant, but a nominal figure that has been estimated for each barrier type is given in Table 5.10.

Table 5.8

Time to Damage Critical Cables (minutes) Using the Modified Version of COMPBRN III

Area	Scenario	Small Fire	Large Fire
Auxiliary Building	Tray at 12 ft	*	2
Cable Vault	Tray at 7 ft	3	3
	Tray at 4 ft	3	3
Emergency Switchgear Room	Tray at 7 ft	3	3
	10 ft and 12 ft Trays	*	3
	Relay Room	*	4
Safeguards	Auxiliary Feedwater	*	3
	Pinch Point	*	3
Mechanical Equipment Room - 3	Cable to Pump	1	1
Charging Pump Service Water Pump Room	Junction Box	1	1
	Anywhere Else	3	2

*No damage predicted (infinite time)

The statistical uncertainty of each estimate, reflecting sampling variation and plant-to-plant variation, is represented by 90 percent confidence bounds. These estimates and confidence bounds are given in Table 5.11 where units of both estimates and bounds are failures/year.

During the confirmatory plant visit scenarios which required barrier failure had those barriers inspected. No plant specific vulnerabilities were noted as a result of this inspection which would require modification of generic barrier failure rates. After multiplying barrier failure rates by the number of penetrations at each appropriate fire zone adjacency and utilizing the probabilities developed in screening Step 4, all remaining barrier failure scenarios did not survive the 10^{-9} per year frequency screening criteria.

5.8 Recovery Analysis

For those remaining cut sets which survived the screening process and where the COMPBRN code predicted fire damage would occur, recovery of random failures and credit for extinguishment of the fire before the COMPBRN predicted time to fire damage was applied.

Table 5.9

Critical Area Ratios

Area	Scenario	Critical Area Ratio Small Fire	Large Fire
Auxiliary Building	Tray at 12 ft	NA	6.34E-4
Cable Vault	Tray at 7 ft	0.022	0.027
	Tray at 4 ft	0.022	0.027
Emergency Switchgear Room	Tray at 7 ft	0.027	0.033
	Tray at 10 ft or 12 ft	NA	0.027
	Relay Room	NA	0.074
Safeguards	Auxiliary Feedwater	NA	8.93E-3
	Pinch Point	NA	5.36E-3
Mechanical Equipment Room - 3	Cable to Pump	0.1	0.1
Charging Pump Service Water Room	Junction Box	1.0	1.0

NA - Not applicable because a small fire will not result in damage for this scenario.

Recovery of random failures (non-fire related) was treated in a similar fashion as in the internal events analysis. All operator recovery actions that were used in the internal events analysis were inspected for use where appropriate in the remaining cut sets. If a sequence was long term (greater than 24 hours), two recovery actions were allowed. In short term (less than 24 hours) sequences only one recovery action was allowed. A recovery action was chosen if the possibility of multiple recovery actions was present and on a hierarchy based on recovery probabilities established by the internal events analysts. For short term sequences recovery action probabilities were modified when deemed appropriate.

In the areas where firefighting activity takes place, no credit was given for local recovery actions until after the fire was extinguished. In non-affected areas, local recovery was allowed for valve manipulation or pump operation when damage to power cabling of an applicable component had not occurred.

Table 5.10

Approximate Number of Barriers at a Plant

Type	Nominal
1	150
2	200
3	3000

Table 5.11

Estimates of Single Barrier Failure Rates

Barrier Type	Barrier/ Unit	Estimate	5% Confidence Bound	95% Confidence Bound
1	150	7.4E-3	0.0	2.4E-1
2	200	2.7E-3	0.0	2.2E-1
3	3000	1.2E-3	0.0	3.7E-2

In conjunction with human factors analysts and the "Handbook of Human Reliability Analysis With Emphasis on Nuclear Power Plant Applications" (Ref. 13), any additional recovery actions not developed by the internal events recovery procedure were quantified. Only one additional recovery action was added for the Surry analysis. This recovery action was necessitated by failure of control cabling in the control room requiring control of the plant from the remote shutdown panel. Even though explicit procedures were in place for this situation, a high stress recovery probability was applied. This was deemed appropriate due to timing of the sequence (less than one hour) and the fact that some amount of time would be required to make the decision to abandon the control room and man the remote shutdown stations.

The probability of manual non-suppression of a fire before the COMPBRN predicted time to damage was quantified using the Wheelis' data base (Ref. 4) which contained information on 69 fire events which had time to suppression associated with them. As part of the Fire Risk Scoping Study (Ref. 3) a distribution was fit to this data. A probability of non-suppression was then associated with any COMPBRN predicted time to fire damage.

Credit was also given for automatic suppression systems in areas where they were located. In the case of Surry the only unscreened area which contained such a system was the cable vault/tunnel. Generic reliability data indicates approximately a 96 percent success rate for such systems (Ref. 14). However, a modification to this reliability value was deemed appropriate due to the predicted short time to damage (~3 minutes), the half minute system actuation time delay, and the fact that five fixed temperature (190°F) heat detectors actuate the system and none was in close proximity to the postulated fire.

5.9 Uncertainty Analysis

Distributions on fire frequency, fire suppression probability, fire code calculations, random failure probability, barrier failure probability, and operator recovery actions, generated uncertainties on fire-induced core damage frequencies.

The uncertainty of these values was propagated through the accident sequence models using two computer codes. A Latin Hypercube Sampling (LHS) algorithm was used to generate the samples for all of the parameter values (Ref. 15). The Top Event Matrix Analysis Code (TEMAC) was used to quantify the uncertainty of the accident sequence equation using the parameter value samples generated by the LHS code (Ref. 16).

LHS is a constrained Monte Carlo technique which forces all parts of the distribution to be sampled. The LHS code is also flexible in that it can sample a variety of random variable distributions. Furthermore, parameter distributions for similar events were correlated. For example, if two similar components (e.g., MOV XX-FTO and MOV YY-FTO) are modeled from the same probability distribution, then the sampling of these two distributions is perfectly correlated, meaning the same value is used for both events in a given sample member. For basic events which are modeled with very similar but slightly different distributions (e.g., MOV XX fails to remain closed for 100 hours and MOV YY fails to remain closed for 200 hours), the LHS code permits an induced correlation between the samples. However, LHS does not allow the correlation coefficient for this case to be equal to 1.0. LHS does permit sampling with a coefficient of 0.99 in these cases.

TEMAC uses the LHS parameter samples and the accident sequence equations (cut sets) as input to quantify the core damage estimates. TEMAC generates a sample of the accident sequence frequency, a point estimate of the frequency, and various importance measures and ranking for the base events.

Uncertainty on fire initiating event frequency was developed when the generic fire frequencies were updated using Surry specific data. This process which was briefly discussed in Section 5.3 is covered in more detail in Reference 5.

Uncertainty on fire non-suppression probabilities ($Q(\tau_G)$) was addressed by modification of COMPBRN predicted time to damage. The COMPBRN Code predicted time to damage and its associated non-suppression curve probability were taken to be a best estimate of a maximum entropy disturbed variable. Fifteen minutes were added and subtracted from the COMPBRN predicted time to allow for uncertainty in its result and the uncertainty in the probability of non-suppression distribution. These probabilities were taken as a minimum and maximum of the maximum entropy distribution respectively.

Uncertainty associated with the fire size estimate factor (f_s) was developed utilizing information associated with an I&E inspector report (see footnote on pg. 5-17) on a survey of different types of combustibles and their amounts found in nuclear power plants. Two fire sizes, a large and small fire were modelled as described in Section 5.6. These fire sizes (BTU content) were compared to the distributions on possible fire sizes developed for the different combustibles from the I&E data. The best estimate for percentage of fires that were either large or small was taken from an average of the different types of combustibles for an equivalent BTU level fire modelled by COMPBRN. This probability was assumed to be the best estimate value of a maximum entropy distribution. Maximum and minimum probabilities for this distribution were assumed to be based on one individual type of combustible with either the maximum and minimum percentage corresponding to applicable fire size (BTU rating).

Random failure events and operator recovery actions were treated identically as in the internal events analysis. Uncertainties and types of distributions were not modified for the fire analysis.

All other factors and their associated uncertainties are not common to all fire sequences and will be addressed individually in the appropriate subsections of Section 5.10.

5.10 Description of Unscreened Fire-Induced Core Damage Scenarios and Their Associated Fire Areas

5.10.1 Introduction

This section will describe the fire scenarios and their associated fire zones which are listed in Table 5.1. All other fire zones and all adjacent fire zone combinations were either screened as described in Section 5.5 or had scenarios that dropped below 10^{-9}/yr after either operator recovery of non-fire related failures, COMPBRN code calculations, or barrier failure probabilities were applied.

5.10.2 Auxiliary Building

One fire scenario in the auxiliary building remained after screening. This scenario was a large fire on the 13-ft elevation which irrecoverably

damaged power or control cables for both the HPI and CCW systems. These fire-related failures with no additional random failures required led to a reactor coolant pump seal LOCA occurrence. The recovery for this particular scenario required the operation of two manual HPI system cross connect valves which were located in the immediate vicinity of the large fire. No recovery was allowed until 15 min after the fire was extinguished. The core damage equation is as follows:

$$\phi_{cm} = \lambda_{aux}\ f_a\ f_s\ Q(\tau_G)\ R_{op}$$

where

ϕ_{cm} = fire-induced core damage frequency for the auxiliary building

λ_{aux} = frequency of auxiliary building fires

f_a = area ratio within the auxiliary building where critical damage occurred

f_s = severity ratio (based on generic combustible fuel loading) for a large fire

$Q(\tau_g)$ = that percentage of fires within the suppression data base where the fire was not manually extinguished before the COMPBRN predicted time to critical damage occurred

R_{op} = failure to cross connect of Unit 2 high pressure injection system to either prevent seal LOCA occurrence or mitigate its effect

Table 5.12 gives the values of each of these factors as well as their associated distribution and upper and lower bounds. In the case of log-normally distributed variables the upper and lower bounds represent the 95th and 5th percentiles of the distribution, respectively, while the best estimate represents the mean value.

5.10.3 Cable Vault/Tunnel

The one remaining scenario which survived screening and is similar to the one described for the auxiliary building in that the postulated fire irrecoverably damages power or control cables for both the HPI and CCW systems leading to a seal LOCA.

Credit was taken for the automatic CO_2 system suppressing the fire before critical damage occurred. COMPBRN predicted 3 min time to damage for this particular scenario. The automatic CO_2 system is actuated by fixed temperature heat detectors at 190°F. There is one heat detector located at the end of the critical area of influence for this scenario. Two

Table 5.12

Auxiliary Building Fire Scenario Factors and Distribution

Factor	Distribution	Lower Bound	Best Estimate	Upper Bound
λ_{aux}	gamma	0.027	0.066	0.16
f_a	maximum entropy	2.4E-4	6.3E-4	1.1E-3
f_s	maximum entropy	0.19	0.30	0.67
$Q(\tau_G)$	maximum entropy	0.69	0.80	1.0
R_{op}	maximum entropy	0.19	0.26	1.0

others are located such that ventilation flow would force the hot gas layer in their direction. The system actuation delay time to allow for evacuation is 30 s. Therefore, the heat detectors must respond to fire ignition and the CO_2 system must suppress the fire within 2.5 min. to prevent critical damage. For these reasons, system reliability data for automatic CO_2 suppression systems was modified to account for this relatively short time to prevent critical damage.

Operator recovery for this scenario is similar to that for the auxiliary building scenario except that the fire is not in the immediate vicinity or even same fire area as where the local recovery actions must take place. Also, since no control room operators respond to the fire itself the same recovery value for operator action was applied as was used in the internal events analysis.

The core damage equation is as follows:

$$\phi_{CM} = \lambda_{CSR}\ f_a\ f_s\ Q(\tau_G)\ Q_{AUTO}\ R_{op}$$

where

ϕ_{CM} = fire-induced core damage frequency for the cable vault/tunnel

λ_{CSR} = frequency of cable vault/tunnel fires

f_a = area ratio within the cable vault/tunnel where critical damage occurred

f_s = severity ratio (based on generic combustible fuel loading)

$Q(\tau_G)$ = that percentage of fires within the data base where the fire was not manually extinguished before the COMPBRN predicted time to critical damage occurred

R_{op} = failure to cross connect of Unit 2 high pressure injection system to either prevent seal LOCA occurrence or mitigate its effect

Q_{AUTO} = probability of the automatic CO_2 not suppressing the fire before COMPBRN predicted time to critical damage occurred

Table 5.13 gives the values of each of these factors as well as their associated distribution and upper and lower bounds.

5.10.4 Control Room

One scenario survived the screening process for the control room. As was the case for the auxiliary building and cable vault/tunnel, no additional random failures were required to lead directly to core damage. This scenario was a fire interior to benchboard 1-1 leading to the spurious actuation of one PORV located on this benchboard. Because of the cabinet configuration within the control room and based on Sandia cabinet fire tests (Ref. 17), the fire was assumed not to spread and damage any components outside of benchboard 1-1. However, due to Sandia large scale enclosure tests (Ref. 18) where smoke engulfed a control room within 5 to 10 min. of time from ignition within a cabinet even with ventilation rates of up to 10 room changes per hour, this scenario postulates forced abandonment of the control room and subsequent plant control from the auxiliary shutdown panel located in the emergency switchgear room.

Credit was given for quick extinguishment of the fire within benchboard 1-1 since the control room is continually staffed. None of the four control room fires in the data base lead to abandonment of the control room. It was assumed that one in ten control room fires would result in abandonment of the control room and a factor of ten reduction in control room fire frequency was the modification made to allow credit for continuous occupation.

The area ratio for fire involvement was developed ratioing the area of benchboard 1-1 to the total cabinet area in the control room. This is warranted based on fire event data that all control room fires have occurred within electrical cabinets. Therefore, this is postulated to be the most likely fire ignition source within the control room.

Table 5.13

Cable Vault/Tunnel Fire Scenario Factors and Distribution

Factor	Distribution	Lower Bound	Best Estimate	Upper Bound
λ_{CSR}	gamma	3.0E-6	7.5E-3	0.016
f_a	maximum entropy	0.011	0.025	0.047
f_s	maximum entropy	0.50	0.99	1.0
$Q(\tau_G)$	maximum entropy	0.69	0.80	1.0
Q_{AUTO}	maximum entropy	0.50	0.70	0.90
R_{op}	maximum entropy	4.4E-3	0.044	0.44

Once abandonment of the control room takes place, operators would control the plant from the auxiliary shutdown panel. However, PORV indication is not provided at this panel and in conversations with the utility it was learned that the PORV disable function on the auxiliary shutdown panel is not electrically independent of the control room. Therefore, it was assumed that the PORV disable function would fail and, consequently, the operators would be in high stress recovery mode.

The core damage equation is as follows:

$$\phi_{CM} = \lambda_{CR}\ f_a\ R_{op}\ f_r$$

where

ϕ_{CM} = fire-induced core damage frequency for the control room

λ_{CR} = frequency of control room fires

f_r = probability that operators will not successfully extinguish the fire before smoke forces abandonment of the control room

f_a = area ratio of benchboard 1-1 to total cabinet area within the control room

R_{op} = probability that operates will unsuccessfully recover the plant from the auxiliary shutdown panel

Table 5.14 gives the values of each of these factors as well as their associated distribution and upper and lower bounds.

Table 5.14

Control Room Fire Scenario Factors and Distribution

Factor	Distribution	Lower Bound	Best Estimate	Upper Bound
λ_{CR}	gamma	1.2E-6	1.8E-3	7.4E-3
f_a	maximum entropy	0.028	0.084	0.12
R_{op}	maximum entropy	7.4E-3	0.074	0.74
f_r	maximum entropy	0.01	0.1	0.25

5.10.5 Emergency Switchgear Room

One fire scenario remained in the emergency switchgear room after screening. This scenario was a fire that damaged either power or control cables for HPI and CCW pumps thus leading to a reactor coolant pump seal LOCA. No additional random failures were required for this scenario to lead directly to core damage.

As was the case for the cable vault/tunnel and auxiliary building, recovery from this scenario was cross connecting HPI from Unit 2. The fire itself would not affect local auxiliary building recovery actions. Therefore, similar to the cable vault/tunnel the same probability for recovery was used as in the internal events analysis.

The core damage equation is as follows:

$$\phi_{CM} = \lambda_{SWGR}\, Q(\tau_G)\, R_{op}\, [f_{a1}\, f_{s1} + f_{a2}\, f_{s2}]$$

where

ϕ_{CM} = fire-induced core damage for the emergency switchgear room

λ_{SWGR} = frequency of emergency switchgear room fires

f_{a1} = area ratio within the emergency switchgear room for a small fire where critical damage occurred

f_{s1} = severity ratio (based on generic combustible fuel loading) of small fires

f_{a2} = area ratio within the emergency switchgear room for a large fire

f_{s2} = severity ratio (based on generic combustible fuel loading) of large fires

$Q(\tau_G)$ = that percentage of fires in the data base where the fire was not manually extinguished before the COMPBRN predicted time to critical damage occurred

R_{op} = failure to cross connect of Unit 2 high pressure injection system to either prevent seal LOCA occurrence or mitigate its effect

Table 5.15 gives the values of each of these factors as well as their associated distribution and upper and lower bounds.

5.10.6 Charging Pump Service Water Pump Room

One fire scenario remained in the charging pump service water pump room after screening. Fire-related component damage included Units 1 and 2 charging pump service water pumps (CPSWP) 10A and control power for Unit 1 CPSWP 10B. As in the internal events analysis it was assumed that one service water pump provides insufficient cooling flow for both units charging pumps given a small LOCA.

Either a large or small fire will fail all cabling and components within this relatively small fire area due to a rapid buildup of a hot gas layer. This scenario requires a PORV demand and subsequent failure to reclose and isolate the leak. The internal events failure rate for the non-isolatable stuck-open PORV was used.

The core damage equation is as follows:

$$\phi_{CM} = \lambda_{PR}\ Q(\tau_G)\ Q_{PORV}$$

where

ϕ_{CM} = fire-induced core damage frequency for the CPSWPR

λ_{PR} = frequency of pump room fires (small pumps only)

$Q(\tau_G)$ = that percentage of fires in the data base where the fire was manually extinguished before the COMPBRN predicted time to critical damage occurred

Q_{PORV}= stuck-open PORV with failure to isolate the leak path

Table 5.15

Emergency Switchgear Room Fire Scenario Factors and Distribution

Factor	Distribution	Lower Bound	Best Estimate	Upper Bound
λ_{SWGR}	gamma	2.0E-5	8.0E-3	0.017
f_{a1}	maximum entropy	0.02	0.039	0.099
f_{s1}	maximum entropy	0.33	0.70	0.81
f_{a2}	maximum entropy	0.051	0.10	0.24
f_{s2}	maximum entropy	0.19	0.30	0.67
$Q(\tau_G)$	maximum entropy	0.67	0.80	1.0
R_{op}	maximum entropy	4.4E-3	0.044	0.44

Note that neither an area or severity ratio factor appear in the core damage equation. This is because a fire of any size no matter where it was located in the room led to the rapid development of a hot gas layer which failed all components and cabling. Therefore, both these factors are taken to be unity.

Table 5.16 gives the values of each of these factors as well as their associated distribution and upper and lower bounds.

Table 5.16

CPSWPR Fire Scenario Factors and Distribution

Factor	Distribution	Lower Bound	Best Estimate	Upper Bound
λ_{CPSWPR}	lognormal	(E.F.=3)	3.7E-3	
$Q(\tau_G)$	maximum entropy	0.67	0.80	1.0
Q_{PORV}	determined by TEMAC computation			

5.11 Conclusion

The overall fire-induced core damage frequency for Surry Unit 1 was found to be 1.13E-5 per year. The dominant contributing plant areas are the (a) emergency switchgear room, (b) auxiliary building, (c) control room, and (d), cable vault/tunnel. These four areas comprise 99% of the total fire risk.

In the case of the emergency switchgear room, cable vault/tunnel, and the auxiliary building, a reactor coolant pump seal LOCA leads to core damage. The fire itself fails cabling for both the HPI and CCW systems resulting in a seal LOCA.

For the control room, a general transient with a subsequent stuck-open PORV leads to a small LOCA. Failure to control the plant from the auxiliary shutdown panel results in core damage.

5.12 References

1. Seabrook Station Probabilistic Safety Assessment, Section 9.4, Public Service Company of New Hampshire and Yankee Atomic Electric Company, December 1983.

2. Severe Accident Risk Assessment Limerick Generating Station, Chapter 4, Main Report, Philadelphia Electric Company, Report #4161, April 1983.

3. J. A. Lambright, S. P. Nowlen, V. F. Nicolette, and M. P. Bohn, Fire Risk Scoping Study: Current Perception of Unaddressed Fire Risk Issues, Sandia National Laboratories, Albuquerque, NM, SAND88-0177, NUREG/CR-5088, December 1988.

4. W. T. Wheelis, Users Guide for a Personal-Computer-Based Nuclear Power Plant Fire Data Base, Sandia National Laboratories, Albuquerque, NM, SAND86-0300, NUREG/CR-4586, August 1986.

5. R. L. Iman, S. C. Hora, Modeling Time to Recovery and Initiating Event Frequency for Loss of Off-Site Power Incidents at Nuclear Power Plants, Sandia National Laboratories, Albuquerque, NM, SAND87-2428, NUREG/CR-5032, January 1988.

6. R. B. Worrell, SETS Reference Manual, Sandia National Laboratories, Albuquerque, NM, SAND83-2675, NUREG/CR-4213, May 1985.

7. D. W. Stack, A SETS User's Manual for Accident Sequence Analysis, Sandia National Laboratories, Albuquerque, NM, SAND83-2238, NUREG/CR-3547, January 1984.

8. N. O. Siu, COMPBRN - A Computer Code for Modeling Compartment Fires, University of California, UCLA-ENG-8257, NUREG/CR-3239, May 1983.

9. V. Ho, N. O. Siu, G. Apostolakis, COMPBRN III - A Computer Code for Modeling Compartment Fires, University of California, UCLA-ENG-8524, November 1985.

10. C. Ruger, J. L. Boccio, and M. A. Azarm, Evaluation of Current Methodology Employed in Probabilistic Risk Assessment (PRA) of Fire Events at Nuclear Power Plants, Brookhaven National Laboratory, NUREG/CR-4229, May 1985.

11. V. F. Nicolette, S. P. Nowlen, J. A. Lambright, Observations Concerning the COMPBRN III Fire Growth Code, Sandia National Laboratories, Albuqueque, NM, SAND88-2160C, Presented at International Topical Meeting, Probability, Reliability, and Safety Assessment, April 1989 in Pittsburgh, PA.

12. V. F. Nicolette, and S. P. Nowlen, A Critical Look at Nuclear Qualified Electrical Cable Insulation Ignition and Damage Thresholds, SAND88-2161C, presented at Operability of Nuclear Systems in Normal and Adverse Environments, Lyon, France, September 18-22, 1989.

13. A. D. Swain, H. E. Guttmann, Handbook of Human Reliability Analysis with Emphasis on Nuclear Power Plant Applications, Sandia National Laboratories, Albuquerque, NM, SAND80-0200, NUREG/CR-1278, August 1983.

14. M. P. Bohn, and J. A. Lambright, Procedures for the External Event Core Damage Frequency Analyses for NUREG-1150, Sandia National Laboratories, Albuquerque, NM, NUREG/CR-4840, November 1990.

15. R. L. Iman, M. J. Shortencarrier, A FORTRAN 77 Program and User's Guide for the Generation of Latin Hypercube and Radom Samples for Use with Computer Models, Sandia National Laboratories, Albuquerque, NM, SAND83-2365, NUREG/CR-3024, March 1984.

16. R. L. Iman, M. J. Shortencarrier, A User's Guide for the Top Event Matrix Analyses Code (TEMAC), Sandia National Laboratories, Albuquerque, NM, SAND86-0960, NUREG/CR-4598, August 1986.

17. J. M. Chavez, An Experimental Investigation of Internally Ignited Fires in Nuclear Power Plant Control Cabinets, Part I - Cabinet Effects Tests, SAND86-0336, NUREG/CR-4527, Albuquerque: Sandia National Laboratories, April 1987.

18. J. M. Chavez, An Experimental Investigation of Internally-Ignited Fires in Nuclear Power Plant Cabinets, Part II - Room Effects Tests, SAND86-0336, NUREG/CR-4527, Albuquerque: Sandia National Laboratories, October 1988.

APPENDIX A

Surry Structural Floor Response Spectra

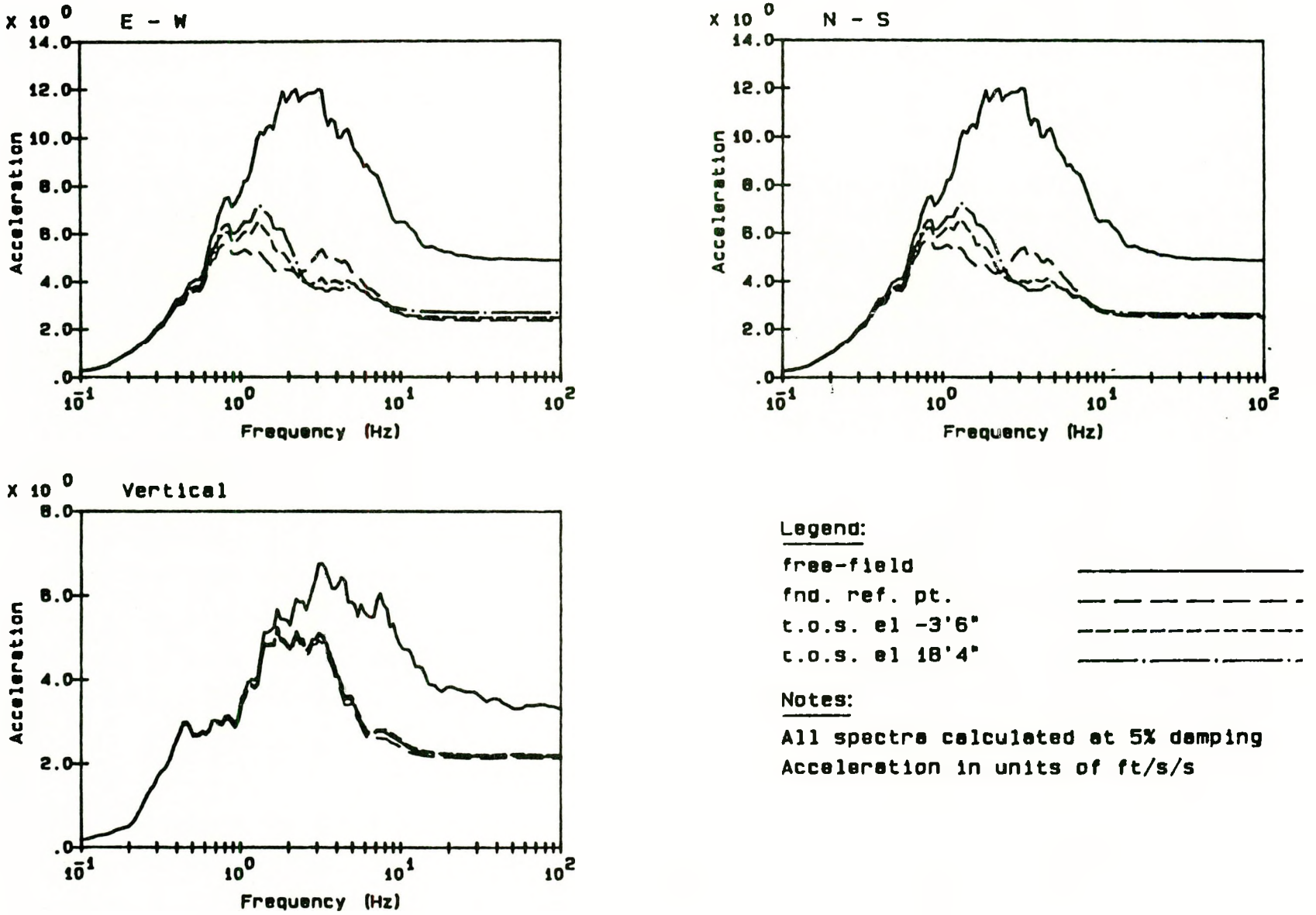

RSPLT V3.00 1rcb1.plt 15:46:44 07-05-88

Figure A.1(a) Surry Nuclear Power Plant Reactor Containment Internal Building Instructure Response Acceleration Range 1

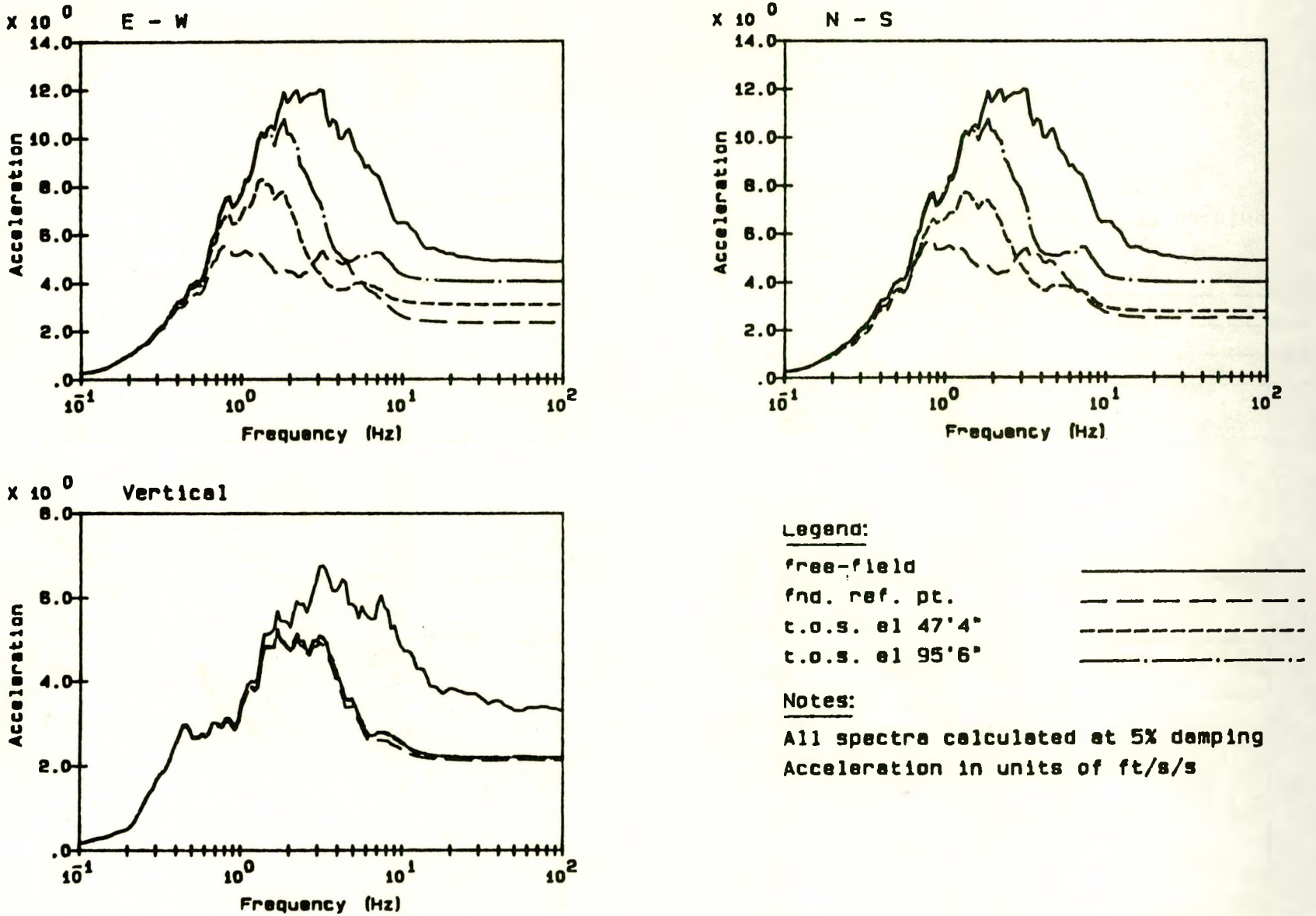

RSPLT V3.00 1rcb2.plt 15:47:25 07-05-88

Figure A.1(b) Surry Nuclear Power Plant Reactor Containment Internal Building Instructure Response Acceleration Range 1

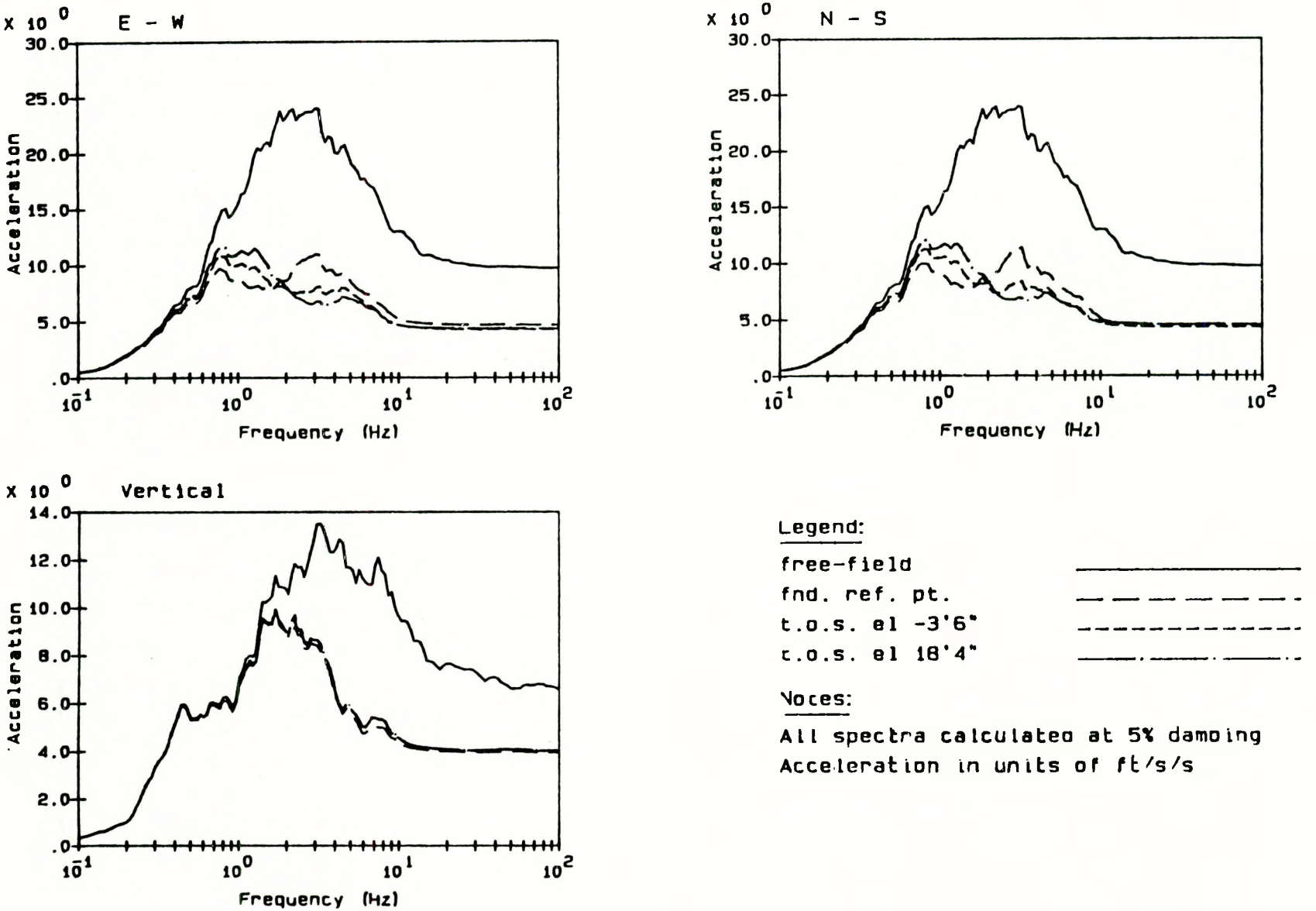

Figure A.2(a) Surry Nuclear Power Plant Reactor Containment Internal Building Instructure Response Acceleration Range 2

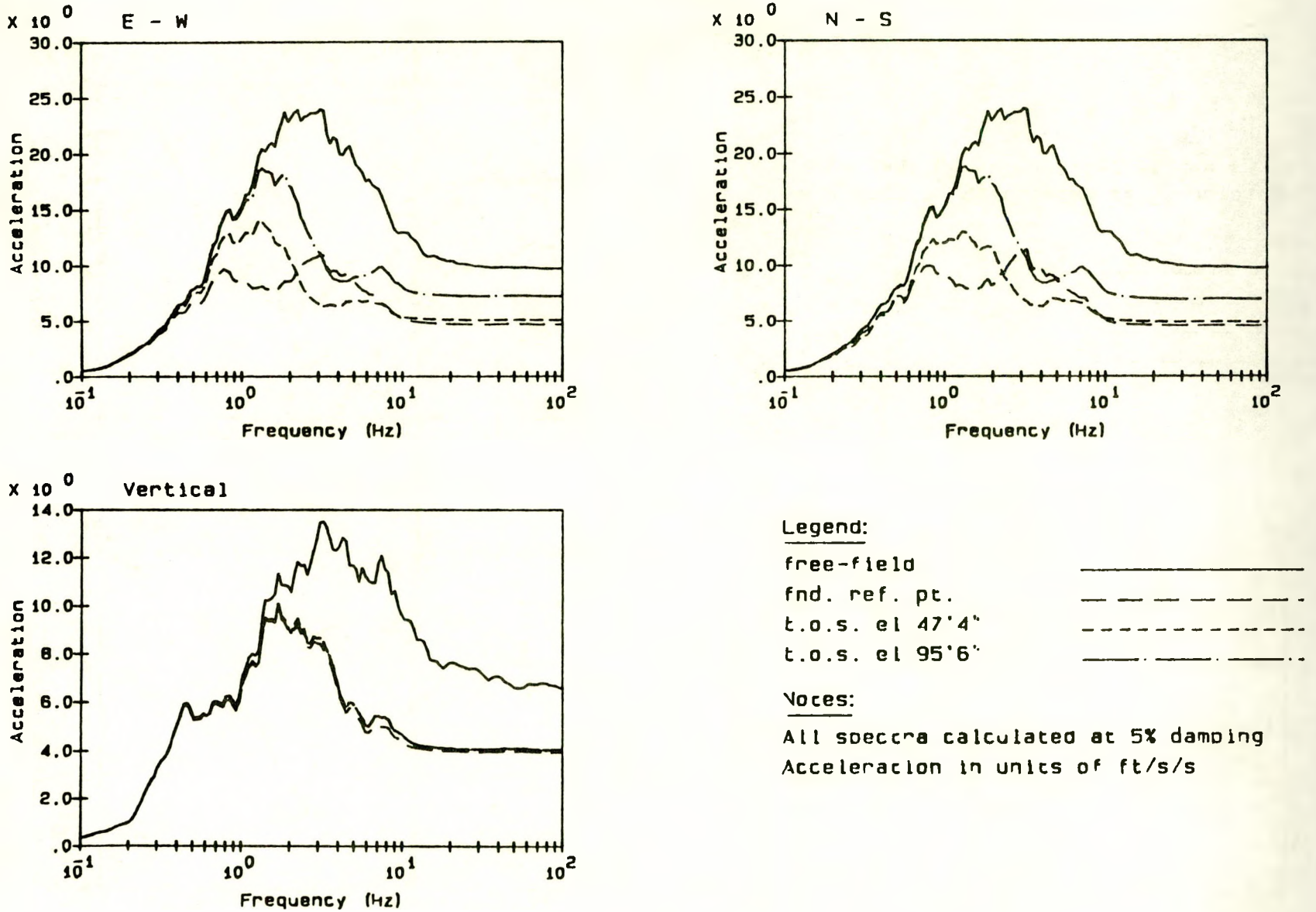

Figure A.2(b) Surry Nuclear Power Plant Reactor Containment Internal Building Instructure Response Acceleration Range 2

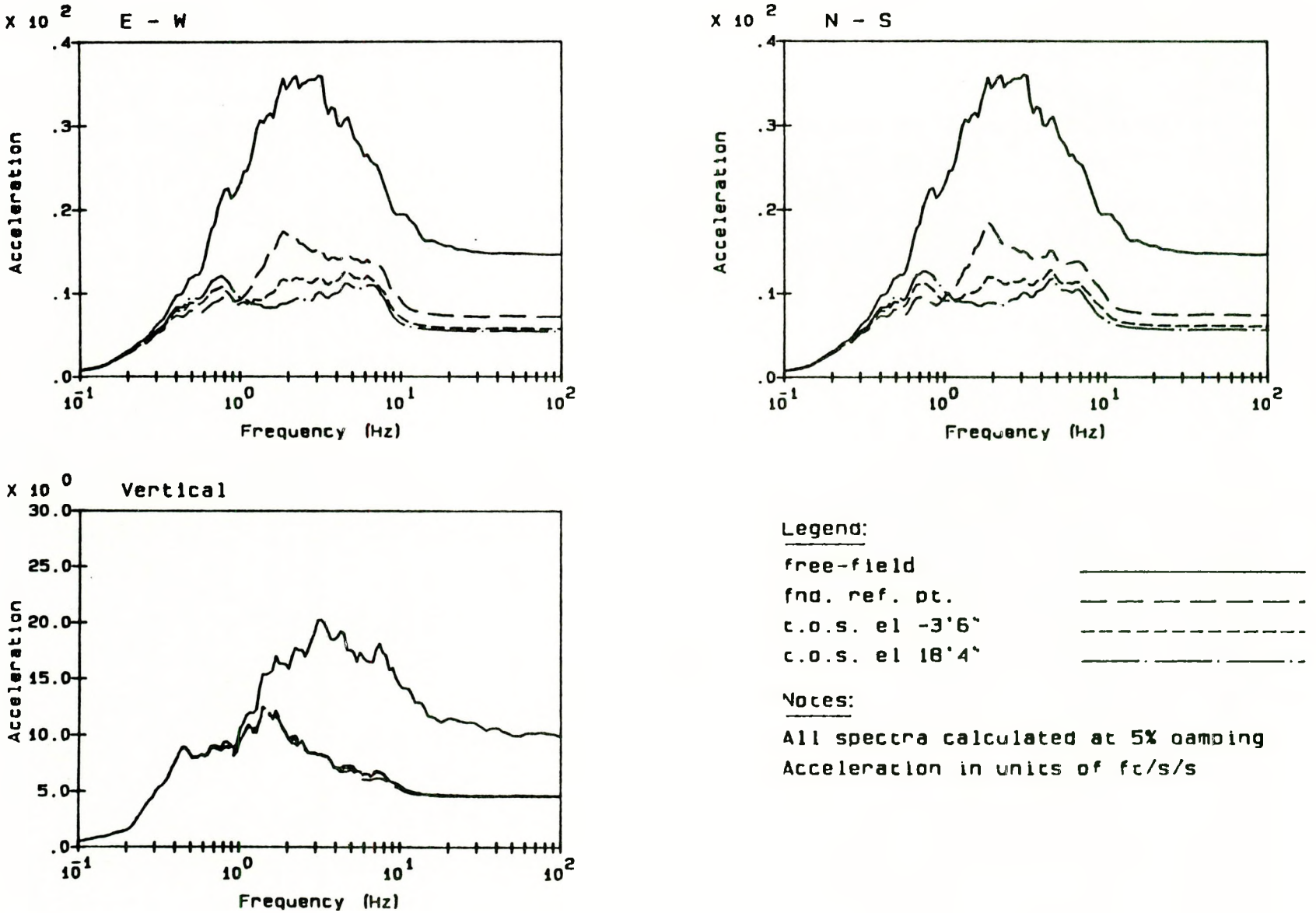

Figure A.3(a) Surry Nuclear Power Plant Reactor Containment Internal Building Instructure Response Acceleration Range 3

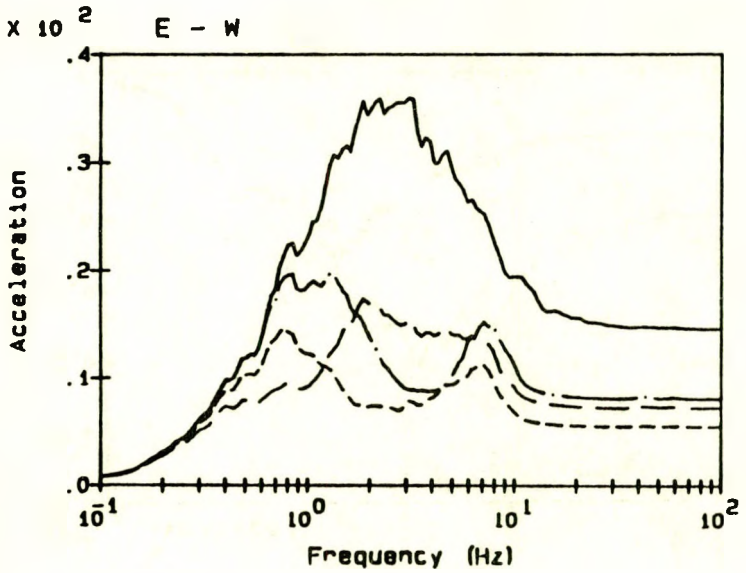

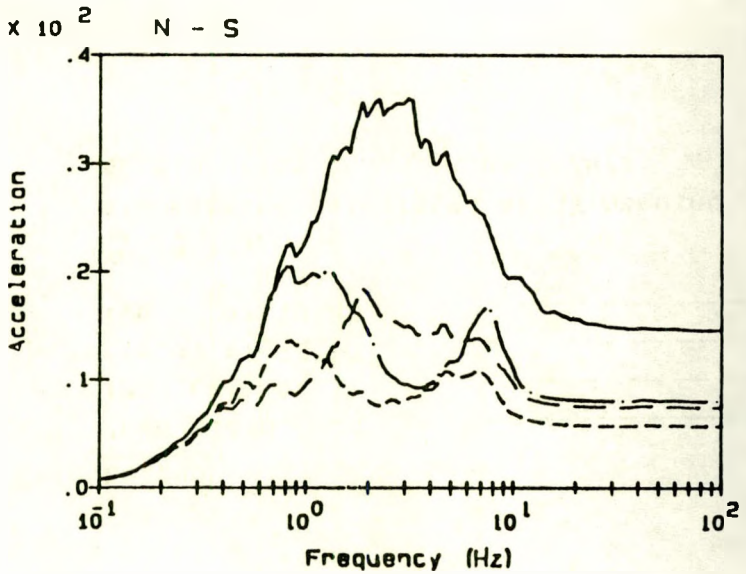

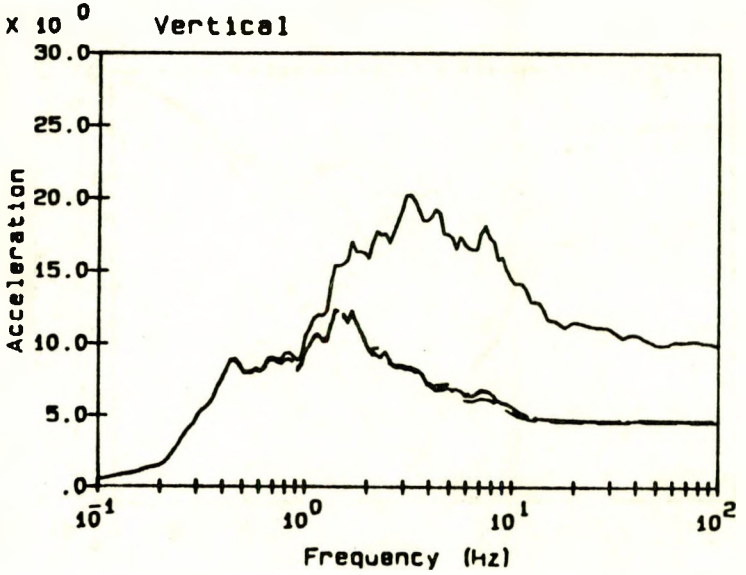

Legend:

free-field

fnd. ref. pt.

t.o.s. el 47'4"

t.o.s. el 95'6"

Notes:

All spectra calculated at 5% damping

Acceleration in units of ft/s/s

RSPLT V3.00 3rcb2.plt 15:51:43 07-05-88

Figure A.3(b) Surry Nuclear Power Plant Reactor Containment Internal Building Instructure Response Acceleration Range 3

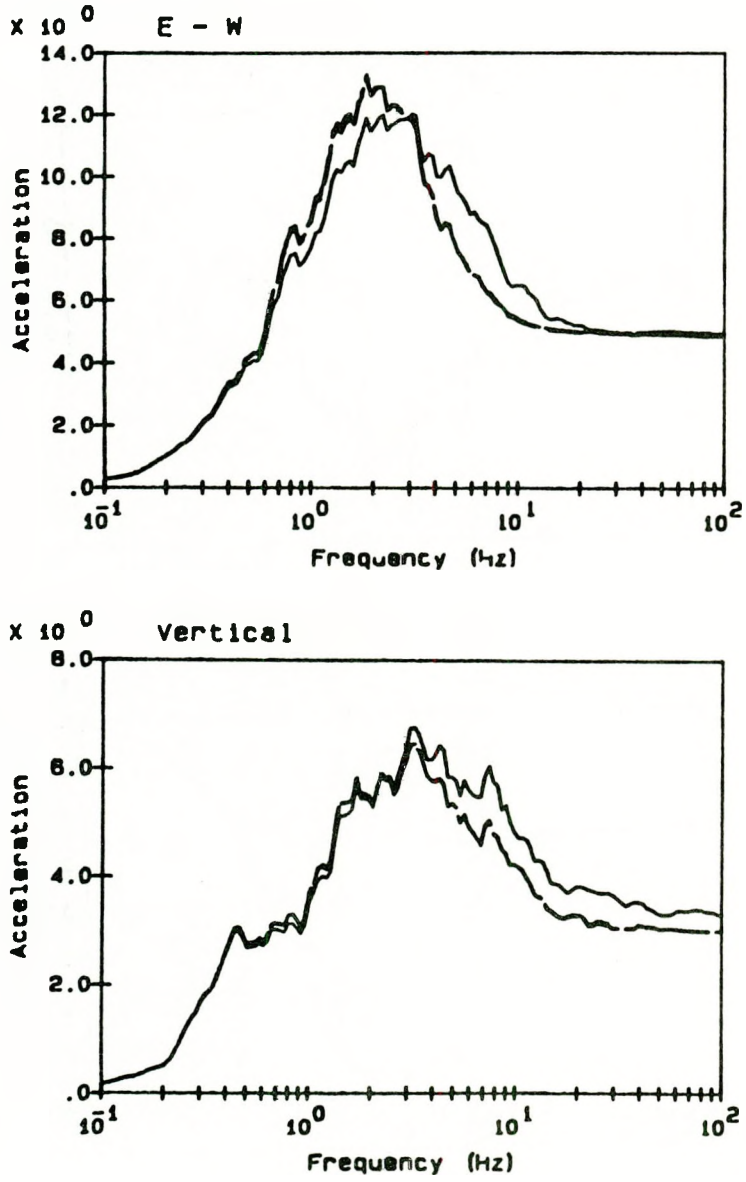

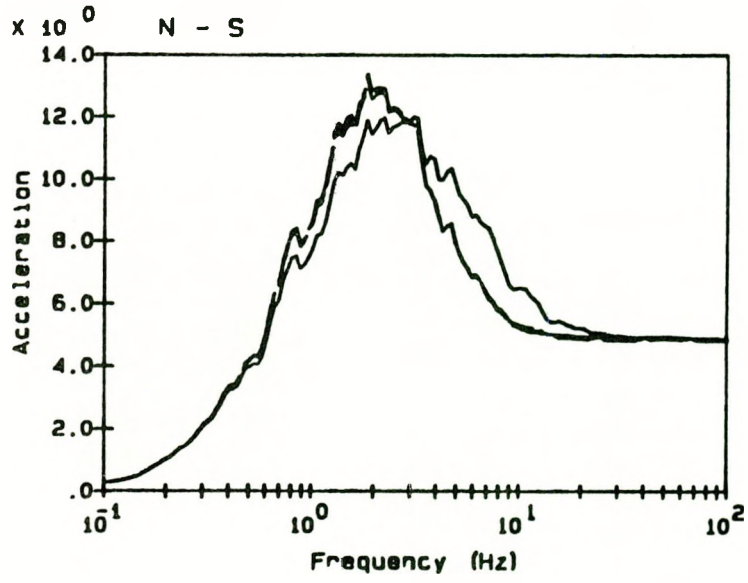

Legend:

free-field
fnd. ref. pt.
t.o.s. el 13'0"
t.o.s. el 27'6"

Notes:

All spectra calculated at 5% damping
Acceleration units in ft/s/s

RSPLT V3.00 1sxb1.plt 13:44:02 02-21-88

Figure A.4(a) Surry Nuclear Power Plant Auxiliary Building
Instructure Response Acceleration Range 1

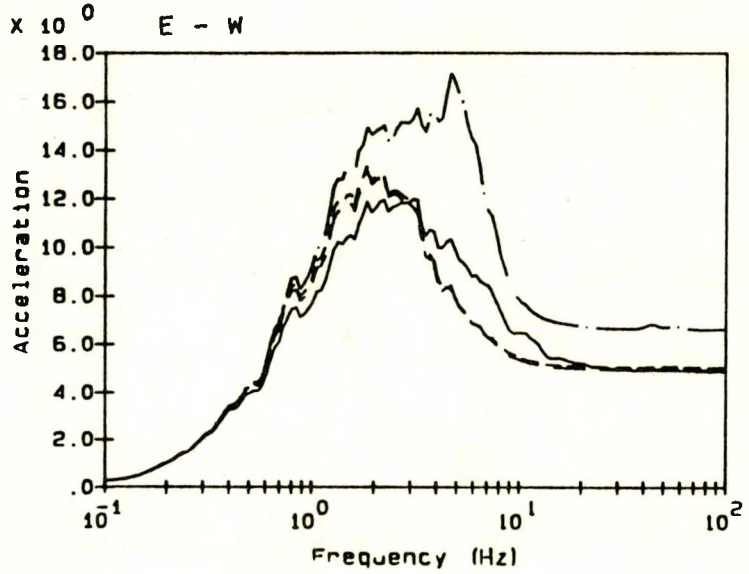

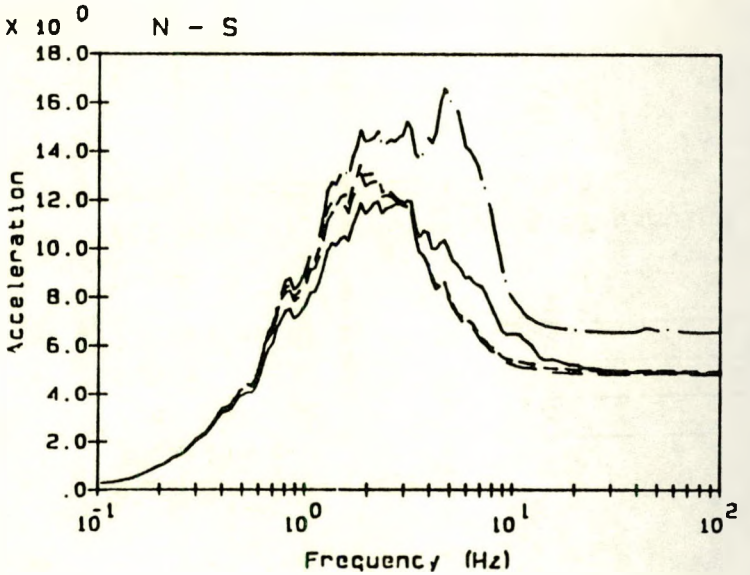

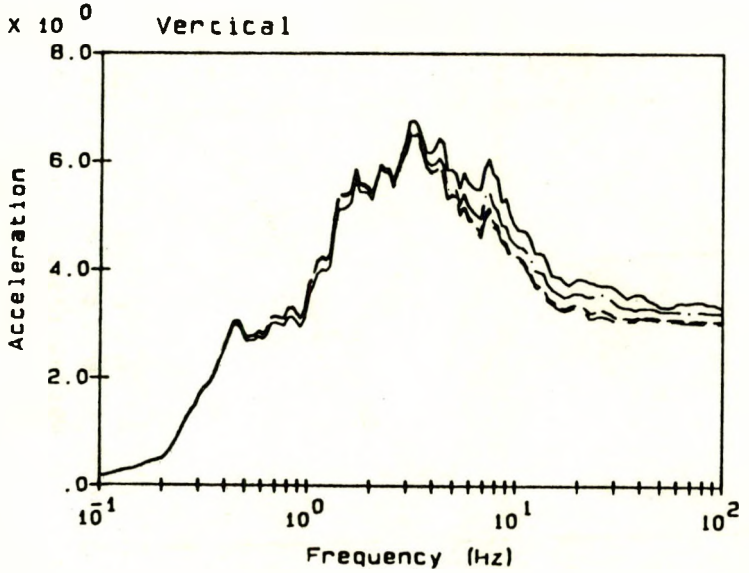

Legend:

free-field
fnd. ref. pt.
t.o.s. el 45'10"
t.o.s. el 66'0"

Notes:

All spectra calculated at 5% damping
Acceleration units in ft/s/s

RSPLT V3.00 1axb2.plt 13:44:44 02-21-88

Figure A.4(b) Surry Nuclear Power Plant Auxiliary Building
Instructure Response Acceleration Range 1

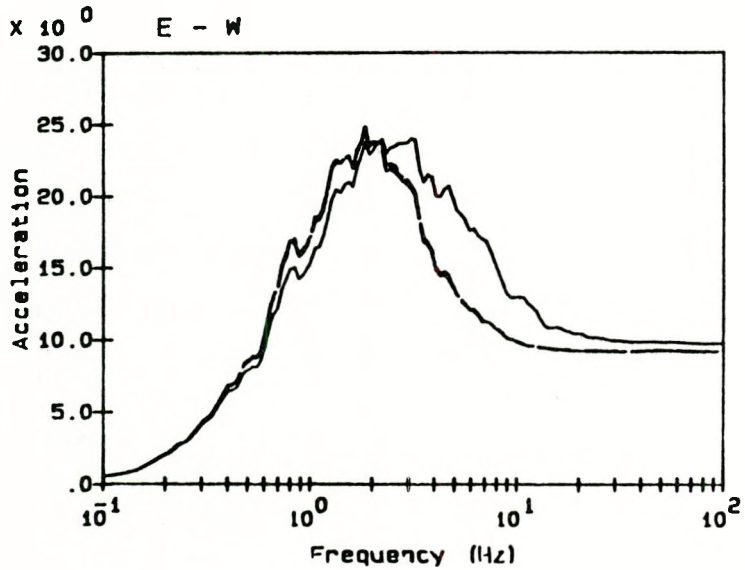

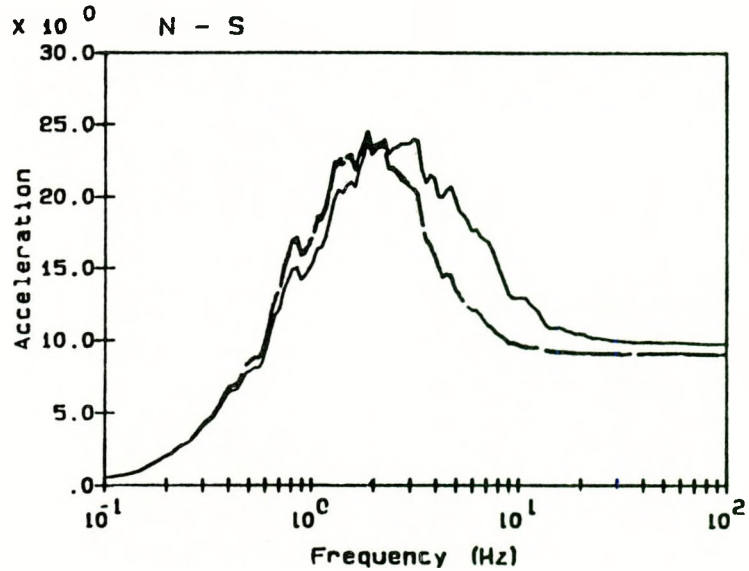

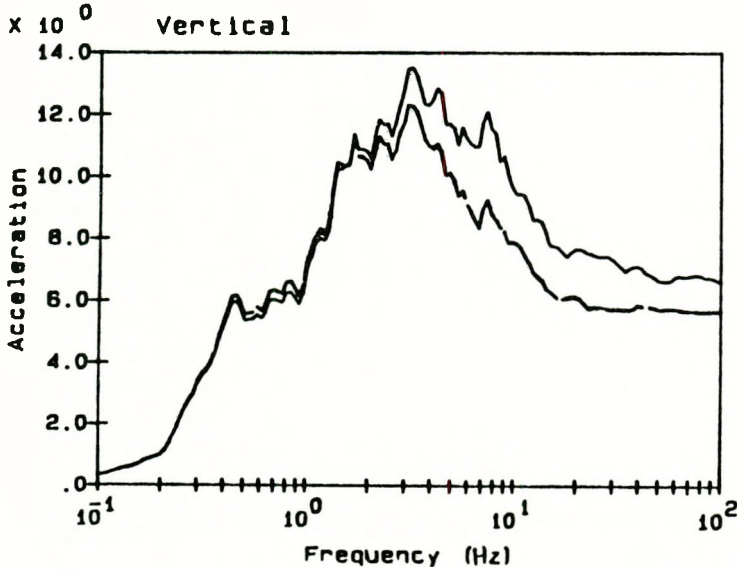

Legend:

free-field ——————————

fnd. ref. pt. — — — — — —

t.o.s. el 13'0" - - - - - - - - - - -

t.o.s. el 27'6" ——.——.——.

Notes:

All spectra calculated at 5% damping

Acceleration units in ft/s/s

RSPLT V3.00 2axb1.plt 09:27:59 07-06-88

Figure A.5(a) Surry Nuclear Power Plant Auxiliary Building
Instructure Response Acceleration Range 2

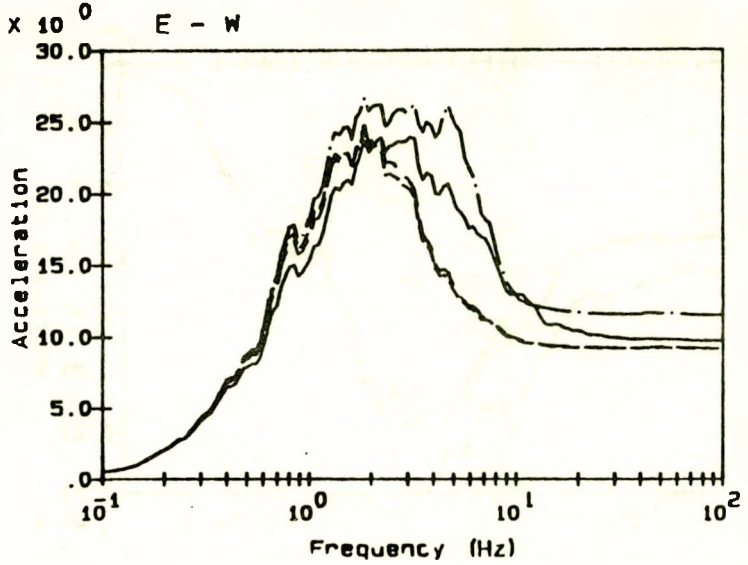

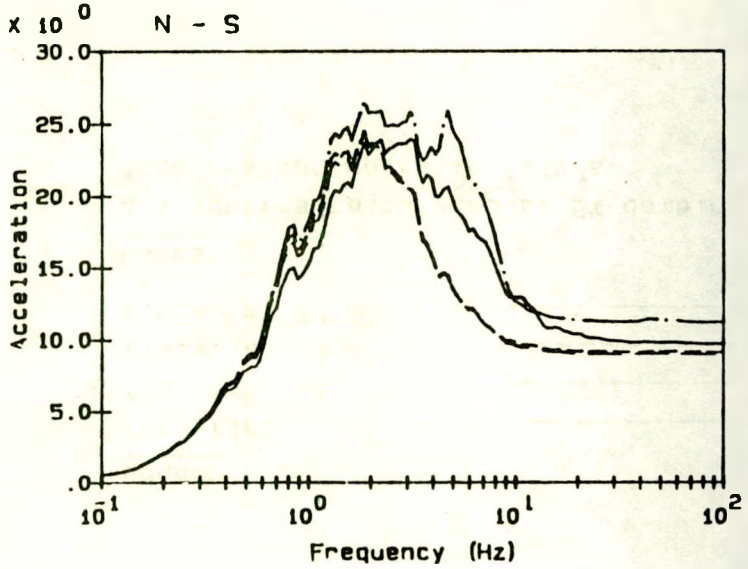

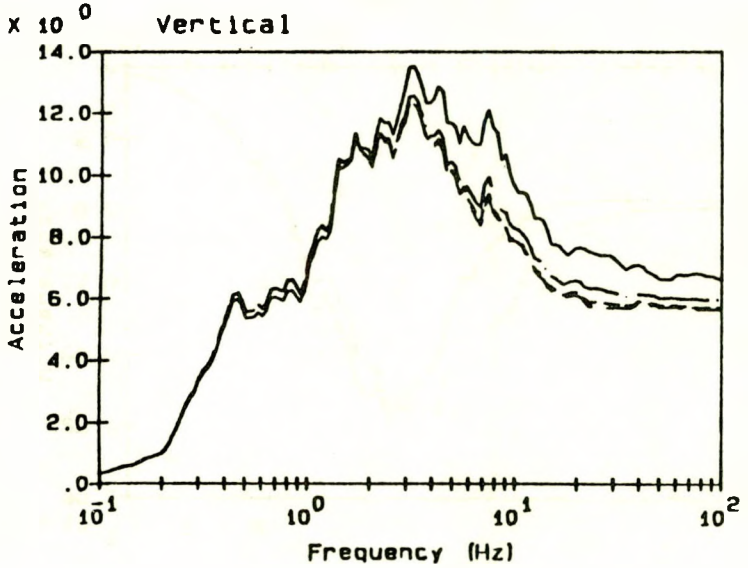

Legend:

free-field
fnd. ref. pt.
t.o.s. el 45'10"
t.o.s. el 66'0"

Notes:

All spectra calculated at 5% damping
Acceleration units in ft/s/s

RSPLT V3.00 2ax02.plt 11:50:41 02-21-88

Figure A.5(b) Surry Nuclear Power Plant Auxiliary Building
Instructure Response Acceleration Range 2

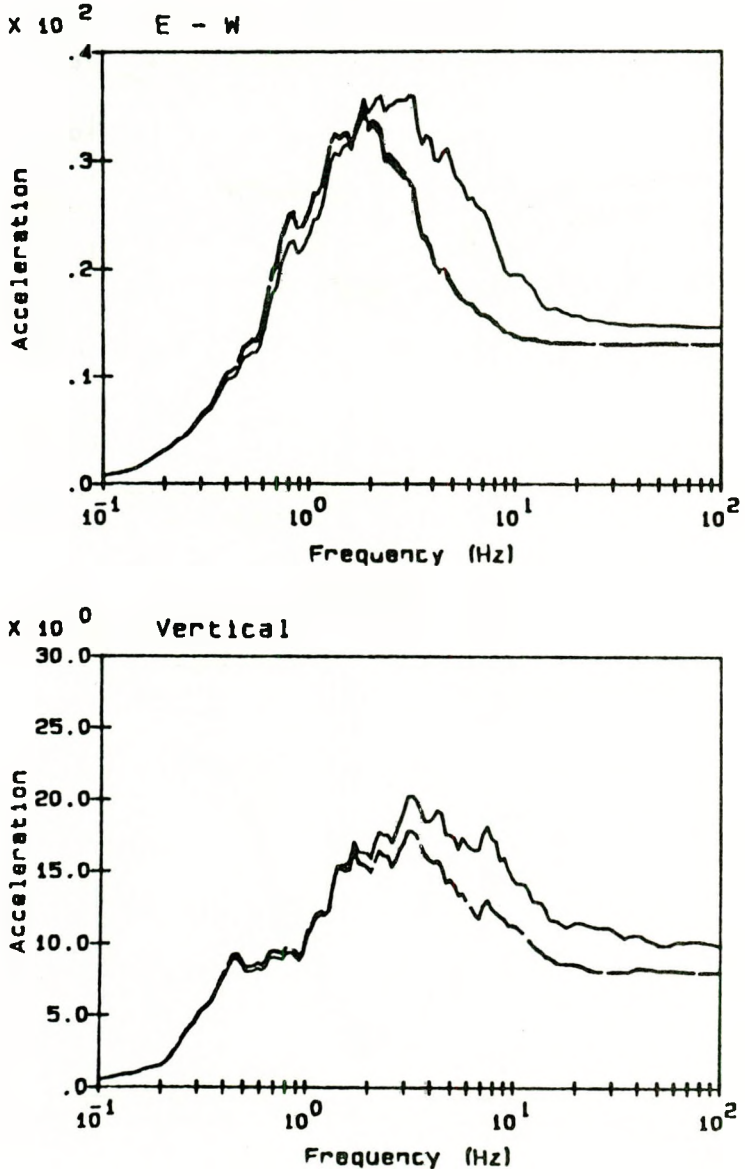

RSPLT V3.00 3axb1.plt 11:51:37 02-21-88

Figure A.6(a) Surry Nuclear Power Plant Auxiliary Building
Instructure Response Acceleration Range 3

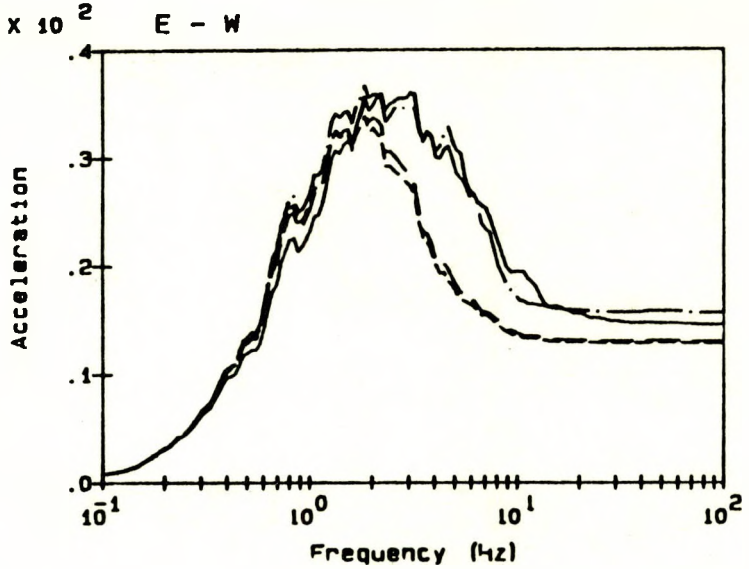

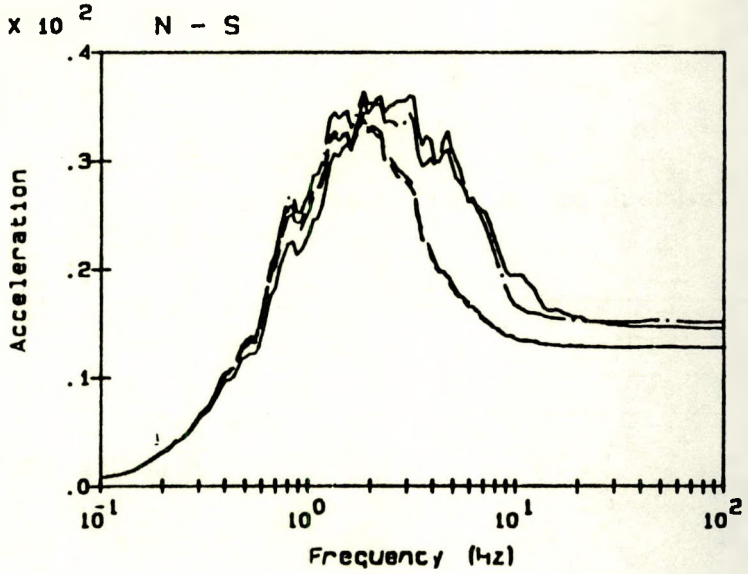

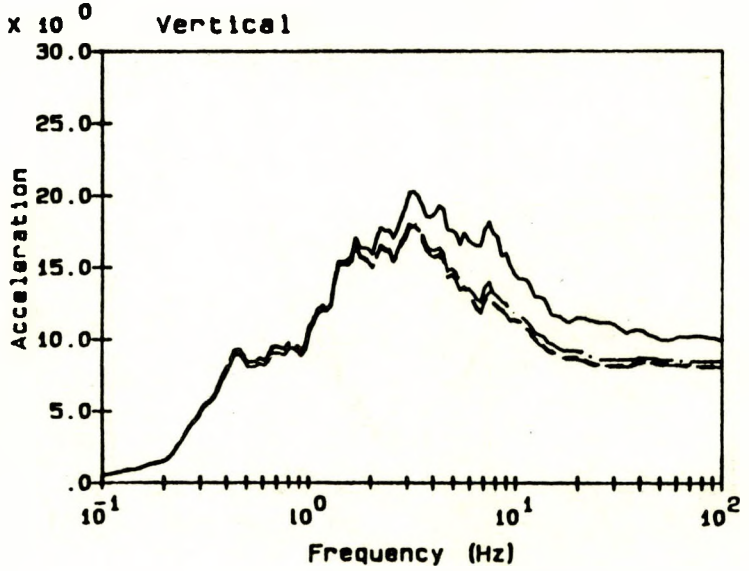

Legend:

free-field

fnd. ref. pt.

t.o.s. el 45'10"

t.o.s. el 66'0"

Notes:

All spectra calculated at 5% damping

Acceleration units in ft/s/s

RSPLT V3.00 3sxb2.plt 11:52:38 02-21-88

Figure A.6(b) Surry Nuclear Power Plant Auxiliary Building
Instrument Bearing Acceleration Range 3

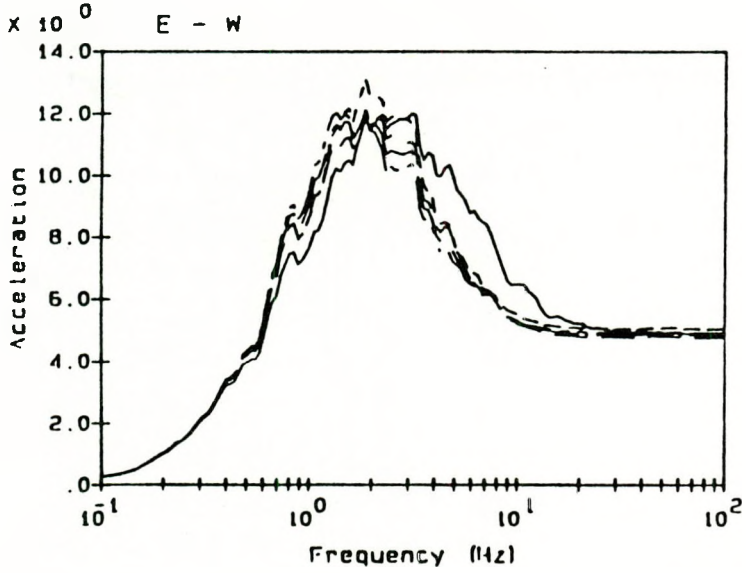

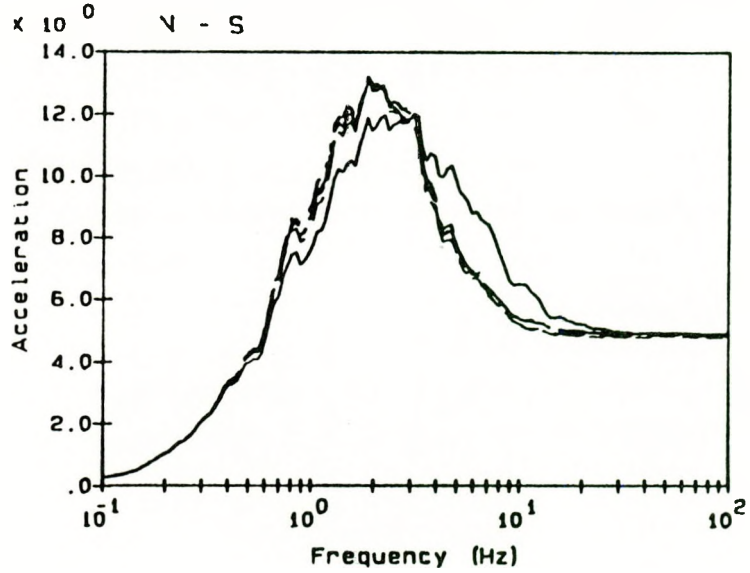

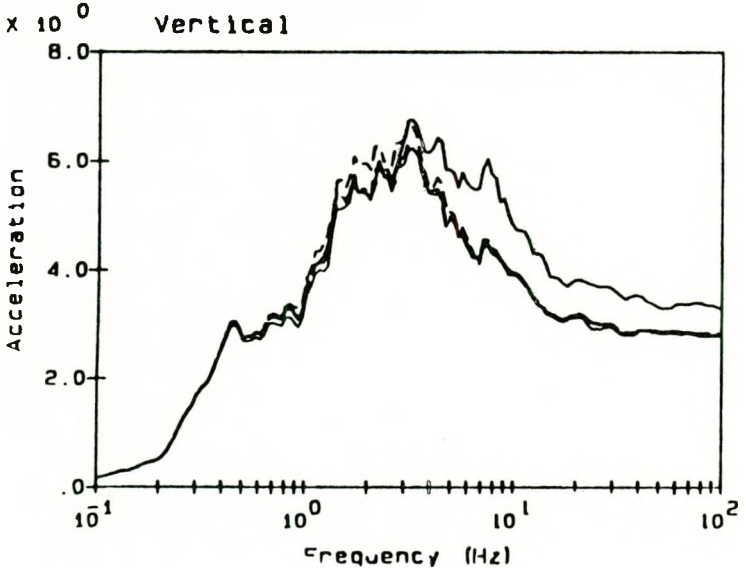

Legend:

free-field
fnd. ref. pt.
t.o.s. el 9'6"
t.o.s. el 27'0"
t.o.s. el 45'3"

Notes:

All spectra calculated at 5% damping
Acceleration units in ft/s/s

RSPLT V3.00 1501.plt 11:18:22 02-21-88

Figure A.7(a) Surry Nuclear Power Plant Control Room Structure
Instructure Responses Acceleration Range 1

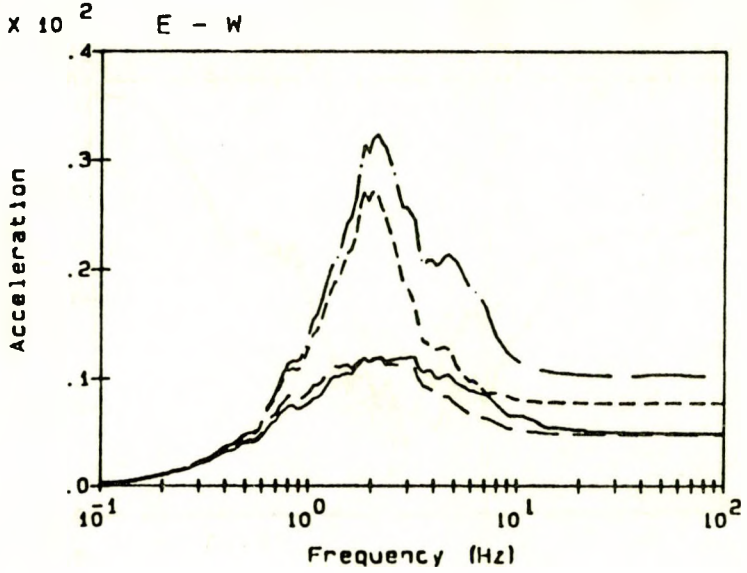

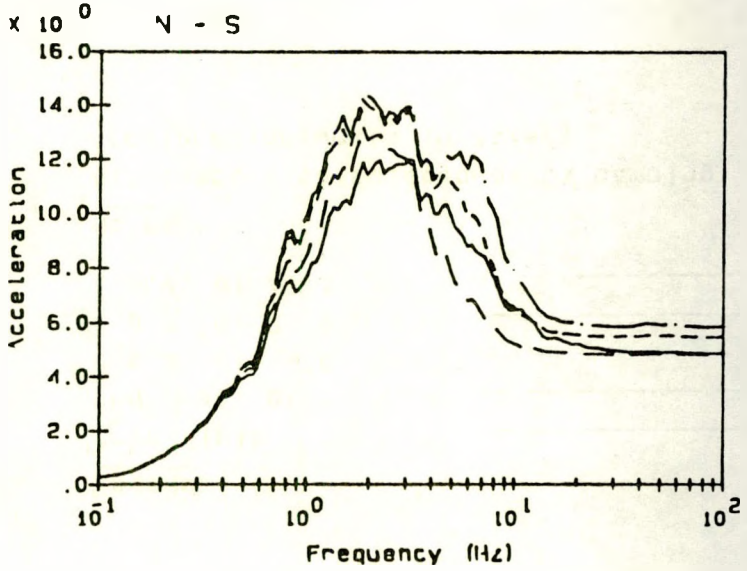

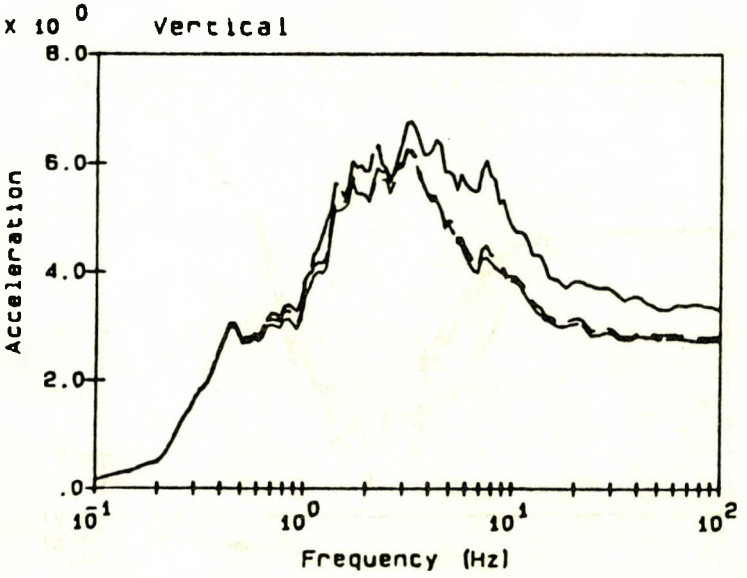

Legend:

free-field

fnd. ref. pt.

t.o.s. el 58'3"

t.o.s. el 77'6"

Notes:

All spectra calculated at 5% damping

Acceleration units in ft/s/s

RSPLT V3.00 1ab2.plt 11:19:15 02-21-88

Figure A.7(b) Surry Nuclear Power Plant Control Room Structure
Instructure Responses Acc. Range 1

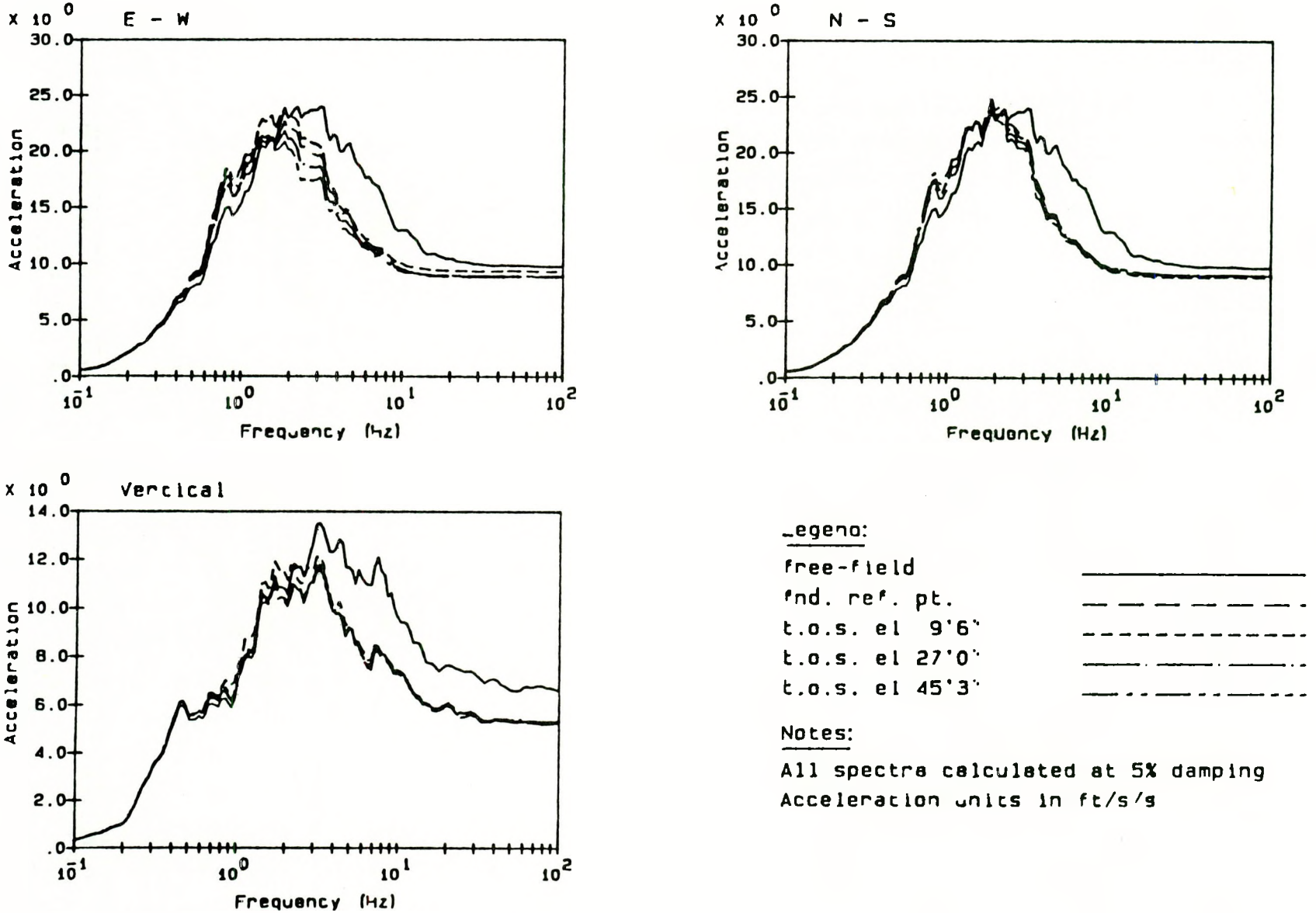

Figure A.8(a) Surry Nuclear Power Plant Control Room Structure
Instructure Responses Acceleration Range 2

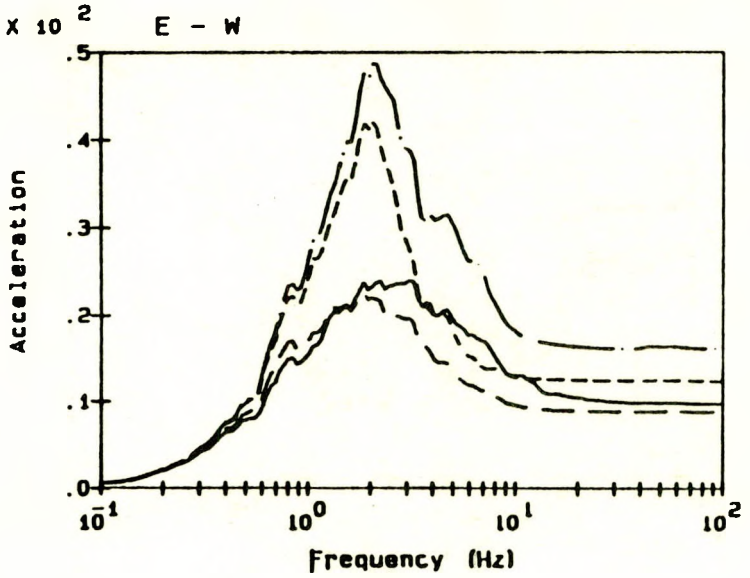

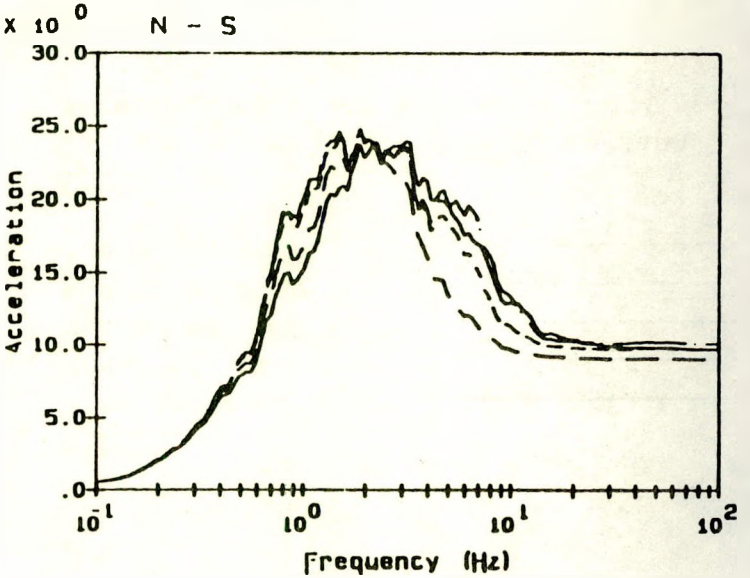

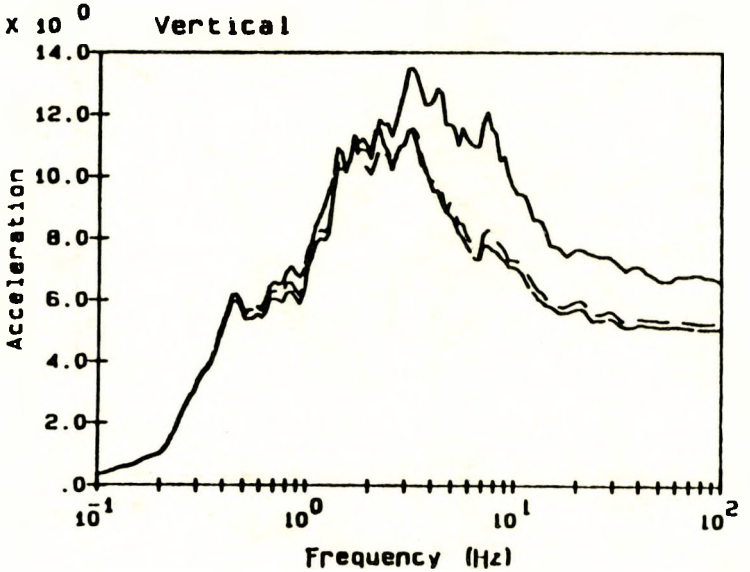

Legend:

free-field
fnd. ref. pt.
t.o.s. el 58'3"
t.o.s. el 77'6"

Notes:

All spectra calculated at 5% damping
Acceleration units in ft/s/s

RSPLT V3.00 3bb2.plt 11:21:32 02-21-88

Figure A.8(b) Surry Nuclear Power Plant Control Room Structure
Instructure Responses Acc Range 2

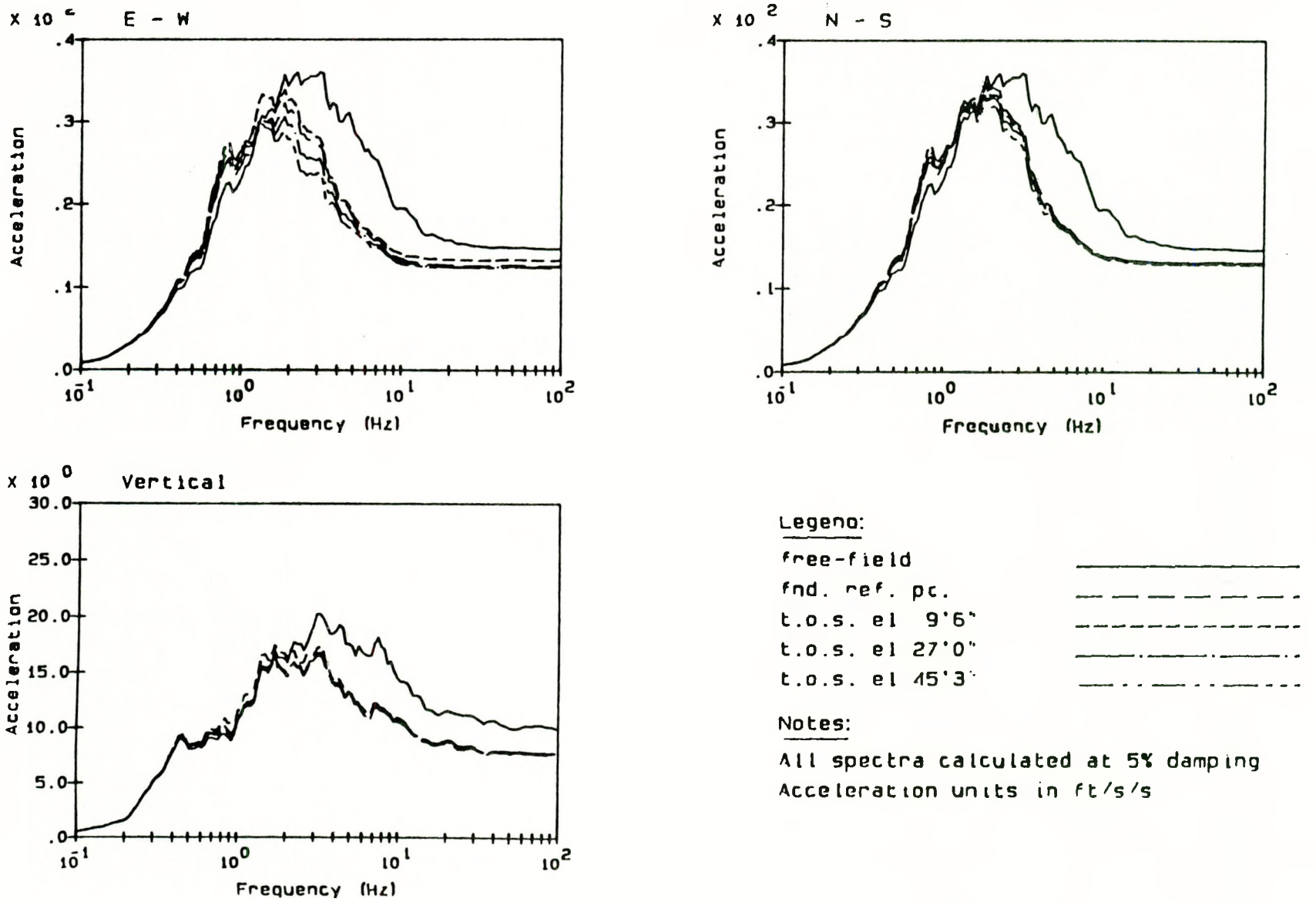

Figure A.9(a) Surry Nuclear Power Plant Control Room Structure
Instructure Responses Acceleration Range 3

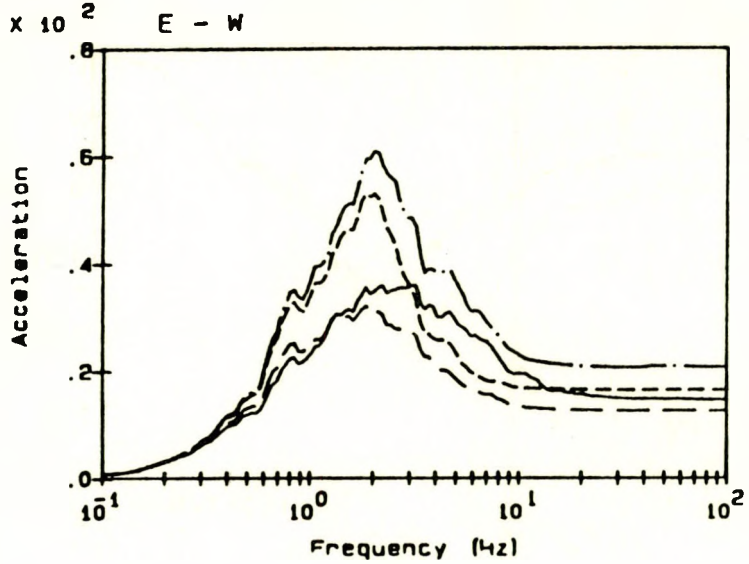

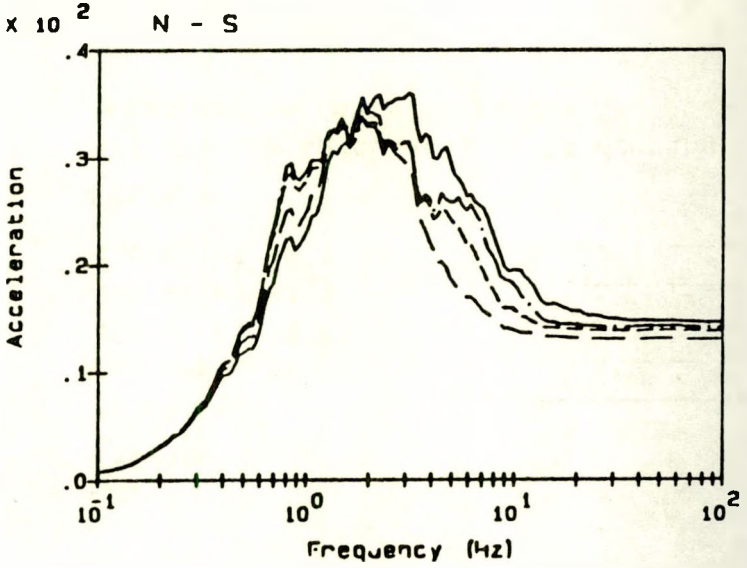

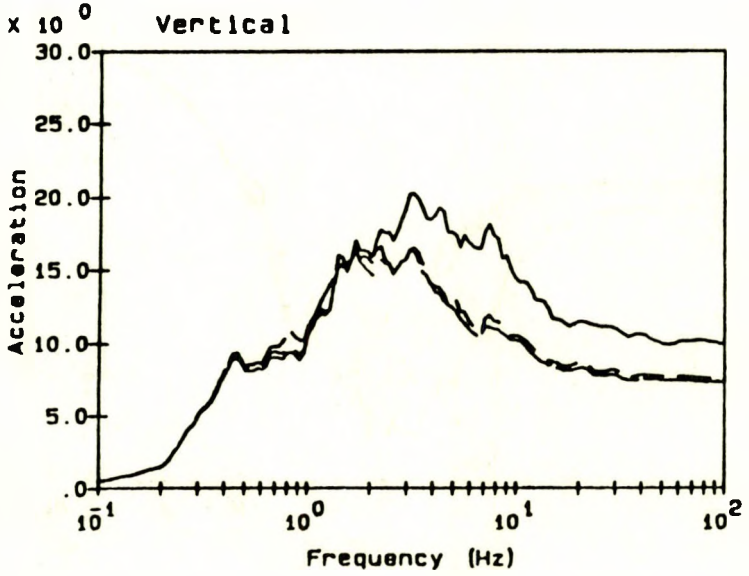

Legend:

free-field

fnd. ref. pt.

t.o.s. el 58'3"

t.o.s. el 77'6"

Notes:

All spectra calculated at 5% damping

Acceleration units in ft/s/s

RSPLT V3.00 3802.plt 10:29:11 02-21-88

Figure A.9(b) Surry Nuclear Power Plant Control Room Structure
Infrastructure Responses Acc. Range 3

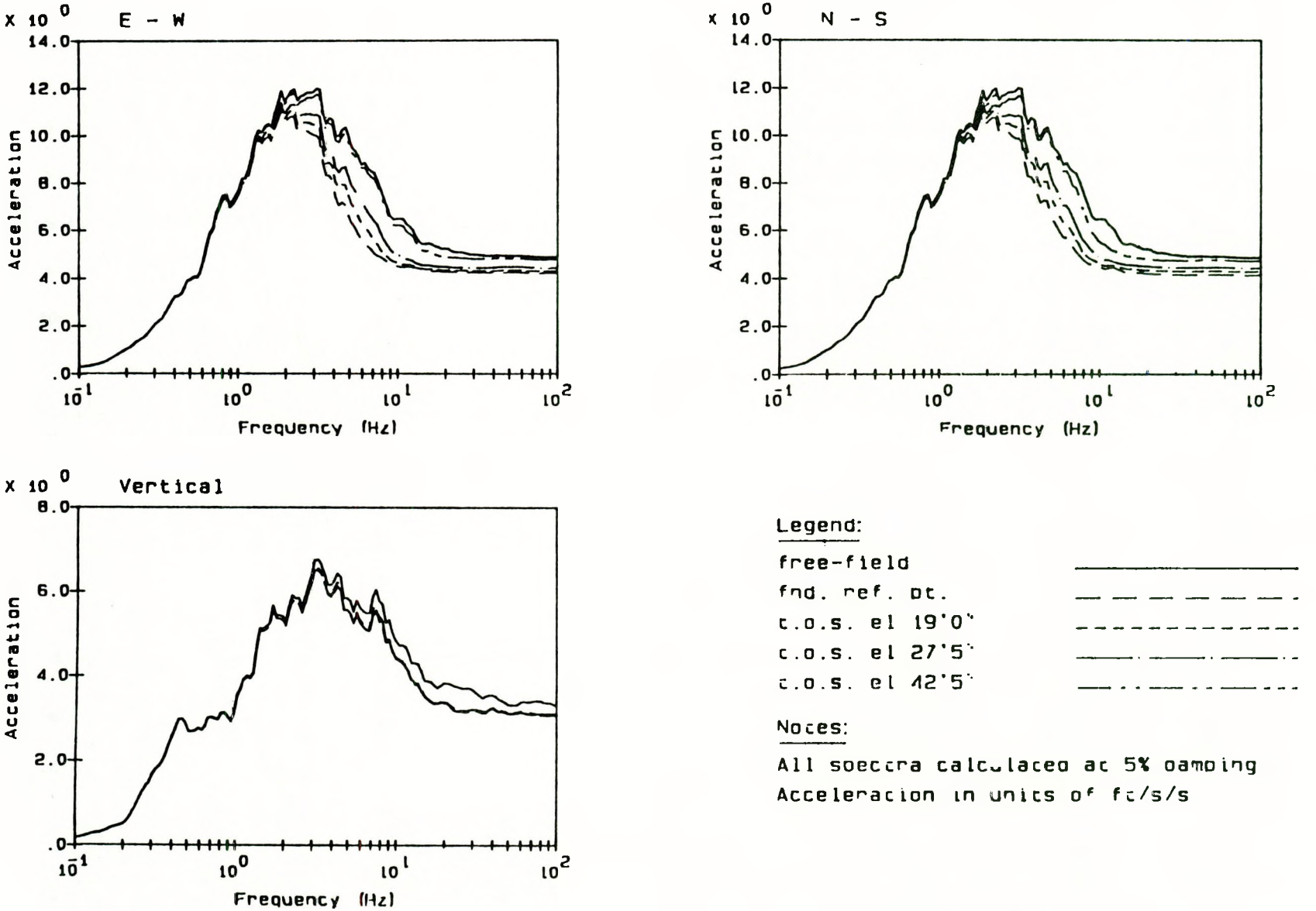

RSPLT V3.00 1001.plt 14:52:48 02-21-88

Figure A.10 Surry Nuclear Power Plant Safeguards Building
Instructure Responses Acceleration Range 1

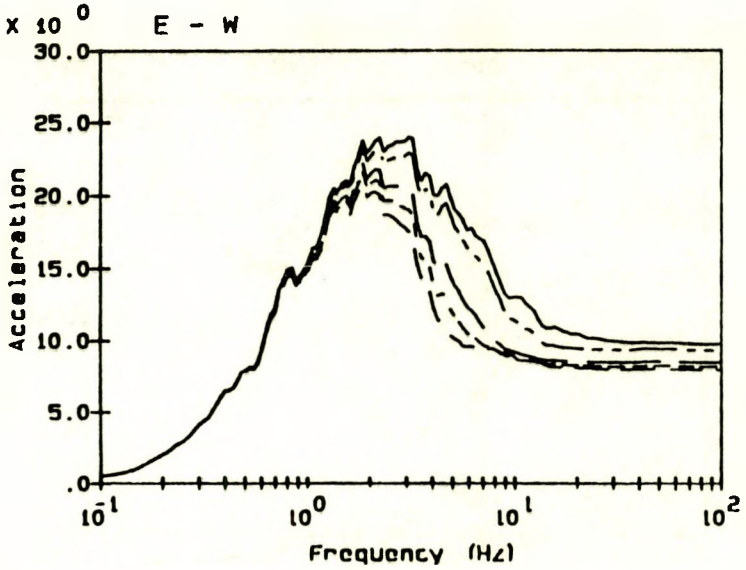

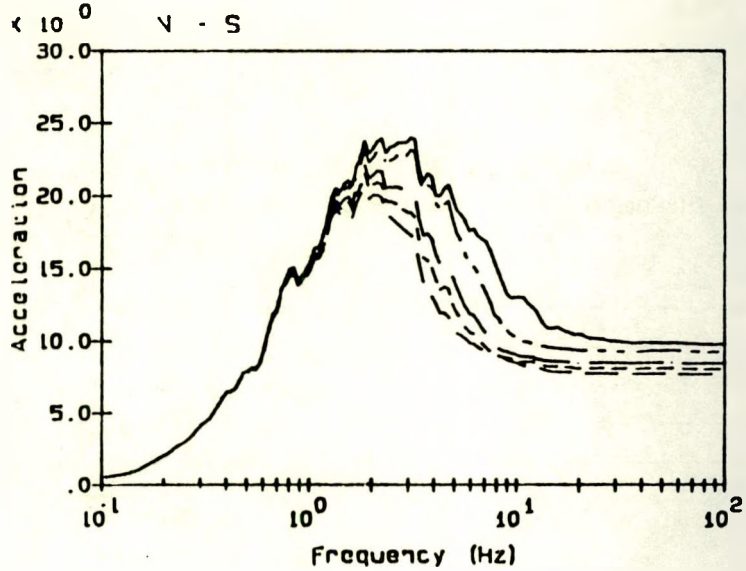

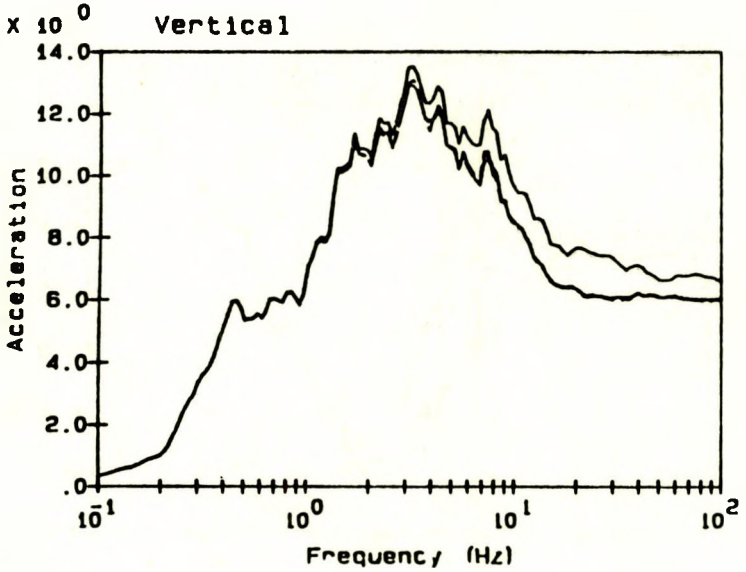

Legend:

free-field
fnd. ref. pt.
t.o.s. el 19'0"
t.o.s. el 27'5"
t.o.s. el 42'5"

Notes:

All spectra calculated at 5% damping
Acceleration in units of ft/s/s

RSPLT V3.00 2991.plt 15:07:34 02-21-88

Figure A.11 Surry Nuclear Power Plant Safeguards Building
Instructure Responses Acceleration Range 2

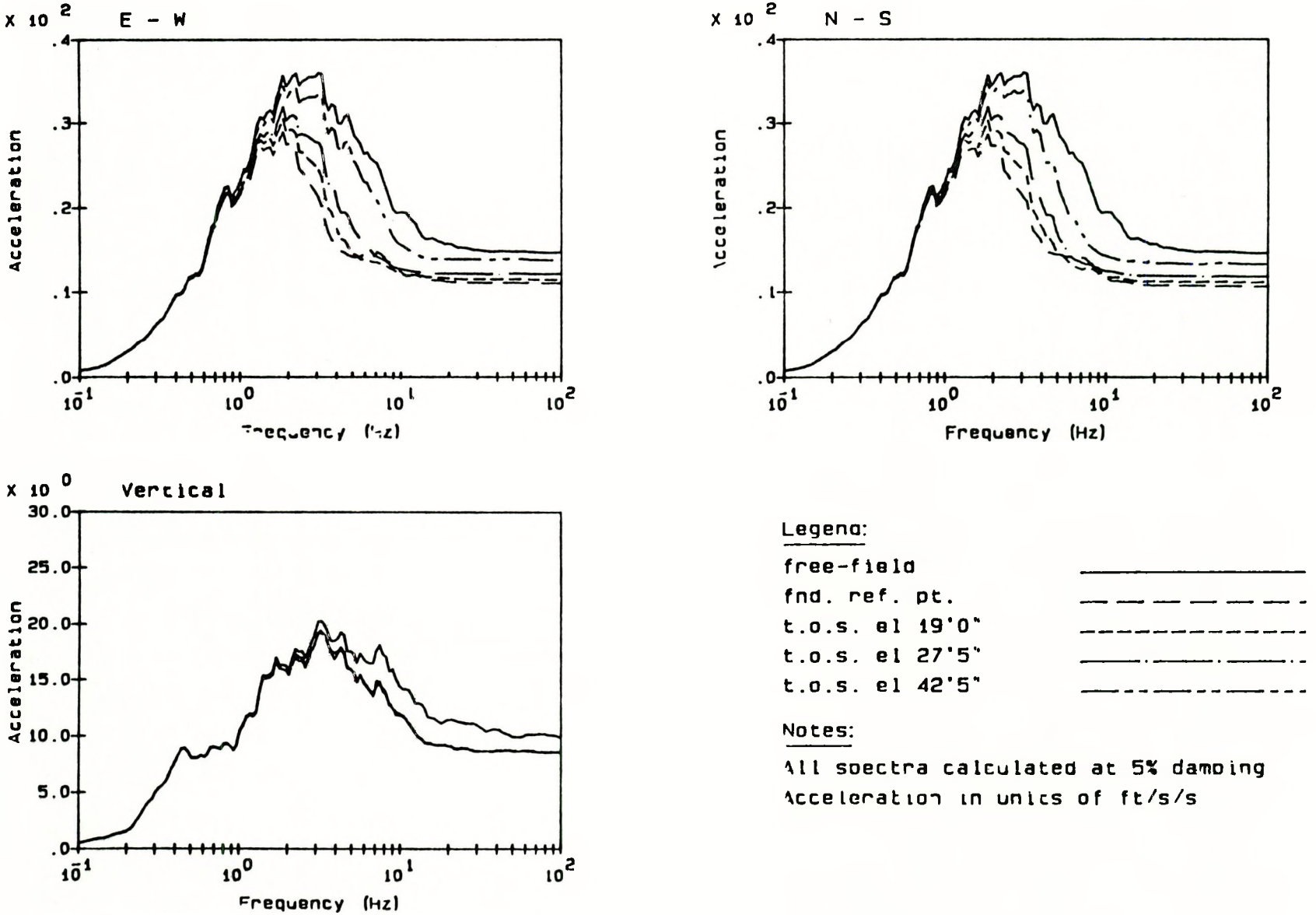

Figure A.12 Surry Nuclear Power Plant Safeguards Building
Instructure Responses Acceleration Range 3

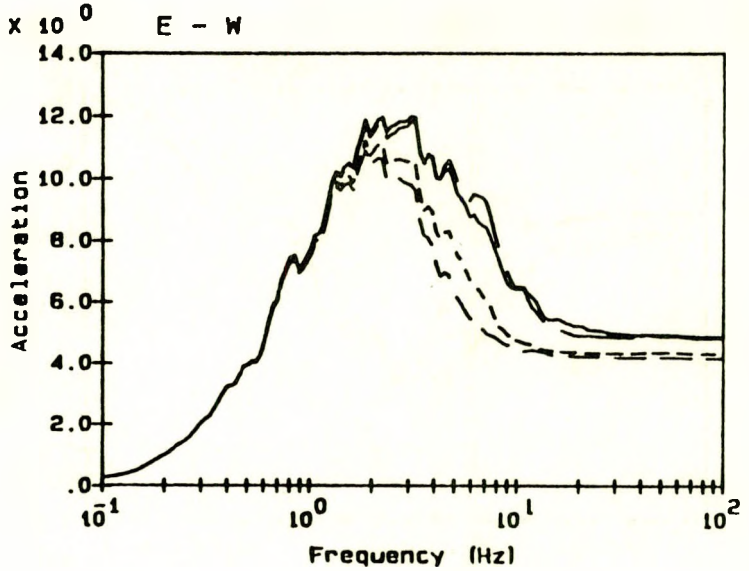

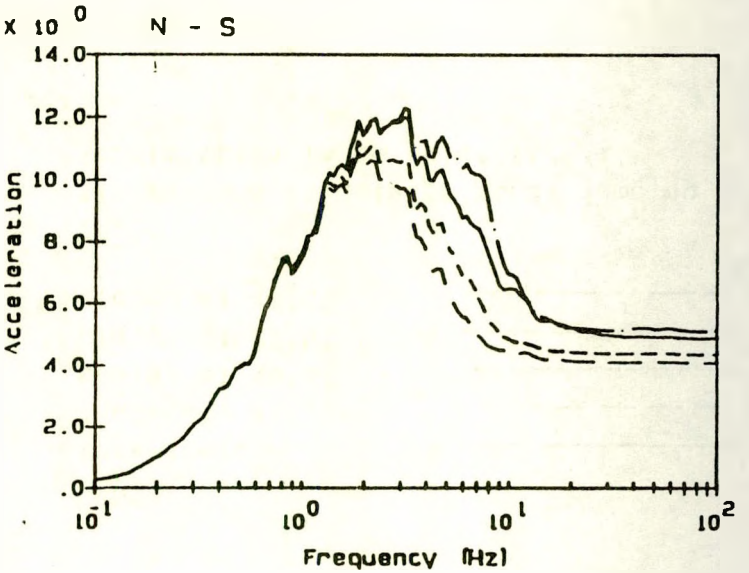

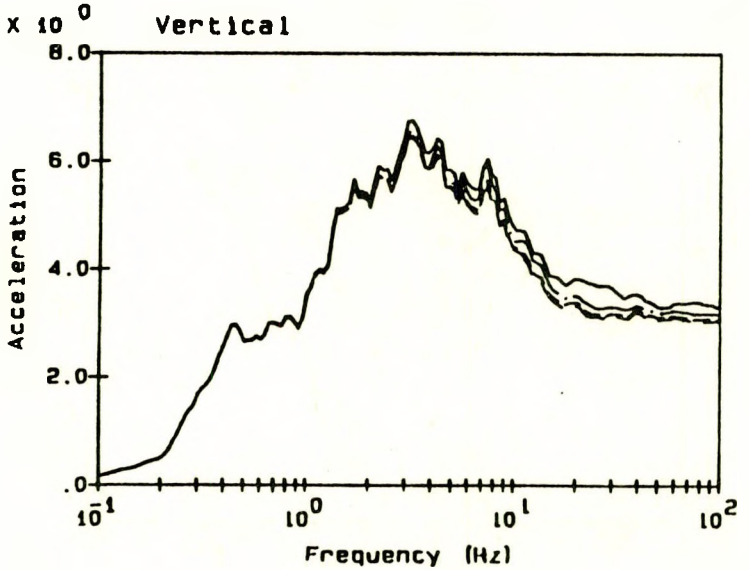

Legend:

free-field

fnd. ref. pt.

t.o.s. el 26'6"

t.o.s. el 52'0"

Notes:

All spectra calculated at 5% damping

Acceleration in units of ft/s/s

RSPLT V3.00 ics1.plt 15:59:19 02-21-88

Figure A.13 Surry Nuclear Power Plant Containment Spray Building
Instructure Responses Acceleration Range 1

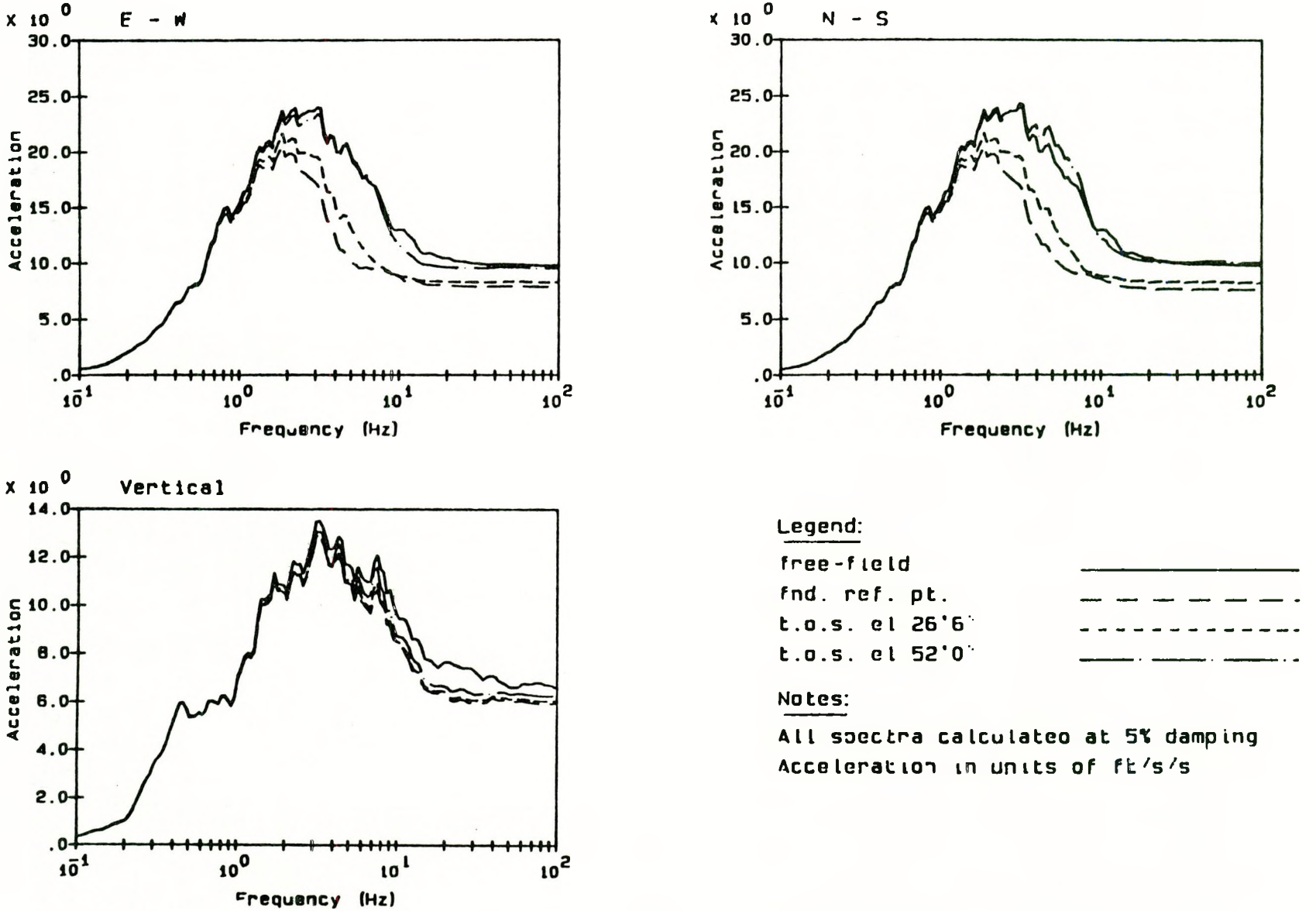

RSPLT V3.00 2ca1.plt 16:16:10 02-21-88

Figure A.14 Surry Nuclear Power Plant Containment Spray Building
Instructure Responses Acceleration Range 2

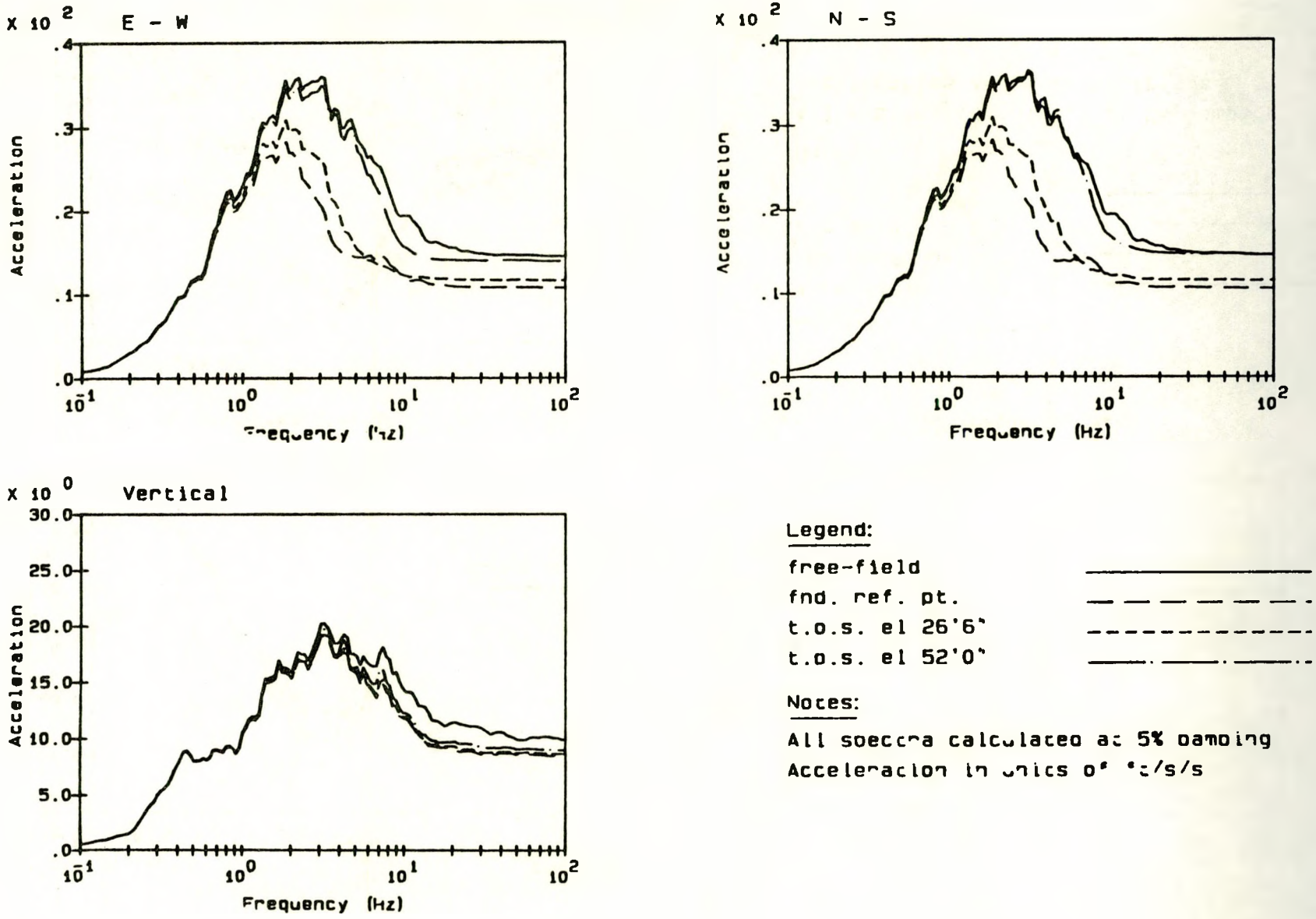

Figure A.15 Surry Nuclear Power Plant Containment Spray Building Instructure Responses Acceleration Range 3

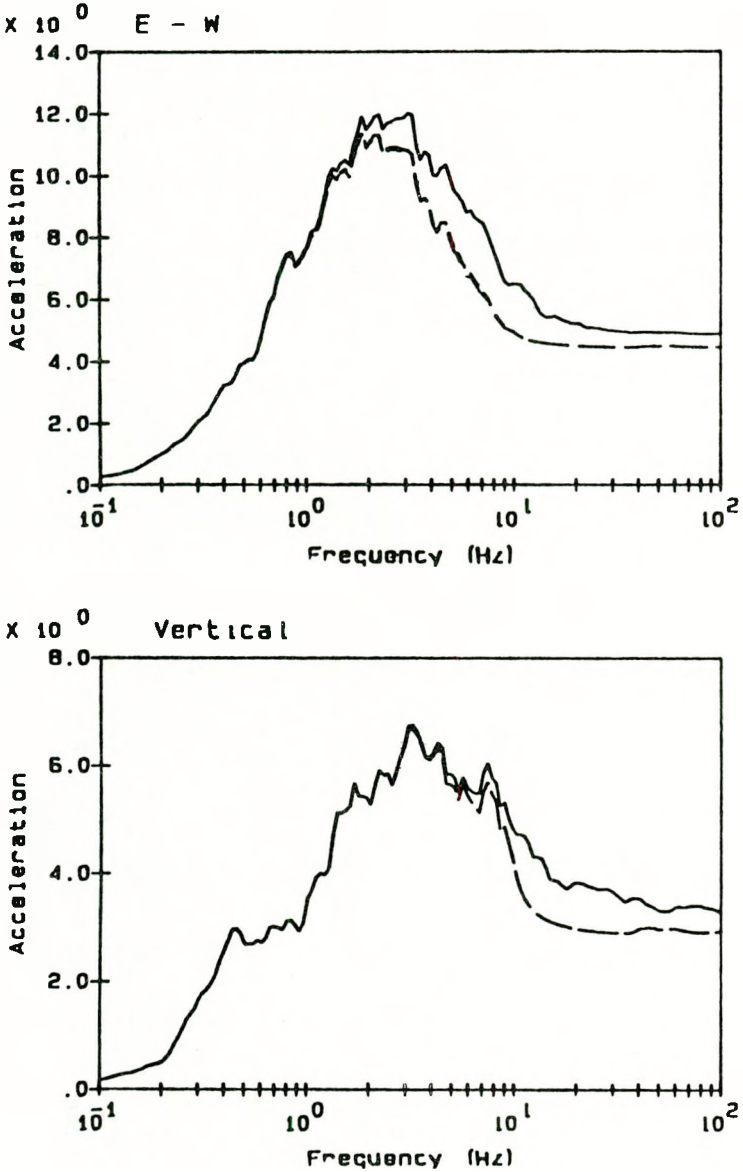

RSPLT V3.00 ege.plt 10:55:45 07-06-88

Figure A.16 Surry Nuclear Power Plant Emergency Generator Enclosure
Instructure Response Acceleration Range 1

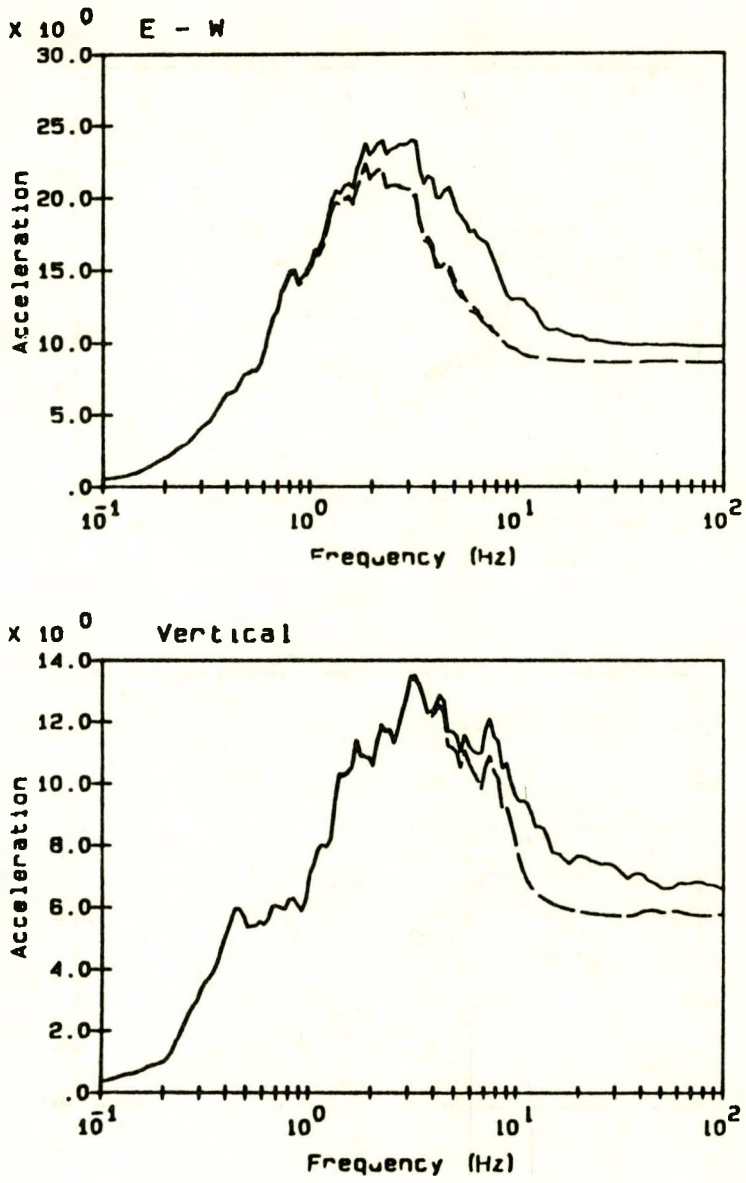

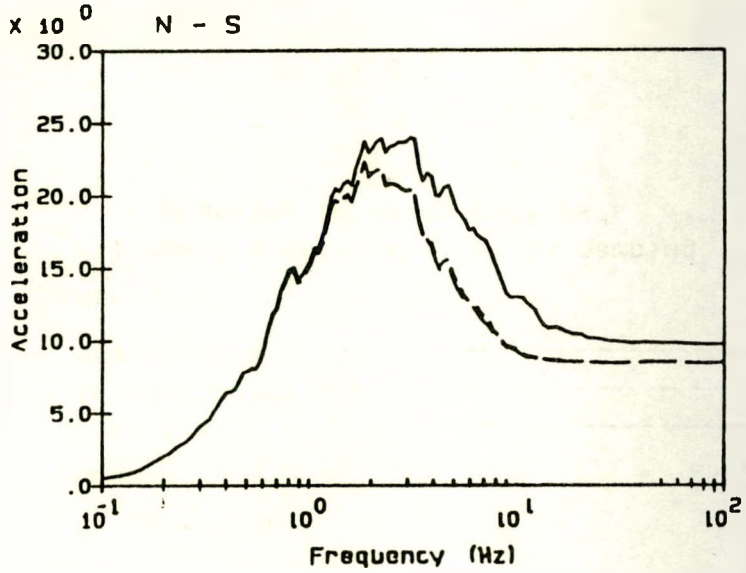

Legend:

free-field ————————

foundation ref. pt. — — — — — —

t.o.s. el 27 - 6 - - - - - - - - - - -

Notes:

all spectra calculated at 5% damping

accelerations in units of ft/s/s

RSPLT V3.00 egs.plt 10:59:05 07-06-88

Figure A.17 Surry Nuclear Power Plant Emergency Generator Enclosure
Instructure Response Acceleration Range 2

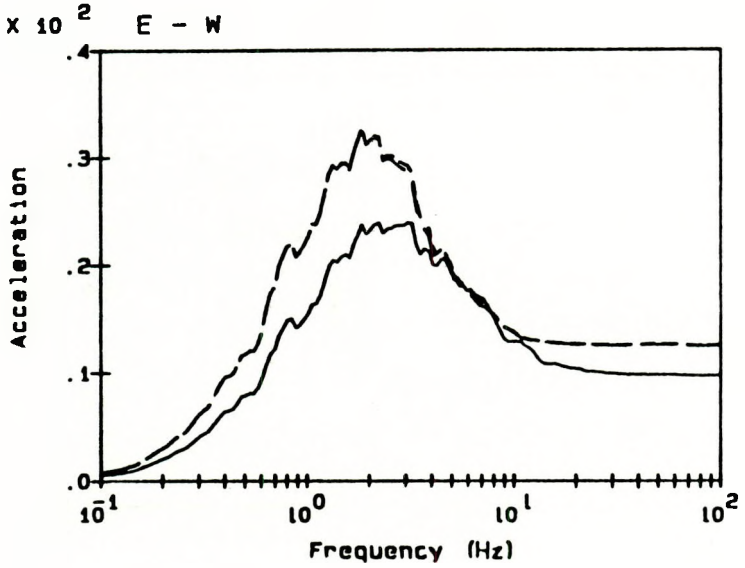

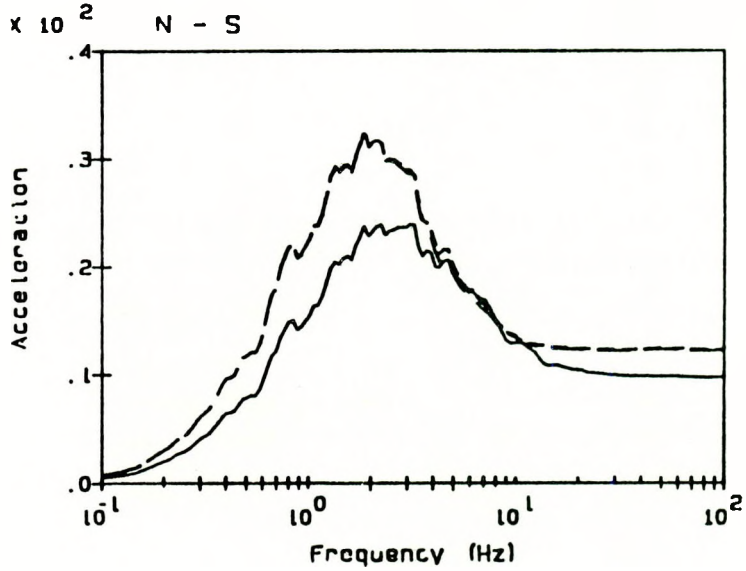

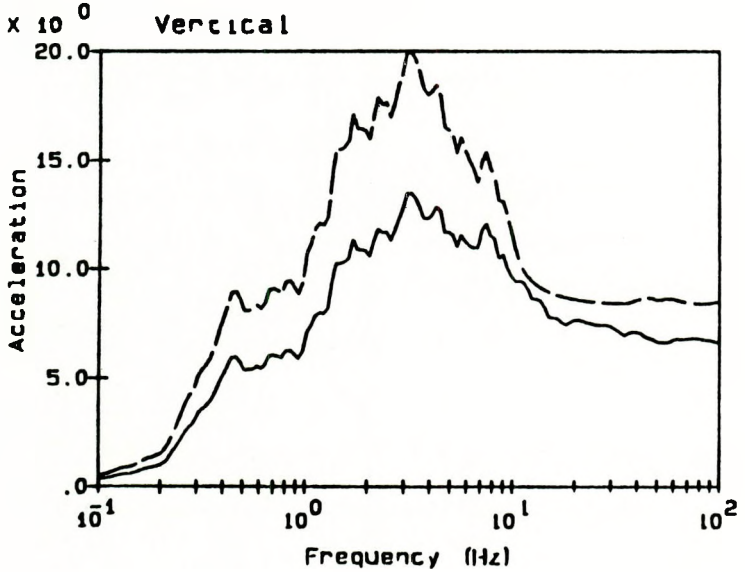

Legend:

free-field ——————————

foundation ref. pt. — — — — — — —

t.o.s. el 27 - 6 - - - - - - - - - - -

Notes:

all spectra calculated at 5% damping

accelerations in units of ft/s/s

RSPLT V3.00 ege.plt 16:32:24 07-06-88

Figure A.18 Surry Nuclear Power Plant Emergency Generator Enclosure Instructure Response Acceleration Range 3

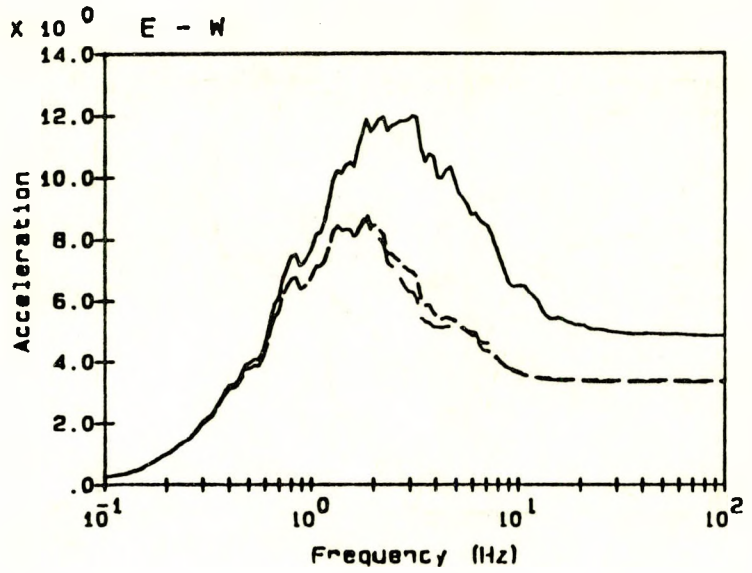

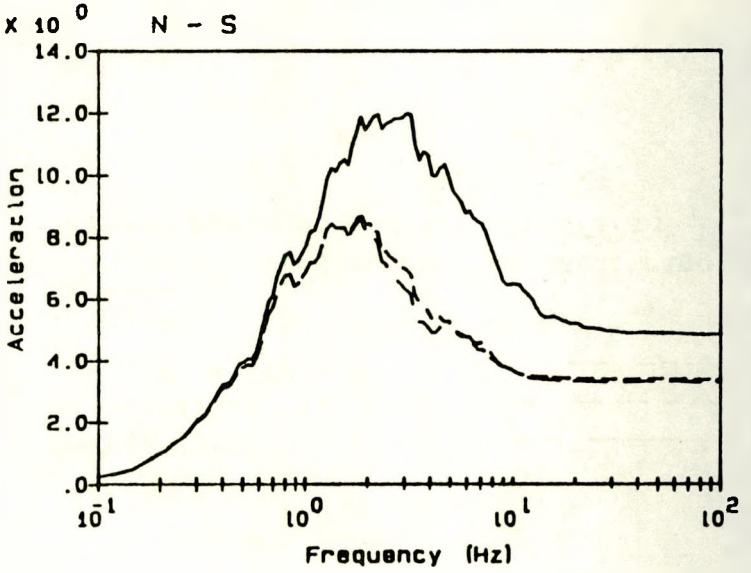

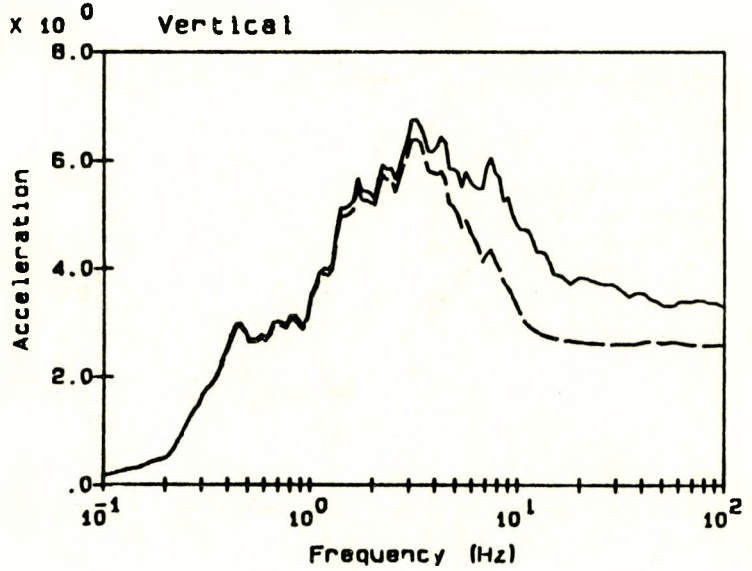

Legend:

free-field ——————————

foundation ref. pt. — — — — — — —

t.o.s. el 27 - 6 - - - - - - - - - - - - -

Notes:

all spectra calculated at 5% damping

accelerations in units of ft/s/s

RSPLT V3.00 Int.plt 11:01:33 07-06-88

Figure A.19 Surry Nuclear Power Plant Intake Structure
Instructure Response Acceleration Range 1

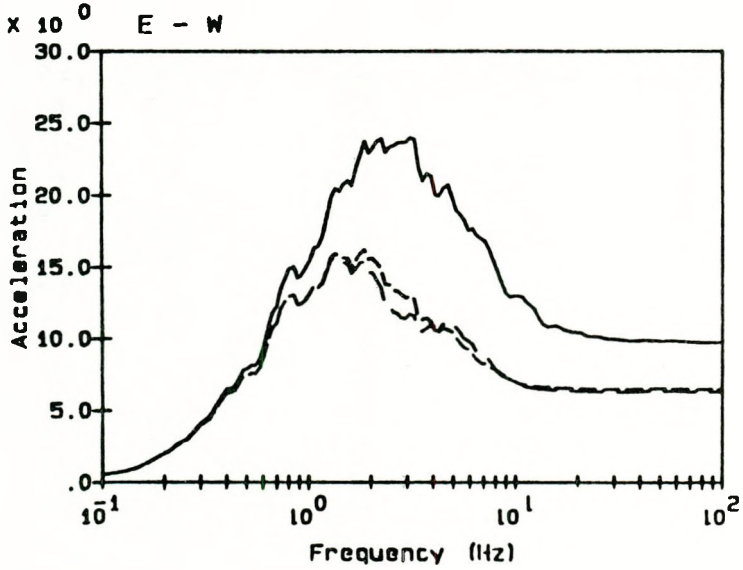

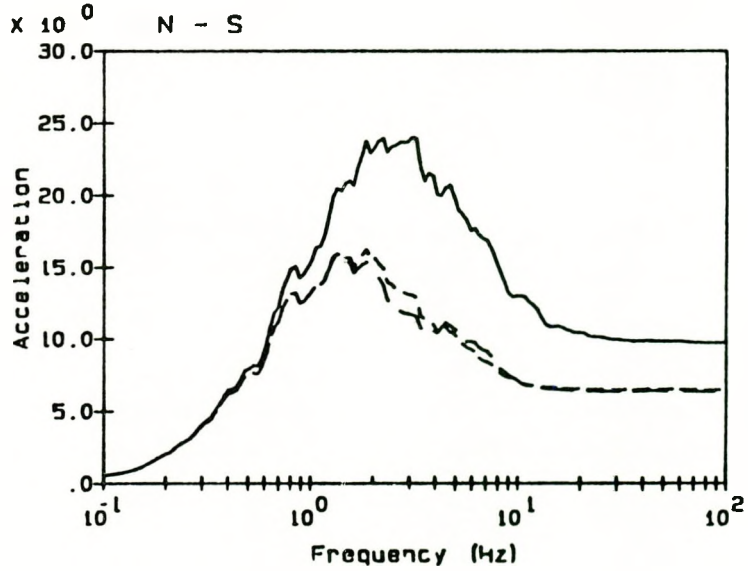

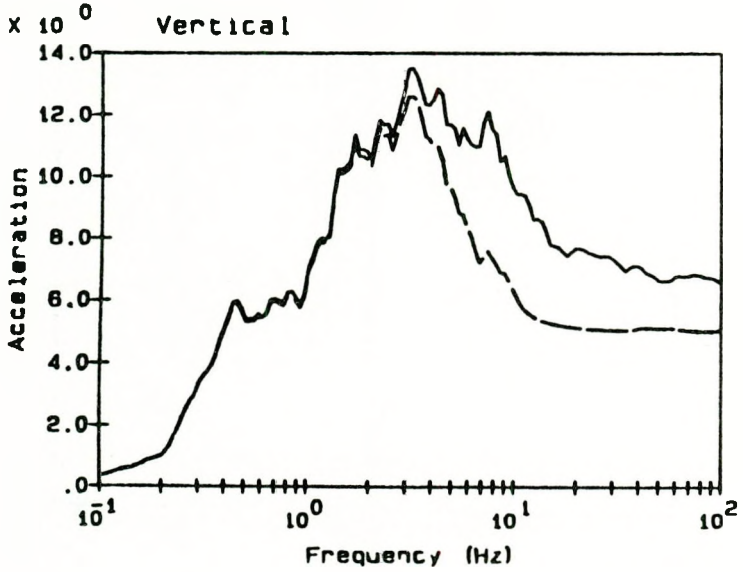

Legend:

free-field ——————————

foundation ref. pt. — — — — — —

t.o.s. el 27 - 6 - - - - - - - - - - -

Notes:

all spectra calculated at 5% damping

accelerations in units of ft/s/s

RSPLT V3.00 int.plt 11:02:44 07-06-88

Figure A.20 Surry Nuclear Power Plant Intake Structure
Instructure Response Acceleration Range 2

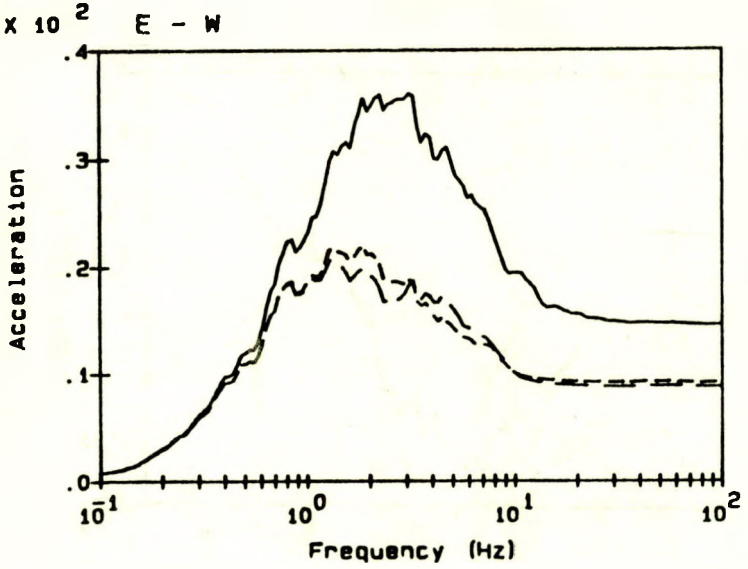

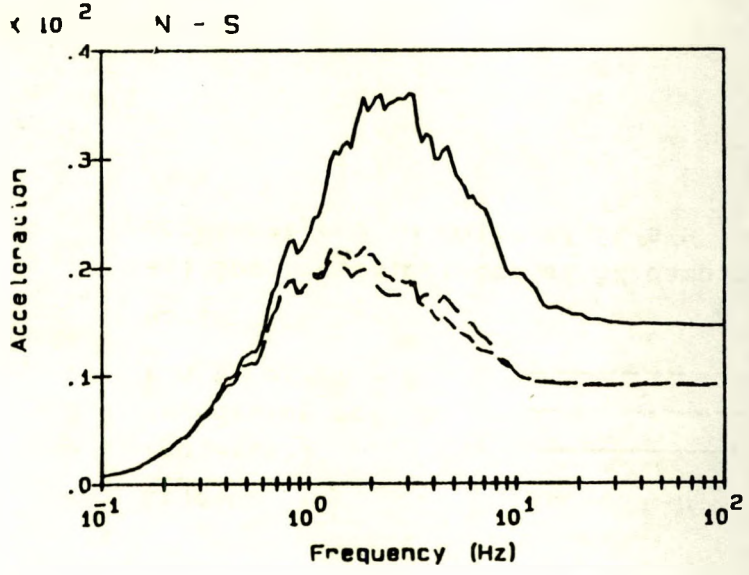

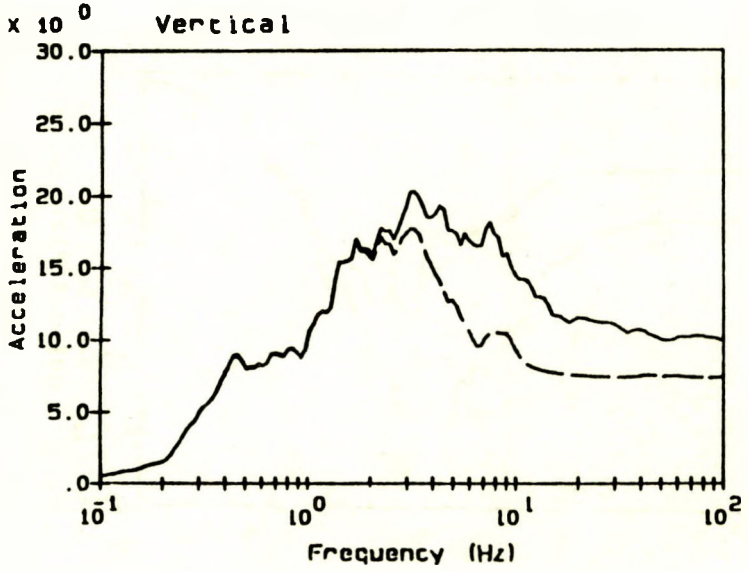

Legend:

free-field ——————————

foundation ref. pt. — — — — — — —

c.o.s. el 27 - 6 - - - - - - - - - - -

Notes:

all spectra calculated at 5% damping

accelerations in units of ft/s/s

RSPLT V3.00 Int.plt 10:08:36 07-06-88

Figure A.21 Surry Nuclear Power Plant Intake Structure
Instructure Response Acceleration Range 3

APPENDIX B

Numerical Values of Building Response at Three Excitation Levels

Table B-1a

Reactor Building Median Response
Acceleration Range 1 (g)

		Frequency				
Elevation	Dir	2-5(Hz)	5-10(Hz)	7 (Hz)	10 (Hz)	zpa
-39'-7"	x	.15	.10	.11	.08	.07
-39'-7"	y	.15	.10	.11	.08	.08
-39'-7"	z	.13	.08	.08	.07	.07
-3'-6"	x	.13	.10	.10	.08	.08
-3'-6"	y	.13	.10	.10	.08	.08
-3'-6"	z	.14	.09	.08	.08	.07
18'-4"	x	.12	.10	.10	.09	.08
18'-4"	y	.12	.10	.10	.09	.08
18'-4"	z	.14	.09	.09	.08	.07
47'-4"	x	.14	.11	.12	.10	.10
47'-4"	y	.14	.11	.11	.09	.09
47'-4"	z	.14	.09	.09	.08	.07
95'-6"	x	.20	.15	.16	.14	.13
95'-6"	y	.20	.15	.17	.13	.12
95'-6"	z	.14	.09	.09	.08	.07

Table B-1b

Reactor Building Median Response
Acceleration Range 2 (g)

		Frequency				
Elevation	Dir	2-5(Hz)	5-10(Hz)	7 (Hz)	10 (Hz)	zpa
-39'-7"	x	.30	.21	.22	.16	.15
-39'-7"	y	.30	.21	.22	.16	.14
-39'-7"	z	.23	.15	.16	.14	.12
-3'-6"	x	.24	.18	.19	.15	.13
-3'-6"	y	.24	.18	.19	.15	.13
-3'-6"	z	.23	.16	.17	.14	.13
18'-4"	x	.21	.18	.19	.14	.14
18'-4"	y	.22	.18	.19	.15	.14
18'-4"	z	.23	.16	.17	.14	.13
47'-4"	x	.22	.19	.21	.17	.16
47'-4"	y	.23	.19	.20	.16	.15
47'-4"	z	.23	.16	.17	.14	.13
95'-6"	x	.32	.28	.30	.25	.23
95'-6"	y	.32	.28	.30	.24	.22
95'-6"	z	.23	.16	.17	.14	.13

Table B-1c

Reactor Building Median Response
Acceleration Range 3 (g)

		Frequency				
Elevation	Dir	2-5(Hz)	5-10(Hz)	7 (Hz)	10 (Hz)	zpa
-39'-7"	x	.46	.38	.42	.28	.23
-39'-7"	y	.46	.38	.42	.30	.23
-39'-7"	z	.24	.18	.19	.16	.14
-3'-6"	x	.36	.31	.34	.22	.18
-3'-6"	y	.36	.31	.34	.24	.19
-3'-6"	z	.25	.20	.21	.17	.14
18'-4"	x	.31	.28	.32	.20	.17
18'-4"	y	.31	.28	.31	.21	.18
18'-4"	z	.25	.20	.20	.17	.14
47'-4"	x	.25	.29	.34	.21	.17
47'-4"	y	.27	.29	.33	.21	.18
47'-4"	z	.25	.20	.21	.17	.14
95'-6"	x	.30	.41	.46	.34	.25
95'-6"	y	.32	.43	.50	.33	.25
95'-6"	z	.25	.20	.20	.17	.15

Table B-2a

Auxiliary Building Median Response
Acceleration Range 1 (g)

		Frequency				
Elevation	Dir	2-5(Hz)	5-10(Hz)	7 (Hz)	10 (Hz)	zpa
-2 - 0"	x	.32	.19	.20	.17	.15
-2 - 0"	y	.32	.19	.19	.16	.15
-2 - 0"	z	.18	.15	.15	.13	.09
13'- 0"	x	.32	.19	.20	.17	.16
13'- 0"	y	.32	.19	.20	.16	.15
13'- 0"	z	.18	.15	.15	.13	.09
27'- 6"	x	.32	.19	.20	.17	.16
27'- 6"	y	.32	.19	.20	.16	.15
27'- 6"	z	.18	.15	.15	.13	.10
45'-10"	x	.31	.19	.20	.17	.16
45'-10"	y	.32	.19	.20	.17	.15
45'-10"	z	.18	.15	.15	.13	.10
66'- 0"	x	.48	.34	.37	.24	.21
66'- 0"	y	.46	.36	.40	.25	.21
66'- 0"	z	.18	.16	.16	.14	.10

Table B-2b

Auxiliary Building Median Response
Acceleration Range 2 (g)

		Frequency				
Elevation	Dir	2-5(Hz)	5-10(Hz)	7 (Hz)	10 (Hz)	zpa
-2 - 0"	x	.56	.35	.35	.31	.29
-2 - 0"	y	.55	.34	.35	.30	.28
-2 - 0"	z	.34	.27	.27	.24	.18
13'- 0"	x	.55	.35	.35	.31	.29
13'- 0"	y	.55	.34	.35	.30	.28
13'- 0"	z	.34	.27	.27	.24	.18
27'- 6"	x	.55	.34	.35	.31	.29
27'- 6"	y	.55	.34	.35	.30	.28
27'- 6"	z	.34	.27	.27	.24	.18
45'-10"	x	.54	.34	.35	.30	.29
45'-10"	y	.55	.34	.35	.30	.29
45'-10"	z	.34	.27	.28	.25	.18
66'- 0"	x	.79	.54	.58	.40	.36
66'- 0"	y	.76	.55	.60	.40	.36
66'- 0"	z	.35	.29	.29	.26	.19

Table B-2c

Auxiliary Building Median Response
Acceleration Range 3 (g)

		Frequency				
Elevation	Dir	2-5(Hz)	5-10(Hz)	7 (Hz)	10 (Hz)	zpa
-2 - 0"	x	.76	.48	.49	.43	.41
-2 - 0"	y	.76	.47	.48	.42	.40
-2 - 0"	z	.49	.38	.38	.35	.25
13'- 0"	x	.76	.48	.49	.43	.41
13'- 0"	y	.75	.47	.48	.42	.40
13'- 0"	z	.49	.38	.39	.35	.25
27'- 6"	x	.75	.47	.48	.42	.40
27'- 6"	y	.75	.47	.48	.42	.40
27'- 6"	z	.49	.38	.38	.35	.25
45'-10"	x	.74	.47	.48	.42	.40
45'-10"	y	.75	.47	.48	.42	.40
45'-10"	z	.50	.39	.39	.35	.26
66'- 0"	x	1.03	.69	.74	.53	.49
66'- 0"	y	1.00	.69	.75	.52	.48
66'- 0"	z	.50	.40	.41	.36	.27

Table B-3a

Control Room Structure Median
Response Acceleration Range 1 (g)

		Frequency				
Elevation	Dir	2-5(Hz)	5-10(Hz)	7 (Hz)	10 (Hz)	zpa
-0 - 0"	x	.30	.19	.20	.16	.15
-0 - 0"	y	.32	.19	.19	.16	.15
-0 - 0"	z	.17	.13	.13	.12	.09
9'- 6"	x	.31	.19	.20	.17	.16
9'- 6"	y	.31	.19	.19	.16	.15
9'- 6"	z	.18	.14	.14	.12	.09
27'- 0"	x	.29	.19	.19	.16	.15
27'- 0"	y	.31	.19	.20	.17	.15
27'- 0"	z	.17	.13	.14	.12	.09
45'- 3"	x	.28	.19	.19	.16	.15
45'- 3"	y	.31	.19	.20	.17	.15
45'- 3"	z	.17	.13	.13	.12	.09
58'- 6"	x	.50	.28	.28	.25	.24
58'- 6"	y	.38	.26	.28	.20	.17
58'- 6"	z	.17	.13	.13	.12	.09
77'- 6"	x	.74	.47	.51	.36	.32
77'- 6"	y	.39	.32	.35	.24	.18
77'- 6"	z	.17	.13	.13	.12	.09

Table B-3b

Control Room Structure
Acceleration Range 2 (g)

		Frequency				
Elevation	Dir	2-5(Hz)	5-10(Hz)	7 (Hz)	10 (Hz)	zpa
-0 - 0"	x	.53	.34	.35	.30	.28
-0 - 0"	y	.56	.34	.35	.30	.28
-0 - 0"	z	.32	.24	.24	.23	.17
9'- 6"	x	.55	.35	.36	.31	.29
9'- 6"	y	.55	.33	.34	.30	.28
9'- 6"	z	.33	.25	.25	.23	.17
27'- 0"	x	.50	.33	.34	.29	.27
27'- 0"	y	.55	.34	.35	.30	.28
27'- 0"	z	.32	.25	.25	.23	.17
45'- 3"	x	.48	.32	.33	.29	.28
45'- 3"	y	.53	.34	.34	.30	.28
45'- 3"	z	.32	.24	.25	.23	.17
58'- 6"	x	.78	.44	.43	.40	.39
58'- 6"	y	.64	.43	.46	.35	.31
58'- 6"	z	.32	.23	.23	.22	.16
77'- 6"	x	1.11	.71	.75	.56	.51
77'- 6"	y	.66	.51	.55	.41	.32
77'- 6"	z	.32	.23	.23	.22	.16

Table B-3c

Control Room Structure
Acceleration Range 3 (g)

		Frequency				
Elevation	Dir	2-5(Hz)	5-10(Hz)	7 (Hz)	10 (Hz)	zpa
-0 - 0"	x	.74	.47	.48	.42	.39
-0 - 0"	y	.78	.48	.49	.43	.41
-0 - 0"	z	.45	.35	.35	.33	.24
9'- 6"	x	.76	.49	.50	.43	.41
9'- 6"	y	.76	.47	.48	.42	.40
9'- 6"	z	.48	.36	.37	.34	.24
27'- 0"	x	.69	.46	.47	.41	.39
27'- 0"	y	.75	.48	.49	.43	.41
27'- 0"	z	.46	.36	.36	.33	.24
45'- 3"	x	.65	.45	.46	.40	.38
45'- 3"	y	.73	.47	.48	.43	.40
45'- 3"	z	.45	.35	.35	.33	.24
58'- 6"	x	.99	.57	.57	.52	.51
58'- 6"	y	.87	.58	.61	.48	.43
58'- 6"	z	.45	.34	.34	.31	.23
77'- 6"	x	1.38	.87	.91	.71	.65
77'- 6"	y	.88	.68	.72	.55	.44
77'- 6"	z	.45	.34	.34	.31	.23

Table B-4a

Safeguards Area Median Response
Acceleration Range 1 (g)

		Frequency				
Elevation	Dir	2-5(Hz)	5-10(Hz)	7 (Hz)	10 (Hz)	zpa
9'- 6"	x	.27	.16	.16	.14	.13
9'- 6"	y	.27	.16	.16	.14	.13
9'- 6"	z	.18	.16	.16	.14	.10
19'- 6"	x	.29	.17	.17	.14	.13
19'- 6"	y	.29	.17	.18	.14	.13
19'- 6"	z	.18	.16	.16	.14	.10
28'- 6"	x	.30	.19	.20	.15	.14
28'- 6"	y	.30	.19	.20	.15	.14
28'- 6"	z	.18	.16	.16	.14	.10
42'- 6"	x	.33	.24	.25	.19	.15
42'- 6"	y	.33	.22	.24	.17	.15
42'- 6"	z	.18	.16	.17	.14	.10

Table B-4b

Safeguards Area Median Response
Acceleration Range 2 (g)

		Frequency				
Elevation	Dir	2-5(Hz)	5-10(Hz)	7 (Hz)	10 (Hz)	zpa
9'- 6"	x	.45	.29	.29	.27	.25
9'- 6"	y	.46	.29	.29	.26	.24
9'- 6"	z	.36	.30	.31	.26	.19
19'- 6"	x	.50	.30	.30	.27	.26
19'- 6"	y	.51	.30	.30	.27	.25
19'- 6"	z	.36	.30	.32	.26	.19
28'- 6"	x	.55	.33	.34	.28	.27
28'- 6"	y	.56	.32	.33	.28	.26
28'- 6"	z	.36	.30	.31	.26	.19
42'- 6"	x	.65	.44	.47	.35	.29
42'- 6"	y	.65	.40	.42	.32	.29
42'- 6"	z	.36	.31	.32	.26	.19

Table B-4c

Safeguards Area Median Response
Acceleration Range 3 (g)

		Frequency				
Elevation	Dir	2-5(Hz)	5-10(Hz)	7 (Hz)	10 (Hz)	zpa
9'- 6"	x	.57	.43	.45	.38	.34
9'- 6"	y	.58	.41	.43	.36	.33
9'- 6"	z	.54	.42	.44	.37	.27
19'- 6"	x	.64	.41	.42	.38	.36
19'- 6"	y	.64	.40	.40	.37	.35
19'- 6"	z	.54	.43	.44	.37	.27
28'- 6"	x	.74	.44	.44	.39	.38
28'- 6"	y	.73	.42	.42	.39	.37
28'- 6"	z	.54	.42	.44	.37	.27
42'- 6"	x	.94	.61	.65	.48	.43
42'- 6"	y	.92	.52	.53	.44	.42
42'- 6"	z	.54	.43	.45	.37	.27

Table B-5a

Containment Spray Pump Enclosure
Median Response Acceleration
Range 1 (g)

		Frequency				
Elevation	Dir	2-5(Hz)	5-10(Hz)	7 (Hz)	10 (Hz)	zpa
9'- 0"	x	.26	.16	.16	.14	.13
9'- 0"	y	.26	.15	.16	.14	.13
9'- 0"	z	.18	.16	.16	.14	.10
27'- 6"	x	.29	.18	.19	.15	.14
27'- 6"	y	.30	.18	.19	.15	.14
27'- 6"	z	.18	.16	.17	.14	.10
52'- 0"	x	.34	.26	.28	.20	.15
52'- 0"	y	.35	.28	.31	.22	.16
52'- 0"	z	.18	.16	.17	.14	.10

Table B-5b

Containment Spray Pump Enclosure
Median Response Acceleration
Range 2 (g)

		Frequency				
Elevation	Dir	2-5(Hz)	5-10(Hz)	7 (Hz)	10 (Hz)	zpa
9'- 0"	x	.44	.29	.29	.27	.25
9'- 0"	y	.45	.28	.28	.26	.24
9'- 0"	z	.36	.30	.32	.26	.19
27'- 6"	x	.53	.31	.31	.27	.26
27'- 6"	y	.54	.32	.32	.27	.26
27'- 6"	z	.36	.31	.32	.27	.19
52'- 0"	x	.67	.47	.52	.36	.30
52'- 0"	y	.70	.51	.56	.38	.31
52'- 0"	z	.37	.32	.34	.28	.20

Table B-5c

Containment Spray Pump Enclosure
Median Response Acceleration
Range 3 (g)

		Frequency				
Elevation	Dir	2-5(Hz)	5-10(Hz)	7 (Hz)	10 (Hz)	zpa
9'- 0"	x	.57	.43	.45	.38	.34
9'- 0"	y	.56	.41	.44	.36	.33
9'- 0"	z	.54	.43	.44	.37	.27
27'- 6"	x	.68	.42	.42	.38	.37
27'- 6"	y	.70	.41	.41	.38	.36
27'- 6"	z	.54	.44	.45	.37	.37
52'- 0"	x	.99	.63	.68	.49	.44
52'- 0"	y	1.03	.67	.72	.52	.46
52'- 0"	z	.55	.45	.48	.39	.28

Table B-6a

Emergency Generator Enclosure
Acceleration Range 1 (g)

		Frequency				
Elevation	Dir	2-5(Hz)	5-10(Hz)	7 (Hz)	10 (Hz)	zpa
13'- 6"	x	.30	.18	.19	.15	.14
13'- 6"	y	.30	.18	.19	.15	.14
13'- 6"	z	.19	.16	.17	.13	.09
27'- 6"	x	.30	.19	.19	.15	.14
27'- 6"	y	.30	.19	.19	.15	.14
27'- 6"	z	.19	.16	.17	.13	.09

Table B-6b

Emergency Generator Enclosure
Acceleration Range 2 (g)

		Frequency				
Elevation	Dir	2-5(Hz)	5-10(Hz)	7 (Hz)	10 (Hz)	zpa
13'- 6"	x	.55	.34	.35	.29	.27
13'- 6"	y	.55	.34	.35	.29	.27
13'- 6"	z	.38	.31	.32	.25	.18
27'- 6"	x	.56	.35	.36	.29	.27
27'- 6"	y	.56	.35	.36	.29	.27
27'- 6"	z	.38	.31	.32	.25	.18

Table B-6c

Emergency Generator Enclosure
Median Response Acceleration
Range 3 (g)

		Frequency				
Elevation	Dir	2-5(Hz)	5-10(Hz)	7 (Hz)	10 (Hz)	zpa
13'- 6"	x	.77	.49	.50	.42	.39
13'- 6"	y	.77	.48	.49	.41	.38
13'- 6"	z	.56	.44	.46	.35	.27
27'- 6"	x	.79	.50	.51	.43	.40
27'- 6"	y	.79	.49	.51	.42	.39
27'- 6"	z	.56	.44	.46	.35	.27

Table B-7a

Intake Structure Median
Response Acceleration Range 1 (g)

		Frequency				
Elevation	Dir	2-5(Hz)	5-10(Hz)	7 (Hz)	10 (Hz)	zpa
-9'- 3"	x	.18	.13	.14	.11	.10
-9'- 3"	y	.18	.13	.14	.11	.10
-9'- 3"	z	.18	.13	.13	.10	.08
27'- 6"	x	.20	.13	.14	.11	.11
27'- 6"	y	.20	.13	.14	.11	.11
27'- 6"	z	.18	.13	.13	.10	.08

Table B-7b

Intake Structure Median Response
Acceleration Range 2 (g)

		Frequency				
Elevation	Dir	2-5(Hz)	5-10(Hz)	7 (Hz)	10 (Hz)	zpa
-9'- 3"	x	.36	.26	.27	.22	.20
-9'- 3"	y	.36	.27	.28	.22	.20
-9'- 3"	z	.35	.23	.23	.19	.16
27'- 6"	x	.37	.25	.26	.22	.20
27'- 6"	y	.37	.25	.26	.22	.20
27'- 6"	z	.35	.23	.23	.19	.16

Table B-7c

Intake Structure Median Response
Acceleration Range 3 (g)

		Frequency				
Elevation	Dir	2-5(Hz)	5-10(Hz)	7 (Hz)	10 (Hz)	zpa
-9'- 3"	x	.54	.39	.41	.31	.28
-9'- 3"	y	.54	.40	.42	.32	.28
-9'- 3"	z	.48	.32	.31	.29	.23
27'- 6"	x	.53	.37	.39	.31	.29
27'- 6"	y	.53	.37	.38	.31	.29
27'- 6"	z	.48	.32	.31	.29	.23

APPENDIX C

Cross-Reference File, Boolean Expressions and Accident Sequences

SURRY FRAGILITY TABLE (12/28/88)

Comp	Median	Beta-r	Beta-u	Name
1	0.25	0.25	.25	CERAMIC INSULATORS
2	4.00	0.48	.75	RELAY CHATTER
3	7.63	0.48	.74	CIRCUIT BREAKER TRIP
4	2.50	0.40	.39	BATTERIES
5	2.29	0.31	.39	BATTERY RACKS
6	2.00	0.26	.35	INVERTORS
7	8.80	0.28	.30	TRANSFORMERS
8	7.63	0.48	.74	MOTOR CONTROL CENTER
9	7.63	0.48	.66	AUX RELAY CABINET
10	6.43	0.29	.66	SWITCHGEAR
11	2.23	0.34	.19	CABLE TRAYS
12	11.50	0.46	.74	CONTROL PANELS AND RACKS
13	7.68	0.20	.35	LOCAL INSTRUMENTS
14	1.00	0.25	.31	DIESEL GENERATOR
15	12.10	0.27	.31	MOTORS-HORIZONTAL
16	2.80	0.25	.27	MOTOR-DRIVEN PUMPS & COMPRESSORS
17	2.21	0.22	.32	LG. VERT. M-D. CENTRIF PUMP
18	6.50	0.26	.60	LMOV
19	4.83	0.26	.60	SMALL MOV & AOVs
20	6.50	0.26	.34	LG. PNEUM/HYD VALVE
21	8.90	0.20	.35	LG. MANUAL,CHECK,RELIEF VALVE
22	12.50	0.33	.43	MISC. SMALL VALVES
23	3.00	0.30	.53	LG. HORIZ. VESSELS
24	1.84	0.25	.45	SM-MED HEAT EXCHANGERS & VESSELS
25	1.46	0.20	.35	LG. VERT VESSELS w/ FORMED HEADS
26	0.45	0.35	.29	LG. VERT. FLAT BOTTOMED TANKS
27	6.90	0.27	.31	AIR HANDLING UNITS
28	0.76	0.25	.3	4kv CB BUS-SLIDING(SURRY)
29	0.68	0.25	.3	same -TIPPING(SURRY)
30	1.65	0.25	.3	480 V MCC-SLIDING(SURRY)
31	0.70	0.25	.3	same -TIPPING(SURRY)
32	0.46	0.34	.3	RWST (SURRY)
33	0.29	0.30	.3	CCW-HTX (SURRY)
34	2.45	0.24	.3	STEAM GENERATOR (ZION-SSMRP)
35	2.65	0.24	.3	REACTOR COOLANT PUMP (ZION-SSMRP)
36	0.95892	0.50	.3	SLOCA FIT (SSMRP)
37	1.4967	0.4681	.3	MLOCA FIT (SSMRP)
38	1.8286	0.40764	.3	ALOCA FIT (MONTE CARLO SG&RCP-ZION)
39	2.2701	0.39086	.3	RVR FIT (MONTE CARLO SG&RCP-ZION)
40	1.8	0.14	.27	CONCRETE INTERNALS(SURRY)
41	1.5	0.06	.23	SAFEGUARDS BLDG(SURRY)
42	1.7	0.05	.24	SERVICE BLDG(SURRY)
43	1.8	0.05	.23	AUXILIARY BLDG(SURRY)
44	99.0	0.3	.3	DUMMY EVENT-CAUSES NO SEISMIC FAILURE
45	0.01	0.3	.3	DUMMY EVENT-CAUSES FAILURE

SURRY RESPONSE TABLE (12/28/88)

Response	Median/pga	Beta-r	Beta-u	Notes
1	1.00	0.25	.25	
2	1.00	0.35	.25	
3	1.20	0.45	.25	
4	1.30	0.35	.25	
5	1.10	0.35	.25	
6	0.90	0.35	.25	
7	1.20	0.45	.25	
8	1.00	0.35	.25	
9	1.50	0.35	.25	
10	1.30	0.35	.25	
11	0.90	0.35	.25	
12	1.20	0.35	.25	
13	1.00	0.35	.25	
14	1.20	0.45	.25	
15	0.50	0.35	.25	
16	0.60	0.35	.25	
17	0.80	0.35	.25	
18	4.00	0.45	.25	
19	1.75	0.36	.25	FREE-FIELD AT 7 hz
20	1.75	0.00	.25	RESPONSE FOR RVR & ALOCA IE
21	1.00	0.00	.25	RESPONSE FOR M & S-LOCA IE
22	0.91	0.25	.25	AUX. AND SERVICE BLDGS
23	0.96	0.25	.25	SAFEGUARDS BLDG
24	0.87	0.25	.25	CONTAINMENT CONCRETE INTERNALS
25	1.00	0.25	.25	RESPONSE FOR CST

********SURRY CROSS-REFERENCE TABLE (XREF)*********

Random Failure	Error Factor	Frag Cat	Resp Cat		Component Name	Component Number
2.2e-4	3.	1	1		LOSP	1
0.0	10.	32	1		RWST	2
0.0	10.	26	25		CST	3
9.0e-5	5.	29	3		4KV1H	4
9.0e-5	5.	29	3		4KV1J	5
9.0e-5	5.	31	3		BAC-1H1-2	6
9.0e-5	5.	31	3		BAC-1J1-2	7
3.0e-3	10.	3	3		CRB-FT-15H3	8
3.0e-3	10.	3	3		CRB-FT-15J3	9
4.6e-2	3.	28	7		DG1-FS	10
4.6e-2	3.	28	7		DG3-FS	11
6.0e-3	10.	0			DG1-MA	12
6.0e-3	10.	0			DG3-MA	13
8.4e-4	3.	28	7	2	OEP-DG-CCF-13	14
3.4e-2	3.	0			OEP-DG3U2	15
7.2e-4	3.	4	2		BATT1A	16
7.2e-4	3.	4	2		BATT1B	17
1.5e-4	3.	19	18		AFW-XCONN	18
3.0e-3	3.	18	18		HPI-MOV-FT-1115B	19
3.0e-3	3.	18	18		HPI-MOV-FT-1115C	20
3.0e-3	3.	18	18		HPI-MOV-FT-1115D	21
3.0e-3	3.	18	18		HPI-MOV-FT-1115E	22
3.0e-3	3.	18	18		HPI-MOV-1867C	23
3.0e-3	3.	18	18		HPI-MOV-1867D	24
1.0e-3	3.	18	18		CPC-AOV-FT-108B	25
3.0e-1	1.01	0			PPS-MOV-FC-1535	26
3.0e-1	1.01	0			PPS-MOV-FC-1536	27
4.0e-2	3.	18	18		PPS-MOV-FT-1535	28
4.0e-2	3.	18	18		PPS-MOV-FT-1536	29
1.0e-3	3.	19	18		PPS-SOV-FT-1455C	30
1.0e-3	3.	19	18		PPS-SOV-FT-1456	31
7.0e-5	3.	19	18	2	PPS-CCF-FT-PORV	32
7.2e-5	10.	33	1		CCW-HTX-LK-E1A	33
7.2e-5	10.	33	1		CCW-HTX-LK-E1B	34
1.4e-4	10.	0			CCW-HTX-PG-E1A	35
1.4e-4	10.	0			CCW-HTX-PG-E1B	36

********SURRY CROSS-REFERENCE TABLE (Cont'd)*********

Random Failure	Error Factor	Frag Cat	Resp Cat		Component Name	Component Number
7.7e-4	10.	0			CPC-CCF-PG-STRAB	37
1.0e-4	30.	0			AFW-CCF-LK-STMBD	38
3.0e-3	3.	18	18		LPR-MOV-FT-1860A	39
3.0e-3	3.	18	18		LPR-MOV-FT-1860B	40
5.2e-3	10.	18	18		LPR-MOV-FT-1862A	41
5.2e-3	10.	18	18		LPR-MOV-FT-1862B	42
3.0e-3	3.	18	18		LPR-MOV-FT-1890A	43
3.0e-3	3.	18	18		LPR-MOV-FT-1890B	44
2.6e-4	3.	18	18	2	LPR-CCF-860AB	45
2.6e-4	3.	18	18	2	LPR-CCF-862AB	46
2.6e-4	3.	18	18	2	LPR-CCF-890AB	47
0.0e-0	3.	34	17		STEAM GEN.(IE)	48
0.0e-0	3.	35	17		R. C. PUMP (IE)	49
0.0e-0	3.	36	21		SLOCA FIT (IE)	50
0.0e-0	3.	37	21		MLOCA FIT (IE)	51
4.0e-2	3.	0			MCW-XHE-FO-FLOW	52
3.0e-4	10.	17	19	2	PCS-CCF-MDP	53
2.7e-5	10.	16	12	2	IAL-CCF-LF-INAIR	54
1.0e-4	10.	20	18	2	PCS-CCF-FT-TRBYP	55
0.0e-0	3.	38	20		ALOCA FIT	56
0.0e-0	3.	39	20		RVR FIT	57
6.0e-2	10.	0			AFW-TDP-FR-24HR	58
1.1e-2	10.	16	12		AFW-TDP-FS-FW2	59
1.0e-4	3.	21	18		AFW-CKV-FT-CV142	60
1.0e-2	10.	0			AFW-TDP-MA-FW2	61
7.0e-5	10.	33	1		CCW-CCF-HTX	62
0.0e-0	3.	29	3	2	OEP-CCF-4KV-HJ	63
0.0e-0	3.	31	3	2	OEP-CCF-1H1&1J1-2	64
3.0e-4	10.	0			RMT-CCF-FA-MSCAL	65
0.0e-0	3.	40	24		CONCRETE-INTERNAL	66
0.0e-0	3.	41	23		SAFEGUARDS-BLDG	67
0.0e-0	3.	42	22		SERVICE-BLDG	68
0.0e-0	3.	43	22		AUXILIARY-BLDG	69
0.730	-1.0	0			SEAL LOCA FRACTN	70
0.0e-0	10.	32	1	2	CCF-RWST-CST	71

******BOOLEAN EXPRESSIONS FOR SURRY INITIATING EVENTS******

RVR Event
IE(1) = RVR + CONCRETE-INTERVALS

LARGE LOCA
IE(2) = ALOCA * $\overline{IE(1)}$

MEDIUM LOCA
IE(3) = MLOCA * $\overline{IE(1)}$ * $\overline{IE(2)}$

SMALL LOCA
IE(4) = SLOCA * $\overline{IE(1)}$ * $\overline{IE(2)}$ * $\overline{IE(3)}$

Transients with Loss of Power Conversion System
IE(5) = LOSP* $\overline{IE(1)}$ * $\overline{IE(2)}$ * $\overline{IE(3)}$ * $\overline{IE(4)}$

General Transient
IE(6) = 1.0 - IE(1) - IE(2) - IE(3) - IE(4) - IE(5)

******SURRY SEISMIC DOMINANT ACCIDENT SEQUENCES (2/5/89)*********

```
BOOL(1) =
RMT-CCF-FA-MSCAL +
BAC-1H1-2 * 4KV1J +
BAC-1J1-2 * 4KV1H +
OEP-CCF-1H1&1J1-2 +
DG1-FS * BAC-1J1-2 * LOSP +
BAC-1H1-2 * DG3-FS * LOSP +
4KV1H * LPR-MOV-FT-1862B +
4KV1J * LPR-MOV-FT-1862A +
BAC-1H1-2 * LPR-MOV-FT-1862B +
BAC-1J1-2 * LPR-MOV-FT-1862A +
4KV1H * LPR-MOV-FT-1890B +
4KV1J * LPR-MOV-FT-1860A +
4KV1J * LPR-MOV-FT-1890A +
4KV1H * LPR-MOV-FT-1860B +
BAC-1J1-2 * LPR-MOV-FT-1890A +
BAC-1H1-2 * LPR-MOV-FT-1860B +
BAC-1H1-2 * LPR-MOV-FT-1890B +
BAC-1J1-2 * LPR-MOV-FT-1860A +
DG1-FS * LOSP * LPR-MOV-FT-1862B +
DG3-FS * LOSP * LPR-MOV-FT-1862A +
DG1-FS * LOSP * LPR-MOV-FT-1890B +
DG1-FS * LOSP * LPR-MOV-FT-1860B +
DG3-FS * LOSP * LPR-MOV-FT-1860A +
DG3-FS * LOSP * LPR-MOV-FT-1890A +
BAC-1H1-2 * OEP-DG3U2 * LOSP +
LPR-CCF-860AB +
LPR-CCF-862AB +
LPR-CCF-890AB


BOOL(2)  =
RWST +
SERVICE-BLDG +
SAFEGUARDS-BLDG +
OEP-CCF-4KV-HJ +
DG3-FS * 4KV1H * LOSP +
DG1-FS * 4KV1J * LOSP +
OEP-DG-CCF-13 * LOSP +
OEP-DG3U2 * 4KV1H * LOSP +
DG1-FS * OEP-DG3U2 * LOSP
```

```
BOOL(11) =
RWST +
SERVICE-BLDG +
OEP-CCF-4KV-HJ +
BAC-1J1-2 * 4KV1H +
BAC-1H1-2 * 4KV1J +
OEP-CCF-1H1&1J1-2 +
DG3-FS * 4KV1H * LOSP +
DG1-FS * 4KV1J * LOSP +
BAC-1H1-2 * DG3-FS * LOSP +
DG1-FS * BAC-1J1-2 * LOSP +
OEP-DG-CCF-13 * LOSP +
HPI-MOV-1867C * 4KV1J +
4KV1H * HPI-MOV-FT-1115E +
HPI-MOV-1867D * 4KV1H +
4KV1J * HPI-MOV-FT-1115C +
4KV1J * HPI-MOV-FT-1115B +
HPI-MOV-1867D * 4KV1H +
CPC-AOV-FT-108B * 4KV1H +
HPI-MOV-FT-1115B * BAC-1J1-2 +
HPI-MOV-FT-1115D * BAC-1H1-2 +
BAC-1H1-2 * HPI-MOV-FT-1115E +
BAC-1J1-2 * HPI-MOV-FT-1115C +
CPC-CCF-PG-STRAB +
HPI-MOV-1867C * DG3-FS * LOSP +
DG1-FS * LOSP * HPI-MOV-FT-1115E +
HPI-MOV-FT-1115D * DG1-FS * LOSP +
DG3-FS * LOSP * HPI-MOV-FT-1115C +
HPI-MOV-FT-1115B * DG3-FS * LOSP +
HPI-MOV-1867D * DG1-FS * LOSP +
CPC-AOV-FT-108B * DG1-FS * LOSP +
OEP-DG3U2 * 4KV1H * LOSP +
BAC-1H1-2 * OEP-DG3U2 * LOSP +
DG1-FS * OEP-DG3U2 * LOSP +
DG1-MA * OEP-DG3U2 * LOSP
```

```
BOOL(14) =
4KV1H * CST * PPS-MOV-FC-1535 +
4KV1J * CST * PPS-MOV-FC-1536 +
BAC-1H1-2 * CST * PPS-MOV-FC-1535 +
BAC-1J1-2 * CST * PPS-MOV-FC-1536 +
DG1-FS * CST * PPS-MOV-FC-1535 +
DG3-FS * CST * PPS-MOV-FC-1536 +
CST * PPS-SOV-FT-1455C +
CST * PPS-SOV-FT-1456 +
4KV1H * AFW-XCONN * PPS-MOV-FC-1535 +
4KV1J * AFW-XCONN * PPS-MOV-FC-1536 +
BAC-1H1-2 * AFW-XCONN * PPS-MOV-FC-1535 +
BAC-1J1-2 * AFW-XCONN * PPS-MOV-FC-1536 +
DG1-FS * AFW-XCONN * PPS-MOV-FC-1535 +
DG3-FS * AFW-XCONN * PPS-MOV-FC-1536 +
CST * PPS-MOV-FC-1535 * PPS-MOV-FT-1535 +
CST * PPS-MOV-FC-1536 * PPS-MOV-FT-1536 +
AFW-XCONN * PPS-SOV-FT-1455C +
AFW-XCONN * PPS-SOV-FT-1456
```

BOOLEAN SEQUENCE 15 INVOLVES L AND D2 FAILURES WITH BOTH EARLY (SEISMIC MECHANICAL) AND LATE (BATT DEPLETION DUE TO SBO) FAILURES OF THE AFWS. BOOLEAN SEQUENCES 26 AND 33 ARE SEAL LOCA SEQUENCES WITH NO FAILURE OF AFWS. THE FRACTION OF SEAL LOCAS GIVEN SBO IS GIVEN BY SLLOCA.

```
SLLOCA = SEAL-LOCA-FRACTN
BATTDP = 1.0 - SLLOCA
```

```
BOOL(15) =
CCF-RWST-CST +
SERVICE-BLDG +
CST * OEP-CCF-4KV-HJ +
CST * 4KV1H * BAC-1J1-2 +
CST * 4KV1J * BAC-1H1-2 +
CST * OEP-CCF-1H1&1J1-2 +
DG3-FS * 4KV1H * CST +
DG1-FS * 4KV1J * CST +
BAC-1H1-2 * DG3-FS * CST +
DG1-FS * BAC-1J1-2 * CST +
OEP-DG-CCF-13 * CST +
RWST * AFW-XCONN +
OEP-CCF-4KV-HJ * AFW-XCONN +
```

```
4KV1H * BAC-1J1-2 * AFW-XCONN +
BAC-1H1-2 * 4KV1J * AFW-XCONN +
OEP-CCF-1H1&1J1-2 * AFW-XCONN +
DG1-FS * 4KV1J * AFW-XCONN +
DG3-FS * 4KV1H * AFW-XCONN +
DG1-FS * BAC-1J1-2 * AFW-XCONN +
BAC-1H1-2 * DG3-FS * AFW-XCONN +
OEP-DG-CCF-13 * AFW-XCONN +
4KV1H * HPI-MOV-FT-1115E * CST +
4KV1H * HPI-MOV-1867D * CST +
4KV1J * HPI-MOV-1867C * CST +
4KV1H * HPI-MOV-FT-1115D * CST +
4KV1J * HPI-MOV-FT-1115C * CST +
4KV1J * HPI-MOV-FT-1115B * CST +
4KV1H * CPC-AOV-FT-108B * CST +
BAC-1H1-2 * HPI-MOV-FT-1115E * CST +
BAC-1J1-2 * HPI-MOV-FT-1115C * CST +
BAC-1J1-2 * HPI-MOV-FT-1115B * CST +
BAC-1H1-2 * HPI-MOV-FT-1115D * CST +
HPI-MOV-FT-1115D * DG1-FS * CST +
DG3-FS * HPI-MOV-FT-1115C * CST +
HPI-MOV-1867C * DG3-FS * CST +
HPI-MOV-FT-1115E * DG1-FS * CST +
HPI-MOV-1867D * DG1-FS * CST +
HPI-MOV-FT-1115B * DG3-FS * CST +
CPC-AOV-FT-108B * DG1-FS * CST +
OEP-DG3U2 * 4KV1H * CST +
BAC-1H1-2 * OEP-DG3U2 * CST +
DG1-FS * OEP-DG3U2 * CST +
OEP-CCF-4KV-HJ * BATTDP +
AUXILIARY-BLDG * BATTDP +
DG1-FS * 4KV1J * BATTDP +
4KV1H * DG3-FS * BATTDP +
OEP-DG-CCF-13 * BATTDP +
OEP-DG3U2 * 4KV1H * BATTDP +
DG1-FS * OEP-DG3U2 * BATTDP


BOOL(26) =
OEP-CCF-4KV-HJ * SLLOCA +
AUXILIARY-BLDG +
CCW-HTX-PG-E1A * CCW-HTX-PG-E1B * CPC-CCF-PG-STRAB +
CCW-CCF-HTX * CPC-CCF-PG-STRAB +
CCW-HTX-LK-E1B * CCW-HTX-PG-E1A * CPC-CCF-PG-STRAB +
CCW-HTX-LK-E1A * CCW-HTX-PG-E1B * CPC-CCF-PG-STRAB
```

```
BOOL(33) =
OEP-CCF-4KV-HJ * SLLOCA +
AUXILIARY-BLDG * SLLOCA +
DG1-FS * 4KV1J * SLLOCA +
4KV1H * DG3-FS * SLLOCA +
OEP-DG-CCF-13 * SLLOCA +
OEP-DG3U2 * 4KV1H * SLLOCA +
DG1-FS * OEP-DG3U2 * SLLOCA +
CCW-HTX-PG-E1A * CCW-HTX-PG-E1B * CPC-CCF-PG-STRAB +
CCW-CCF-HTX * CPC-CCF-PG-STRAB +
CCW-HTX-LK-E1B * CCW-HTX-PG-E1A * CPC-CCF-PG-STRAB +
CCW-HTX-LK-E1A * CCW-HTX-PG-E1B * CPC-CCF-PG-STRAB +
RWST * CCW-CCF-HTX


KBAR = 1.0
QBAR = 1.0

M =
MCW-XHE-FO-FLOW +
PCS-CCF-MDP +
IAL-CCF-LF-INAIR +
PCS-CCF-TRBYPTRBYP

AFW =
AFW-XCONN +
AFW-CCF-LK-STMBD +
CST +
AFW-TDP-FR-24HR * OEP-CCF-4KV-HJ +
AFW-TDP-FS-FW2 * OEP-CCF-4KV-HJ +
AFW-CKV-FT-CV142 * OEP-CCF-4KV-HJ +
AFW-TDP-MA-FW2 * OEP-CCF-4KV-HJ +
AFW-TDP-FR-24HR * OEP-DG-CCF-13 * LOSP +
AFW-TDP-FS-FW2 * OEP-DG-CCF-13 * LOSP +
AFW-CKV-FT-CV142 * OEP-DG-CCF-13 * LOSP

AFW = 1.0-AFW
LBAR = 1.0-AFW
D5BAR = 1.0
D2BAR = 1.0 - BOOL(11)
D6BAR = 1.0
```

```
ACC(1) = IE(5)*BOOL(15)*KBAR*QBAR
ACC(2) = IE(5)*BOOL(14)*KBAR*QBAR*D2BAR
ACC(3) = IE(5)*BOOL(33)*KBAR*QBAR*LBAR
ACC(4) = IE(6)*BOOL(26)*KBAR*QBAR*LBAR
ACC(5) = IE(4)*BOOL(11)*KBAR
ACC(6) = IE(2)*BOOL(2)*D5BAR
ACC(7) = IE(1)
ACC(8) = IE(3)*BOOL(11)
ACC(9) = IE(2)*BOOL(1)*D5BAR*D6BAR
ACC(10)= IE(6)*KBAR*QBAR
         * ( (SERVICE-BLDG) + ((OEP-CCF-4KV-HJ)*(BATTDP)) )
```

Appendix D

Critical Components by Fire Area

Appendix D

Critical Components by Fire Area

Fire Area	Component Description
1	Large quantity of safety-related control and power cables for equipment required for safe shutdown, including: CPC motor driven pumps CC2A and CC2B; HPI motor driven charging pumps CH1A, CH1B, and CH1C; HPR motor driven charging pumps CH1A, CH1B, and CH1C; LPI motor driven pumps SI1A and SI1B; AFW motor driven pumps 3A and 3B; AFW turbine driven pump 2P; CSS motor driven pumps 1A and 1B; CCW motor driven pumps CC-P1A and CC-P1B; ISR motor driven pumps RS1A and RS1B; OSR motor driven pumps RS2A and RS2B; AC circuit breakers FE9BJ and FE9BK; RHR motor driven pumps 1A and 1B.
3	Large quantity of safety-related electrical equipment associated with the following: CPC motor driven pumps CC2A and CC2B; CPC motor driven pumps SW10A and SW10B; HPI motor driven charging pumps CH1A, CH1B, and CH1C; HPR motor driven charging pumps CH1A, CH1B, and CH1C; LPI motor driven pumps SI1A and SI1B; AFW motor driven pumps 3A and 3B; AFW turbine driven pump 2P; CSS motor driven pumps 1A and 1B; CCW motor driven pumps CC-P1A and CC-P1B; ISR motor driven pumps RS1A and RS1B; OSR motor driven pumps RS2A and RS2B; various AC circuit breakers, transformers, battery chargers, rectifiers, inverters, and buswork; various DC batteries, circuit breakers, buswork; RHR motor driven pumps 1A and 1B; auxiliary shutdown panel.
5	Contains controls, cabling, and electrical equipment associated with the following: AFW cross-connect control; AFW AOV-MS102A and B actuation; AFW actuation for pumps 3A and 3B; CPC actuation signals; CPC motor driven pumps CC2A and CC2B; CPC motor driven pumps SW10A and SW10B; CLCS actuation; SIS actuation; RMTS actuation; HPI motor driven charging pumps CH1A, CH1B, and CH1C; HPR motor driven charging pumps CH1A, CH1B, and CH1C; LPI motor driven pumps SI1A and SI1B; AFW motor driven pumps 3A and 3B; AFW turbine driven pump 2P; CSS motor driven pumps 1A and 1B; CCW motor driven pumps CC-P1A and CC-P1B; ISR motor driven pumps RS1A and RS1B; OSR motor driven pumps RS2A and RS2B; various AC transformers and buswork; RHR motor driven pumps 1A and 1B.

Appendix D

Critical Components by Fire Area (Continued)

Fire Area	Component Description
6	Emergency Diesel generator #1
7	Emergency Diesel Generator #2
8	Emergency Diesel Generator #3
15	RCS PORV solenoids PCV 1455C and 1456; PORV block valves 1535 and 1536; ISR motor driven pumps RS1A and RS1B; RHR MOV's 1700, 1701, 1720A, and 1720B; RHR SRV 1721.
17	The following components and/or associated power and control cabling are located in this fire area: CPC motor driven pump CC2A; HPI motor driven pumps CH1A, CH1B, and CH1C; HPI MOV's 1115B, 1115C, 1115D, and 115E, 1350, 1867C, 1867D; HPR motor driven pumps CH1A, CH1B, and CH1C; CPC motor driven pump CC2B; CVC motor driven boric acid transfer pump; CCW motor driven pumps CC-P1A and CC-P1B.
19	CSS MOV's 101A, 101B, 101C, and 101D; CSS motor driven pumps CS1A and CS1B; SWS header cross-connect; LPI motor driven pumps SI1A and SI1B; AFW motor driven pumps 3A and 3B; AFW turbine driven pump 2P; LPR MOV's 1860A, 1860B, 1862A, 1862B, 1863A, 1863B, 1890A, 1980B; SWS MOV's 103A, 103B, 103C, and 103D; ISR motor driven pumps RS1A and RS1B; OSR motor driven pumps RS2A and RS2B; RHR motor driven pumps 1A and 1B.
31	Cabling for the following system motor driven pumps is routed through this fire area: LPI pump SI1A; AFW pumps 3A and 3B; CPC pumps SW10A and SW10B; CSS pump 1A; OSR pump RS2A; RHR pump 1A.

Appendix D

Critical Components by Fire Area (Concluded)

Fire Area	Component Description
45	Charging pump service water motor driven pump SW10B and power and control cabling for pump SW10A; power and control cables for EDG's #2 and #3.
54	Charging pump service water motor driven pump SW10A.

Appendix E

Fire Event Data

Appendix E. Surry Fire Event Data Table--Auxiliary Building Fires

Plant Name	Date of Occurrence	Plant Status	Fire Type	Remarks
San Onofre 1	2/7/68	Power Operation	Cable	Thermally overloaded 480 V cables caught fire - 55 cables damaged.
San Onofre 1	3/9/68	Power Operation	Cable	Thermally overloaded cables in switchgear room.
Palisades	6/25/71	Cold Shutdown	Air Dryer Filter	Low flow of air through air dryer resulted in temperature buildup and ignition of filter.
LaCrosse	7/15/72	Power Operation	Circulation Pump	Oil on pump lagging ignited by hot pump casing.
Turkey Point 3	12/16/72	Power Operation	Battery Charger	Battery charger overheated and a small fire occurred in the transformer winding insulation.
Robinson 2	4/19/74	Power Operation	Expansion Joint	Cigarette or welding slag from construction workers ignited combustible expansion joint material.
Robinson 2	4/19/74	Power Operation	Expansion Joint	Same type of event as previous event - occurred one week apart.

Appendix E. Surry Fire Event Data Table--Auxiliary Building Fires (Continued)

Plant Name	Date of Occurrence	Plant Status	Fire Type	Remarks
Turkey Point 3	5/75	Power Operation (100%)	Battery Charger	Transformer overheated igniting insulation. Similar to previous event on 12/14/72.
Millstone 2	3/24/76	Hot Shutdown	Motor Control Center	Fire resulted from arcing of a supply lead. Extinguished by de-energizing MCC.
Dresden 2	4/76	Cold Shutdown	Circuit Breaker	ECCS Jockey Pump control feed breaker caught fire from a burned-out contacter coil.
Fitzpatrick	6/11/76	Power Operation (93%)	Circuit Breaker	Overload in HPCI valve circuit breaker. Extinguished by de-energizing breaker.
Millstone 2	11/15/76	Hot Shutdown	Relay-MCC	Relay fire in motor control center.
Pilgrim 1	3/77	Hot Shutdown	Circuit Breaker	Circuit breaker under-voltage coil burnt due to high floating charge on station battery.
Fitzpatrick	4/4/77	Power Operation (88%)	Circuit Breaker	Coil failed by fire in HPCI test valve breaker and extinguished by de-energizing. Similar to 7/28/75 event.

Appendix E. Surry Fire Event Data Table--Auxiliary Building Fires (Continued)

Plant Name	Date of Occurrence	Plant Status	Fire Type	Remarks
Arnold	5/7/77	Refueling Outage	Circuit Breaker	Breaker relay failed, burning open and starting phase burner material above it on fire.
Salem 1	6/30/77	Power Operation	Relay - Cabinet	Fire detection instrumentation panel fire due to relay failure.
Unknown	4/13/78	Power Operation	Circuit Breaker - MCC	Failure breaker contact due to improper maintenance - occurred in motor control center.
Robinson 2	7/16/78	Power Operation	Battery	Resistance heating of terminal connection ignited plastic tops of two cells of a battery.
Unknown	7/27/78	Power Operation	Battery Terminal	Defective terminal or connections not secured.
Arkansas Nuclear One 1	8/16/78	Cold Shutdown	Pump Motor	LPSI pump motor on fire (being used for shutdown cooling) due to incorrect installation of motor bearings resulting in shorting of rotor with the stator.
Salem 1	1/79	Power Operation (95%)	Transformer	Moisture in the windings resulted in a short and subsequent fire.

Appendix E. Surry Fire Event Data Table--Auxiliary Building Fires (Continued)

Plant Name	Date of Occurrence	Plant Status	Fire Type	Remarks
Palisades	4/4/79	Power Operation (100%)	Battery	Battery burst due to internal explosion of hydrogen ignited by a test lead being used to measure voltage.
San Onofre 1	11/27/79	Power Operation (100%)	Switchgear	Rodents shorted two phases of a 480V bus in the switchgear room.
Hatch 2	4/80	Cold Shutdown	Cable	A loose connection resulted in a wire of an RPS motor generator set breaker burning.
Unknown BWR	4/15/80	Power Operation	Bus	Fire involving supply bus occurred in switchgear room.
Peach Bottom 1	6/3/80	Power Operation (100%)	Transformer	A filtering capacitor in a vital bus transformer caught fire damaging the transformer.
Unknown PWR	7/6/80	Power Operation	Circuit Breaker	Circuit breaker caught fire when it failed to close properly because contacts were out of adjustment.
Unknown PWR	10/2/80	Power Operation	Valve Motor	Air sample inlet valve motor issued smoke. Power was removed from motor.

Appendix E. Surry Fire Event Data Table--Auxiliary Building Fires (Continued)

Plant Name	Date of Occurrence	Plant Status	Fire Type	Remarks
Trojan	12/31/80	Power Operation (100%)	Circuit Breaker	Breaker stab misaligned causing ignition of plastic dust collector by arcing.
Palisades	1/24/81	Power Operation (98%)	Pump Motor	Component cooling water pump motor caught fire due to bearing failure from loss of lubricating oil.
San Onofre 1	7/17/81	Cold Shutdown	Gas Decay Tank	Explosion of H_2 in recombiner.
Indian Point 2	8/10/81	Power Operation (100%)	Pump Motor	Short circuit within SI pump caused fire and an overload trip of its supply breaker.
North Anna 1	11/11/81	Power Operation	Pump	Main feedwater pump fire.
Hatch 1	11/23/81	Cold Shutdown	Relay	Insulation breakdown caused fire in a reactor low-low RPS relay.
Point Beach 1	10/15/82	Power Operation (78%)	Circuit Breaker	Supply breaker for MG set caught fire.

Appendix E. Surry Fire Event Data Table--Auxiliary Building Fires (Continued)

Plant Name	Date of Occurrence	Plant Status	Fire Type	Remarks
Salem 1	11/9/82	Cold Shutdown	Relay	Relay failure resulted in a fire in a fire detection instrumentation panel. Fire detectors for switchgear rooms, battery room, and DG area were rendered inoperable.
Brunswick 1	11/27/82	Power Operation (68%)	Battery Charger	Resistor on charger amplifier board opened causing a voltage increase and capacitor failure.
Oconee 2	2/3/83	Power Operation (100%)	Pump Motor	Loss of lubrication oil resulted in high bearing temperature and smoke.
Brunswick 1	4/26/83	Refueling	Transformer	Following a loss of offsite power, a fire occurred in a transformer between emergency buses.
Oconee 3	5/25/83	Power Operation (100%)	Cable and Conduit	Welding operation started a fire in conduit surrounding a cable (letdown valve).

Appendix E. Surry Fire Event Data Table--Auxiliary Building Fires (Concluded)

Plant Name	Date of Occurrence	Plant Status	Fire Type	Remarks
Salem 2	6/20/83	Cold Shutdown	Transformer	Transformer breaker tripped on overcurrent and was reclosed. Fire occurred immediately thereafter.
Peach Bottom 1	9/9/83	Power Operation (100%)	Control Panel	Water entered a control room ventilation chiller control panel shorting motor starter contacters.
Yankee Rowe	8/2/84	Power Operation (100%)	Circuit Breaker	High resistance in the main disconnecting contacts of the center phase of the breaker caused an arc to propagate to outside phases.

Appendix E. Surry Fire Event Data Table--Control Room Fires

Plant Name	Date of Occurrence	Plant Status	Fire Type	Remarks
Unknown	7/4/78	Power Operation	Diode	Zener diode failed in an RPS circuit.
Three Mile Island 2	7/12/79	Cold Shutdown	Circuit Board	Overheated resistor caused fire in a radiation monitoring readout panel. Extinguished immediately.
Hatch 1*	3/12/83	Power Operation (94%)	Relay	Low reactor water level RPS relay burned causing a 1/2 scram (failed safe). Extinguished by operators.
Hatch 1*	3/30/83	Power Operation (34%)	Relay	Scram discharge volume high level RPS relay burned a 1/2 scram (failed causing safe). Extinguished by operators. Same type of relay as in previous event.

*Counted as one event for quantification of fire frequency.

Appendix E. Surry Fire Event Data Table--Cable Spreading Room Fires

Plant Name	Date of Occurrence	Plant Status	Fire Type	Remarks
Browns Ferry 1&2	3/22/75	Power Operation (100%)	Cable Fire	Spread from cable spreading room to reactor building in Unit 1 and affected Unit 2.
Peach Bottom 3	4/18/77	Power Operation (25%)	Relay Fire	Fire in PCIS logic and RHR valve relay.

Appendix E. Surry Fire Event Data Table--Switchgear Room Fires

Plant Name	Date of Occurrence	Plant Status	Fire Type	Remarks
Unknown PWR	11/7/79	Power Operation	480 V Bus	Fire involved 480 V bus; short circuit caused by rodent bridging two energized phases.
Unknown BWR	4/15/80	Power Operation	Bus	Fire involved supply bus in switchgear room.
Unknown PWR	7/6/80	Power Operation	Circuit Breaker	Fire involving switchgear room breaker. Out of adjustment control circuit completed
Yankee Rowe	8/2/84	Power Operation (100%)	Circuit Breaker	A fault occurred in the 480 V supply ACB to bus 4-1; high resistance in the main disconnecting contacts caused an arc to propagate from the center phase to the outside phases.

APPENDIX F

Soils Liquefaction Analysis for Surry

by

Maurice S. Power
Principal Engineer

GeoMatrix Consultants, Inc.

TABLE OF CONTENTS

1. INTRODUCTION

This report describes a liquefaction fragility assessment conducted for the Surry nuclear power plant, Virginia. The specific objectives of the study are to estimate median values of free field ground surface peak acceleration required to cause liquefaction at the site and the associated consequences of liquefaction. It is our understanding that the critical structures at the site are the reactor building, control building, and auxiliary building. Therefore, our assessments have focused on liquefaction potential beneath these structures as well as in the free field. The results of this study will be used in a probabilistic risk assessment (PRA) of the plant.

A number of documents furnished by Sandia National Laboratories and by EQE Incorporated have been reviewed and utilized in conducting this study. These documents included the following:

1. Surry Plant Final Safety Analysis Report (FSAR), Section 2.4 Geology, dated 12-1-69, and Section 2.5 Seismology, dated 12-1-69 and 2-13-70.

2. Surry Plant Preliminary Safety Analysis Report (PSAR), Supplement S9.12, pp. S9.12-1 to S9.12-6, dated 11-15-67; Appendix S9.12A, pp. S9.12 A-1 to S9.12A-8, dated 12-5-67; Appendix S9.12B, pp. S9-12B-1 and S9.12B-2 dated 11-16-67, Appendix 9.12C, pp. S9.12C-1 to S9.12C-5, dated 11-15-67, Table S9.12C-1, and Figure S9.12C-1 dated 11-22-67; Appendix S9.12D, pp. S9.12D-1 to S9.12D-6 dated 11-24-67 and Figures S9.12D-1 to S9.12D-3 dated 11-22-67.

3. Surry Plant PSAR, Amendment 5, dated 12-7-67.

4. Dames and Moore report dated November 17, 1967, "Report Environmental Studies, Proposed Power Plant, Surry, Virginia, Virginia Electric and Power Company."

5. R.V. Whitman report dated 8-11-67 to Stone & Webster Engineers on Foundation Dynamics

6. EQE Incorporated letter of July 28, 1988 to M.S. Power, Geomatrix Consultants re: Median peak accelerations, base shear forces, and static bearing pressures for structures included in the Probabilistic Risk Analysis performed by EQE.

7. EQE Incorporated letter of August 16, 1988 to M.S. Power, Geomatrix Consultants re: Base shear stresses for structures included in the Probabilistic Risk Analysis performed by EQE.

2. SUBSURFACE CONDITIONS

The plan arrangement of the nuclear power plant complex is shown in Figure 1. Cross sections that show the facilities in relation to the subsurface soil conditions are presented in Figures 2 and 3. The foundation soils of interest for this study are:

Sand A: The layer typically exists between elevations 0 and -10 feet (26.5 to 36.5 feet below the plant finished grade). The layer does not underlie the critical structures. It was included in the analysis for completeness because its liquefaction potential had been addressed in the PSAR and FSAR.

Sand B: The layer typically exists between elevations -20 and -40 feet (46.5 to 66.5 feet below plant finished grade). It underlies the auxiliary building and the control building (both founded at elevation -2 feet) at depth, but the reactor building extends below the layer.

Sand C: Sand C is found at approximately elevation -58 feet on the average (approximately 85 feet below plant finished grade). The layer is typically interlensed with clay and the cumulative thickness of sand lenses is typically 5 feet or less. Sand C (where present) is approximately 18 feet below the mat foundation of the reactor building (at elevation -40).

Select fill: Beneath the auxiliary building and the control building, as well as beneath the fuel building, Sand A was excavated and replaced with select granular fill. The fill was reported in the FSAR to be compacted to a density equal to or exceeding 95 percent of the maximum density obtained using ASTM compaction test method 1557-66. The select fill provides direct bearing support for the mat foundations of the auxiliary building and the control building.

Groundwater levels were reported in the FSAR to be at elevation +5 feet in the free field. A permanent dewatering system was installed around the perimeter of the reactor buildings. The dewatering system is reported (FSAR) to maintain piezometric levels at or below elevation -30 feet beneath the reactor building and at or below elevation -7 feet beneath the auxiliary building and control building. In liquefaction potential evaluations originally carried out for the plant (PSAR and FSAR), the aforementioned piezometric levels were assumed; however, for the auxiliary building and control building, analyses were also carried out for a piezometric level of +5 feet to cover the possibility of the drainage system ceasing to depress the piezometric head in Sand B.

3. ASSESSMENT OF LIQUEFACTION RESISTANCE OF SOILS

Assessment of free field peak ground accelerations required to cause liquefaction requires two evaluations: (1) an evaluation of the cyclic shear stress, τ_L, or the cyclic stress ratio, $(\tau/\bar{\sigma})_L$ (where $\bar{\sigma}$ is the pre-earthquake effective vertical stress), required to cause liquefaction of the soils; and (2) an evaluation of the earthquake-induced cyclic shear stress or stress ratio $(\tau/\bar{\sigma})_E$ as a function of the free field peak acceleration at the ground surface. From these two evaluations, the acceleration levels causing the induced stresses or stress ratios to equal those causing liquefaction are obtained. The assessment of the cyclic stress ratios required to cause liquefaction is summarized in sections 3.1 through 3.3. Section 4 summarizes the assessment of the stress ratios induced by the earthquake ground shaking and the corresponding acceleration levels causing liquefaction.

3.1 Liquefaction Resistance of Sand A and Sand B

The present state of practice of evaluating the liquefaction potential of insitu soil layers generally relies on insitu measurements of the resistance of the soils to a penetration device and empirical correlations relating the penetration resistance to the cyclic stress ratio required to cause liquefaction. Typically, the resistance measure is the number of blows per foot required to drive a standard sampler into the soil at the base of a drill hole (Standard Penetration Test, SPT). The resistance to penetration of a static cone penetrometer (Cone Penetrometer Test, CPT) is also often used as a resistance measure.

At the Surry plant site, there are a number of SPT results in Sands A and B. These were used to assess the liquefaction resistance of these soil layers. The empirical correlation that was used to relate the normalized SPT penetration resistance, N_1 (i.e. the penetration resistance adjusted to a common effective vertical stress of 2 ksf), to the cyclic stress ratio causing liquefaction is the widely used correlation developed by Seed and his coworkers. The current version of this correlation for a magnitude 7-1/2 earthquake is shown in Figure 4 (Seed and others, 1985). As shown, the cyclic stress ratio causing liquefaction for a given magnitude earthquake is a function of the percentage of silty and clayey fines in the sand as well as the penetration resistance. Factors are presented by Seed and others (1985) to adjust the ordinates of the curves in Figure 4 to magnitudes other than 7-1/2. The factors result in increasing values of $(\tau/\bar{\sigma})_L$ with decreasing magnitudes.

One other adjustment should be made to the values of cyclic stress ratio obtained from Figure 4. It has been found that these stress ratios decrease somewhat with increasing effective vertical stress, $\bar{\sigma}$, and the values in Figure 4 are applicable to $\bar{\sigma}$ = 2 ksf. A relationship recently developed by Seed and his coworkers (Seed, 1988, personal communication) was used to make this adjustment.

The normalized penetration resistance values obtained from SPT tests in the plant site borings (summarized in the FSAR) are shown in Figures 5 and 6 for Sands A and B, respectively. In obtaining these plots, the blow counts have not only been normalized to an effective overburden pressure of 2 ksf (using the chart presented by Seed and others, 1985), they have also been adjusted to those of a clean sand (i.e. sand with ≤ 5 percent fines) using the relative position of the curves in Figure 4 along with data presented in the FSAR describing the fines contents of the sands. These data indicate that the fines content of Sand A and Sand B are typically equal to or greater than 10 percent and 25 percent, respectively. Based on Figure 4, an upward N_1 adjustment of 2 blows/foot for Sand A and 5 to 7 blows/foot for Sand B (depending on the unadjusted N_1 value) was made to adjust the N_1 values to those of a clean sand.

In assessing the cyclic stress ratios causing liquefaction in Sands A and B, representative or characteristic blow counts for the layers must be selected from the scattergrams in Figures 5 and 6. Seed (personal communication, 1984 and 1988) indicated that a characteristic blow count that is consistent with how the empirical correlation was developed is the 33rd percentile blow count of the distribution after eliminating obvious outliers. Accordingly, the N_1 values selected for Sands A and B from the plots in Figures 5 and 6 are equal to 15 and 18, respectively. Using these N_1 values, the curve for clean sand in Figure 4, and appropriate adjustment factors for earthquake magnitude and effective vertical stress, values of cyclic stress ratio causing liquefaction in Sand A and in Sand B were obtained.

Seed and others (1985) describe the sensitivity of N_1 values to the exact techniques used in conducting Standard Penetration Tests. In fact, the designation $(N_1)_{60}$ in Figure 4 refers to a specific type of drophammer used for the SPT that delivers on the average 60 percent of the theoretical free-fall energy to the rods to which the sampler is attached. Since the details of the techniques used in conducting SPT tests at the site are not known, there are some uncertainties in the cyclic stress ratios causing liquefaction.

The influence of these uncertainties on values of peak ground acceleration causing liquefaction is discussed in Section 4.

The PSAR and FSAR contain dynamic (cyclic) test results on undisturbed samples of sand from layers A and B and an evaluation of the cyclic stress ratios causing liquefaction using these test results. The test results are few and widely scattered. Experience since the late 1960's when these facts were made has demonstrated the extreme difficulty in obtaining cyclic test results representative of insitu conditions, which has, in turn, spurred the development and utilization of empirical correlations and insitu test data in characterizing liquefaction resistance, as summarized above. Nevertheless, previous cyclic test results and interpretations were reviewed during the present study. It was found that when the cyclic test results were interpreted using correction factors established in later years, the cyclic stress ratios causing liquefaction interpreted from these tests are in good agreement with those interpreted during this study from the empirical correlations and insitu test data.

3.2 Liquefaction Resistance of Sand C

There are virtually no insitu test data nor laboratory test data in Sand C due in part to the lenticular nature of the deposit and its slight thickness (equal to or less than 5 feet thick). Based on the fact that the layer is relatively old geologically (of Miocene age, whereas the overlying Sands A and B are of Pleistocene age) and thin, it is judged that this layer has a high resistance to liquefaction and does not pose a significant hazard to the plant structures.

3.3 Liquefaction Resistance of Select Fill

Based on the minimum degree of compaction requirement for the fill stated in the FSAR, it is judged that the relative density of the fill should be approximately equal to or greater than 80 percent. The cyclic shear resistance of the fill was estimated using published laboratory cyclic test results for granular soils compacted to various relative densities (Seed, 1979; Lee and Seed, 1967) along with consideration of the beneficial effect of aging of

the fill since placement (Seed, 1979). In addition, the liquefaction resistance of the fill was estimated on the basis of an assumed N_1 value for the fill; for a well compacted granular fill, it is judged that N_1 should be approximately 25 blows/foot or higher. The effect of possible variations in the liquefaction resistance of the fill on the acceleration levels to cause liquefaction is discussed in the following section.

4. ASSESSMENT OF EARTHQUAKE-INDUCED STRESS RATIOS AND PEAK GROUND ACCELERATIONS CAUSING LIQUEFACTION

For free-field conditions, the ratio of the earthquake induced cyclic shear stress to the pre-earthquake effective vertical stress, $(\tau/\bar{\sigma})_E$, can be obtained using the widely used simplified procedure (Seed and Idriss, 1971; Seed and others, 1983):

$$(\frac{\tau}{\bar{\sigma}})_E = a \cdot \frac{\sigma}{\bar{\sigma}} \cdot r_d \cdot 0.65 \qquad (1)$$

where a = peak acceleration at the ground surface in the free field

σ = total vertical stress at a depth of interest below the ground surface

$\bar{\sigma}$ = effective vertical stress at the same depth

r_d = depth-dependant shear stress reduction factor (mainly accounting for the reduction of peak ground acceleration with depth below the ground surface)

0.65 = factor to obtain average shear stress from peak shear stress

By equating the earthquake-induced stress ratio, $(\tau/\bar{\sigma})_E$, to the stress ratio required to cause liquefaction, $(\tau/\bar{\sigma})_L$, the peak ground acceleration, a, causing liquefaction is obtained.

For conditions beneath structures, a modified form of Equation (1) was used to incorporate the shear stresses induced in the soil by the structures' response to the earthquake ground motions:

$$\left(\frac{\tau}{\bar{\sigma}}\right)_E = \left[\frac{\tau_b}{\bar{\sigma}} + \frac{a_B \cdot r_d \cdot \sigma_s}{\bar{\sigma}}\right] \cdot 0.65 \qquad (2)$$

where τ_b - shear stress induced in the soil at a depth of interest below the structure due to the structure's base shear stress, τ_B, at the foundation-soil interface.

a_B - peak acceleration at the base of the structure.

σ_s - component of the total vertical stress due to the soil weight between the base of the structure and the depth of interest ($\sigma_s = \gamma_t \cdot z$ where γ_t is the total unit weight of soil and z is the depth below the base of the structure).

and other parameters are as defined previously.

In essence, the first term on the right hand side of Equation 2 represents the shear stress induced in the soil layer due to base shear transmitted by the responding structures and the second term represents the shear stress induced in the soil layer by the inertial response of the soils beneath the structure.

Values for the base shear stress, τ_B, transmitted by the structures and the acceleration at the base of the structures, a_B, as a function of the free-field ground surface acceleration, a, were provided by EQE from their soil-structure interaction (SSI) analyses carried out for the PRA. In the SSI analyses, embedment effects (if any) were neglected for the auxiliary building and the control building, which may be conservative. The shear stress, τ_b, induced at some depth beneath the structure due to the structures' base shear was estimated using elastic, static shear stress influence factors.

In evaluating the vertical effective stress, $\bar{\sigma}$, elastic solutions were also used to obtain the stress distribution with depth resulting from the structures' bearing pressures. Bearing pressures were provided by EQE. The variation of r_d with depth below the structures was assumed to be the same as the variation with depth below the ground surface in the free field (i.e. structure-foundation soil interface taken as zero depth).

Using Equation 2, values of the induced cyclic stress ratio, $(\tau/\bar{\sigma})_E$, were obtained as a function of free-field peak ground surface acceleration, a. (The relationships between $(\tau/\bar{\sigma})_E$ and a are nonlinear because of nonlinear relationships between a and a_B, and a and τ_B obtained in the SSI analyses by EQE.) Values of a causing liquefaction were then obtained by equating $(\tau/\bar{\sigma})_E$ with the cyclic stress ratio required to cause liquefaction, $(\tau/\bar{\sigma})_L$. Because Equation 2 involves greater uncertainty in the estimates than those obtained using the free-field formulation of Equation 1, the results were interpreted somewhat conservatively.

Table 1 provides a summary of the free-field ground surface peak accelerations causing liquefaction obtained from the analyses. Estimated peak accelerations causing liquefaction are summarized for four earthquake magnitudes (5, 5.5, 6, and 6.5) for Sands A and B in the free-field and for the select fill and Sand B beneath the auxiliary building and control building. Consistent with prior analyses presented in the FSAR, peak accelerations are presented for two piezometric levels in the soils below the auxiliary building and the control room — elevation -7, which is the expected highest piezometric level beneath these structures due to the influence of the permanent dewatering system; and elevation +5, which is the level that would exist beneath the structures if the dewatering system were not draining the soils beneath the structures as expected. (The latter water level would thus appear to represent an unlikely condition.) Analyses are not presented for Layer C because, as previously noted, it is judged that this layer is very resistant to liquefaction and any consequences of liquefaction in the layer would be insignificant. The SSI results for the reactor building obtained by EQE are also indicative of very low shear stresses induced in Sand C by the reactor building.

Possible ranges in the estimated values of peak ground acceleration causing liquefaction due to uncertainties in the cyclic shear resistances of the soils are summarized in the entries in parentheses in Table 1. For natural Sands A and B, the ranges reflect our judgment as to a possible range of N_1 values due to unknown details of conducting the Standard Penetration Tests at the site. Considering the geologic age of these sands, it is also our judgment that values in the upper half of the ranges are more likely than values in the lower half. For select fill, the ranges in the table reflect our judgment as to a possible range of relative densities to which the fill was compacted (given that it was compacted to the compaction standard stated in the FSAR) or corresponding range of N_1 values.

The peak accelerations summarized in Table 1 are median (50th percentile) values because the correlation for liquefaction resistance (Figure 4) has been interpreted by its developer as a median curve (Seed, 1988, personal communication) and the estimates of induced stress ratios are also considered to be median estimates. In a previous study (Power and others, 1986), a probabilistic distribution was developed for the liquefaction resistance curves. Development of the distribution involved quantification of the expert judgment of the developer of the correlation, Professor H.B. Seed. However, since that work was done, data have been added and reinterpreted and the correlation has been revised. With regard to the current correlation (Figure 4), Professor Seed's preliminary judgment (Seed, 1988, personal communication) is that the band of uncertainty about the median line has narrowed such that the 5th and 95th percentiles of the distribution for $(\tau/\bar{\sigma})_L$ may vary by a factor of only about 1.15 to 1.2 from the median curve. Liao and others (1988) recently quantified the uncertainty in the cyclic stress ratio causing liquefaction; however, the correlation they derived is different from the correlation in widespread general use that is shown in Figure 4.

The foregoing observations suggest that, for purposes of the present PRA, uncertainty in the liquefaction correlation could be included as summarized above. It could be assumed that the variation of peak accelerations about

median values is about the same as the variation in the liquefaction resistance, i.e., a variation by a factor of 1.15 to 1.2 from median values at the 5th and 95th percentile levels. A log-normal distribution could reasonably be used to model the uncertainty. The uncertainty could be increased to incorporate uncertainty in the induced stress ratios. It is judged that this would increase the overall uncertainty to a factor of about 1.25 at the 5th and 95th percentile levels. In addition to the variation about median values, uncertainty in the median values, as discussed previously and summarized in Table 1 due to uncertainty in the N_1 values or relative density of the soil, could be included.

5. CONSEQUENCES OF LIQUEFACTION

The estimated consequences of liquefaction in Sand B and in the select fill, which are the susceptible soils underlying the critical structures of the auxiliary building and the control building, are settlements of the overlying structures due to post-earthquake dissipation of pore pressures in the liquefied soils. These reconsolidation settlements would tend to occur rather slowly after the earthquake, perhaps over a period of several hours or days. Based on data presented by Lee and Albaisa (1974) and Tokimatsu and Seed (1987), the magnitude of the reconsolidation settlements is estimated to be approximately 1 percent of the thickness of the layer of liquefied soil. This could lead to maximum total settlements of approximately 3 inches in the event of liquefaction of Layer B and 1½ inches in the event of liquefaction of the select fill. Differential settlement could occur across the building widths due to variations in the soil layer thicknesses. All of the total settlements could be differential with respect to adjacent non-settling Category 1 structures (reactor building and pile-supported fuel building). In addition to these reconsolidation settlements, some shear distortional differential settlements could occur within the select fill because that layer is the direct bearing support for the auxiliary building and control building. However, it is judged that such distortional settlements should be minor because of the dense nature of the fill and the thinness of the layer relative to the foundation width.

An assessment was also made of the potential for lateral movements of the structures toward the slope of the discharge canal (Figure 1) in the event of liquefaction. Simplified Newmark-type procedures as presented by Makdisi and Seed (1978) were utilized in estimating the deformations. It was assumed that the water level elevation in the canal was approximately equal to the ground water elevation. Based on these analyses, it is judged that lateral movements of the structures would be small (less than 1 inch) for levels of peak ground acceleration equal to or less than 1.5 times the accelerations required to cause liquefaction.

REFERENCES

Liao, S.C., D. Veneziano, and R.V. Whitman,(1988) "Regression Models for Evaluating Liquefaction Probability", Journal of Geotechnical Engineering, ASCE, 111 (4): 389-411.

Lee, K.L., and A. Albaisa (1974) "Earthquake Induced Settlement in Saturated Sands", Journal of the Soil Mechanics and Foundations Division ASCE 100(GT4): 387-406.

Makdisi, F. and Seed, H.B. (1987) "Simplified Procedure for Estimating Dam and Embankment Earthquake-induced Deformations", Journal of the Geotechnical Engineering Division, ASCE 104 (GT7): 849-867.

Power, M.S., V. Berger, R.R. Youngs, K.J. Coppersmith, and D.W. Streiff (1986) "Evaluation of Liquefaction opportunity and liquefaction Potential in the San Diego, California Urban Area", Report submitted by Woodward-Clyde Consultants to the U.S. Geological Survey under contract 14-08-0001-20607.

Seed, H.B. (1979) "Soil Liquefaction and Cyclic Mobility Evaluation for Level Ground During Earthquakes," Journal of the Geotechnical Engineering Division, ASCE 105(GT2): 201-255.

Seed, H.B., and I.M. Idriss (1971) "Simplified Procedure for Evaluating Soil Liquefaction Potential," Journal of the Soil Mechanics and Foundations Division, ASCE 97(SM9): 1249-1273.

Seed, H.B., I.M. Idriss, and I. Arango (1983) "Evaluation of Liquefaction Potential Using Field Performance Data," Journal of Geotechnical Engineering, ASCE 109(3): 458-482.

Seed, H.B., K. Tokimatsu, L.F. Harder, and R.M. Chung (1985) "Influence of SPT procedures in Soil Liquefaction Resistance Evaluations", Journal of Geotechnical Engineering, ASCE, 111 (12): 1425-1445.

Tokimatsu, K. and Seed, H.B. (1978) "Evaluation of Settlements in Sands due to Earthquake Shaking ", Journal of Geotechnical Engineering, ASCE 113 (8): 861-878.

REFERENCES

Liao, S.C., D. Veneziano, and R.V. Whitman,(1988) "Regression Models for Evaluating Liquefaction Probability", Journal of Geotechnical Engineering, ASCE, 111 (4): 389-411.

Lee, K.L., and A. Albaisa (1974) "Earthquake Induced Settlement in Saturated Sands", Journal of the Soil Mechanics and Foundations Division ASCE 100(GT4): 387-406.

Makdisi, F. and Seed, H.B. (1987) "Simplified Procedure for Estimating Dam and Embankment Earthquake-induced Deformations", Journal of the Geotechnical Engineering Division, ASCE 104 (GT7): 849-867.

Power, M.S., V. Berger, R.R. Youngs, K.J. Coppersmith, and D.W. Streiff (1986) "Evaluation of Liquefaction opportunity and liquefaction Potential in the San Diego, California Urban Area", Report submitted by Woodward-Clyde Consultants to the U.S. Geological Survey under contract 14-08-0001-20607.

Seed, H.B. (1979) "Soil Liquefaction and Cyclic Mobility Evaluation for Level Ground During Earthquakes," Journal of the Geotechnical Engineering Division, ASCE 105(GT2): 201-255.

Seed, H.B., and I.M. Idriss (1971) "Simplified Procedure for Evaluating Soil Liquefaction Potential," Journal of the Soil Mechanics and Foundations Division, ASCE 97(SM9): 1249-1273.

Seed, H.B., I.M. Idriss, and I. Arango (1983) "Evaluation of Liquefaction Potential Using Field Performance Data," Journal of Geotechnical Engineering, ASCE 109(3): 458-482.

Seed, H.B., K. Tokimatsu, L.F. Harder, and R.M. Chung (1985) "Influence of SPT procedures in Soil Liquefaction Resistance Evaluations", Journal of Geotechnical Engineering, ASCE, 111 (12): 1425-1445.

Tokimatsu, K. and Seed, H.B. (1978) "Evaluation of Settlements in Sands due to Earthquake Shaking ", Journal of Geotechnical Engineering, ASCE 113 (8): 861-878.

TABLE 1

ESTIMATED MEDIAN VALUES OF FREE-FIELD
GROUND SURFACE PEAK ACCELERATIONS
REQUIRED TO CAUSE LIQUEFACTION

	Median Acceleration to Cause Liquefaction (g)			
	M5	M5.5	M6	M6.5
Free field (Groundwater Level at El +5)				
Sand A	0.34 (± 20%)	0.31 (± 20%)	0.28 (± 20%)	0.25 (± 20%)
Sand B	0.40 (± 15%)	0.37 (± 15%)	0.34 (± 15%)	0.30 (± 15%)
Beneath Auxiliary Building and Control Building				
(a) Groundwater Level at El -7				
Select Fill	>0.8 (>0.8)	>0.8 (0.75->0.8)	>0.8 (0.69->0.8)	>0.73 (0.60->0.8)
Sand B	0.40 (± 15%)	0.37 (± 15%)	0.34 (± 15%)	0.30 (± 15%)
(b) Groundwater Level at El +5				
Select Fill	0.78 (0.65->0.8)	0.72 (0.59->0.8)	0.65 (0.53-0.76)	0.56 (0.46-0.66)
Sand B	0.35 (± 15%)	0.32 (± 15%)	0.29 (± 15%)	0.26 (± 15%)

Note: Values in parentheses represent a possible range about the estimated accelerations due to uncertainties in the cyclic shear resistances of the soils.

FIG. 2.4-7
DEC. 1, 1969

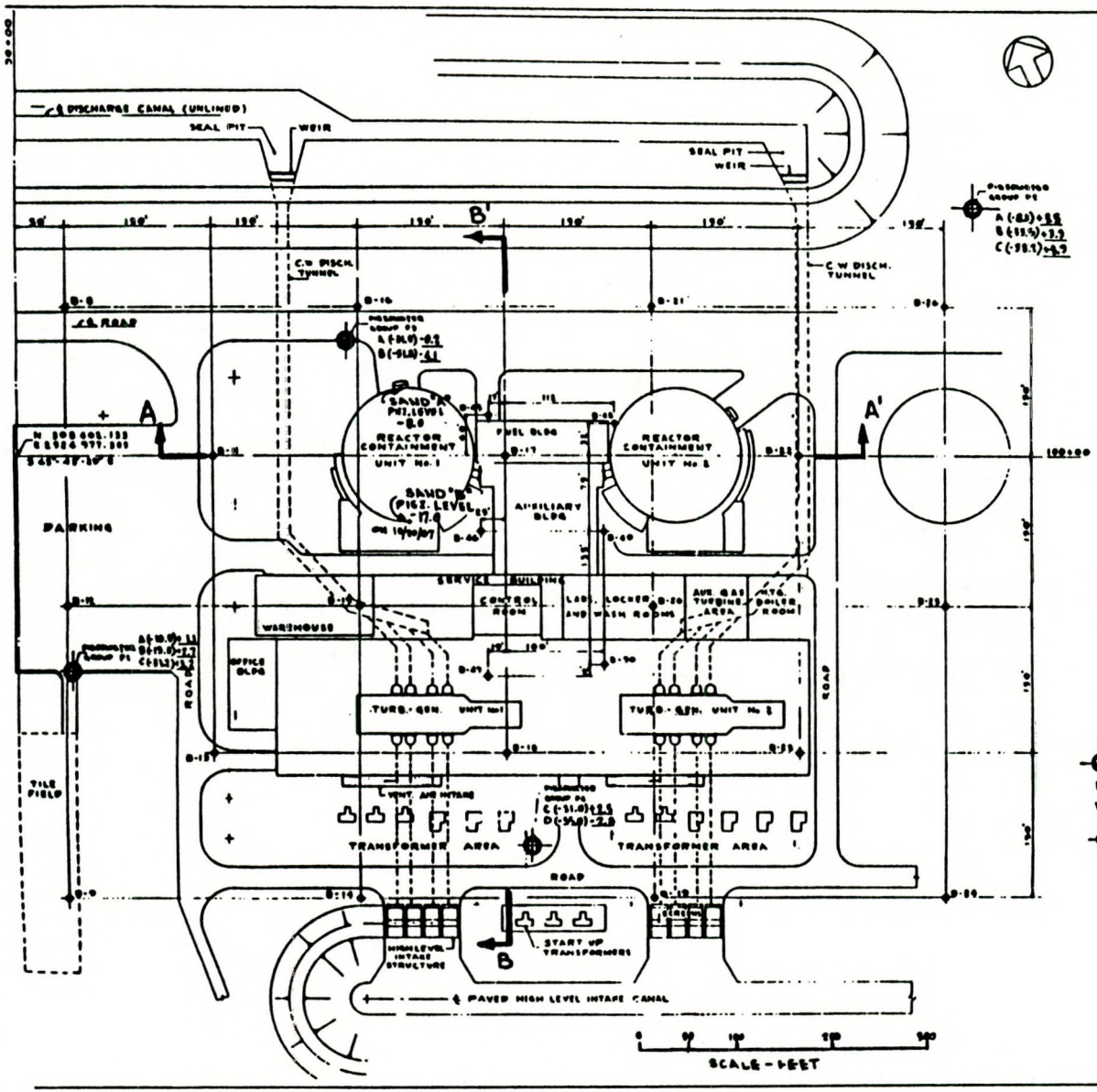

PIEZOMETER LEVELS 11-2-67

NO.	TIP	ELEV.
P1A	-10.0	+1.1
P1B	-19.0	+1.3
P1C	-31.2	+1.9
P2A	-8.1	+3.7
P2B	-33.5	+3.5
P2C	-38.2	+3.2
P3A	-31.0	-17.8
P3B	-51.0	-17.2
P4C	-31.0	+2.2
P4D	-55.0	-3.3
P5A	-7.0	+5.0
P5B	-37.0	+5.3

COFFERDAM NO.1		
SAND	N. WALL	S. WALL
A	-7.0	-9.0
B	-22.0	-24.0

DENOTES LOCATION OF PIEZOMETER GROUP
PIEZOMETER TIP EL. SHOWN IN PARENTHESIS ( )
WATER LEVEL AS OF 10-3-67 SHOWN UNDERLINED

DENOTES BORINGS

PLAN OF POWER PLANT
From FSAR

GEOMATRIX

Figure 1

Project No. 1134A

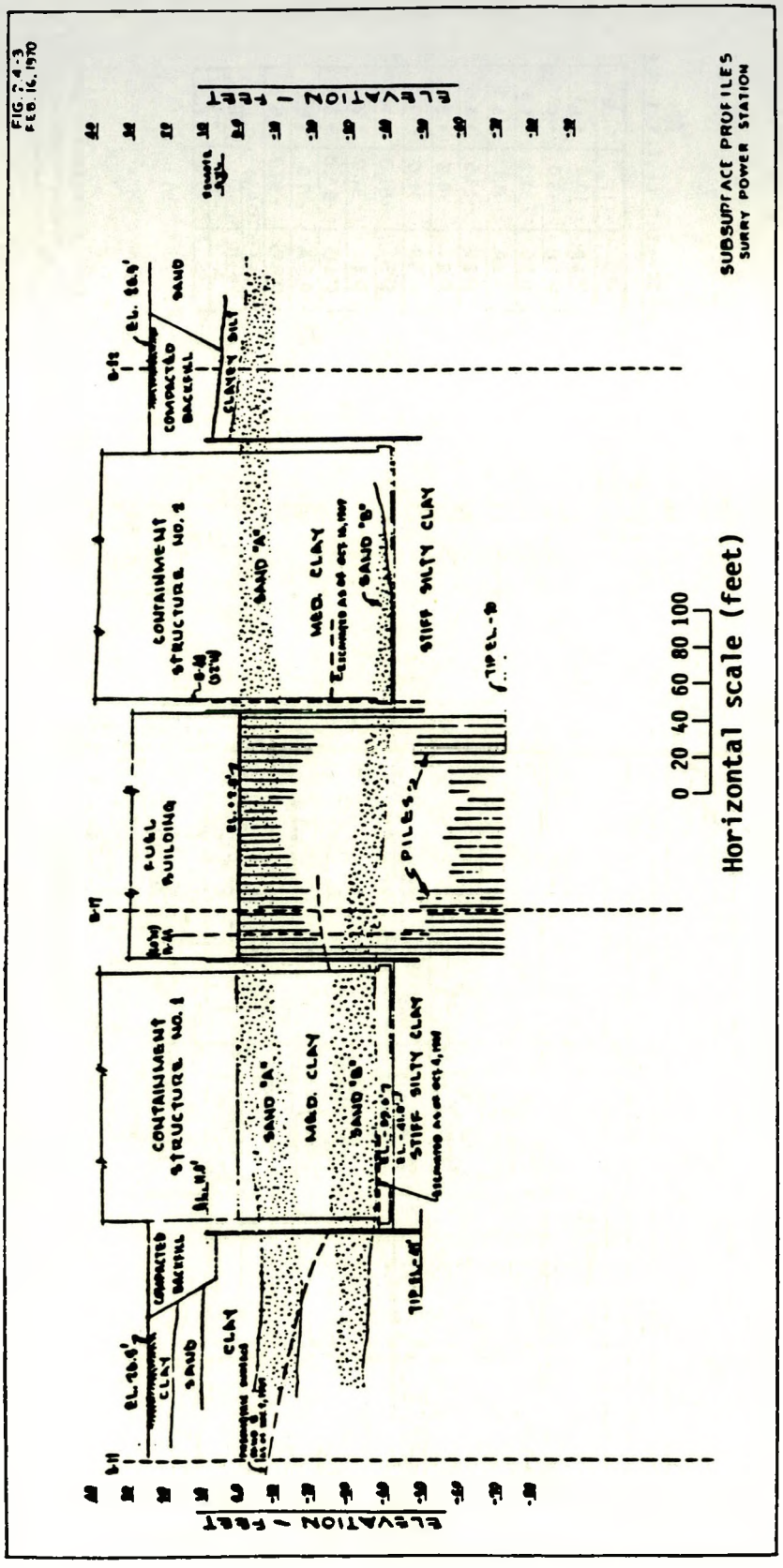

GEOMATRIX

SECTION A-A'
From FSAR

Figure
2

Project No.
1134A

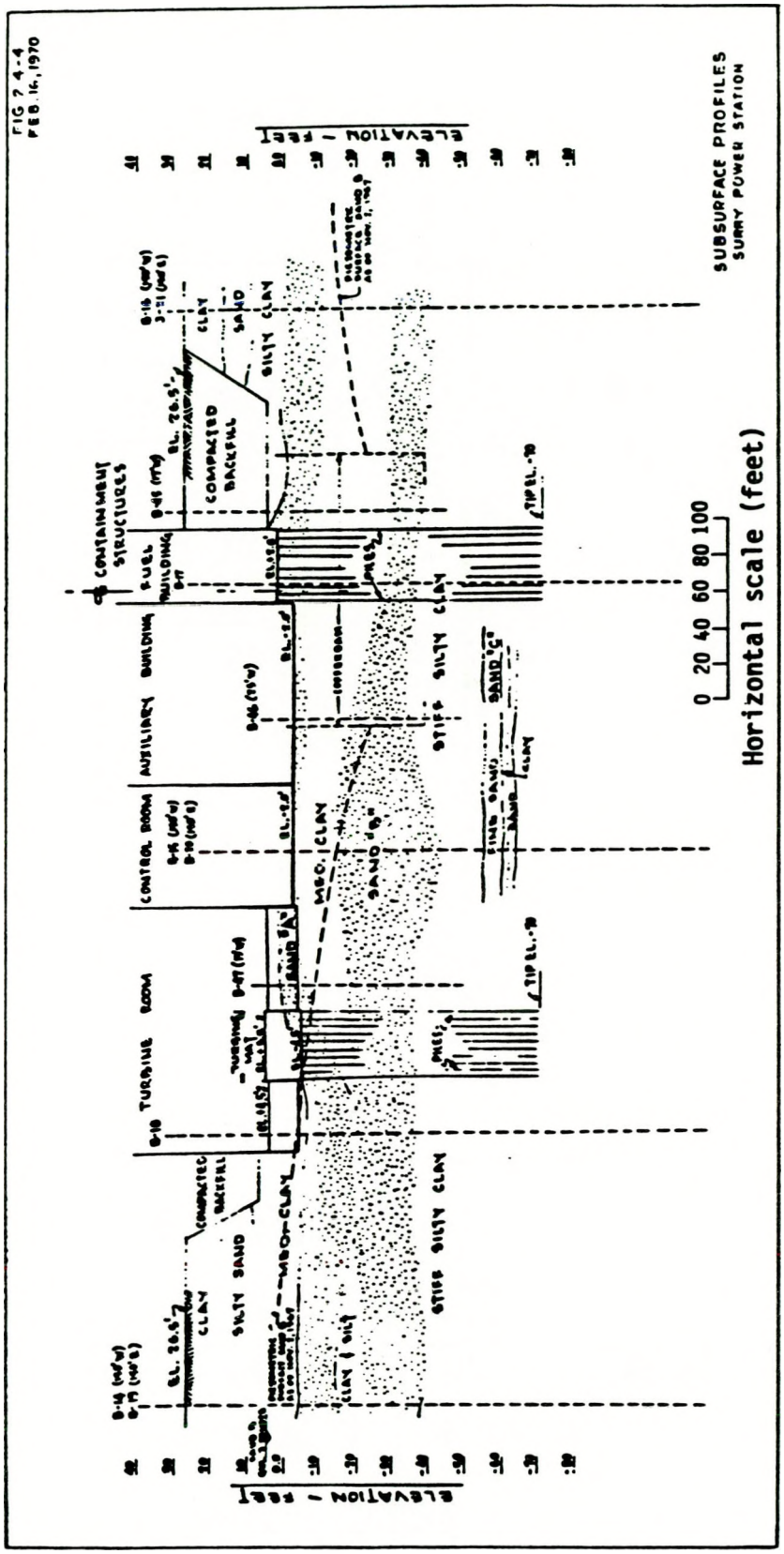

GEOMATRIX

SECTION B-B'
From FSAR

Figure
3

Project No.
1134A

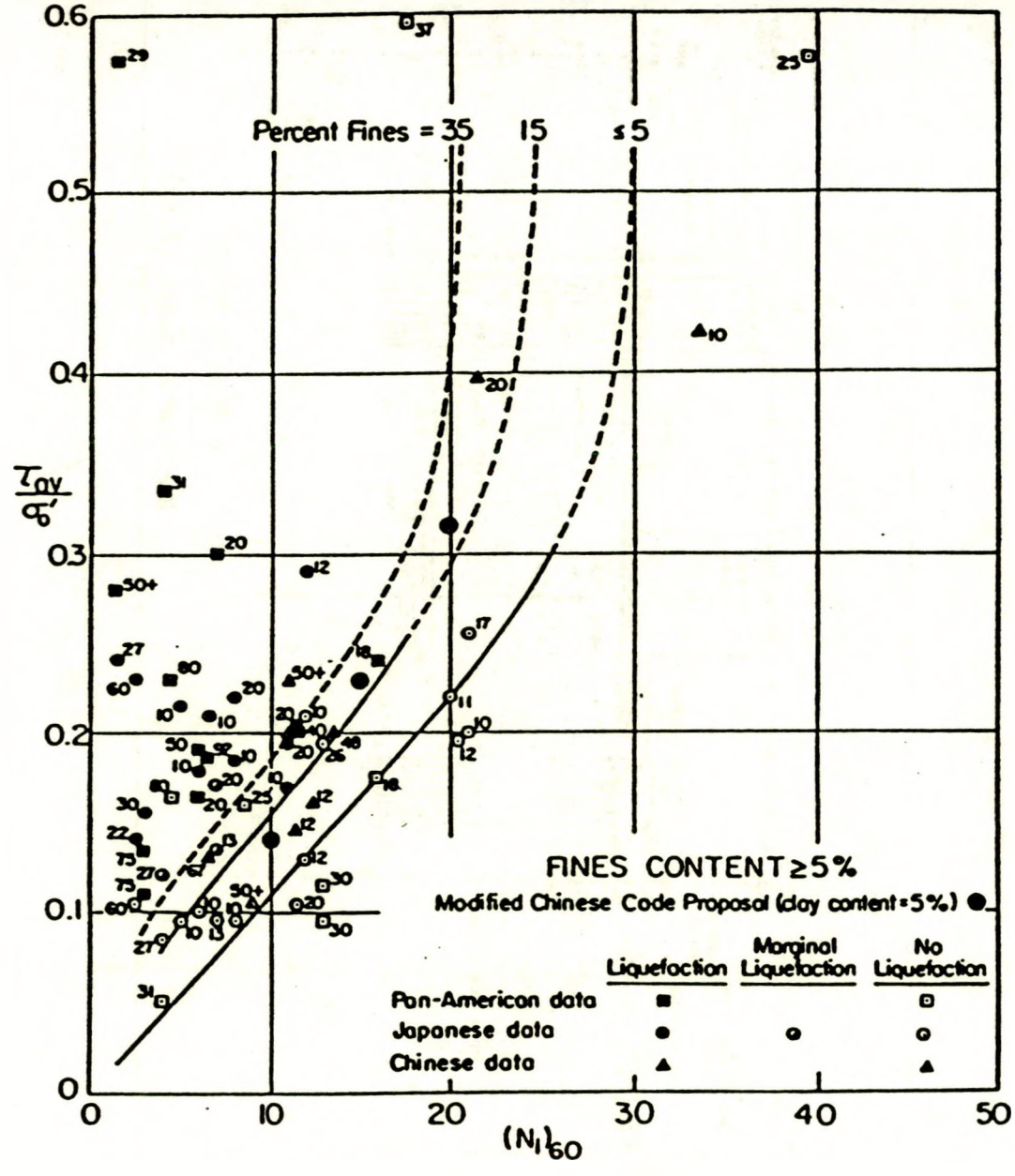

GEOMATRIX

RELATIONSHIP BETWEEN STRESS RATIOS CAUSING LIQUEFACTION AND N_1 VALUES FOR $M = 7\text{-}1/2$ EARTHQUAKES FROM SEED AND OTHERS, 1985

Figure 4

Project No. 1134A

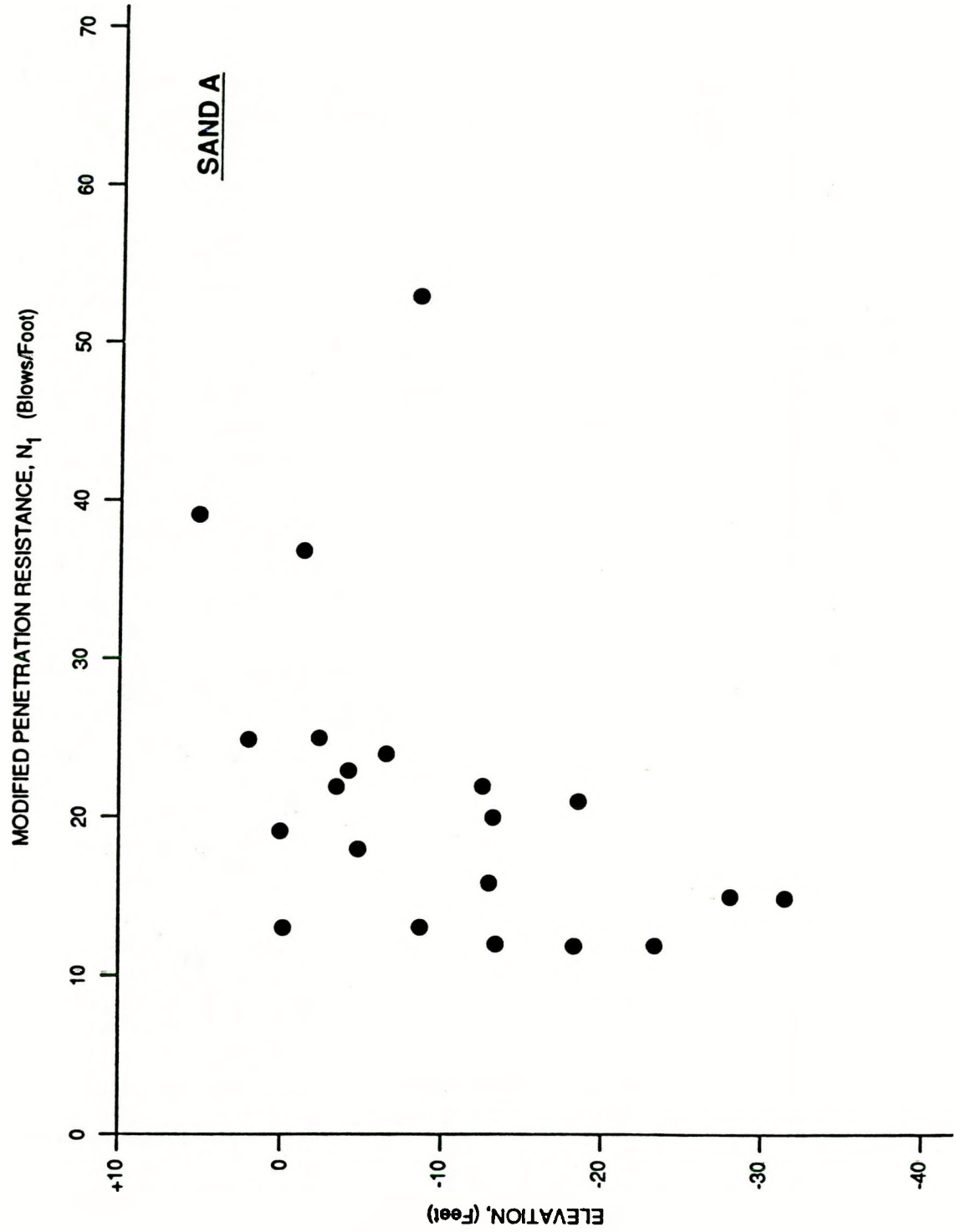

GEOMATRIX

MODIFIED PENETRATION RESISTANCE VALUES
VERSUS ELEVATION FOR SAND A

Figure
5

Project No.
1134A

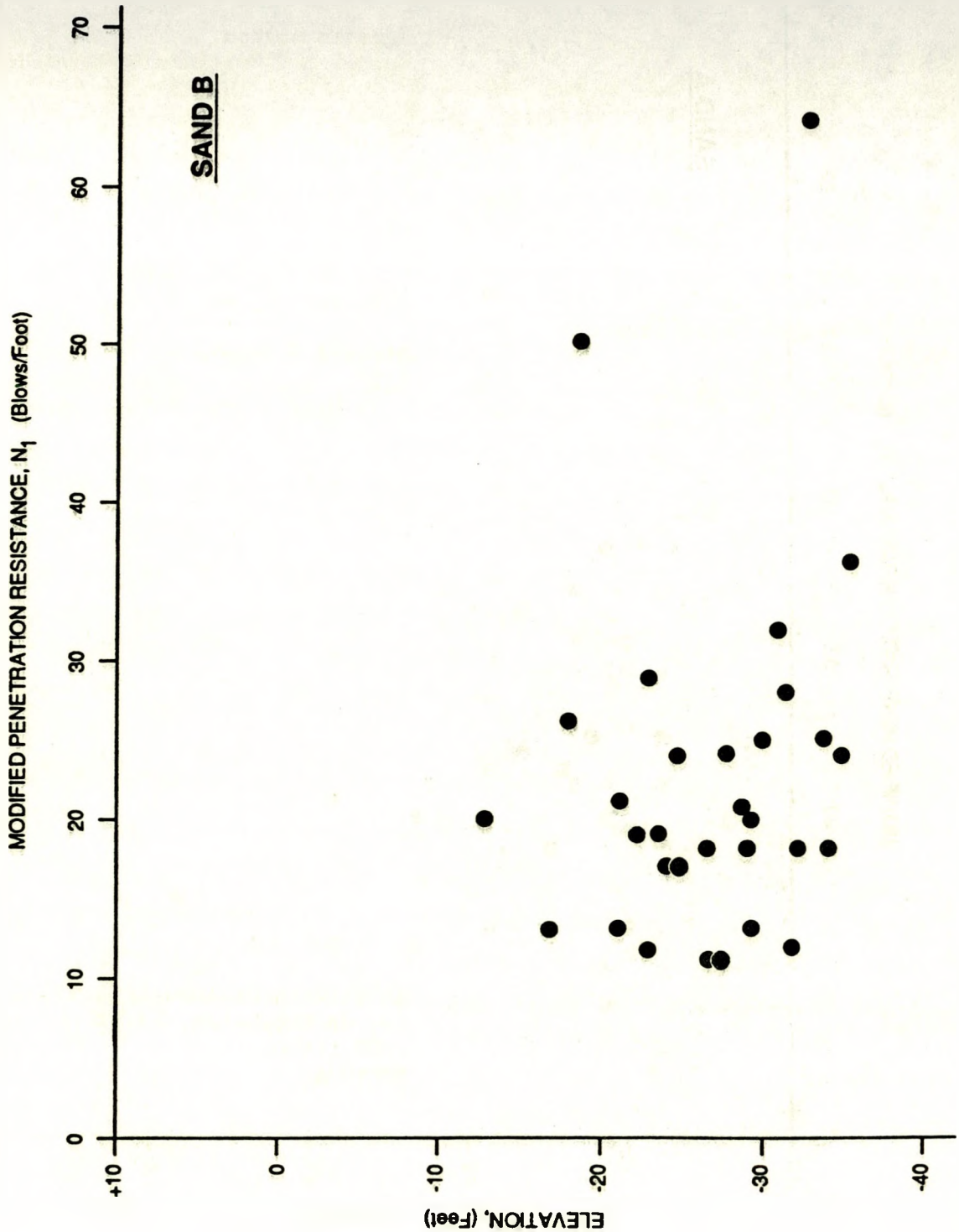

GEOMATRIX

MODIFIED PENETRATION RESISTANCE VALUES
VERSUS ELEVATION FOR SAND B

Figure
6

Project No.
1134A

DISTRIBUTION:

Frank Abbey
U. K. Atomic Energy Authority
Wigshaw Lane, Culcheth
Warrington, Cheshire, WA3 4NE
ENGLAND

Kiyoharu Abe
Department of Reactor Safety Research
Nuclear Safety Research Center
ToKai Research Establishment
JAERI
Tokai-mura, Naga-gun
Ibaraki-ken,
JAPAN

Ulvi Adalioglu
Nuclear Engineering Division
Cekmece Nuclear Research and Training Centre
P.K.1, Havaalani
Istanbul
TURKEY

Bharat Agrawal
USNRC-RES/AEB
MS: NL/N-344

Kiyoto Aizawa
Safety Research Group
Reactor Research and Development Project
PNC
9-13m 1-Chome Akasaka
Minatu-Ku
Tokyo
JAPAN

Oguz Akalin
Ontario Hydro
700 University Avenue
Toronto, Ontario
CANADA M5G 1X6

David Aldrich
Science Applications International Corporation
1710 Goodridge Drive
McLean, VA 22102

Agustin Alonso
University Politecnica De Madrid
J Gutierrez Abascal, 2
28006 Madrid
SPAIN

Christopher Amos
Science Applications International Corporation
2109 Air Park Road SE
Albuquerque, NM 87106

Richard C. Anoba
SAIC
4900 Motors Edge Drive, Suite 255
Raleigh, NC 27606

George Apostolakis
UCLA
Boelter Hall, Room 5532
Los Angeles, CA 90024

James W. Ashkar
Boston Edison Company
800 Boylston Street
Boston, MA 02199

Donald H. Ashton
Bechtel Power Corporation
P.O. Box 2166
Houston, TX 77252-2166

J. de Assuncao
Cabinete de Proteccao e Seguranca Nuclear
Secretario de Estado de Energia
Ministerio da Industria
av. da Republica, 45-6°
1000 Lisbon
PORTUGAL

Mark Averett
Florida Power Corporation
P.O. Box 14042
St. Petersburg, FL 33733

Raymond O. Bagley
Northeast Utilities
P.O. Box 270
Hartford, CT 06141-0270

Juan Bagues
Consejo de Seguridad Nucleare
Sarangela de la Cruz 3
28020 Madrid
SPAIN

George F. Bailey
Washington Public Power Supply System
P. O. Box 968
Richland, WA 99352

H. Bairiot
Belgonucleaire S A
Rue de Champ de Mars 25
B-1050 Brussels
BELGIUM

Louis Baker
Reactor Analysis and Safety Division
Building 207
Argonne National Laboratory
9700 South Cass Avenue
Argonne, IL 60439

H-P. Balfanz
TUV-Norddeutschland
Grosse Bahnstrasse 31,
2000 Hamburg 54
FEDERAL REPUBLIC OF GERMANY

Patrick Baranowsky
USNRC-NRR/OEAB
MS: 11E-22

H. Bargmann
Dept. de Mecanique
Inst. de Machines Hydrauliques et de Mecaniques des Fluides
Ecole Polytechnique de Lausanne
CH-1003 Lausanne
M.E. (ECUBLENS)
CH. 1015 Lausanne
SWITZERLAND

Robert A. Bari
Brookhaven National Laboratory
Building 130
Upton, NY 11973

Richard Barrett
USNRC-NRR/PRAB
MS: 10A-2

Kenneth S. Baskin
S. California Edison Company
P.O. Box 800
Rosemead, CA 91770

J. Basselier
Belgonucleaire S A
Rue du Champ de Mars 25, B-1050
Brussels
BELGIUM

Werner Bastl
Gesellschaft Fur Reaktorsicherheit
Forschungsgelande
D-8046 Garching
FEDERAL REPUBLIC OF GERMANY

Anton Bayer
BGA/ISH/ZDB
Postfach 1108
D-8042 Neuherberg
FEDERAL REPUBLIC OF GERMANY

Ronald Bayer
Virginia Electric Power Co.
P. O. Box 26666
Richmond, VA 23261

Eric S. Beckjord
Director
USNRC-RES
MS: NL/S-007

Bruce B. Beckley
Public Service Company
P.O. Box 330
Manchester, NH 03105

William Beckner
USNRC-RES/SAIB
MS: NL/S-324

Robert M. Bernero
Director
USNRC-NMSS
MS: 6A-4

Ronald Berryman [2]
Virginia Electric Power Co.
P. O. Box 26666
Richmond, VA 23261

Robert C. Bertucio
NUS Corporation
1301 S. Central Ave, Suite 202
Kent, WA 98032

John H. Bickel
EG&G Idaho
P.O. Box 1625
Idaho Falls, ID 83415

Peter Bieniarz
Risk Management Association
2309 Dietz Farm Road, NW
Albuquerque, NM 87107

Adolf Birkhofer
Gesellschaft Fur Reaktorsicherheit
Forschungsgelande
D-8046 Garching
FEDERAL REPUBLIC OF GERMANY

James Blackburn
Illinois Dept. of Nuclear Safety
1035 Outer Park Drive
Springfield, IL 62704

Dennis C. Bley
Pickard, Lowe & Garrick, Inc.
2260 University Drive
Newport Beach, CA 92660

Roger M. Blond
Science Applications Int. Corp.
20030 Century Blvd., Suite 201
Germantown, MD 20874

Simon Board
Central Electricity Generating
Board
Technology and Planning Research
Division
Berkeley Nuclear Laboratory
Berkeley Gloucestershire, GL139PB
UNITED KINGDOM

Mario V. Bonace
Northeast Utilities Service Company
P.O. Box 270
Hartford, CT 06101

Gary J. Boyd
Safety and Reliability Optimization
Services
9724 Kingston Pike, Suite 102
Knoxville, TN 37922

Robert J. Breen
Electric Power Research Institute
3412 Hillview Avenue
Palo Alto, CA 94303

Charles Brinkman
Combustion Engineering
7910 Woodmont Avenue
Bethesda, MD 20814

K. J. Brinkmann
Netherlands Energy Res. Fdtn.
P.O. Box 1
1755ZG Petten NH
NETHERLANDS

Allan R. Brown
Manager, Nuclear Systems and
Safety Department
Ontario Hydro
700 University Ave.
Toronto, Ontario M5G1X6
CANADA

Robert G. Brown
TENERA L.P.
1340 Saratoga-Sunnyvale Rd.
Suite 206
San Jose, CA 95129

Sharon Brown
EI Services
1851 So. Central Place, Suite 201
Kent, WA 98031

Ben Buchbinder
NASA, Code QS
600 Maryland Ave. SW
Washington, DC 20546

R. H. Buchholz
Nutech
6835 Via Del Oro
San Jose, CA 95119

Robert J. Budnitz
Future Resources Associates
734 Alameda
Berkeley, CA 94707

Gary R. Burdick
USNRC-RES/DSR
MS: NL/S-007

Arthur J. Buslik
USNRC-RES/PRAB
MS: NL/S-372

M. Bustraan
Netherlands Energy Res. Fdtn.
P.O. Box 1
1755ZG Petten NH
NETHERLANDS

Nigel E. Buttery
Central Electricity Generating Board
Booths Hall
Chelford Road, Knutsford
Cheshire, WA168QG
UNITED KINGDOM

Jose I. Calvo Molins
Probabilistic Safety Analysis Group
Consejo de Seguridad Nuclear
Sor Angela de la Cruz 3, Pl. 6
28020 Madrid
SPAIN

J. F. Campbell
Nuclear Installations Inspectorate
St. Peters House
Balliol Road, Bootle
Merseyside, L20 3LZ
UNITED KINGDOM

Kenneth S. Canady
Duke Power Company
422 S. Church Street
Charlotte, NC 28217

Lennart Carlsson
IAEA A-1400
Wagramerstrasse 5
P.O. Box 100
Vienna, 22
AUSTRIA

Annick Carnino
Electricite de France
32 Rue de Monceau 8EME
Paris, F5008
FRANCE

G. Caropreso
Dept. for Envir. Protect. & Hlth.
ENEA Cre Casaccia
Via Anguillarese, 301
00100 Roma
ITALY

James C. Carter, III
TENERA L.P.
Advantage Place
308 North Peters Road
Suite 280
Knoxville, TN 37922

Eric Cazzoli
Brookhaven National Laboratory
Building 130
Upton, NY 11973

John G. Cesare
SERI
Director Nuclear Licensing
5360 I-55 North
Jackson, MS 39211

S. Chakraborty
Radiation Protection Section
Div. De La Securite Des Inst. Nuc.
5303 Wurenlingen
SWITZERLAND

Sen-I Chang
Institute of Nuclear Energy Research
P.O. Box 3
Lungtan, 325
TAIWAN

J. R. Chapman
Yankee Atomic Electric Company
1671 Worcester Road
Framingham, MA 01701

Robert F. Christie
Tennessee Valley Authority
400 W. Summit Hill Avenue, W10D190
Knoxville, TN 37902

T. Cianciolo
BWR Assistant Director
ENEA DISP TX612167 ENEUR
Rome
ITALY

Thomas Cochran
Natural Resources Defense Council
1350 New York Ave. NW, Suite 300
Washington, D.C. 20005

Frank Coffman
USNRC-RES/HFB
MS: NL/N-316

Larry Conradi
NUS Corporation
16835 W. Bernardo Drive
Suite 202
San Diego, CA 92127

Peter Cooper
U.K. Atomic Energy Authority
Wigshaw Lane, Culcheth
Warrington, Cheshire, WA3 4NE
UNITED KINGDOM

C. Allin Cornell
110 Coquito Way
Portola Valley, CA 94025

Michael Corradini
University of Wisconsin
1500 Johnson Drive
Madison, WI 53706

E. R. Corran
Nuclear Technology Division
ANSTO Research Establishment
Lucas Heights Research Laboratories
Private Mail Bag 7
Menai, NSW 2234
AUSTRALIA

James Costello
USNRC-RES/SSEB
MS: NL/S-217A

George R. Crane
1570 E. Hobble Creek Dr.
Springville, UT 84663

Mat Crawford
SERI
5360 I-55 North
Jackson, MS 39211

Michael C. Cullingford
Nuclear Safety Division
IAEA
Wagramerstrasse, 5
P.O. Box 100
A-1400 Vienna
AUSTRIA

Garth Cummings
Lawrence Livermore Laboratory
L-91, Box 808
Livermore, CA 94526

Mark A. Cunningham
USNRC-RES/PRAB
MS: NL/S-372

James J. Curry
7135 Salem Park Circle
Mechanicsburg, PA 17055

Peter Cybulskis
Battelle Columbus Division
505 King Avenue
Columbus, OH 43201

Peter R. Davis
PRD Consulting
1935 Sabin Drive
Idaho Falls, ID 83401

Jose E. DeCarlos
Consejo de Seguridad Nuclear
Sor Angela de la Cruz 3, Pl. 8
28016 Madrid
SPAIN

M. Marc Decreton
Department Technologie
CEN/SCK
Boeretang 200
B-2400 Mol
BELGIUM

Richard S. Denning
Battelle Columbus Division
505 King Avenue
Columbus, OH 43201

Vernon Denny
Science Applications Int. Corp.
5150 El Camino Real, Suite 3
Los Altos, CA 94303

J. Devooget
Faculte des Sciences Appliques
Universite Libre de Bruxelles
av. Franklin Roosevelt
B-1050 Bruxelles
BELGIUM

R. A. Diederich
Supervising Engineer
Environmental Branch
Philadelphia Electric Co.
2301 Market St.
Philadelphia, PA 19101

Raymond DiSalvo
Battelle Columbus Division
505 King Avenue
Columbus, OH 43201

Mary T. Drouin
Science Applications International
Corporation
2109 Air Park Road S.E.
Albuquerque, NM 87106

Andrzej Drozd
Stone and Webster
Engineering Corp.
243 Summer Street
Boston, MA 02107

N. W. Edwards
NUTECH
145 Martinville Lane
San Jose, CA 95119

Ward Edwards
Social Sciences Research Institute
University of Southern California
Los Angeles, CA 90089-1111

Joachim Ehrhardt
Kernforschungszentrum Karlsruhe/INR
Postfach 3640
D-7500 Karlsruhe 1
FEDERAL REPUBLIC OF GERMANY

Adel A. El-Bassioni
USNRC-NRR/PRAB
MS: 10A-2

J. Mark Elliott
International Energy Associates,
Ltd., Suite 600
600 New Hampshire Ave., NW
Washington, DC 20037

Farouk Eltawila
USNRC-RES/AEB
MS: NL/N-344

Mike Epstein
Fauske and Associates
P. O. Box 1625
16W070 West 83rd Street
Burr Ridge, IL 60521

Malcolm L. Ernst
USNRC-RGN II

F. R. Farmer
The Long Wood, Lyons Lane
Appleton, Warrington
WA4 5ND
UNITED KINGDOM

P. Fehrenback
Atomic Energy of Canada, Ltd.
Chalk River Nuclear Laboratories
Chalk River Ontario, K0J1P0
CANADA

P. Ficara
ENEA Cre Casaccia
Department for Thermal Reactors
Via Anguillarese, 301
00100 ROMA
ITALY

A. Fiege
Kernforschungszentrum
Postfach 3640
D-7500 Karlsruhe
FEDERAL REPUBLIC OF GERMANY

John Flack
USNRC-RES/SAIB
MS: NLS-324

George F. Flanagan
Oak Ridge National Laboratory
P.O. Box Y
Oak Ridge, TN 37831

Karl N. Fleming
Pickard, Lowe & Garrick, Inc.
2260 University Drive
Newport Beach, CA 92660

Terry Foppe
Rocky Flats Plant
P. O. Box 464, Building T886A
Golden, CO 80402-0464

Joseph R. Fragola
Science Applications International Corporation
274 Madison Avenue
New York, NY 10016

Wiktor Frid
Swedish Nuclear Power Inspectorate
Division of Reactor Technology
P. O. Box 27106
S-102 52 Stockholm
SWEDEN

James Fulford
NUS Corporation
910 Clopper Road
Gaithersburg, MD 20878

Urho Fulkkinen
Technical Research Centre of Finland
Electrical Engineering Laboratory
Otakaari 7 B
SF-02150 Espoo 15
FINLAND

J. B. Fussell
JBF Associates, Inc.
1630 Downtown West Boulevard
Knoxville, TN 37919

John Garrick
Pickard, Lowe & Garrick, Inc.
2260 University Drive
Newport Beach, CA 92660

John Gaunt
British Embassy
3100 Massachusetts Avenue, NW
Washington, DC 20008

Jim Gieseke
Battelle Columbus Division
505 King Avenue
Columbus, OH 43201

Frank P. Gillespie
USNRC-NRR/PMAS
MS: 12G-18

Ted Ginsburg
Department of Nuclear Energy
Building 820
Brookhaven National Laboratory
Upton, NY 11973

James C. Glynn
USNRC-RES/PRAB
MS: NL/S-372

P. Govaerts
Departement de la Surete Nucleaire
Association Vincotte
avenue du Roi 157
B-1060 Bruxelles
BELGIUM

George Greene
Building 820M
Brookhaven National Laboratory
Upton, NY 11973

Carrie Grimshaw
Brookhaven National Laboratory
Building 130
Upton, NY 11973

H. J. Van Grol
Energy Technology Division
Energieonderzoek Centrum Nederland
Westerduinweg 3
Postbus 1
NL-1755 Petten ZG
NETHERLANDS

Sergio Guarro
Lawrence Livermore Laboratories
P. O. Box 808
Livermore, CA 94550

Sigfried Hagen
Kernforschungzentrum Karlsruhe
P. O. Box 3640
D-7500 Karlsruhe 1
FEDERAL REPUBLIC OF GERMANY

L. Hammar
Statens Karnkraftinspektion
P.O. Box 27106
S-10252 Stockholm
SWEDEN

Stephen Hanauer
Technical Analysis Corp.
6723 Whittier Avenue
Suite 202
McLean, VA 22101

Brad Hardin
USNRC-RES/TRAB
MS: NL/S-169

R. J. Hardwich, Jr.
Virginia Electric Power Co.
P.O. Box 26666
Richmond, Va 23261

Michael R. Haynes
UKAEA Harwell Laboratory
Oxfordshire
Didcot, Oxon., OX11 ORA
ENGLAND

Michael J. Hazzan
Stone & Webster
3 Executive Campus
Cherry Hill, NJ 08034

A. Hedgran
Royal Institute of Technology
Nuclear Safety Department
Bunellvagen 60
10044 Stockholm
SWEDEN

Sharif Heger
UNM Chemical and Nuclear
Engineering Department
Farris Engineering
Room 209
Albuquerque, NM 87131

Jon C. Helton
Dept. of Mathematics
Arizona State University
Tempe, AZ 85287

Robert E. Henry
Fauske and Associates, Inc.
16W070 West 83rd Street
Burr Ridge, IL 60521

P. M. Herttrich
Federal Ministry for the
Environment, Preservation of
Nature and Reactor Safety
Husarenstrasse 30
Postfach 120629
D-5300 Bonn 1
FEDERAL REPUBLIC OF GERMANY

F. Heuser
Giesellschaft Fur Reaktorsicherheit
Forschurgsgelande
D-8046 Garching
FEDERAL REPUBLIC OF GERMANY

E. F. Hicken
Giesellschaft Fur Reaktorsicherheit
Forschungsgelande
D-8046 Garching
FEDERAL REPUBLIC OF GERMANY

D. J. Higson
Radiological Support Group
Nuclear Safety Bureau
Australian Nuclear Science and
Technology Organisation
P.O. Box 153
Rosebery, NSW 2018
AUSTRALIA

Daniel Hirsch
University of California
A. Stevenson Program on
Nuclear Policy
Santa Cruz, CA 95064

H. Hirschmann
Hauptabteilung Sicherheit und
Umwelt
Swiss Federal Institute for
Reactor Research (EIR)
CH-5303 Wurenlingen
SWITZERLAND

Mike Hitchler
Westinghouse Electric Corp.
Savanna River Site
Aiken, SC 29808

Richard Hobbins
EG&G Idaho
P. O. Box 1625
Idaho Falls, ID 83415

Steven Hodge
Oak Ridge National Laboratory
P.O. Box Y
Oak Ridge, TN 37831

Lars Hoegberg
Office of Regulation and Research
Swedish Nuclear Power Inspectorate
P. O. Box 27106
S-102 52 Stockholm
SWEDEN

Lars Hoeghort
IAEA A-1400
Wagranerstraase 5
P.O. Box 100
Vienna, 22
AUSTRIA

Edward Hofer
Giesellschaft Fur Reaktorsicherheit
Forschurgsgelande
D-8046 Garching
FEDERAL REPUBLIC OF GERMANY

Peter Hoffmann
Kernforschingszentrum Karlsruhe
Institute for Material
Und Festkorperforsching I
Postfach 3640
D-7500 Karlsruhe 1
FEDERAL REPUBLIC OF GERMANY

N. J. Holloway
UKAEA Safety and Reliability
Directorate
Wigshaw Lane, Culcheth
Warrington, Cheshire, WA34NE
UNITED KINGDOM

Stephen C. Hora
University of Hawaii at Hilo
Division of Business Administration
and Economics
College of Arts and Sciences
Hilo, HI 96720-4091

J. Peter Hoseman
Swiss Federal Institute for
Reactor Research
CH-5303, Wurenlingen
SWITZERLAND

Thomas C. Houghton
KMC, Inc.
1747 Pennsylvania Avenue, NW
Washington, DC 20006

Dean Houston
USNRC-ACRS
MS: P-315

Der Yu Hsia
Taiwan Atomic Energy Council
67, Lane 144, Keelung Rd.
Sec. 4
Taipei
TAIWAN

Alejandro Huerta-Bahena
National Commission on Nuclear
Safety and Safeguards (CNSNS)
Insurgentes Sur N. 1776
Col. Florida
C. P. 04230 Mexico, D.F.
MEXICO

Kenneth Hughey [2]
SERI
5360 I-55 North
Jackson, MS 39211

Won-Guk Hwang
Kzunghee University
Yongin-Kun
Kyunggi-Do 170-23
KOREA

Michio Ichikawa
Japan Atomic Energy Research
Institute
Dept. of Fuel Safety Research
Tokai-Mura, Naka-Gun
Ibaraki-Ken, 319-1
JAPAN

Sanford Israel
USNRC-AEOD/ROAB
MS: MNBB-9715

Krishna R. Iyengar
Louisiana Power and Light
200 A Huey P. Long Avenue
Gretna, LA 70053

Jerry E. Jackson
USNRC-RES
MS: NL/S-302

R. E. Jaquith
Combustion Engineering, Inc.
1000 Prospect Hill Road
M/C 9490-2405
Windsor, CT 06095

S. E. Jensen
Exxon Nuclear Company
2101 Horn Rapids Road
Richland, WA 99352

Kjell Johannson
Studsvik Energiteknik AB
S-611 82, Nykoping
SWEDEN

Richard John
SSM, Room 102
927 W. 35th Place
USC, University Park
Los Angeles, CA 90089-0021

D. H. Johnson
Pickard, Lowe & Garrick, Inc.
2260 University Drive
Newport Beach, CA 92660

W. Reed Johnson
Department of Nuclear Engineering
University of Virginia
Reactor Facility
Charlottesville, VA 22901

Jeffery Julius
NUS Corporation
1301 S. Central Ave, Suite 202
Kent, WA 98032

H. R. Jun
Korea Adv. Energy Research Inst.
P.O. Box 7, Daeduk Danju
Chungnam 300-31
KOREA

Peter Kafka
Gesellschaft Fur Reaktorsicherheit
Forschungsgelande
D-8046 Garching
FEDERAL REPUBLIC OF GERMANY

Geoffrey D. Kaiser
Science Application Int. Corp.
1710 Goodridge Drive
McLean, VA 22102

William Kastenberg
UCLA
Boelter Hall, Room 5532
Los Angeles, CA 90024

Walter Kato
Brookhaven National Laboratory
Associated Universities, Inc.
Upton, NY 11973

M. S. Kazimi
MIT, 24-219
Cambridge, MA 02139

Ralph L. Keeney
101 Lombard Street
Suite 704W
San Francisco, CA 94111

Henry Kendall
Executive Director
Union of Concerned Scientists
Cambridge, MA

Frank King
Ontario Hydro
700 University Avenue
Bldg. H11 G5
Toronto
CANADA M5G1X6

Oliver D. Kingsley, Jr.
Tennessee Valley Authority
1101 Market Street
GN-38A Lookout Place
Chattanooga, TN 37402

Stephen R. Kinnersly
Winfrith Atomic Energy Establishment
Reactor Systems Analysis Division
Winfrith, Dorchester
Dorset DT2 8DH
ENGLAND

Ryohel Kiyose
University of Tokyo
Dept. of Nuclear Engineering
7-3-1 Hongo Bunkyo
Tokyo 113
JAPAN

George Klopp
Commonwealth Edison Company
P.O. Box 767, Room 35W
Chicago, IL 60690

Klaus Koberlein
Gesellschaft Fur Reaktorsicherheit
Forschungsgelande
D-8046 Garching
FEDERAL REPUBLIC OF GERMANY

E. Kohn
Atomic Energy Canada Ltd.
Candu Operations
Mississauga
Ontario, L5K 1B2
CANADA

Alan M. Kolaczkowski
Science Applications International Corporation
2109 Air Park Road, S.E.
Albuquerque, NM 87106

S. Kondo
Department of Nuclear Engineering
Facility of Engineering
University of Tokyo
3-1, Hongo 7, Bunkyo-ku
Tokyo
JAPAN

Herbert J. C. Kouts
Brookhaven National Laboratory
Building 179C
Upton, NY 11973

Thomas Kress
Oak Ridge National Laboratory
P.O. Box Y
Oak Ridge, TN 37831

W. Kroger
Institut fur Nukleare Sicherheitsforschung
Kernforschungsanlage Julich GmbH
Postfach 1913
D-5170 Julich 1
FEDERAL REPUBLIC OF GERMANY

Greg Krueger [3]
Philadelphia Electric Co.
2301 Market St.
Philadelphia, PA 19101

Bernhard Kuczera
Kernforschungzentrum Karlsruhe
LWR Safety Project Group (PRS)
P. O. Box 3640
D-7500 Karlsruhe 1
FEDERAL REPUBLIC OF GERMANY

Jeffrey L. LaChance
Science Applications International Corporation
2109 Air Park Road S.E.
Albuquerque, NM 87106

H. Larsen
Riso National Laboratory
Postbox 49
DK-4000 Roskilde
DENMARK

Wang L. Lau
Tennessee Valley Authority
400 West Summit Hill Avenue
Knoxville, TN 37902

Timothy J. Leahy
EI Services
1851 South Central Place, Suite 201
Kent, WA 98031

John C. Lee
University of Michigan
North Campus
Dept. of Nuclear Engineering
Ann Arbor, MI 48109

Tim Lee
USNRC-RES/RPSB
MS: NL/N-353

Mark T. Leonard
Science Applications International Corporation
2109 Air Park Road, SE
Albuquerque, NM 87106

Leo LeSage
Director, Applied Physics Div.
Argonne National Laboratory
Building 208, 9700 South Cass Ave.
Argonne, IL 60439

Milton Levenson
Bechtel Western Power Company
50 Beale St.
San Francisco, CA 94119

Librarian
NUMARC/USCEA
1776 I Street NW, Suite 400
Washington, DC 80006

Eng Lin
Taiwan Power Company
242, Roosevelt Rd., Sec. 3
Taipei
TAIWAN

N. J. Liparulo
Westinghouse Electric Corp.
P. O. Box 355
Pittsburgh, PA 15230

Y. H. (Ben) Liu
Department of Mechanical Engineering
University of Minnesota
Minneapolis, MN 55455

Bo Liwnang
IAEA A-1400
Swedish Nuclear Power Inspectorate
P.O. Box 27106
S-102 52 Stockholm
SWEDEN

J. P. Longworth
Central Electric Generating Board
Berkeley Gloucester
GL13 9PB
UNITED KINGDOM

Walter Lowenstein
Electric Power Research Institute
3412 Hillview Avenue
P. O. Box 10412
Palo Alto, CA 94303

William J. Luckas
Brookhaven National Laboratory
Building 130
Upton, NY 11973

Hans Ludewig
Brookhaven National Laboratory
Building 130
Upton, NY 11973

Robert J. Lutz, Jr.
Westinghouse Electric Corporation
Monroeville Energy Center
EC-E-371, P. O. Box 355
Pittsburgh, PA 15230-0355

Phillip E. MacDonald
EG&G Idaho, Inc.
P.O. Box 1625
Idaho Falls, ID 83415

Jim Mackenzie
World Resources Institute
1735 New York Ave. NW
Washington, DC 20006

Richard D. Fowler
Idaho Nat. Engineering Laboratory
P.O. Box 1625
Idaho Falls, ID 83415

A. P. Malinauskas
Oak Ridge National Laboratory
P.O. Box Y
Oak Ridge, TN 37831

Giuseppe Mancini
Commission European Comm.
CEC-JRC Eraton
Ispra Varese
ITALY

Lasse Mattila
Technical Research Centre of Finland
Lonnrotinkatu 37, P. O. Box 169
SF-00181 Helsinki 18
FINLAND

Roger J. Mattson
SCIENTECH Inc.
11821 Parklawn Dr.
Rockville, MD 20852

Donald McPherson
USNRC-NRR/DONRR
MS: 12G-18

Jim Metcalf
Stone and Webster Engineering Corporation
245 Summer St.
Boston, MA 02107

Mary Meyer
A-1, MS F600
Los Alamos National Laboratory
Los Alamos, NM 87545

Ralph Meyer
USNRC-RES/AEB
MS: NL/N-344

Charles Miller
8 Hastings Rd.
Momsey, NY 10952

Joseph Miller
Gulf States Utilities
P. O. Box 220
St. Francisville, LA 70775

William Mims
Tennessee Valley Authority
400 West Summit Hill Drive.
W10D199C-K
Knoxville, TN 37902

Jocelyn Mitchell
USNRC-RES/SAIB
MS: NL/S-324

Kam Mohktarian
CBI Na-Con Inc.
800 Jorie Blvd.
Oak Brook, IL 60521

James Moody
P.O. Box 641
Rye, NH 03870

S. Mori
Nuclear Safety Division
OECD Nuclear Energy Agency
38 Blvd. Suchet
75016 Paris
FRANCE

Walter B. Murfin
P.O. Box 550
Mesquite, NM 88048

Joseph A. Murphy
USNRC-RES/DSR
MS: NL/S-007

V. I. Nath
Safety Branch
Safety Engineering Group
Sheridan Park Research Community
Mississauga, Ontario L5K 1B2
CANADA

Susan J. Niemczyk
1545 18th St. NW, #112
Washington, DC 20036

Pradyot K. Niyogi
USDOE-Office of Nuclear Safety
Washington, DC 20545

Paul North
EG&G Idaho, Inc.
P. O. Box 1625
Idaho Falls, ID 83415

Edward P. O'Donnell
Ebasco Services, Inc.
2 World Trade Center, 89th Floor
New York, NY 10048

David Okrent
UCLA
Boelter Hall, Room 5532
Los Angeles, CA 90024

Robert L. Olson
Tennessee Valley Authority
400 West Summit Hill Rd.
Knoxville, TN 37902

Simon Ostrach
Case Western Reserve University
418 Glenman Bldg.
Cleveland, OH 44106

D. Paddleford
Westinghouse Electric Corporation
Savanna River Site
Aiken, SC 29808

Robert L. Palla, Jr.
USNRC-NRR/PRAB
MS: 10A-2

Chang K. Park
Brookhaven National Laboratory
Building 130
Upton, NY 11973

Michael C. Parker
Illinois Department of Nuclear Safety
1035 Outer Park Dr.
Springfield, IL 62704

Gareth Parry
NUS Corporation
910 Clopper Road
Gaithersburg, MD 20878

J. Pelce
Departement de Surete Nucleaire
IPSN
Centre d'Estudes Nucleaires du CEA
B.P. no. 6, Cedex
F-92260 Fontenay-aux-Roses
FRANCE

G. Petrangeli
ENEA Nuclear Energy ALT Disp
Via V. Brancati, 48
00144 Rome
ITALY

Marty Plys
Fauske and Associates
16W070 West 83rd St.
Burr Ridge, IL 60521

Mike Podowski
Department of Nuclear Engineering and Engineering Physics
RPI
Troy, NY 12180-3590

Robert D. Pollard
Union of Concerned Scientists
1616 P Street, NW, Suite 310
Washington, DC 20036

R. Potter
UK Atomic Energy Authority
Winfrith, Dorchester
Dorset, DT2 8DH
UNITED KINGDOM

William T. Pratt
Brookhaven National Laboratory
Building 130
Upton, NY 11973

M. Preat
Chef du Service Surete Nucleaire et Assurance Qualite
TRACTEBEL
Bd. du Regent 8
B-100 Bruxells
BELGIUM

David Pyatt
USDOE
MS: EH-332
Washington, DC 20545

William Raisin
NUMAEC
1726 M St. NW
Suite 904
Washington, DC 20036

Joe Rashid
ANATECH Research Corp.
3344 N. Torrey Pines Ct.
Suite 1320
La Jolla, CA 90237

Dale M. Rasmuson
USNRC-RES/PRAB
MS: NL/S-372

Ingvard Rasmussen
Riso National Laboratory
Postbox 49
DK-4000, Roskilde
DENMARK

Norman C. Rasmussen
Massachusetts Institute of
Technology
77 Massachusetts Avenue
Cambridge, MA 02139

John W. Reed
Jack R. Benjamin & Associates, Inc.
444 Castro St., Suite 501
Mountain View, CA 94041

David B. Rhodes
Atomic Energy of Canada, Ltd.
Chalk River Nuclear Laboratories
Chalk River, Ontario K0J1P0
CANADA

Dennis Richardon
Westinghouse Electric Corporation
P.O. Box 355
Pittsburgh, PA 15230

Doug Richeard
Virginia Electric Power Co.
P.O.Box 26666
Richmond, VA 23261

Robert Ritzman
Electric Power Research Institute
3412 Hillview Avenue
Palo Alto, CA 94304

Richard Robinson
USNRC-RES/PRAB
MS: NL/S-372

Jack E. Rosenthal
USNRC-AEOD/ROAB
MS: MNBB-9715

Denwood F. Ross
USNRC-RES
MS: NL/S-007

Frank Rowsome
9532 Fern Hollow Way
Gaithersburg, MD 20879

Wayne Russell
SERI
5360 I-55 North
Jackson, MS 39211

Jorma V. Sandberg
Finnish Ctr. Rad. Nucl. and Safety
Department of Nuclear Safety
P.O. Box 268
SF-00101 Helsinki
FINLAND

G. Saponaro
ENEA Nuclear Engineering Alt.
Zia V Brancati 4B
00144 ROME
ITALY

M. Sarran
United Engineers
P. O. Box 8223
30 S 17th Street
Philadelphia, PA 19101

Marty Sattison
EG&G Idaho
P. O. Box 1625
Idaho Falls, ID 83415

George D. Sauter
Electric Power Research Institute
3412 Hillview Avenue
Palo Alto, CA 94303

Jorge Schulz
Bechtel Western Power Corporation
50 Beale Street
San Francisco, CA 94119

B. R. Sehgal
Electric Power Research Institute
3412 Hillview Avenue
Palo Alto, CA 94303

Subir Sen
Bechtel Power Corp.
15740 Shady Grove Road
Location 1A-7
Gaithersburg, MD 20877

S. Serra
Ente Nazionale per l'Energia
Electtrica (ENEL)
via G. B. Martini 3
Rome
ITALY

Bonnie J. Shapiro
Science Applications International Corporation
360 Bay Street
Suite 200
Augusta, GA 30901

H. Shapiro
Licensing and Risk Branch
Atomic Energy of Canada Ltd.
Sheridan Park Research Community
Mississauga, Ontario L5K 1B2
CANADA

Dave Sharp
Westinghouse Savannah River Co.
Building 773-41A, P. O. Box 616
Aiken, SC 29802

John Sherman
Tennessee Environmental Council
1719 West End Avenue, Suite 227
Nashville, TN 37203

Brian Sheron
USNRC-RES/DSR
MS: NL/N-007

Rick Sherry
JAYCOR
P. O. Box 85154
San Diego, CA 92138

Steven C. Sholly
MHB Technical Associates
1723 Hamilton Avenue, Suite K
San Jose, CA 95125

Louis M. Shotkin
USNRC-RES/RPSB
MS: NL/N-353

M. Siebertz
Chef de la Section Surete' des Reacteurs
CEN/SCK
Boeretang, 200
B-2400 Mol
BELGIUM

Melvin Silberberg
USNRC-RES/DE/WNB
MS: NL/S-260

Gary Smith
SERI
5360 I-55 North
Jackson, MS 39211

Gary L. Smith
Westinghouse Electric Corporation
Hanford Site
Box 1970
Richland, WA 99352

Lanny N. Smith
Science Applications International Corporation
2109 Air Park Road SE
Albuquerque, NM 87106

K. Soda
Japan Atomic Energy Res. Inst.
Tokai-Mura Naka-Gun
Ibaraki-Ken 319-11
JAPAN

David Sommers
Virginia Electric Power Company
P. O. Box 26666
Richmond, VA 23261

Herschel Spector
New York Power Authority
123 Main Street
White Plains, NY 10601

Themis P. Speis
USNRC-RES
MS: NL/S-007

Klaus B. Stadie
OECD-NEA, 38 Bld. Suchet
75016 Paris
FRANCE

John Stetkar
Pickard, Lowe & Garrick, Inc.
2216 University Drive
Newport Beach, CA 92660

Wayne L. Stiede
Commonwealth Edison Company
P.O. Box 767
Chicago, IL 60690

William Stratton
Stratton & Associates
2 Acoma Lane
Los Alamos, NM 87544

Soo-Pong Suk
Korea Advanced Energy Research Institute
P. O. Box 7
Daeduk Danji, Chungnam 300-31
KOREA

W. P. Sullivan
GE Nuclear Energy
175 Curtner Ave., M/C 789
San Jose, CA 95125

Tony Taig
U.K. Atomic Energy Authority
Wigshaw Lane, Culcheth
Warrington, Cheshire, WA3 4NE
UNITED KINGDOM

John Taylor
Electric Power Research Institute
3412 Hillview Avenue
Palo Alto, CA 94303

Harry Teague
U.K. Atomic Energy Authority
Wigshaw Lane, Culcheth
Warrington, Cheshire, WA3 4NE
UNITED KINGDOM

Technical Library
Electric Power Research Institute
P.O. Box 10412
Palo Alto, CA 94304

Mark I. Temme
General Electric, Inc.
P.O. Box 3508
Sunnyvale, CA 94088

T. G. Theofanous
University of California, S.B.
Department of Chemical and Nuclear Engineering
Santa Barbara, CA 93106

David Teolis
Westinghouse-Bettis Atomic Power Laboratory
P. O. Box 79, ZAP 34N
West Mifflin, PA 15122-0079

Ashok C. Thadani
USNRC-NRR/SAD
MS: 7E-4

Garry Thomas
L-499 (Bldg. 490)
Lawrence Livermore National Laboratory
7000 East Ave.
P.O. Box 808
Livermore, CA 94550

Gordon Thompson
Institute for Research and Security Studies
27 Ellworth Avenue
Cambridge, MA 02139

Grant Thompson
League of Women Voters
1730 M. Street, NW
Washington, DC 20036

Arthur Tingle
Brookhaven National Laboratory
Building 130
Upton, NY 11973

Rich Toland
United Engineers and Construction
30 S. 17th St., MS 4V7
Philadelphia, PA 19101

Brian J. R. Tolley
DG/XII/D/1
Commission of the European Communities
Rue de la Loi, 200
B-1049 Brussels
BELGIUM

David R. Torgerson
Atomic Energy of Canada Ltd.
Whiteshell Nuclear Research Establishment
Pinawa, Manitoba, ROE 1LO
CANADA

Dr. Alfred F. Torri
1421 Hymettus Avenue
Leucadia, CA 92024

Klau Trambauer
Gesellschaft Fur Reaktorsicherheit
Forschungsgelande
D-8046 Garching
FERERAL REPUBLIC OF GERMANY

Nicholas Tsoulfanidis
Nuclear Engineering Dept.
University of Missouri-Rolla
Rolla, MO 65401-0249

Chao-Chin Tung
c/o H.B. Bengelsdorf
ERC Environmental Services Co.
P. O. Box 10130
Fairfax, VA 22030

Brian D. Turland
UKAEA Culham Laboratory
Abingdon, Oxon OX14 3DB
ENGLAND

Takeo Uga
Japan Institute of Nuclear Safety
Nuclear Power Engineering Test Center
3-6-2, Toranomon
Minato-ku, Tokyo 108
JAPAN

Stephen D. Unwin
Battelle Columbus Division
505 King Avenue
Columbus, OH 43201

A. Valeri
DISP
ENEA
Via Vitaliano Brancati, 48
I-00144 Rome
ITALY

Harold VanderMolen
USNRC-RES/PRAB
MS: NL/S-372

G. Bruce Varnado
ERC International
1717 Louisiana Blvd. NE, Suite 202
Albuquerque, NM 87110

Jussi K. Vaurio
Imatran Voima Oy
Loviisa NPS
SF-07900 Loviisa
FINLAND

William E. Vesely
Science Applications International Corporation
655 Metro Place South, Suite 745
Dubbin, OH 43017

J. I. Villadoniga Tallon
Div. of Analysis and Assessment
Consejo de Seguridad Nuclear
c/ Sor Angela de la Cruz, 3
28020 Madrid
SPAIN

Willem F. Vinck
Kapellestract 25
1980
Tervuren
BELGIUM

R. Virolainen
Office of Systems Integration
Finnish Centre for Radiation and Nuclear Safety
Department of Nuclear Safety
P.O. Box 268
Kumpulantie 7
SF-00520 Helsinki
FINLAND

Raymond Viskanta
School of Mechanical Engineering
Purdue University
West Lafayette, IN 47907

S. Visweswaran
General Electric Company
175 Curtner Avenue
San Jose, CA 95125

Truong Vo
Pacific Northwest Laboratory
Battelle Blvd.
Richland, WA 99352

Richard Vogel
Electric Power Research Institute
P. O. Box 10412
Palo Alto, CA 94303

G. Volta
Engineering Division
CEC Joint Research Centre
CP No. 1
I-21020 Ispra (Varese)
ITALY

Ian B. Wall
Electric Power Research Institute
3412 Hillview Avenue
Palo Alto, CA 94303

Adolf Walser
Sargent and Lundy Engineers
55 E. Monroe Street
Chicago, IL 60603

Edward Warman
Stone & Webster Engineering Corp.
P.O. Box 2325
Boston, MA 02107

Norman Weber
Sargent & Lundy Co.
55 E. Monroe Street
Chicago, IL 60603

Lois Webster
American Nuclear Society
555 N. Kensington Avenue
La Grange Park, IL 60525

Wolfgang Werner
Gesellschaft Fur Reaktorsicherheit
Forschungsgelande
D-8046 Garching
FEDERAL REPUBLIC OF GERMANY

Don Wesley
IMPELL
1651 East 4th Street
Suite 210
Santa Ana, CA 92701

Detlof von Winterfeldt
Institute of Safety and Systems Management
University of Southern California
Los Angeles, CA 90089-0021

Pat Worthington
USNRC-RES/AEB
MS: NL/N-344

John Wreathall
Science Applications International Corporation
655 Metro Place South, Suite 745
Dubbin, OH 43017

D. J. Wren
Atomic Energy of Canada Ltd.
Whiteshell Nuclear Research Establishment
Pinawa, Manitoba, ROE 1LO
CANADA

Roger Wyrick
Inst. for Nuclear Power Operations
1100 Circle 75 Parkway, Suite 1500
Atlanta, GA 30339

Kun-Joong Yoo
Korea Advanced Energy Research Institute
P. O. Box 7
Daeduk Danji, Chungnam 300-31
KOREA

Faith Young
Energy People, Inc.
Dixou Springs, TN 37057

Jonathan Young
R. Lynette and Associates
15042 Northeast 40th St.
Suite 206
Redmond, WA 98052

C. Zaffiro
Division of Safety Studies
Directorate for Nuclear Safety and Health Protection
Ente Nazionale Energie Alternative
Via Vitaliano Brancati, 48
I-00144 Rome
ITALY

Mike Zentner
Westinghouse Hanford Co.
P. O. Box 1970
Richland, WA 99352

X. Zikidis
Greek Atomic Energy Commission
Agia Paraskevi, Attiki
Athens
GREECE

Bernhard Zuczera
Kernforschungszentrum
Postfach 3640
D-7500 Karlsruhe
FEDERAL REPUBLIC OF GERMANY

1521 J. R. Weatherby
3141 S. A. Landenberger [5]
3151 W. I. Klein
5214 D. B. Clauss
6344 E. D. Gorham
6001 D. D. Carlson
6001 R. J. Breeding
6001 D. M. Kunsman
6400 D. J. McCloskey
6410 D. A. Dahlgren
6412 A. L. Camp
6412 S. L. Daniel
6412 T. M. Hake
6412 L. A. Miller
6412 D. B. Mitchell
6412 A. C. Payne, Jr.
6412 T. T. Sype
6412 T. A. Wheeler
6412 D. W. Whitehead
6413 T. D. Brown
6413 F. T. Harper [2]
6415 R. M. Cranwell
6415 W. R. Cramond [3]
6415 R. L. Iman
6418 J. E. Kelly
6418 K. J. Maloney
6419 M. P. Bohn
6419 J. A. Lambright
6422 D. A. Powers
6424 K. D. Bergeron
6424 J. J. Gregory
6424 D. R. Bradley
6424 D. C. Williams
6425 S. S. Dosanjh
6453 J. S. Philbin
6900 A. W. Snyder
6460 J. V. Walker
6463 M. Berman
6463 M. P. Sherman
6471 L. D. Bustard
6473 W. A. von Riesemann
8524 J. A. Wackerly